

Final Report for the AISC Fellowship Project

Development of Long Span Floor Systems for Multi-Story Residential Structures

Devin Huber and Amit Varma

Ph.D. Student and Associate Professor

Purdue University

School of Civil Engineering

West Lafayette

Indiana 47906

November 2008

TABLE OF CONTENTS

	Page
LIST OF TABLES	x
LIST OF FIGURES	xii
ABSTRACT	xxi
CHAPTER 1. INTRODUCTION	1
1.1. General Overview of Traditional Floor Systems in Steel Construction	1
1.1.1. Advantages of Steel Deck-Concrete Slab Composite Floor Systems.....	1
1.1.2. Disadvantages	2
1.2. Objectives and Goals of Research	2
CHAPTER 2. LITERATURE REVIEW AND FURTHER BACKGROUND	5
2.1. Introduction.....	5
2.2. Previous Research.....	5
2.2.1. Widjaja Deep Deck Research	5
2.2.2. Hillman and Murray Deck-on-Deck System	6
2.2.3. Sandwich Panel Systems.....	7
2.3. Alternatives to Traditional Composite Floor Systems in Steel Construction	9
2.3.1. Stub Girder System	9
2.3.2. <i>Slimdek</i> System	10
2.4. <i>Girder Slab</i> Floor System	11
2.5. Synopsis/Evaluation.....	12
2.6. Floor Vibration Requirements and Research.....	13
2.6.1. Modeling Human Motion	13
2.6.2. Structural Modeling for Vibration Analysis	14
2.6.3. Acceptance Criteria.....	17
2.7. UK Guidelines – Differences from U.S. Guidelines	17

	Page
2.8. Comments on Guidelines.....	20
2.9. Fire Resistance Requirements and Research	20
2.9.1. Fire Resistant Design – Prescriptive Approach	20
2.9.2. Performance Based (PB) Fire Resistant Design	23
2.9.3. Comments of Fire Resistant Design	24
2.10. Scope and Limits of Research	24
CHAPTER 3. OVERVIEW OF DEVELOPED FLOOR SYSTEMS	45
3.1. Introduction/Overview.....	45
3.2. Sandwich Type Composite Floor Systems	45
3.2.1. Double Skin Composite System	45
3.2.2. Profiled Double Skin Composite (DSC) System	46
3.3. Advanced Metal Deck Systems	47
3.3.1. Composite Cellular Deep Deck (CC-DD) System.....	48
3.3.2. Shored Composite Deep Deck (SC-DD) System.....	50
3.3.3. Sandwich Metal Deck System	51
3.3.4. Reduced Weight Composite Deep Deck (RW-DD) System.....	52
3.4. Pre-Loaded Self-Shoring (PLSS) System.....	52
3.4.1. Case Study	54
3.4.2. System Development	55
3.5. Ratings of Proposed Systems.....	56
CHAPTER 4. COMPOSITE CELLULAR DEEP DECK SYSTEMS.....	70
4.1. Summary of CC-DD System	70
4.2. Analysis and Design of CC-DD System – Strength and Stiffness	70
4.2.1. Code-Based Design Approach	70
4.2.2. Non-Linear Inelastic Analysis	73
4.2.3. 3D Finite Element Analysis – No Slip.....	78
4.2.4. Discussion of Three Analysis Methods	80
4.3. Other Design Issues – Floor Vibrations and Fire Resistance	80
4.4. Experimental Setup – Composite Cellular Deep Deck Systems Structural Tests .	81
4.4.1. Composite Deep Deck Structural Tests	82
4.4.2. Frequency Determination Test.....	85
4.4.3. Test Matrix of CC-DD Systems.....	86

	Page
4.5. Construction Phase and Dynamic Testing	87
4.5.1. Construction Phase Results and Discussion	87
4.5.2. Modal Impact Testing Results and Discussion	88
4.6. Ultimate Load Testing Results	91
4.6.1. CC-DD Specimen 1 Results and Discussion	91
4.6.2. Specimen 2 Results and Discussion.....	94
4.6.3. CC-DD Specimen 3 Results and Discussion	96
4.6.4. CC-DD Specimen 4 Test Results and Discussion	99
4.7. General Discussion Points of CC-DD Test Results.....	101
4.7.1. Construction Phase Results Discussion Points	102
4.7.2. Dynamic/Modal Impact Testing Results Discussion Points.....	102
4.7.3. Ultimate Load Testing Results Discussion Points	103
CHAPTER 5. ELEVATED TEMPERATURE TESTING OF CC-DD SPECIMENS ..	162
5.1. Test Setup for Heat Transfer Tests	162
5.2. Heat Transfer Test Results.....	163
5.3. Summary of Findings.....	164
5.4. Combined Thermal and Mechanical Loading Behavior of CC-DD Specimen ...	164
5.4.1. Test Setup.....	164
5.4.2. Experimental Results – Combined Heating and Loading Test.....	166
5.4.3. General Discussion Points of Combined Heating and Loading Test.....	169
CHAPTER 6. SHORED COMPOSITE DEEP DECK SYSTEM	193
6.1. Summary of the Shored Composite Deep Deck System	193
6.2. Preliminary Analysis and Design of SC-DD System	193
6.2.1. Code-Based Design Approach	193
6.2.2. Numerical Non-Linear Inelastic Analysis.....	195
6.2.3. Finite Element Analysis	196
6.3. Experimental Setup.....	196
6.4. Experimental Results and Discussion.....	197
6.4.1. Construction Phase Results and Discussion	197
6.4.2. Modal Impact Testing Results and Discussion.....	198
6.4.3. Ultimate Load Test	199

	Page
CHAPTER 7. REDUCED WEIGHT DEEP DECK SYSTEM	221
7.1. Summary of RW-DD System	221
7.2. Preliminary Analysis and Design	221
7.2.1. Design Code Based Approach	221
7.2.2. Numerical Non-Linear Inelastic Analysis.....	222
7.2.3. Finite Element Analysis	222
7.3. Experimental Setup.....	223
7.4. Experimental Results and Discussion.....	223
7.4.1. Construction Phase Results and Discussion	223
7.4.2. Modal Impact Testing Results and Discussion.....	224
7.4.3. Ultimate Load Test Results and Discussion	224
CHAPTER 8. PRE-LOADED SELF-SHORED SYSTEM.....	234
8.1. Analysis and Design of System – Construction Phase	234
8.1.1. Phase 1	234
8.1.2. Phase 2	235
8.1.3. Phase 3	237
8.1.4. Determination of ideal upward force and deflection	238
8.1.5. Analysis and Design of System – Composite Phase.....	239
8.1.6. Design Example for Pre-Loaded Self-Shored System.....	239
8.2. Experimental Setup – PLSS System.....	242
8.2.1. Overall Test Setup.....	242
8.3. Experimental Results and Discussion – PLSS System.....	244
8.3.1. Construction Phase.....	244
8.3.2. Composite Phase Results	245
CHAPTER 9. FURTHER ANALYSIS AND DESIGN STUDIES ON STRUCTURAL BEHAVIOR OF COMPOSITE DEEP DECK SYSTEMS.....	261
9.1. Analysis of Ultimate Load Testing Results – Deep Deck Systems	261
9.1.1. Fiber Models and FEM Models – No Construction or Slip Effects	261
9.1.2. Fiber and FEM models accounting for Construction Effects	263
9.1.3. Modeling Approaches for Partial Composite Action – Interfacial Slip in Fiber Based Model.....	266
9.1.4. Partial Composite Action – FEM Approach.....	271
9.1.5. Results of interfacial Slip (Partial Composite) Models	272

	Page
9.2. General Discussion of Structural Analytical Models for Deep Deck Systems....	274
CHAPTER 10. COMPOSITE DEEP DECK FLOOR VIBRATION SYSTEM STUDY	297
10.1. Parametric Study Using US and UK Guidelines	297
10.1.1. AISC Guidelines	298
10.1.2. Steel Construction Institute Criteria.....	299
10.1.3. Discussion Points and Issues with Evaluation Guidelines.....	300
10.2. Finite Element Investigation of Floor Vibrations for Deep Deck Systems	300
10.2.1. Predicted Dynamic Parameters for Developed Models	302
10.2.2. Other Possible Applications of Modeling Technique	305
CHAPTER 11. ANALYSIS AND DESIGN RECCOMENDATIONS FOR COMPOSITE DEEP DECK SYSTEMS	322
11.1. Recommendations for Strength and Serviceability Evaluation of Composite Deep Deck Systems.....	322
11.1.1. Composite Strength of Long Span Composite Deep Deck Systems	324
11.1.2. Recommendations for serviceability criteria	327
11.1.3. Fire Resistance and Behavior.....	328
CHAPTER 12. SUMMARY, CONCLUSIONS, AND FUTURE WORK	330
12.1. Background and Literature Review	330
12.2. Overview of Developed Floor Systems	331
12.3. Composite Cellular Deep Deck Systems Experimental Validation.....	331
12.4. Shored Composite Deep Deck (SC-DD) System Experimental Validation	334
12.5. Pre-Loaded Self-Shored (PLSS) System	335
12.6. Analysis and Design Studies for Structural Behavior of Composite Deep Deck Systems	336
12.7. Floor Vibration Parametric Studies and FEM Modeling.....	337
12.8. Analysis and Design Recommendations for Composite Deep Deck Systems ..	338
12.9. Recommendations.....	339
12.9.1. Recommendations for Long Span Floor Systems.....	339
12.9.2. Recommendations for Future Work.....	339
LIST OF REFERENCES	341
APPENDICES	
Appendix A.....	346
Appendix B.....	366
Appendix C.....	375

LIST OF TABLES

Table	Page
Table 2.1: Table of suggested distributed weights based on structure. [Murray, Allen, and Ungar 2003].....	26
Table 2.2: Parameters suggested by Murray, Allen, and Ungar [2003] for use in calculating the peak acceleration of the floor system in a given structure.....	26
Table 2.3: Results of Easterling and Widjaja research (Widjaja, 1997).....	26
Table 2.4: Loading for common rhythmic activities [Allen, Onysko, and Murray 1999].	27
Table 2.5: Values for L_{eff} and S used in determining the effective mass of the Floor (re-produced from SCI Publication 076).....	27
Table 2.6: Response Factors for SCI Guidelines (SCI, 1989).....	28
Table 2.7: Fire resistant ratings and temperature criteria for standard fire tests on floor systems (reproduced from(Cedeno, 2006)).....	28
Table 2.8: Fire resistant ratings and temperature criteria for standard fire tests on floor systems (reproduced from (Cedeno, 2006)).....	29
Table 3.1: Increase in stiffness from increase steel deck depths	58
Table 3.2: W Sections Used In Study	58
Table 3.3: Parameters Used In Study.....	58
Table 3.4: Ratings of proposed systems	59
Table 4.1: Design Checks of CC-DD System.....	104
Table 4.2: Assumed nominal material properties used for models.....	104
Table 4.3: Relevant results of numerical non-linear inelastic analysis.....	104
Table 4.4: Results for floor vibration analysis on CC-DD Systems.....	104
Table 4.5: Fire Ratings based on UL Assembly D903 for 4.5, 6, and 7.5 in. deep deck assemblies.....	105
Table 4.6: Specifications for steel strain gauges used (reproduced from Texas Measurements website www.straingauge.com).....	105
Table 4.7: Specifications for concrete strain gauges used (reproduced from Texas Measurements website www.straingauge.com).....	105
Table 4.8: Testing matrix for CC-DD systems	106
Table 4.9: Summary of construction phase results for CC-DD Specimens.....	106
Table 4.10: Measured and Calculated Natural Frequencies for Tested Specimens.....	106
Table 4.11: Estimated damping at first resonant frequency for CC-DD Specimens	107
Table 4.12: Output Spectra values for heel drops on CC-DD Spectra 3	107

Table	Page
Table 4.13: Relative Stiffness Parameters of Specimen 1	107
Table 4.14: R^2 values for strain distribution at various loading values CC-DD Specimen 1	107
Table 4.15: Relative Stiffness Parameters of CC-DD Specimen 2.....	108
Table 4.16: R^2 values for strain distribution at various loading values CC-DD Specimen 2.....	108
Table 4.17: Relative Stiffness Parameters of CC-DD Specimen 3.....	108
Table 4.18: R^2 values for strain distribution at various loading values CC-DD Specimen 3	109
Table 4.19: Relative stiffness parameters of CC-DD Specimen 4.....	109
Table 4.20: R^2 values for strain distribution at various loading values CC-DD Specimen 4	109
Table 6.1: Design checks for SC-DD System using code based approach.....	203
Table 6.2: Change in Microstrain readings from removal of shoring.....	203
Table 6.3: Relative stiffness parameters of SC-DD Specimen	203
Table 6.4: R^2 values for strain distribution at various loading values for SC-DD Specimen	204
Table 7.1: Design Checks of RW-DD System.....	226
Table 7.2: Summary of construction phase measurements for RW-DD Specimen.....	226
Table 8.1: Construction phase results for PLSS System.....	247
Table 9.1: Geometric and material properties for CC-DD Specimens	275
Table 9.2: Predicted and Experimental un-cracked (UC) and cracked (C) stiffness for CC-DD Specimens	275
Table 9.3: Predicted and Experimental capacities for CC-DD Specimens – Full Composite Models	275
Table 9.4: Capacity and stiffness prediction for SC-DD Specimen – Full Composite Models	276
Table 9.5: Predicted and Experimental capacities for CC-DD Specimens – Full Composite Models with construction effects.....	276
Table 9.6: Predicted and Experimental capacities for SC-DD Specimen.....	276
Table 9.7: Predicted and experimental capacities for CC-DD Specimens models that account for interfacial slip and construction effects	276
Table 9.8: Predicted and experimental capacities for SC-DD Specimen that account for interfacial slip and construction effects.....	277
Table 10.1: Results from AISC Parameter Study 1	306
Table 10.2: Results from AISC Parameter Study 2	306
Table 10.3: Results from AISC Parameter Study 3	306
Table 10.4: SCI Criteria Results	307
Table 10.5: First 12 resonant frequencies for FEM models (no additional loading).....	307
Table 10.6: Modal effective mass ratios for various models – first 12 modes of vibration	308
Table 10.7: Modal effective mass ratio for 9 bay model – first 20 modes of vibration	309
Table 11.1: Shoring factors (ASCE, 1992).....	329

Table	Page
Table 11.2: Predicted and actual capacities	329
Table A.1: Design Forces for Cellular Sandwich System	360
Table C.1: Measured yield stress and tensile stress for 14 gage steel material taken from CC-DD Specimens	382
Table C.2: Measured yield stress and tensile stress for 16 gage steel material taken from CC-DD Specimens	382
Table C.3: Measured yield stress and tensile stress for 18 gage steel material taken from CC-DD Specimens	382
Table C.4: Measured yield stress and tensile stress for 20 gage steel material taken from CC-DD Specimens	383
Table C.5: Measured yield stress and tensile stress for 18 gage steel material taken from CC-DD Specimens	383

LIST OF FIGURES

Figure	Page
Figure 1.1: Typical Steel Deck Profiles Used in Floor Systems (Canam Steel, 2002)	4
Figure 1.2: Typical Steel Deck System (Buckner, 2002)	4
Figure 2.1: Profiles used in Widjaja research (Widjaja, 1997).....	30
Figure 2.2: Test setup for Widjaja research (Widjaja, 1997).....	30
Figure 2.3: Load-deflection results for LSS1 (Widjaja, 1997)	31
Figure 2.4: Load-deflection results for LSS2 (Widjaja, 1997)	31
Figure 2.5: Conceptual floor systems for use in steel construction conceived by Hillman and Murray (Hillman & Murray, 1990)	32
Figure 2.6: Hillman/Murray Deck-on-Deck 30 ft by 30 ft prototype system (Hillman & Murray, 1990).....	33
Figure 2.7: Measured frequencies for Deck-on-Deck prototype specimen (Hillman, 1990) 33	
Figure 2.8: DSC with (a) traditional shear studs and (b) Bi-Steel System (McKinley & Boswell, 2002).....	34
Figure 2.9: SPS system (Kennedy & Kennedy, 2004).....	34
Figure 2.10: Schematic of SPS system used for bridge deck application (Kennedy & Kennedy, 2004).....	35
Figure 2.11: Proposed SPS floor layout by Intelligent Engineering (Kennedy & Kennedy, 2004)	36
Figure 2.12: Connection details for SPS floor system (Kennedy & Kennedy, 2004)	36
Figure 2.13: Schematic of Stub Girder System (Wang, Padmanaban, & Shanmugam, 1995)	37
Figure 2.14: Construction photos of structure using Stub Girder System (a) prior to deck placement and (b) after deck placement (Colaco, 1972).....	37
Figure 2.15: SD 225 profile (Lawson, Mullet, & Rackham, 1997)	38
Figure 2.16: Original Slimflor system (Corus, 2002).....	38
Figure 2.17: Slimdek Flooring System with SD 225 deck and rolled ASB (Corus, 2002)	39
Figure 2.18: Schematic of <i>Girder Slab</i> System (Naccarato, 1999)	39
Figure 2.19: D-Beam Girder (Girder Slab Technologies, 2002)	40

Figure	Page
Figure 2.20: Scale factors to determine the forcing of a floor system due to walking as given by Murray, Allen, and Ungar [2003] (left) and Wyatt [1989] (right).....	40
Figure 2.21: Model of forcing due to walking taking into account high frequency content (Taken from Pavic and Reynolds 2002b after Ohlsson, 1988).	41
Figure 2.22: Idealized Lumped SDOF Dynamic System	41
Figure 2.23: (a) Bay of Structure and (b) Simply Supported Beam Idealization of System.....	42
Figure 2.24: Conventional Steel Deck-Concrete Slab System (a) isometric schematic and (b) Typical Interior Bay.....	42
Figure 2.25: Peak acceleration levels as recommended by the International Standards Organization (left) (from [Murray, Allen, and Ungar 2003]) and the Canadian annoyance criteria chart (from [Wyatt 1989]).	43
Figure 2.26: Typical Fundamental Mode Shapes for Composite Floor Systems (SCI, 2004).....	43
Figure 2.27: First Vibration Mode of Deep Deck Floor System (SCI, 2004)	44
Figure 2.28: UL Fire Design No. 858 (UL, 2003).....	44
Figure 3.1: Schematic of DSC Floor Panel.....	60
Figure 3.2: DSC Layout in Typical Bay	61
Figure 3.3: DSC panel for 30 ft spans.....	61
Figure 3.4: Sandwich System Using 1.5 or 2 in. Cellular Deck Profiles.....	61
Figure 3.5: (a) 1.5 in. and (b) 2 in. cellular floor deck profiles	62
Figure 3.6: Composite deep deck system cross section – 30 ft. Span	62
Figure 3.7: Possible End Detail for Composite Deep Deck System.....	63
Figure 3.8: Shear Stud Placed in Test Specimen	63
Figure 3.9: Test Specimen with 5/8” Puddle Welds.....	64
Figure 3.10: Cross-section of shored composite deep deck system (self weight of 78 psf with NWC and 62 psf with LWC)	64
Figure 3.11: Plan view of interior bay with shoring at mid-span	65
Figure 3.12: Schematic of Sandwiched Metal Deck System.....	65
Figure 3.13: Reduced weight composite deck system.....	66
Figure 3.14: $I_{actual} / I_{required}$ for Construction and Composite Phase - 8 ft Spacing and 30 ft Span.....	66
Figure 3.15: $I_{actual} / I_{required}$ for Construction and Composite Phase - 10 ft Spacing and 30 ft Span.....	67
Figure 3.16: $Z_{actual} / Z_{required}$ for Construction and Composite Phase - 8 ft Spacing and 30 ft Span.....	68
Figure 3.17: $Z_{actual} / Z_{required}$ for Construction and Composite Phase-10 ft Spacing and 30 ft Span.....	69
Figure 3.18: Conceptual Schematic of self Shoring System.....	69
Figure 4.1: Composite deep deck system cross section – 30 ft. Span	110
Figure 4.2: Fiber discretization for cross-section and assumptions for strain and stress.....	110
Figure 4.3: Flowchart for finding section moment-curvature relationship.....	111

Figure	Page
Figure 4.4: Beam member discretized into stations.....	111
Figure 4.5: Flow chart for finding load-deflection of beam	112
Figure 4.6: Predicted load-deflection behavior for 30 ft. span CC-DD systems with uniform loading and nominal material properties.....	113
Figure 4.7: Schematic of meshed structural FEM models for CC-DD systems	114
Figure 4.8: View of mesh for (a) steel components and (b) concrete.....	114
Figure 4.9: Cross-section of steel deck used in FEM models for (a) full geometry and (b) simplified geometry	115
Figure 4.10: Steel Material Model used in FEM	115
Figure 4.11: Concrete material property models used in FEM models (Simulia, 2007)	115
Figure 4.12: Almusallam curve for 4 ksi lightweight concrete	116
Figure 4.13: Load-deflection behavior of CC-DD systems with uniform loading and a 30 ft span	117
Figure 4.14: Plan View of Test Setup with CC-DD specimen	118
Figure 4.15: Schematic side view of sensor layout for deep deck tests (half span shown – symmetric).....	119
Figure 4.16: Strain Gage Locations in Specimen Cross-section at Mid-Span and quarter points.....	119
Figure 4.17: CC-DD Floor System Specimen (a) Before and (b) After Concrete Placement	120
Figure 4.18: Sensor and overall layout in the (a) construction phase and (b) composite phase	121
Figure 4.19: Schematics of (a) 603 Duncan potentiometer and (b) 606 Duncan potentiometer (BEI Duncan, 2008)	122
Figure 4.20: 1 in. stroke potentiometers used for measuring end slips showing (a) schematic and (b) actual sensor (BEI Duncan, 2008).....	123
Figure 4.21: Schematic of slip sensor setup.....	123
Figure 4.22: Photograph of slip sensor on CC-DD specimen.....	124
Figure 4.23: Schaevitz clinometers with manufacturer’s specifications (Measurement Specialties, 2008).....	124
Figure 4.24: Picture showing clinometer attached to test specimen.....	125
Figure 4.25: Schematic of CC-DD test specimens	126
Figure 4.26: Modal Impact Hammer and Specifications (PCB , 2008).....	127
Figure 4.27: Seismic Accelerometer used for Acquiring Data with Specifications (PCB , 2008).....	128
Figure 4.28: Applying Impact with Modal Hammer to test Specimen.....	128
Figure 4.29: Specimen with Accelerometers Attached.....	129
Figure 4.30: Data Acquisition Box with Specifications (National Instruments, 2008)	129
Figure 4.31: Strains during concrete pour and for 24 hours following pour on CC- DD Specimen 2	130
Figure 4.32: Frequency response magnitude for CC-DD Specimen 2 taken from mid-span hit showing north third point and mid-span accelerometer responses	131

Figure	Page
Figure 4.33: Frequency response magnitude for CC-DD Specimen 3 taken from mid-span hit showing north and south third point and mid-span accelerometer responses	132
Figure 4.34: Frequency response magnitude for CC-DD Specimen 4 taken from mid-span hit showing north and south third point and mid-span accelerometer responses	133
Figure 4.35: Frequency response magnitude for CC-DD Specimen 4 taken from south third span hit showing south third point accelerometer response to show second bending mode frequency	134
Figure 4.36: Illustration of estimating damping with half-power method.....	135
Figure 4.37: FRFs for CC-DD Specimen 3 with: (a) no loads, (b) 10 psf equivalent loading, and (c) 20 psf equivalent loading	136
Figure 4.38: Output Spectra for CC-DD Specimen 3 resulting from heel drops (y-axis is log scale)	137
Figure 4.39: Load vs. mid-span displacement plot for CC-DD Specimen 1	138
Figure 4.40: Displacement vs. time plot for north and south sensors at 6 th and load points over first 350 seconds – Specimen 1	139
Figure 4.41: Average load vs. measured rotation plot	140
Figure 4.42: Specimen 1 with approximately 6 in. of deflection at mid-span and 23 kips of load applied at each load point (load cycle 1).....	140
Figure 4.43: Cracks that formed at south support (a) top view and (b) side view.....	141
Figure 4.44: Close-up of southeast support crack during re-loading of Specimen 1.....	141
Figure 4.45: Specimen 1 strain gage profiles through depth at mid-span for various load levels.....	142
Figure 4.46: Specimen 1 strain gage profiles through depth at south end for various load levels.....	143
Figure 4.47: Load vs. mid-span displacement plot for CC-DD Specimen 2	144
Figure 4.48: Crack the formed over north support of Specimen 2	144
Figure 4.49: CC-DD Specimen 2 with approximately 8 in. of deflection at mid-span and 23 kips of load applied at each load point.....	145
Figure 4.50: Applied average load vs. measured end rotations for CC-DD Specimen 2	145
Figure 4.51: Mid-Span moment vs. average curvature of CC-DD Specimen 2	146
Figure 4.52: Average applied load vs. measured end slip for CC-DD Specimen 2	147
Figure 4.53: CC-DD Specimen 2 strain gage profiles through depth at mid-span for various load levels	148
Figure 4.54: CC-DD Specimen 2 strain gage profiles through depth at north load point for various load levels	149
Figure 4.55: Load vs. mid-span deflection plot for CC-DD Specimen 3	150
Figure 4.56: Shear bond failure crack that formed on CC-DD Specimen 3	150
Figure 4.57: Propagation of shear bond failure to north end	151
Figure 4.58: Average load vs. measured slip for CC-DD Specimen 3	151
Figure 4.59: Average load vs. measured end rotations for CC-DD Specimen 3	152
Figure 4.60: Mid-Span moment vs. average curvature of CC-DD Specimen 3	153

Figure	Page
Figure 4.61: CC-DD Specimen 3 strain gage profiles through depth at mid-span for various load levels	154
Figure 4.62: CC-DD Specimen 3 strain gage profile through depth at north end for various load levels	155
Figure 4.63: Load vs. mid-span displacement plot for CC-DD Specimen 4	156
Figure 4.64: Picture of crack that formed at south support.....	156
Figure 4.65: Applied average load vs. measured end rotations for CC-DD Specimen 4	157
Figure 4.66: Mid-Span moment vs. average curvature of CC-DD Specimen 4	157
Figure 4.67: Applied average load vs. measured slip plot.....	158
Figure 4.68: CC-DD Specimen 4 strain gage profile through depth at mid-span for various load levels.....	159
Figure 4.69: CC-DD Specimen 4 strain gage profile through depth at north end for various load levels.....	160
Figure 4.70: CC-DD Specimen 4 strain gage profile through depth at south end for various load levels	161
Figure 5.1: Side View Schematic of Heat Transfer Tests.....	170
Figure 5.2: Heat transfer specimen (a) after concrete pour and (b) during testing	170
Figure 5.3: Temperature vs. time curve for unprotected side of heat transfer specimen.....	171
Figure 5.4: Temperature vs. time curve for protected side of heat transfer specimen.....	172
Figure 5.5: Heating of unprotected side of heat transfer specimen showing deformations of bottom plate	172
Figure 5.6: Picture of specimen showing cracks in concrete.....	173
Figure 5.7: Top view schematic of combined heating and loading test.....	173
Figure 5.8: Overall Specimen view showing loading frame and heaters attached to specimen.....	174
Figure 5.9: Front view schematic of loading frame for combined heating and loading test	175
Figure 5.10: Photograph showing displacement transducer	176
Figure 5.11: Photographs of (a) generator used to power heaters and (b) heater control box	177
Figure 5.12: Overall view of specimen just prior to testing showing protective polycarbonate plastic.....	178
Figure 5.13: Measured bottom steel temperatures vs. time for first 50 minutes of heating	178
Figure 5.14: Photograph showing local upward bowing of bottom plate.....	179
Figure 5.15: Measured steel web temperatures vs. time for first 50 minutes of heating	179
Figure 5.16: Measured displacements for first 50 minutes of heating.....	180
Figure 5.17: Measured rotations for first 50 minutes of heating	181
Figure 5.18: Photograph showing vertical side crack on specimen.....	181

Figure	Page
Figure 5.19: Measured bottom steel temperatures vs. time for second heating cycle	182
Figure 5.20: Measured temperatures in steel profile for second heating cycle	183
Figure 5.21: Measured displacements in second heating phase	184
Figure 5.22: Measured rotations in second heating phase	185
Figure 5.23: Measured temperatures over all heating cycles.....	186
Figure 5.24: Measured vertical deflections over both heating cycles.....	187
Figure 5.25: Measured rotations over both heating cycles	188
Figure 5.26: Crack that formed at north end at end of heating	188
Figure 5.27: Displacements on Specimen.....	189
Figure 5.28: Load vs. vertical mid-span deflection of specimen.....	190
Figure 5.29: Growth of crack at north end during load test.....	190
Figure 5.30: Vertical separation of slab from deck during load test.....	191
Figure 5.31: Specimen at 7 in. of deflection.....	191
Figure 5.32: Buckled steel deck near mid-span (concrete was removed).....	192
Figure 6.1: Schematic of SC-DD system showing (a) the deck profile, and (b) a cross-section with concrete cast	204
Figure 6.2: Structural analysis for two-span condition showing equations for calculating (a) positive and negative bending moments, (b) deflections, and (c) reactions (Steel Deck Institute , 2002).....	205
Figure 6.3: Non-Linear inelastic analysis results showing the CC-DD systems and the SC-DD system.....	206
Figure 6.4: Schematic of meshed structural FEM models for SC-DD	207
Figure 6.5: Comparison of FEM models and fiber based model for SC-DD System	208
Figure 6.6: SC-DD Specimen ends before concrete casting (note shear studs at ends).....	208
Figure 6.7: SC-DD Specimen prior to concrete casting	209
Figure 6.8: Vertical displacement of shoring system during concrete pour	209
Figure 6.9: Measured strains in deck profile at mid-span during concrete pour and for first twelve hours	210
Figure 6.10: Measured strains at mid-span over first four days after concrete casting	210
Figure 6.11: Measured mid-span deflection vs. time after concrete pour and shore removal for SC-DD Specimen	211
Figure 6.12: Measured strains vs. time for mid-span bottom gages	211
Figure 6.13: Measured strains vs. time for mid-span top gages	212
Figure 6.14: Measured strains vs. time for mid-span web gages.....	212
Figure 6.15: Frequency response plot for SC-DD Specimen taken from mid-span hammer hit showing data from south third point accelerometer, mid-span accelerometer, and north third point accelerometer	213
Figure 6.16: Applied load vs. mid-span deflection plot for SC-DD Specimen	214
Figure 6.17: Average applied load vs. measured slip plot.....	214
Figure 6.18: View of north load point just prior to shear bond failure.....	215

Figure	Page
Figure 6.19: SC-DD Specimen with approximately 11 kips (220 psf) applied and 4.5 in. of deflection	215
Figure 6.20: Concrete cracking at north support of SC-DD Specimen	216
Figure 6.21: Average applied load vs. measured end rotation for SC-DD Specimen	216
Figure 6.22: Plot of moment vs. measured curvature for SC-DD Specimen.....	217
Figure 6.23: SC-DD Specimen strain gauge profiles through depth at mid-span for various load levels.....	218
Figure 6.24: SC-DD Specimen strain gauge profiles through depth at north loading point for various load levels.....	219
Figure 6.25: SC-DD Specimen strain gauge profiles through depth at south loading point for various load levels.....	220
Figure 6.26: Schematic showing web distortion of deep deck cross-section	220
Figure 7.1: Reduced weight composite deck system.....	227
Figure 7.2: Predicted load vs. deflection behavior for RW-DD System for Non-linear inelastic analysis	227
Figure 7.3: Schematic of meshed structural FEM models for RW-DD system.....	228
Figure 7.4: Predicted load vs. deflection behavior for RW-DD System for Non-linear inelastic analysis and FEM model	228
Figure 7.5: View of specimen with shear studs placed.....	229
Figure 7.6: End view of RW-DD System prior to concrete pour showing mineral wool placement	229
Figure 7.7: Frequency Response Function (FRF) for RW-DD System.....	230
Figure 7.8: Output Spectrum for RW-DD Specimen from two people walking simultaneously (log scale).....	231
Figure 7.9: Applied load vs. measured mid-span deflection for RW-DD Specimen	232
Figure 7.10: Separation of concrete from steel and concrete buckling.....	232
Figure 7.11: Displaced shape of specimen as failure occurred.....	233
Figure 8.1: Free body diagram in phase 1.....	248
Figure 8.2: Free Body Diagram in Phase 2.....	248
Figure 8.3: Interior bay layout for design example.....	249
Figure 8.4: Side view schematic of self-shoring test setup.....	249
Figure 8.5: Top view schematic of PLSS test setup	250
Figure 8.6: Side view of double angle connection on PLSS test setup.....	250
Figure 8.7: End fixture for self-shoring specimen showing (a) schematic of double angle connection, (b) photograph of double angle connection, (c) front view schematic of end fixture and (d) photograph of end fixture.....	251
Figure 8.8: Schematic of mid-span fixture used on PLSS Specimen	252
Figure 8.9: Mid-Span fixture for PLSS lab specimen.....	252
Figure 8.10: Possible mid-span configuration for PLSS system (assumed in design example).....	253
Figure 8.11: Photograph showing overall self-shoring apparatus	253
Figure 8.12: View of composite system after PLSS system removed.....	254

Figure	Page
Figure 8.13: Photograph showing attachment of rotation clinometers and slip sensor.....	254
Figure 8.14: Loading frame for PLSS Specimen (a) in first load cycle and (b) second load cycle	255
Figure 8.15: Measured load vs. mid-span deflection data for PLSS Specimen.....	256
Figure 8.16: Measured Load vs. End Rotations for PLSS Specimen	257
Figure 8.17: Photograph showing prying action occurring at connection	258
Figure 8.18: Measured Load vs. north and south third point displacements	258
Figure 8.19: Applied load vs. measured end slip for PLSS Specimen	259
Figure 8.20: Photograph from above of PLSS Specimen at 6.5 in. of mid-span deflection.....	259
Figure 8.21: Side view of PLSS Specimen with 7.5 in. of mid-span deflection	260
Figure 9.1: Comparison of analytical models to test results for CC-DD Specimen 1 – Models assuming no effects from concrete pour or interfacial slip	277
Figure 9.2: Comparison of analytical models to test results for CC-DD Specimen 2 – Models assuming no effects from concrete pour or interfacial slip	278
Figure 9.3: Comparison of analytical models to test results for CC-DD Specimen 3 – Models assuming no effects from concrete pour or interfacial slip	279
Figure 9.4: Comparison of analytical models to test results for CC-DD Specimen 4 – Models assuming no effects from concrete pour or interfacial slip	280
Figure 9.5: Comparison of analytical models to test results for SC-DD Specimen – Models assuming no effects from concrete pour or interfacial slip	281
Figure 9.6: Comparison of models with construction effects included to test data for CC-DD Specimen 1	282
Figure 9.7: Comparison of models with construction effects included to test data for CC-DD Specimen 2	283
Figure 9.8: Comparison of model with construction effects included to test data for CC-DD Specimen 3	284
Figure 9.9: Comparison of model with construction effects included to test data for CC-DD Specimen 4	285
Figure 9.10: Comparison of model with construction effects included to test data for SC-DD Specimen	286
Figure 9.11: Differential element of composite cross section showing distribution of shear stresses at interface	286
Figure 9.12: Distribution of strains for (a) fully composite section and (b) after slip occurs with two materials having the same curvature.....	287
Figure 9.13: Rigid-Plastic relationship assumed for interfacial shear stress behavior.....	288
Figure 9.14: Test configuration and resulting transverse shear and bending moment diagrams	289
Figure 9.15: Internal force distribution for test specimens	290
Figure 9.16: CC-DD Specimen 2 load vs. end slip plot showing indication of first measurable slip.....	290
Figure 9.17: Shear bond surface model implemented in <i>Abaqus</i>	291

Figure	Page
Figure 9.18: Load vs. mid-span deflection for interfacial slip models and CC-DD Specimen 1	291
Figure 9.19: Load vs. mid-span deflection for interfacial slip models and CC-DD Specimen 2	292
Figure 9.20: Load vs. mid-span deflection for interfacial slip models and CC-DD Specimen 3	293
Figure 9.21: Load vs. mid-span deflection for interfacial slip models and CC-DD Specimen 4	294
Figure 9.22: Load vs. mid-span deflection for interfacial slip models and SC-DD Specimen	295
Figure 9.23: Comparison of fiber based slip models and FEM based slip model to test results – CC-DD Specimen 2	296
Figure 10.1: Typical Level Framing Plan – Structural (AISC 2004)	310
Figure 10.2: Typical Architectural Floor Plan for Prototype Structure (AISC 2004)	311
Figure 10.3: Floor Evaluation Calculation Procedure (reproduced from AISC Design Guide 11, 2003)	312
Figure 10.4: Schematic showing model of single cell for FEM model	313
Figure 10.5: Schematic showing model of entire bay	313
Figure 10.6: Schematic showing model of entire bay with flexible girder included	314
Figure 10.7: Schematic showing multiple bays modeled for vibrations	314
Figure 10.8: Schematic of 9 bay model	315
Figure 10.9: Modes 1-6 of vibration for single unit model	315
Figure 10.10: Modes 7-12 of vibration for single unit model	316
Figure 10.11: Modes 1-6 of vibration for single bay model with rigid supports	316
Figure 10.12: Modes 7-12 of vibration for single bay model with rigid supports	317
Figure 10.13: Modes 1-6 of vibration for single bay model with flexible girders	317
Figure 10.14: Modes 7-12 of vibration for single bay model with flexible girders	318
Figure 10.15: Modes 1-6 of vibration for multi-bay model	318
Figure 10.16: Modes 7-12 of vibration for multi-bay cruciform model	319
Figure 10.17: Modes 1-4 of vibration for 9 bay model	319
Figure 10.18: Modes 5-8 of vibration for 9 bay model	320
Figure 10.19: Modes 9-12 of vibration for 9 bay model	320
Figure 10.20: Modes 13-16 of vibration for 9 bay model	321
Figure 10.21: Modes 17-20 of vibration for 9 bay model	321
Figure 11.1: Typical shear-bond plot showing reduced regression line for m and k (ASCE, 1992)	329
Figure A.1: Sandwich Beam Schematic	361
Figure A.2: Cross Section View of Sandwich Beam	361
Figure A.3: Shear Stress Distribution in Sandwich Panel	362
Figure A.4: Effects of Shear Deformations on Sandwich Panel (Allen H. G., 1969)	362
Figure A.5: Cross Section of DSC Panel	363
Figure A.6: Two Dimensional Thermal Analysis Results	363

Figure	Page
Figure A.7: Side View of DSC Panel	364
Figure A.8: Possible Connection Between Panels	364
Figure A.9: Possible DSC to Girder Connection	365
Figure A.10: Cellular Deck Sandwich System Profile	365
Figure C.1: Concrete batch ticket for CC-DD Specimen 1	376
Figure C.2: Concrete batch ticket for CC-DD Specimen 4	376
Figure C.3: Concrete batch ticket for SC-DD Specimen	376
Figure C.4: Concrete batch ticket for combined heating and loading Specimen.....	377
Figure C.5: Concrete batch ticket for PLSS System.....	377
Figure C.6: Mill Certification for 14 gage deck material used in CC-DD Specimens	378
Figure C.7: Mill Certification for 16 gage bottom plate material used in CC-DD Specimens	379
Figure C.8: Mill Certification for 18 gage steel deck material used in CC-DD Specimens	380
Figure C.9: Mill Certification for 20 gage bottom plate material used in CC-DD Specimens	381
Figure C.10: Nominal dimensions of steel deck tension coupons	384
Figure C.11: Engineering stress vs. measured elongation CC-DD 14 Gage Material Coupon 1.....	385
Figure C.12: Engineering stress vs. measured elongation CC-DD 14 Gage Material Coupon 2.....	386
Figure C.13: Engineering stress vs. measured elongation CC-DD 14 Gage Material Coupon 3.....	387
Figure C.14: Engineering stress vs. measured elongation CC-DD 16 Gage Material Coupon 1.....	388
Figure C.15: Engineering stress vs. measured elongation CC-DD 16 Gage Material Coupon 2.....	389
Figure C.16: Engineering stress vs. measured elongation CC-DD 18 Gage Material Coupon 1.....	390
Figure C.17: Engineering stress vs. measured elongation CC-DD 18 Gage Material Coupon 2.....	391
Figure C.18: Engineering stress vs. measured elongation CC-DD 20 Gage Material Coupon 1.....	392
Figure C.19: Engineering stress vs. measured elongation CC-DD 20 Gage Material Coupon 2.....	393
Figure C.20: Engineering stress vs. measured elongation SC-DD 14 Gage Material Coupon 1.....	394
Figure C.21: Engineering stress vs. measured elongation SC-DD 14 Gage Material Coupon 2.....	395
Figure C.22: Engineering stress vs. measured elongation SC-DD 14 Gage Material Coupon 3.....	396
Figure C.23: Engineering stress vs. measured elongation SC-DD 14 Gage Material Coupon 4.....	397

Figure	Page
Figure C.24: Engineering stress vs. measured elongation SC-DD 14 Gage Material Coupon 5.....	398
Figure C.25: Engineering stress vs. measured elongation SC-DD 14 Gage Material Coupon 6.....	399
Figure C.26: Engineering stress vs. measured elongation SC-DD 14 Gage Material Coupon 7.....	400
Figure C.27: Engineering stress vs. measured elongation SC-DD 14 Gage Material Coupon 8.....	401

ABSTRACT

Typical steel deck-concrete slab floor systems used in multi-story steel construction require intermediate filler or support beams (14 in. or deeper) and are limited to span of 8-12 ft depending on deck depth. The goal of the research was to develop and validate innovative long span floor systems capable of spanning up to 30 ft with total depths up to 12 in. or less. Several long-span floor systems were conceived and considered. These floor systems were evaluated based on their ability to achieve certain performance objectives. To accomplish these objectives, the project has been conducted in four tasks. The first task focused on conducting a literature review and survey of existing long-span slab systems. This task was conducted to determine the state-of-art for existing floor systems in steel construction. It helped in identifying existing solutions that have been proposed or implemented in steel construction. The second task of the research focused on conceptual development and design of long span floor systems. A suite of different floor system types were developed and proposed. The systems were ranked by the researchers and an oversight committee based on their technical merit and potential to achieve the prescribed performance objectives. The systems were analyzed and designed using analytical tools and methods including the finite element method (FEM), numerical analysis, and existing design codes. Based on the rankings, floor systems were selected for further development and experimental validation. The third task for the research project focused on the experimental validation of the floor system candidates. The testing focused on three different aspects for the floor systems. The aspects included strength and serviceability characteristics at ambient temperature levels, the fundamental heat transfer of certain specimen, and the effects of combined mechanical and thermal loading. The fourth task focused on numerical investigations and analytical parametric studies of the long-span floor system candidates. Analysis methods were developed and used for structural evaluation and evaluation for floor vibrations. Three different systems were found to present merit as potential long span systems. Two used 7.5 in. deep steel decks acting composite with either a 2.5 in. or 3 in. concrete slab on top to achieve 30 ft spans with a 10 or 11 in. depth. The other modified existing steel deck-concrete slab systems with new type of self-shoring system to achieve 30 ft spans with a 12.5 in. depth.

CHAPTER 1. INTRODUCTION

1.1. General Overview of Traditional Floor Systems in Steel Construction

The most common type of flooring system used currently in steel building construction is the steel deck and concrete slab composite floor system. This floor system was developed in the 1920s and has evolved into a thoroughly tried, tested, and efficient floor system. The most commonly used floor system involves the placement of a cold-formed steel deck upon structural beams, and then placement of concrete over the steel deck. The steel deck is typically ribbed with embossments to delay slipping of the concrete slab. It is connected to floor beams via shear connectors, and thus a composite system is developed. Some common composite steel deck profiles are shown in Figure 1.1. A schematic of a composite system is shown in Figure 1.2

The steel deck is ribbed with embossments, which allows for less concrete to be used and aids in bonding the concrete to the steel deck. The steel deck also acts as reinforcing steel in positive moment regions (if designed as a composite system) while the metal fabric mesh acts as shrinkage reinforcement. Most conventional steel decks have a rib height of 1.5 to 3 in. with rib spacing of 4.5 to 6 in. Un-shored spans of the steel deck-concrete slab system typically range from 6 to 10 ft for standard deck profiles with 5-7 in. of total concrete depth (Easterling, 2002).

If the steel deck-concrete slab system is used in structures with large bays, (i.e., spans greater than ten feet) then filler beams are required to provide support to the steel deck. The use of intermediate filler beams allows for un-shored construction (temporary construction level supports), but increases the total depth of the floor system, and thus the story height. It also requires the use of more structural steel. Typically, these filler beams range in depth from 16 to 20 in. The filler beams reduce the useable headroom and increase the floor-to-floor (story) height of the structure. This limitation makes steel structures less efficient for multistory residential construction as compared to reinforced concrete systems where shallower floor system depths can readily be achieved via flat plate construction, post-tensioning, etc.

1.1.1. Advantages of Steel Deck-Concrete Slab Composite Floor Systems

There are definite advantages to using steel deck-concrete slab flooring systems. These include:

- 1) Steel decks are readily available throughout North America. In the United States alone, there are over two-dozen companies that manufacture steel decks (SDI, 2002).

- 2) Once the deck is placed, it provides a workable platform for workers to use before concrete is placed leading to a safer construction environment and allowing for efficient construction.
- 3) The deck acts as permanent formwork and tension reinforcement for the concrete slab. As a result; these two costly aspects of construction are greatly reduced.
- 4) The composite floor system has good fire resistance as shown by the Cardington compartment fire tests (Lawson, 2000) and the AISC Design Guide 19 (AISC, 2003), which is based on the standard fire tests.

1.1.2. Disadvantages

The limitations of the steel deck-concrete slab composite floor system are as follows:

- 1) The requirement of intermediate filler beams when spans exceed 10 – 12 ft. For most modern steel frames this means that anywhere from 2 – 4 filler beams could be required in each bay of the structure.
- 2) Filler beams reduce head room and increase story height
- 3) The additional cost incurred from the additional members and required connections when filler beams are needed

Several approaches have been used to solve the issues associated with the above steel deck systems. Certain systems have completely eliminated using composite steel decks while others have tried to optimize thin gaged deck profiles to achieve longer spans. A review of some of these systems is given in Chapter 2.

1.2. Objectives and Goals of Research

The goal of this research project is to develop and investigate new types of long span floor systems to be used in multi-story residential steel construction and determine the important aspects in designing and developing them. The American Institute of Steel Construction (AISC) has funded the project. The project has focused on the conception, development, and validation of long-span floor systems (span up to 30ft. unsupported) for multistory residential construction. Several long-span floor systems have been conceived and considered. These floor systems were evaluated based on their ability to achieve certain performance objectives that were established by the research team (Huber & Varma, 2005). These performance objectives include:

- 1) Ability to achieve long spans of up to 30 ft. unsupported.
- 2) Achieve minimum floor-to-floor height requirements.
- 3) Utilize un-shored construction (preferred) or provide minimal shoring.
- 4) Achieve strength and serviceability criteria during the construction phase.
- 5) Achieve strength and serviceability criteria during the service phase of the structure.

- 6) Achieve adequate performance with respect to floor vibrations.
- 7) Achieve adequate fire resistance.
- 8) Use relatively simple connection systems.
- 9) Provide cost-effective fabrication and erection.
- 10) Provide adequate diaphragm action for transferring lateral loads.

The primary objective of this research is to develop new types of floor systems that satisfy the above performance criterion. To accomplish this objective, the project has been conducted in four tasks. The first task focused on conducting a literature review and survey of existing long-span slab systems. This task was conducted to determine the state-of-art for existing floor systems in steel construction. It helped in identifying existing solutions that have been proposed or implemented in steel construction. This literature review is given in chapter 2 of this dissertation.

The second task of the research focused on conceptual development and design of long span floor systems. A suite of different floor system types were developed and proposed. The systems were ranked by the researchers and an oversight committee based on their technical merit and potential to achieve the performance objectives noted above. The systems were analyzed and designed using analytical tools and methods including the finite element method (FEM), numerical analysis, and existing design codes. Based on the rankings, floor systems were selected for further development and experimental validation. The development of the chosen systems is presented within Chapter 3.

The third task for the research project focused on the experimental validation of the floor system candidates. The testing focused on three different aspects for the floor systems. The first aspect is the strength and serviceability characteristics at ambient temperature levels. Next, the fundamental heat transfer of certain specimens has been investigated. Finally, the effects of combined mechanical and thermal loading have been investigated. The details of the experimental setup, testing procedures, instrumentation, etc. are described in Chapters 4 through 8 for the various developed systems

The fourth task has focused on numerical investigations and analytical parametric studies of the long-span floor system candidates. Details of the analysis methods used for structural evaluation are highlighted in Chapter 9. Chapter 10 describes approaches used in evaluation for floor vibrations. Chapter 11 presents recommendations based on the experimental work and analytical investigations. These include: (a) design guidelines and recommendations for the floor systems, (b) recommendations for implementing the developed systems into multi-story residential structures, and (c) guidelines for modeling these systems for future research and engineering development if needed. Chapter 12 is a summary of the work, recommendations for future work, and general conclusions.

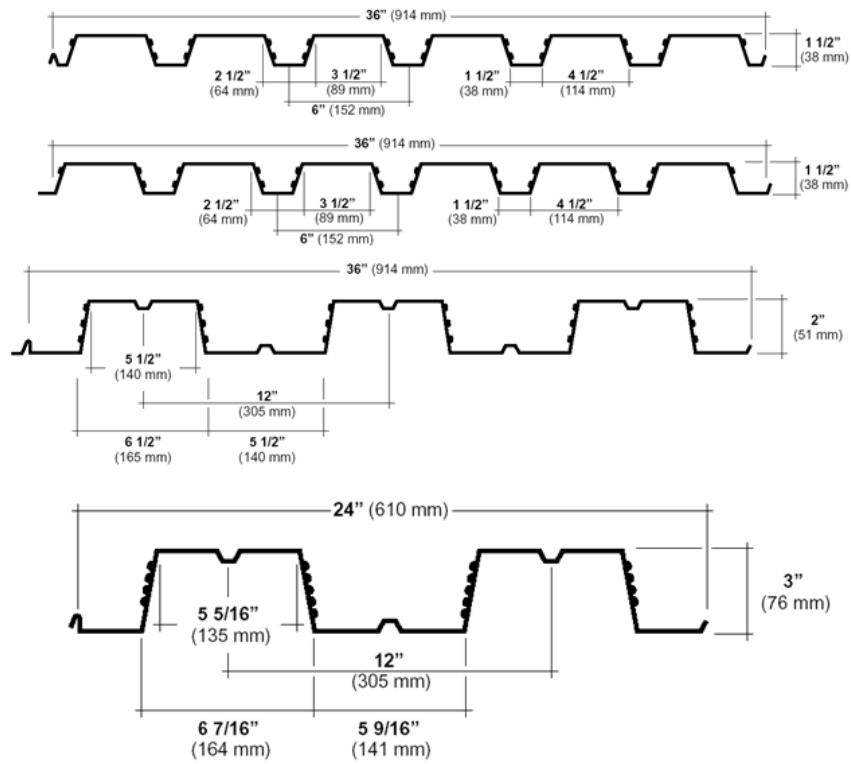


Figure 1.1: Typical Steel Deck Profiles Used in Floor Systems (Canam Steel, 2002)

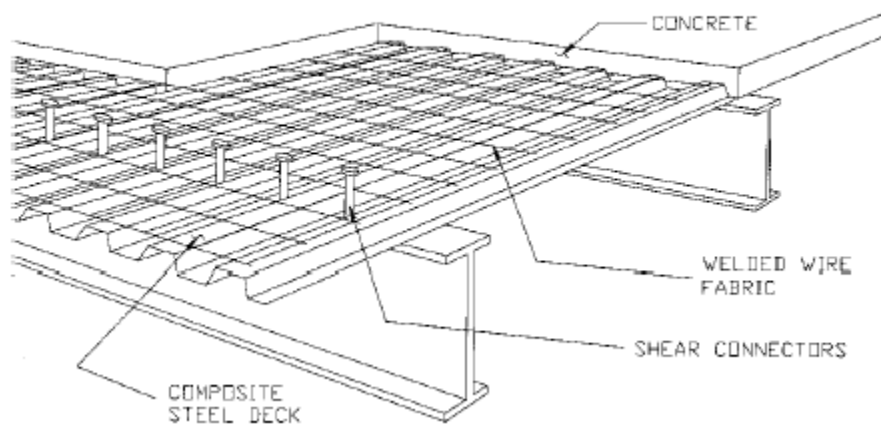


Figure 1.2: Typical Steel Deck System (Buckner, 2002)

CHAPTER 2. LITERATURE REVIEW AND FURTHER BACKGROUND

2.1. Introduction

This chapter presents a background related to previous work done on long span floor systems and some of the key issues related to them. The first part of this chapter discusses some previous research that has investigated the use of alternative systems for achieving long spans and reduced depths in steel construction. The second part of the chapter discusses and highlights some current alternative floor systems being implemented in steel construction. Finally, a review of some key issues related to long span systems beyond just pure structural considerations are presented in more detail. From this chapter an understanding of what has been done previously can be understood. Furthermore, the review of previous work helps to highlight what considerations need be made for developing new type of floor systems for use in multi-story steel construction.

2.2. Previous Research

2.2.1. Widjaja Deep Deck Research

The most notable recent research in long span floor systems in the U.S. has been carried out by Widjaja (1997) at Virginia Polytechnic Institute. In this research, the use of *deep* steel deck profiles was investigated and compared to conventional steel decks in an effort to determine the benefits of using the deeper decks. Figure 2.1 shows the profiles (1 and 2) used in the study. Figure 2.1 also includes a standard metal deck (Profile 3 for comparison). Profile 1 is a 6 in. deep 16-gage deck that was manufactured specially for the project. Profile 2 is a 4.5 in. deep 16-gage commercially available roof deck (Widjaja, 1997).

In this research, the deck slabs had unsupported spans of 20 ft. as shown in Figure 2.2. Both profiles were used with a 2.5 in. normal weight concrete cover. Slab 1 used deck Profile 1, and as shown in Figure 2.2 (a), it was setup as two simply supported spans of 20 ft. each. This was due to a limitation on the length (25 ft max) of the manufactured system. Slab 2 used metal deck profile 2 and as shown in Figure 2.2(b), it was setup as two continuous spans of 20 ft each. The two systems were tested under a uniformly distributed load (using an air bladder) until failure or excessive deflections occurred.

Research Findings

The results of these tests are summarized in Table 2.3 where LSS1a and b correspond to two tests of Slab 1 and LSS2a and b correspond to two tests of slab 2. Load deflection curves for the tests are shown in Figure 2.3 and Figure 2.4. As shown in figures, both specimens had excess of strength and good behavior. Table 2.3 shows the load ultimate

load capacity, load at allowable deflection, ultimate load divided by 50 psf, and ultimate load divided by 150 psf. The table shows that the specimens had a great excess of strength and were adequate for deflection serviceability criteria. The results of this research also made apparent some key issues related to the design of long spanning slab systems. Both systems had excess capacity when looking purely at strength, as shown in Table 2.3. However, it was reported that construction level deflections were the limiting design criteria for the specimens. Some vibration testing in the form of measuring frequency and acceleration response was done on the systems. The findings were somewhat inconclusive but it was believed that vibrations could be problematic if not properly accounted for in composite deep deck systems. Therefore, long span metal decks with concrete slabs could have more issues related to serviceability limits of deflection and floor vibrations (while not mentioned in this research, fire resistance also plays a key role in design), not strength. Overall, this research indicates that more research should be conducted on deep steel deck systems as a means of developing a long span slab system (Easterling, 2002).

2.2.2. Hillman and Murray Deck-on-Deck System

Description

Hillman and Murray conducted research on several alternative floor systems for use in steel construction (Hillman, 1990), (Hillman & Murray, 1990). Most of these systems were developed only in concept and were meant to heighten interest in new types of floor systems for use in steel framing. Some of the systems investigated are shown in Figure 2.5. As shown, all the systems were variations of existing composite steel deck construction. System (c) from Figure 2.5, the long span cold formed deck-composite slab system, was also experimentally investigated (herein called the deck-on-deck system). This system consisted of existing 7.5 in. deep 14 gage thick roof deck sections with a 9/16 in. deep 24 gauge thick form deck running transverse to the deep deck. The form deck was attached to the deep deck sections via stand-off screws. A 2 in. normal weight concrete slab was poured on top of the form deck. The overall system was intended to act as a composite section. The deep deck sections were existing roof deck profiles that were inverted to place more steel in tension. The system self weight was 35 psf, which is a significant reduction as compared to traditional floor systems with an intended span of 30 ft.

Experimental Verification

The experimental verification of the deck-on-deck system involved the construction of a 30 ft by 30 ft prototype system. A photograph of the specimen being constructed is shown in Figure 2.6. The system was placed on 8 in. block concrete masonry unit (CMU) walls, which acted as simple supports. Load was added to the system using concrete blocks up to a load of 70 psf. At this point there was a recorded mid-span deflection of 0.8 in. No further loading was applied beyond this point. Thus, an overall capacity of the system could not be verified.

The system's susceptibility to floor vibrations was also investigated for the system. Heel drops were induced at mid-span of the system with responses measured by accelerometers placed at mid-span and quarter points on the system. A Fast Fourier Transform (FFT) algorithm was then implemented to determine natural frequencies, which are shown in Figure 2.7. As shown, the measured frequencies were comparable to theoretical values computed for the system. The floor vibration behavior, however, was difficult to evaluate based on existing models. This is because multiple modes with similar energy were contributing to the floor system behavior. Existing guidelines for investigating floor systems were based on one dominant mode contributing to the response. Thus, it was difficult to make solid conclusions about the floor vibration behavior of the floor system.

This work helped in showing how deep deck systems could be implemented as alternative long-span floor systems. The developed system showed merit in becoming a viable long-span system. Unfortunately, there was not any found follow-up work on the system beyond the initial research project. The ideas and concepts presented did help in motivating the work on deep deck systems within the current project.

2.2.3. Sandwich Panel Systems

Sandwich panel construction has been used for many years throughout the United States and Europe. Some of the more common engineering uses have been in the use of wall panels, bridge decks, blast resistant structures, maritime applications and stadium risers (McKinley & Boswell, 2002). The concept of sandwich construction is quite simple. A 'soft' core is sandwiched between two thin 'stiff' plates to form an extremely efficient structural system. The core is analogous to the web of a beam, while the top and bottom plates act as top and bottom flanges. When used to resist bending, the core need only be strong enough to resist induced shear stresses while the plates resist bending. The stiffness of a sandwich system comes from the stiffness of the top and bottom plates and how far they are spaced apart (therefore increasing the section's moment of inertia). The most common face plate material used in sandwich construction is steel, due to its inherent stiffness. Common core filler materials include lightweight foams, mineral wools, and polystyrene (Davies, 2001).

The last half of the 20th century has brought upon a sharp increase in sandwich construction. The advent of new types of lightweight and strong materials used as core materials, along with more advanced manufacturing techniques has propelled the increase in use. Recently, both the UK and United States have developed sandwich panel type systems to be used in civil engineering applications. These systems helped in motivating the development of some proposed systems for the current research. Therefore, some sandwich type systems that have been developed are presented. Sandwich panel systems could present a very viable solution for achieving long spans in a floor system.

Double Skin Composite (DSC) Systems Research

DSC or steel-concrete-steel sandwich construction was conceived over 15 years ago in the UK for use in submerged tunnel construction (McKinley & Boswell, 2002). It has recently been more extensively developed and marketed by Corus Inc. of the UK for

further applications including wall panels, building cores, and protective structures. Originally, DSC panels were constructed as two separate steel plates with shear studs welded to the face of the plates to transfer shear stresses between the core and face plates. Concrete was then poured between the plates to form the sandwich structure.

Recent manufacturing advances in the UK have brought about the Bi-Steel system for construction of DSC panels. These panels are made by simultaneous friction welding of cut lengths of round steel bars to both top and bottom plates in a factory environment (McKinley & Boswell, 2002). Traditional DSC and Bi-Steel panels are shown in Figure 2.8. Bi-Steel panels are then filled with concrete in the field and placed accordingly. Bi-Steel panels have become more economical to use than the systems using shear studs due to their streamlined fabrication process.

DSC systems present merit for use as a floor system in multi-story residential steel construction. Previous research has investigated and experimentally tested the flexural behavior of DSC elements. This research has shown that DSC panels behave in a ductile and predictable manner similar to reinforced concrete, if properly designed (Wright, 1991).

Sandwich Plate System

Intelligent Engineering Inc. of Canada has recently developed its patented Sandwich Plate System (SPS) system. This system has an elastomeric composite core sandwiched between two thin steel plates, as shown in Figure 2.9. The system is currently used extensively for stadium risers, maritime applications, and bridge decks. A schematic of a bridge deck application is shown in Figure 2.10 (Kennedy & Kennedy, 2004). The SPS system is beginning to gain more popularity due to its strength/weight ratio.

A system of this nature could possibly be used for a floor system in multi-story residential steel construction. Its strength and stiffness is apparent from its uses in bridge decks. Intelligent Engineering has recently proposed a floor system using SPS panels. The proposed layout is for a 10 m by 10 m bay (33 by 33 ft), as shown in Figure 2.11. The numbers shown in the figure correspond to thickness of the face-core-face materials used (all dimensions in mm). For example, the edge panels have a top face thickness of 10 mm (0.4 in.), core thickness of 100 mm (4 in.) and bottom face thickness of 10 mm. The connection details between the panels are shown in Figure 2.12. As shown, back to back channels are placed between sections and then welded together.

Intelligent Engineering reports that the self weight of this system would be 47 psf. They also report the system exhibits adequate stiffness and vibration characteristics. A maximum expected deflection under 100 psf loading is approximately $L/500$ (0.75 in.) and acceleration responses of 0.3% g are expected based on using existing current vibration guidelines (discussed in section 2.6). The main issue with the system is the resistance of the elastomer core in a fire event. The core experiences extensive softening at elevated temperatures. The onset of this softening occurs at much lower temperatures than if a concrete filler material were used. Also, de-bonding between the face plates and core would likely cause premature failure in the event of a fire. Nonetheless, the SPS system is quite novel and shows some merit as a new type of flooring system.

2.3. Alternatives to Traditional Composite Floor Systems in Steel Construction

As mentioned in chapter 1, the steel deck-concrete slab system is the most common type of floor system used in steel construction. Alternative systems have been developed and implemented in steel construction, and warrant review. It is important to understand their salient features, corresponding design provisions for strength and serviceability, identify advantages and disadvantages of each system, and use this knowledge to aid in the design of new innovative long span systems.

2.3.1. Stub Girder System

Description

The stub girder system was developed in the early 1970s by engineer Joseph Colaco (Colaco, 1972). The intent of the system was to improve construction economy by integrating electrical and mechanical service ducts into the flooring system itself. Hence, allowing for a more efficient use of space and reducing floor to ceiling heights. Furthermore, the system is capable of long spans (up to 50 feet) and is composed completely of steel components. However, multiple lines of shoring is required when constructing the system (Viest, Colaco, Griffis, Leon, & Wylie, 1997). A key element in the composite system is a special element known as a ‘stub.’ The stub is fabricated from standard hot-rolled wide flange shapes. Welding these stubs on top of longitudinal floor girders forms the composite system. Stubs are 3-7 ft in length and the longitudinal floor girder acts as the ‘bottom chord’ of the stub girder. A steel deck, which acts as formwork and positive moment reinforcement for the concrete slab, is then connected to the stubs via shear studs. A schematic of a stub girder system is shown in Figure 2.13. Construction photos of a stub-girder system are shown in Figure 2.14.

The space between the girders and transverse floor beams allows for utility ducts to be placed, as shown in Figure 2.13, which results in a more efficient use of all components of the system. The stubs also help to provide additional stiffness. Thus, composite level deflections are usually not the limiting design parameter. The performance of the system is not greatly affected by the lengths of the stubs as long as a reasonable range is not exceeded (i.e. 3 – 7 ft.). The stub girder system can span up to 50 feet with span preferred between 35 and 45 ft. When spans approach 50 ft the dead load becomes excessive which causes the slab to govern the overall design. Transverse floor beam spacing needs to be maintained between 8 and 12 ft. This limitation is based on the span limitations of the steel deck being utilized (Viest, Colaco, Griffis, Leon, & Wylie, 1997).

Advantages of System

- 1) The integration of the ductwork and other mechanical components within the system helps reduce floor-to-floor heights.
- 2) Relatively simple design provisions. The various components are all designed according either the AISC LRFD or the ACI code.
- 3) System can also be designed to be a lateral load resisting system

- 4) All connections are simple and shapes are conventional, reducing the possibility of construction errors in the field.

Disadvantages of System

- 1) Multiple lines of shoring per bay are required for construction. This leads to increased construction costs.
- 2) The stub-girder system trades a reduction in steel weight for increased shop labor, which is not an economical trade-off in current steel construction.
- 3) The availability of deeper W shapes is more common than when the system was conceived. Furthermore, the use of web openings in these shapes is common practice (Liddy, 2004).
- 4) The fire resistance and floor vibration performance of the system has not been investigated.

Essentially, the stub-girder system has become outdated in recent years. Reduced material costs and availability of deeper W shapes that can accommodate web openings has all but eliminated the need for the system. It is however one of the first systems to try and address the issue of excessive structural depth in conventional steel structures.

2.3.2. *Slimdek* System

Description

There are many long span shallow flooring systems, collectively known as slim floors, which are being used in practice in the UK. The most popular of these systems is the proprietary *Slimdek* system produced and sold by the Corus Group in the UK. The *Slimdek* system is designed for exclusive use with a deep steel deck. The steel deck known as SD 225 is used for the *Slimdek* system. A profile of this deck, shown in Figure 2.15 (*note: All units in figure are mm*), shows the 9 in. depth and 24 in. width of the deck. The figure also shows vertical embossments to aid in composite action, and indicates a deck thickness of 0.05 in. or equal to 20 gage (Lawson & Mullet, 1999).

Originally, a universal column (UC) section with a plate welded to its bottom flange as shown in Figure 2.16 was used as the support beam. The deck component rested on the on the plate welded to the bottom flange. Advances in rolling technology have allowed for the fabrication of a more efficient asymmetric beam. The Asymmetric Slimflor Beam (ASB), which is more commonly known as a *Slimdek* beam has a narrower top flange which has a ribbed pattern rolled into it to provide composite action between the concrete slab and beam. Also, it does not require a plate to be welded to its bottom flange. A *Slimdek* system including the ASB is shown schematically in Figure 2.17. The system is capable of 20 ft. un-shored spans in both directions when the SD 225 deck is used with the ASB.

Advantages of System

- 1) System is capable of spanning up to 20 ft. without the use of shoring (assumed live load of 50 psf and the use of lightweight concrete).
- 2) HVAC systems, conduit, and other mechanical services can be integrated right into the *Slimdek* system. Special sleeves are available for integrating ductwork (see Figure 2.16).
- 3) System shown in Figure 2.17 is capable of 60 minutes of fire resistance (Lawson & Mullet, 1999).

Disadvantages

- 1) System is restrictive in the sense that the SD 225 deck must always be used.
- 2) Currently system availability in U.S. is restricted since deck profile and ASB is rolled in the U.K.

2.4. Girder Slab Floor System

The *Girder Slab* system is a steel-precast concrete system that uses long span hollow-core pre-cast concrete slabs with an integral steel 'D' beam to form the floor system. The system is a composite system and is designed for un-shored construction. The system is capable of spans up to 28 ft. in the plank longitudinal direction. Spans are limited to around 15 ft in the D-beam spanning direction. The hollow core slabs are pre-cast in widths of 4 or 8 ft with a depth of 8 inches. Figure 2.18 shows a schematic of the system (Girder Slab Technologies, 2002). The system was conceived by Peter Naccarato, John Costanza, and Dan Fisher. The *Girder Slab* system is very similar to the *Slimdek* system with the exception that it uses concrete planks rather than a deep steel deck.

The D-beam is an inverted T-beam that is made by: (a) castellating a conventional W-shape beam with openings in the web of each tee, and (b) welding a plate to the top of the castellated web. Figure 2.19 shows more detail of the D-beam. As shown, the openings in the beam allow for the free-flow of grout into the pre-cast hollow core slab. The D-beams are connected to columns as simple (pinned) connections and span the length of the slab in the transverse direction (Naccarato, 1999). The D-beam is the only component of the slab system that is actually designed since the system utilizes pre-cast concrete sections. D-beams come in 8 and 9 in. depths, depending on whether or not a concrete topping is required. Composite action is developed between the beam and the plank once grout has been pumped into the planks. The grout also serves as the connection between the floor sections in the longitudinal direction. Thus, the composite action of the system relies only on the grout that is placed.

Advantages

- 1) Ease of construction and use of pre-fabricated sections. Once the steel frame has been placed, the pre-cast planks are simply set in place and then the grout is placed into the system.
- 2) The controlled environment in which the pre-cast sections are fabricated reduces flaws within materials (related to concrete).
- 3) The shallow depth of the system (8 – 10 in.) allows for reduced floor-to-floor heights.
- 4) Unrestrained Assembly and Unrestrained Beam fire ratings of two hours are achieved when spray-on fire protection is used with system (Girder Slab Technologies, 2002).

Disadvantages

- 1) The use of the pre-cast plank sections could alter the costs of the system based on regional availability of materials.
- 2) The D-beam limits the transverse span of the system due to its reduced depth.
- 3) If a 2 in. topping is placed on top of the system the dead load can become excessive on the D-beam. Special pre-cautions need to then be made for the D-beam during construction (Veitas, 2002).

2.5. Synopsis/Evaluation

Several alternative floor systems have either been researched or implemented into steel construction. However, it is apparent that there is a need for more innovative floor systems in steel construction. Many of the aforementioned systems only partially address the issues with conventional and long span flooring systems in steel construction. These issues were described in Chapter 1. If a system can be developed that address these issues, it has definite great potential for widespread use.

Many of the issues listed are commonly encountered in any structural engineering application. However floor vibrations and fire resistance are issues often not well known to many structural engineers in practice. Often it is assumed that these issues are already addressed and need no more further consideration. For example, most deck companies publish that their deck profiles with a certain amount of cover will meet recommendations for floor vibrations based on the American Institute of Steel Construction (AISC) Design Guide 11 (AISC, 2003). The design guide provides recommendations in mitigating floor vibrations in steel structures. Similarly, a particular steel deck-concrete slab assembly will be stated to have a certain fire rating (i.e. one hour, two hour, etc.) associated with it. Thus, the engineer can simply select one of these systems and make sure it also meets structural requirements. In developing new systems, however, it is required to know the relevant issues related to both of these phenomena. The next two sections present relevant background and details to both floor vibrations and fire resistance.

2.6. Floor Vibration Requirements and Research

The most important factor in the design of almost any structure is ensuring it can sustain the anticipated loadings it will be subjected too. This principle does not change when designing a building to minimize floor vibrations due to human activities. This section highlights, based on existing literature, how floor vibrations are accounted and designed for (to ensure they are not problematic) in modern structure design within the United States and United Kingdom.

2.6.1. Modeling Human Motion

The loadings imposed on a floor system by human movement can be quite complex in nature. Walking, for example, itself is fairly complex and varies both in the force it imparts on the structure and in frequency (between 1.4 and 2.5 Hz) depending on a variety of factors (SCI, 1989). Modeling this excitation for general application is thus a difficult task and is typically accomplished by assuming that walking produces a time dependent harmonic forcing function (AISC, 2003). Therefore, force spectra at harmonics of the walking frequency are often used to model the input to the structure in cases where vibration due to ambulation exists. Two different frequency domain representations of the forces due to walking are shown in Figure 2.20. The left plot shows the scale factors for each harmonic of the walking frequency used by AISC Design Guide 11 (AISC, 2003) which, when multiplied by the weight of an individual, gives the forcing imparted on the structure by due to walking.

On the right plot in Figure 2.20 are frequency domain scaling functions for each harmonic of the walking frequency as given by Rainer, Pernica, and Allen (1988) for the forces imparted on footbridges due to walking. While the two plots appear significantly different, the values of the calculated forces are comparable at most frequencies. However, other models take into account the heel strikes that occur during walking and also take into account the higher frequency content of this impulsive loading as seen in Figure 2.21. This may play a significant role for floors with higher fundamental frequencies (above 8 Hz) or for floors in which higher modes contribute significantly to the response.

There are various other rhythmic human activities that must be considered when designing floor systems. For example aerobics, dancing, concerts, and other activities that involve large scale coordinated movements can cause very large forces and can have significant harmonics (Naeim, 1991). The loading functions shown in Table 2.4 are recommended by Allen, Onysko, and Murray (1999) for several rhythmic activities. Note the especially high scale factors for all harmonics of aerobics in comparison to those for walking shown in Figure 2.20. In general, these activities cause high levels of vibration and often the only alternative is to ensure that excitation of a resonance does not occur is by designing the structure such that the natural frequency is higher than the third harmonic of the main frequency component of the forcing (AISC, 2003). These activities are not of as much interest to the current study but do suggest special considerations must be made when designing for activities other than walking.

2.6.2. Structural Modeling for Vibration Analysis

Once the type of input has been modeled it is also necessary to properly model the structure of interest. Because of the many different types of possible floor structures, creating a universal criterion for all is difficult if not impossible. However, most models focus on creating acceleration based indices that utilize the natural frequency of the flooring system itself. For instance, AISC Design Guide 11 (2003) proposes a widely used method to determine whether problems due to walking are likely to occur. The first assumption in this process is that only the first natural frequency is important to the response to walking. This assumption of the first natural frequency dominating the response is often true when the natural frequency lies between 3 and 9 Hz. Most steel-concrete composite floor systems have first natural frequencies in this range. The natural frequency (f_n) is calculated using equation 2.1.

$$f_n = 0.18 \sqrt{\frac{g}{\Delta}} \quad 2.1$$

Where:

g Acceleration due to gravity.
 Δ Mid-span deflection of the member under consideration due to the supported weight.

The above equation comes from using a simple single degree of freedom model, shown in Figure 2.22, where the floor system is assumed to exhibit beam behavior, as shown in Figure 2.23. The stiffness is assumed based on a uniformly loaded simply supported beam.

The frequency calculated from the above equation is that of the floor system only. It does not consider the contribution of frequency from the girders supporting the floor system. The contribution of the girder frequencies can be included via the Dunkerly relationship (AISC, 2003) shown in equation 2.2.

$$\frac{1}{f_n^2} = \frac{1}{f_1^2} + \frac{1}{f_2^2} \quad 2.2$$

Where:

f_1 Frequency of floor system alone
 f_2 Frequency of girders

This results in an estimate of the first natural frequency of the overall system (f_n) that is always lower than the natural frequency of the floor system alone (i.e. if an assumption of infinitely stiff girders was made). Typically, the two elements used in Dunkerly's relationship are the natural frequencies of the joists or filler beams and girders in the floor framing structure. Assuming Dunkerly's method applies for the structural system of

interest, the frequency of the combined system can then be calculated from static deformations as:

$$f_c = 0.18 \sqrt{\frac{g}{\Delta_1 + \Delta_2}} \quad 2.3$$

Where

- Δ_1 The static deformation of the flooring system alone under assumed supported weight.
- Δ_2 The static deformation of the supporting girders under the supported weight.

These equations assume uniform loading and if the load is assumed concentrated at mid-span then the corresponding deflection should be multiplied by $4/\pi$. The suggested applied loads when using this method are based on the type of structure under investigation. They are often a small portion of the full design loads. Table 2.1 summarizes the recommended values for various structure types. As shown, residential applications have a recommended value of 6 psf. This would be the additional loading on the system for most day to day activities.

This estimation of the natural frequency may then be used in conjunction with several other parameters in order to determine if vibrations due to ambulatory motion may be problematic for the given system. The metric that is used to determine the ratio of peak acceleration to gravity due to these vibration problems is given in equation 2.4 (AISC, 2003).

$$\frac{a_p}{g} = \frac{P_0 \exp(-0.35 f_n)}{\beta W} \quad 2.4$$

Where:

- a_p Acceleration introduced into the system from the imposed excitation.
- P_0 Assumed force from a foot drop causing dynamic excitation in the system
- β The damping ratio for the system

Table 2.2 shows recommended values for the above parameters.

- W Effective panel weight of the structure and can be calculated using equation 2.5.

$$W = wBL \quad 2.5$$

Where:

- w Supported weight per unit area
- L Span of the given member

B Effective width for the mode type model used

The effective width concept is calibrated for conventional composite floor systems utilizing composite decks with concrete slabs or steel joists with concrete slabs. A typical conventional system is shown schematically in Figure 2.24. The joist or beam mode is when the deck and filler beams oscillate together as was shown in Figure 2.23. The effective width for this mode is found using equation 2.6

$$B_j = C_j \left(\frac{D_s}{D_j} \right)^{\frac{1}{4}} L_j \quad 2.6$$

Where:

C_j	A calibration factor accounting for bay location. It is 2.0 for joists or beams in most areas and 1.0 for joists or beams parallel to an interior edge.
D_s	Transformed slab moment of inertia per unit width
D_j	Joist or beam transformed moment of inertia per unit width
L_j	Joist or beam span

Similarly, for the girder mode the effective width is found using equation 2.7.

$$B_g = C_g \left(\frac{D_j}{D_g} \right)^{\frac{1}{4}} L_g \quad 2.7$$

Where:

C_g	Factor to account for beam connection to the girders. 1.6 for girders supporting joists connected to the girder flange. 1.8 for girders supporting beams connected to the girder web.
D_g	Girder transformed moment of inertia per unit width equal to I_g/L_j for all but edge girders and $2 I_g/L_j$ for edge girders.
L_g	Girder span

Once the effective widths are found, the effective weight of the complete system is approximated with equation 2.8.

$$W = \frac{\Delta_1}{\Delta_1 + \Delta_2} W_j + \frac{\Delta_2}{\Delta_1 + \Delta_2} W_g \quad 2.8$$

Where:

W_j	The effective weight for the joist or beam component
W_g	The effective weight for the girder component

2.6.3. Acceptance Criteria

Once the peak acceleration has been calculated by a method such as that outlined above, it must now be determined whether this level of acceleration would prove problematic for a given structure. The quantification of such a phenomena is quite difficult as the perception of a vibration as unpleasant can range for different individuals and in different situations. For instance, the acceleration level limits suggested by the International Standards Organization (International Standard ISO 2631-2, 1989) are shown on the left side of Figure 2.25 and vary depending on the type of activity that is taking place in or on the structure. These are the most widely accepted standards in the United States and are commonly used in practice. However, other criteria are used such as the Canadian annoyance criteria chart (Figure 2.25 right) which modifies the maximum acceleration levels based on the type of excitation and the damping in the structure. The maximum acceleration levels for walking are based on the heel impact test. Furthermore, the reason higher peak acceleration levels are allowed for systems with higher damping is because an impulsive event damps out more quickly (SCI, 1989). While this criterion is only applicable to quiet offices and residential settings it is suggested that the levels be increased by a factor of 3 for occupancies such as shopping malls etc. (AISC, 2003). For residential applications, AISC Design Guide 11 recommends the a_p/g ratio found from equation 2.4 not exceed 0.5% of g .

The information presented in the section above was the basis for Guidelines published within the United States. The two primary guidelines are *AISC Design Guide 11: Floor Vibrations Due to Human Activity* (AISC, 2003) and *Applied Technology Council (ATC) Design Guide 1: Minimizing Floor Vibration* (ATC, 1999). Much of the same background information was used in developing guidelines published in the UK by the Steel Construction Institute (SCI). However, there are some key differences between the two guidelines and these differences are highlighted in the section below.

2.7. UK Guidelines – Differences from U.S. Guidelines

When using the SCI recommendations for evaluating floor vibrations due to walking excitation, a similar procedure as outlined in *AISC Design Guide 11* is followed with some modifications. The modifications relate to the assumed fundamental modes of vibration and acceptance criterion. Two primary modes of vibration in a composite floor system are defined in the SCI guidelines, the secondary beam mode and primary beam mode. These mode shapes are shown in Figure 2.26. For the secondary beam mode, the primary beams in the system form nodal lines (have zero deflection) and the secondary beams vibrate as simply supported members as shown in Figure 2.26a. For this case, the slab flexibility is affected by approximately equal deflections at the supports (secondary beams). Because of this assumption, the slab frequency is evaluated on a basis that fixed-ended boundary conditions exist. In the primary beam mode the primary beams vibrate about the columns as simply-supported members as shown in Figure 2.26b. Because of the approximately equal deflections at their supports, the secondary beams are assessed on the basis that fixed ended boundary conditions exist and the slab is also assumed fixed (SCI, 2004).

In the case where no secondary beams are present, the *SCI Publication 331: Design Guide on the Vibration of Floors in Hospitals* (2004) has a suggested procedure. Their procedure is based on evaluating floor systems that make use of the *Slimdek* (described previously in Section 2.3.2) system. SCI suggest evaluating the slab component of the system as fixed ended for vibration and the supporting members as pinned ended, which leads to higher estimates of natural frequency as compared to AISC guidelines. The first vibration mode of the slab system is shown schematically in Figure 2.27. The 331 Publication also suggests modifications to the effective length and width of the floor system. These modifications are presented below.

The acceptability criterion for the SCI recommendations is also slightly different than those published by the AISC. The criteria states that the root mean square acceleration (a_{rms}) should be calculated. For floor systems with a fundamental frequency less than 10 Hz, it is assumed the floor exhibits a single dominant resonant response and a_{rms} can be found with equation 2.9.

$$a_{rms} = \frac{\alpha_n P_o}{2\sqrt{2}M\zeta} = \frac{\alpha_n P_o}{2\sqrt{2}mL_{eff}S\zeta} \quad 2.9$$

Where:

α_n	The Fourier coefficient of the n^{th} harmonic component of the walking activity, assumed to be 0.1 for systems with a first natural frequency between 4 and 8 Hz.
ζ	The damping ratio. Assumed to be 1.1% for bare floors, 3% for floors in normal use, and 4.5% for a floor where partitions will be located to interrupt relevant modes of vibration.
P_o	The person's weight, taken as 746 N (167 lbs)
M	The effective modal mass given by $M = mL_{eff}S$.
m	The floor distributed mass that comprises of the self weight, the superimposed dead load, and 10% of the imposed load.

The effective floor length (L_{eff}) and effective floor width (S) have different recommended values based on two different SCI publications. Both sets of values were used for evaluation.

SCI 076 Recommendations

Based on recommendations in SCI Publication 076 (1989), the values reproduced in Table 2.5 are recommended for effective floor length and widths. From this table the following terms need definition.

$RF_{main\ beam}$	Relative flexibility of the primary beam
S^*	Effective width of the floor participating in the vibration. This is calculated from equation 2.10.

$$S^* = 4.5 \left(\frac{EI_1}{mf_0^2} \right)^{1/4} \quad 2.10$$

Where:

- EI_1 The dynamic flexural rigidity of the slab component. For the *Slimdek* this is the stiffness of the top concrete portion alone – as this represents the transverse stiffness.
- f_0 The combined frequency of the floor system
- L^* The effective span of the secondary beam participating in the vibration, given by equation 2.11.

$$L^* = 3.8 \left(\frac{EI_b}{mbf_0^2} \right)^{1/4} \quad 2.11$$

- EI_b The dynamic flexural rigidity of the composite secondary beam.

SCI 331 Recommendations

$$L_{eff} = n_y L_y.$$

Where

- n_y the number of bays in the direction of the secondary beam and L_y is the secondary beam span (m).
- S The effective floor width found using equation 2.12.

$$S = C \left(\frac{EI_1}{mf_0^2} \right)^{1/4} < W \quad 2.12$$

Where:

- C Factor that accounts for structural framing arrangement
- EI_1 Dynamic flexural rigidity of the slab (per unit width)
- W The building width

The a_{rms} is then weighted based on the range of frequency which the floor system lies. This weighted a_{rms} equals that calculated in the above equation for frequency ranges between 4 and 8 Hz. A ratio of a_{rms} and a value calculated from a curve given in British Standard is then found. This value is 0.5% g for most cases. The ratio is known as the Response Factor (R). It is found using equation 2.13.

$$R = \frac{a_{rms}}{0.005g} \quad 2.13$$

This Response Factor is then compared to acceptable limits that are summarized in Table 2.6. As shown, the R value is 4 for residential applications.

2.8. Comments on Guidelines

The likelihood of floor vibration problems in a structure is estimated by comparing the peak accelerations calculated via models or experimentation to criteria such as those described above. However, the true applicability of such criteria and modeling techniques is not firmly established. Some reasons for this are methods for predicting the natural frequency of 2-way spanning floor systems is unreliable. Also, simple methods of modeling the walking inputs are difficult to develop and apply (Caverson, Waldron, & Williams, 1994).

A further complication is that for some floor systems a model such as that described above may be wholly inadequate because the response contains significant contributions from multiple modes. For example, the testing of the deck-on-deck system described earlier had two modes that were located at approximately 6 and 10 Hz when no live load was applied. Both of these modes showed significant contributions during a heel drop test. This suggests that a model of the type above may not be applicable to a floor with such a construction and a different model may need to be developed (Hillman, 1990). Therefore, the extension of criteria such as those just presented to new slender floor designs must be evaluated experimentally and analyzed.

2.9. Fire Resistance Requirements and Research

Another key issue related to properly developing new floor systems performance under elevated temperature (fire). Existing knowledge of fire behavior for structural members is somewhat limited among structural engineers within the United States. The reasoning for this is often it is not something that needs to be analyzed when prescriptive approaches are used (as described later in this chapter). The current research was not intended to specifically examine and analyze fire behavior of floor systems. However, determining a proper way to investigating fire resistance for the developed systems is important and was considered. Experimental approaches to investigating fire resistance and behavior were implemented to explore new means of evaluating a structural system under elevated temperature. The purpose of this section is to present some background on the current approaches related to fire resistant design and behavior of structural members. Issues of fire resistance and behavior related to flooring systems, in particular, are also highlighted.

2.9.1. Fire Resistant Design – Prescriptive Approach

The prescriptive approach for fire resistant design is the most common methodology used in the United States. A particular system is subjected to a standard ASTM E119

(ASTM, 2000) fire test and a fire rating is given in terms of time (1 hour, 2 hour, etc.) based on the test. The intended use of the structure determines what sort of fire rating is required is needed. Thus, the required fire rating of a particular system must first be known in a prescriptive approach. Next, what sort of rating a particular system provides needs to be determined for the prescriptive methodology.

In steel construction, the amount of fire resistance needed is governed by the type of structure being built and is set forth by relevant building codes. The most common code adhered to in steel construction is the International Building Code (International Code Council, 2003). The IBC code for classifying a structure and determining required fire resistance is as follows:

- 1) The occupancy and use of the building is determined (residential, business, educational, etc.).
- 2) The type of construction than must be determined. IBC classifies five construction types based on combustibility of the components. Steel structures are classified as Type I or II, which are both noncombustible.
- 3) The dimensions of the building such as base area, building height, story area, and total area are determined.
- 4) With these parameters known, relevant IBC tables can be used to determine the required fire protection of the structure.

Once the amount of fire protection required (commonly known as the fire resistance rating [FRR]) is known, how this fire resistance is provided is determined by the engineer. The engineer must deem whether restrained or unrestrained ratings need to be met when determining fire protection. Restrained and unrestrained classifications refer to how the structural system behaves in the event of a fire and is defined in ASTM E119 (ASTM, 2000). A restrained classification accounts for continuity provided by the floor system and structural system that allows for substantial thermal expansion (i.e. deformations) to occur in the event of a fire. Unrestrained ratings refer to when a structural element's ends are free to rotate and expand and they are often not related to the load capacity of the structure in a fire event. Thus, meeting unrestrained requirements involves the use of more fire protection compared to restrained requirements. A summary of the fire resistance ratings for different restrained and unrestrained assemblies as given per ASTM E119 are shown in Table 2.7 and Table 2.8. In general, almost all steel structures are considered to be of the restrained classification (AISC, 2003).

The other aspect to be considered when designing for fire resistance is the type of protection that will be used. Fire protection is classified as either passive or active protection. Passive protection includes the resistance of the structural components and the use of externally applied materials such as spray applied fire resistant materials (SFRM) and gypsum board. There are many combinations of passive protection that can be employed to meet rating requirements. However, several agencies publish rated designs that have been developed to meet specified rating requirements. Active protection includes such devices as smoke detectors and sprinkler systems. Most steel structures employ some form of both passive and active protection.

Determination of Required Fire Resistance: W/D Criteria

One of the most common ways to design a structural member for fire resistance is the use of W/D criteria. The use of this method is based on tests that investigated the rate of thermal transfer through a steel member. Results from these tests indicate that the rate of temperature change is proportional to the beams exposed surface area and inversely proportional to its mass (AISC, 2003). This relationship can be expressed in the weight (W) to the inside perimeter of the fire protection material (D) ratio (W/D ratio) of a steel member. Those members with higher W/D ratios are more resistant to thermal transfer than those with lower ratios.

One common application of the W/D criteria is for the application of SFRM. Underwriters Laboratories (UL) has come up with required thicknesses of SFRM to meet certain requirements based on tested beams. Thickness of SFRM can be adjusted for different size sections using a thickness adjustment equation, given as (UL, 2003):

$$T_1 = \frac{\left(\frac{W_2}{D_2} + 0.6\right) T_2}{\left(\frac{W_1}{D_1} + 0.6\right)} \quad 2.14$$

Where,

T	Thickness of spray applied material (in.)
W	Weight of beam (lb/ft)
D	Perimeter of protection
Subscript 1	Desired beam size and required material thickness
Subscript 2	Given beam size and material thickness

This equation is valid with the following conditions:

- 1) The W/D ratio is greater than 0.37
- 2) T_1 is greater than 0.375 (3/8) in.
- 3) Unrestrained and restrained beam rating is not less than 1 hour
- 4) Sections used are compact

To aid in the design process, UL has published a catalog of approved designs for given required ratings based on the ASTM E119 testing standard. These designs are categorized based on the type of construction used, what sort of member or system is being investigated, and what sort of protection they use (SFRM, gypsum board, etc.). A typical UL design for a two hour rating on a composite metal deck system is shown below in Figure 2.28. As shown, the design specifies the type of fire protection needed and what components should be present in the system.

Comments on Prescriptive Based Approach

The prescriptive approach for determining the fire resistance of a structural member is straightforward to use, but provides little insight into the actual behavior of a member under elevated temperature. The use of the E119 curve limits the known fire resistance of the structural system to that of the E119 time-temperature curve. In reality, a structure could be subjected to any sort of temperature variation in a fire event. The provided fire ratings for a particular system are given only as a time that the system 'resisted' the E119 curve. The ratings do not discuss the mode of failure and the overall response of the component. The use of performance based design helps address some of these shortcomings. This approach is described in the next section.

2.9.2. Performance Based (PB) Fire Resistant Design

The use of performance based design for fire resistance has recently been implemented into relevant building codes. The provisions of performance-based design focus on two main components:

- 1) The estimation of realistic fires for compartment fire events.
- 2) The thermal response of structural components to realistic fire scenarios.

The primary performance requirement for a given structure is that it can withstand this 'realistic' fire exposure long enough that occupants can be evacuated and emergency workers be able to perform their duties (Parkinson, 2002). Much work has been done on properly modeling compartment fires in structures. Within a compartment fire there are four distinct stages that can be summarized (AISC, 2003):

- 1) Incipient Stage – Ignition takes place and fire begins.
- 2) Growth Stage – The fire grows along with a rise in temperature. If enough combustible material is present than flashover occurs.
- 3) Burning Stage – Fire has engulfed entire compartment.
- 4) Decay Stage – Occurs when the exhaustion of combustible materials has occurred. This stage is characterized by a decrease of temperatures and eventual termination of the fire.

Attempts to model these compartment fires have been done by different researchers. It is beyond the scope of this research to detail all the various models, but they are described in Parkinson (2002). It suffices to say that those attempts to model more realistic fires vary quite a bit from the typical ASTM 119 curve used in UL rated designs.

Performance based (PB) design also focuses on the thermal response of structural components. It is obvious that the thermal response of structural member relies heavily upon how it is thermally loaded. Therefore, modeling of compartmental fires has an important influence on the evaluation of the effects of realistic fires on structures. All current models in PB design represent the fire by using time-temperature curves (In lieu of incident heat fluxes on structural members, which are the more fundamental measure of heat induced on the structural elements). These curves are used as loads to determine

the thermal response of structural components using a non-linear heat transfer analysis (using either the finite element method or finite difference method) coupled with heat balance equations. The results from these analyses include the complete thermal response and temperatures throughout the structural components and these temperatures are then used to establish and design test specimens based on the performance criteria set forth by the relevant building code. Performance based approaches are presented in more detail in Parkinson (2002).

The main drawback to using performance based design (especially in the context of the current research) is there is little knowledge pertaining to the behavior of steel-concrete composite structures. The developed systems presented later are primarily steel-concrete composite systems so evaluating them using performance based approaches is somewhat difficult. However, experiments using new approaches for simulating heating were conducted and helped provide insight into behavior of one of the developed systems. The experimental work related to elevated temperature is presented in Chapter 5.

2.9.3. Comments of Fire Resistant Design

The previous sub-sections described two general approaches used for designing structural members against elevated temperature. The prescriptive approach allows for a structural engineer to select a fire rated assembly and implement it directly into a structure. Little insight into the actual behavior is provided from this approach. Performance based design allows for more realistic fire scenarios to be implemented in design. It also allows for a more thorough understanding of the structures response to the fire event. However, estimating a fire event can be difficult as all fires are different compared to one another and current models are somewhat limited. Furthermore, there is little knowledge as it pertains to steel-concrete composite structures. Which is the better approach is debatable. Within the context of the current research it was sought to understand the current state of the art for fire resistant design and how it could be implemented for the developed floor systems.

2.10. Scope and Limits of Research

A thorough background and review of existing floor systems and issues pertaining to them have been highlighted so far. This research attempted to address as many of these issues as possible when developing new type of floor systems. However, it was also realized that not all issues could be resolved within the context of the study. The scope of this project includes:

- 1) Identify existing and researched floor systems to help in developing new types of systems.
- 2) Develop new systems for use in multi-story residential steel construction.
- 3) Evaluate experimentally the structural behavior of chosen floor system.

- 4) Develop analytical tools for evaluating the structural characteristics of developed systems.
- 5) Based on testing and developed models provide recommendations for design of developed systems.
- 6) Experimentally investigate dynamic properties of floor systems.
- 7) Use existing guidelines to evaluate the developed systems for floor vibrations. Suggest any modifications to existing guidelines based on experimental observation, modeling, and engineering judgment.
- 8) Investigate a new experimental means for evaluating proposed floor systems at evaluated temperatures.

The above scope was chosen so that systems could be properly developed without focusing completely on one issue. As an example, it was not intended to develop detailed models of floor systems at elevated temperature. This issue was deemed too complex to properly address in the issue of the various systems development. It was also understood that every issue that may occur for systems could not be remedied within the context of the study. Most of these issues pertain to issues that may occur in the field if a particular system was used. By performing large scale experimentation most of these issues were believed to be identified. Any limitations that may exist for particular systems are highlighted when presenting them.

Table 2.1: Table of suggested distributed weights based on structure. [Murray, Allen, and Ungar 2003]

Structure Type	Live Load (psf)
Office floors with desks, file cabinets, bookcases etc.	11
Residential floors	6
Footbridges, gymnasiums and shopping centers	0 or nearly so

Table 2.2: Parameters suggested by Murray, Allen, and Ungar [2003] for use in calculating the peak acceleration of the floor system in a given structure.

Building Use	ao/g (%)	Damping (β)	Po (lbs)
Residential, office, or church	0.5	0.02 – 0.05*	65
Shopping mall	1.5	0.02	65
Outdoor footbridges	5	0.01	92

*0.02 for floors with few non-structural components
0.03 for floors with few non-structural components, but with small partitions
0.05 for full height partitions

Table 2.3: Results of Easterling and Widjaja research (Widjaja, 1997)

Slab #	Ultimate Load Capacity (psf)	Load at allowable deflection (psf)	Test Load/50		Test Load/150	
			Ultimate Load Capacity	Load at allowable deflection	Ultimate Load Capacity	Load at allowable deflection
LSS1a	621	245	12.42	4.9	4.14	1.63
LSS1b	559	210	11.18	4.2	3.73	1.4
LSS2a	498	163	9.96	3.26	3.32	1.09
LSS2b	455	121	9.1	2.43	3.03	0.81

Table 2.4: Loading for common rhythmic activities [Allen, Onysko, and Murray 1999].

Activity	Distributed weight of participants	α_1 , (range Hz)	α_2 , (range Hz)	α_3 , (range Hz)
Dancing	12 psf	0.5, (1.5-3)	NA	NA
Concert or Sporting Event	30 psf	0.25, (1.5-3)	0.05, (3-5)	NA
Aerobics	4 psf	1.5, (2-2.75)	0.6, (4-5.5)	0.1 (6-8.25)

Table 2.5: Values for L_{eff} and S used in determining the effective mass of the Floor (reproduced from SCI Publication 076)

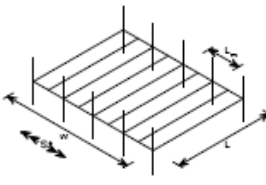
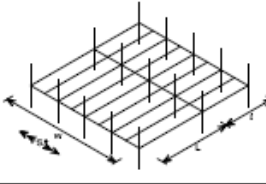
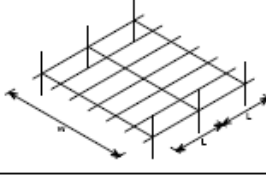
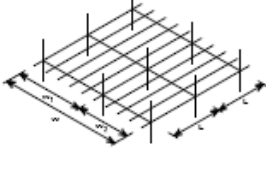
Indicative floor layout		Qualifying conditions	L_{eff} (m)	S (m)
Mode shape governed by motion of secondary beams	Case 1 	$RF_{main\ beam} < 0.2$	L	S^* but $\leq W$
		$RF_{main\ beam} > 0.2$	L	Greater of S^* or L_m but $\leq W$
Mode shape governed by motion of primary beams	Case 2 	$l = L$	$2L$	As for Case (1) above
		$0.8L < l < L$	$1.7L$	
		$l < 0.8L$	L	
Mode shape governed by motion of primary beams	Case 3 	$RF_{main\ beam} < 0.6$	$2L$	W
		$RF_{main\ beam} > 0.6$	L^* but $\leq L_{max}$	
Mode shape governed by motion of primary beams	Case 4 	$W_2 = W_1$	As for Case (3) above	$2W_1$
		$W_2 > 0.8W_1$		$1.7W_1$
		$W_2 < 0.8W_1$		W_1

Table 2.6: Response Factors for SCI Guidelines (SCI, 1989)

Building Type	Limiting response factor
General Office	8
Residential	4
Special Office	4
Busy Office	12

Table 2.7: Fire resistant ratings and temperature criteria for standard fire tests on floor systems (reproduced from(Cedeno, 2006))

Tested Member or Assembly	FRR Type	Maximum Temperature °F (°C)	Maximum Temperature and Location	Comment on Temperature Criteria
Unloaded and Restrained or Unrestrained Beam	Unrestrained beam	1000 (538)	Average at any section	Achieved at the end of the fire resistant rating
		1200 (649)	At any one of the measured points	
Loaded and Restrained Beam	Unrestrained beam	1100 (593)	Average at any section	Achieved at the end of the fire resistant rating
		1300 (704)	At any location	
		800 (427)	Average at any section for prestressing steel	
		1100 (593)	Average at any section for reinforcing steel	
	Restrained beam	1100 (593)	Average at any section	Achieved at the greater between 1 hour and half of the fire resistant rating
		1300 (704)	At any location	
Loaded Unrestrained Floor Assembly	Unrestrained beam	Same as classification for Loaded and Restrained Beam		
	Unrestrained floor	250 (139)	Average rise above initial value on unexposed surface	Achieved at the end of the fire resistant rating

Table 2.8: Fire resistant ratings and temperature criteria for standard fire tests on floor systems (reproduced from (Cedeno, 2006))

Tested Member or Assembly	FRR Type	Separation of steel beams, joists, etc	Maximum Temperature °F (°C)	Maximum Temperature and Location	Comment on Temperature Criteria
Loaded Restrained Floor Assembly	Unrestrained floor system	Any	250 (139)	Average rise above initial value on unexposed surface	Achieved at the end of the fire resistant rating
		More than 4ft (1.2m)	1100 (593)	Average at any section	
			1300 (704)	At any location	
		4ft (1.2m) or less	1100 (593)	Average of all beams or joists	
		Any	800 (427)	Average at any section for prestressing steel	
	Any	1100 (593)	Average at any section for reinforcing steel		
	Restrained floor system	Any	250 (139)	Average rise above initial value on unexposed surface	Achieved at the end of the fire resistant rating
		More than 4ft (1.2m)	1100 (593)	Average at any section	Achieved at the greater between 1 hour and half of the fire resistant rating
			1300 (704)	At any location	
		4ft (1.2m) or less	1100 (593)	Average of all beams or joists	
		Any	800 (427)	Average at any section for prestressing steel	
	Any	1100 (593)	Average at any section for reinforcing steel		
	Unrestrained beam	Any	Same as classification for Loaded and Restrained Beam		

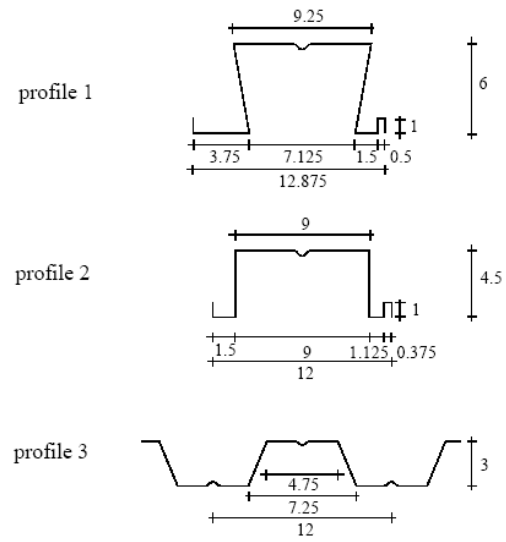


Figure 2.1: Profiles used in Widjaja research (Widjaja, 1997)

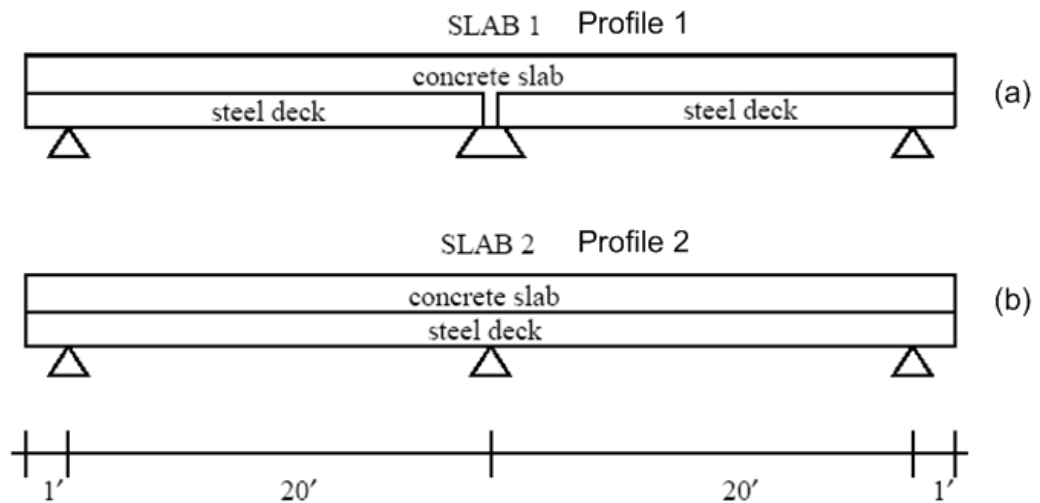
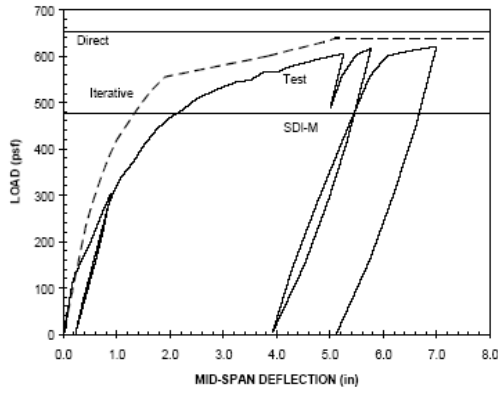
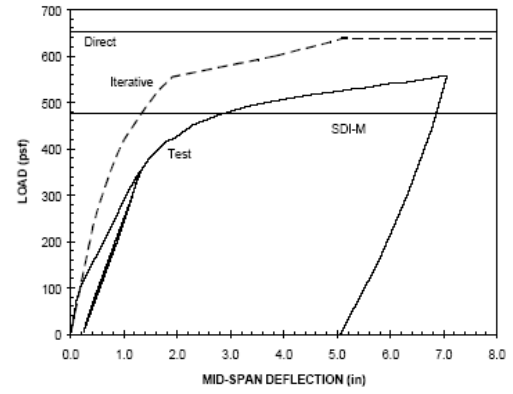


Figure 2.2: Test setup for Widjaja research (Widjaja, 1997)

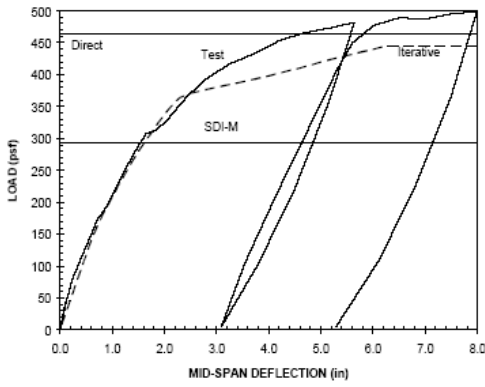


(a) 1st test

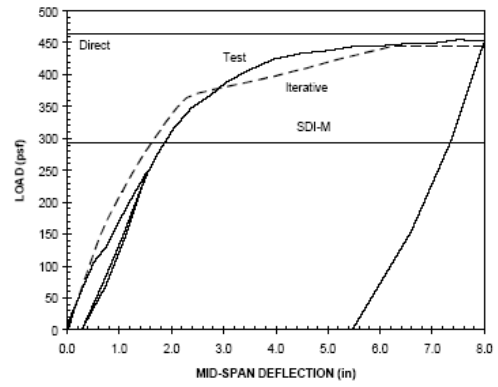


(b) 2nd test

Figure 2.3: Load-deflection results for LSS1 (Widjaja, 1997)

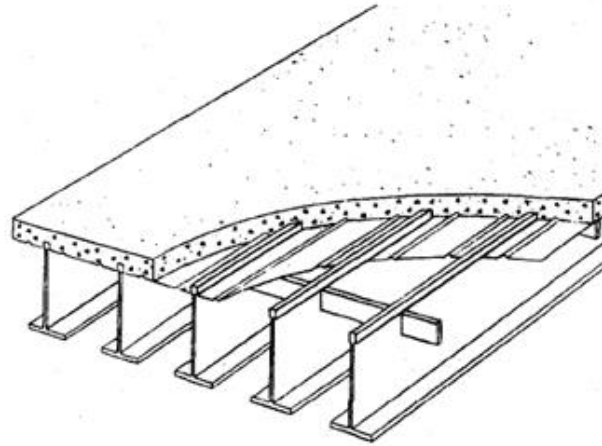


(a) 1st test

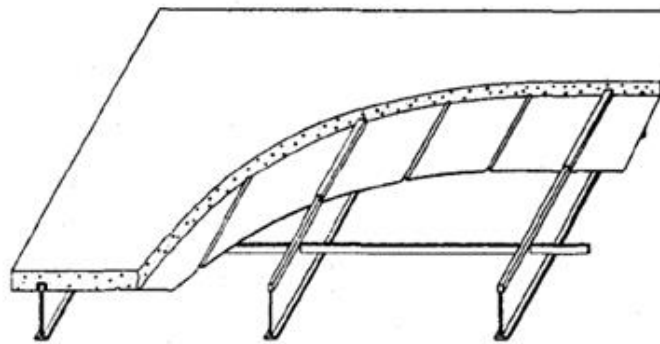


(b) 2nd test

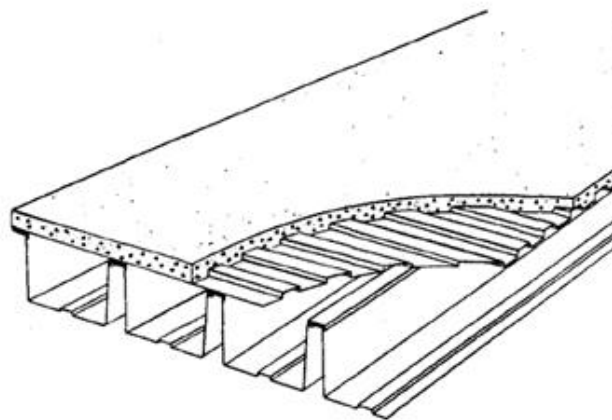
Figure 2.4: Load-deflection results for LSS2 (Widjaja, 1997)



(a) Long-Span Steel Grid Floor System



(b) Steel Grid with Profiled Deck & Concrete Slab



(c) Long Span Cold-Formed Deck/Composite Slab

Figure 2.5: Conceptual floor systems for use in steel construction conceived by Hillman and Murray (Hillman & Murray, 1990)



Figure 2.6: Hillman/Murray Deck-on-Deck 30 ft by 30 ft prototype system (Hillman & Murray, 1990)

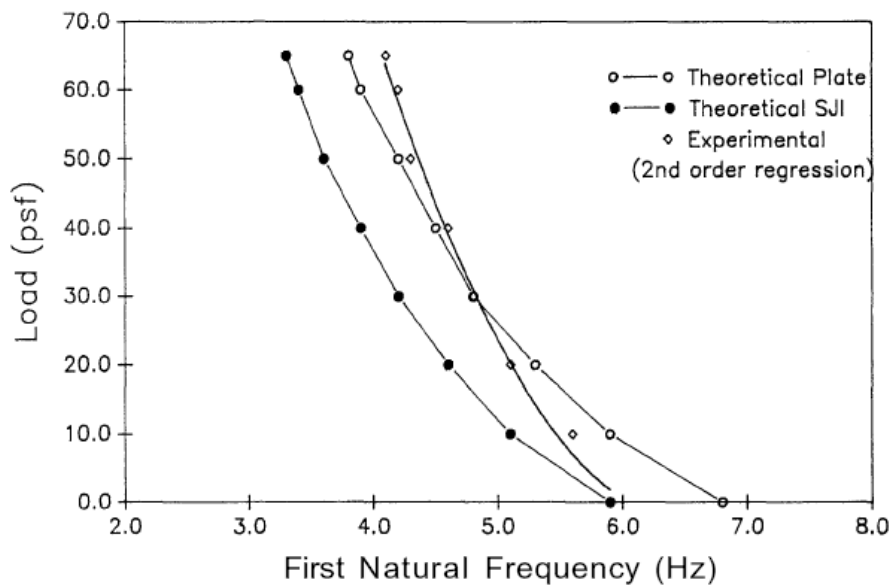


Figure 2.7: Measured frequencies for Deck-on-Deck prototype specimen (Hillman, 1990)



Figure 2.8: DSC with (a) traditional shear studs and (b) Bi-Steel System (McKinley & Boswell, 2002)



Figure 2.9: SPS system (Kennedy & Kennedy, 2004)

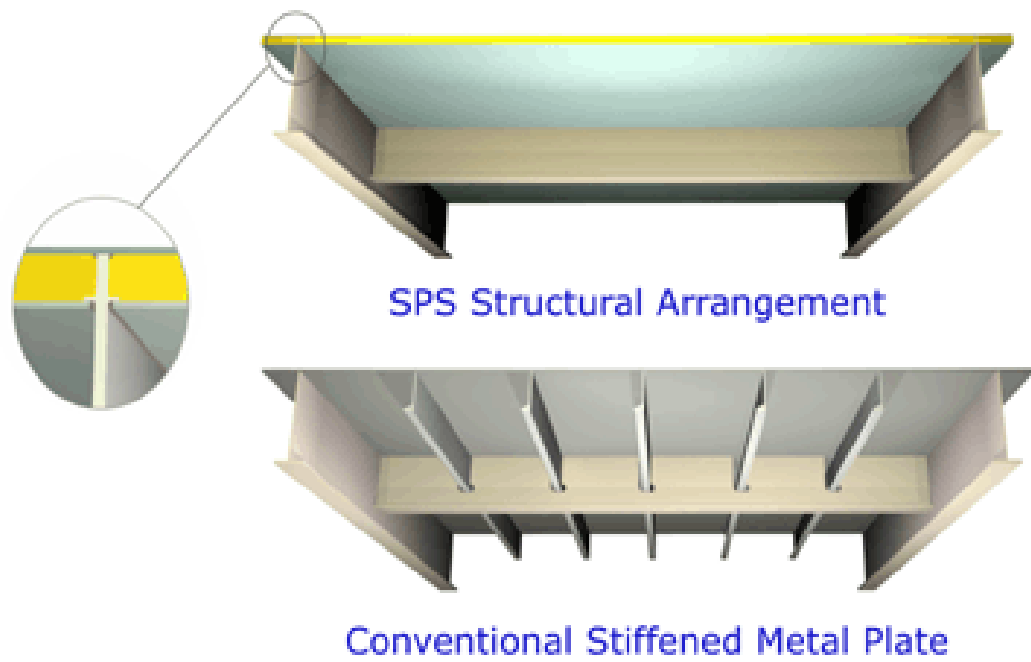


Figure 2.10: Schematic of SPS system used for bridge deck application (Kennedy & Kennedy, 2004)

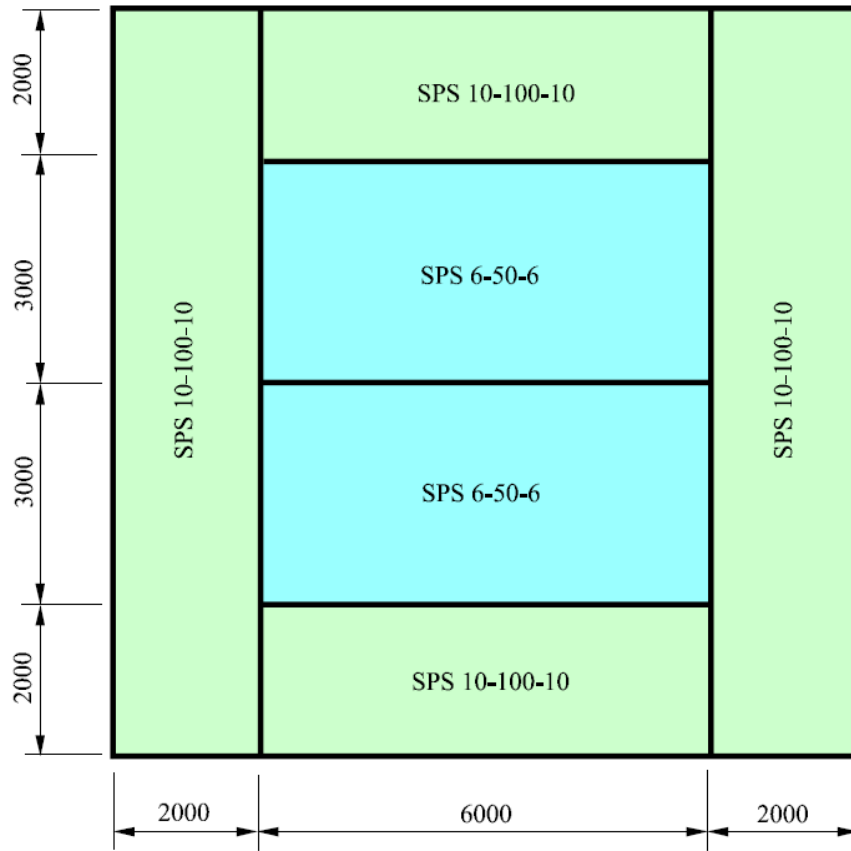


Figure 2.11: Proposed SPS floor layout by Intelligent Engineering (Kennedy & Kennedy, 2004)

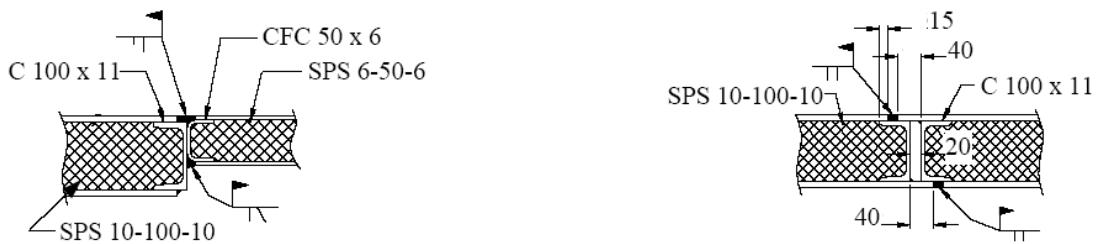


Figure 2.12: Connection details for SPS floor system (Kennedy & Kennedy, 2004)

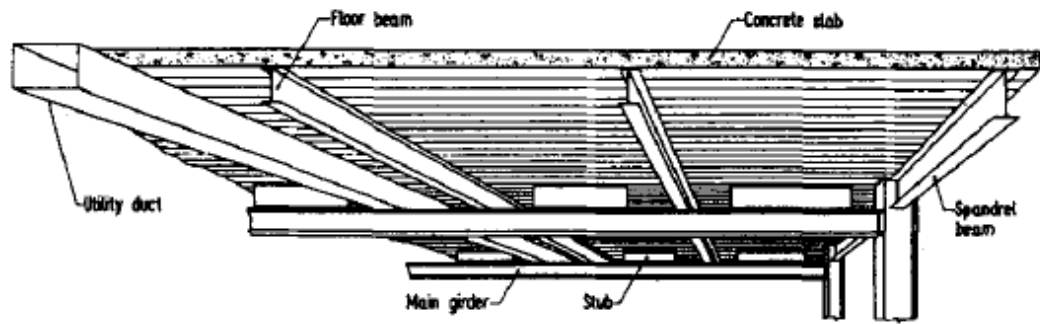


Figure 2.13: Schematic of Stub Girder System (Wang, Padmanaban, & Shanmugam, 1995)

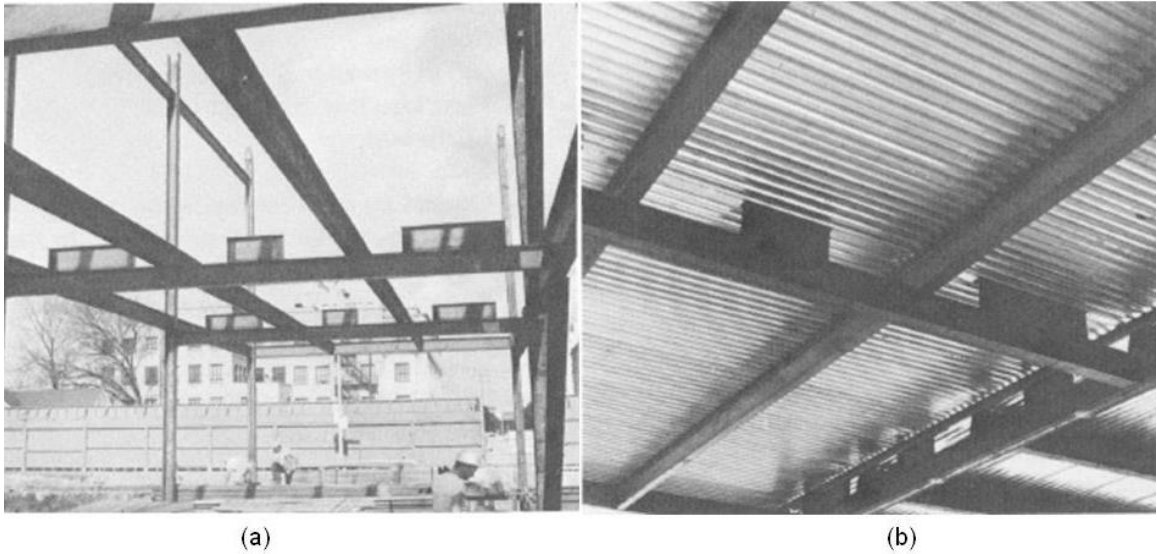


Figure 2.14: Construction photos of structure using Stub Girder System (a) prior to deck placement and (b) after deck placement (Colaco, 1972)

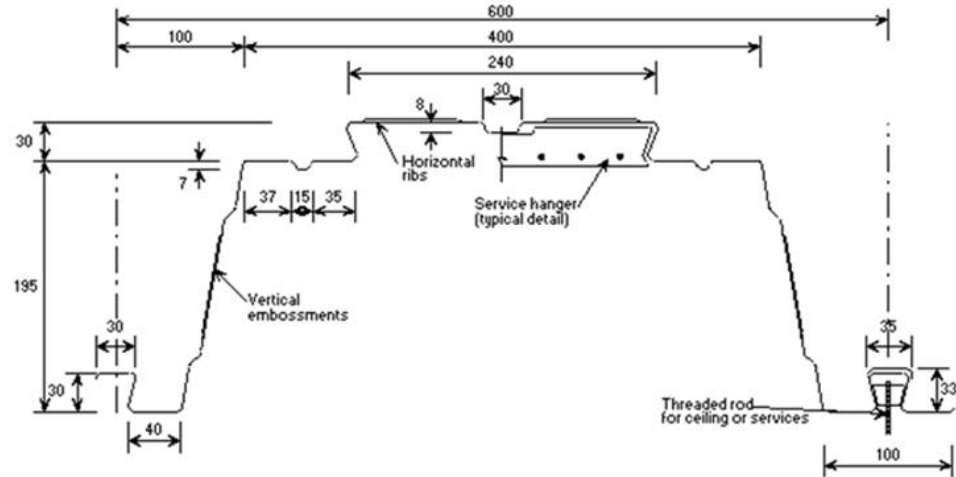


Figure 2.15: SD 225 profile (Lawson, Mullet, & Rackham, 1997)

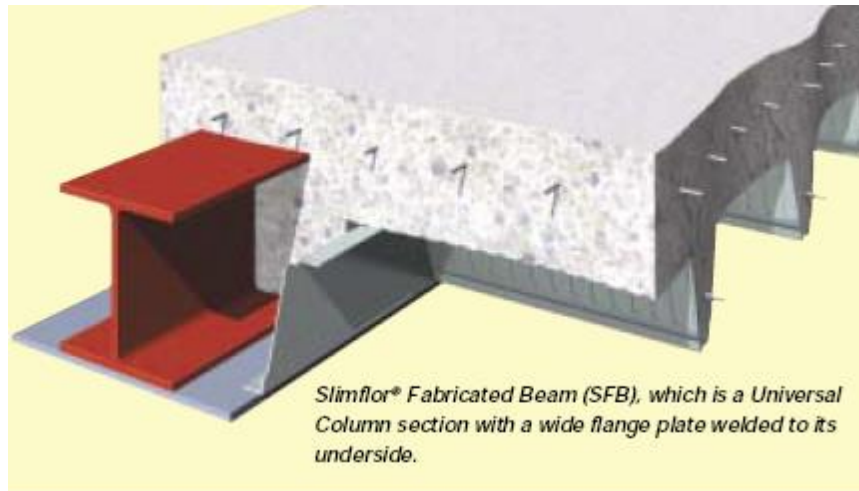


Figure 2.16: Original Slimflor system (Corus, 2002)

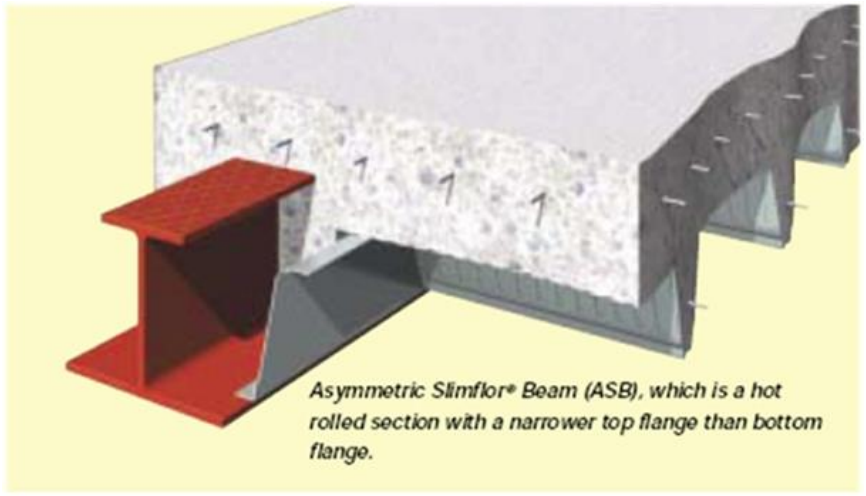


Figure 2.17: Slimdek Flooring System with SD 225 deck and rolled ASB (Corus, 2002)

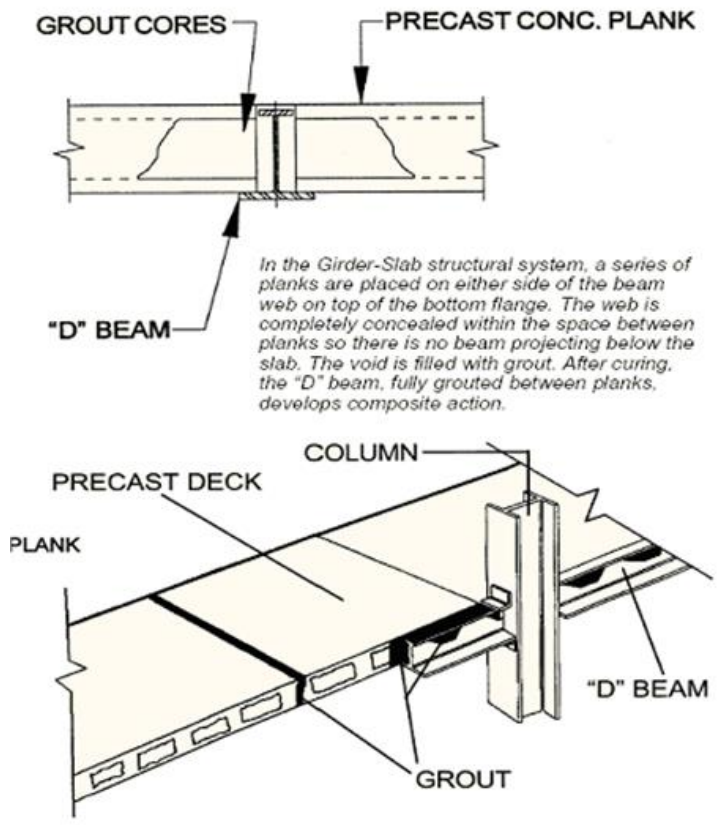


Figure 2.18: Schematic of Girder Slab System (Naccarato, 1999)

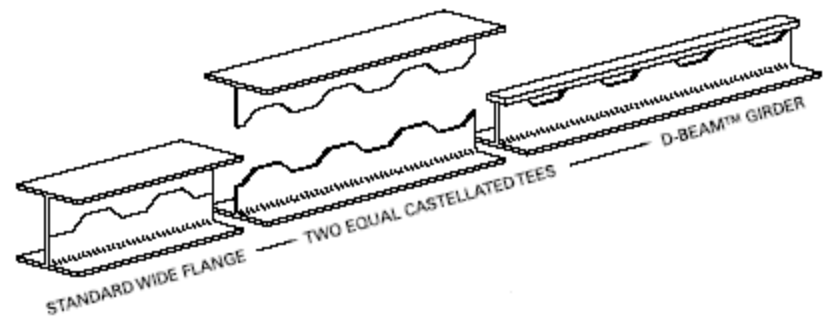


Figure 2.19: D-Beam Girder (Girder Slab Technologies, 2002)

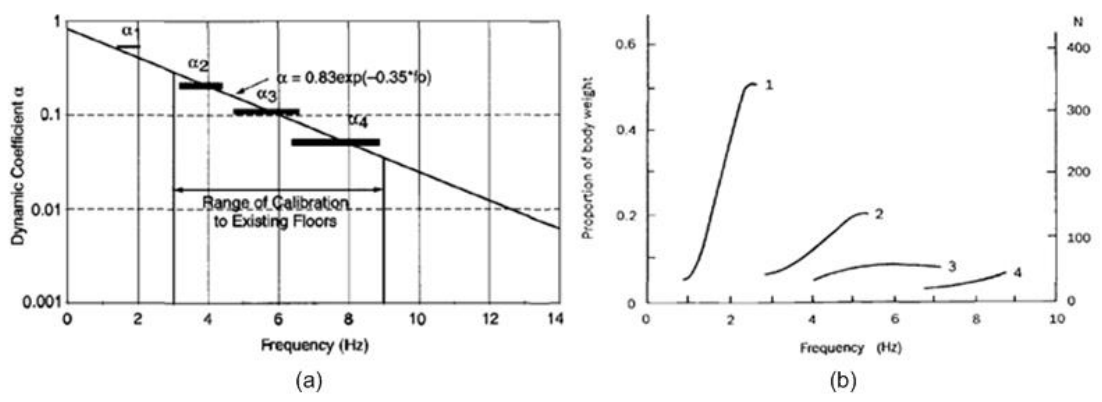


Figure 2.20: Scale factors to determine the forcing of a floor system due to walking as given by Murray, Allen, and Ungar [2003] (left) and Wyatt [1989] (right).

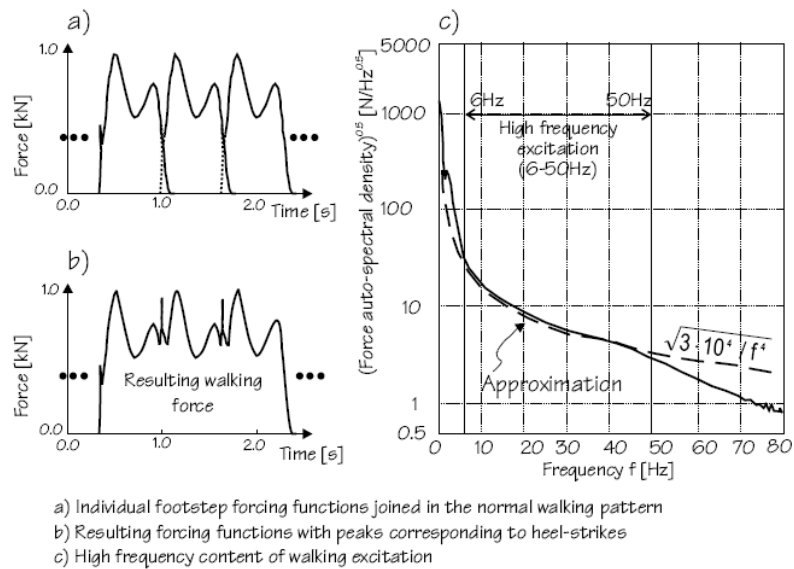


Figure 2.21: Model of forcing due to walking taking into account high frequency content (Taken from Pavic and Reynolds 2002b after Ohlsson, 1988).

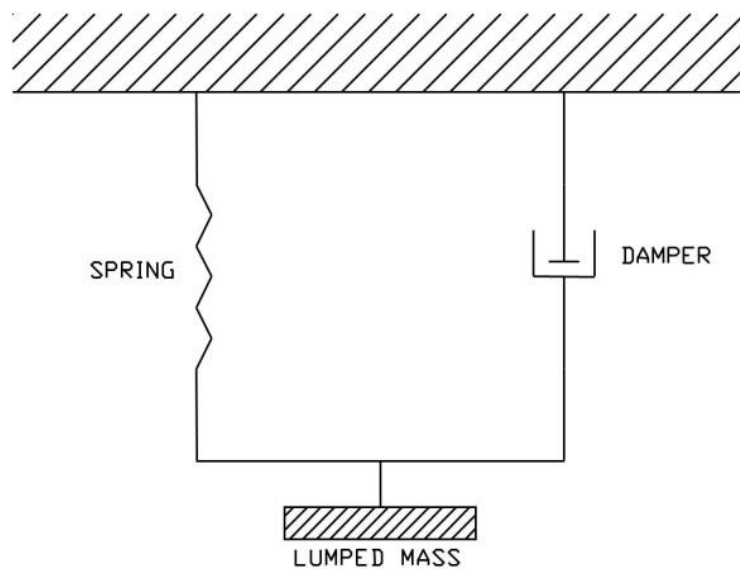


Figure 2.22: Idealized Lumped SDOF Dynamic System

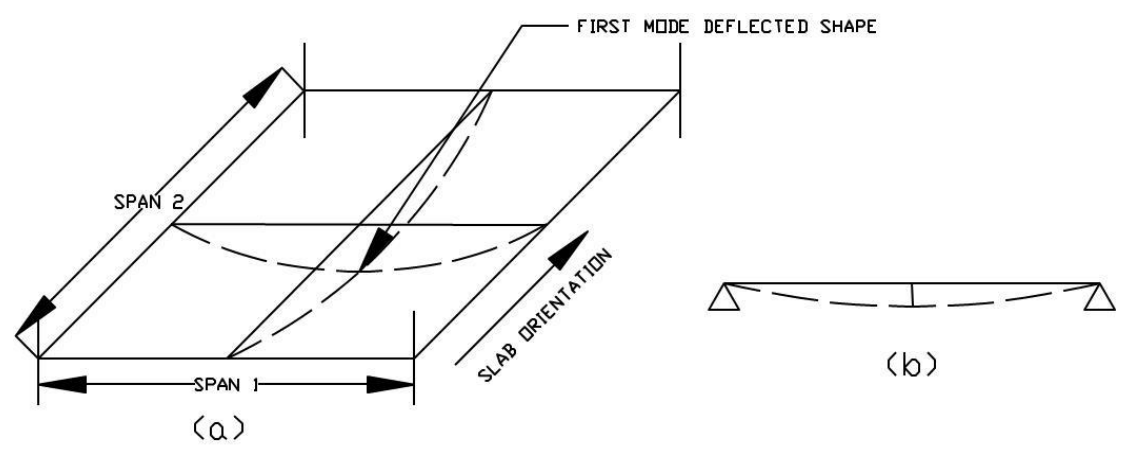


Figure 2.23: (a) Bay of Structure and (b) Simply Supported Beam Idealization of System

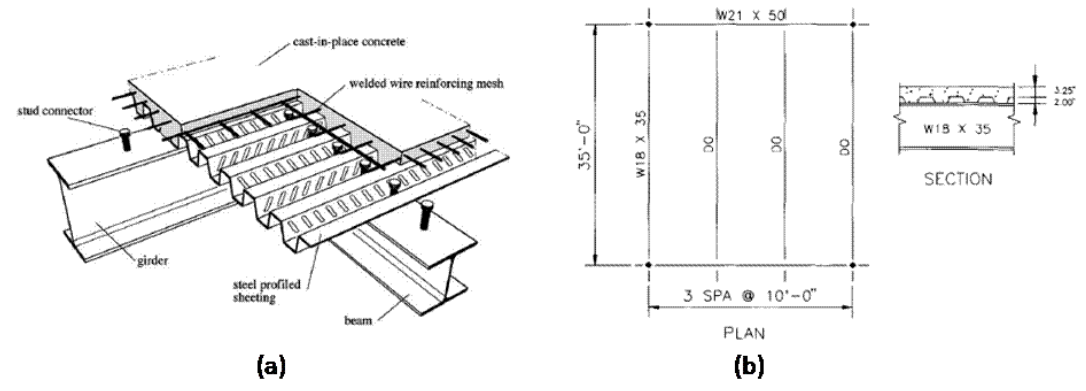


Figure 2.24: Conventional Steel Deck-Concrete Slab System (a) isometric schematic and (b) Typical Interior Bay

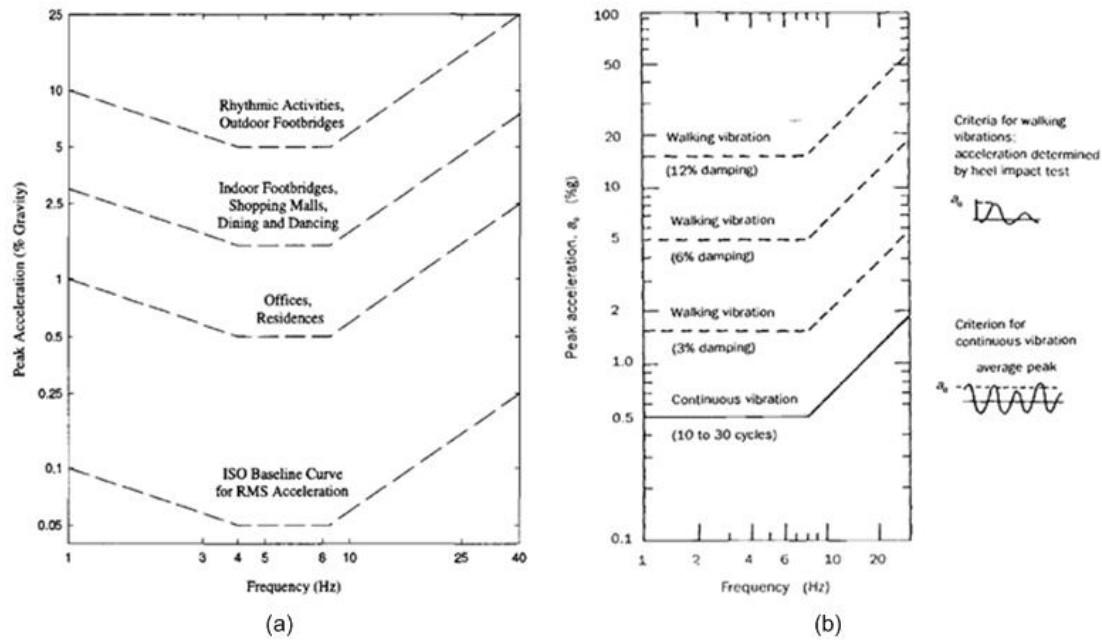
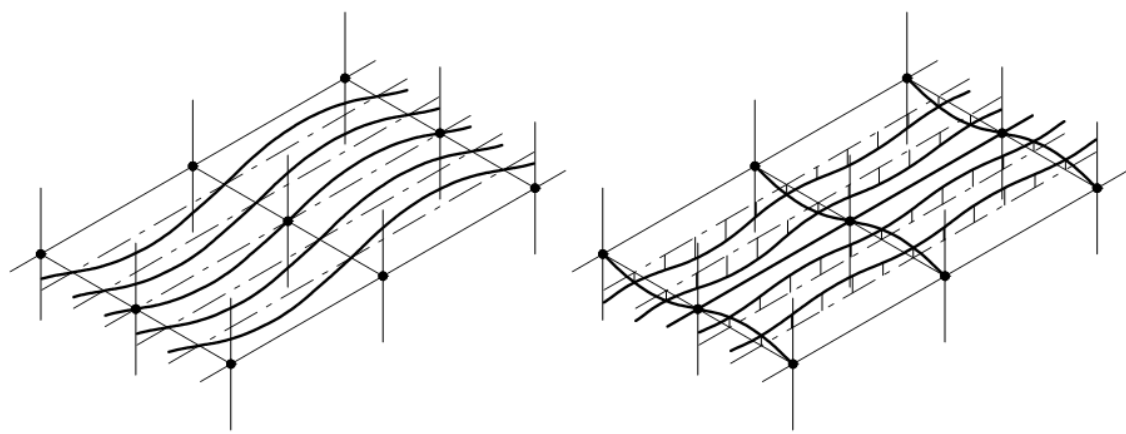


Figure 2.25: Peak acceleration levels as recommended by the International Standards Organization (left) (from [Murray, Allen, and Ungar 2003]) and the Canadian annoyance criteria chart (from [Wyatt 1989]).



(a) governed by secondary beam flexibility (b) governed by primary beam flexibility

Figure 2.26: Typical Fundamental Mode Shapes for Composite Floor Systems (SCI, 2004)

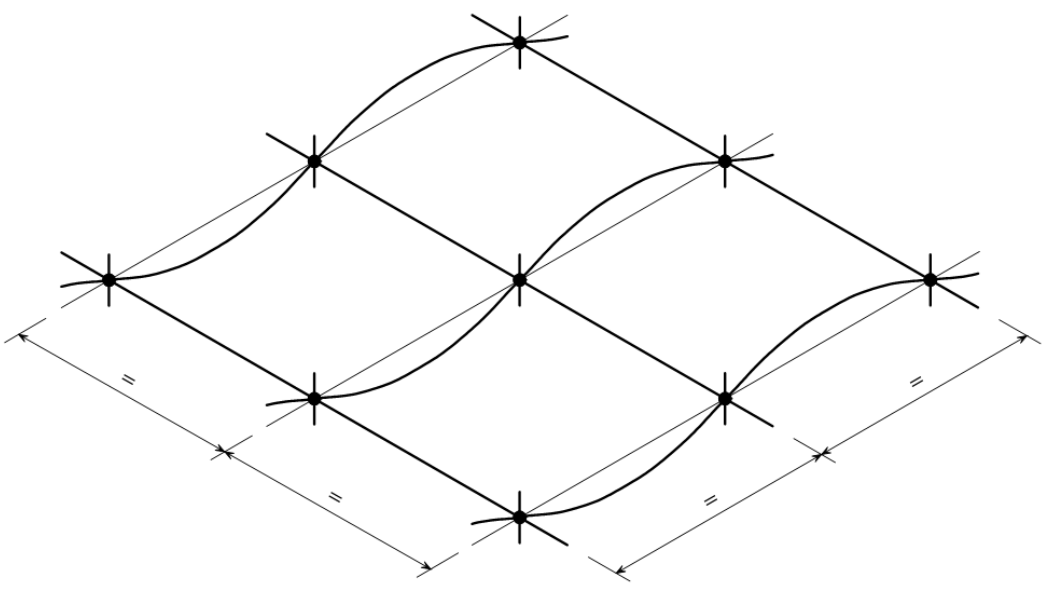
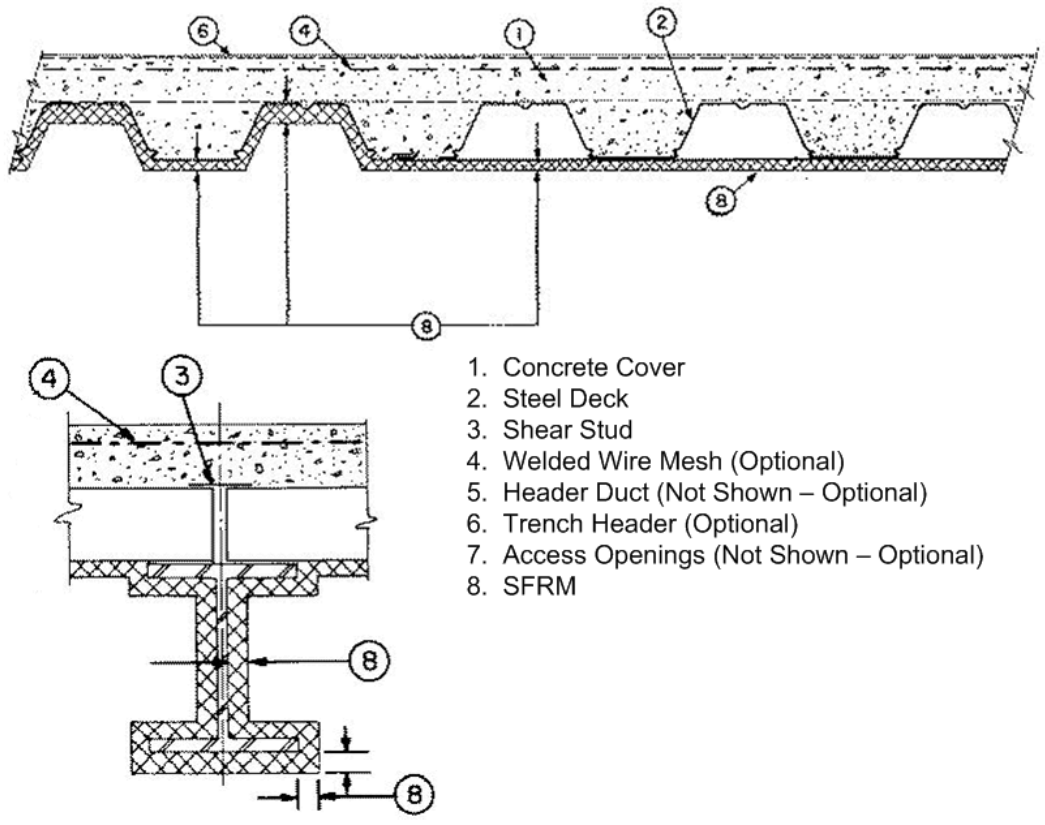


Figure 2.27: First Vibration Mode of Deep Deck Floor System (SCI, 2004)



- 1. Concrete Cover
- 2. Steel Deck
- 3. Shear Stud
- 4. Welded Wire Mesh (Optional)
- 5. Header Duct (Not Shown - Optional)
- 6. Trench Header (Optional)
- 7. Access Openings (Not Shown - Optional)
- 8. SFRM

Figure 2.28: UL Fire Design No. 858 (UL, 2003)

CHAPTER 3. OVERVIEW OF DEVELOPED FLOOR SYSTEMS

3.1. Introduction/Overview

The first two chapters have focused on background information related to different types of floor systems used in steel construction. Existing systems have been reviewed to highlight their salient features and identify possible issues related to developing new types of floor systems. Based on this information a suite of different floor systems were developed to varying degrees of completion. The systems were chosen based on their technological merits and viability as a floor system in steel construction. The systems were investigated further for economic feasibility, and final systems were selected for further experimental and analytical investigation.

This chapter presents an overview of new types of floor systems that were developed for residential multi-story steel construction. The key features of the systems are presented along with the reasoning behind their development. The systems were developed to varying degrees of completion depending on their overall merit as judged by the research team and oversight committee for the project. Section 3.2 focuses on sandwich type composite floor systems. Section 3.3 focuses on advanced metal deck systems. Section 3.4 presents the pre-loaded self-shoring system. Section 3.5 presents the ratings of the developed systems. The following chapters (4 onwards) focus on floor systems that received the highest rating. The chapters include experimental and analytical investigations of these highest rated systems.

3.2. Sandwich Type Composite Floor Systems

The first group of floor systems developed were those using sandwich construction for structural integrity. The advantages of sandwich type structures were highlighted in Chapter 2. Two types of sandwich systems are presented in the following sub-sections.

3.2.1. Double Skin Composite System

Chapter 2 included a review of sandwich structural systems that have been developed and used for different engineering applications. Based on the designs of existing sandwich systems, merit exists for a double skin composite (DSC) system can be designed and implemented as a floor system. The top and bottom steel plates could be attached and made composite with a lightweight concrete core using shear studs. Figure 3.1 shows a schematic of the proposed DSC panels for floor systems. The concrete would be cast before placing the DSC panels into the structure. Thus, it would essentially be a pre-cast system. The pre-cast planks could be lifted by crane and set in the steel frame and connected appropriately. Figure 3.2 shows a possible layout of DSC panels within a steel frame. Figure 3.3 shows DSC panels designed for a 30 ft. span. As

shown, the top and bottom surface plates are 0.25 in. thick, and the concrete core is 6 in. thick. The shear studs are 0.5 in. diameter and have a spacing of 1 ft in both directions.

Advantages

- 1) System uses readily available construction materials and components.
- 2) Sandwich construction is structurally quite efficient as depths of 6 in. are possible for 30 ft. spans.
- 3) The concrete between the steel plates would provide desirable thermal and insulating characteristics, which would improve fire resistance. The damping properties and mass would improve the floor vibration characteristics.
- 4) The bi-steel system in the UK has shown that mass production of double skin composite systems is feasible.

Issues and Discussion

A conceptual design of a structurally efficient DSC panel system utilizing lightweight concrete sandwiched between steel plates was developed. The system performs adequately from a structural standpoint and could present merit for use in multi-story residential steel construction. However, since a system of this type has not been used in the U.S., there are some issues that would need to be investigated including:

- 1) The overall cost for fabricating and constructing the system could be prohibitive. Studies would need to focus on the best way to fabricate and erect a system of this nature.
- 2) Connection systems to supporting girders would need to be investigated to ensure this would be feasible.
- 3) The self weight of the pre-cast system ranges from 75-95 psf (depending on whether lightweight or normal weight concrete is used). This is significantly higher than the self-weight of metal deck systems, but comparable to pre-cast plank systems (~75-85 psf). This is a major issue for these DSC panel systems, and may prevent them from being used.

3.2.2. Profiled Double Skin Composite (DSC) System

As an alternative to using top and bottom steel plates for the DSC panel system, it is possible to use cellular metal decks on top and bottom with lightweight concrete sandwiched between them. This concept is shown in Figure 3.4. This system would either need to be pre-cast or shored if it were to be used in practice. If an embossed deck profile is used, there may be sufficient bond strength between the deck and concrete to resist the horizontal shear that would develop in the composite section. Figure 3.5 shows the 1.5 and 2 in. profiles that were considered in the design. These profiles are manufactured by CSI, and all deck components are 16 gage material. The typical self-weight of the profiled DSC system is 84-87 psf, which is slightly higher than many pre-cast systems. The maximum width of the panel varies from 24-36 in. because that is the maximum width of manufactured cellular decks (as shown in Figure 3.5).

Issues and Discussion

The above profiled DSC design is an alternative to the DSC panel design presented in Section 3.2.1. Both systems have the same fundamental behavior and similar designs. The profiled DSC system is slightly heavier than the DSC system because it uses much less steel, and requires more concrete depth. From a fabrication standpoint, the profiled DSC system may present the advantage that it uses metal decks with embossments instead of flat steel plates, and may not require additional shear studs. The main issues for the profiled DSC are:

- 1) The current side-lap connections used on the metal deck profiles may inhibit casting of concrete into the system. If a grout key could be added, it would help in transferring shear for diaphragm action. The use of intermittently welded steel plates is also a possibility.
- 2) The bond strength between the deck profiles and the concrete core can be an issue. If the bond strength is not adequate, then slip may occur and the system might lose much of its strength. Determining this capacity would require testing to determine the bond-slip behavior of the profiles.

The profiled DSC system is an efficient way to construct a sandwich system utilizing readily available products and technologies. While it is somewhat heavier than the DSC system, the additional mass further enhances floor vibration resistance characteristics. It is also innovative in how it utilizes both sandwich construction and cellular steel decks in the structural system. If using a flat plate DSC type system were to be too expensive (due to steel thickness), then the profiled DSC system presents a viable alternative.

3.3. Advanced Metal Deck Systems

As previously noted, conventional floor systems consist of 1.5-3.0 in. deep steel deck profiles that serve as formwork and reinforcement for the concrete slab. These floor systems are supported by floor beams every 6-10 ft. depending on the depth and geometry of the metal deck. The maximum unsupported span is limited to 10-12 ft. due to the: (1) 3 in. depth limit for conventional metal decks, (2) the concrete slab weight, and (3) the low stiffness of metal deck in the direction perpendicular to the ribs. Despite these limitations, metal deck systems continue to be the dominant type of floor system used in steel structures. Their popularity comes more from existence of manufacturing techniques and the ease of design, fabrication, and erection in steel framing.

Systems using modified metal decks to achieve longer spans and maintain low overall depth were investigated in the current research project. These systems are referred to as advanced metal deck (AMD) systems. The AMD systems developed include systems that: (a) utilize a concrete slab for composite action, and (b) those that use all steel structural components. Some of the AMD systems utilize sandwich construction, where now a steel deck is sandwiched between two steel plates (in lieu of concrete). The target bay sizes for these various systems were set at 30 ft (in the strong direction span), which

are typical for multi-story residential construction. The use of intermediate filler beams was eliminated for all systems developed.

Previous chapters have discussed in detail the issues related to existing composite steel deck-concrete slab floor systems. The primary issue with the deck profiles is their manufactured depths of 1.5 to 3 in. limit their ability to achieve spans greater than 12 ft (for typical slab depths). These metal deck depths provide limited stiffness in the non-composite phase, which often governs the design of composite slab systems.

Chapter 2 highlighted previous research in the use of deep deck systems along with those which have been used commercially to a certain extent. The *Slimdek* system is the most well known system in the UK. It has demonstrated how deeper decks can improve span capabilities for composite steel-concrete floor systems. The span increases result from the much greater non-composite stiffness that deeper decks can provide. Table 3.1 shows the moment of inertia increase for deck profiles as the depth of the deck increases. The steel decks shown in this table are 18 gage thick profiles available from Consolidated Systems Inc. The 1.5 - 3 in. profiles are used for composite floor systems, while the 4.5 - 7.5 in. profiles are used for roof decks. The table illustrates that as the depth is increased from 1.5 in. to 4.5 in. there is 13.5 times increase in the flexural stiffness.

The composite deep deck systems investigated in the current study were intended for spans ranging from 20 to 30 ft. The longer spans were achieved by using deck profiles with nominal depths between 6 in. and 7.5 in. Existing roof deck profiles manufactured by Consolidated Systems Inc. (CSI) were used in the development of deep deck systems.

3.3.1. Composite Cellular Deep Deck (CC-DD) System

One of the composite deep deck floor system candidates that has been investigated in detail is referred to as the composite cellular deep deck (CC-DD) system. The CC-DD system consists of a deeper cellular deck profile that is composite with the concrete slab on top. The CC-DD system can achieve un-shored spans of up to 30 ft. by using cellular deck profiles with a nominal depth of 7.5 in. The cellular profiles are manufactured in two ft widths, and they can be connected at side-lap connections using typical screws, welds, or button punch. The cellular deep decks provide greater stiffness in the construction (non-composite) phase, which typically governs the overall design. The cellular (bottom) plate provides more steel area in tension in the composite phase, thus enhancing the stiffness and capacity of the section.

Figure 3.6 shows the CC-DD system cross-section that was designed for an unsupported span of 30 ft. As shown, there are two similar deck cross sections with different thickness components. Option 1 consists of a 7.5 in. deep cellular deck profile with 14-gage thickness metal deck and 16 gage thick bottom plate, and 2.5 in. thick concrete slab on top. Option 2 consists of a 7.5 in. deep cellular deck profile with 18 gage thickness and 20 gage bottom plate. The two options will yield construction level deflections of $L/360$ and $L/220$ based on simple span conditions. The CC-DD system was designed assuming simply supported end conditions in both composite and construction level phases. Lightweight concrete (LWC – 110-120 pcf nominal unit weight) was used for the 30 ft. span CC-DD system. It was used to reduce the self-weight of the system and to achieve the deflection requirements in the construction phase, which

usually governs the deck design. The use of lightweight concrete is also desirable from a fire resistance standpoint. The desired fire rating requirements can be achieved using smaller thickness lightweight concrete slabs over the metal deck.

The connections between the CC-DD system and the supporting (end) girders were designed to be similar to existing deck to beam connections. Two connection types were considered: (i) using shear studs, and (ii) using puddle welds alone without shear studs. The connections using shear studs would be more efficient in preventing end slip and maintaining composite action between the deck and concrete slab. This connection type is shown schematically in Figure 3.7. As shown, the flutes of the deck are aligned and butted against one another for an interior condition. Holes are fabricated in the bottom flutes of the cellular deep deck profile because of the overall thickness of the deck profiles. Deck profiles thicker than 14 gage are difficult to weld a stud through, and hence it is not recommended to weld a stud directly through these profiles. The shear studs are welded to the supporting girder flanges through holes fabricated in the bottom plates of the cellular deep deck. Figure 3.8 shows a shear stud placed on an actual test specimen. For the puddle weld connection, 5/8 in. puddle welds can be placed in place of the shear studs as shown in Figure 3.9.

Advantages of System

The major advantage of the CC-DD system is that it eliminates the need for intermediate floor beams for spans up to 30 ft. This reduces the total depth of the floor systems. For example, the total depth of the CC-DD system designed for 30 ft. span is 10 in., which is a significant reduction compared to standard metal deck systems. The drawback of the CC-DD system is that it uses more weight of steel deck per foot as compared to conventional floor systems. The steel weights of the deep deck profiles are approximately 2.5 to 3.0 times the weights of steel deck profiles (1.5 - 3.0 in. deep) used for conventional floor systems. Hence, their associated costs will also be higher than those for conventional deck profiles. Some of these costs will be offset by: (a) eliminating intermediate floor beams and the shear studs associated with them, and (b) reducing floor-to-floor heights. Another advantage of CC-DD systems is that the total weight of the floor system (with concrete) is comparable to the total weight of conventional floor systems. The total weight of the CC-DD floor system is much lower (approximately 47%) than the weight of floor systems using pre-cast planks that span up to 30 ft. (8 in. plank with 2 in. topping).

Another advantage of this system is the ability to achieve long spans with already existing products. The deck profiles used in design are existing roof deck profiles available from Consolidated Steel (CSI). However other similar deep deck profiles are manufactured by other companies such as United Steel and Epic Metals. The use of readily available products is desirable as it presents the possibility of implementation in a timely manner if the system is proven to have merit.

Issues for Discussion and Further Investigation

Some of the possible issues that need to be further investigated for this system include:

- 1) The possibility of slip between the deck and concrete. Since there are no embossments on the deck, the possibility of interfacial slip exists. Using shear studs will help in delaying localized end slip. This was included in the experimental investigation.
- 2) Investigation of the system's susceptibility to floor vibrations induced by human motion.
- 3) Investigation into behavior at elevated temperatures
- 4) The cellular deep deck profile spanning 30 ft may be too heavy for workers to lift, thus requiring the use of a crane. This could become an issue on jobsites where crane time is at a premium. One possibility to help with this would be to assemble several units together on the ground and then lift them into place.

3.3.2. Shored Composite Deep Deck (SC-DD) System

A second type of system utilizing a non-cellular deep steel deck acting composite with a concrete slab was developed for up to span lengths of 30 ft. The difference with this type of system is that it uses a single line of shoring at mid-span to reduce deflection in the construction phase. Figure 3.10 shows a cross-section of the SC-DD system. As shown, a 7.5 in. deep 14 gauge thick deck is utilized with a 3.5 in. lightweight concrete slab on top for a total depth of 11 in. The concrete depth helps in meeting the fire rating requirements, provides additional mass for damping out floor vibrations, and also adds some structural capacity to the system.

The addition of a line of shoring in the construction phase helps in achieving longer spans while reducing the amount of steel needed. Shoring is usually avoided in the construction process if multiple lines of shoring are required. For the SC-DD system, only one line of shoring is required so that the additional costs can be minimized.

Advantages

Using the SC-DD system offers the primary advantage of reducing the steel material used while maximizing spans. Compared to the cellular system there is not only a reduction in the material, but the added cost of attaching the bottom plate is also eliminated. While a 7.5 in. 14 gauge deck profile was used in this design, it is also possible to use thinner gauges and smaller deck depths such as 4.5 in. or 6 in. deep profiles. The 7.5 in. deck offers the advantage of maximizing the efficiency of steel material used, while minimizing concrete material above the deck to get desirable structural characteristics.

Issues for discussion and further investigation

The shored composite deck system has certain issues associated with it that merit further investigation. These issues include:

- 1) The amount of deflection that occurs after shore removal must be accounted for to avoid unlevel floor finishes. Cracking of the concrete may occur from shore removal. This would reduce the initial stiffness of the system. More issues

related to shrinkage and creep deflections are plausible since the composite section is subjected to stresses due to shore removal.

- 2) There would likely be hesitation by certain erectors to use any type of shored system due to perceived limitations and problems. However, many of these perceptions are based on using shoring with traditional deck systems, which often involve multiple lines of shoring in a given bay.

3.3.3. Sandwich Metal Deck System

Figure 3.12 shows a schematic of the sandwich metal deck system. This system combines the structural characteristics of sandwich construction along with the benefits of using lightweight cold-formed steel deck. An existing cellular deck profile that has a 7.5 in. nominal depth is used with *another top steel plate* attached to the system (attached with screws or welded). A topping of lightweight concrete, gypcrete, or other material can be used as a non-structural walking surface. The additional topping also helps in contributing mass and damping for mitigating floor vibrations. It is also recommended for this system that concrete be placed in the lower flutes over supporting girders and for a nominal distance past the support to enhance the connection strength of the system and allow for helping to transfer lateral loads.

Advantages of System

- 1) A significant reduction in self weight as compared to traditional deck systems and composite deep deck systems.
- 2) Sandwich construction is structurally very efficient in how it utilizes the steel components of the system.
- 3) Reduced amount of concrete leads to material savings.

Issues for discussion and further investigation

Some of the issues that provide advantages for this system also lead to possible problems. These include:

- 1) The reduction in self weight could possibly lead to issues with floor vibrations. This comes from the reduction of effective mass that could help to dampen motions excited by human motion.
- 2) The addition of the top plate would cause an increase in production cost of the system. The cellular profile is already manufactured but the plate would need to be added as a separate process. Current manufacturing techniques for deck producers do not allow for the production of system of this nature.

After consulting with deck manufacturers, it was determined that currently this system would not be economically efficient. Therefore, a modified version of this system was developed. It is presented in the next section.

3.3.4. Reduced Weight Composite Deep Deck (RW-DD) System

The reduced weight composite deep deck system also uses a 7.5 in. deep deck profile to span 30 ft. However, in this system the concrete in the lower flutes is replaced by a lightweight filler material (for this project, mineral wool) to help in reducing the self-weight of the system. Figure 3.13 shows a cross section of the system. As shown, the deep deck profile is inverted to maximize the area of steel in tension, while minimizing the self weight. Assuming normal weight concrete, a self weight of 34 psf can be achieved. This is a significant reduction over the previous systems. It is recommended to use concrete in the lower flutes over the connection region and a small distance past the connection region to enhance its strength.

Advantages of System

The system shares many of the advantages of the Sandwich metal deck system including the reduction in self-weight and amount of concrete needed. Additionally, by replacing the top steel plate of the sandwich metal deck system with a concrete plate, the issues related to manufacturing the system are eliminated. Also, by inverting the deck profiles there is more steel area in tension and additional room for placing shear studs over the connections.

Issues for Further Discussion and Investigation

Issues that need further consideration include:

- 1) The reduction in mass and increased span may cause floor vibration related issues. It may be difficult to quantify this experimentally as full scale specimens would be needed to investigate vibration response including the effects of contributing mass and damping
- 2) Sound transmission (or absorption) through the floor system. The removal of concrete from the lower flutes may make the system susceptible to excessive sound transmission.
- 3) Overall structural behavior of system. Since the concrete is placed only above the metal deck, there is a reduction in bond area between the concrete and steel deck. This could lead to partial composite action and an overall reduction in capacity.
- 4) The thermal (heat transfer) behavior of this system is unclear. The placement of the mineral wool material into the flutes would change how heat would disperse through the cross-section; as compared to a system with concrete throughout.

3.4. Pre-Loaded Self-Shoring (PLSS) System

Introduction and Motivation

From an economy standpoint, the most ideal flooring system utilizes existing and readily available construction technologies in its fabrication, erection, and final implementation. These types of systems are desirable because they are easily implementable in the market for multistory residential/commercial steel framing. In

essence, these solutions modify and improve existing systems to address some of the inherent drawbacks within them.

The conventional steel deck/concrete slab floor system was selected for further modification/development because it is the most popular system within the U.S. A review of traditional composite deck systems was given previously in Chapter 1. The major advantages of this system are the strength and stiffness provided in the composite phase (i.e. between the steel deck, concrete slab, and steel framing). Furthermore, the use of concrete provides fire resistance and floor vibration control. When considering only the composite phase of this system it would seem to be a near ideal system. However, the major drawbacks of this system occur in the construction or non-composite phase.

In the non-composite construction phase, the steel deck/concrete system must be designed with the following considerations:

- 1) The steel deck must have adequate strength and stiffness to support the construction live loads and the self-weight of the wet (curing) concrete.
- 2) The steel girder and intermediate floor beams should provide adequate strength and stiffness for the construction live loads and self-weight of the curing concrete.

The strength and stiffness of the steel decks is controlled by their depth, thickness, and span configuration (i.e. single, double, or triple span). Most commercially available decks have depths ranging from 1.5 to 3 in., with thicknesses ranging from 22-18 gage. For these commonly used decks, the unsupported spans range from 8-12 ft. The spans are usually limited by excessive deflections. For large bays (30 to 40 ft), intermediate floor beams provide the support needed by the decks. The span limitations for deck profiles are given in the design tables provided by steel deck manufacturers. These tables provide deck section properties to allow for ease in design and implementation. Thus, there is not much deviation that can be made from what is available from deck manufacturers.

The second design aspect that must be considered is the strength and stiffness of the steel beams and girders being used in the floor system. In the non-composite phase the steel beams alone must provide the required strength and stiffness to the slab system if shoring is not used. For moderately loaded structures (i.e., 50 – 100 psf live loading), it is often the construction phase that governs the design of steel beams. Furthermore, deflections in the construction phase tend to govern, especially for long spans (~30 ft). For non-shored systems, the floor beams themselves can be quite deep (16 – 18 in.). When this depth is combined with that of the deck and concrete slab the structural system alone can approach depths of 24 – 30 in. The use of deeper beams reduces the weight of the steel needed. This is desirable from a steel weight economy standpoint, but increases the floor-to-floor height. This is undesirable for multi-story residential structures.

In summary, the following issues are inherent in composite slab systems:

- 1) The limitation of unsupported spans due to the use of relatively shallow deck systems.
- 2) Significant overall depths within the floor system caused by the requirement for deep floor beams (16 – 18 in.).

- 3) The need for shoring in the non-composite phase for span larger than 30 ft.

The limit on unsupported span lengths for decks can be remedied if deck manufacturers would more readily manufacture deeper decks for use in floor systems, thus making it more economical for use. Chapter 2 highlighted some deep deck systems that help increase the span of the deck itself. Additional details of advanced metal deck systems were presented in Section 3.3. This section focuses on the development of a long span floor system using conventional metal decks.

3.4.1. Case Study

To investigate how conventional composite construction can be improved, a study was undertaken to determine how the construction and composite loads affect overall design. It was desired to determine how non-composite loading influences overall design from both a serviceability and strength perspective. The aspect looked at specifically was the design of intermediate floor beams supporting a steel deck-concrete slab composite system. To conduct the study, a range of W shapes that are commonly used as beams with 8, 10, 12, 14, and 16 in. structural depths were investigated to determine their overall efficiency in both the non-composite and composite phase. These structural depths are listed in Table 3.2.

In conducting the study, some constant inputs were used to see their corresponding influence on different variables. These parameters are shown in Table 3.3. They include the slab depth, deck and slab weight, construction live load, span, and spacing. These parameters were used to calculate the actual and required moments of inertia (I_x) and plastic modulus (Z_x) in both the non-composite and composite phases. The ratios of the above values to the required stiffness and strength for both the construction and composite phases were then investigated. The required construction level stiffness ($I_{required}$) was the stiffness needed to meet an $L/240$ limit from the weight of the concrete. The required composite level stiffness ($I_{req-comp}$) was the stiffness needed to meet an $L/360$ limit for applied live loading. The required construction level strength was based on the combined construction and concrete loading in the non-composite phase. The required composite level strength was based on factored loads including the dead and live loading assumed. The ratios of the above values were then plotted against one another for the range of W shapes shown in Table 3.2. These plots are shown in Figure 3.14 - Figure 3.17.

Figure 3.14 and Figure 3.15 show the required stiffness for the construction and composite phase for 8 and 10 ft beam spacing at a 30 ft span. The y-axis is the ratio of lower bound moment of inertia to the required composite stiffness. The x axis is the ratio of the moment of inertia of the steel section to the required construction moment of inertia. As seen in the figures, three main areas are highlighted. The zones are for sections inadequate in both the construction and composite phase (lower left hand part of the figure), sections inadequate in the construction phase but adequate in the composite phase (upper left hand quadrant), and sections that are adequate in both phases. The figures show that many of the sections 12 in. depth or less are adequate for the composite

phase but not in the construction phase. Also, many of the deeper W16 shapes are providing enough stiffness for both phases.

Figure 3.16 and Figure 3.17 are similar plots, but are showing strength parameters for 8 and 10 ft spacing with 30 ft span. As shown many more of the sections have adequate strength in both the construction and composite phases. Thus, the deflections in the construction phase tend to be governing the design of the steel sections. For example, while only 8% of the W8 sections are adequate for the non-composite phase with 8 ft spacing, 69% are adequate when only considering strength. As the sections get deeper, a closer correlation between serviceability and strength is observed, due to the larger capacities that can be achieved with less weight in steel.

Common between all the sections is the fact that deflections in the construction phase govern the overall design of the steel. Because of this, sections with larger moments of inertia are needed only to resist these loads. Once composite action occurs, the composite section is inefficient and over-designed from the standpoint that oftentimes it has both a great excess of strength and stiffness. This is evident in Figures 3.14-3.17, as many sections are greatly over designed in the composite phase, but construction load levels are still limiting the design. Properly addressing this issue could lead to improved and more efficient composite construction.

3.4.2. System Development

The study of the overall efficiency of steel sections as floor beams highlighted that many shallower steel sections were adequate when considering only the composite phase. Therefore an ideal solution would be achieved if a given section could be supported temporarily in the construction phase, but without slowing construction speed. Conventional shoring is not desirable because of economic and construction delay considerations. Conventional shores transfer load to lower floors and need to stay in place until concrete reaches 75% of its compressive strength. For this reason, oftentimes only one floor can be constructed during this time to avoid excessive loads being placed on shores.

Cambering of steel beams can be done to steel shapes in lieu of shoring. However, cambering can be expensive and is often difficult to inspect and ensure proper camber has been used. If too much camber is induced then the floor slab may be too thin at critical sections, which can lead to inadequate cover of shear connectors. Furthermore, camber can be lost between the time of the cambering and the placement of the concrete due to stress relaxation. This loss is almost impossible for a designer to predict as it depends on circumstances such as shipping distance and support during shipping (Buckner, 2002).

Both shoring and cambering allow for smaller steel sections to be used in floor beams. However, the problems with these techniques are described above. A self-shoring system would not have these problems, so it could present significant merit in composite construction. Thus, if a self-shoring system (shoring supported on itself, not on other floors) could be designed and built it could provide great benefits for the steel construction industry.

The objective of the modified system is to either boost the moment of inertia of the steel beam in the non-composite phase to counteract deflections, or support it. One

possibility is a system that could induce a counteracting moment that varies linearly by inducing an upwards point load at mid-span. There are several ways to induce a point load at mid-span of the beam to provide the needed bending moment. A screw jack could be placed beneath the beam at mid-span to provide the needed force. Figure 3.18 shows a schematic of the possible system. Another way of providing this force would be by using a turnbuckle in conjunction with clevises and threaded rods to support a steel shape at mid-span. The turnbuckles could be adjusted until the desired force is achieved.

Advantages

- 1) The PLSS system utilizes existing materials and products.
- 2) The system can essentially cut floor beam depths in half when implemented properly. This leads to lower floor-to-floor heights and more useable real estate along the height of the structure.
- 3) The self-shoring system induces no additional weight on floors below. All forces are self reacting within the beam member itself.

Issues for Further Discussion and Investigation

Despite the perceived advantages of this system there are issues that need to be investigated.

- 1) The system would need to be optimized from an erection standpoint. If used the self-shoring system would need to have quick and relatively easy installation and removal.
- 2) Maintaining stability of the system while it is in use. While the upward load is being applied it cannot be disturbed or accidentally knocked out from its location.
- 3) The use of reduced depth floor beams may be problematic from a floor vibration standpoint. It must be checked that reducing the beam depth does not adversely affect the dynamic behavior of the slab system.
- 4) Connections at the end will need to properly be examined. The reduction in beam depth leads to lesser area for shear tab type connections between the beam web and girder. Examining these connections and ensuring adequate performance is vital to the system.

In general, these systems have significant potential for reducing the depths of floor beams and thus the overall depths of floor systems in multi-story residential construction.

3.5. Ratings of Proposed Systems

The new floor systems of Sections 3.2, 3.3, and 3.4 were presented to an oversight committee that consisted of steel fabricators, erectors, design engineers, steel deck manufacturers, and researchers. They ranked all the systems based on the criteria of technological merit, feasibility merit, and economic merit (as perceived by them). The ratings were based on a 1-10 scale where 10 represented the highest possible rating. The ratings are presented in Table 3.4. As shown, the lowest ranking went to the double-skin

composite probably because of its excessive use of steel material (0.25 in. thick steel plates), need for fabrication (shear studs, etc.), and self-weight. The profiled DSC system was ranked slightly higher because of its more efficient use of steel material. But, it was still ranked low because of its self-weight. The next was the reduced weight deep deck system. It was ranked in the middle probably due to concerns regarding its structural behavior and issues pertaining to floor vibrations. The pre-loaded self shoring system was ranked second because of its perceived economy and efficiency. The composite deep deck systems were ranked highest due to their overall design, efficiency, and economy. Based on these rankings, the top three ranked systems were selected for additional development and analytical investigations. These are the deep deck systems, the pre-loaded self-shoring system, and the reduced weight deck system. Additional work on DSC systems was halted. Appendix A includes details of the research on DSC systems up to this point. Chapters 4, 5, and 6 focus on further development of the composite deep deck systems and structural experimental investigation. Chapter 7 details elevated temperature testing of deep deck systems. Chapter 8 presents the pre-loaded self-shoring system including experimental investigations.

Table 3.1: Increase in stiffness from increase steel deck depths

Deck Depth (in.)	I_x (in. ⁴ /ft)	Relative Flexural Stiffness Increase
1.5	0.29	-
2	0.53	2
3	1.32	4.5
4.5	3.97	13.5
6	7.68	26
7.5	12.84	44

Table 3.2: W Sections Used In Study

W8 Shapes	W10 Shapes	W12 Shapes	W14 Shapes	W16 Shapes
W8x10	W10x12	W12x16	W14x22	W16x26
W8x13	W10x15	W12x19	W14x26	W16x31
W8x15	W10x17	W12x22	W14x30	W16x36
W8x18	W10x19	W12x26	W14x34	W16x40
W8x21	W10x22	W12x30	W14x38	
W8x24	W10x26	W12x35		
W8x28	W10x30	W12x40		
	W10x33			

Table 3.3: Parameters Used In Study

Slab Depth (in.)	Deck and Slab Weight (psf)	Construction Live Load (psf)	Composite Live Load (psf)	Span (ft)	Spacing (ft)	Deck Depth (in.)	E_s (ksi)	f'_c (ksi)	F_y (ksi)
2.5	45	20	40	30	8/10	2	29000	4	50
3	50								
4	62.5								
5	75								

Table 3.4: Ratings of proposed systems

System	Overall Ratings			
	Technological Merit	Feasibility Merit	Economic Merit	Overall Merit
DSC	6.9	5.1	4.5	5.5
Profiled DSC	7.4	5.2	5.4	6
Composite Deep Deck	8.2	8.2	7.3	7.9
Reduced Weight Deep Deck	7.3	6.7	6.4	6.8
Pre-Loaded Self-Shored	7.8	7.9	7.3	7.7

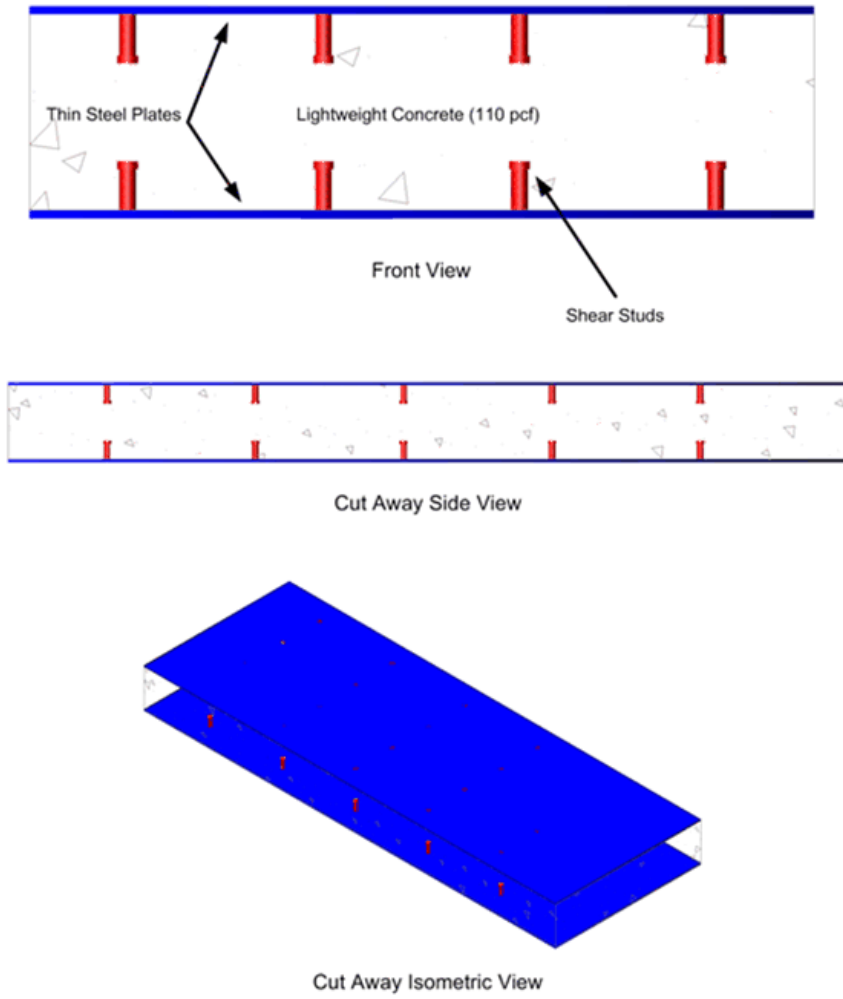
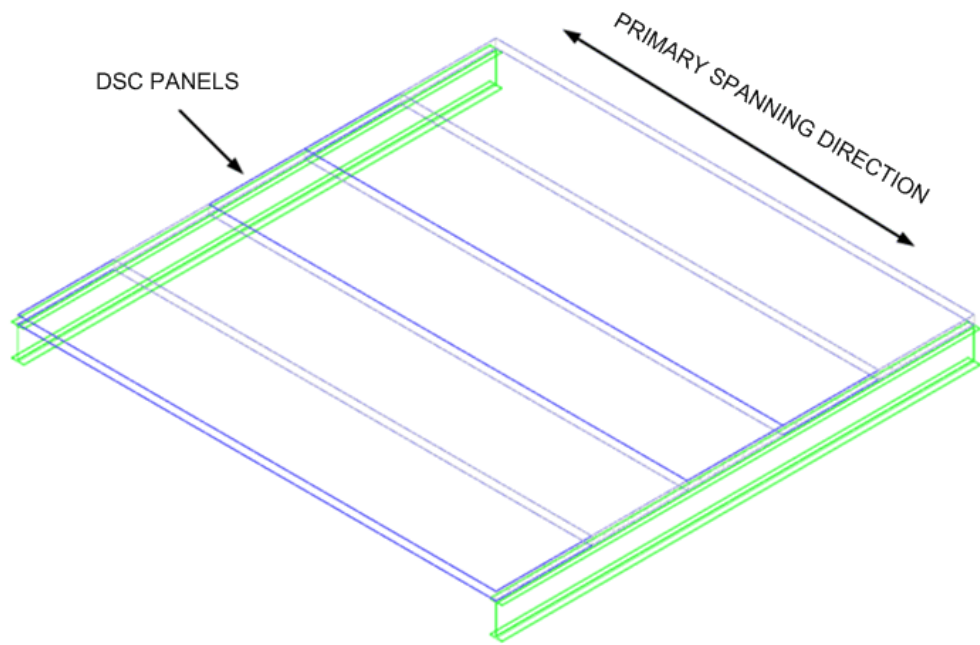


Figure 3.1: Schematic of DSC Floor Panel



30 FT. SPAN IN BOTH DIRECTIONS
COLUMNS NOT SHOWN FOR CLARITY

Figure 3.2: DSC Layout in Typical Bay

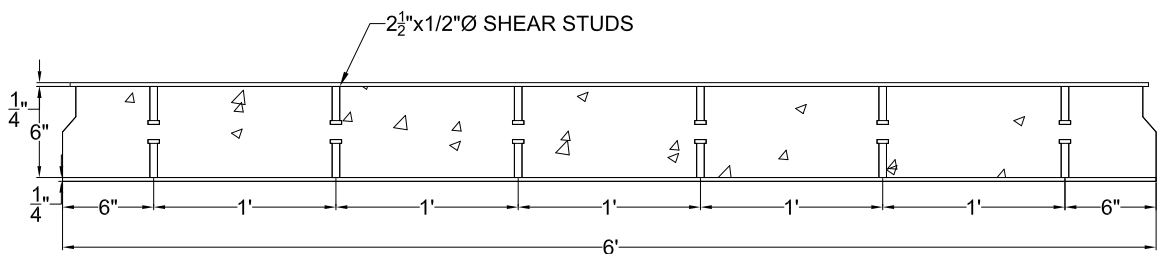


Figure 3.3: DSC panel for 30 ft spans

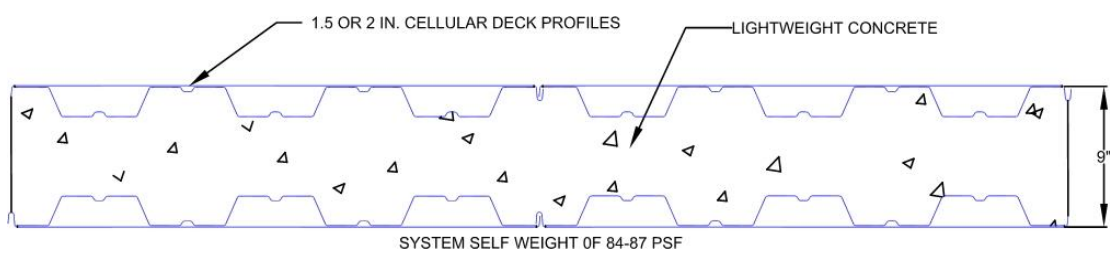


Figure 3.4: Sandwich System Using 1.5 or 2 in. Cellular Deck Profiles

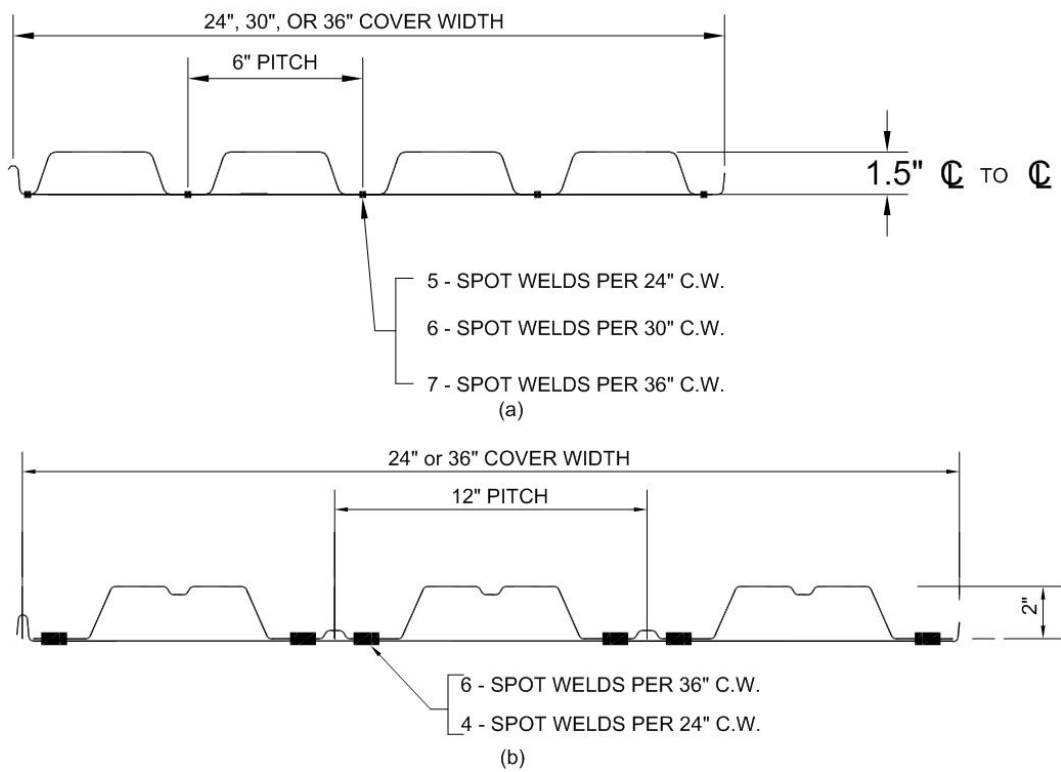


Figure 3.5: (a) 1.5 in. and (b) 2 in. cellular floor deck profiles

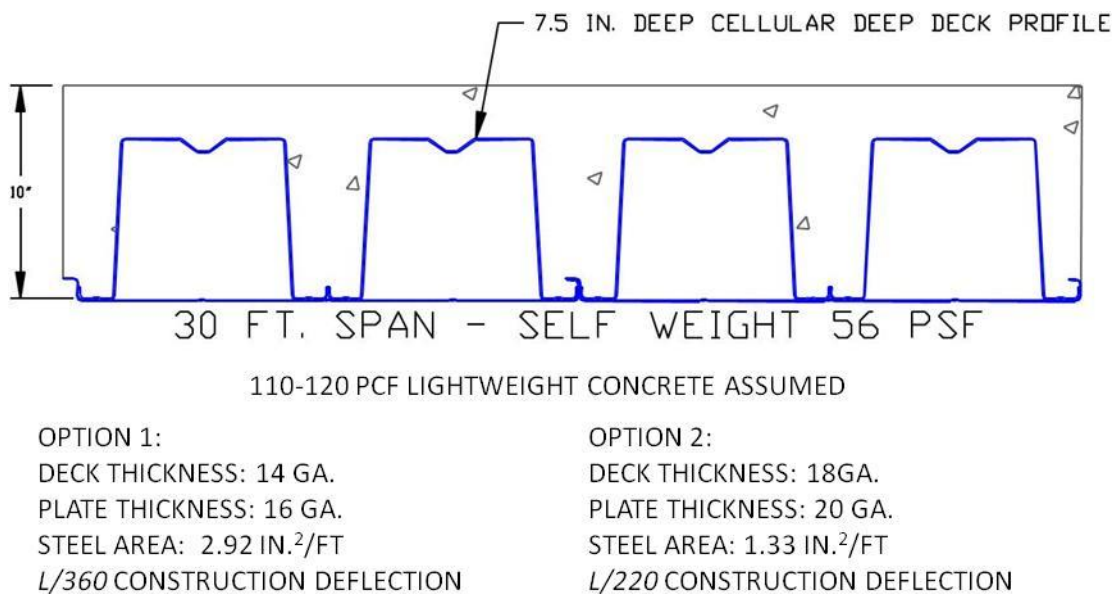
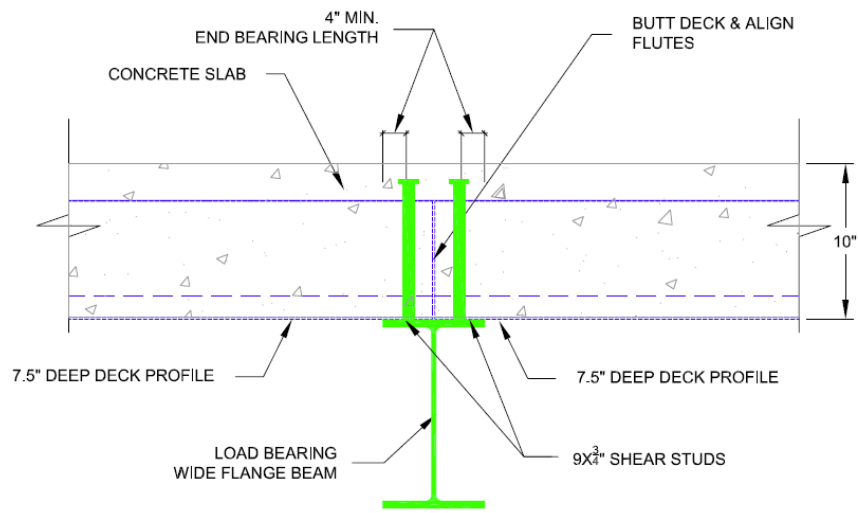


Figure 3.6: Composite deep deck system cross section – 30 ft. Span



7.5" CELLULAR PROFILE ON LOAD BEARING WIDE FLANGE BEAM
INTERIOR CONDITION

Figure 3.7: Possible End Detail for Composite Deep Deck System



Figure 3.8: Shear Stud Placed in Test Specimen

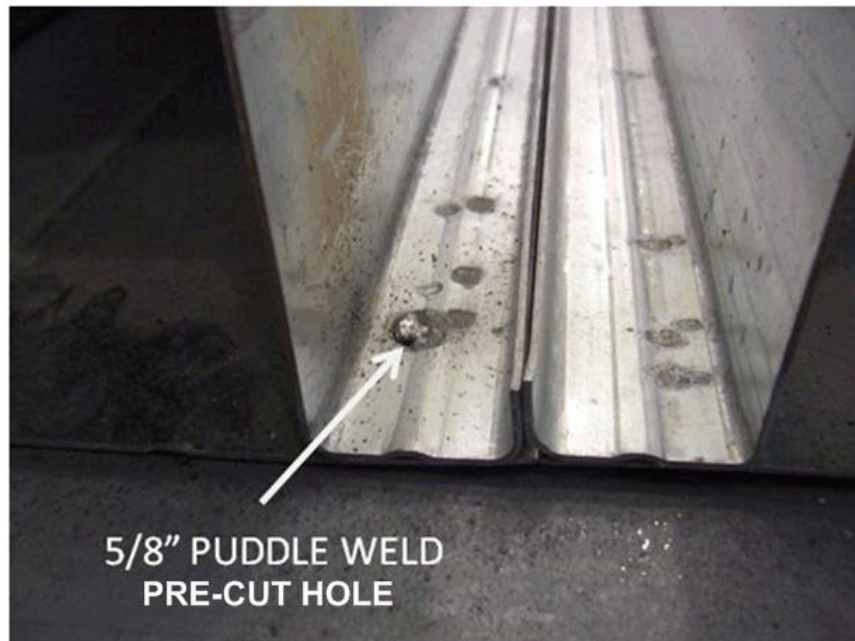


Figure 3.9: Test Specimen with 5/8" Puddle Welds

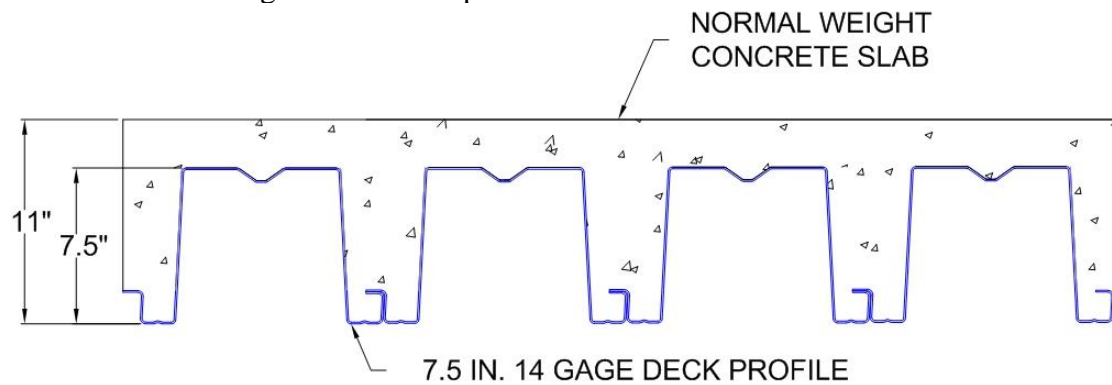


Figure 3.10: Cross-section of shored composite deep deck system (self weight of 78 psf with NWC and 62 psf with LWC)

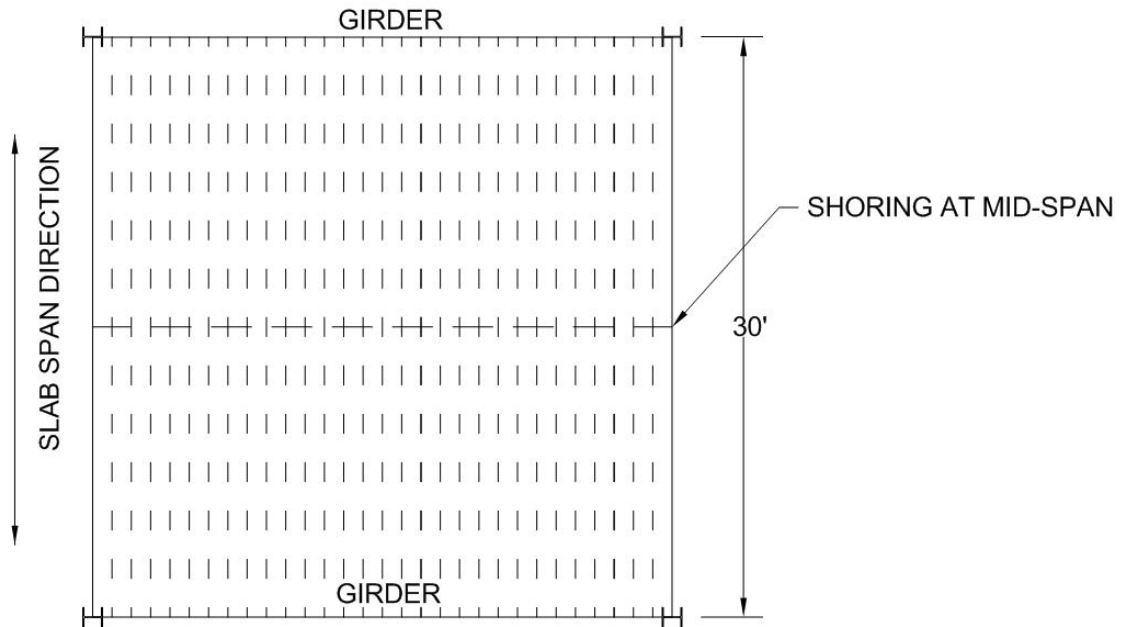


Figure 3.11: Plan view of interior bay with shoring at mid-span

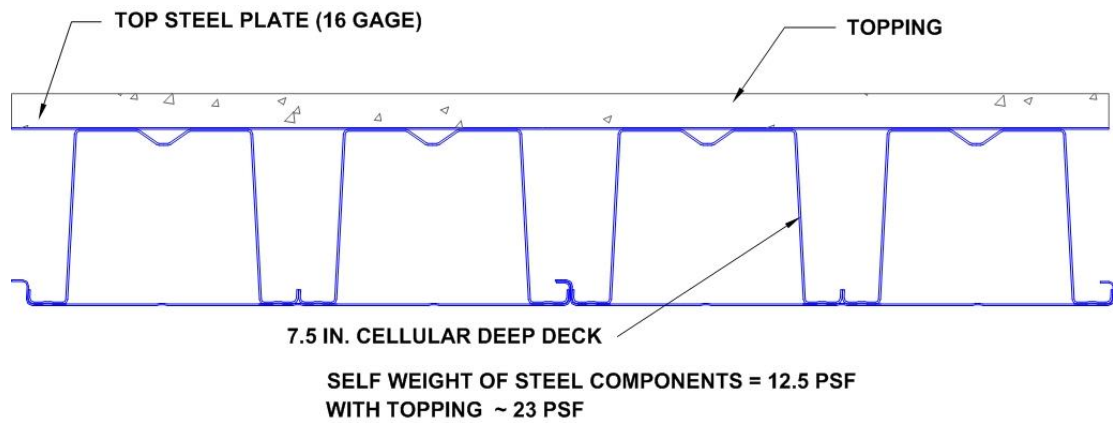


Figure 3.12: Schematic of Sandwiched Metal Deck System

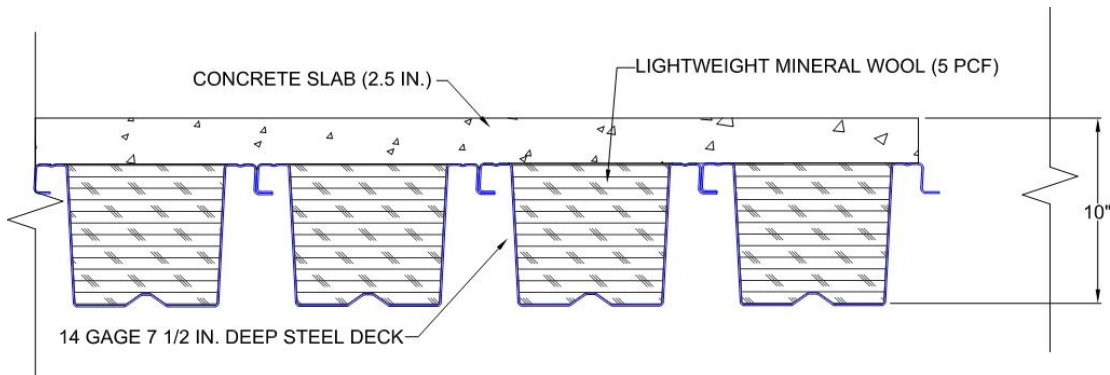


Figure 3.13: Reduced weight composite deck system

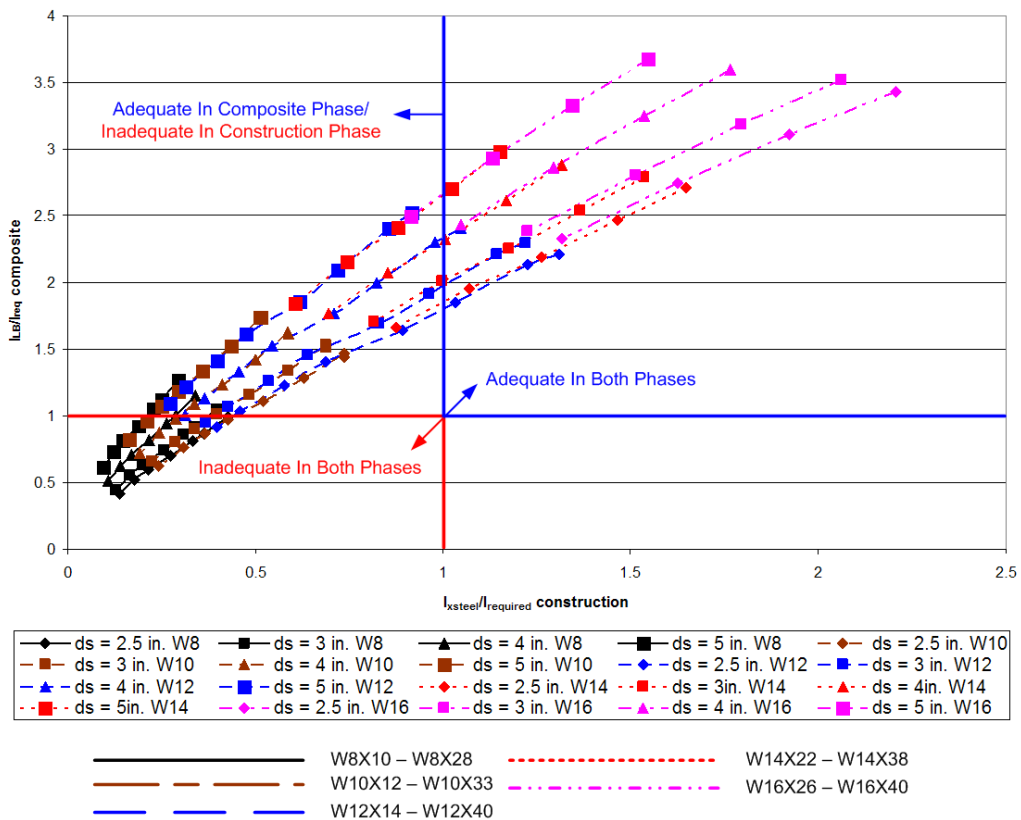


Figure 3.14: $I_{actual} / I_{required}$ for Construction and Composite Phase - 8 ft Spacing and 30 ft Span

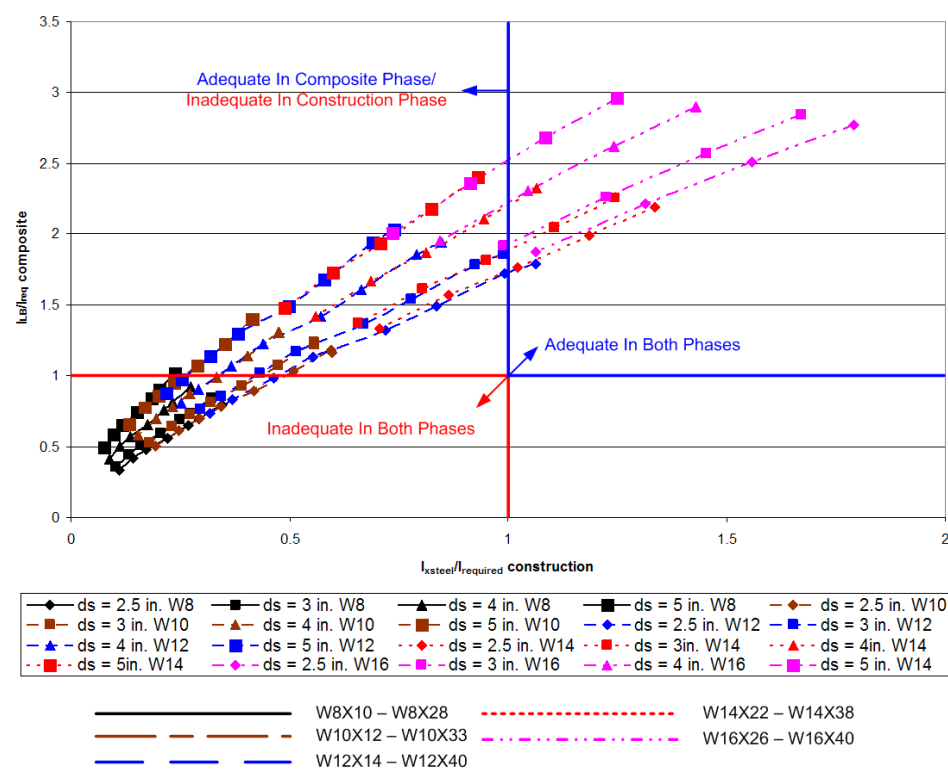


Figure 3.15: $I_{actual} / I_{required}$ for Construction and Composite Phase - 10 ft Spacing and 30 ft Span

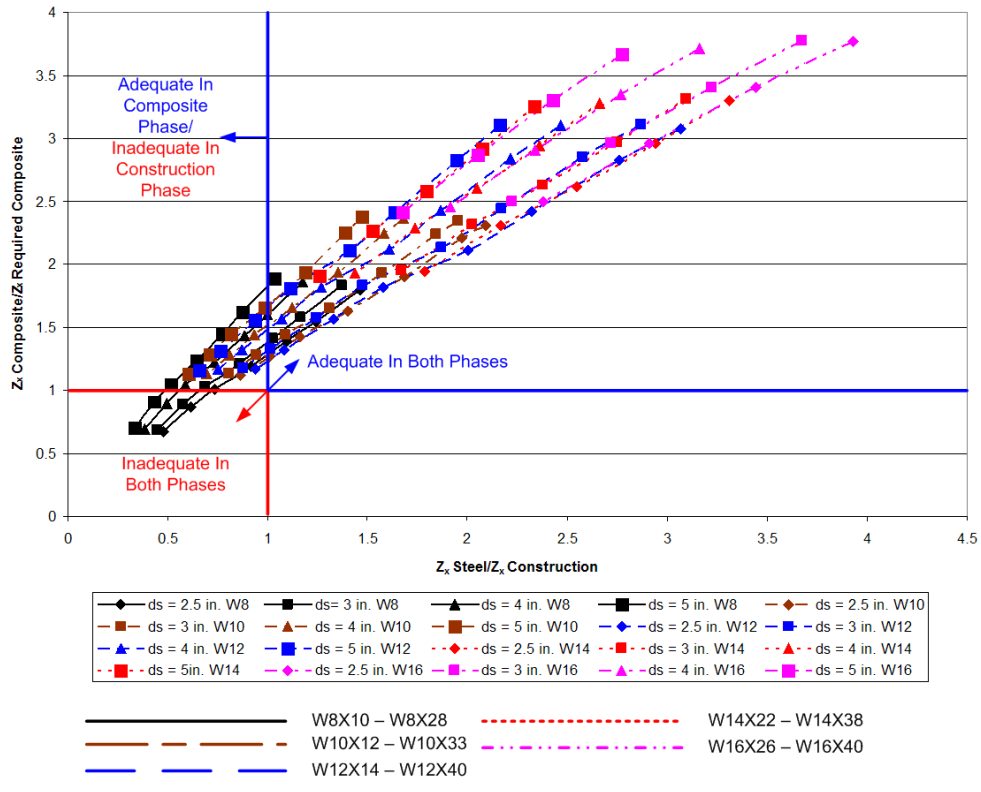


Figure 3.16: $Z_{actual} / Z_{required}$ for Construction and Composite Phase - 8 ft Spacing and 30 ft Span

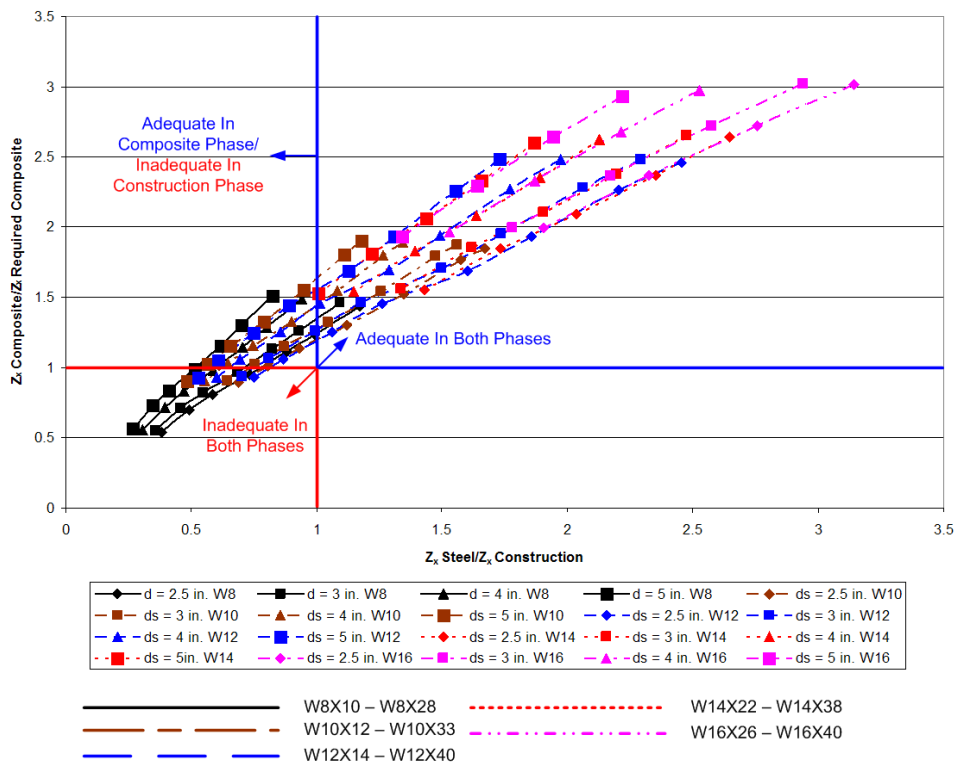


Figure 3.17: $Z_{actual} / Z_{required}$ for Construction and Composite Phase-10 ft Spacing and 30 ft Span

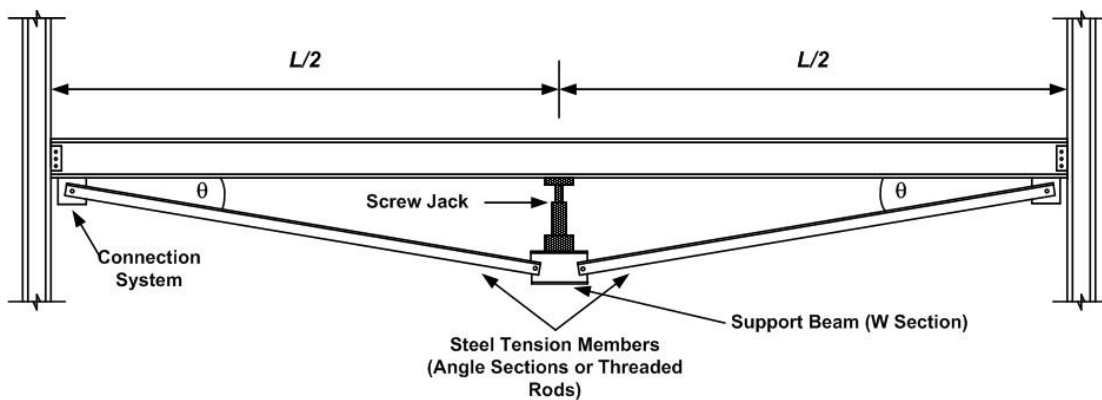


Figure 3.18: Conceptual Schematic of self Shoring System

CHAPTER 4. COMPOSITE CELLULAR DEEP DECK SYSTEMS

This chapter presents further details and experimental validation of the previously described composite cellular deep deck (CC-DD) system. The CC-DD system has been systematically analyzed, designed, and tested to develop an optimized floor system for long spans. Based on the analysis and design there were three different types of CC-DD systems that were experimentally investigated. The details of the analysis and design are highlighted, followed by a description of the finalized systems. The experimental setup, results, and discussion are presented.

4.1. Summary of CC-DD System

Chapter 3 highlighted the development of the CC-DD system. It was shown that a 7.5 in. deep cellular profile with a 2.5 in. concrete slab is capable of an un-shored span of 30 ft. Two different cross-sections (option 1 and option 2) were developed as shown again in Figure 4.1. It was previously highlighted that the thinner profile deck would have larger deflections and stresses in the non-composite (construction) phase, but it would optimize the use of steel material while eliminating the need for intermediate supports or shoring. The effects of different end conditions including: (1) Shear studs welded to the supporting girders through the CC-DD System and (2) Puddle welds connecting the CC-DD systems to the supporting girders were also evaluated experimentally. The use of the CC-DD system helps in achieving low floor-to-floor heights by providing shallow floor depths and eliminating the need for floor beams in spans up to 30 ft.

4.2. Analysis and Design of CC-DD System – Strength and Stiffness

Three different approaches were used to analyze and design the CC-DD system. These approaches ranged in complexity from a code-based design approach to 3D finite element models for capturing material and geometric non-linearity. The details of these three approaches are summarized below.

4.2.1. Code-Based Design Approach

The first approach used the Steel Deck Institute provisions (SDI, 2002) to analyze and design the CC-DD system. The recommendations provided by SDI are based on Standards published by the American Society of Civil Engineers (ASCE) in *ASCE 3-91*:

Standards for the Structural Design of Composite Slabs (ASCE, 1992). The SDI provisions included simple design equations to analyze the behavior in the non-composite phase, and recommended the use of reinforced concrete design theory (American Concrete Institute, 2005) to analyze the behavior of the composite sections. This approach was used to develop preliminary estimates of flexural stiffness and strength of CC-DD systems in the non-composite and composite phases.

Construction Phase – Design Code Based Approach

Strength and deflection criteria should be considered for design with un-shored construction. SDI has two main criteria that must be considered for un-shored construction. The non-composite deck should have adequate flexural strength to support worker weight and other construction loads. The flexural strength of the deck for a single span must be greater than those calculated using equations 4.1 and 4.2.

$$M = 0.25PL + 0.125W_1L^2 \quad 4.1$$

And

$$M = 0.125(W_1 + W_2)L^2 \quad 4.2$$

Where:

M	The applied design bending moment
P	150 lb concentrated worker load
W_1	$1.5 \times (\text{slab weight}) + \text{deck weight} \leq \text{slab weight} + 30 \text{ psf} + \text{deck weight}$
W_1	slab weight + deck weight, psf
W_2	20 psf construction load
L	Clear span length, ft

The SDI recommends that the maximum deflection of the non-composite deck should be smaller $L/180$ or 0.75 in. For the current long span decks being considered, the 0.75 in. limit will be too stringent. Hence, the deflection limit of $L/240$ was used in lieu of the 0.75 in. deflection limit. The maximum deflection of the system can then be calculated using equation 4.3:

$$\Delta = \frac{0.130W_1L^4}{EI_{deck}} (1728) \quad 4.3$$

When un-shored construction is used the stresses from the concrete pour will permanently remain in the deck. These locked-in stresses from the casting can have a significant influence on the overall capacity of the system in the composite phase. Initially, the effects of these locked in stresses from the construction phase on the

strength in the composite were not considered. Analytical models were developed later to look at these effects. These models will be described later in Sections 4.2.2 and 4.2.3.

Composite Phase – Code Based Approach

The composite stage (after concrete sets) rarely governs conventional deck design because of the additional stiffness and strength from composite action with the concrete slab. The span limitations and deck design are governed by deflection requirements in the construction phase. To check for these criteria in the composite phase, SDI recommends using reinforced concrete theory to analyze the section. For strength, the moment capacity can be found using an equivalent section modulus (S_c) calculated knowing the neutral axis location and the cracked moment of inertia. Deflections can be estimated using the averages of the cracked and un-cracked moments of inertia, and elastic deflection equations. These calculations were carried out to compute the design of the proposed specimen.

Assumptions in Analysis

The following assumptions were made when carrying out design and analysis of the CC-DD systems.

- 1) 4000 psi compressive strength 115 pcf lightweight concrete is used.
- 2) 40 ksi yield strength steel is used.
- 3) Non-composite moment capacity and stiffness are that of the steel deck alone.
- 4) Composite stiffness requirement is based on an $L/360$ deflection limit for applied live loads. L corresponds to length of the system.
- 5) Any reduction of the composite capacity strength from construction effects was ignored.

Results of Code Based Approach

Table 4.1 summarizes the results of the code-based design and analysis for the construction and composite phases of the CC-DD systems. Table 4.1 includes the flexural strength (ϕM_{nc}) and stiffness (I_{cons} , I_{comp}) for the construction and composite phases. The ratios ($\phi M_{nc}/M_{u*}$, $\phi M_{nc}/M_u$, $I_{con}/I_{req-con}$, and I_{comp}/I_{reqd}) are also included in the table. In these ratios M_{u*} , $I_{req-con}$, M_u , and I_{reqd} are the required flexural strengths and stiffnesses for the construction and composite phases. The results and comparisons for both options (1) and (2) presented earlier are included in the table. As shown by the comparisons, both options (1) and (2) met the requirements and are adequate for both the construction and composite phases. The ratio $I_{cons}/I_{req-con}$ is the lowest and governing factor for both options. Option (2) has been optimized with the governing ratio $I_{cons}/I_{req-con}$ equal to 1.0.

Inherent in the code based design approach are assumptions that must be discussed. The first and most important assumption being made is that the deck-concrete system acts composite all the way up to ultimate load. Since the deck profiles used were not intended for composite floor systems it is likely that some degree of slip between the deck and

concrete may occur. The structural tests conducted on these systems investigated this phenomenon and are described later.

4.2.2. Non-Linear Inelastic Analysis

The second approach used in analyzing the composite deep deck systems was a non-linear inelastic analysis. This method allowed for determination of the complete load-deflection behavior of the composite floor system. Fiber models were developed for the floor system cross-section assuming full composite action, i.e., no slip. These models were analyzed to determine the moment-curvature ($M-\phi$) response of the cross-section. The complete load-deflection behavior of the system was calculated by discretizing the entire length into several section points, satisfying static equilibrium at each of the section points, and using the central difference approach for determining curvatures, rotations, and the deflections at different load levels. A summary of this procedure used for models with no slip (i.e. full composite action) is given in the following sub-sections.

Development of Cross-Section Moment-Curvature Relationship

The first step in conducting the non-linear analysis is generating the moment-curvature relationship for the given cross section. A fiber based approach was used to develop this relationship. In this approach the cross-section is discretized into a series of 'fibers' through the depth of the section. If residual stresses are present then they can be accounted using horizontally distributed fibers. For the composite deep deck systems, no residual stresses were assumed so only vertically distributed fibers were needed. Once the cross-section is discretized into fibers, it is necessary to tabulate the area of the fibers (A_f) and the distance of the fiber from a datum point, which was selected to be located at the lower left hand corner of the cross-section (y_f). Figure 4.2 shows these parameters graphically.

Principles of statics and strength of materials were applied to find the moment-curvature relationship once the geometric parameters of the fibers were defined. These principles and assumptions are:

- 1) Plane sections remain plane before and after bending – a neutral axis of zero strain is thus present.
- 2) The variation of longitudinal bending strains in the cross-sections vary linearly throughout the depth (see Figure 4.2).
- 3) The cross-section must maintain static equilibrium and thus internal forces should sum to zero and moments sum to a non-zero value corresponding to the curvature (ϕ).

Further assumptions used in developing the moment-curvature relationship for the CC-DD systems include:

- 1) Steel exhibits elastic-perfectly plastic behavior.
- 2) Steel strains should not exceed 20%.

- 3) The steel deck is adequately restrained by the concrete slab such that buckling will not occur.
- 4) Concrete is assumed to exhibit elastic behavior up to 70% of f'_c and beyond that point Popovics curve (Popovics, 1973) is assumed for normal weight concrete and a curve developed by Almusallam (Almusallam & Alsayed, 1995) is used for lightweight concrete.
- 5) Concrete in tension is assumed to contribute strength and stiffness up to reaching 10% of f'_c and beyond that is assumed to have zero contribution.
- 6) Concrete crushing is assumed to occur at a strain value of 0.003.

With these assumptions and principles, the moment-curvature ($M-\phi$) response of the cross section can be found with the following procedure:

- 1) An initial curvature value (ϕ) is assumed for the cross-section.
- 2) A strain is then assumed at some point in the cross-section. For the given model the strain at the centroid of the cross-section was assumed.
- 3) The strain in the top fiber of the cross-section can be found with equation 4.4.

$$\varepsilon_{top} = \varepsilon_c - \phi(y_{top} - y_c) \quad 4.4$$

Where:

ε_{top}	Strain in top fiber
ε_c	Strain assumed at centroid of cross-section
ϕ	Assumed curvature
y_{top}	Vertical distance from lower left hand corner of cross-section to centroid of top fiber
y_c	Vertical distance from lower left hand corner of cross-section to centroid of cross-section

Strains in the fibers below this can be found using equation 4.5.

$$\varepsilon_f = \varepsilon_{top} - \phi(y_f - y_{top}) \quad 4.5$$

Where:

ε_f	Strain in fiber
y_f	Vertical distance from lower left hand corner of cross-section to centroid of current fiber

The stresses in the fibers (σ_f) were found based on the strains that were calculated and the material relationships that were assumed. Forces (F_f) in each fiber can be calculated using Equation 4.6. The internal moments contributed by each fiber can be calculated

using Equation 4.7. The forces and moment contributed by all the fibers can be calculated using Equation 4.8.

$$F_f = \sigma_f \times A_f \quad 4.6$$

$$M_f = F_f \times y_f \quad 4.7$$

$$F_{total} = \sum_{F_f=1}^{F_f=n} F_f \quad 4.8$$

$$M_{total} = \sum_{M_f=1}^{M_f=n} M_f$$

Where the fiber contributions are summed from the top fiber (1) to the nth fiber at the bottom of the cross section.

- 1) If the sum of the forces does not equal to zero, a new centroidal strain value is assumed. This is done until the summation of force (F_{total}) approaches zero to a reasonable degree of precision or tolerance.
- 2) Once the summation of forces has approached zero the corresponding summation of internal moments (M_{total}) and curvature (ϕ) value are stored.
- 3) A new higher curvature value is assumed and steps 1-7 above are repeated. The process is repeated until the limiting strain value in the concrete top fiber is reached (0.003 as stated earlier) or any portion of the steel reaches 0.02 strain.

Figure 4.3 shows a flowchart for generating the section's M - ϕ relationship.

Predicting the Load-Deflection Behavior

Once the moment-curvature relationship is obtained the complete load deflection behavior of a beam made of the same cross-section can be predicted using the numerical integration procedure and the central difference approach. A description of the background behind this procedure and the process to carry it out is described below.

For the derivation of the procedure we will consider a simply supported beam member with an arbitrary loading on it. The rotation (θ) along any point can be expressed as the change in vertical deflection (y) over some horizontal distance (x). Equation 4.9 expresses this in differential form.

$$\theta = \frac{dy}{dx} \quad 4.9$$

The curvature can then be described as the change in rotation over a certain distance x , or the second derivative of the deflection with respect to distance. Equation 4.10 expresses the curvature in differential form.

$$\phi = \frac{d^2 y}{dx^2} = \frac{d\theta}{dx} \quad 4.10$$

Using the above relationships and using double integration procedures a closed form solution for bending moments, shears, and deflections can be found applying proper boundary conditions to solve the equations. However, a numerical integration procedure can be implemented and programmed more efficiently to calculate the complete load-deflection behavior of a flexural member using the section moment-curvature relationship.

Consider a simply supported beam of length L . The first step for finding the load-deflection behavior of this beam is to divide the beam into a reasonable amount of stations as shown in Figure 4.4. We will assume that deflection of interest to find is that of station 3 shown in the figure. For finding the deflection at this point the rotations at intermediate points between stations 2 and 3 can be expressed using equation 4.11.

$$\begin{aligned} \theta_{1.5} &= \frac{y_2 - y_1}{\Delta x} \\ \theta_{2.5} &= \frac{y_3 - y_2}{\Delta x} \end{aligned} \quad 4.11$$

Where:

$\theta_{1.5}$	Rotation between stations 1 and 2
$\theta_{2.5}$	Rotation between stations 2 and 3
Δx	The distance between the stations
y_3	The deflection at station 3
y_2	The deflection at station 2

The curvature at station 2 can then be expressed using equation 4.12, which can be rearranged into equation 4.13 to calculate the deflection at station 3.

$$\phi_2 = \frac{\theta_{2.5} - \theta_{1.5}}{\Delta x} = \frac{y_1 - 2y_2 + y_3}{(\Delta x)^2} \quad 4.12$$

$$y_3 = -y_1 + 2y_2 + \phi_2(\Delta x)^2 \quad 4.13$$

Similarly, the deflection at station 2 can be found for a simply supported beam with zero vertical deflection at the support. It can be expressed as:

$$y_2 = 2y_1 + \phi_1(\Delta x)^2 \quad 4.14$$

In general, the deflection at a station n (as shown in Figure 4.4) can be expressed using Equation 4.15.

$$y_n = -(y_{n-2}) + 2(y_{n-1}) - \phi_{n-1}(x_n - x_{n-1})^2 \quad 4.15$$

Using the above relationships, the deflections at each point can be solved using the following procedure:

- 1) The member is divided into a reasonable amount of stations (stations were placed every ft for the 30 ft beam specimens).
- 2) Based on the loading condition the moments applied to the member are calculated and tabulated at each station.
- 3) The curvature at each station is found based on the calculated moment and the previously acquired moment-curvature relationship.
- 4) An initial guess for the deflection at station 1 (shown in Figure 4.4) is made.
- 5) The deflections at stations 2,3 ... n are found based on equations 4.13 - 4.15
- 6) If the deflection at station n does not equal zero (for a simply supported beam) than a new guess for the deflection at station 1 is made.
- 7) After the procedure has converged satisfactorily, all values are stored and then the load is incremented higher until the complete load-deflection behavior is calculated.

It can thus be seen that the procedure is somewhat iterative and is easily programmable. The algorithm for the procedure is shown in the flowchart in Figure 4.5.

Prediction of Load-Deflection Behavior from Non-Linear Inelastic Method

The key advantage to using this method is that the complete load deflection behavior can be predicted. Variables such as steel yield strength, concrete compressive strength, loading conditions, and geometric parameters can be changed to determine their overall affect on the structural behavior. The initial models assumed that no slip occurred between the steel deck and concrete slab components. Prior to testing it was not known to what level slip would affect the overall behavior. Hence, full bond models were assumed initially.

For the initial predictions of load-deflection behavior some assumptions needed to be made. First, it was assumed that uniform loading would be applied to the sections. This gives a good starting point for evaluation and is the most common design loading condition encountered. The models can be easily modified to account for different loading conditions. Nominal material properties also needed to be assumed. The assumed properties are shown in Table 4.2. These properties were chosen as they are

believed to be typical for the concrete used in slabs and cold formed steel deck. Based on these material properties and the procedure described above the load-deflection behavior of the CC-DD floor systems was predicted.

Figure 4.6 shows the predicted load-deflection behavior of the CC-DD systems subjected to uniform loading. The nominal material properties shown in Table 4.2 were used. Again, these models assumed complete interaction between the steel deck and concrete slab. As shown, the flexural capacity of both deck systems is well above the design factored loads ($166 \text{ psf} = 1.2D + 1.6L$). The stiffness is also adequate for the design level nominal live loads of 40 psf. A summary of key findings from the analysis are given in Table 4.3. In the table w_u is the maximum design factored loads. It is observed that the composite deep deck systems are adequate in the construction and composite phases assuming full composite action (i.e. bond) is maintained between the steel deck and concrete.

4.2.3. 3D Finite Element Analysis – No Slip

The third approach to analyze and design the CC-DD systems was the finite element method. 3D finite element models of the composite deep deck specimens were developed and analyzed to predict the complete load-deflection behavior. The 3D finite element models accounted for the cross-section geometries of the floor systems, non-linear material and geometric properties, and the simply supported end conditions. All FEM models were created and analyzed using the commercial software package *Abaqus* (Simulia, 2007). The models assumed full composite action, i.e., no slip between the deck and the concrete. The results from the finite element analyses included the complete load-deflection behavior and stress states of the floor systems.

Note: The finite element models were modified later to account for the effects of slip between the deck and the concrete. Experimental results were used to define or calibrate the behavior of the slip interface model between the deck and the concrete. These models are described later in section 9.1.4.

FEM Models – Description

A single ‘unit’ cell of the composite deep deck specimens was modeled and analyzed. The steel deck was modeled using four-noded reduced integration 3D shell elements (called S4R elements in *Abaqus*) with six degrees of freedom at each node. The concrete slab was modeled using solid eight-noded ‘brick’ elements (C4D8 in *Abaqus*) with only displacement degrees of freedom at each node.

An illustration of a typical finite element model is shown in Figure 4.7. Mesh layouts for the steel and concrete components are further illustrated in Figure 4.8. As shown, symmetry conditions were used at mid-span to reduce model size. The loads and results were scaled appropriately to determine the load-deflection behavior. Two models were developed and analyzed. One used the full geometry of the deck including flange stiffeners and side laps. The other used a more ‘simplified’ geometry where the deck was idealized to allow for easier convergence and lesser element complexity in the model. Figure 4.9 shows (a) full, and (b) simplified geometry.

Material Models in FEM Models

Abaqus allows for complex material models to be implemented that can accurately represent material non-linearity. Material models with the ability to capture non-linearity were implemented for both concrete and steel. For steel, an elastic-perfectly plastic model with a Von Mises yield surface and kinematic hardening was implemented. The assumed steel stress-strain curve is shown in Figure 4.10.

The concrete material was modeled using the damaged plasticity model developed by Lee and Fenves (1998). This model uses the concrete compressive stress-strain curve and tension stiffening stress-strain curve along with some parameters to define the concrete multi-axial stress-strain behavior. The concrete compression curve was based on the Almusallam (Almusallam & Alsayed, 1995) model for LWC, where linear elastic behavior was assumed up to 70% of the compressive strength. Beyond this point, the equations developed by Almusallam were used to define stress-strain behavior. Figure 4.12 shows the compressive stress-strain behavior input. The tension properties were defined using a rigid plastic model. The tensile capacity was assumed to be 10% of the compressive strength (f'_c). Both the compressive and tensile concrete models are shown in Figure 4.11.

Comments on Bond Behavior

It has been noted that all models developed thus far have assumed full bond between the steel deck and concrete components. However, maintaining this full bond is a key issue with the deep deck systems. It was believed in the development of these systems that only partial composite action would occur. However, without experimental results it is difficult to what degree the slip may affect the overall structural behavior. Previous studies on deep decks by Widjaja (1997) showed that the use of shear studs at supports helps in enhancing composite action between the deck and concrete and near full composite strength is realized by using them. Thus, full composite action is expected to occur up to large load levels for composite deep decks with studs at the ends. The specimens without shear studs will probably not maintain composite action up to ultimate load levels. Experimental investigations of both types of systems were done to evaluate their flexural behavior and strength, and the extent of composite action.

Results from Preliminary Finite Element Analyses

The described FEM models were analyzed to determine the stress and strain states of the composite deep decks at various load levels and were analyzed to determine the complete behavior of the systems. Figure 4.13 shows the load vs. mid-span displacement results for the two different deck profiles (options 1 and 2 mentioned earlier). The results using both the simple geometry (SG) and the complete geometry (CG) are included in the figure. The figure also includes the results from the non-linear inelastic analyses. The figure shows that when the complete geometry of the deck is included in the FEM model higher flexural capacity is achieved. This was expected since more steel material is included by the complete geometry. The difference in predicted load capacity between the simple and complete geometries is around 10% for both these profiles. Thus, the simplified geometry models do a reasonable job of capturing behavior of the CC-DD systems and predicting the load capacity.

The FEM results are comparable to those obtained from the non-linear inelastic analysis fiber based models. The FEM models did encounter some convergence problems at higher displacement levels as large geometric and material non-linearity was present in the model. However, the models did a reasonable job in predicting the flexural capacity and initial stiffness of the models. It is also important to note that both the initial FEM models and fiber based models did not consider the effects of the stresses caused by construction load in the non-composite phase. As mentioned earlier, the un-shored steel deck alone must carry the wet concrete weight prior to the concrete curing. Thus, there would be some additional stresses locked in the deck due to construction loads. The effect of these stresses on the flexural capacity is presented in greater detail in later chapters.

4.2.4. Discussion of Three Analysis Methods

A comprehensive understanding of the structural behavior of the composite deep deck systems (assuming full composite action) was obtained from the three different types of analyses performed. This allowed for confidence in the structural characteristics of the composite system. However, if slip between the deck and concrete were to occur than there would be a reduction in the predicted capacity of the systems. Thus, this slip was monitored during experimental investigations as described later. Ways to model the effects of slip, or partial interaction between the steel deck and concrete components, was also investigated.

Another aspect that was not considered with the initial models was construction effects. These are the strains and stress the deck experiences and maintains after the concrete is poured. These effects change depending on the span, aspect ratio, and self-weight of the given system. For the CC-DD systems it is predicted that the maximum stresses the deck would experience is around 8 ksi for Option 1 and 12 ksi for option 2. These are the maximum tensile steel stresses at mid-span of the specimen. Thus, away from mid span towards the support the stresses would decrease. How these effects were considered and their overall effects are discussed later as more detailed analysis were conducted and compared to testing results.

A final point of discussion that can be taken away from the analyses conducted relates to designing new profiles. The 3D FEM models showed that relatively simple trapezoidal cross-sections can be used to idealized what may be a more complicated cross-section with stiffeners, etc. The predicted capacity varied by about 10% but was conservative. Thus, a 3D FEM model assuming full bond could be used to help in coming up with new profiles for deep deck systems.

4.3. Other Design Issues – Floor Vibrations and Fire Resistance

The final two issues investigated in the preliminary design phase were floor vibrations and fire resistance. For evaluating floor vibrations the guidelines presented in Chapter 2 were used to initially evaluate the proposed systems. In particular the guidelines from AISC Design Guide 11 (2003) were used in the initial evaluation. A

determination of the floor system's susceptibility to annoying floor vibrations can be made once the frequency is known along with a few simplifying assumptions. The assumptions involved include:

- 1) The boundary conditions are simply supported
- 2) The mass contributing to the floor system comes only from the bay in which is being considered. This is a conservative assumption
- 3) The effects of girder stiffness are included by assuming girder deflections of 0.25 in. This deflection value is based on the girder acting composite with the floor system. It has been found that even if a girder is not designed as composite with the floor system, it is often assumed composite when being analyzed for floor vibration. This assumption stems from the fact that the floor girder often acts as a composite section for the small magnitudes of loading present when floor vibration occur. (AISC, 2003).
- 4) The floor system will have between 3 to 5% damping when used in residential construction. Common damping values assumed for damping in structures range from 3 to 5% depending on the application. 4% damping can be readily achieved from the presence of furniture and partial height partitions (AISC, 2003). Thus, the equation was checked for damping between 3 and 5%.

Continuing with these assumptions, equation 2.4 can be used to solve for the ratio of peak acceleration (a_p) to gravitational acceleration (g). The acceptable ratio given from the design guide is 0.5%. The results of the analysis are highlighted in Table 4.4. It can be seen that for CC-DD Option 1 and 2 the system meets AISC requirements for most common damping ratios in residential applications. In fact, the required damping ratios for options 1 and 2 were found to be 3.1 and 3.7 %, respectively. The analysis included several assumptions which will be investigated in later chapters.

With respect to fire resistance of the CC-DD systems it is difficult to say much without experimental verification. There are existing UL ratings for the deck profiles used in development of the CC-DD system. They are given in the UL catalog and are summarized in Table 4.5. For the cellular deep deck developed it can be seen that with 2.5 in. of lightweight concrete topping a fire rating of 1 hour is obtained based on the UL rating. From a structural behavior under fire loading standpoint it is difficult what this values signifies. However, as a starting point it is already known that the CC-DD units will meet a 1 hour rating. Also, by adding an additional inch of lightweight of concrete a 2 hour rating is achieved.

4.4. Experimental Setup – Composite Cellular Deep Deck Systems Structural Tests

This Section provided details of the experimental program implemented for the composite cellular deep deck (CC-DD) systems. The section is divided into descriptions of the structural tests for the CC-DD systems, the test setup and specimen layouts, sensor descriptions and instrumentation layout, and the test matrix.

The experiments focused on determining the structural behavior of the CC-DD systems. The structural behavior measured included the deflections, longitudinal strains

and stress, and end slip: (a) during construction and after concrete placement, (b) at service-level loads, (c) at ultimate loads, and (d) for monotonically increasing loading up to failure or excessive deflections. Additionally, floor vibration tests were conducted to determine the fundamental frequency the floor system by subjecting it to impulse excitation and measuring accelerations and displacement-time histories. The following sub-sections describe the sensor layout for the various phases of the structural tests that were conducted.

4.4.1. Composite Deep Deck Structural Tests

Figure 4.14 shows a schematic plan view of the test-setup for subjecting the CC-DD specimens to structural loading (4 point loading). As shown, the tested CC-DD system specimens were 4 ft. wide and 30 ft. long. They were supported at the ends by reaction frames identified in Figure 4.14. Two loading frames were placed close to the 1/3 point (9 ft. from each end) of the floor system specimens. 100 kip capacity Enerpac hydraulic rams were attached to the loading frames and used to apply concentrated loads to the floor system specimens. The bending moment distribution produced by the applied loading was trapezoidal with the middle third subjected to uniform bending moment. This trapezoidal bending moment distribution closely approximates the parabolic moment distribution produced by a uniformly distributed load. The concentrated loading (P) can be used to compute an equivalent uniformly distributed surface loading (w) by equating the mid-span bending moment for both cases. The equivalent w (in psf) is computed as the applied load P (in kips) multiplied by 20. The portion of the specimens between the support locations and the load point has constant shear and is referred to as the shear span.

A typical instrumentation layout for the floor system specimens is shown in Figure 4.14 and Figure 4.15. The floor system specimens were instrumented to measure displacements and longitudinal strains in the construction (non-composite) and ultimate (composite) for monotonically increasing loading. Most of the instrumentation is attached prior to placing the concrete. Figure 4.16 shows the location of the longitudinal strain gauges in the floor system cross-section at the mid-span and quarter points. As shown, longitudinal strain gauges are attached to the steel deck, bottom plate, and concrete slab. Figure 4.17 shows photographs of a specimen before and after placing the concrete.

Construction (Non-Composite) Phase Test

The construction phase behavior was investigated experimentally by: (a) subjecting the non-composite specimen to loads simulating the standard construction loading, and (b) monitoring the behavior of the specimen during construction and concrete placement. The standard construction load (w), specified by SDI (2002) as 20psf, was applied by subjecting the non-composite specimen to concentrated loads equal to 1-kip at the loading frame locations (via concrete blocks). The deflections and longitudinal strains in the specimens were monitored after applying the loading, and also during construction and concrete placement. Figure 4.18 (a) shows a typical specimen with sensors attached while casting concrete.

Ultimate Load Test

The ultimate load test was conducted by subjecting the floor system specimen to monotonically increasing loading using hydraulic rams attached to the loading frames as shown in Figure 4.18 (b). Each ram had 100 kip load capacity and 10 in. of displacement stroke. The loading was applied monotonically in load control until the system started deforming non-linearly. Further loading was applied in displacement control until the mid-span deflections reached about 8-10 in., corresponding to the limiting stroke of the actuators.

Additional Details of Sensors and Data Acquisition

Displacement Transducers

BEI Duncan linear position potentiometers were used for a majority of the displacement measurements on the CC-DD specimens. The potentiometers used for vertical displacement measurements were '600' series models with stroke ranges of 3 in., 4in., 6 in., and 10 in. (corresponding to model numbers of 603, 604, 606, and 610). The sensors were 10 volt input and output sensors. Other specifications for the sensors are given in Figure 4.19. Additional details of the sensors are available via the manufacturer's website [<http://www.beiduncan.com> (BEI Duncan, 2008)]. A UniMeasure 20 in. stroke wire pot was also used for measuring mid-span displacements. It was a model number P510-20 and had 10 volt output with 15 volt input. Additional information is available via the manufacturer's website [<http://www.unimeasure.com> (UniMeasure, 2008)]. The sensors on the actual specimen can be seen in Figure 4.18. The wire pot was screwed to a wood piece that was then weighted to the floor with steel plates. The other potentiometers were attached to custom made steel frames that were clamped to the strong floor via threaded rods.

End slips were monitored primarily by using 1 in. stroke potentiometers that were also manufactured by BEI Duncan. These potentiometers were model number 9610 and were chosen for their ability to capture quite small movements and small overall size (making them easier to install). Schematics of the sensor are shown in Figure 4.20 (a) with an actual sensor shown in Figure 4.20 (b). Again, more information is available from the Duncan website for these sensors. For all specimens slip gauges were placed near the end support. CC-DD Specimens 3 and 4 (described later) also placed slip gauges near the loading point, but still in the shear span region.

For most specimens (1 exception as described below) the potentiometer was set in a small aluminum U-channel that was then glued to a steel plate which was in turn epoxied to the specimen. This fixture was epoxied to the top of the concrete near beam ends and near load points. A 1/4 in. diameter threaded rod was welded to the top of the deck and 1" diameter piece of steel tube was placed around it to protect the rod during the concrete pour. A schematic of the slip sensor setup is shown in Figure 4.21 and a fixture on an actual specimen is shown in Figure 4.22. Two of the CC-DD specimens also used ± 1 in. LVDTs in conjunction with the potentiometers to try and measure slip. It was found that rotations of the specimen were causing the brass rods threaded into the LVDTs to bend and thus yield unreliable results.

Clinometer Details

Clinometers were also attached to CC-DD specimens to measure rotations at critical points. For all tests they were placed near end supports to monitor end rotations. For most specimens (1 specimen excluded as described later) they were also placed near load points and the measurements were used to determine curvature of the specimen during the testing. The type of clinometer used was a Schaevitz AccuStar $\pm 60^\circ$ sensor. A picture of the type of clinometers with specifications is given in Figure 4.23. The clinometers were attached to small aluminum plates which were then epoxied to the CC-DD specimens as shown in Figure 4.24.

Determination of Curvature from Clinometers

An experimental means of determining the curvature of the uniform moment region of the CC-DD specimens was measured experimentally using clinometers attached near the loading points on the specimens. Consider the idealized schematic of the CC-DD test specimens shown in Figure 4.25. Considering the dimensions given in the figure (b) the curvature can be calculated from the measured rotations using equation 4.16.

$$\phi_m = \frac{(\theta_1 - \theta_2) \left(\frac{\pi}{180} \right)}{x_d} \quad 4.16$$

Where:

ϕ_m	Measured curvature from test specimen
θ_1	Rotation in degrees at clinometer 1
θ_2	Rotation in degrees at clinometer 2
x_d	Distance between clinometers

The corresponding moment at each load point can be computed (assuming a pinned-pinned condition) using equation 4.17.

$$\begin{aligned} M_{p1} &= 0.3R_s L \\ M_{p2} &= 0.3R_n L \end{aligned} \quad 4.17$$

Where R_s and R_n correspond to the north and south reaction forces. The moment at mid-span can then be found using equation 4.18.

$$M_{0.5L} = \left(\frac{M_{p1} - M_{p2}}{0.4L} \right) (0.2L) + M_{p2} \quad 4.18$$

Where:

M_{p1}	The moment at the location of P ₁
----------	--

M_{p2}	The moment at the location of P ₂
$M_{0.5L}$	The moment at mid-span

Strain Gage Details

The strain gages used to monitor strains on steel material were Texas Measurements post-yield gauges (YEF series). The gages were 5 mm in length and 2 mm in width and 120 Ohm nominal resistance with 5 m lead wires attached. Additional details of the gauges are given in Table 4.6. The concrete gages were also Texas Measurements gauges. However, they were polyester foil gages (PF series) and 30 mm length by 2.3 mm width. They were also 120 ohm nominal resistance. Additional details are given in Table 4.7.

Note: All strain gages were applied to material of interest based on recommendations and procedures published by Vishay Micro-Measurements

4.4.2. Frequency Determination Test

The fundamental frequencies of the CC-DD specimens were determined by: (a) subjecting it to impulse excitation using a calibrated impact hammer, and (b) measuring its response using accelerometers. The acceleration response of the specimen is transformed into the frequency domain by performing a Fast Fourier Transform (FFT). The details of the FFT procedure is not given here, but a detailed description of it can be found in Brigham (1988). The results from the FFT can then be used to determine the fundamental frequency of the floor system. This type of testing is more commonly known as modal impact testing.

For this series of tests three PCB seismic accelerometers (1000 mV/g resolution) were attached with wax at the third points and at mid-span of the specimen. A sampling rate of 1 kHz was used to ensure frequency aliasing was not an issue. Hammer impacts were averaged over 5 hits and hits were applied at 1 ft increments along the length of the specimen. The calculated frequency response functions (FRFs) can then be used for determining natural frequencies, damping, and modal shapes, and other modal parameters of the component or structure in question.

Input Excitation

Three different types of input or excitation were used in studying the CC-DD systems; a modal sledge hammer, heel drops, and walking excitation. Some specimens had more excitation sources than others and this is highlighted as needed. The first type of excitation used was a tuned modal impact sledge hammer (modal sledge hammer). The modal sledge hammer is like a normal sledge hammer except that it has a load cell in the tip for measuring input force. A picture of the modal sledge hammer with specifications is given in Figure 4.26. As shown in the figure there are different tips that can be used on the hammer tip. Different frequency ranges can be captured based on the hardness of the tip (harder tips provide more input energy).

Another type of input excitation used in the experimental portion of the work was heel drops applied by a person at the longitudinal and transverse mid-span of the specimen. These heel drops were meant to simulate a person impacting the slab

specimen. The last type of excitation used was walking along the specimen by one and two persons. From these tests an idea of what frequencies were dominant from walking motion could be captured.

Response Sensors and Sensor Placement

The sensors used for measuring the acceleration response of the specimens were Model 393A03 Seismic Accelerometers manufactured by PCB Electronics. A picture of one of these accelerometers with specifications is given in Figure 4.27. Hit locations for applying the hammer impact varied depending on the required parameter of interest. Impacts were done located at the transverse mid-span of the specimen. Hits were then taken at various increments in the longitudinal direction depending on the specimen. Any of these hammer impacts could be used in correlation with a given acceleration response when determining the FRFs of the system. A picture of the modal sledge hammer in use is shown in Figure 4.28. Heel drop locations were always applied at the longitudinal and transverse mid-span of the specimen. Walking excitation was provided by one or two persons walking longitudinally along the middle third of the specimen.

Accelerometer placement also varied depending on what parameters of interest were to be captured. In general, two of the accelerometers were placed at third points (10 ft from the ends) along the length, and the other was placed at the longitudinal mid-span of specimen. The accelerometers were attached to the top of the specimen (concrete side) using wax. A specimen with the attached accelerometers is shown in Figure 4.29.

Data Acquisition System

Data acquisition for the testing was done with a 4 channel National Instruments cRIO-9233 data acquisition box attached via a USB interface to a laptop computer. This DAQ box has a sampling rate of 50Ks/s and a combination of digital and analog filters to ensure the signal is not aliased. The DAQ box with specifications is shown in Figure 4.30. The software used for data acquisition was a custom made GUI programmed within the commercial software *Matlab* (Yoder, 2006).

4.4.3. Test Matrix of CC-DD Systems

Large scale experiments were performed on 4 CC-DD specimens. The testing matrix is shown in

Table 4.8. As shown, all the CC-DD specimens were 30 ft in length, which was the target un-supported span length for this research. The first 3 specimens used 14 gauge deck with a 16 gauge bottom plate. Specimens 1 and 2 were essentially identical, i.e. repeat specimens with some slight modification in sensor layout. As shown in

Table 4.8, these specimens used shear studs at the ends to attach the CC-DD specimens to the supporting beams. Specimen 3 was also similar to Specimens 1 and 2 with the exception that it was attached to the support beams with puddle welds. The fourth specimen used thinner 18 gauge deck and 20 gauge bottom plate.

Specimens 1-3 had the Option 1 design for the CC-DD Specimens mentioned earlier. Specimen 4 had the optimized Option 2 design. It was attached to the supporting beams using shear studs similar to Specimens 1 and 2. All the Specimens 1-4 used lightweight concrete with a dry unit weight of 115 pcf and specified compressive strength of 4000 psi. The experimental results and from the tests conducted on the four CC-DD Specimens are presented in the following sections. Section 4.5 presents the results from the construction loading tests and dynamic floor vibration tests. Section 4.6 presents the results from the ultimate load tests of the four CC-DD Specimens.

4.5. Construction Phase and Dynamic Testing

This section presents the experimental results and relevant discussion for all four CC-DD specimens.

4.5.1. Construction Phase Results and Discussion

Table 4.9 summarizes the results from the construction phase for the CC-DD test specimens. For each of the specimens (1-4), Table 4.9 includes the results from the static construction loading tests and the concrete casting operations. As mentioned earlier, the construction load tests were conducted by placing 1 kip concrete blocks at the two load points. The concrete casting included the effects of the weight of the concrete and the construction workers. The residual deflections were measured upon removal of the construction loads (1 kip blocks) and also after the completion of the concrete casting operation.

As shown in Table 4.9, CC-DD specimen 1 had a mid-span deflection of 0.43 in. for the construction loading (1 kip blocks). All of the deflection was recovered upon removal of the concrete blocks. The maximum tensile strain induced in the bottom steel plate of the CC-DD Specimen at mid-span was equal to 105 microstrain. During the concrete casting operation of Specimen 1, the maximum deflection caused by the wet concrete and construction workers was 1.5 in. The residual deflection caused by the concrete weight alone was equal to 1.1 in. The maximum tensile strain induced by the concrete casting was 370 microstrain. The corresponding stress was 11 ksi. The residual strain after completion of the concrete casting process was equal to 320 microstrain or 9.5 ksi. As shown in Table 4.9, similar results were obtained for specimens 2 and 3. For specimens 1-3 the residual deflection after concrete casting was 0.9 to 1.1 in., which is approximately $L/360$. Specimen 3 had slightly less displacement during the concrete casting operation. This may have occurred because of the puddle welds provided slightly more end restraint than the shear studs. Specimen 4 had the Option 2 optimized design with the 18 gauge deck and 20 gauge bottom plate. The thinner gauge components reduced the flexural stiffness, which caused higher displacements up to 1.7 in. ($L/200$) during the construction (non-composite) phase for this specimen.

These results indicate that the CC-DD systems perform adequately during un-shored construction. The maximum strains experienced during the concrete casting operation were well below the yield stress of the deck. Current SDI requirements call for a

maximum deflection of $L/180$ or 0.75 in. maximum. As mentioned previously, these restrictions were based on the use of 1.5 to 3 in. deck profiles where maximum expected spans were 10-15 ft. Thus, the maximum deflection requirement of 0.75 in. is believed too stringent for the longer span systems investigated.

One other aspect that was investigated in this phase was variation in the measured strains during the concrete hardening. The residual strains reported in Table 4.9 were measured 24 hours after concrete casting. During the first 12 hours after casting, the strains rose higher than the residual values. This was due to the increase in the temperature of the concrete and consequently the deck due to the hydration of the concrete, which is an exothermic reaction. The temperature increase induced thermal strains that were measured as the apparent strains by the strain gauges. The strains reached the residual value as the concrete hardened and the temperature decreased between 24 and 48 hours after casting and remained constant thereon. Figure 4.31 shows this for the strains measured in the bottom plate of CC-DD Specimen 2 over the first 24 hours after casting.

Key Observations and Discussion for Construction Level Testing

- 1) Measured deflections and strains during the construction loading test and the concrete casting operation were within acceptable limits.
- 2) Specimen 3 exhibited slightly less deflection than specimens 1 and 2. This may have occurred because the puddle welds provided slightly higher end restraint initially than the shear studs.
- 3) The residual strains after concrete casting were measured and reported at least 24 hours after the initial concrete pour. The concrete heat of hydration caused thermal strains in the first few hours (12-24 hours) after casting. These thermal strains decreased as the concrete hardened and set, and the strains reduced to the residual value.

4.5.2. Modal Impact Testing Results and Discussion

Modal impact testing was performed to determine the fundamental frequencies of the CC-DD test specimens. The one exception was specimen 1. Modal impact equipment was not available for this specimen. However, accelerometers were mounted on the specimen and the data was used to estimate the first natural frequency of the specimen. For other specimens more frequencies and other modal properties could be estimated. A measured frequency response function (FRF) spectrum for CC-DD specimen 2 is shown in Figure 4.32. The figure shows the FRF from a third point and mid-span accelerometer with a mid-span hammer hit. Similarly, FRFs are shown for Specimen 3 in Figure 4.33 and Specimen 4 in Figure 4.34. These FRFs are from mid-span hits. The second bending mode is difficult to capture from mid-span hits as the first and third bending mode dominate for that location. Hence, Figure 4.35 shows a FRF spectrum for Specimen 4 based on a third point hammer hit and third point accelerometer. This figure shows the second bending mode frequency that was not appearing in Figure 4.34.

The peaks in the frequency responses correspond to the natural frequencies of the various specimens. Table 4.10 shows the natural frequencies for the CC-DD Specimens. As shown, for the first CC-DD Specimen, the second and third frequencies could not be measured. For Specimen 2 the first, second, and third natural frequencies were 6 Hz, 22.6 Hz, and 49.2 Hz, respectively. For Specimen 3 the natural frequencies were 6.2 Hz, 23 Hz, and 50 Hz. The values for Specimen 4 were 5.8 Hz, 21.9 Hz, and 46.7 Hz. Specimen 3 had slightly higher measured frequencies that are due to slightly more restraint being present from the puddle weld connections. Specimen 4 had the lowest measured frequencies because of its lower stiffness as compared to the first 3 specimens. Table 4.10 includes the natural frequencies estimated using a single-degree of freedom model recommended by AISC and presented in Section 2.6.2. The results in the table show good comparison between the calculated and measured natural frequencies.

Estimate of Damping

The modal impact testing results were also used to estimate the damping at each of the natural frequencies of the CC-DD Specimens. The half-power method was used to estimate damping from the modal impact data. This method estimates damping by seeking the half-power points on either side of a resonant frequency. These half power points correlate to the point where the response is equal to the resonant response divided by $\sqrt{2}$ (Thomson, 1988). The damping ratio of the system is then estimated with equation 4.19.

$$\xi = \frac{f_b - f_a}{2f_n} \quad 4.19$$

Where:

ξ	The estimated damping ratio
f_b	Frequency at $0.707*f_n$ on right side of the resonant frequency
f_a	Frequency at $0.707*f_n$ on left side of the resonant frequency
f_n	The resonant frequency of interest

The half power concept is shown graphically in Figure 4.36. In this figure ξ is the damping ratio.

Table 4.11 summarizes the damping ratios calculated for the first natural frequencies of Specimens 2, 3, and 4. The damping ratio for Specimen 1 could not be calculated. As shown, the estimated damping ratios were between 0.7 and 0.9%. These values are representative of the damping of a bare floor system. These values are comparable to values reported in existing literature that indicate damping ratios between 1 to 2% for existing composite steel deck-concrete systems (Allen, Onsyko, & Murray, 1999).

CC-DD Specimen 3 was subjected to an equivalent load of 10 psf and modal impact testing was repeated. The 10 psf equivalent load was applied by setting concrete blocks at third points on the specimen. The modal impact test was repeated to measure the natural frequencies and damping. After this, an additional 10 psf of loading was added to the specimen and the modal impact testing was repeated. Figure 4.37 shows the

frequency response from the mid-span accelerometers and a mid-span hammer hit on Specimen 3 with no loading, 10 psf equivalent loading, and 20 psf equivalent loading. The results in Table 4.11 and Figure 4.37 indicate that as weight is added to the system the frequency shifts lower and damping ratios decrease for the resonant frequency. However, the overall response at the resonant frequencies also reduces. Intuitively, the shift in frequency is reasonable. The kinetic energy needed to bring the system to equilibrium has increased and thus the frequency shift. Furthermore, if we consider Equation 2.4 for evaluating the floor system, then if both the response and frequency of the system are reducing, then the amount of damping needed would also reduce.

It was also of interest to look at the response of various frequencies. It was mentioned in Chapter 2 that for floor system evaluation of steel-concrete composite systems there are some characteristics that the floor system should exhibit to use those guidelines. Those characteristics included a natural frequency between 4 and 10 Hz, adequate spacing between the first and higher modes, and the first mode response should be dominant. The results from the modal impact tests indicate that for the CC-DD Specimens, the first natural frequency is between 4 and 10 Hz, and there is adequate spacing between modes of vibration.

The final consideration for evaluating dynamic behavior was determining the dominant frequency in the overall response of the structure. Looking only at normalized FRFs can be misleading as the normalization techniques used can make some modes appear more dominant than others. The auto power or output spectra can provide more insight into the overall dominance of certain modes. For CC-DD Specimen 3 heel drop amplitudes were used as one of the excitation types. The output spectra from heel drops were examined since they are typically used in measuring floor response (Allen, Onsyko, & Murray, 1999). Figure 4.38 shows the measured response spectra for heel drop excitation on CC-DD Specimen 3. In Figure 4.38, the output spectra G_{yy} has units of acceleration squared (g^2). It is defined using Equation 4.20 (Allemang, 1999).

$$G_{yy} = X_p X_p^* \quad 4.20$$

Where:

X_p The spectrum of the p^{th} response
 X_p^* The complex conjugate of X_p at the frequency of interest

G_{yy} is thus a representation of the energy being output in each mode of vibration. Figure 4.38 shows that for all accelerometers the first mode is the dominant mode. Table 4.12 shows the output spectra values and ratios of G_{yy} of the first mode to higher modes for the first three frequencies of the CC-DD Specimens. The table shows that the first vibration mode has at least 8 times more energy than higher modes. Thus, in general, the first mode is dominant in overall dynamic response of the specimen.

Discussion of Results

As described above, the primary relevant dynamic property that could be determined from the modal impact tests were the natural frequencies of the CC-DD Specimens. The results were also used to estimate the damping for the natural frequencies of the

specimens. However, the dynamic behavior of a composite slab floor system in a building structure depends on the contributing mass and damping from the adjoining bays, the presence of partitions and other elements that could dissipate vibrations, and the structural configuration. These elements obviously could not be captured from the performed modal impact testing. Furthermore, the supporting girders for the CC-DD floor system will play a vital role in the dynamic behavior of the complete floor system. The CC-DD System alone may not be prone to annoying vibrations, but if the floor system is supported by relatively flexible girders then problems could arise.

The CC-DD Systems satisfy the key assumptions made by AISC and SCI in using their guidelines for floor vibration evaluation. These assumptions are (1) The first fundamental frequency is in the 4 – 10 Hz. range (2) the first frequency is adequately distanced from other frequencies such that modal coupling does not occur and (3) floor vibration induced by walking excitation is dominated by the first natural frequency and mode.

Key Observations and Discussion for Modal Impact Testing

- 1) The measured natural frequencies were close to those calculated using a simple SDOF model.
- 2) The first mode of vibration and natural frequency was much lower than higher modes, and seemed to be the dominant mode for heel drop and modal impact excitation.
- 3) The floor vibration behavior of the CC-DD systems can be evaluated using guidelines published by the AISC and SCI.

4.6. Ultimate Load Testing Results

All specimens used the same general setup for applying loads and measuring behavior (as previously described). Some aspects did change between different experiments and these changes are explained as needed in the following sections

4.6.1. CC-DD Specimen 1 Results and Discussion

Background Information

CC-DD Specimen 1 was 30 ft long and 4ft wide as described previously. The Specimen was subjected to 4 point loading with the load points located approximately 9 ft from the supports. The compressive strength of the concrete on the date of test was 5767 psi. This was determined by testing 4in. by 8 in. concrete cylinders. The steel material yield strengths were reported in the mill certificates as 48 ksi for both the deck and bottom plate steel. Uniaxial tension tests according to ASTM E8 (ASTM, 2004) were performed on machined tension coupons taken from the deck and bottom plate. These tests indicated a yield stress of 53 ksi for the deck and 46 ksi for the bottom plate.

Additional concrete batch mixes, mill certifications and measurements from tension tests are given in Appendix C.

Displacement and Rotation Data

Figure 4.39 shows the applied load vs. mid-span deflection plot for CC-DD Specimen 1. The figure includes the estimated equivalent distributed loading psf on the right hand side of the ordinate (y) axis. The figure includes loads applied by the north and south hydraulic rams and the average of these loads plotted with respect to the mid-span displacements. It can be seen that the initial load vs. deflection for the north hydraulic ram has an unexpected shape. The reason for this is response is perhaps that the south ram began contacting the specimen slightly sooner than the north ram. This can be seen by examining the displacements at the $L/6$ points (5 ft from the ends) on the north and south side and the displacements measured under the north and south loads. Figure 4.40 shows these measured displacements for the duration of 350 seconds up to around 7 kips of applied load. It can be seen from the figure that the south side deflections were initially larger than the north side deflection. The north and south deflection converge closer around 5 kips of loading. At 7 kips of loading (at each point) the values are almost identical to each other. After this convergence, the specimen was initially loaded to around 6.5 in. of deflection being reached at mid-span. This corresponds to approximately 23 kips or 460 psf of loading on the specimen. A picture of the specimen with approximately 6 in. of mid-span deflection is shown in Figure 4.42. The specimen was then unloaded and it had a residual deflection of approximately 3 in. The specimen was then reloaded to approximately 8 in. of mid-span deflection. At this point the hydraulic rams had reached their stroke capacity and the test was terminated.

The measured loads and mid-span deflections were used to estimate the stiffness of the specimen. The stiffnesses were estimated for the un-cracked concrete and cracked concrete phases. The cracked concrete stiffness was estimated at the point when flexural cracks were observed in the specimen. This occurred at approximately 8 kips of loading (at each load point). Un-cracked stiffness was estimated for loading prior to this level. The stiffness was estimated as the north, south, and average loads divided by the mid-span deflection. The estimated stiffnesses are shown in Table 4.13 for the cracked and un-cracked phases of CC-DD Specimen 1. The numerical values are difficult to interpret, but the relative values in Table 4.13 show that there is approximately a 30 % change in stiffness due to concrete cracking.

The specimen end rotations were also monitored during the load test. Figure 4.41 shows the average (north and south) load vs. end rotations. The figure shows that end rotations were consistent up to around 18 kips (360 psf) of loading (averaged for two loading rams). Beyond this point north and south end rotations were slightly different from each other. At the end of the first loading cycle, the north end rotations were slightly greater than the south end rotation. However, upon reloading the rotations at the southeast end of the specimen increased more rapidly. This corresponded to the occurrence of a significant crack in the concrete at the southeast end of the specimen over the interior edge of the support beam. The crack is shown in Figure 4.43 and Figure 4.44.

The end slip was also measured for CC-DD Specimen 1. Unfortunately for this specimen the end slips could not be measured consistently using the displacement transducers. This was due to the factors related to how the slip transducers were mounted

on the specimen. The 1 in. stroke potentiometers and 1 in. stroke LVDTs were mounted to the support beam and small metal angles were mounted to the side of the concrete. The slip measurements were based on the relative movement between the metal angle and the sensors attached to the beam. However, the beam end rotations caused the sensors to capture rigid body rotations in their measurements. This rigid body rotation can be seen in Figure 4.43b. The slip sensors for the remaining specimens were 1 in. potentiometers mounted as described previously in this Chapter.

Strain Gage Data

As described in Section 4.4 and shown in Figure 4.16, strain gages were attached at various locations throughout the depth of the cross section at the loading points and mid-span of the specimen. The gages were attached to steel at the underside of the bottom plate, on the web of the deck, and on the top of the steel deck. Concrete gages were also placed on the top of the concrete. Figure 4.45 shows plots of the measured strains throughout the depth of the section at various load levels. Similarly, Figure 4.46 shows plots of the measured strains through the section depth at the south load point. It is important to note that the strains were re-zeroed (balanced) for the load test. Therefore, the plots show only the composite level strains that were observed.

Figures 4.45 and 4.46 highlight a few important observations for the test. First, when the loading was terminated, the entire cross section had not yielded at the mid-span when loading was terminated and the concrete had not reached crushing strains (0.003). The results show relatively linear strain distributions over the cross-section depth. The strain linearity is more pronounced at the mid-span than at the south load point at higher load levels, which is reasonable because the mid-span section is subjected to uniform moments and negligible shear. This can be proven by finding the square of the Pearson product-moment correlation coefficient (R^2) values of the strain values. The R^2 values for the strains measured at various load point are given in Table 4.14. It can be seen from the table that at the south end the R^2 value is near 1 (indicating a perfect linear relationship) up until around 20 kips of load then it reduces significantly. For the mid-span section the R^2 value stays near 1 through the duration of loading. A lower R^2 value would be a likely indicator of slip having occurred between the two specimens. Thus, it could be stated that slip began occurring in the shear span of the specimen at around 20 kips of load (at each point) based on the strain gage data obtained there.

Key Observations and Discussion for CC-DD Specimen 1 Load Test

- 1) The specimen exhibited adequate capacity for anticipated residential loading.
- 2) The specimen exhibited very ductile behavior.
- 3) End slip was not believed to occur until higher levels of loading. The observation of a large crack over the south support indicated some separation between the deck and concrete.
- 4) Strain observations indicate near full composite action until higher levels of loading
- 5) There was approximately a 30% reduction in stiffness from concrete cracking.

- 6) End slip was not properly measured for the specimen using slip gauges. This led to a change in sensor layout for subsequent specimens in measuring end slip.
- 7) The loading fixtures for transferring load from the hydraulic rams to the specimen could not accommodate the large rotations that were occurring on the specimen. Thus, new fixtures were constructed for subsequent tests.

4.6.2. Specimen 2 Results and Discussion

Background Information

CC-DD Specimen 2 was a replica and a repeat of the first specimen. The changes were in some of the sensor layouts and the use of new cylindrical bearings for transferring the loads from the hydraulic rams to the load spreader beam on the specimen. The slip sensors for this specimen were mounted as described in section 4.4. As mentioned earlier, this mounting technique allowed for more accurate measurement of the slip the deck and concrete components. The compressive strength of the concrete on the date of test was 6222 psi. This was determined by testing 4in. by 8 in. concrete cylinders. The steel material yield strengths were reported in the mill certificates as 48 ksi for both the deck and bottom plate steel. Uniaxial tension tests according to ASTM E8 (ASTM, 2004) were performed on machined tension coupons taken from the deck and bottom plate. These tests indicated a yield stress of 53 ksi for the deck and 46 ksi for the bottom plate. Additional concrete batch mixes, mill certifications and measurements from tension tests are given in Appendix C.

Displacement and Rotation Data

Figure 4.47 shows the applied load vs. mid-span displacements for CC-DD Specimen 2. It includes the loads applied by the north and south rams and the average load vs. mid-span displacement responses of the Specimen. The ordinate on the right hand side of the figure expresses the applied load in equivalent distributed loading (in psf). Up to around 10 kips (200 psf) of loading both the north and south load followed very closely to one another. Beyond this point the north load is consistently lower than the south load by anywhere from 1 up to around 5 kips at higher load levels. The reason for this reduction in load between the two ends is that, similar to the first specimen, a crack began forming near the north support end and continued to grow as loading and deflection increased. Figure 4.48 shows a picture of the crack that formed at the north end of the Specimen. The Specimen was initially loaded to around 22 kips of average load and 6 in. of deflection. It was unloaded to about 2.75 in. of permanent deflection. It was then re-loaded to about 23 kips and 9 in. of total deflection. Loading was terminated when the stroke limit in the hydraulic rams (10 in.) was reached. The load-deflection curve had plateaued and the estimated capacity of the system was 23 kips (average) per load point equivalent to 460 psf distributed loading. A photograph of the specimen at 23 kips of load and 8 in. of deflection is shown in Figure 4.49.

The measured loads and mid-span deflections were used to estimate the stiffness of the specimen. The stiffnesses were estimated for the un-cracked concrete and cracked concrete phases. The cracked concrete stiffness was estimated at the point when flexural

cracks were observed in the specimen. This occurred at approximately 8 kips of loading (at each load point). Un-cracked stiffness was estimated for loading prior to this level. The stiffness was estimated as the north, south, and average loads divided by the mid-span deflection. The estimated stiffnesses are shown in Table 4.15 for the cracked and un-cracked phases of CC-DD Specimen 1. The numerical values are difficult to interpret, but the relative values in Table 4.15 show that there is approximately a 30 % change in stiffness due to concrete cracking.

Figure 4.50 shows the average load vs. measured end rotations for the Specimen. The end rotations were approximately equal to each other up to around 22 kips of applied load. Beyond this point the north end rotations were larger than the rotations of the south end of the Specimen. The crack forming over the north end support was the likely cause for this change in the rotations. Clinometers were also used to determine the average curvature of the uniform moment region of the Specimen (between the load points). The clinometers were placed near the loading points of the specimen as described previously. The average curvature between the loading points was calculated using Equation 4.16. The mid-span moment vs. average curvature plot is shown in Figure 4.51.

Figure 4.52 shows the average load vs. end slip measured using the 1 in. slip sensors. The positive direction of slip in the figures indicates slip towards the mid-span of the specimen. The figure shows that the end slip at the north end of the Specimen was much more significant than the slip at the south end. Measureable slip was observed around 20 kips of loading, and it increased continuously until the applied loading was terminated. The end slip did not cause a shear-bond type failure in the specimen. As explained later, in the behavior of Specimen 3, a shear bond failure causes a large crack to originate from the load point and propagate across the shear interface to the specimen end, and the cause the entire end of the specimen to slip outwards (towards the support point) as the concrete slab delaminates from the steel deck. The experimental results indicated that shear bond failure did not occur in Specimen 2, probably because the end shear studs ‘anchored’ the concrete slab to the steel deck and prevented delamination type failure.

Strain Gage Data

Figure 4.53 shows plots of the strains measured in the steel deck and the concrete slab at the mid-span section at different load levels. The strain measurements are shown as variations over the section depth at different load levels. Figure 4.54 shows plots of the strains measured in steel deck and the concrete slab at the north load point. It is important to note that all the strains were re-zeroed at the beginning of the load test. Therefore, the plots show the strains induced in the composite section by applied loads.

Figure 4.53 and Figure 4.54 show that strain distributions are mostly linear over the cross-section. Non-linearity occurs as the loads are increased, and the slope of the strain diagram in the steel deck section becomes different from the slope of the strain diagram in the concrete slab. This indicates the occurrence of slip and partial composite action between the steel deck and the concrete slab. Figure 4.53 and Figure 4.54 also indicate that reasonable portions of the cellular deep deck had yielded at ultimate loads (although the entire cross-section had not yielded completely). Table 4.16 reports the R^2 values for the strains shown in Figures 4.51 and 4.52. As shown, the linearity of strain profiles measured by the R^2 value decreased as the loads were increased. The strain values shown

in the figure also indicate the maximum concrete strain (at top) has not reached the crushing strain (0.003), while the bottom plate of the cellular deep deck has yielded significantly.

Key Observations from CC-DD Specimen 2 Load Test

- 1) The load-deflection behavior of the repeat specimen was very similar to the behavior of CC-DD Specimen 1.
- 2) The mid-span displacement for service level load of 40 psf (equivalent concentrated loadings of 2 kips) was equal to 0.25 in. This is well within the acceptable range of deflections (typically $L/360$ at applied live loading) for floor systems.
- 3) The maximum load capacity of the specimen was equal to 23 kips (equivalent uniform loading of 460 psf). This is much greater than the ultimate factored loads anticipated on the floor system of 160 psf.
- 4) End slip was not observed until close to the maximum loading, and much after the anticipated ultimate (factored) loading.
- 5) End slip sensors indicated measureable slip close to around 20 kips (400 psf) of loading.
- 6) A crack formed over the north end support and was opening significantly when loads approached 20 kips (400 psf). The crack likely formed prior to this but was not clearly visible. The crack likely formed from the concrete bearing against the shear studs as shear forces increased.
- 7) Strain measurements indicate full composite action until higher levels of loading (around 20 kips or 400 psf).
- 8) When end slips occurred, the specimen did not have a shear bond failure. The end shear studs enhanced behavior and ductility by 'anchoring' the concrete slab to the steel deck.

4.6.3. CC-DD Specimen 3 Results and Discussion

Background Information

CC-DD Specimen 3 had the same cellular deep deck profile and concrete depth as the first two specimens. The only difference was with respect to end conditions. This specimen was attached to the support beams using puddle welds only, i.e., no shear studs at the ends. The pour stops were left in place at the ends like the previous two specimens. Thus, the end condition changed from shear studs to puddle welds. The loading setup and the sensor layout were similar to those for CC-DD Specimen 2. An additional slip sensor was added near the loading point. The resulting slip measurements were used to evaluate the consistency of slip between the ends and within the shear span. The compressive strength of the concrete on the date of test was 5295 psi. This was

determined by testing 4in. by 8 in. concrete cylinders. The steel material yield strengths were reported in the mill certificates as 48 ksi for both the deck and bottom plate steel. Uniaxial tension tests according to ASTM E8 (ASTM, 2004) were performed on machined tension coupons taken from the deck and bottom plate. These tests indicated a yield stress of 53 ksi for the deck and 46 ksi for the bottom plate. Additional concrete batch mixes, mill certifications and measurements from tension tests are given in Appendix C.

Displacement and Rotation Data

Figure 4.55 shows the measured load vs. mid-span displacement data for CC-DD Specimen 3. The figure includes the loads from north and south loading rams, and also the average loading. It shows that the north and south loads were quite close and approximately equal to each other throughout the duration of the test. It is also evident from Figure 4.55 that the behavior of CC-DD Specimen 3 is much different than the behavior of the first two CC-DD Specimens with shear studs. As shown in the figure, the displacement for service level loading (2 kips equivalent to 40 psf) was equal to 0.2 in. The displacement for ultimate factored load level (8 kips equivalent to 160 psf) was equal to 1.1 in. The peak load capacity of the specimen was equal to 18 kips (equivalent to 360 psf). The specimen failed after reaching the peak load at a mid-span displacement of approximately 4.8 in. due to shear bond failure. Figure 4.56 shows the shear bond failure that occurred in CC-DD Specimen 3. Shear bond failure originated as a shear crack from one of the loading points as shown in Figure 4.56. After originating, the crack propagated through the shear interface between the deck and the concrete slab in a brittle (abrupt) manner. The crack propagated to the north support end as shown in Figure 4.57, and delaminated the concrete slab from the steel deck thus constituting a shear bond failure. The north end concrete slab was displaced so much that it pushed away the welded pour stop at the north end as shown in Figure 4.57. The shear bond failure caused the brittle (sudden) drop in capacity observed in Figure 4.55.

The measured loads and mid-span displacements were used to estimate the stiffness of the specimen. The stiffnesses were estimated for the un-cracked concrete and cracked concrete phases. The cracked concrete stiffness was estimated at the point when flexural cracks were observed in the specimen. This occurred at approximately 8 kips of loading (at each load point). Un-cracked stiffness was estimated for loading prior to this level. The stiffness was estimated as the north, south, and average loads divided by the mid-span deflection. The estimated stiffnesses are shown in Table 4.13 for the cracked and un-cracked phases of CC-DD Specimen 1. As shown, and similar to the previous two specimens, an approximate 30% reduction in stiffness occurred from the concrete cracking.

Figure 4.58 shows the measured end slip behavior of the specimen. It includes slips measured at the north and south ends of the specimen, and at the north load point (within the shear span). The figure indicates measureable slip occurred at the north and south end and the north load point at approximately 15 kips (300 psf) of applied loading. The slip values increased gradually with increasing loading. Positive values of slip indicate slip or movement towards the mid-span of the specimen, similar to the first two specimens. As the peak load (and approximately 0.2 in. of measured slip), shear bond

failure occurred along with a reversal of slip back towards the end of the specimen as shown in Figure 4.58. Slip reversal occurred at the north end of the specimen where shear bond failure had propagated to as shown in Figure 4.57. The sensor at the north loading point failed during the specimen unloading. The slip sensor at the north end reached its maximum stroke and the weld attaching the target rod to the deck cracked after the sudden load drop and the movement of the concrete slab at the north end.

Figure 4.59 shows the measured average load vs. end rotation responses for CC-DD Specimen 3. The measured end rotations are almost identical up to the peak load, after which the north end rotation increases much more than the south end rotation. This behavior is expected since the failure occurred at the north end shear span. Figure 4.60 shows the mid-span moment-curvature response of CC-DD Specimen 3. The average curvature of the region between the load points and subjected to uniform moment was calculated using the measured rotations near the north and south load points as mentioned previously in Section 4.6.2. The moment-curvature response of the mid-span region unloads elastically after reaching the peak load because brittle (shear bond) failure occurs in the shear span region.

Strain Gage Data

Figure 4.61 shows plots of the strains measured in the steel deck and the concrete slab at the mid-span section at different load levels. The strain measurements are shown as variations over the section depth at different load levels. Figure 4.62 shows plots of the strains measured in steel deck and the concrete slab at the north load point. It is important to note that all the strains were re-zeroed at the beginning of the load test. Therefore, the plots show the strains induced in the composite section by applied loads.

Figure 4.61 and Figure 4.62 show that strain distributions are mostly linear over the cross-section. Non-linearity occurs as the loads are increased, and the slope of the strain diagram in the steel deck section becomes different from the slope of the strain diagram in the concrete slab. This indicates the occurrence of slip and partial composite action between the steel deck and the concrete slab. Figure 4.61 and Figure 4.62 also indicate that reasonable portions of the cellular deep deck had yielded at ultimate loads (although the entire cross-section had not yielded completely).

Table 4.17 reports the R^2 values for the strains shown in Figure 4.61 and Figure 4.62. As shown, the linearity of strain profiles measured by the R^2 value decreased as the loads were increased. The strain values shown in the figure also indicate the maximum concrete strain (at top) has not reached the crushing strain (0.003), while the bottom plate of the cellular deep deck has yielded some. The strains at the mid-span section indicate composite action while the strains at the north loading point (in the shear span) indicate significant slip between the steel deck and the concrete slab. This difference in the strains is significant at the 18 kip load level. Both the mid-span and load point sections have similar strain profiles at the 15 kip load level, but the difference in strains at 18 kips is drastic (just prior to the shear bond failure occurring).

Key Observations from CC-DD Specimen 3 Load Test

- 1) The load-deflection behavior of CC-DD Specimen 3 was similar to the first two specimens up to around 18 kips (360 psf) of applied loading.
- 2) The mid-span displacement for service level load of 40 psf (equivalent concentrated loadings of 2 kips) was equal to 0.2 in. This is well within the acceptable range of deflections (typically $L/360$ at applied live loading) for floor systems.
- 3) Strain measurements indicate full composite action until levels of loading around 15 kips (300 psf).
- 4) The maximum load capacity of the specimen was equal to 18 kips (equivalent uniform loading of 360 psf). This is much greater than the ultimate factored loads anticipated on the floor system of 160 psf.
- 5) End slip was first observed at 15 kips of loading. A shear bond failure occurred at 18 kips (360 psf) of loading. The failure originated as a shear crack under the load and propagated abruptly (in a brittle manner) through the shear interface between the concrete slab and steel deck delaminating them all the way to the support.

4.6.4. CC-DD Specimen 4 Test Results and Discussion

Background Information

CC-DD Specimen 4 used the optimized (Option 2) design for the composite cellular deep deck systems. As mentioned earlier, the 7.5 in. deep cellular deck profile was made from 18 gage material, and the bottom plate was made from 20 gage material. The section design was optimized for a 30 ft unsupported span. The compressive strength of the concrete on the date of test was 5770 psi. This was determined by testing 4 in. by 8 in. concrete cylinders. The steel material yield strengths were reported in the mill certificates as 48 ksi for both the deck and bottom plate steel. Uniaxial tension tests according to ASTM E8 (ASTM, 2004) were performed on machined tension coupons taken from the deck and bottom plate. These tests indicated a yield stress of 48 ksi for the deck and 42 ksi for the bottom plate. Additional concrete batch mixes, mill certifications and measurements from tension tests are given in Appendix C.

Displacement and Rotation Data

Figure 4.63 shows the applied load vs. mid-span displacement for CC-DD Specimen 4. It includes the loads applied by the north and south hydraulic rams and the average of the two load values. The right hand ordinate axis expresses the applied load (kips) in an equivalent uniformly distributed load in psf. As shown in Figure 4.63, the mid-span displacement for the service level live loading was equal to 0.35 in., which is less than the suggested limit of $L/360$. The displacement for ultimate (factored) loading of 160 psf was equal to 1.86 in. Flexural cracking was observed in the concrete between service and ultimate loading.

The specimen was subjected to monotonically increasing loading up to the peak load of 15 kips (300 psf) and mid-span displacement of 7.5 in. The loads applied by the north and south rams deviated slightly from each other after the loads exceeded 12 kips.

Cracking was observed over the south support near this load level. Figure 4.64 shows the cracking over the south end support. The crack became wider as the loads were increased. The loading was terminated because the specimen load capacity had plateaued, the cracks over the south end support had become substantial, and the hydraulic rams had reached their stroke limit. As shown, the residual displacement after unloading was approximately 3.75 in.

The measured loads and mid-span displacements were used to estimate the stiffness of the specimen. The stiffnesses were estimated for the un-cracked concrete and cracked concrete phases. The cracked concrete stiffness was estimated at the point when flexural cracks were observed in the specimen. This occurred at approximately 4 kips of loading (at each load point). Un-cracked stiffness was estimated for loading prior to this level. The stiffness was estimated as the north, south, and average loads divided by the mid-span deflection. The estimated stiffnesses are shown in Table 4.19 for the cracked and un-cracked phases of CC-DD Specimen 4. The relative values in Table 4.19 show that there is approximately a 30 % change in stiffness due to concrete cracking.

Figure 4.65 shows the average load vs. measured end rotations for the Specimen. The end rotations were approximately equal to each other up to around 15 kips of applied load and around 3 degrees of rotations. Beyond this point the south end rotations were slightly larger than the rotations of the north end of the Specimen. The crack forming over the south end support was the likely cause for this change in the rotations. Clinometers were also used to determine the average curvature of the uniform moment region of the Specimen (between the load points). The clinometers were placed near the loading points of the specimen as described previously. The average curvature between the loading points was calculated using Equation 4.16. The mid-span moment vs. average curvature plot is shown in Figure 4.66.

Figure 4.67 shows the average load vs. end slip measured using the 1 in. slip sensors. The positive direction of slip in the figures indicates slip towards the mid-span of the specimen. The figure shows that the end slip at the south end of the Specimen was much more significant than the slip at the north end. Measureable slip was observed around 14 kips of loading, and it increased continuously until the applied loading was terminated. The end slip did not cause a shear-bond type failure in the specimen, probably because the end shear studs ‘anchored’ the concrete slab to the steel deck and prevented delamination type failure (similar to what happened in CC-DD Specimens 1 and 2). Compared to CC-DD Specimens 1&2 the magnitude of slip was much less for this specimen.

Strain Gage Data

Figure 4.68 shows plots of the strains measured in the steel deck and the concrete slab at the mid-span section at different load levels. The strain measurements are shown as variations over the section depth at different load levels. Figure 4.54 shows plots of the strains measured in steel deck and the concrete slab at the north load point. Figure 4.70 shows plots of the strains measured in the steel deck and concrete slab at the south load point. It is important to note that all the strains were re-zeroed at the beginning of the load test. Therefore, the plots show the strains induced in the composite section by applied loads.

Figure 4.68, Figure 4.69, and Figure 4.70 show that significant yielding of the bottom plate occurred at all sections at the peak load. However, the concrete does not reach crushing strains at the top of the slab and the web and top of the steel deck did not reach yielding at peak loads. The strain profiles over the mid-span section are mostly linear and indicate almost full composite action up to peak load. This is expected since the mid-span section is located in the uniform moment region with no shear. The strain profiles over the sections at the north and south load points (in the shear span regions) show increasing nonlinearity with loads. At the peak load, the strain profiles at the north and south load points indicate slip between the steel deck and concrete slab. This is evidenced by the different slopes of the strain profiles in steel deck and concrete slab. Table 4.20 reports the R^2 values for the strains shown in Figure 4.68, Figure 4.69, and Figure 4.70. As shown, the linearity of strain profiles measured by the R^2 value decreased as the loads were increased.

Key Observations from CC-DD Specimen 4 Load Test

- 1) The load-deflection behavior of CC-DD Specimen 4 was very similar to the behavior of CC-DD Specimens 1 and 2, with a lower overall capacity.
- 2) The mid-span deflection for service level load of 40 psf (equivalent concentrated loadings of 2 kips) was equal to 0.35 in. This is well within the acceptable range of deflections (typically $L/360$ at applied live loading) for floor systems.
- 3) The maximum load capacity of the specimen was equal to 15 kips (equivalent uniform loading of 300 psf). This is much greater than the ultimate factored loads anticipated on the floor system of 160 psf.
- 4) End slip was not observed until close to the maximum loading, and much after the anticipated ultimate (factored) loading.
- 5) End slip sensors indicated measureable slip close to around 14 kips (280 psf) if loading.
- 6) A crack formed over the south end support and was opening significantly when loads approached 12 kips (240 psf). The crack likely formed prior to this but was not clearly visible. The crack likely formed from the concrete bearing against the shear studs as shear forces increased (similar to CC-DD Specimens 1 and 2).
- 7) Strain measurements indicate full composite action until higher levels of loading (around 14 kips or 280 psf).
- 8) When end slips occurred, the specimen did not have a shear bond failure. The end shear studs enhanced behavior and ductility by ‘anchoring’ the concrete slab to the steel deck.

4.7. General Discussion Points of CC-DD Test Results

The experimental investigation of the CC-DD specimens investigated three different behavioral aspects for the system. These were the structural behavior in the construction phase, the dynamic behavior as it relates to floor vibrations in the composite phase, and the overall structural behavior in the composite phase. Important observations were

made for all phases and helped in shaping the more advanced analyses investigated and other recommendations for the systems.

4.7.1. Construction Phase Results Discussion Points

- 1) Measured deflections and strains during the construction loading test and the concrete casting operation were within acceptable limits for all specimens. The cellular deep deck systems proved efficient in resisting the imposed construction (non-composite) loads for 30 ft spans. The optimized system, Specimen 4, had construction levels on the order of $L/200$. This was the most optimized design for construction. It used less steel material than other specimens and would hence be more economical.
- 2) Specimen 3 exhibited slightly less deflection than Specimens 1 and 2 during the concrete casting operation. The only difference between the specimens was end support conditions. Specimen 3 was attached to the support beam only with puddle welds. The welds likely provided slightly more restraint to end connection. Hence, if there was a desire to reduce construction level deflections puddle welds in conjunction with shear studs could be utilized.
- 3) The residual strains after concrete casting were measured and reported at least 24 hours after the initial concrete pour. The concrete heat of hydration caused thermal strains in the first few hours (12-24 hours) after casting. These thermal strains decreased as the concrete hardened and set, and the strains reduced to the residual value.

4.7.2. Dynamic/Modal Impact Testing Results Discussion Points

- 1) The measured natural frequencies were close to those calculated using a simple SDOF model for all specimens. Some likely non-linear behavior was observed in higher frequencies as indicated by some double peaks in the FRFs. However, these modes did not contribute significantly to the dynamic response of the specimens.
- 2) The first mode of vibration and natural frequency was much lower than higher modes for all specimens, and seemed to be the dominant mode for heel drop and modal impact excitation. Also, there was significant spacing between modes and the first mode was dominant. Hence, the floor vibration behavior of the CC-DD systems can likely be evaluated using guidelines published by the AISC and SCI.
- 3) Damping was estimated between 0.7 and 0.9% for the CC-DD Specimens at the first fundamental frequency. This is comparable to estimates made of existing composite flooring systems. The actual damping present in a structure however would also be heavily dependent on the presence of non-structural elements, floor bay layouts, and occupancy of a structure.
- 4) A reduction in acceleration response and a decrease in damping were observed when additional mass was added to CC-DD Specimen 3. The frequency shift occurred because the kinetic energy needed to bring the system to equilibrium increased. Furthermore, if we consider Equation 2.4 for evaluating the floor system, then if both the response and frequency of the system are reducing, then the amount of damping needed would also reduce.

4.7.3. Ultimate Load Testing Results Discussion Points

- 1) The presence of shear studs at the support provides additional capacity and ductility to the CC-DD specimens. This was evident from comparing the results from specimens 1, 2 and 4 to Specimen 3. The capacity of the non-studded specimen (3) was around 20% less than the studded option and it experienced a brittle shear-bond failure. This type of failure is undesirable as it appears suddenly and with little warning. The failure occurred at 18 kips (360 psf), which is well above design loads and hence the specimen still had much reserve capacity. To avoid this failure mode either shear studs at the end should be used or some other means to prevent the onset of slip that would cause the brittle failure mode.
- 2) All specimens with shear studs experienced cracks that opened over one of their support points. This crack likely formed due to the concrete bearing against the shear stud. As forces increased the interfacial shear demand increased. This increased the longitudinal forces induced on the shear studs. The force of the stud bearing on the concrete bearing on the concrete caused the concrete to split locally in the area of the stud. This crack could be prevented by providing some hoop type reinforcement around the shear studs. Preventing or delaying this crack would likely enhance capacity and overall behavior of the systems.
- 3) Strain observations indicated mostly linear behavior through the profile depths until higher load levels for shear studded specimens. Linearity in the strains dropped near ultimate loads and high levels of mid-span displacement. The drop in linearity indicates partial composite behavior of the specimen. The drop in linearity was more pronounced in the shear span region of the specimens, as was expected. The non-studded option also experienced mostly linear strains up to near ultimate loads. However, the specimen experienced a sudden and brittle shear bond failure.
- 4) All specimens were observed to have reserve capacity for factored ultimate loads. CC-DD Specimen 1 and 2 were quite overdesigned while Specimen 4 had a more efficient design (for both the construction and composite level phases). Hence, the most efficient design would use the CC-DD Specimen 4 profile for the 30 ft span. Furthermore, using puddle welds and shear studs at the ends and providing some hoop reinforcement around the studs would likely yield the most desirable construction and composite level behavior.

Table 4.1: Design Checks of CC-DD System

System	Construction Phase				Composite Phase			
	ϕM_{nc} (kip-ft/ft)	$\phi M_{nc}/M_u^*$	I_{cons} (in. ⁴ /ft)	$I_{cons}/I_{reqd.}$	ϕM_n (kip-ft/ft)	$\phi M_n/M_u$	I_{comp} (in. ⁴ /ft)	$I_{comp}/I_{reqd.}$
Option 1	28	2.5	29	1.5	54	3.1	79.4	3.2
Option 2	17.3	1.54	18	1.0	36.3	2.1	60	2.4

Table 4.2: Assumed nominal material properties used for models

Property	Assumed Value
Yield strength of steel (f_y)	40 ksi
Young's Modulus of steel (E_s)	29,500 ksi
Compressive Concrete Strength (f'_c)	4 ksi
Elastic Modulus of Concrete	3000 ksi
Density of Concrete	115 pcf

Table 4.3: Relevant results of numerical non-linear inelastic analysis

Deck Profile	Predicted Capacity (w_n -psf)	w_n/w_u	Predicted deflection at nominal live loads (Δ_{II} -in.)
1	475	2.9	0.25
2	320	1.9	0.3

Table 4.4: Results for floor vibration analysis on CC-DD Systems

CC-DD System	Estimated first natural frequency	a_p/g for 3% damping	a_p/g for 4% damping	a_p/g for 5% damping	Required Damping (%)
Option 1	6.0	0.052	0.039	0.031	3.1
Option 2	5.5	0.061	0.0461	0.037	3.7

Table 4.5: Fire Ratings based on UL Assembly D903 for 4.5, 6, and 7.5 in. deep deck assemblies

Rating (hours)	Non-Cellular Units	
	Normal Weight Concrete Required Thickness (in.)	Lightweight Concrete Required Thickness (in.)
1	3	2.75
1.5	3.5	3
2	4.25	3.5
3	-	4
Rating (hours)	Cellular Units	
	Normal Weight Concrete Required Thickness (in.)	Lightweight Concrete Required Thickness (in.)
1	2.75	2.5
1.5	3.25	2.75
2	4	3
3	-	3.75

Table 4.6: Specifications for steel strain gauges used (reproduced from Texas Measurements website www.straingauge.com)

Main Test Materials	Metal	Materials Backing	Special Plastics
Operating Temperature	-20 to +80	Materials Element	Cu-Ni alloy foil
Compensation Range	NA	Strain limit	10 to 15%
Bonding Adhesive	CN, CN-Y*	Fatigue life at room temperature	5x10 ⁵

*CN is a standard super glue adhesive and CN-Y is for post yield applications. CN-Y was used for all specimens.

Table 4.7: Specifications for concrete strain gauges used (reproduced from Texas Measurements website www.straingauge.com)

Main Test Materials	Metal, Mortar	Materials Backing	Polyester
Operating Temperature	-20 to +80	Materials Element	Cu-Ni alloy foil
Compensation Range	+10 to +80C	Strain limit	2%
Bonding Adhesive	CN	Fatigue life at room temperature	1x10 ⁶

Table 4.8: Testing matrix for CC-DD systems

Specimen Designation	Span (ft.)	Nominal Deck Depth (in.)	Total Slab Depth (in.)	Deck and Bottom Plate Thickness (Ga.)	Specified Concrete Type and Strength	End Conditions
CC-DD-1	30	7.5	10	14/16	LWC – 115 pcf f _c =4 ksi	Shear Studs Pour Stop
CC-DD-2	30	7.5	10	14/16	LWC – 115 pcf f _c =4 ksi	Shear Studs Pour Stop
CC-DD-3	30	7.5	10	14/16	LWC – 115 pcf f _c =4 ksi	Puddle Welds Pour Stop
CC-DD-4	30	7.5	10	18/20	LWC – 115 pcf f _c =4 ksi	Shear Studs Pour Stop

Table 4.9: Summary of construction phase results for CC-DD Specimens

	Specimen 1		Specimen 2		Specimen 3		Specimen 4	
	Construction Load	Pour	Construction Load	Pour	Construction Load	Pour	Construction Load	Pour
Max Deflection During Construction (in.)*	0.43	1.5	0.42	1.67	0.5	0.9	0.76	1.7
Residual Mid-Span Deflection (in.)	0	1.1	0	1.1	0	0.9	0	1.7
Max Tensile Strain (μs)	105	370 (11 ksi)	100	319 (9.4 ksi)	120	200 (6 ksi)	185	473 (14 ksi)
Residual Tensile Strain (μs)	0	320 (9.5 ksi)	0	280 (8.2 ksi)	0	200 (6 ksi)	0	420 (12 ksi)

* Measured unit weight at time of pour was 120 pcf±1pcf for all specimens

Table 4.10: Measured and Calculated Natural Frequencies for Tested Specimens

Specimen #	Measured First Natural Frequency (Hz.)	Measured Second Natural Frequency (Hz.)	Measured Third Natural Frequency (Hz.)	Calculated Natural Frequency (Hz.)
1	6.0	-	-	6.2
2	6.0	22.6	49.2	6.2
3	6.2	23	50	5.9
4	5.8	21.9	46.7	5.7

Table 4.11: Estimated damping at first resonant frequency for CC-DD Specimens

Specimen #	Estimated Damping at First Resonant Frequency (%)	Damping at Resonant Frequency with 10/20 psf Applied (%)	Frequency with 10/20 psf load (Hz.)
2	0.86	NA	NA
3	0.72	0.58/0.48	5.6/5.1
4	0.72	NA	NA

Table 4.12: Output Spectra values for heel drops on CC-DD Spectra 3

Accelerometer Location	G_{yy} at fn_1 (6.2 Hz)	G_{yy} at fn_2 (23 Hz)	G_{yy} at fn_3 (50 Hz)	G_{yy1}/G_{yy2}	G_{yy2}/G_{yy3}
South Third Point	2.9×10^{-4}	3.38×10^{-5}	1.40×10^{-6}	8.6	207
Mid-Span	8.2×10^{-4}	4.9×10^{-8}	1.45×10^{-6}	Inf*	565
North Third Point	5.6×10^{-4}	3.4×10^{-5}	9.0×10^{-8}	16	Inf*

*inf indicates two order of magnitudes or greater

Table 4.13: Relative Stiffness Parameters of Specimen 1

Type of Stiffness	North Load / Mid-Span Displacement (kips/in.)	South Load / Mid-Span Displacement (kips/in.)	Average Load / Mid-Span Displacement (kips/in)	Reduction in Stiffness from Concrete Cracking
Concrete Un-Cracked	4.5	11.3	7.9	30%
Concrete Cracked	5.6	5.7	5.65	

Table 4.14: R^2 values for strain distribution at various loading values CC-DD Specimen 1

Average Load Value (kips)	Average Load / Measured Capacity	R^2 value for strains at south end	R^2 value for strains at mid-span	R^2 value for strains at north end
2	0.083	0.99	0.99	0.99
5	0.22	0.99	0.99	0.99
10	0.43	0.99	0.99	0.98
20	0.87	0.97	0.99	NA*
23	0.96	0.93	0.98	NA*

*Strain gauge was no longer reading at this point

Table 4.15: Relative Stiffness Parameters of CC-DD Specimen 2

Type of Stiffness	North Load / Mid-Span Displacement (kips/in.)	South Load / Mid-Span Displacement (kips/in.)	Average Load / Mid-Span Displacement (kips/in)	Reduction in Stiffness from Concrete Cracking
Concrete Un-Cracked	8.2	8.1	8.15	30%
Concrete Cracked	5.4	6.2	5.8	

Table 4.16: R² values for strain distribution at various loading values CC-DD Specimen 2

Average Load Value (kips)	Average Load / Measured Capacity	R ² value for strains at south end*	R ² value for strains at mid-span	R ² value for strains at north end
2.5	0.10	NA	0.97	0.97
8	0.33	NA	0.96	0.98
10	0.42	NA	0.95	0.99
13	0.54	NA	0.96	0.98
21	0.875	NA	0.92	0.93

*Two strain gauges stopped reading after the concrete pour and thus R² values could not be estimated for these gauges

Table 4.17: Relative Stiffness Parameters of CC-DD Specimen 3

Type of Stiffness	North Load / Mid-Span Displacement (kips/in.)	South Load / Mid-Span Displacement (kips/in.)	Average Load / Mid-Span Displacement (kips/in)	Reduction in Stiffness from Concrete Cracking
Concrete Un-Cracked	8.25	8.6	8.4	30%
Concrete Cracked	6.05	6.2	6.1	

Table 4.18: R^2 values for strain distribution at various loading values CC-DD Specimen 3

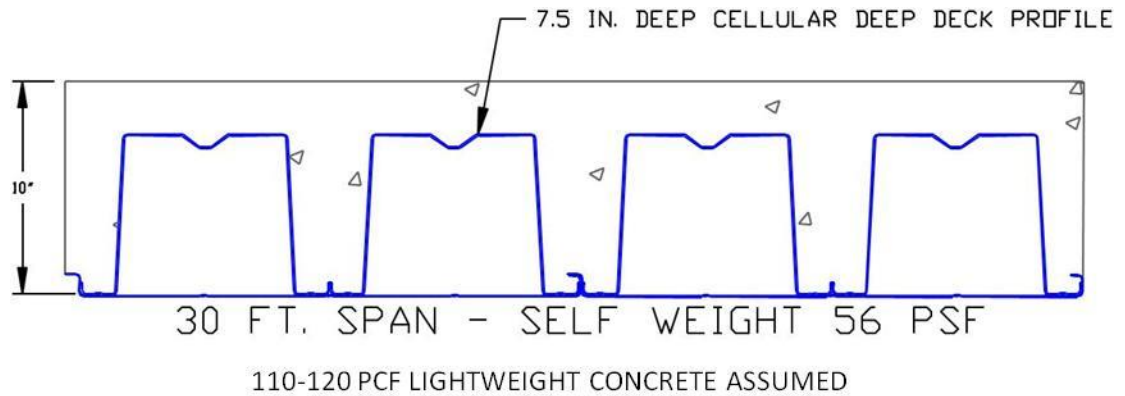
Average Load Value (kips)	Average Load / Measured Capacity	R^2 value for strains at south end	R^2 value for strains at mid-span	R^2 value for strains at north end
2.5	0.14	0.98	0.99	0.99
5	0.28	0.97	0.98	0.98
10	0.55	0.97	0.98	0.99
15	0.83	0.97	0.98	0.94
18	1	0.96	0.98	0.78

Table 4.19: Relative stiffness parameters of CC-DD Specimen 4

Type of Stiffness	North Load / Mid-Span Displacement (kips/in.)	South Load / Mid-Span Displacement (kips/in.)	Average Load / Mid-Span Displacement (kips/in)	Reduction in Stiffness from Concrete Cracking	Average Stiffness (kips/in.)
Concrete Un-Cracked	6.8	6.4	6.6	32.5%	5.5
Concrete Cracked	4.5	4.4	4.45		

Table 4.20: R^2 values for strain distribution at various loading values CC-DD Specimen 4

Average Load Value (kips)	Average Load / Measured Capacity	R^2 value for strains at south end	R^2 value for strains at mid-span	R^2 value for strains at north end
2.5	0.17	0.97	0.99	0.93
5	0.33	0.93	0.99	0.95
8	0.53	0.94	0.99	0.97
12	0.80	0.91	0.99	0.97
15	1	0.86	0.99	0.90



OPTION 1:
 DECK THICKNESS: 14 GA.
 PLATE THICKNESS: 16 GA.
 STEEL AREA: 2.92 IN.²/FT
 L/360 CONSTRUCTION DEFLECTION

OPTION 2:
 DECK THICKNESS: 18GA.
 PLATE THICKNESS: 20 GA.
 STEEL AREA: 1.33 IN.²/FT
 L/220 CONSTRUCTION DEFLECTION

Figure 4.1: Composite deep deck system cross section – 30 ft. Span

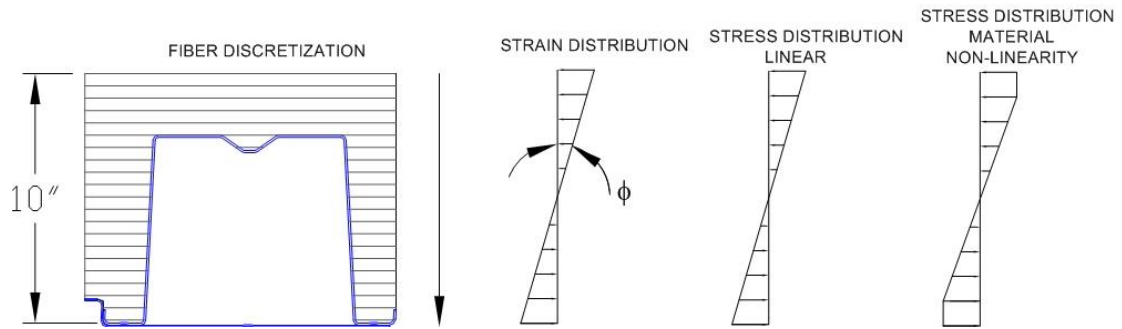


Figure 4.2: Fiber discretization for cross-section and assumptions for strain and stress

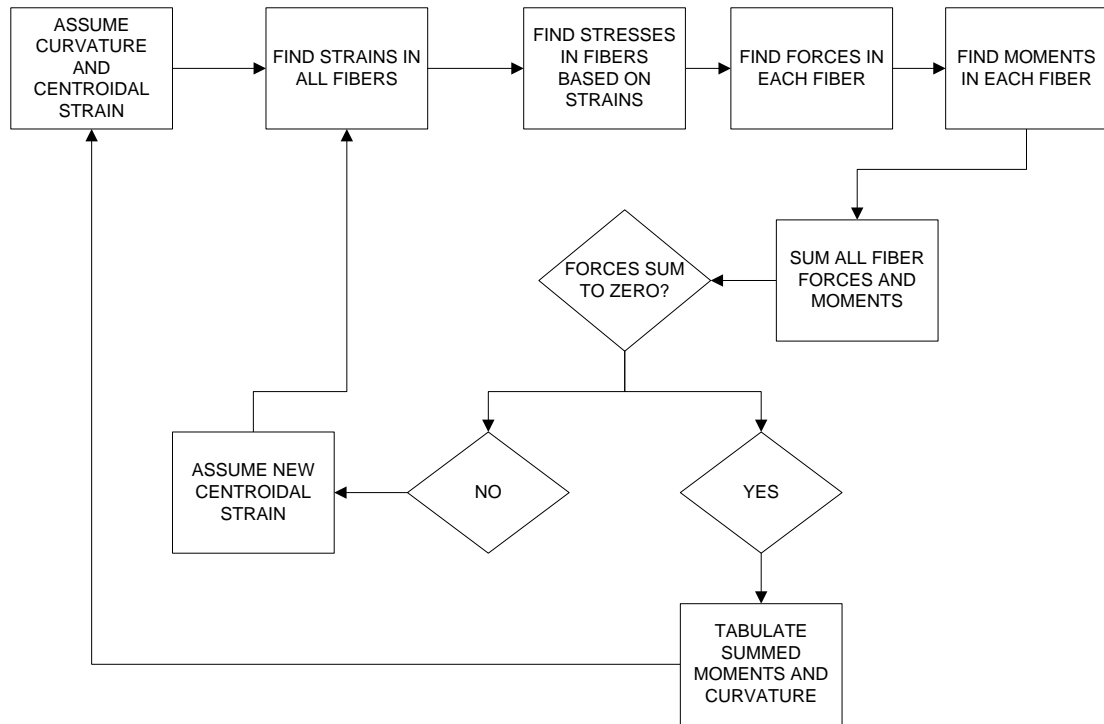


Figure 4.3: Flowchart for finding section moment-curvature relationship

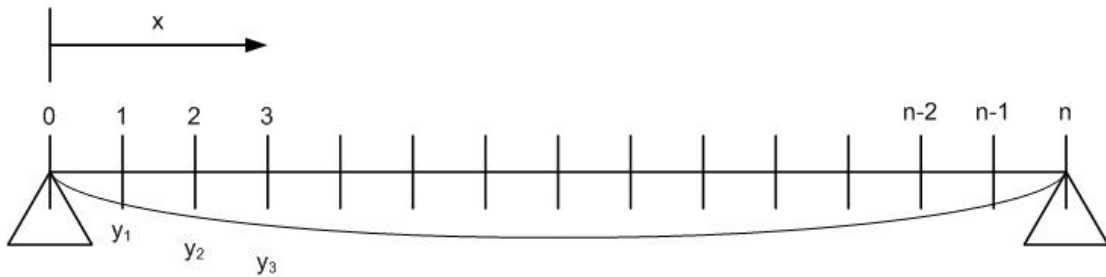


Figure 4.4: Beam member discretized into stations

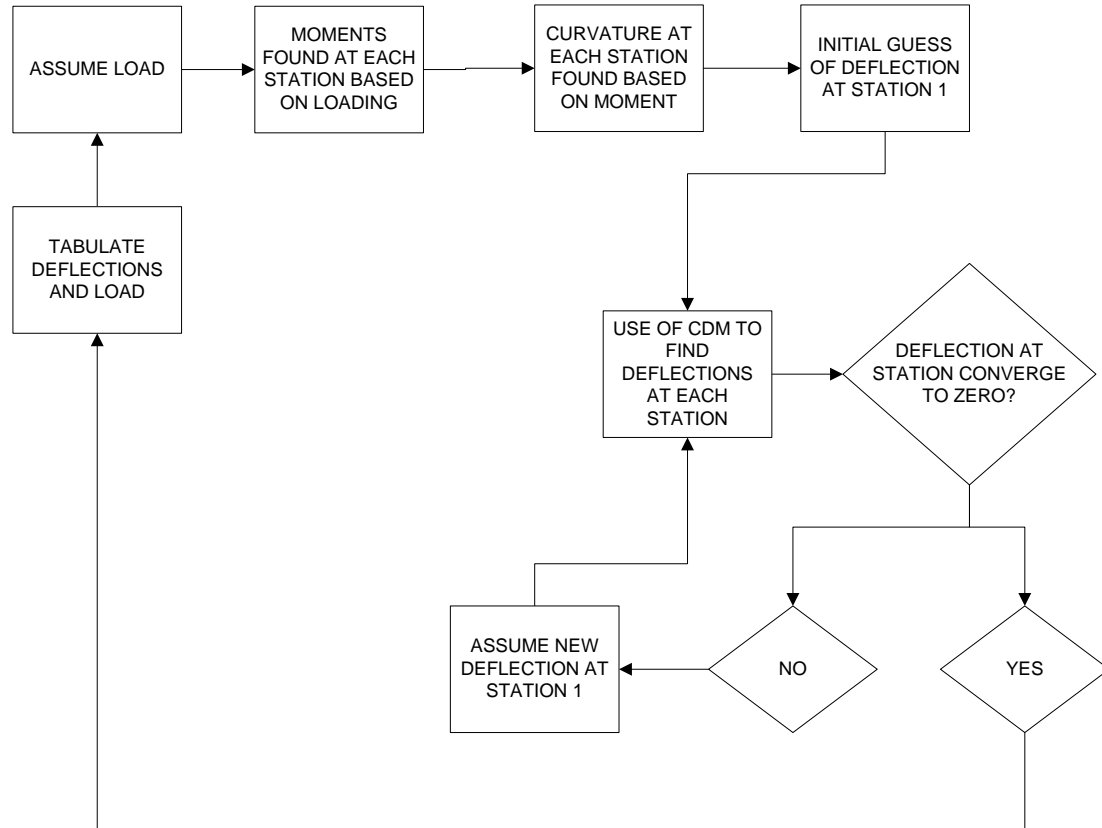


Figure 4.5: Flow chart for finding load-deflection of beam

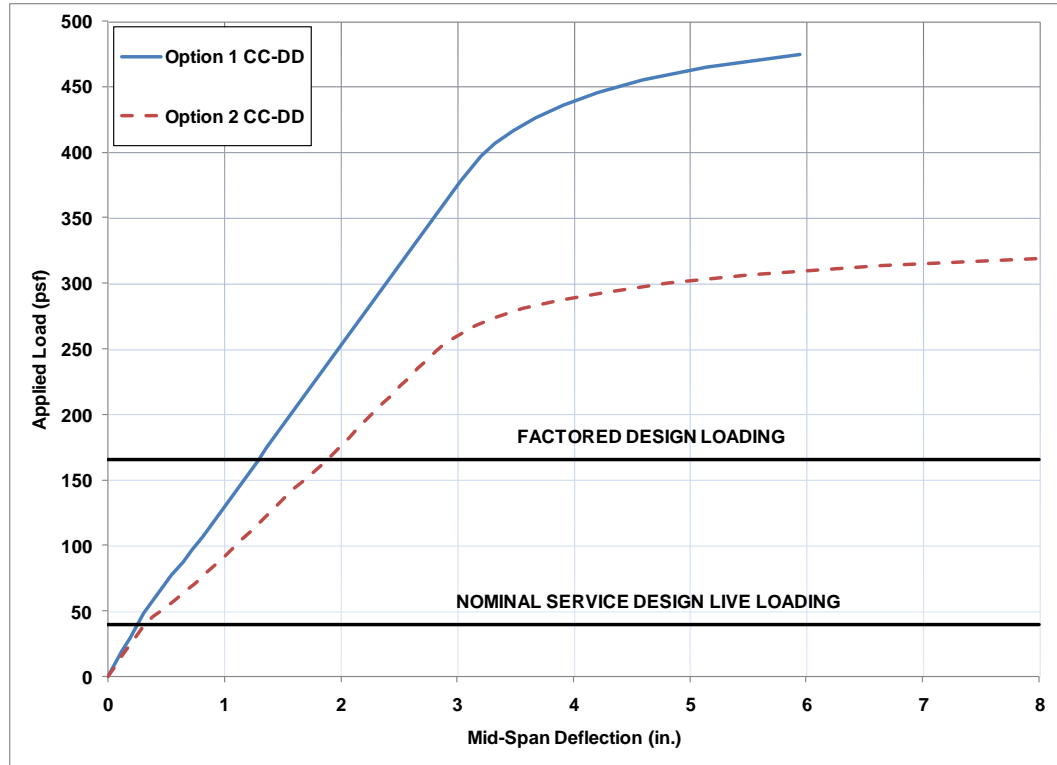


Figure 4.6: Predicted load-deflection behavior for 30 ft. span CC-DD systems with uniform loading and nominal material properties

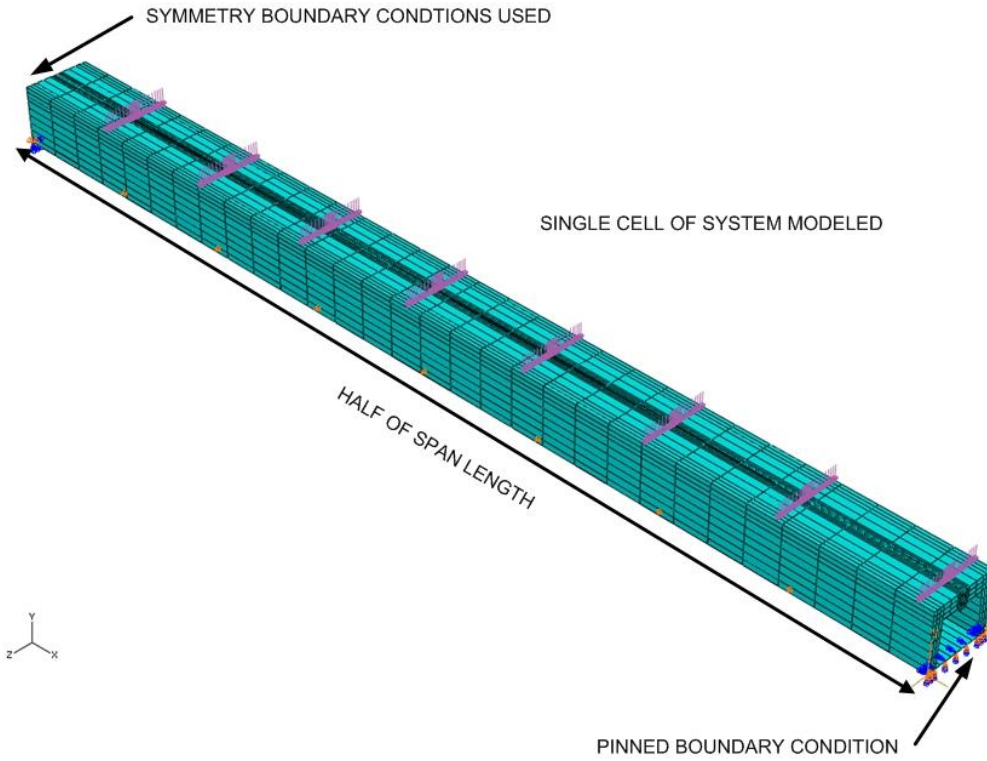


Figure 4.7: Schematic of meshed structural FEM models for CC-DD systems

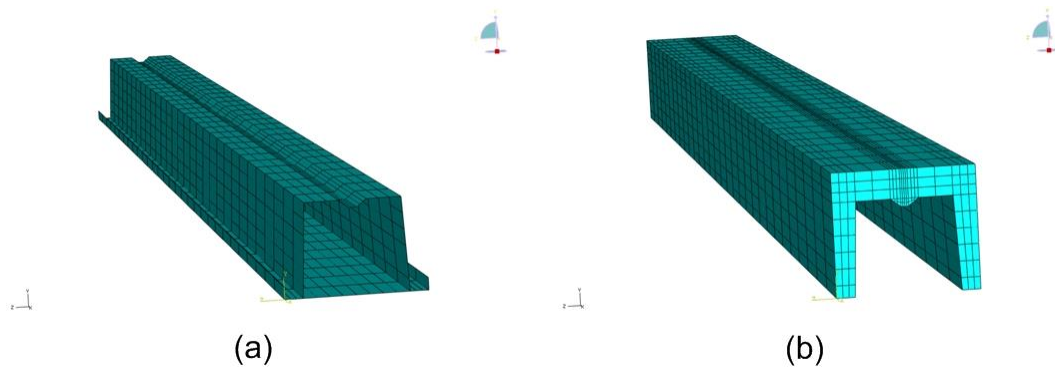


Figure 4.8: View of mesh for (a) steel components and (b) concrete

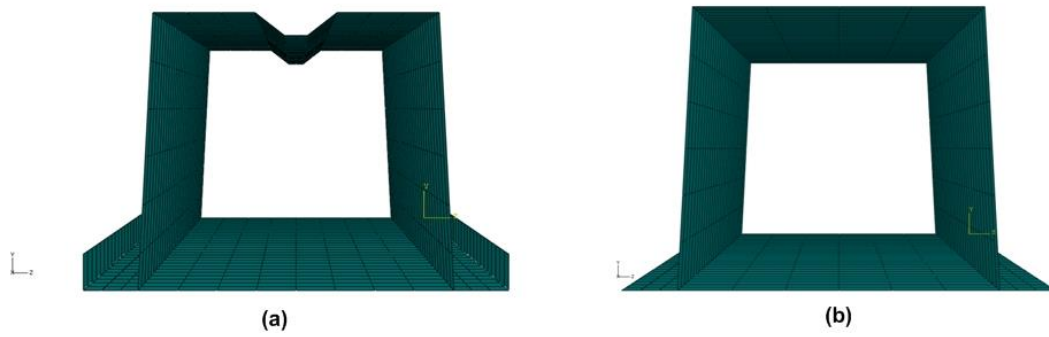


Figure 4.9: Cross-section of steel deck used in FEM models for (a) full geometry and (b) simplified geometry

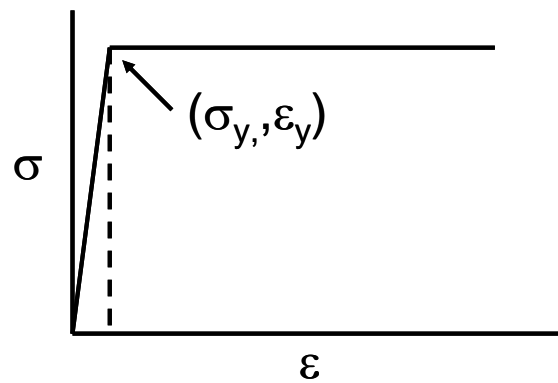


Figure 4.10: Steel Material Model used in FEM

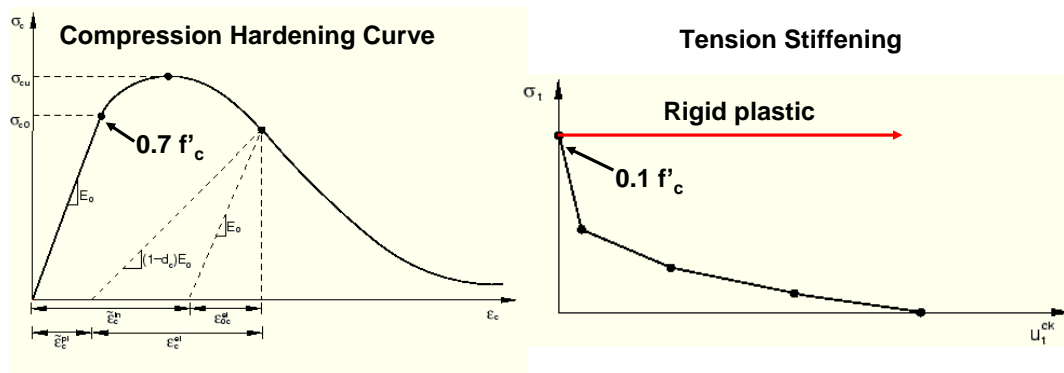


Figure 4.11: Concrete material property models used in FEM models (Simulia, 2007)

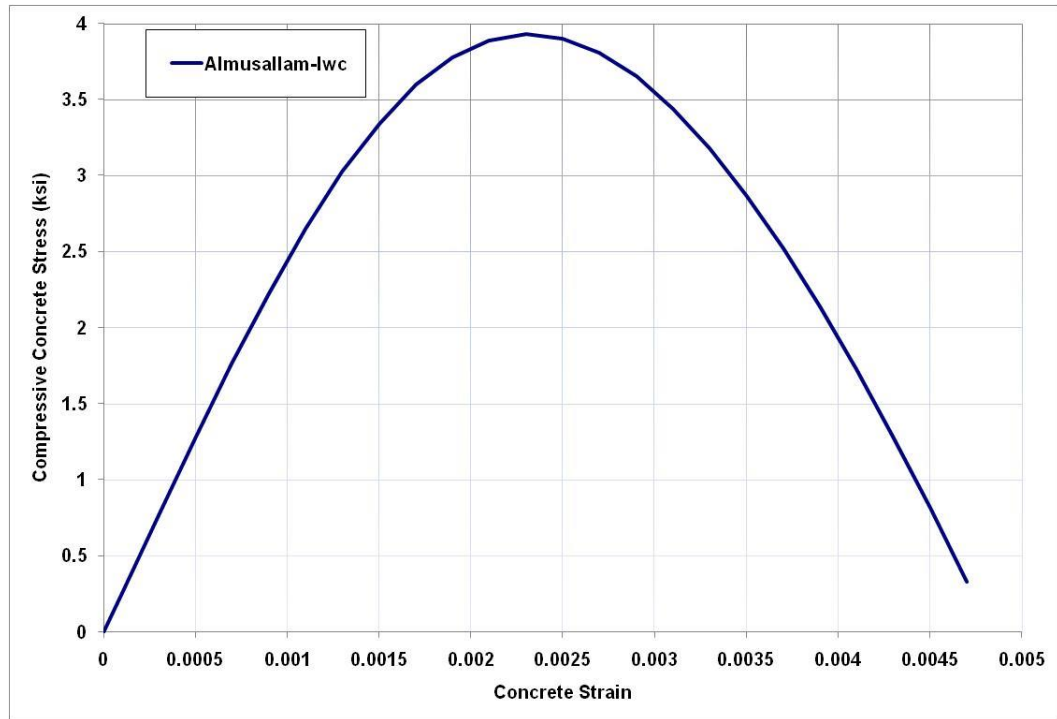


Figure 4.12: Almusallam curve for 4 ksi lightweight concrete

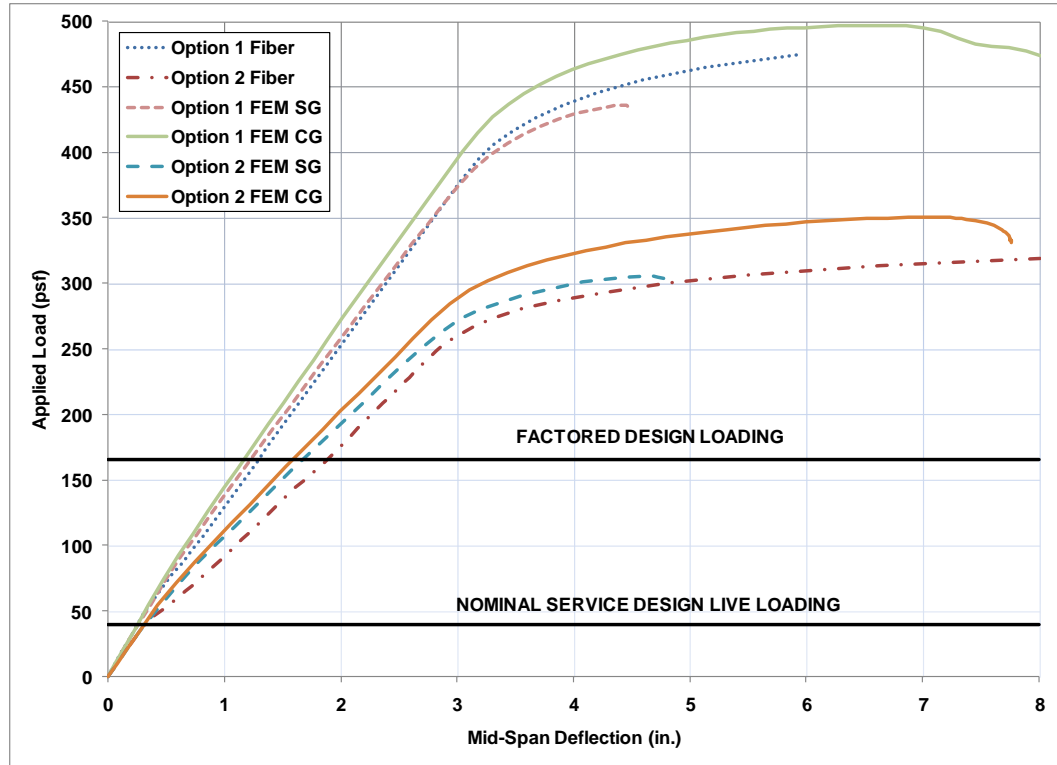


Figure 4.13: Load-deflection behavior of CC-DD systems with uniform loading and a 30 ft span

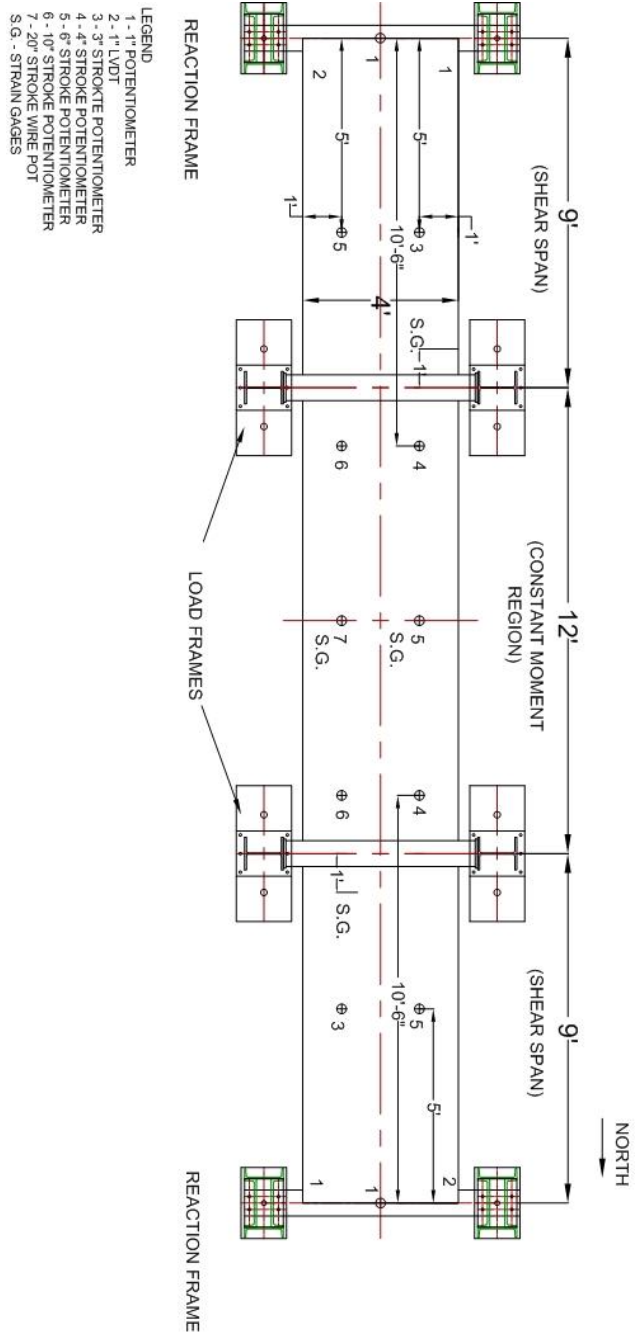


Figure 4.14: Plan View of Test Setup with CC-DD specimen

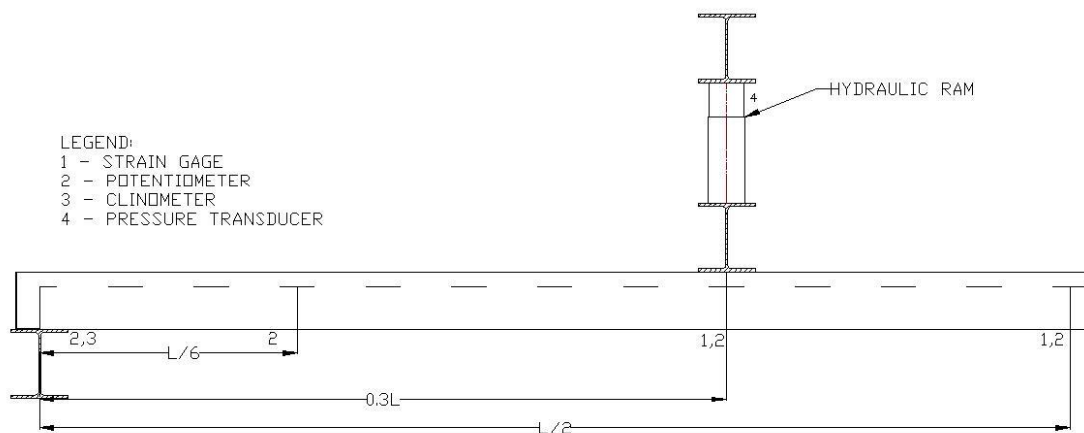


Figure 4.15: Schematic side view of sensor layout for deep deck tests (half span shown – symmetric)

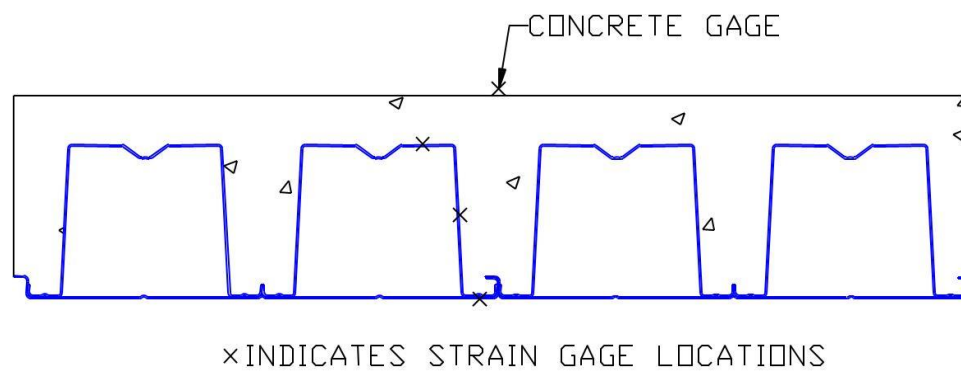
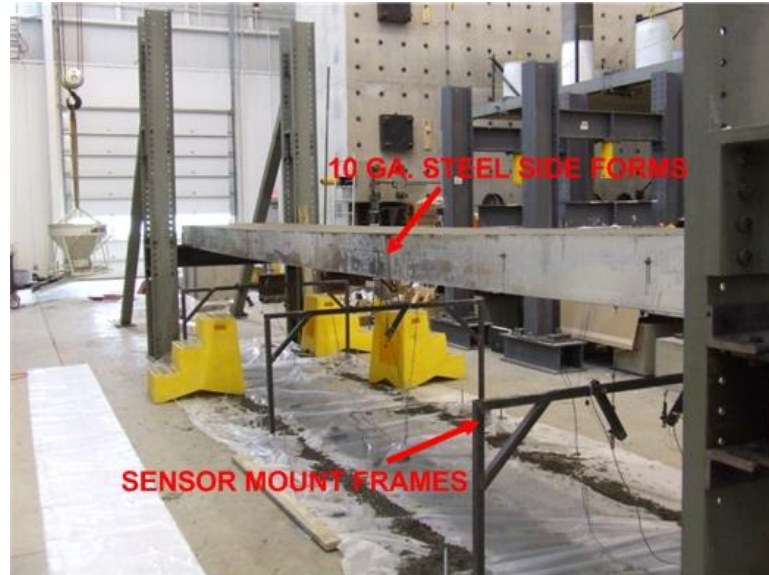


Figure 4.16: Strain Gage Locations in Specimen Cross-section at Mid-Span and quarter points



Figure 4.17: CC-DD Floor System Specimen (a) Before and (b) After Concrete Placement

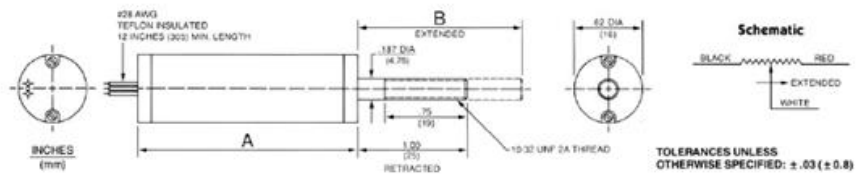


(a) Concrete Pour

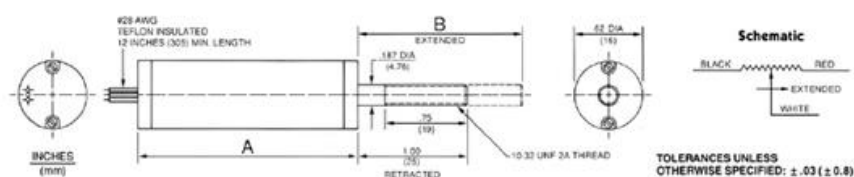


(b) Load Testing

Figure 4.18: Sensor and overall layout in the (a) construction phase and (b) composite phase

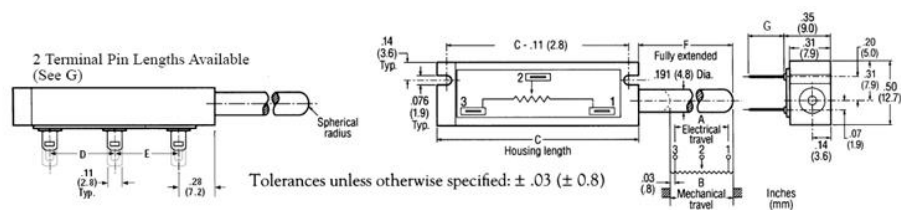


(a)



(b)

Figure 4.19: Schematics of (a) 603 Duncan potentiometer and (b) 606 Duncan potentiometer (BEI Duncan, 2008)



(a)



(b)

Figure 4.20: 1 in. stroke potentiometers used for measuring end slips showing (a) schematic and (b) actual sensor (BEI Duncan, 2008)

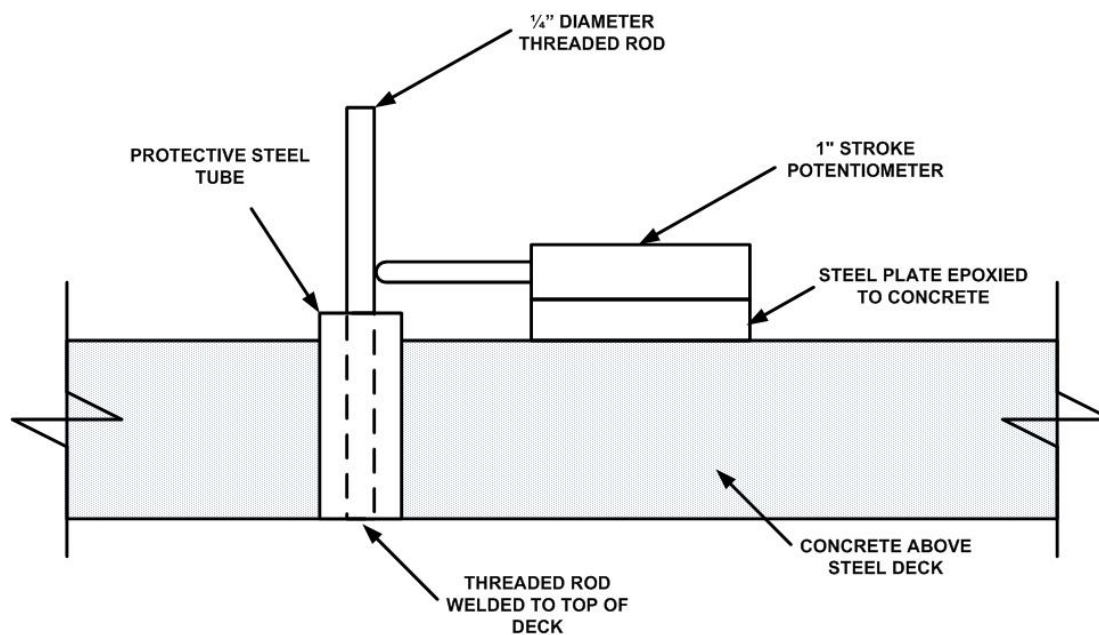


Figure 4.21: Schematic of slip sensor setup



Figure 4.22: Photograph of slip sensor on CC-DD specimen



performance specifications

Total Range	$\pm 60^\circ$
Linear Range	$\pm 45^\circ$
Threshold	0.001°
Linearity	
Null to 10°	$\pm 0.1^\circ$
10 to 45°	$\pm 1\%$
45 to 60°	Monotonic
Null Repeatability	0.05°
Cross Axis Error	$<1\%$ up to 45°
Time Constant	0.3 sec
Freq. Response (-3db)	0.5 Hz
RF Susceptibility	$\leq \pm 2^\circ$

Figure 4.23: Schaevitz clinometers with manufacturer's specifications (Measurement Specialties, 2008)

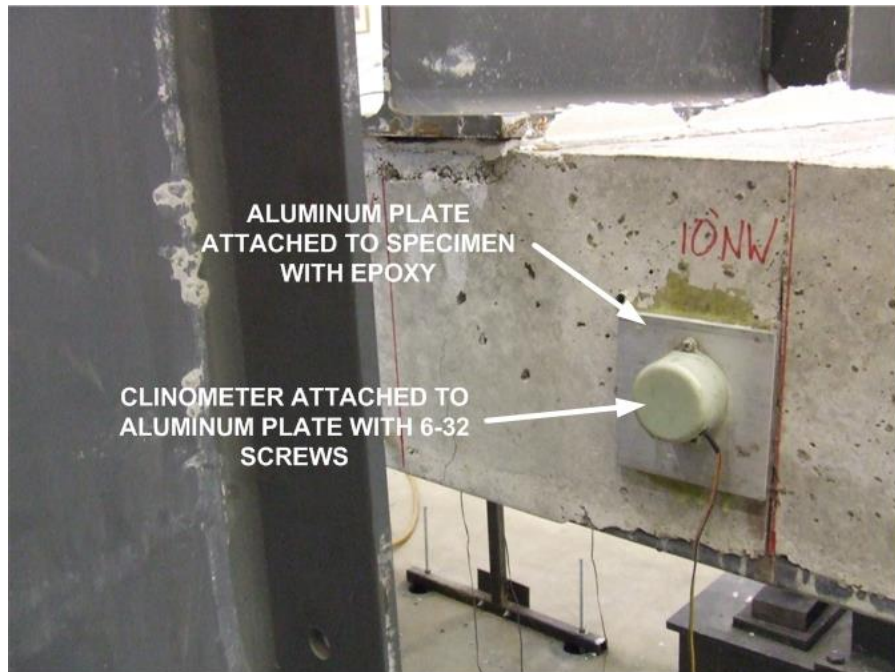
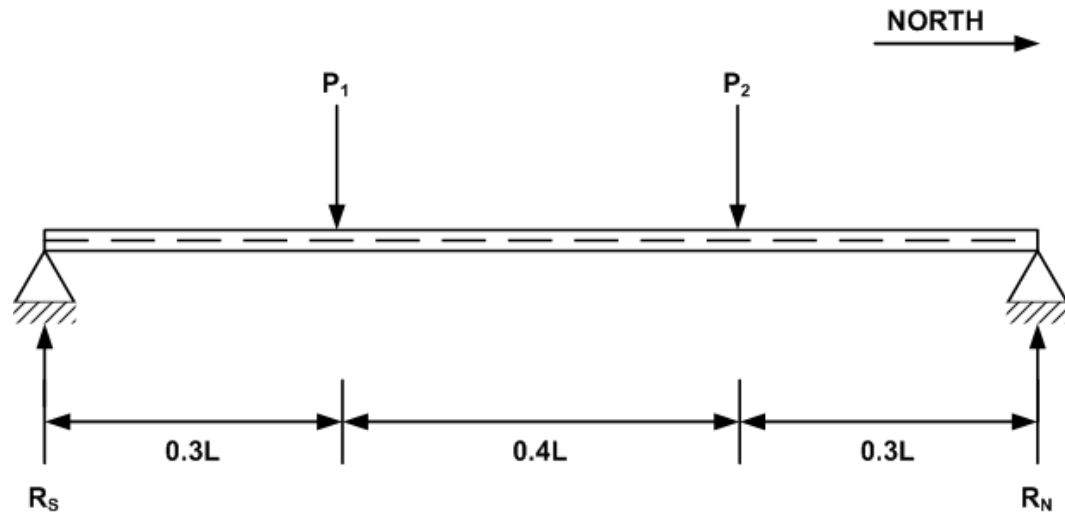
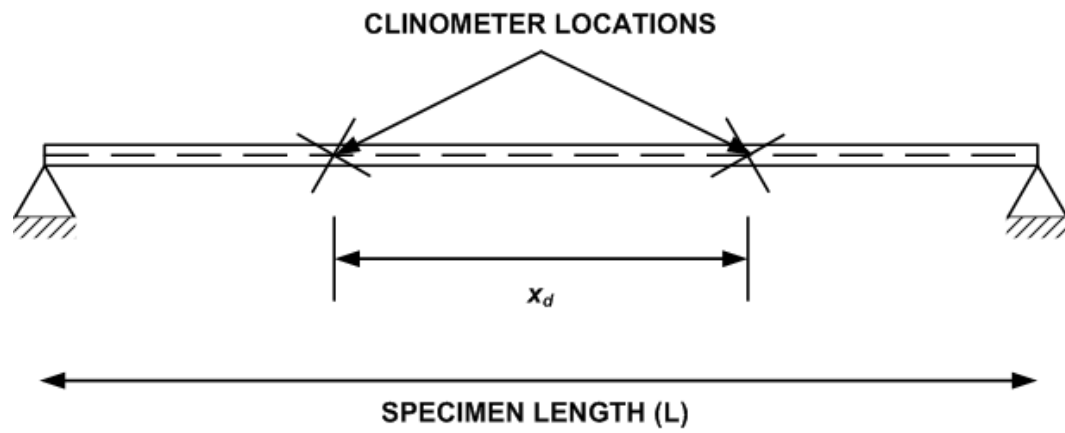


Figure 4.24: Picture showing clinometer attached to test specimen



(a)



(b)

Figure 4.25: Schematic of CC-DD test specimens



MODEL 086C42 IMPACT HAMMER

Sensitivity: 1 mv/lbf
Measurement range: ± 5000 lbf
Hard Tip Frequency Range: 750 Hz
Medium Tip Frequency Range: 650 Hz
Soft Tip Frequency: 350 Hz
Super Soft Tip Frequency: 250 Hz

Figure 4.26: Modal Impact Hammer and Specifications (PCB , 2008)



MODEL 393A03 SEISMIC ACCELEROMETER

Sensitivity ($\pm 5\%$): 1000 mV/g
Frequency Range ($\pm 5\%$): 0.5 to 2000 Hz
Broadband Resolution (1 to 10,000 Hz): 0.00001 g rms

Figure 4.27: Seismic Accelerometer used for Acquiring Data with Specifications (PCB , 2008)



Figure 4.28: Applying Impact with Modal Hammer to test Specimen



Figure 4.29: Specimen with Accelerometers Attached



NI MODEL USB-9233 DATA ACQUISITION BOX

Number of Channels: 4
 Sample Rate: 50 ks/s/channel
 A/D Resolution: 24 bits
 Signal Conditioning: Anti-Aliasing Filter, Current Excitation

Figure 4.30: Data Acquisition Box with Specifications (National Instruments, 2008)

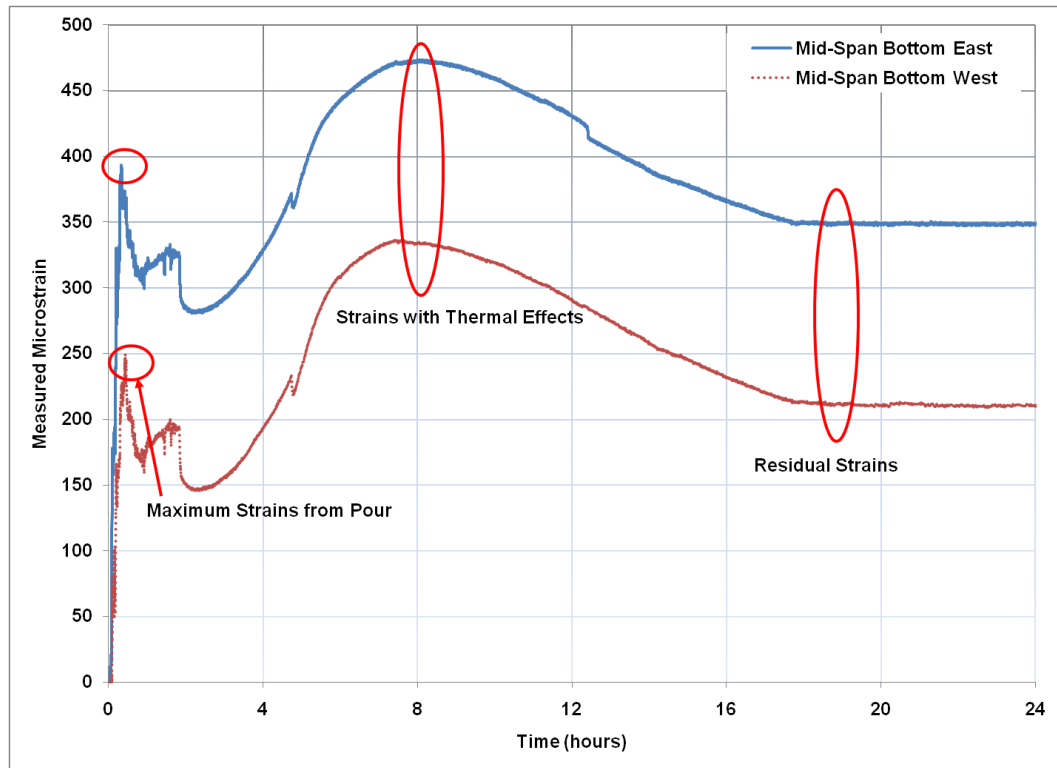


Figure 4.31: Strains during concrete pour and for 24 hours following pour on CC-DD Specimen 2

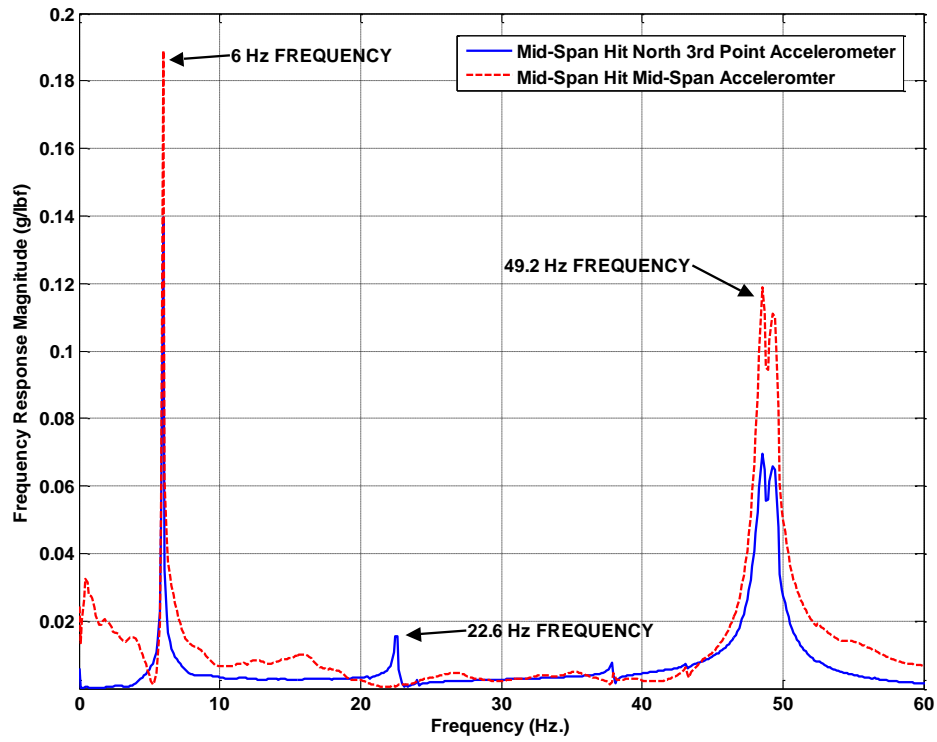


Figure 4.32: Frequency response magnitude for CC-DD Specimen 2 taken from mid-span hit showing north third point and mid-span accelerometer responses

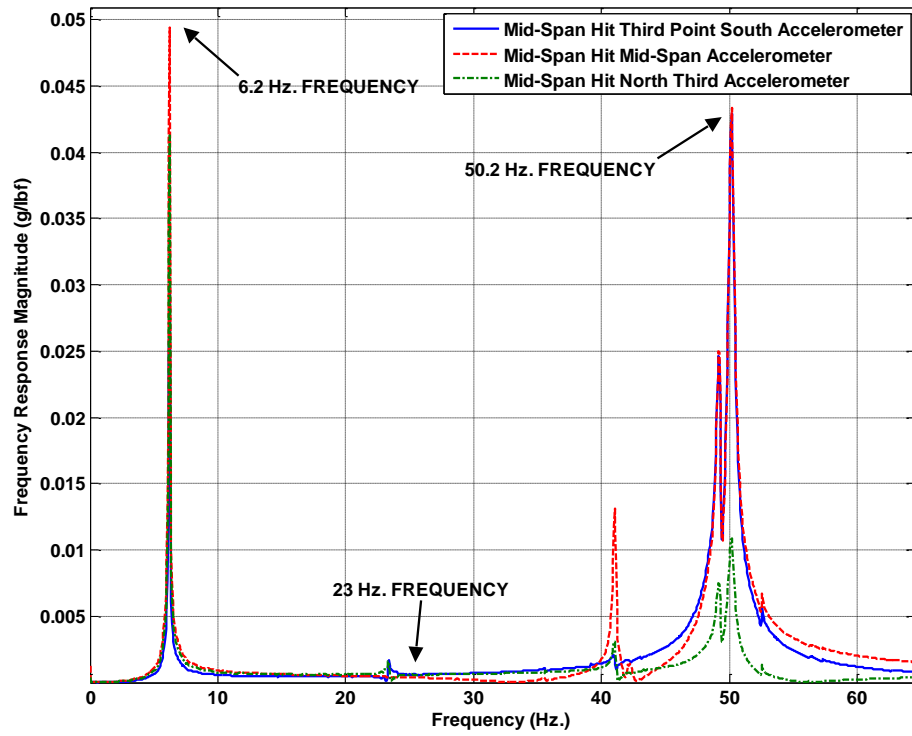


Figure 4.33: Frequency response magnitude for CC-DD Specimen 3 taken from mid-span hit showing north and south third point and mid-span accelerometer responses

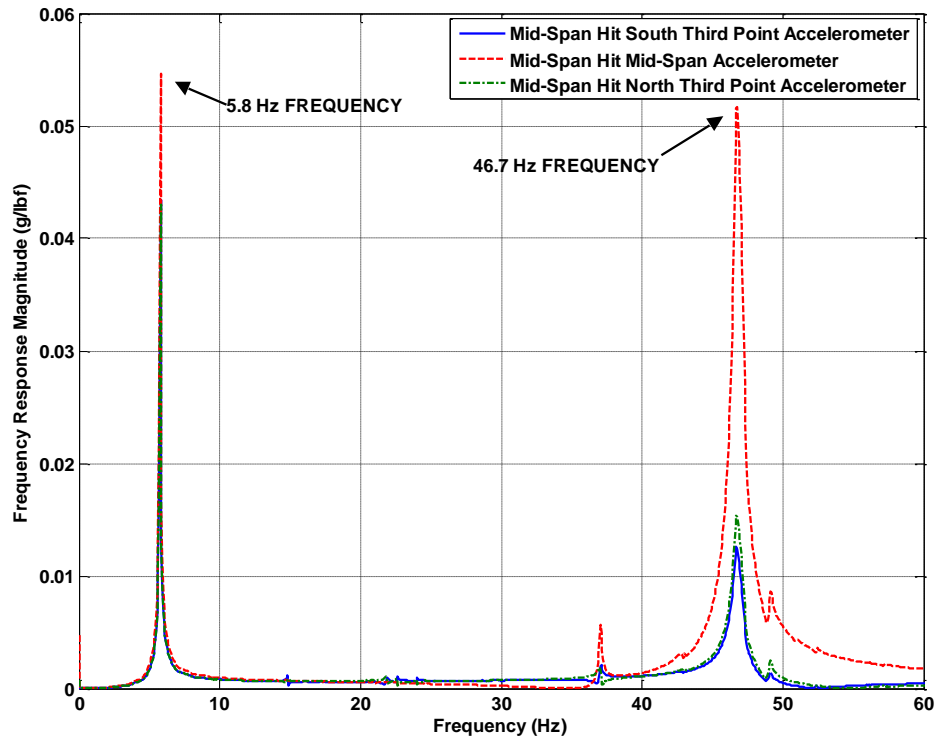


Figure 4.34: Frequency response magnitude for CC-DD Specimen 4 taken from mid-span hit showing north and south third point and mid-span accelerometer responses

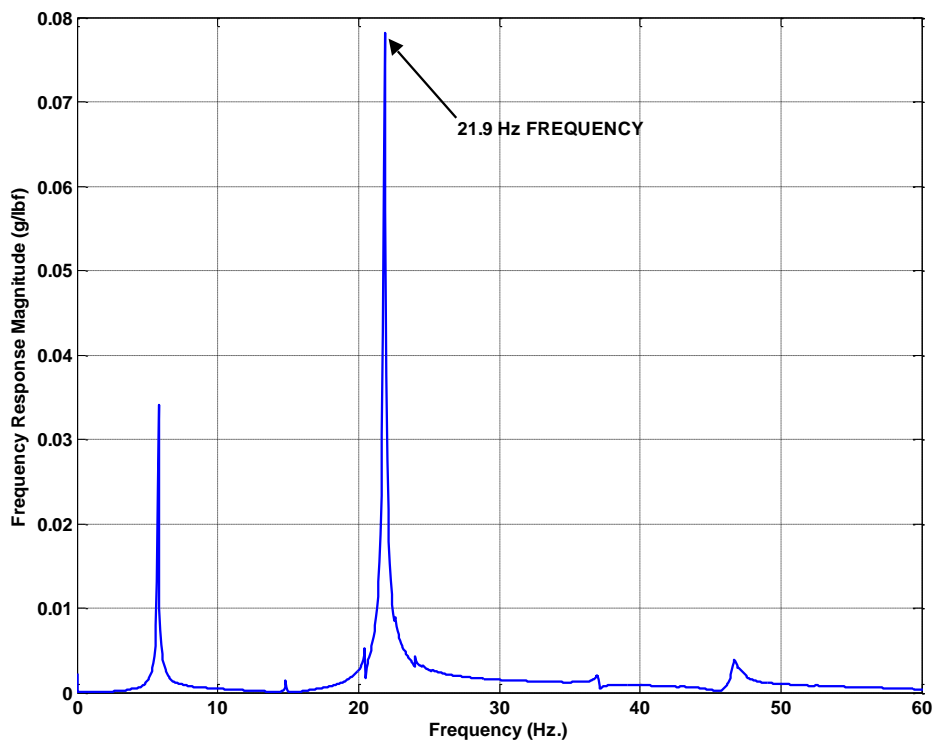


Figure 4.35: Frequency response magnitude for CC-DD Specimen 4 taken from south third span hit showing south third point accelerometer response to show second bending mode frequency

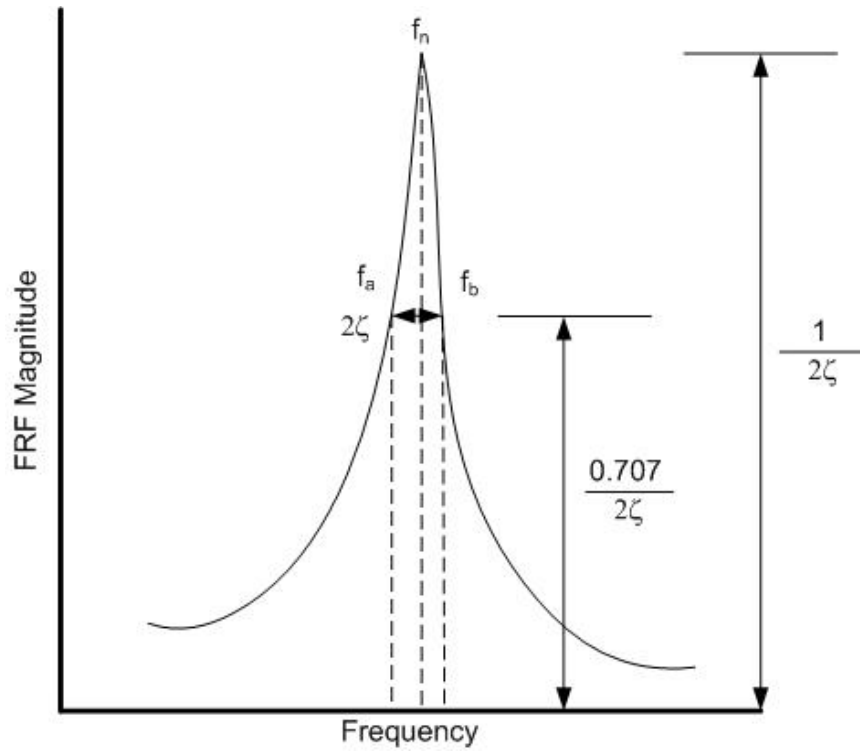


Figure 4.36: Illustration of estimating damping with half-power method

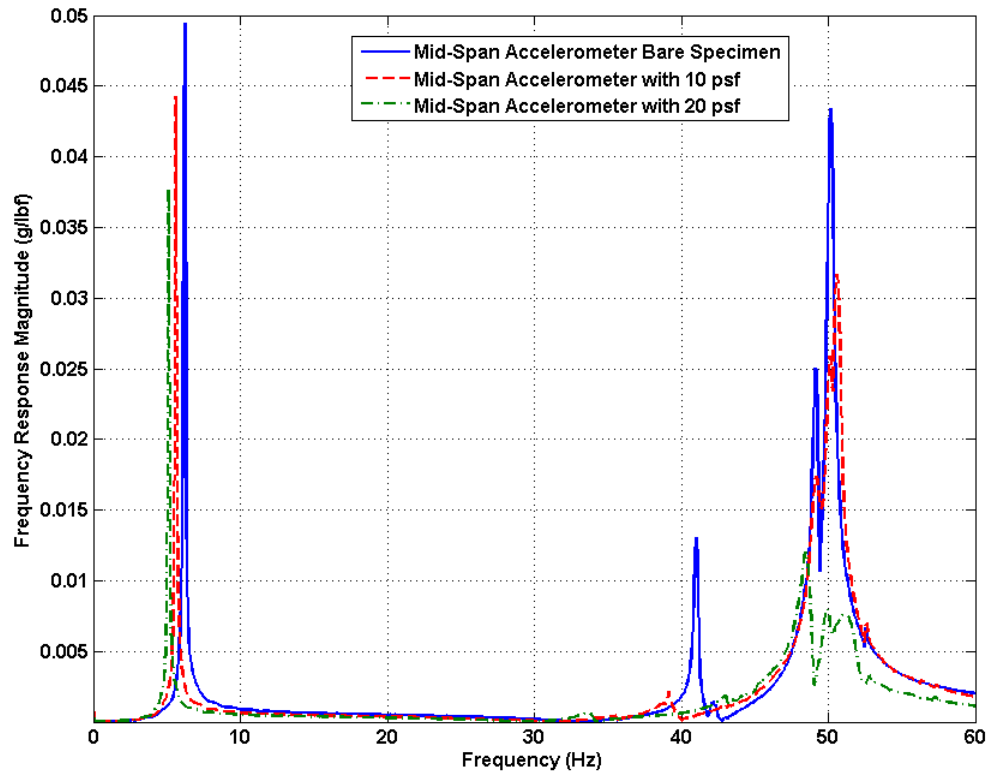


Figure 4.37: FRFs for CC-DD Specimen 3 with: (a) no loads, (b) 10 psf equivalent loading, and (c) 20 psf equivalent loading

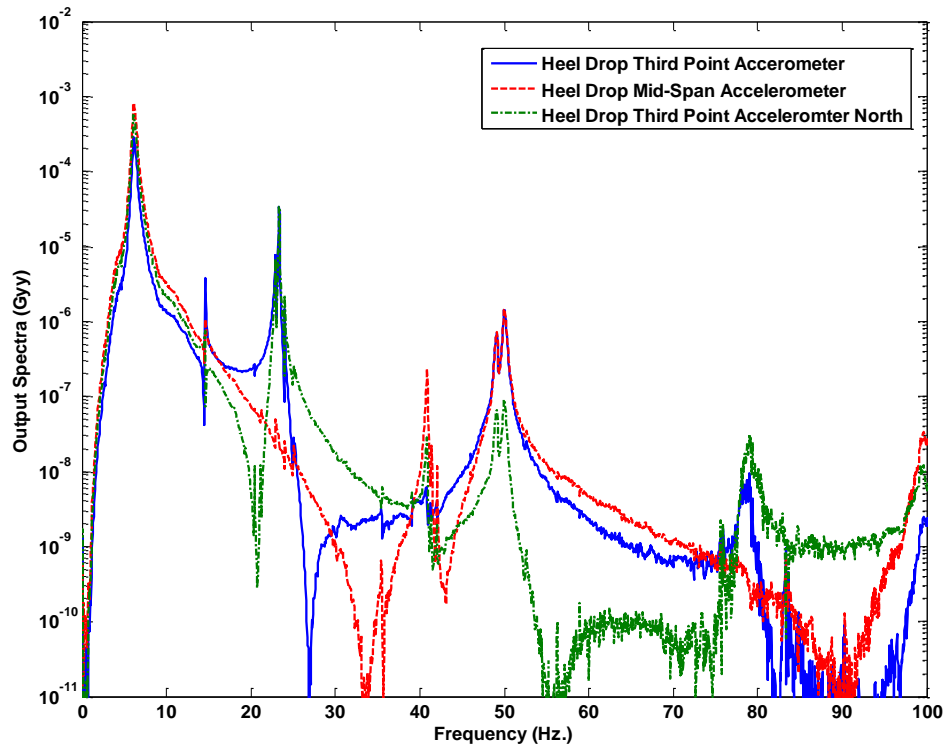


Figure 4.38: Output Spectra for CC-DD Specimen 3 resulting from heel drops (y-axis is log scale)

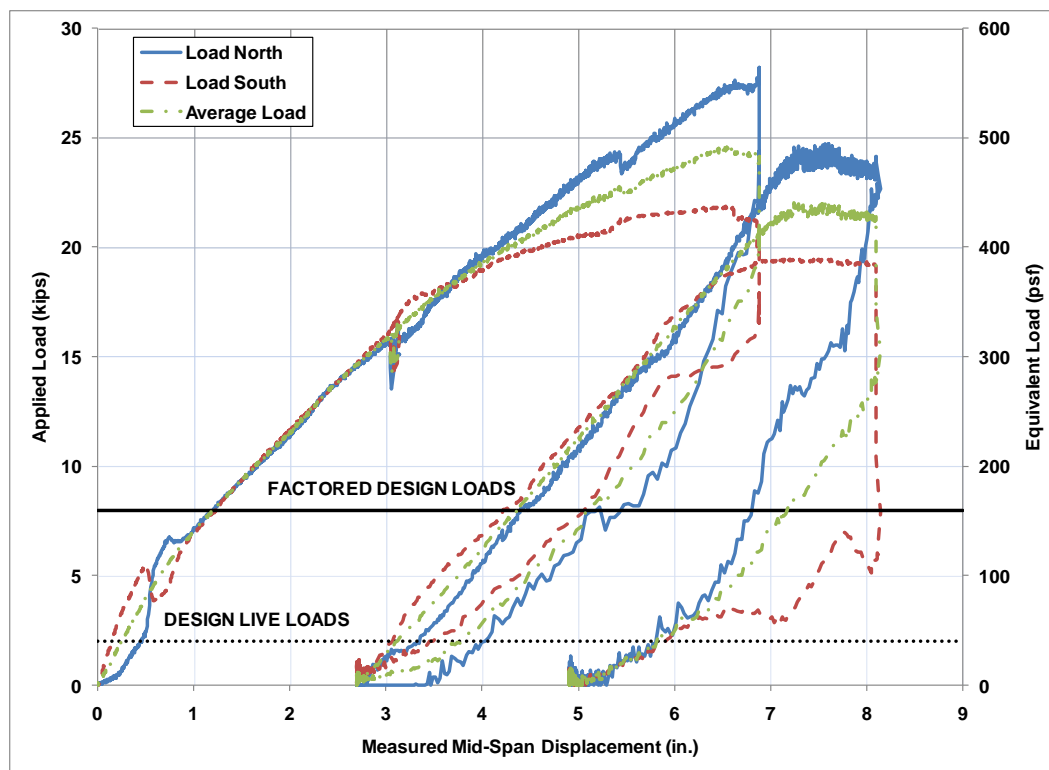


Figure 4.39: Load vs. mid-span displacement plot for CC-DD Specimen 1

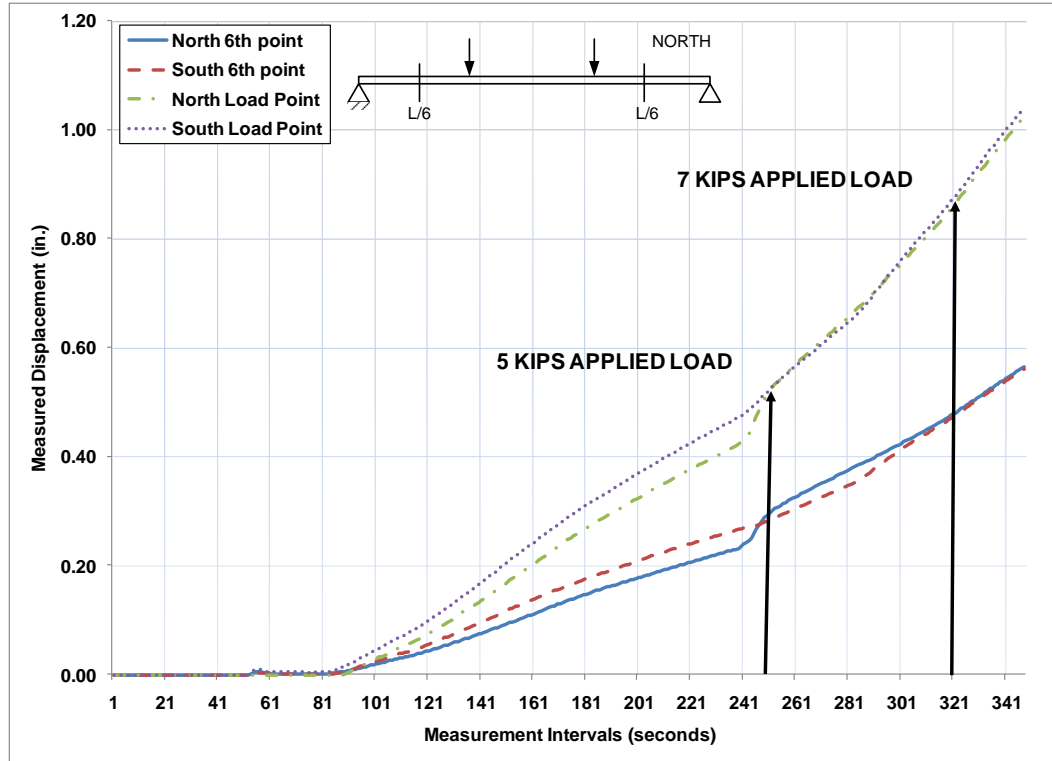


Figure 4.40: Displacement vs. time plot for north and south sensors at 6th and load points over first 350 seconds – Specimen 1

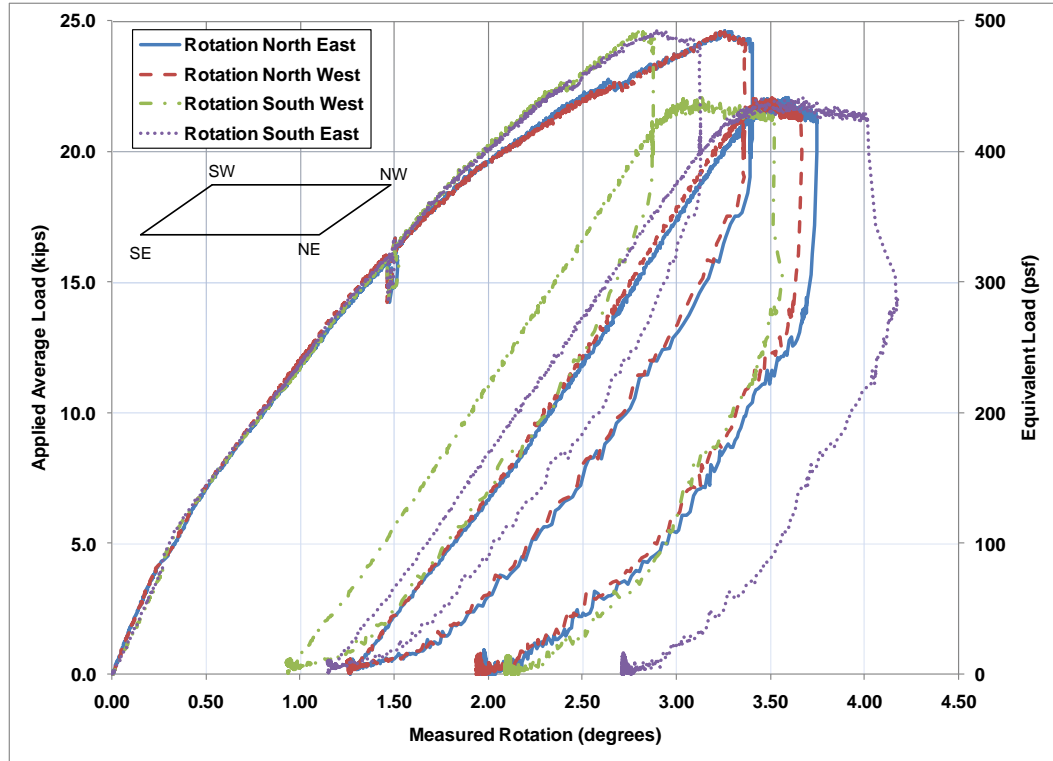


Figure 4.41: Average load vs. measured rotation plot



Figure 4.42: Specimen 1 with approximately 6 in. of deflection at mid-span and 23 kips of load applied at each load point (load cycle 1)

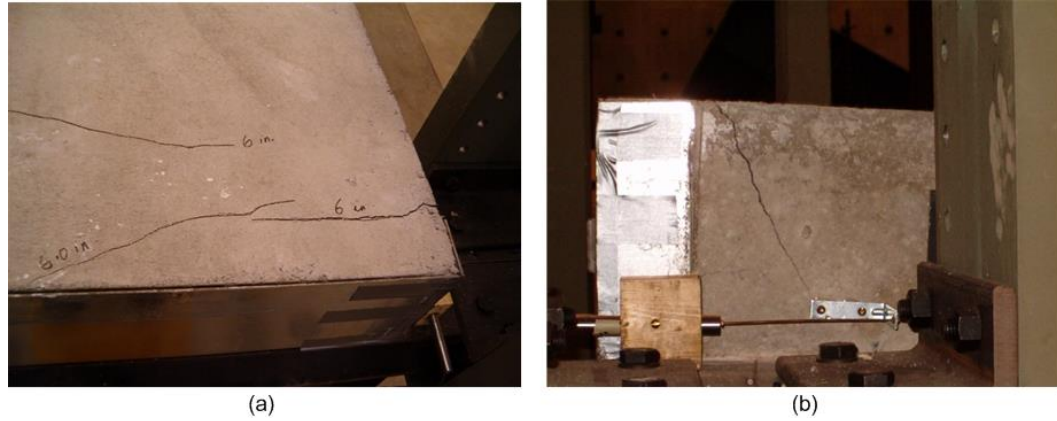


Figure 4.43: Cracks that formed at south support (a) top view and (b) side view



Figure 4.44: Close-up of southeast support crack during re-loading of Specimen 1

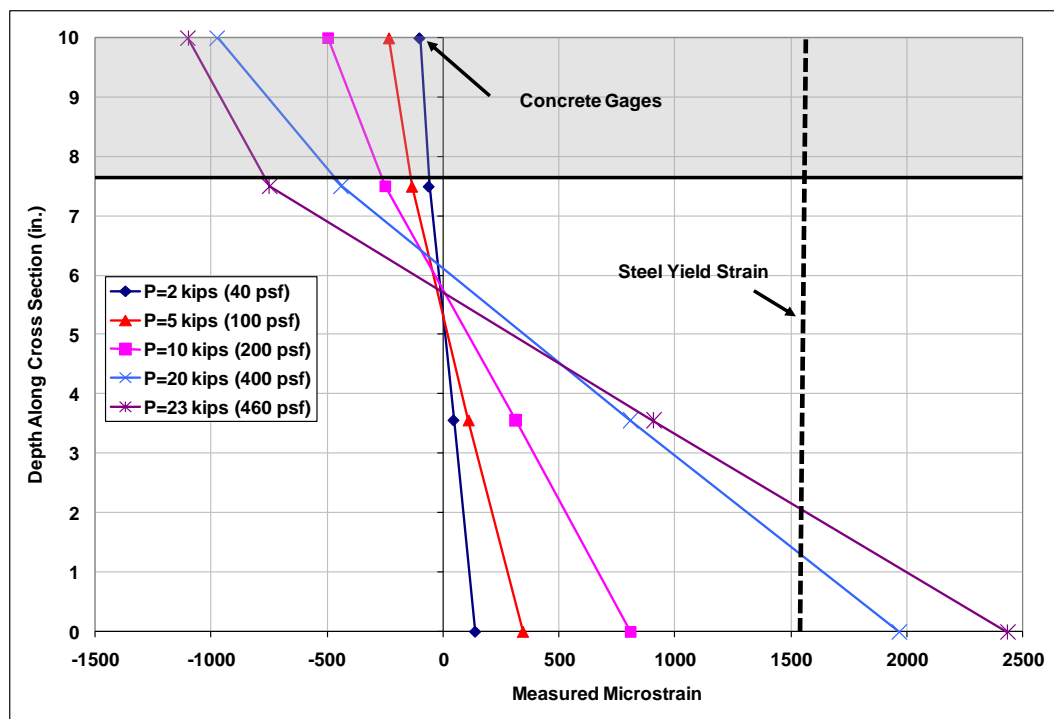


Figure 4.45: Specimen 1 strain gage profiles through depth at mid-span for various load levels

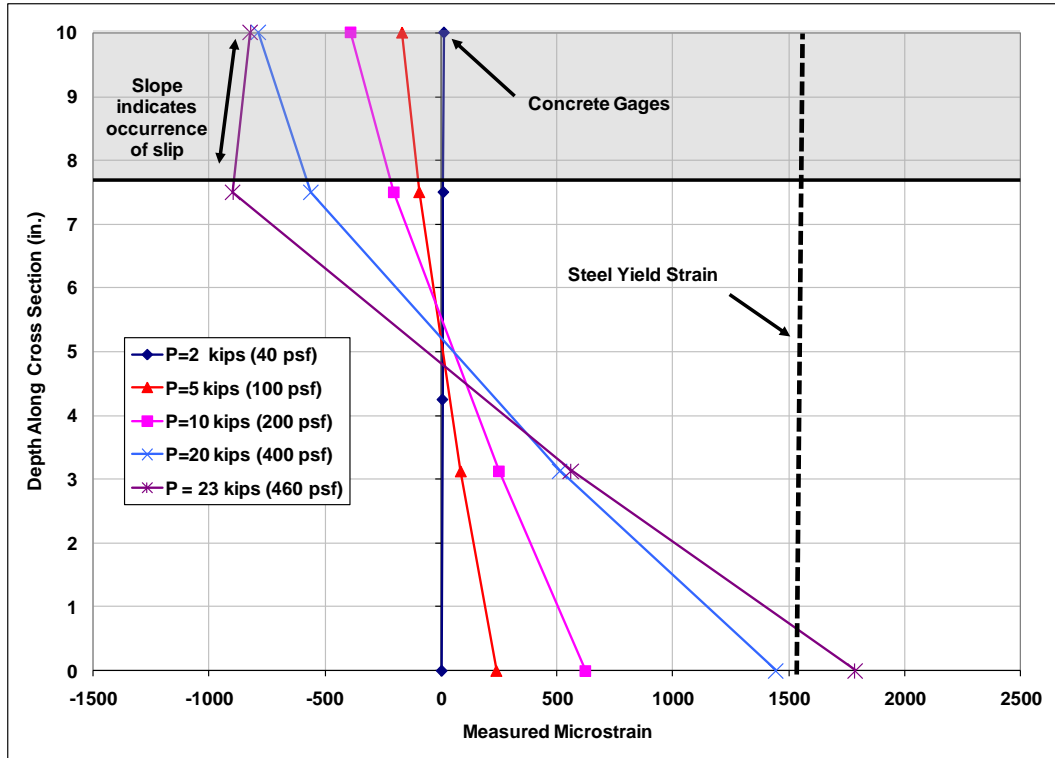


Figure 4.46: Specimen 1 strain gage profiles through depth at south end for various load levels

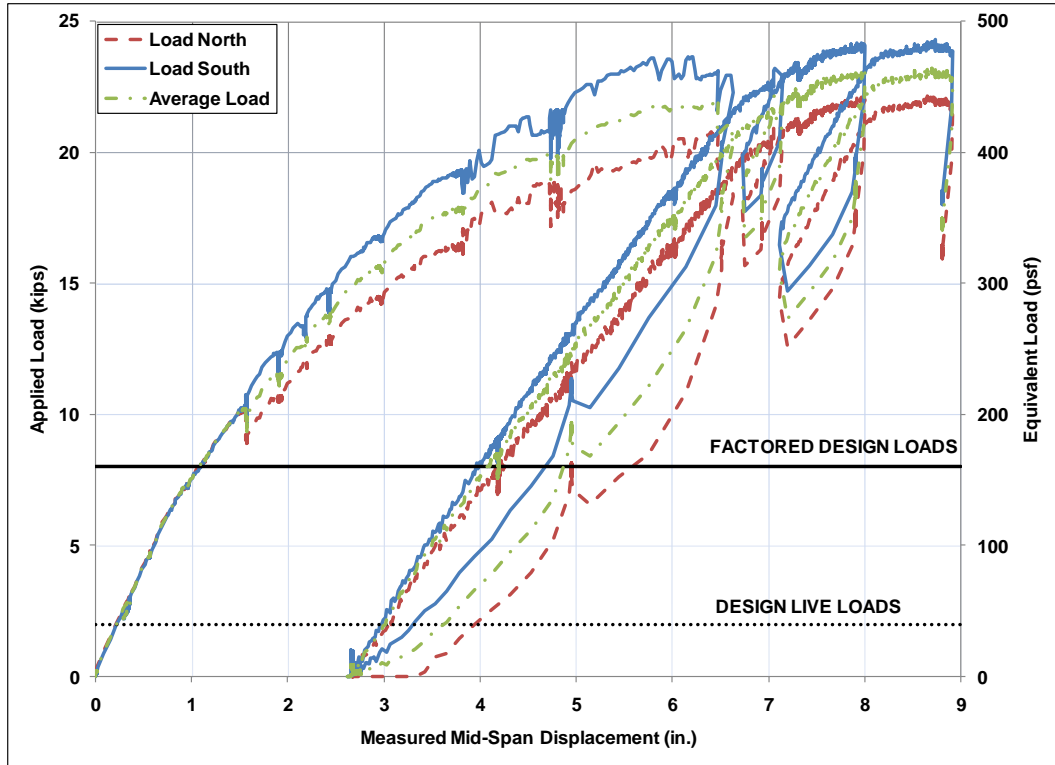


Figure 4.47: Load vs. mid-span displacement plot for CC-DD Specimen 2



Figure 4.48: Crack the formed over north support of Specimen 2



Figure 4.49: CC-DD Specimen 2 with approximately 8 in. of deflection at mid-span and 23 kips of load applied at each load point

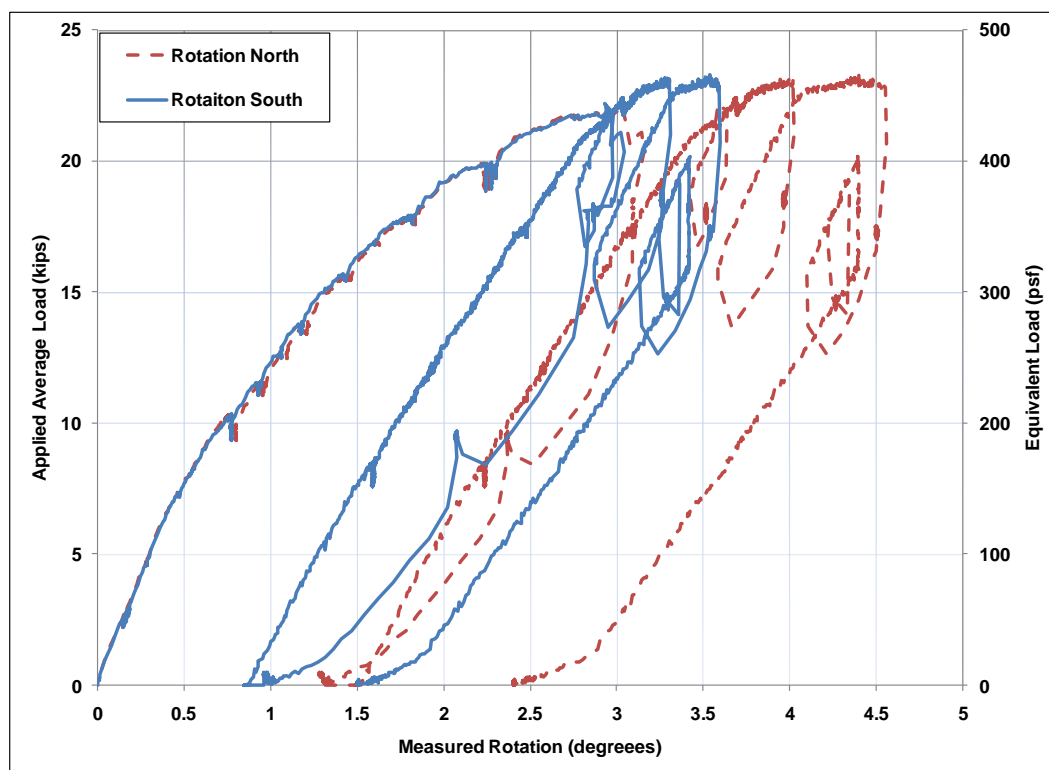


Figure 4.50: Applied average load vs. measured end rotations for CC-DD Specimen 2

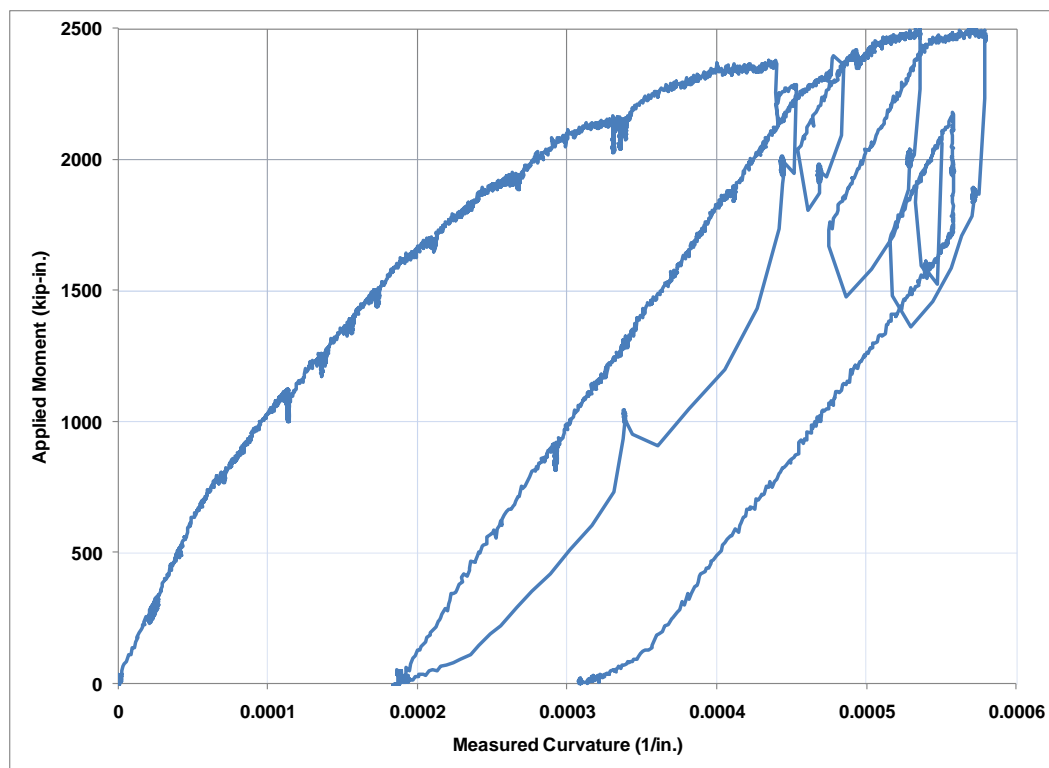


Figure 4.51: Mid-Span moment vs. average curvature of CC-DD Specimen 2

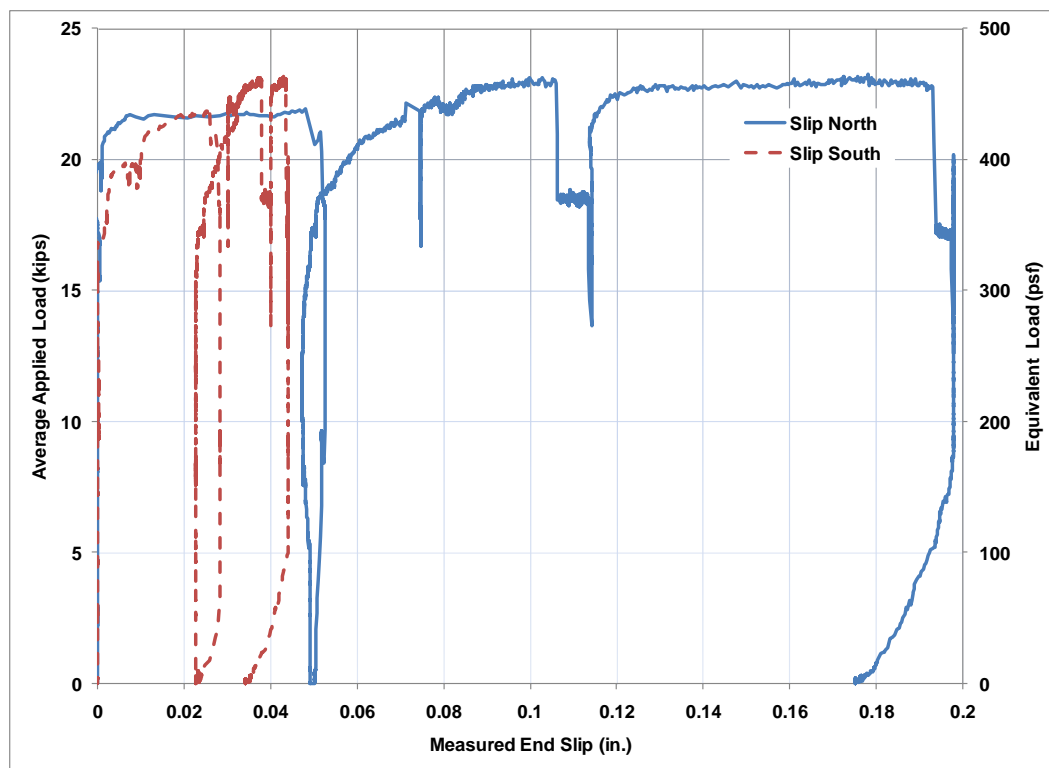


Figure 4.52: Average applied load vs. measured end slip for CC-DD Specimen 2

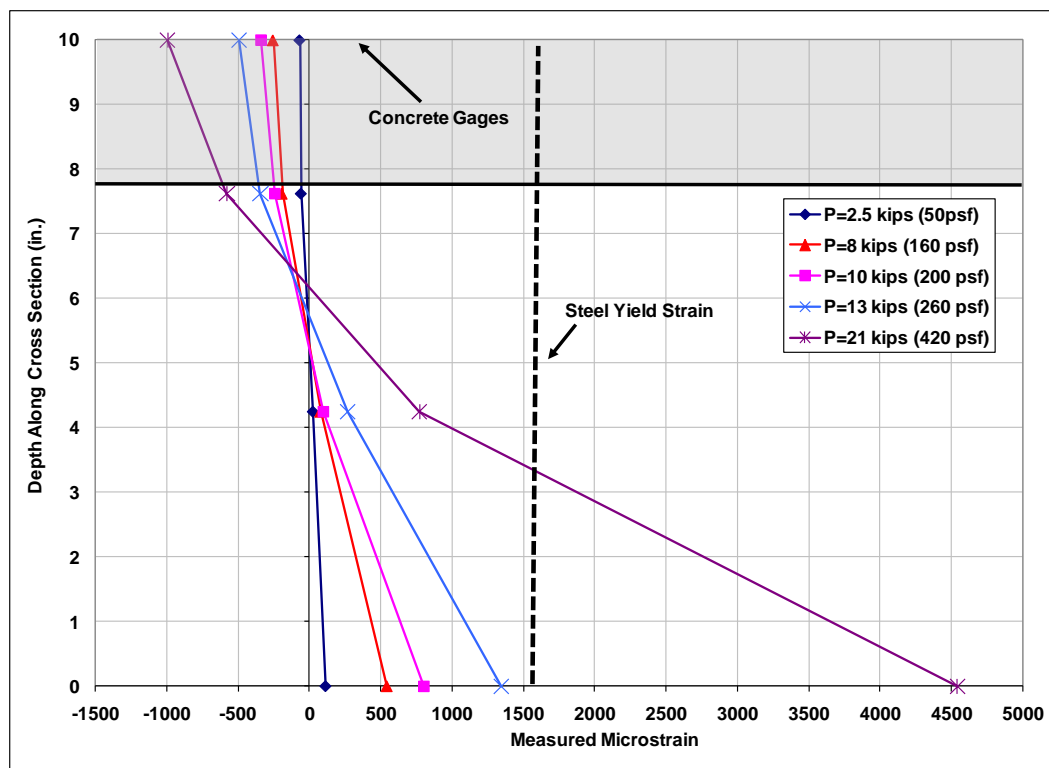


Figure 4.53: CC-DD Specimen 2 strain gage profiles through depth at mid-span for various load levels

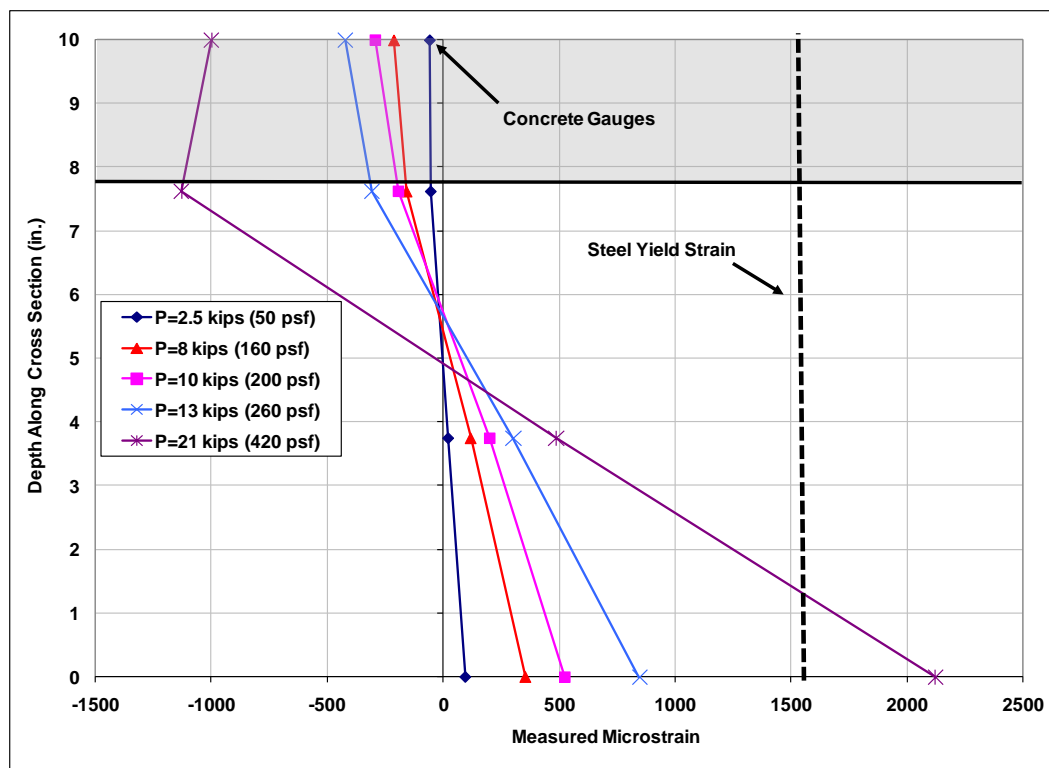


Figure 4.54: CC-DD Specimen 2 strain gage profiles through depth at north load point for various load levels

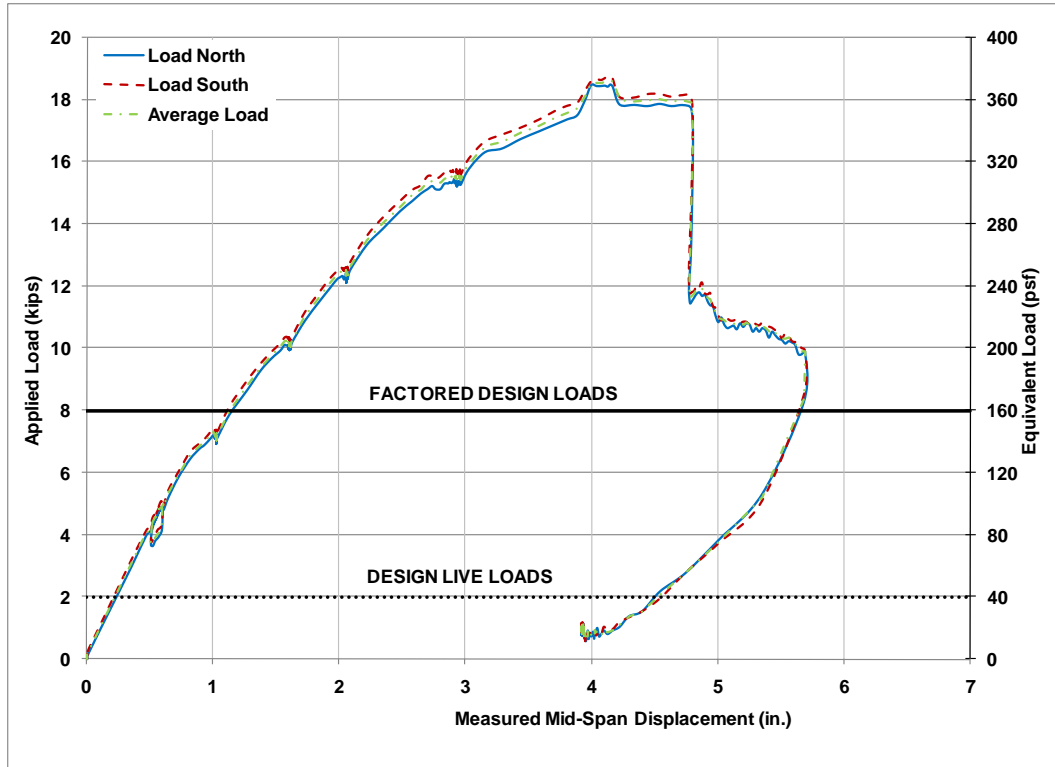


Figure 4.55: Load vs. mid-span deflection plot for CC-DD Specimen 3

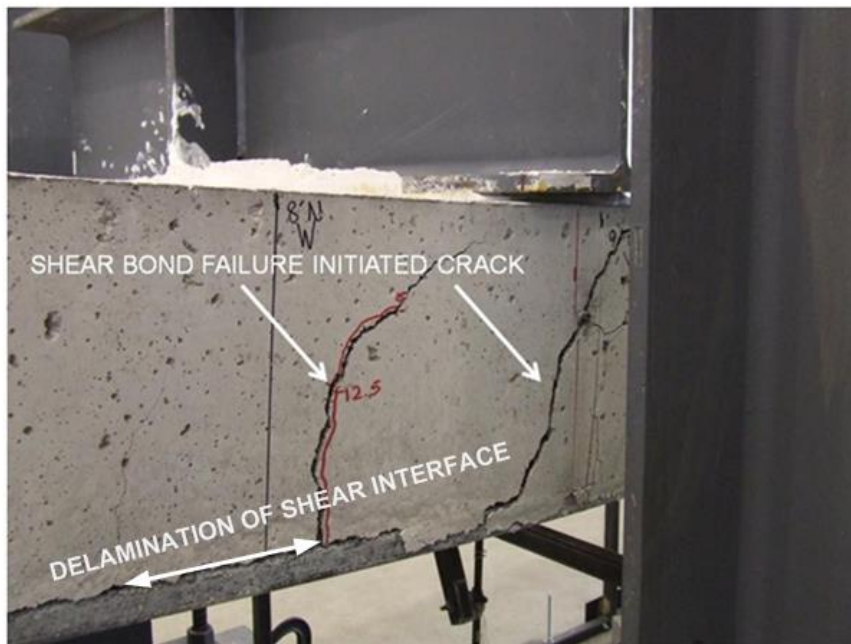


Figure 4.56: Shear bond failure crack that formed on CC-DD Specimen 3



Figure 4.57: Propagation of shear bond failure to north end

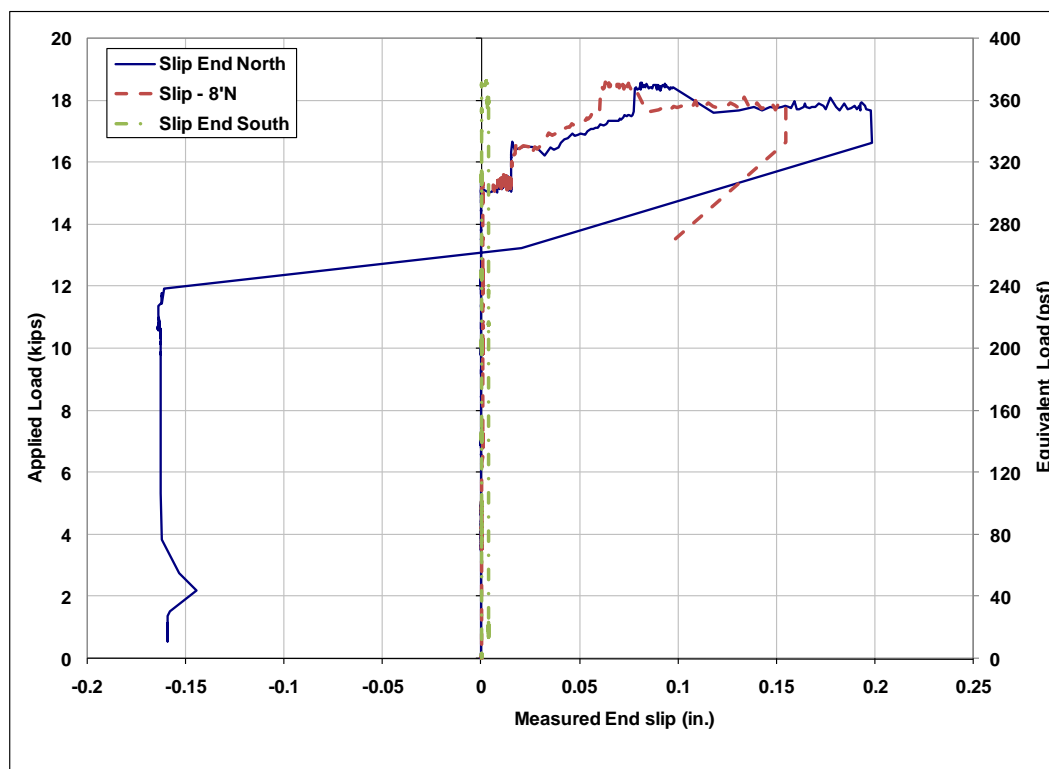


Figure 4.58: Average load vs. measured slip for CC-DD Specimen 3

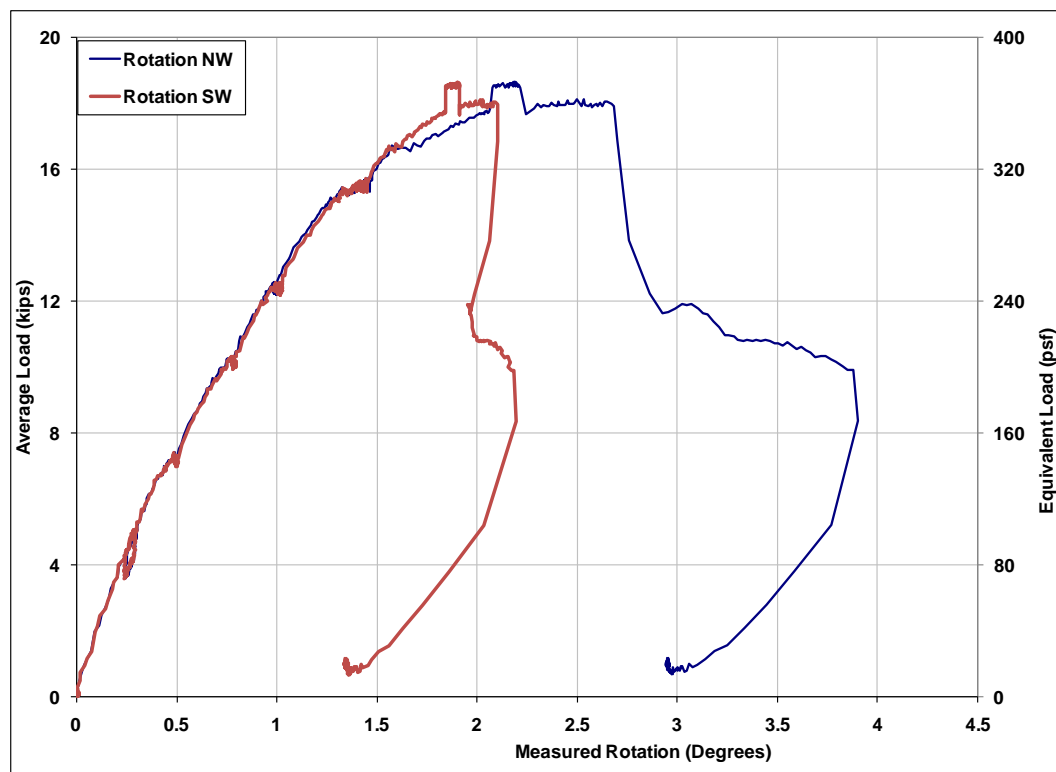


Figure 4.59: Average load vs. measured end rotations for CC-DD Specimen 3

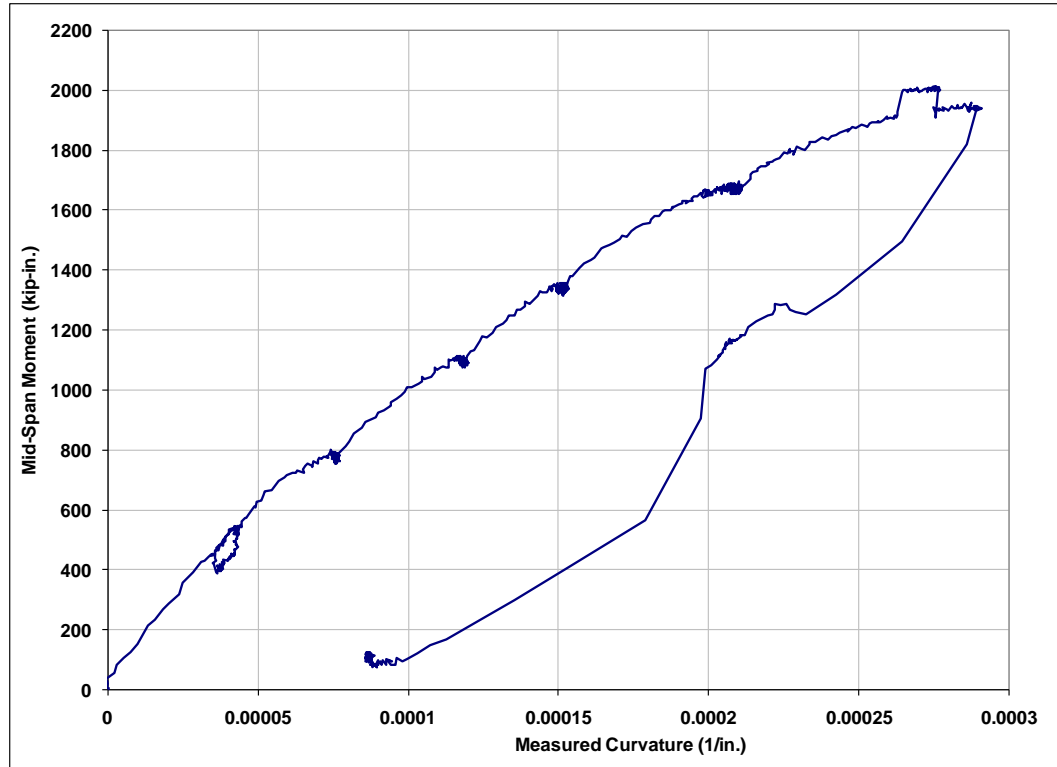


Figure 4.60: Mid-Span moment vs. average curvature of CC-DD Specimen 3

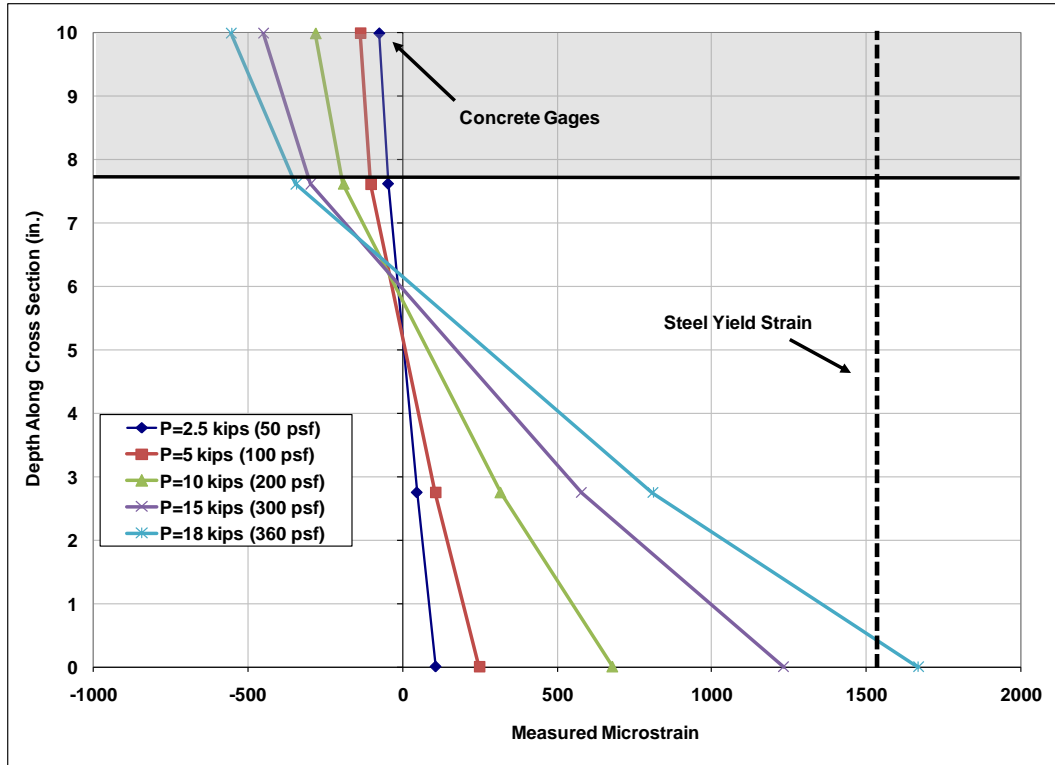


Figure 4.61: CC-DD Specimen 3 strain gage profiles through depth at mid-span for various load levels

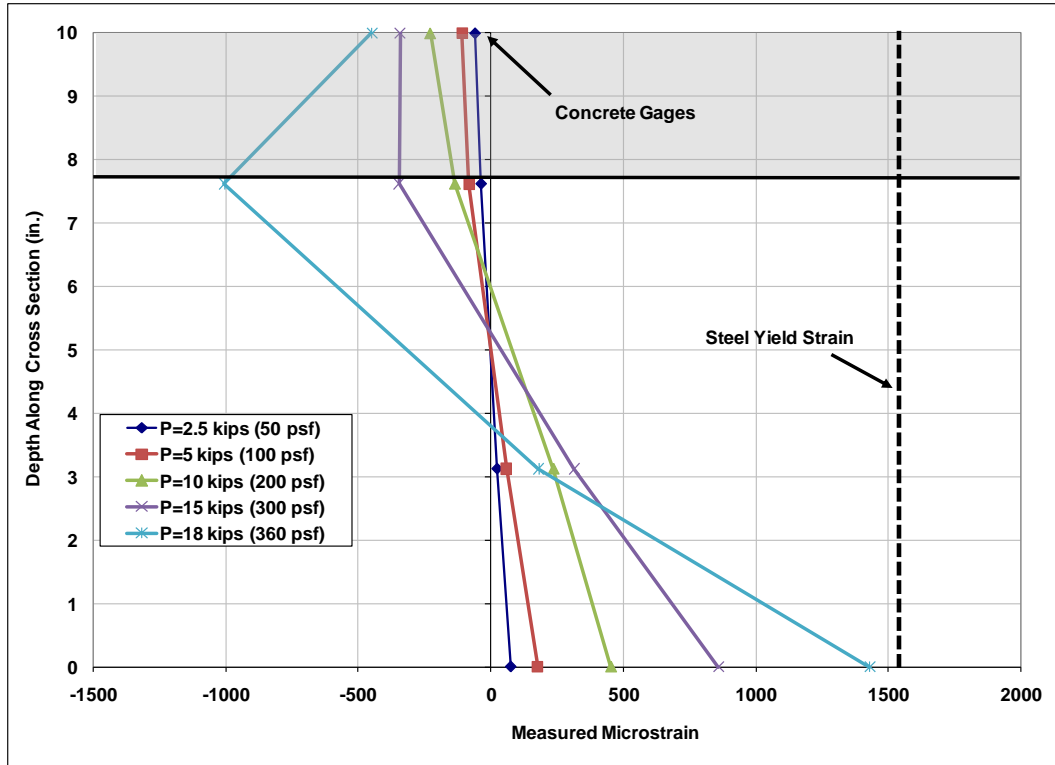


Figure 4.62: CC-DD Specimen 3 strain gage profile through depth at north end for various load levels

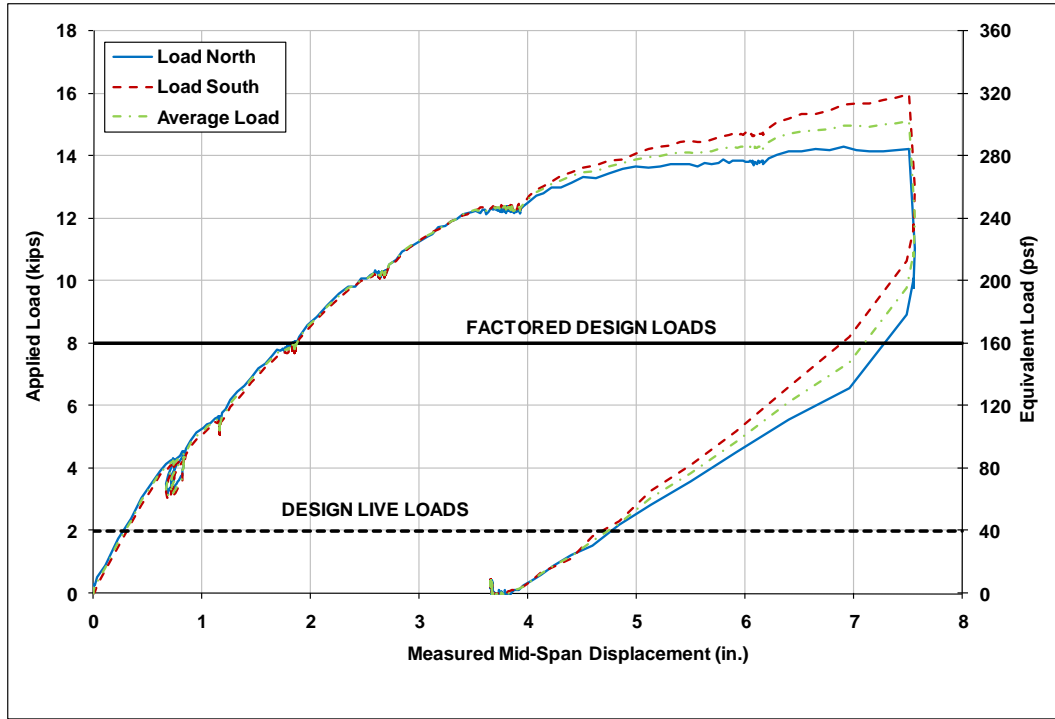


Figure 4.63: Load vs. mid-span displacement plot for CC-DD Specimen 4



Figure 4.64: Picture of crack that formed at south support

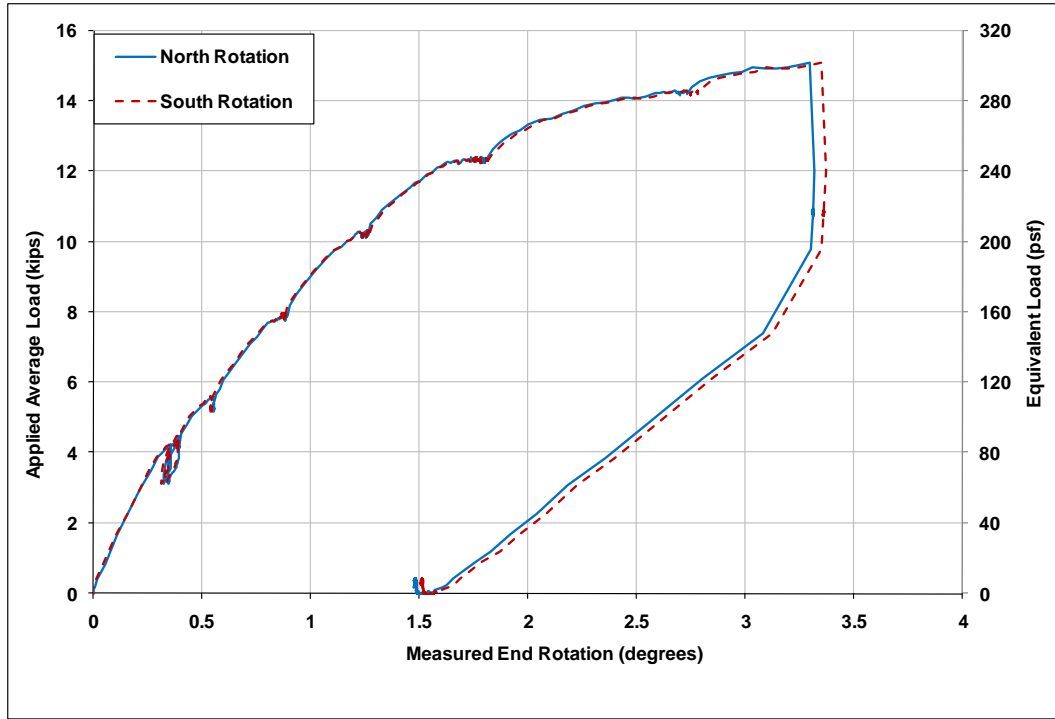


Figure 4.65: Applied average load vs. measured end rotations for CC-DD Specimen 4

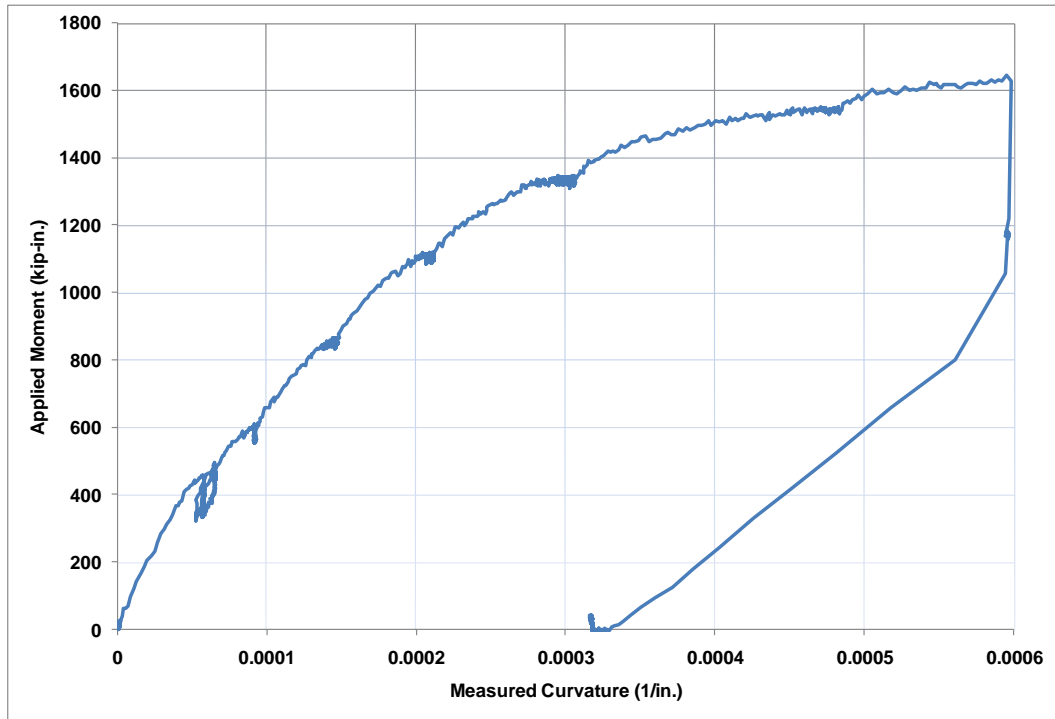


Figure 4.66: Mid-Span moment vs. average curvature of CC-DD Specimen 4

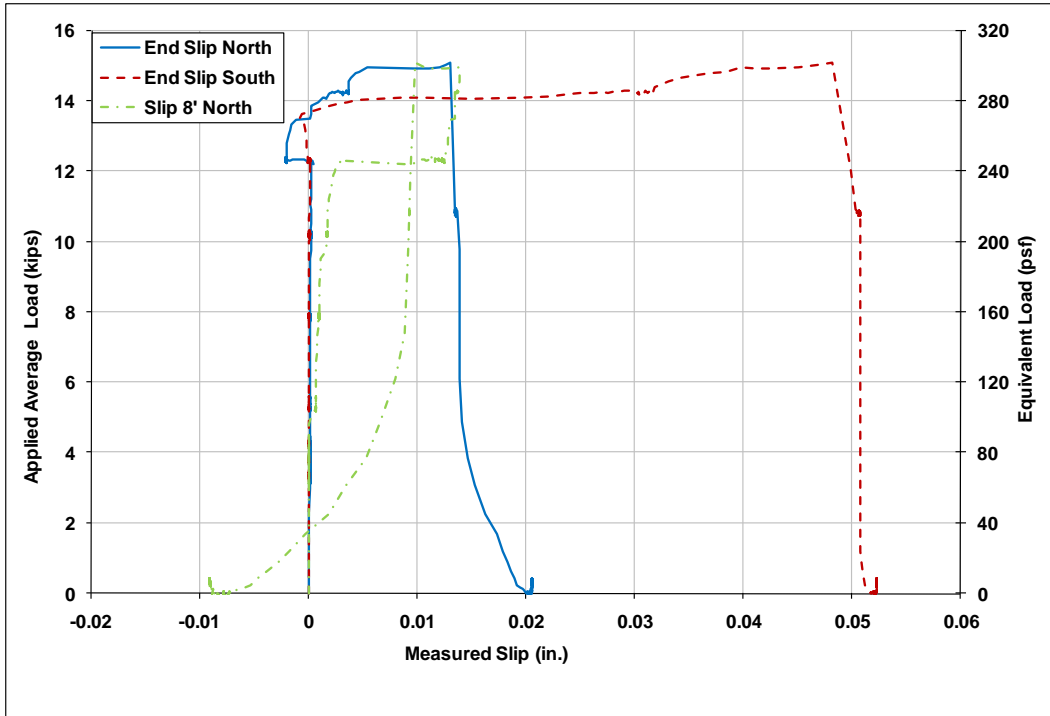


Figure 4.67: Applied average load vs. measured slip plot

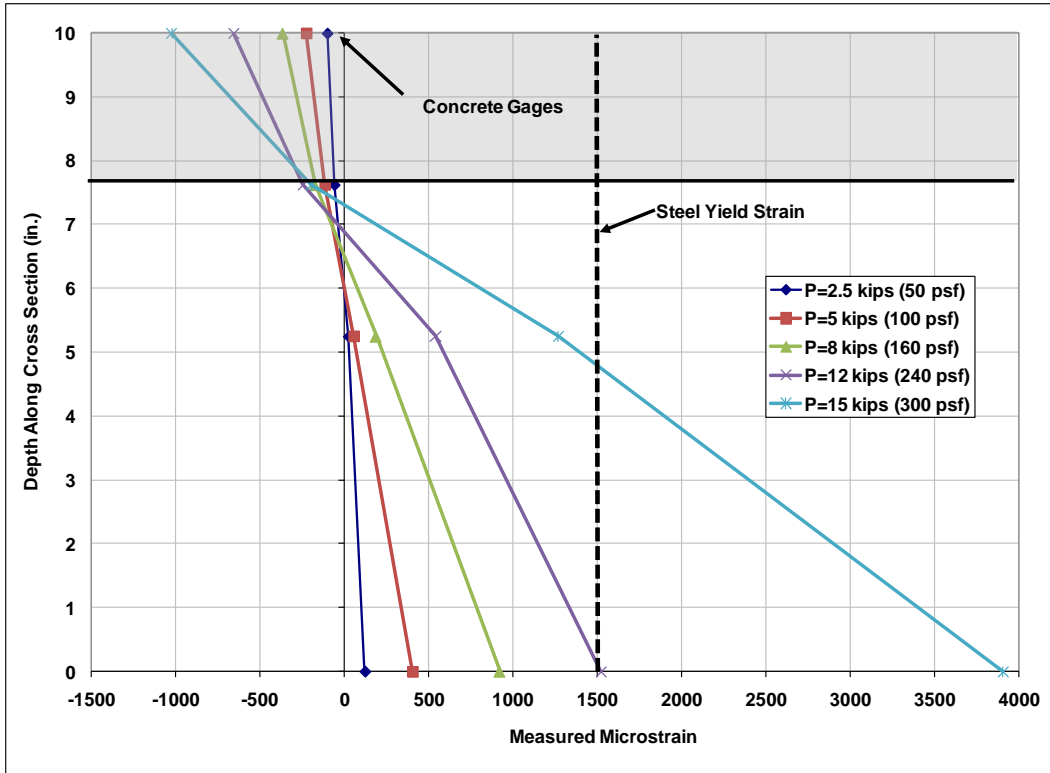


Figure 4.68: CC-DD Specimen 4 strain gage profile through depth at mid-span for various load levels

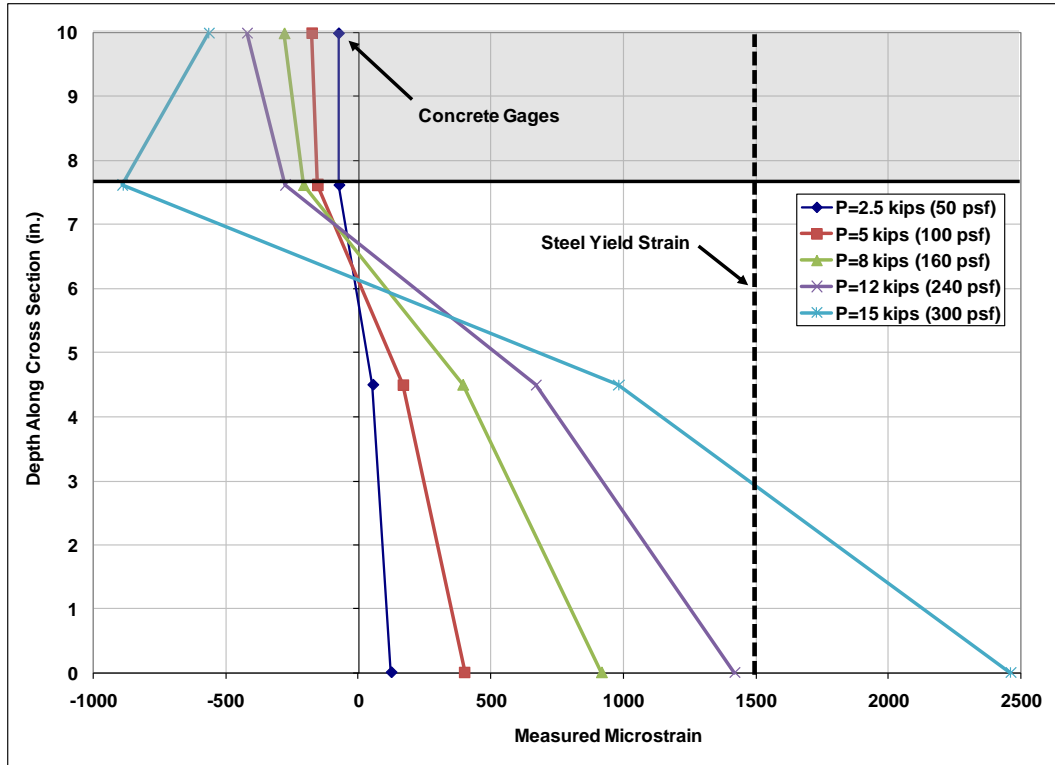


Figure 4.69: CC-DD Specimen 4 strain gage profile through depth at north end for various load levels

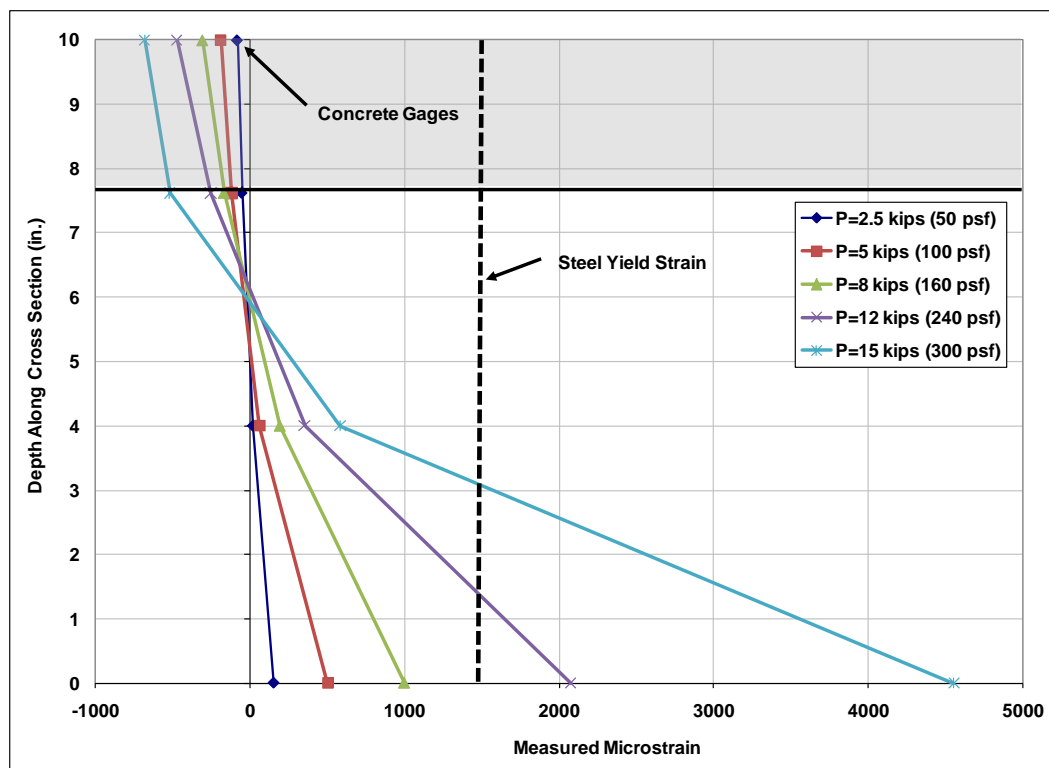


Figure 4.70: CC-DD Specimen 4 strain gage profile through depth at south end for various load levels

CHAPTER 5. ELEVATED TEMPERATURE TESTING OF CC-DD SPECIMENS

This chapter focuses on evaluating the thermal and structural behavior of a CC-DD floor system subjected to temperatures according to the ASTM E119 (ASTM, 2000) temperature-time ($T-t$) curve. The thermal behavior was evaluated by subjecting short (48 in.) spans of the CC-DD Specimens to heating, following the E119 $T-t$ curve from the underside. The heat transfer through the composite CC-DD Specimen was measured using thermocouples that were attached to the steel deck and embedded within the concrete. The thermal behavior is presented in Section 5.2. The structural behavior was evaluated by subjecting a long (240 in.) span of the CC-DD Specimen to combined service level structural loading and heating following the E119 $T-t$ curve from the underside. The thermal and structural behavior of the long span specimen was measured and is presented in Section 5.4.

5.1. Test Setup for Heat Transfer Tests

Figure 5.1 shows a schematic of the test setup used to conduct the heat transfer tests. As shown, the setup consisted of two 4 ft (48 in.) long slab specimens that were supported by two exterior and one interior W8x35 beam. The CC-DD specimens consisted of a 7.5 in. deep cellular deck with 2.5 in. of lightweight concrete on top. The cellular deep deck consisted of a 14 gage, 7.5 in. deep deck friction welded to a 16 gage bottom plate, which was presented earlier and used for CC-DD Specimen 1-3 in Chapter 4. The CC-DD specimens were connected to the supporting beams using shear studs similar to the CC-DD Specimens 1 and 2 in Chapter 4.

One of the slab specimens had fire protection, while the other one did not. The fire protection consisted of 1 in. thick autoclaved aerated concrete (AAC) tiles that were attached to the bottom plate of the CC-DD Specimen. The 1 in. thick AAC tiles have a reported thermal conductivity (k) of 0.14 watts/meter*Kelvin (W/mk) (Tanner, 2003), and hence were equivalent to a 3/8 in. thick layer of spray applied fire resistant material (SFRM), that has a reported k of 0.043 W/mK at 24°C (Cafco International, 2004). AAC tiles were selected to provide fire protection because they provide excellent acoustic or sound dampening, were easy to install using screws, provide for a ceiling finish, and have low self weight with a reported density of 40 pcf (3 psf for 1 in. thick panels).

Type K thermocouples were placed at various locations in the cross-section for measuring temperatures. The thermocouples used were model number CHAL-032-BW manufactured by Omega Inc. The thermocouples were rated up to 1200°C and thus intended for high temperature applications. For both specimens (i.e., with and without fire protection), the type-K thermocouples were placed on the exposed underside of the

bottom steel plate, and top, web, and bottom (over-side) of the steel deck, and the top surface of the concrete slab. For the specimen with fire protection, thermocouples were also attached to the exposed underside of the 1 in. thick AAC tiles. All the thermocouples were placed at the section between the ends (i.e. 2 ft in). The thermocouple locations were based on the E119 standard fire test.

The specimens were subjected to heating from the underside only. This is recommended by E119 for the standard fire test. It simulates the effect of the floor system being the ceiling of a fire compartment. The remaining surfaces of the specimens were exposed to ambient (open air) conditions. The heating was applied using radiant heater panels that have to be located very close (within 1 in. or less) from the surface (i.e. bottom plate) being heated. The heaters were controlled to subject the exposed surface of the specimens (bottom plate for the unprotected specimen, and the AAC tile surface of the fire protected specimen) to the E119 $T-t$ curve. The description of radiant heater panels are presented in (Booth et al 2008) and beyond the scope of this dissertation.

5.2. Heat Transfer Test Results

Figure 5.3 and Figure 5.4 shows the temperatures measured by the thermocouples at the mid-span section (2 ft from either support). Figure 5.3 shows the temperature measured for the specimen without fire protection, and Figure 5.4 shows the temperature for the specimen with fire protection. As shown in Figure 5.3, the bottom steel plate was initially being heated very close to the E119 $T-t$ curve. However at approximately 325°C, the bottom plate buckled due to the elevated temperatures and restraints. The wave-type buckling mode shown in Figure 5.5 caused portions of the bottom plate to move closer to the heater panel, and other portions to move away. The heater panels were moved away from the bottom plate to prevent contact that would have caused a short circuit. As the distance between the heater surface and the bottom plate had to be increased the heating became inefficient and the bottom steel plate temperature could not be increased to follow the E119 $T-t$ curve. As shown in Figure 5.3, after two hours of heating, the bottom plate temperature reached a maximum value of 740 °C. The maximum temperature of the bottom deck in contact with the concrete was equal to 650°C. The temperature profiles of the remaining points (points 3, 4, and 5 shown in the figure) are also included in the figure. As shown, the maximum temperature of the deck top (point 4) was 300°C and the maximum temperature of the concrete was equal to 80°C. These temperature profiles indicate that the bottom steel plate acts as a sacrificial layer between the CC-DD system and heating. It provides some fire protection and reduces the temperature of the deck top and concrete slab significantly. The temperatures are reduced further by the depth of the concrete slab (10 in. in the ribs) and the 7.5 in. deep air gap between the bottom plate and deck top. Figure 5.6 shows some cracking at the top of the concrete slab and moisture evaporating after 2 hours of heating.

Figure 5.4 shows the temperatures of the specimen with fire protection. As shown, the fire protection surface was heated to follow the E119 $T-t$ curve very closely. The apparent differences are caused by the fact that the E119 is a gas phase (air) $T-t$ curve, while the measured is a solid surface temperature. As shown in Figure 5.4 the maximum temperature measured anywhere within the cross-section after 3 hours of heating was less

then 300°C (approximately). The temperatures of the deck top and concrete slab were even lower. Since the temperature of the bottom plate did not increase beyond 300°C, there was not local buckling of the bottom plate, and the heating methodology worked successfully as designed.

5.3. Summary of Findings

Both the specimens with and without fire protection performed well under thermal loading. The behavior of the specimen with fire protection was excellent even after 3 hours of heating. The 1 in. thick AAC tiles are recommended for fire protection of CC-DD and comparable systems particularly the deep deck systems without a bottom plate. The AAC tiles will provide a finished ceiling and some of the other advantages mentioned earlier.

The behavior of the specimens without fire protection was also quite good after two hours of heating. The concrete slab temperature on top (unheated side) was less than 80°C after two hours of heating, which meets the thermal limits required by the ASTM E119 Standard test. Some minor cracking of concrete and moisture migration and evaporation from the cracks was observed. But, the temperatures were quite low (less than 80°C) compared to the E119 limit of 250°C for unrestrained ratings.

5.4. Combined Thermal and Mechanical Loading Behavior of CC-DD Specimen

The thermal and structural behavior of the CC-DD floor system subjected to the combined effects of mechanical and fire loading was experimentally investigated. The goals of this test were to: (1) demonstrate a new testing methodology for conducting elevated temperature (fire) tests of long span floor systems, and (2) to develop insight into the elevated temperature behavior of the CC-DD specimens. The previously described radiant heater panels were used to perform the elevated temperature tests, thus eliminating the need for a large gas-based furnace. Radiant heater panels were used to apply the standard ASTM E119 *T-t* curve to the exposed underside of a CC-DD specimen. Additionally, the specimen was subjected to a concentrated loading at mid-span that was equivalent to the nominal service loads. The following sub-sections describe the test setup for conducting the combined thermal-structural tests, the experimental results, and the final discussion of the results.

5.4.1. Test Setup

This section describes the test setup for conducting the combined heating and mechanical load testing. The CC-DD specimen was a 7.5 in. deep cellular deck profile with 2.5 in. of concrete cover on top, providing an overall depth of 10 in. The CC-DD profile consisted of an 18 gage steel deck with a 20 gage bottom plate thickness. This is the same profile that was specified for CC-DD Specimen 4. Only a 2 ft width of the CC-DD profile was used in the test. The length of the CC-DD specimen was equal to 20 ft.

Figure 5.7 shows a top view schematic of the test setup. As shown, the specimen was heated using six radiant heater panels. These panels were attached to the specimen using a specially design fixture, the discussion of which is beyond the scope. Figure 5.8 shows a photograph of the overall specimen with heaters attached and load frame in place. The specimen had no fire protection attached, similar to the first heat transfer specimen

Loading Fixture and Displacement Sensors

The loading fixture consisted of the setup shown in Figure 5.9. As shown, the loading fixture consisted of a W4x13 steel beam that was attached to a base fixture using two 1 in. diameter threaded rods. The base fixture was attached to the laboratory strong floor using two 1 in. diameter threaded rods. A 10-ton hydraulic ram was placed between the specimen and the loading fixture as shown in Figure 5.9. Figure 5.8 shows a photograph of the overall specimen with the loading frame in place and heaters attached. The loading fixture was used to apply concentrated loading at mid-span. Concentrated loading was applied at the mid-span to provide minimal interference with the heater frames. The applied concentrated load was 1.2 kips, which is equivalent to 60 psf distributed loading (40 psf live load plus 20 psf dead load).

Vertical displacements were measured at three locations along the length of the specimen, i.e., at the longitudinal third points and the mid-span. Displacement transducers, which were Duncan potentiometers with 10 in. stroke, were used to monitor the south side third point and mid-span displacement, and a 6 in. stroke Duncan potentiometer to measure north side third point displacement. The displacement transducers were attached to custom made steel frames that were mounted to the strong floor and canopied over the specimen. They were attached to the specimen using angle brackets mounted to the top of the slab. This helped in keeping the transducers away from the heated surface. Figure 5.10 shows this setup for the displacements transducers. Clinometers were placed at the ends of the specimen to measure rotations. The clinometers were mounted to a custom made steel fixture mounted to the specimen to avoid heating the sensors. Finally, 1 in. stroke potentiometers were placed at the ends of the specimen to measure the inwards or outward movement of the support beams (longitudinally). These potentiometers were placed at the mid-span of the support beams on the top and bottom flanges.

Heaters and Other Equipment

The radiant heater panels were 16 in. in width and 36 in. in length. They were constructed within specially made metal fixtures to ensure safe operation. The heaters were powered by a diesel generator that ran to a specially constructed control box with capability to control up to 24 heaters. Photographs of both the generator and heater control box are shown in Figure 5.11. The heaters were controlled by measuring the temperature of the surface exposed to heating directly by the panels. Type K thermocouples were used to measure the temperatures of the heated surfaces. One thermocouple was centered over the heating area covered by each radiant heater, and were used to control its performance. The temperatures of the heated surfaces measured by those thermocouples were also stored in the data acquisition system.

Due to the high temperatures being generated during the test, some additional protective measures were also installed. The specimen was surrounded by 1/4 in. thick polycarbonate plastic to protect from possible explosive concrete spalling. Figure 5.12 shows a photograph of the protective polycarbonate sheeting. Finally, mineral wool was placed on the sides of the specimen between the top of the heaters and bottom of the specimen. This was done to reduce heat losses to the surrounding atmosphere.

5.4.2. Experimental Results – Combined Heating and Loading Test

The combined heating and load testing on the CC-DD Specimen proved to be very challenging. Ensuring that the sensors were reading properly and monitoring the specimen while applying extreme heating involved caution and attention. The experiment was conducted in two separate heating cycles due to some problems that occurred while loading the specimen. After approximately 50 minutes of heating in the first cycle, the hydraulic pump malfunctioned and did not allow for any loading to be added or released into the system. This led to difficulties in maintaining constant loading on the specimen. As a result, the heating had to be halted temporarily to replace the hydraulic pump. The specimen was then loaded and heated again in heating cycle 2. The experimental results and data will be presented for the first heating cycle, and then the second heating cycle.

First Heating Cycle

Figure 5.13 shows the measured bottom steel plate temperature-time curves for the first heating cycle. From the figure it would initially appear that the heaters were not working properly due to the scatter in measured temperatures. However, the thermocouples and temperatures measured on the surface exposed to heaters 3 and 5 were problematic, not the heaters. These thermocouples malfunctioned periodically throughout the test. The reason for this was that as the specimen deformed, these thermocouples were often coming into contact with other metal components causing problematic readings. The temperature measurements for the surfaces heated by heater 1 were relatively close to the E119 curve for most of the test. The temperature readings for surfaces heated by Heaters 2, 4, and 6 were lagging, but relatively consistent. For heaters 4 and 6, the bottom plate location to which the thermocouples were attached began deflecting upwards due to local buckling (distortion) discussed earlier in Section 5.2. A photograph showing the local distortion of the bottom plate is shown in Figure 5.14. Thus, the measured temperatures were somewhat lower as they were further away from the heaters.

The temperatures measured at the center of the surfaces heated by Heaters 1 and 2 are the most representative of bottom steel temperatures. Figure 5.15 shows the temperatures in the steel web and the top of the steel deck during the first 50 minute heating cycle. As shown, all the maximum temperatures are less than 180°C. Since the temperatures are close to the water evaporation range (80-150°C) the measured temperatures have some scatter. This scatter is caused by the transmigration of moisture and steam through the section. As shown, after 50 minutes of heating, the steel deck temperatures did not get very high. This is probably because the bottom steel plate was acting as the sacrificial

fire protection layer between the heating and composite section. This was discussed earlier in Section 5.2.

Figure 5.16 shows a plot of measured displacements vs. time. As can be seen in the figure the displacements at the north and south third point are consistent with one another. This is an indicator of relatively uniform heating over the specimen length. The maximum deflection of 1 in. downward recovered to -0.12 in. (upward) as loading was removed to fix the hydraulics. Figure 5.17 shows the measured end rotations over the first 50 minutes of heating. As shown, the rotations are consistent with one another and approximately equal to one another.

During this heating cycle several cracks formed in the concrete slab. The cracks provided avenues for the evaporation of moisture (steam). These cracks were typically vertical initiating on the side of the specimen and then travelling across the width of the section. Figure 5.18 shows a crack of this nature. The formation of these cracks was accompanied by a large popping sound. A similar type of flexural cracking was induced by the thermal gradient through the specimen depth including a negative (hogging) moment on the specimen. Figure 5.14 shows an example of this crack on the northwest end of the specimen.

Second Heating Cycle

After the hydraulic pump was replaced, the CC-DD specimen was subjected to combined heating and mechanical loading again. The heaters were controlled to subject the bottom steel plate to the E119 *T-t* curve and concentrated load equal to 1.2 kips was applied to the specimen mid-span. Figure 5.19 shows the measured temperatures on the bottom steel plate during the second heating cycle. The heating was applied for 120 minutes and then the last 1 hour was cooling of the specimen. The temperatures measured by thermocouples corresponding to Heaters 1 and 2 were the most representative of the actual bottom steel temperature. The others were having problems with the deck warping locally and/or thermocouples contacting other metal pieces on the specimen. As shown in Figure 5.19, the temperatures measured by the thermocouples corresponding to heaters 1 and 2 did a reasonable job of approximating the E119 Curve. Heater 5 is observed to have numerous spikes corresponding to thermocouple malfunctions.

Figure 5.20 shows the measured temperatures within the cross-section of the specimen. As shown, the temperatures measured in the south web and mid-span web are consistent with one another. The maximum temperatures in the web are 336°C for the south third point and 270°C for the mid-span web. The measured temperature at the top of the steel deck cross-section at mid-span and the top of the concrete was equal to 270°C and 85°C, respectively. This shows the thermal gradient through the specimen and the delay in heat rise through the specimen. Also, it is shown that the temperature of the steel components in the cross-section never reach above 350°C.

The measured displacements over time for the second heating cycle are shown in Figure 5.21. As shown, the maximum displacement occurs at 140 minutes of heating, where mid-span displacement was equal to 1.1 in. The north and south third displacements were equal to 0.9 and 0.8 in., respectively. Figure 5.21 shows that the north third point displacement increase was consistent with the south third point until

approximately 105 minutes of heating. The north third point displacement began increasing more beyond this point. This is likely because the large crack that formed near the north support continued to open wider as heating time increased. Figure 5.22 shows the measured end rotations in the second heating cycle. The rotations in the second heating cycle were consistent with one another until around 70 minutes of heating. The figure shows the south rotation to increase more than the north end until approximately 130 minutes of heating. The rotations were consistently increased at the same rate until 140 minutes of heating, after this point the north rotation increased more rapidly and had a maximum rotation 0.15 degrees. The maximum south rotation was equal to 0.09 degrees. Rotations began to decrease as the specimen cooled down, as shown in the figure.

Both Heating Cycles Data

The data for both heating and loading cycles was combined and presented. The measured temperatures vs. time are in Figure 5.23, the measured displacements over time are shown in Figure 5.24, and measured rotations over time are shown in Figure 5.25. Only heaters 1 and 2 are shown in Figure 5.23 as they are believed to be the most representative of the bottom plate steel temperatures. It can be seen from the figures that the heating in the second cycle was consistent with the first cycle. Figure 5.24 shows the displacements continue to rise as the heating plateaus on the bottom steel. This is occurring due the temperature gradient through the specimen cross-section and the effects of end restraint. The thermal crack induced on the north end of the specimen due to the thermal gradient continued to grow during re-heating. A picture of the crack at the end of heating is shown in Figure 5.26.

The cool-down period of the specimen was also monitored for several hours after the heating stopped. The plot of the measured displacements over time is shown in Figure 5.27. As shown, after 10 hours cooling, the north and south third point displacement were -0.3 and -0.25 in. (upward). The final mid-span displacement was -0.35 in. upward.

Load Test of Elevated Temperature Specimen

For a matter of completeness, a load capacity test of the CC-DD Specimen was conducted. The load test was conducted after the specimen had been allowed to cool for 24 hours. All heaters were removed from the specimen prior to applying any load. The only sensors placed on the specimen were displacement potentiometers at the mid-point and north and south third point. The loading fixture was used to apply monotonically increasing to the specimen mid-span. The load vs. measured mid-span deflection of the specimen is shown in Figure 5.28. As shown, the maximum load capacity was 12 kips or 600 psf equivalent loading. 3.5 in. of mid-span displacement was observed at maximum load levels. Figure 5.28 shows there is a drop in applied load from 12 kips to 9 kips immediately at 3.5 in. of mid-span displacement. The specimen continued to slowly reduce in load carrying capacity until loading was removed at 7 in. of mid-span deflection. The negative moment crack that had formed from heating continued to open up, and had traversed the entire width of the specimen at 12 kips of applied load. The slab at the north end began to separate vertically from the steel deck as shown in Figure 5.30 as displacements increased. The vertical separation grew larger and also large

flexural cracks formed near the mid-span as displacements increased. The compression flange of the steel deck was also observed to buckle where the concrete was separated. Figure 5.31 shows the specimen with 7 kips of applied load and 7 in. of displacement (just prior to removing the load). Figure 5.32 shows the buckled steel deck after concrete was removed upon test completion.

The specimen was ductile and the failure load was around 70% of what was predicted assuming an undamaged specimen. The reduction in capacity is a result of reduced material properties in the bottom plate steel due to heating, and the numerous cracks induced in the concrete from heating. The large negative moment crack induced by heating initiated the vertical separation of the slab from the deck. However, the system still performed adequately considering the extreme temperatures to which it was exposed.

5.4.3. General Discussion Points of Combined Heating and Loading Test

- 1) It is recommended that a better way of attaching the thermocouples used in controlling the heaters. Keeping thermocouples functioning properly was the most difficult aspect of the experiment. Otherwise, the heaters did a good job of applying the standard E119 Curve.
- 2) A maximum mid-span displacement of 1 in. (downward) occurred from heating of the specimen. This displacement was a result of the thermal gradient in the specimen and end restraint present. After cooling, mid-span displacements equal to -0.35 in. (upward) were observed.
- 3) According to E119 criteria, there are two failure modes possible: (1) failure based on thermal criteria where the top concrete surface temperature exceeds 250°C or (2) a structural failure in which the specimen experiences a collapse. The specimen was able to resist the applied heating and load without experiencing either of these failures.
- 4) A load test on the specimen after the heating was done showed that the specimen retained 70% of its undamaged capacity. The reduction in capacity is a result of the bottom plate becoming a 'sacrificial' fire protection layer. The bottom properties were changed from the extreme temperatures, but the bottom plate helped shield other material in the cross-section from damage. This inherent fire resistance is an advantage to using cellular deep deck systems.

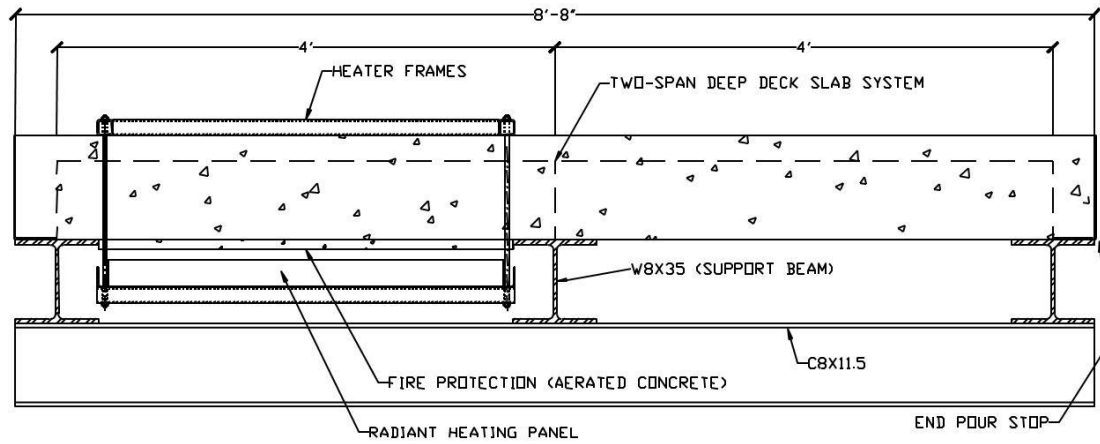


Figure 5.1: Side View Schematic of Heat Transfer Tests



Figure 5.2: Heat transfer specimen (a) after concrete pour and (b) during testing

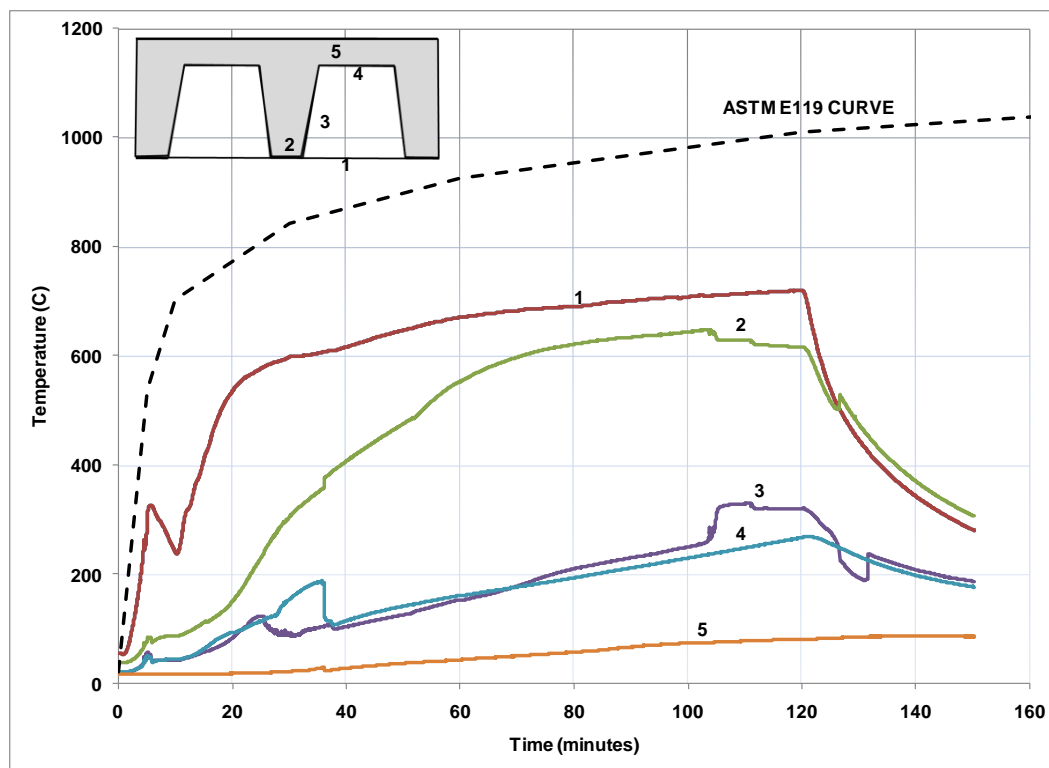


Figure 5.3: Temperature vs. time curve for unprotected side of heat transfer specimen

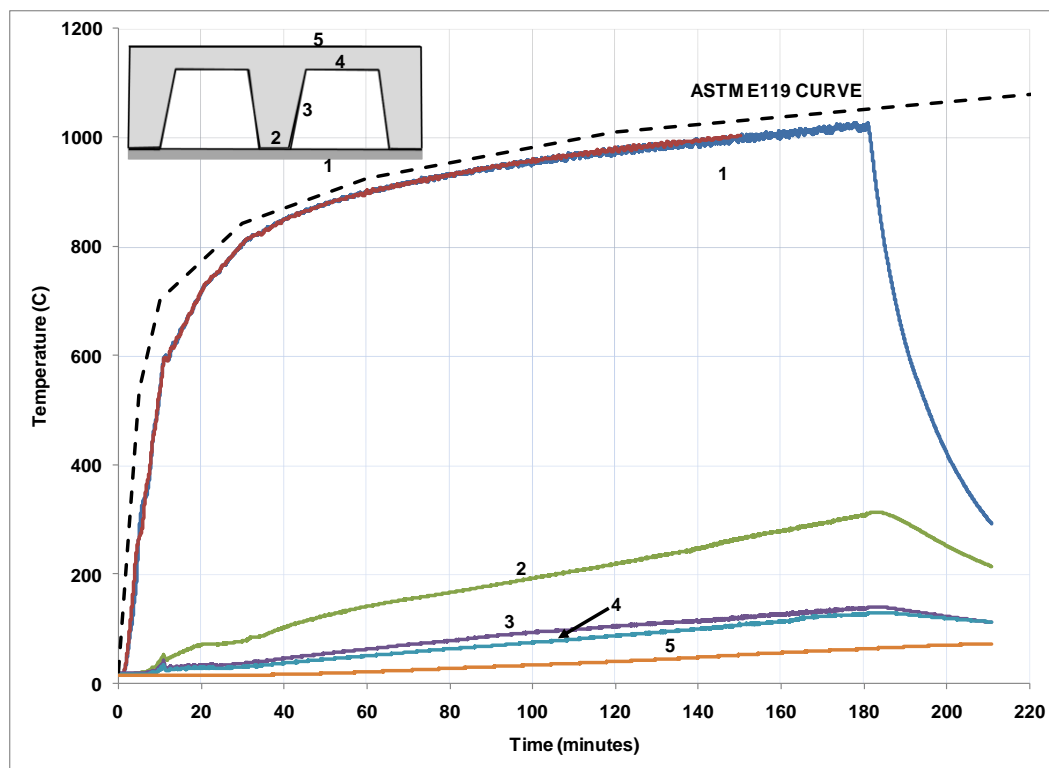


Figure 5.4: Temperature vs. time curve for protected side of heat transfer specimen



Figure 5.5: Heating of unprotected side of heat transfer specimen showing deformations of bottom plate



Figure 5.6: Picture of specimen showing cracks in concrete

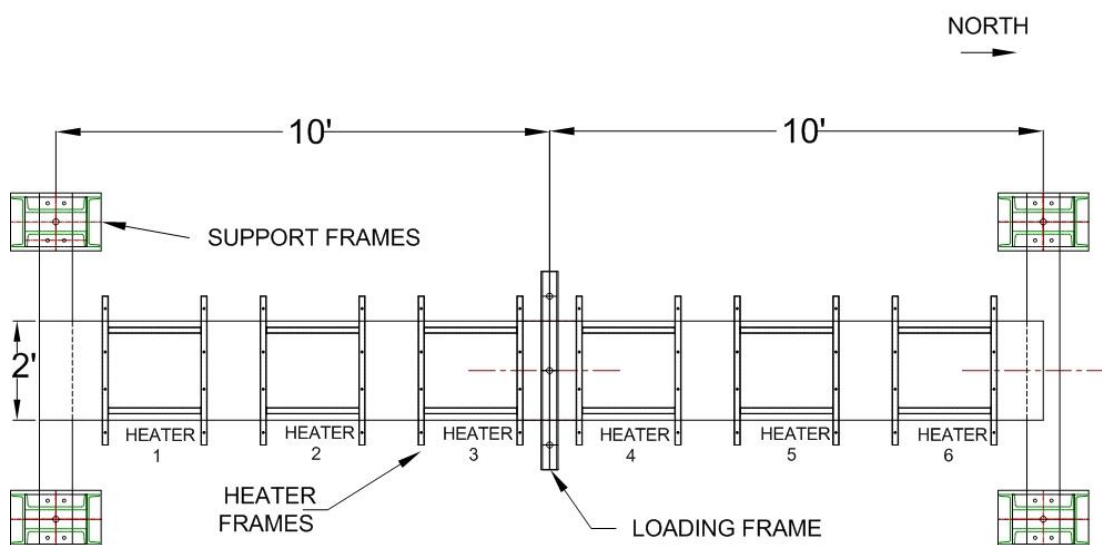


Figure 5.7: Top view schematic of combined heating and loading test



Figure 5.8: Overall Specimen view showing loading frame and heaters attached to specimen

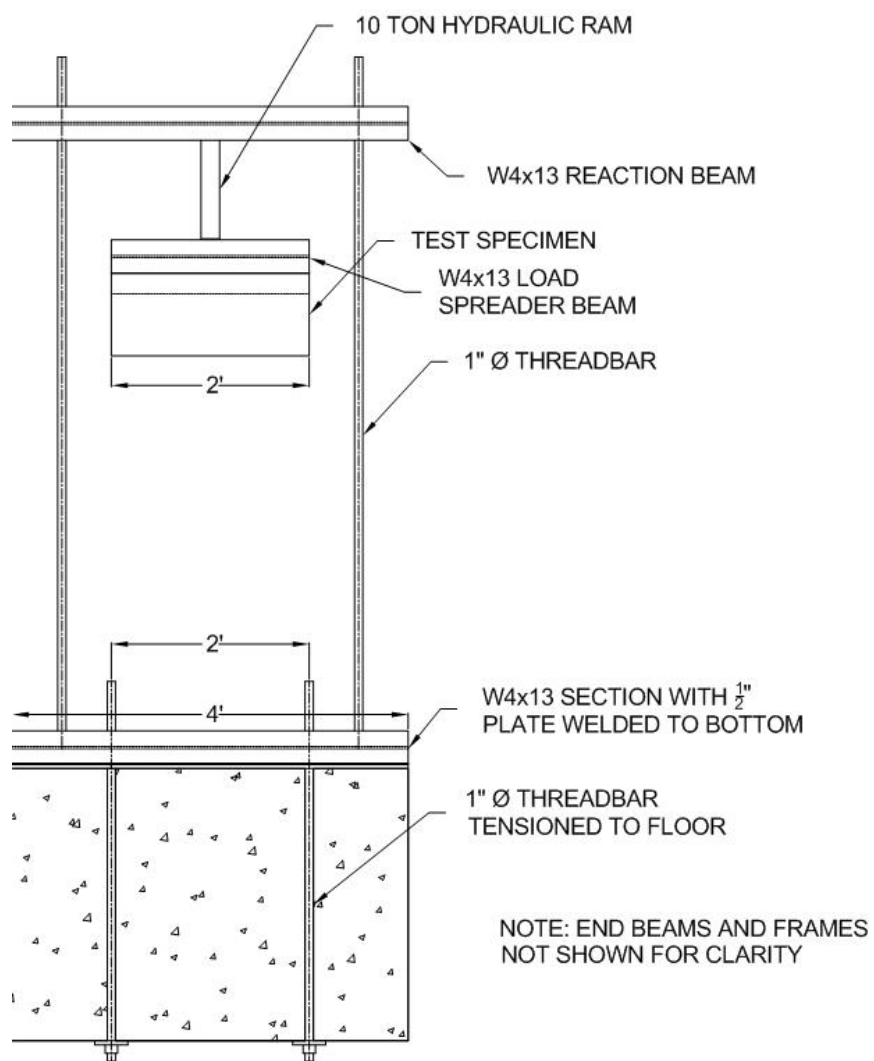


Figure 5.9: Front view schematic of loading frame for combined heating and loading test



Figure 5.10: Photograph showing displacement transducer



(a)



(b)

Figure 5.11: Photographs of (a) generator used to power heaters and (b) heater control box



Figure 5.12: Overall view of specimen just prior to testing showing protective polycarbonate plastic

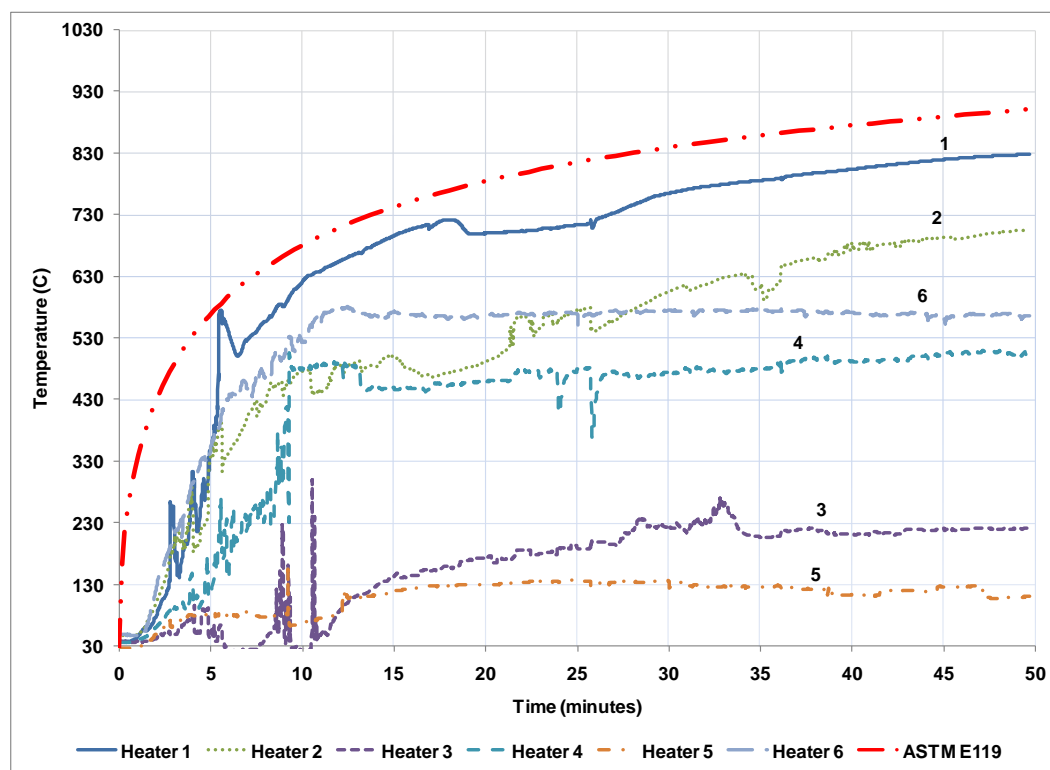


Figure 5.13: Measured bottom steel temperatures vs. time for first 50 minutes of heating



Figure 5.14: Photograph showing local upward bowing of bottom plate

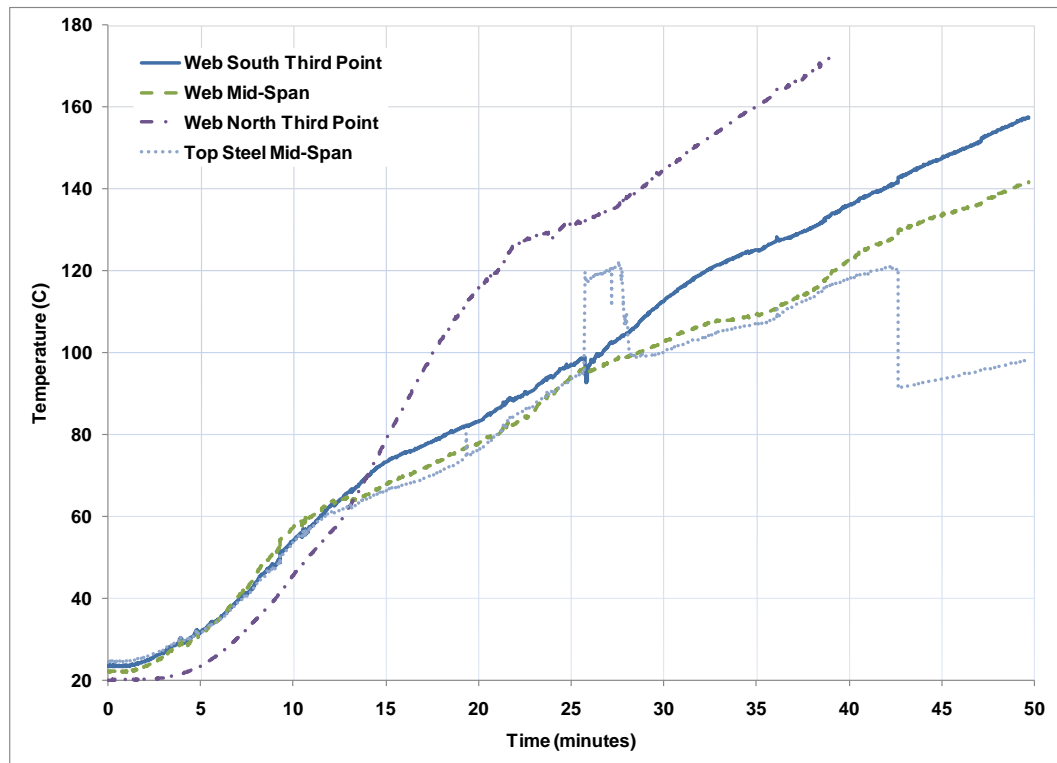


Figure 5.15: Measured steel web temperatures vs. time for first 50 minutes of heating

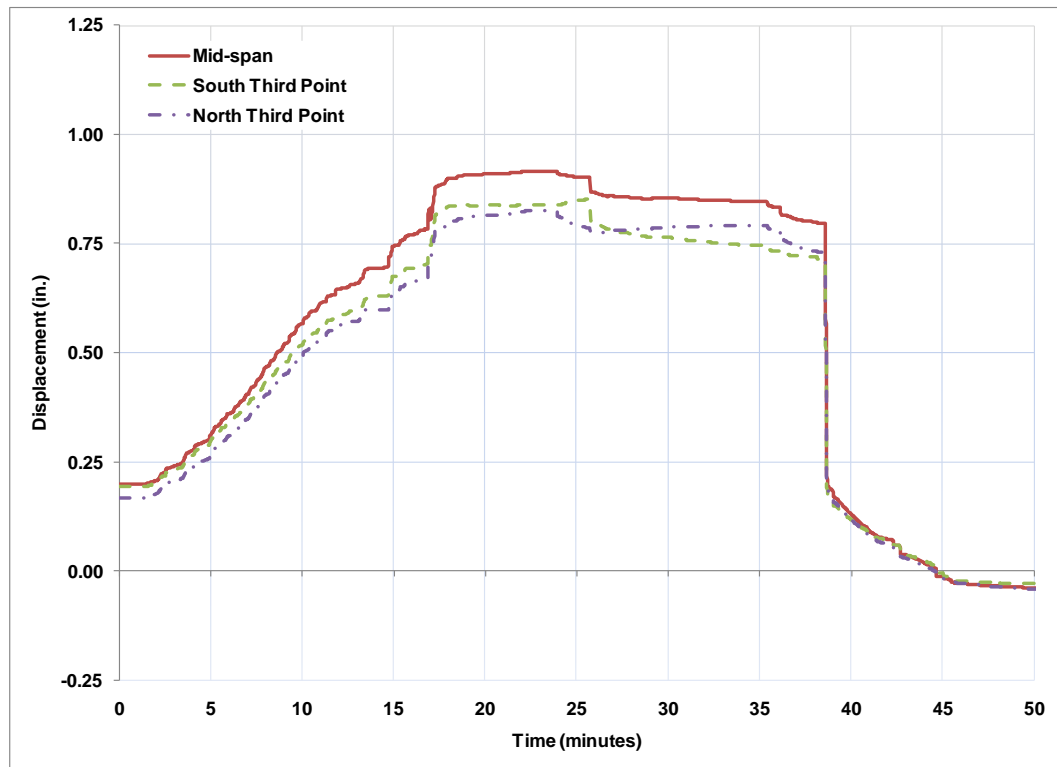


Figure 5.16: Measured displacements for first 50 minutes of heating

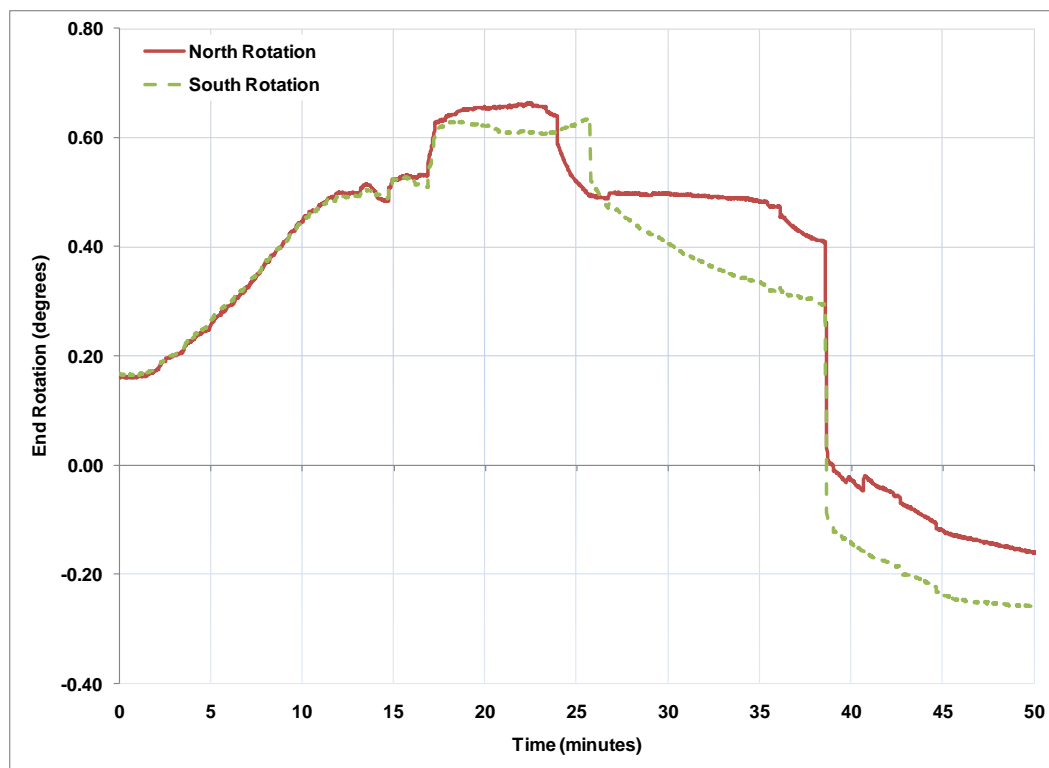


Figure 5.17: Measured rotations for first 50 minutes of heating



Figure 5.18: Photograph showing vertical side crack on specimen

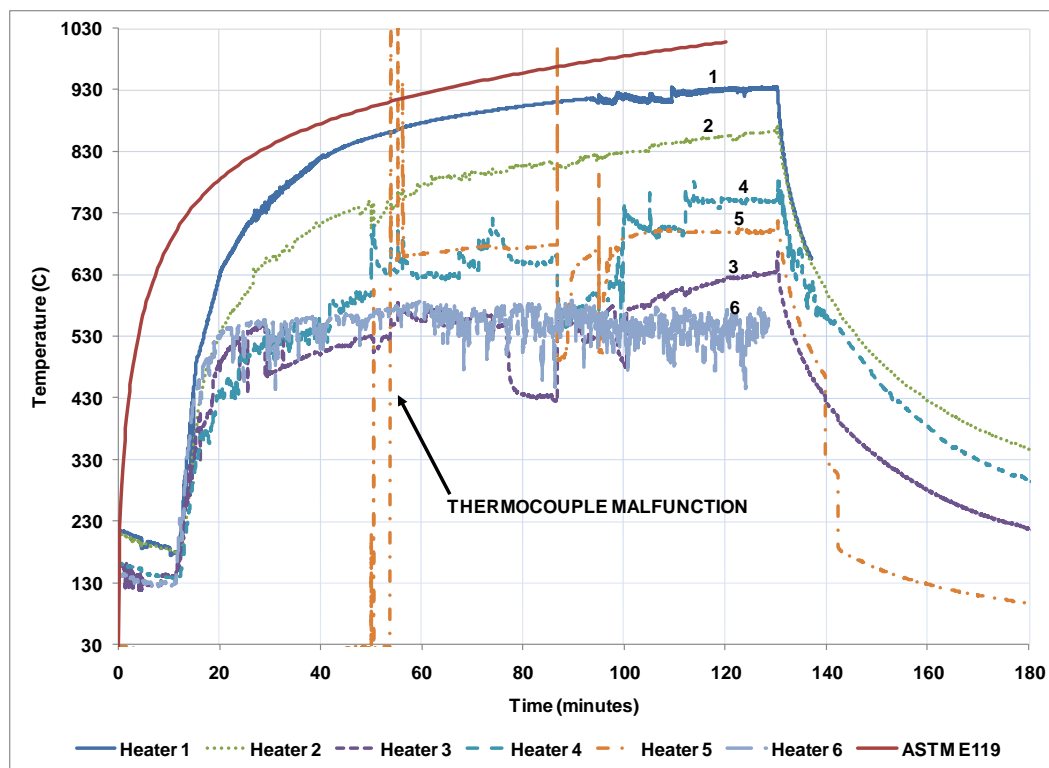


Figure 5.19: Measured bottom steel temperatures vs. time for second heating cycle

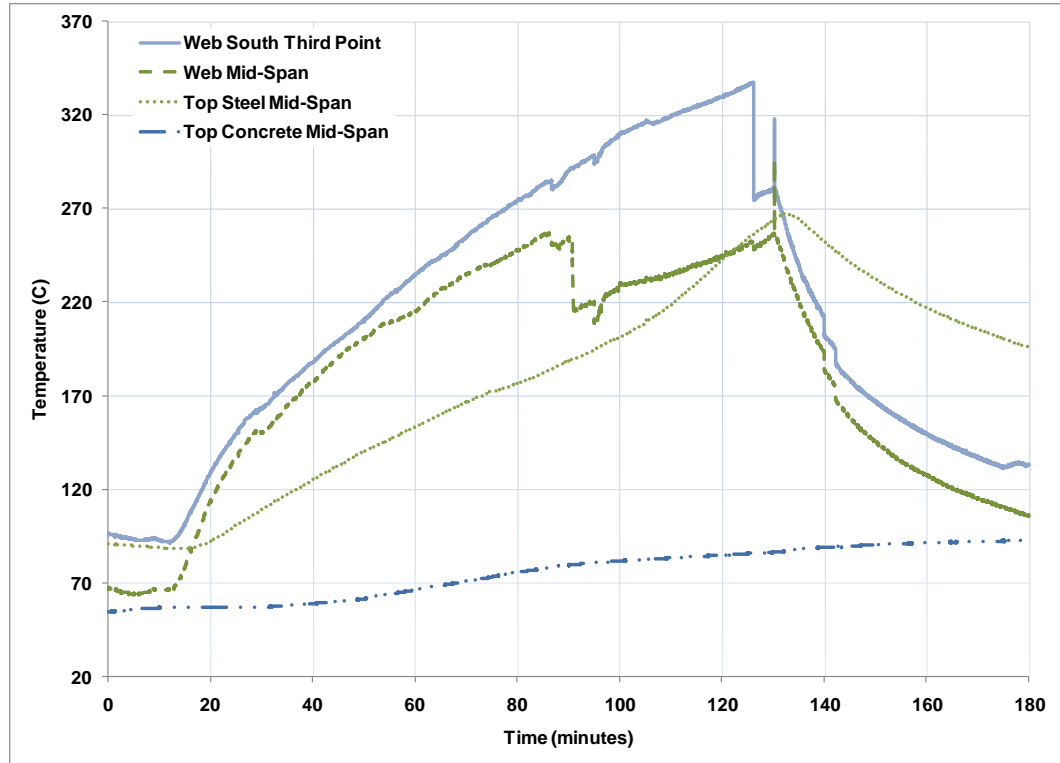


Figure 5.20: Measured temperatures in steel profile for second heating cycle

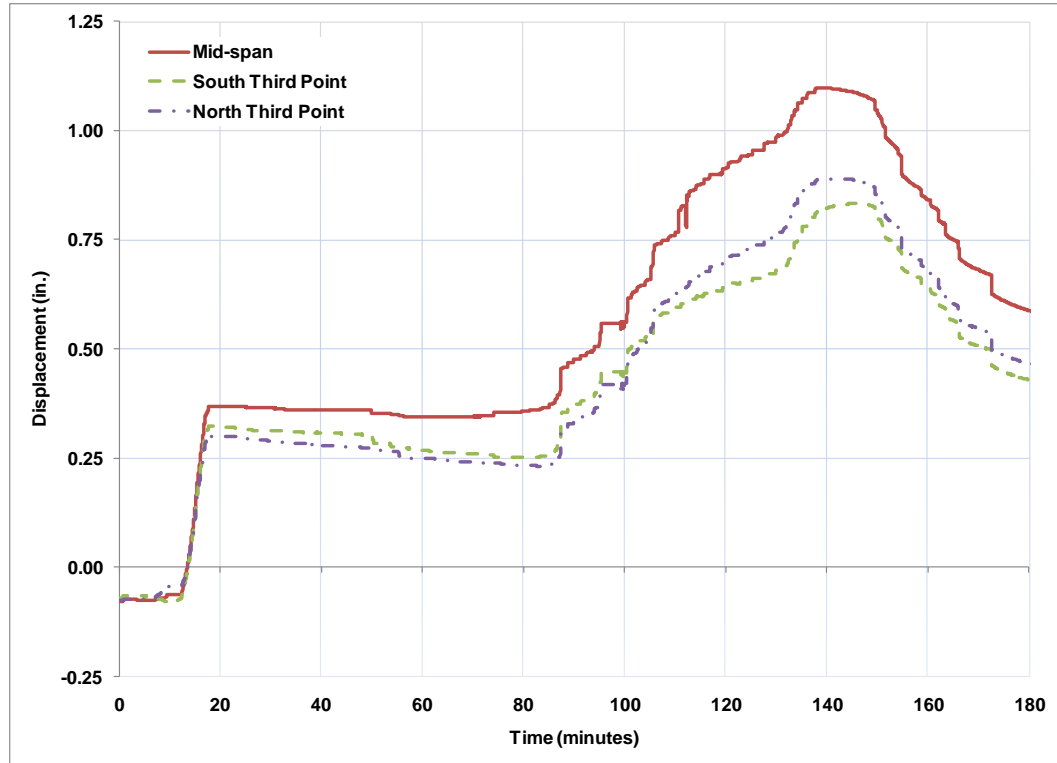


Figure 5.21: Measured displacements in second heating phase

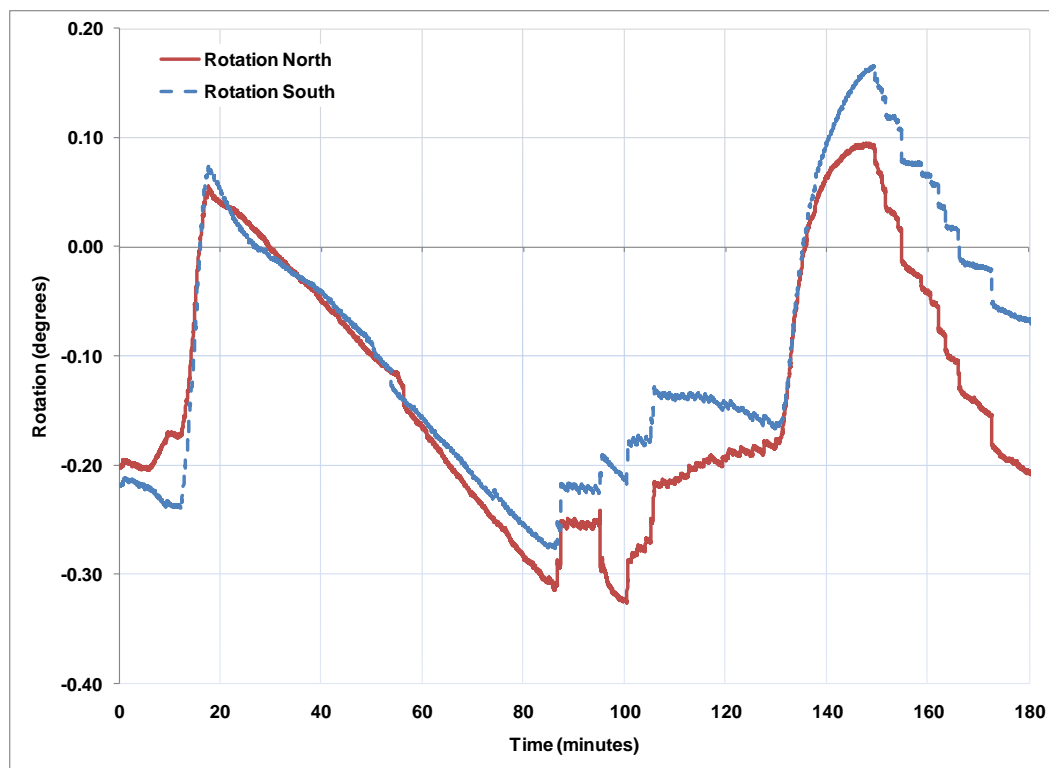


Figure 5.22: Measured rotations in second heating phase

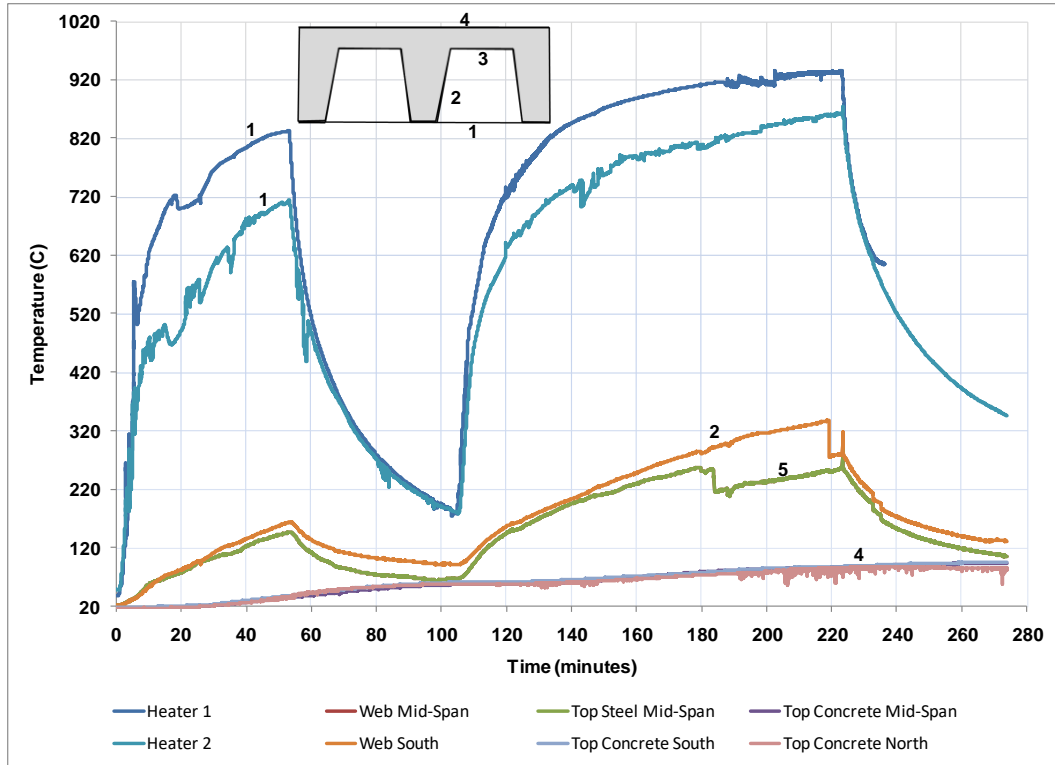


Figure 5.23: Measured temperatures over all heating cycles

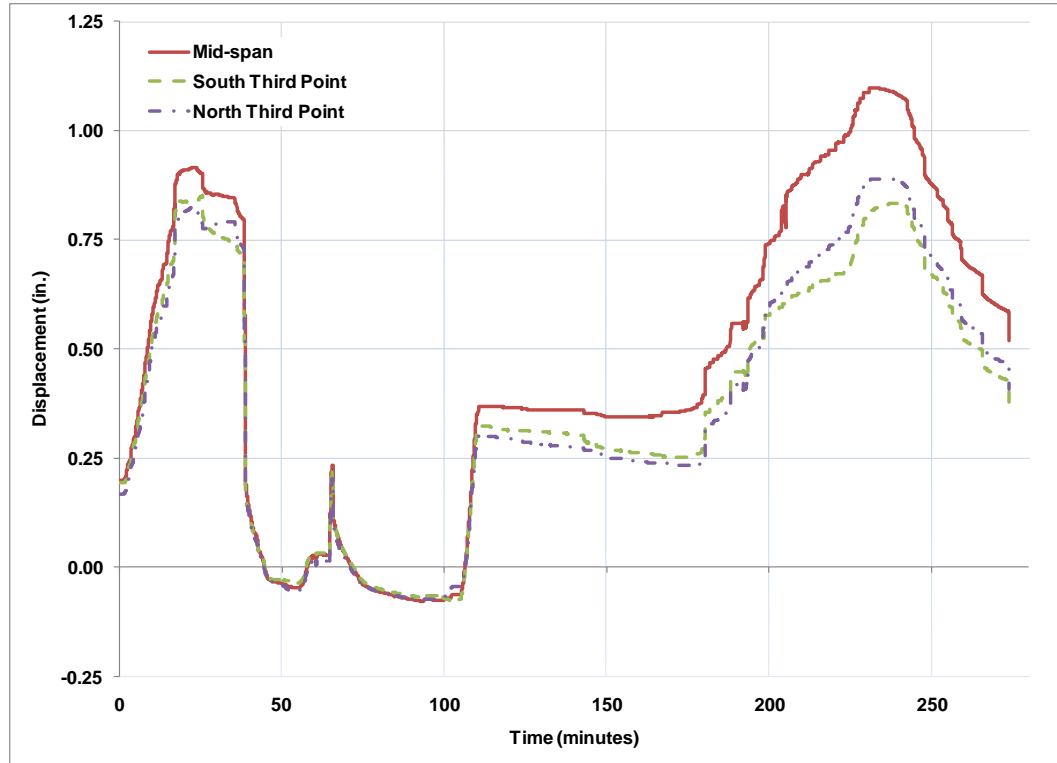


Figure 5.24: Measured vertical deflections over both heating cycles

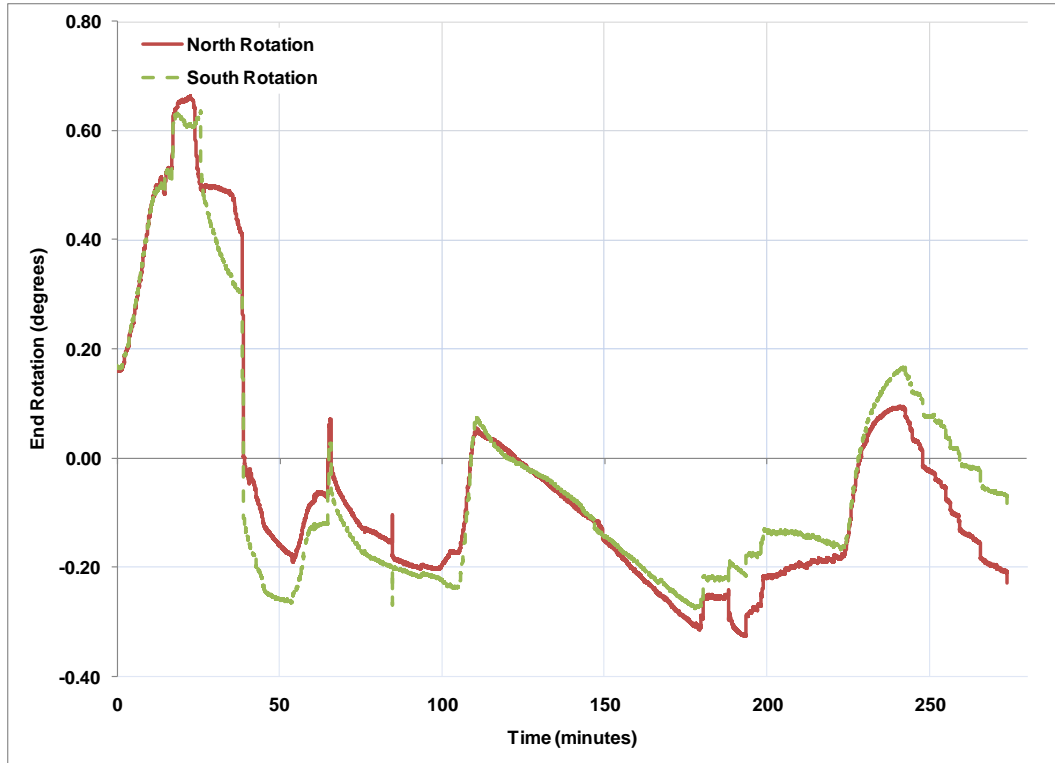


Figure 5.25: Measured rotations over both heating cycles



Figure 5.26: Crack that formed at north end at end of heating

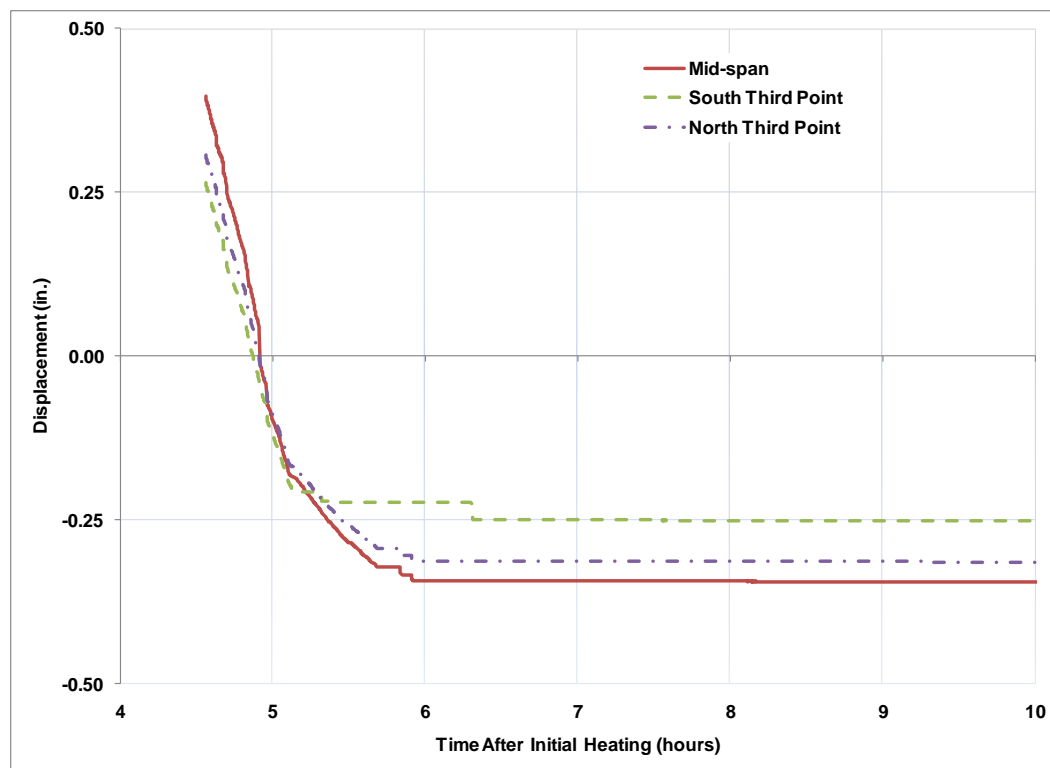


Figure 5.27: Displacements on Specimen

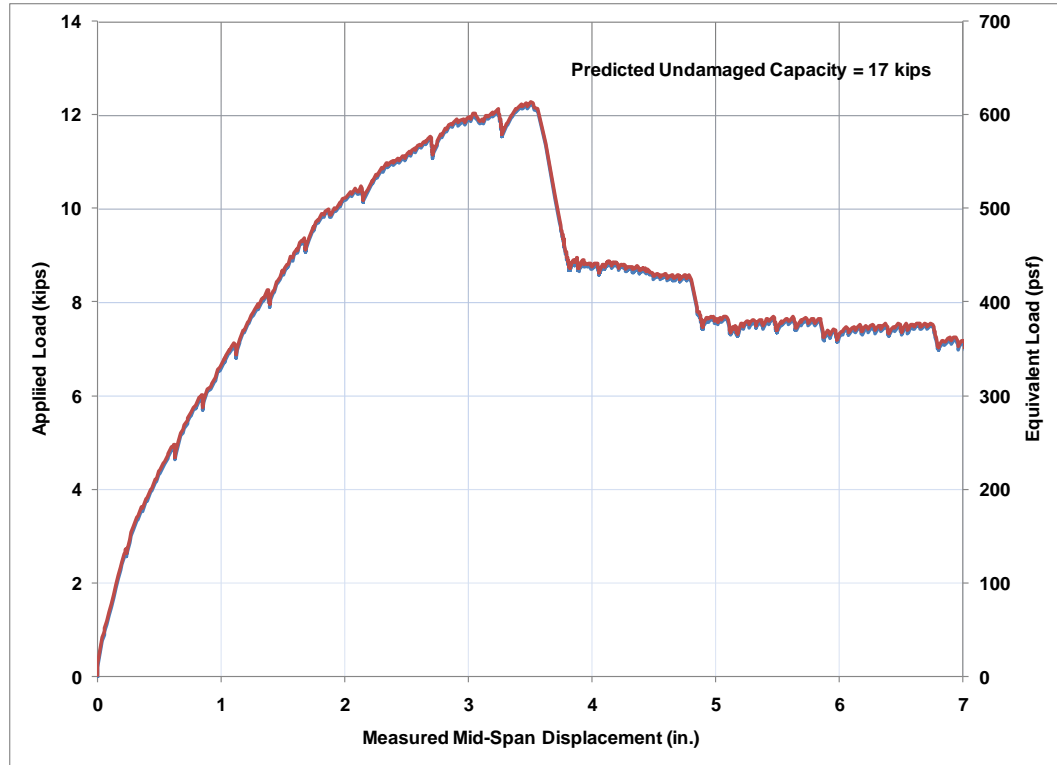


Figure 5.28: Load vs. vertical mid-span deflection of specimen



Figure 5.29: Growth of crack at north end during load test



Figure 5.30: Vertical separation of slab from deck during load test



Figure 5.31: Specimen at 7 in. of deflection



Figure 5.32: Buckled steel deck near mid-span (concrete was removed)

CHAPTER 6. SHORED COMPOSITE DEEP DECK SYSTEM

This chapter presents further details including the preliminary analysis and design and large scale experimental evaluation of the Shored Composite Deep Deck (SC-DD) floor system. This system was described previously in Chapter 3. It is similar to other deep deck systems with the exception that it is non-cellular and requires shoring during the construction phase. Section 6.1 presents a summary of the SC-DD System described earlier in Chapter 3. Section 6.2 presents the preliminary analysis and design of the specimen using methods with different levels of complexity. Section 6.3 presents the details of the experimental investigations including the test setup and behavior of different phases of testing. Section 6.4 presents the summary of findings from the various sections.

6.1. Summary of the Shored Composite Deep Deck System

As mentioned in Chapter 3, the SC-DD system consisted of a 14 gage thickness, 7.5 in. deep steel deck with 3.5 in. of lightweight concrete (LWC) slab on top. The total depth of the system was a total of 11 in. The 7.5 in. deep deck is currently manufactured as individual ‘hat’ sections that are 1 ft wide and connected together. Figure 6.1 shows sketches of the individual deep deck section and a series of the four deck sections connected together and concrete cast.

6.2. Preliminary Analysis and Design of SC-DD System

The preliminary analysis and design of the SC-DD systems was conducted similar to that of the previous deep deck systems presented in chapter 4. However, the effects of shoring in the non-composite (construction) phase, and shore removal in the composite phase had to be included. A simple code based design approach was used initially to evaluate the SC-DD system. This was followed by more detailed evaluation using fiber based models and then 3D FEM models.

6.2.1. Code-Based Design Approach

The same recommendations and specifications from SDI (Steel Deck Institute , 2002) and ACI (American Concrete Institute, 2005) were used to design and evaluate the SC-DD system as were for the CC-DD systems in Chapter 4. The major difference was the

inclusion of the effects of shoring and its effects in the construction and composite phases. This is described further in the following sub-sections.

Construction Phase – Code-Based Design Approach

The 30 ft length of the deck will be provided one line of shoring at mid-span. This will lead to a continuous 2-span condition for the 30 ft long deck. The positive moments and deflections in each 15 ft span, and the negative moments at the shoring and the reaction at the supports would have to be checked for design. These checks are summarized in the SDI manual (Steel Deck Institute, 2002) and shown in Figure 6.2 for completeness. The terms used in Figure 6.2 were also used and described previously in Section 4.2.1. The main difference now is that the negative moment must be checked. Construction level deflections will likely not govern since the span for deflection is reduced and the system acts as a continuous beam in this phase.

Composite Phase – Code Based Approach

The composite phase of the SC-DD system must be checked for service level deflection and ultimate (factored) strength limits. The removal of the shoring at mid-span converts the system from a two-span continuous condition to a simply supported single span condition. The effects of shore removal can be simulated by applying a downward force that is equal and opposite to the upward reaction provided by the shoring. The magnitude of this force can be estimated using equation 6.1.

$$P_{shore} = 1.25W_l \left(\frac{L}{2} \right) \quad 6.1$$

Where:

P_{shore} The downward force simulating shore removal = upward shore reaction after concrete casting

W_l The slab and deck weight (defined previously in Section 4.2.1)

The resulting moment acting on the composite section at mid-span from shore removal can be found using 6.2.

$$M_{SR} = P_{shore} \left(\frac{L}{2} \right) \quad 6.2$$

The composite cross-section will have locked in stresses (residual) from the construction and shore removal phases. For the previous CC-DD systems, only the steel deck had locked-in stresses from the concrete casting. These stresses were small and hence ignored in the initial analysis and design phase. The effects of locked-in stresses due to shore removal were included in the analysis and design of SC-DD that was conducted in Chapter 9.

Results of Code Based Approach

Table 6.1 summarizes the results of the code-based design and analysis for the construction and composite phases of the CC-DD systems. The table includes the flexural strength for both positive and negative moment (ϕM_n^+ and ϕM_n^-) and stiffness (I_{cons} , I_{comp}) for the construction and composite phases. The required positive and negative moment capacities (M_u^+ and M_u^-) and stiffness (I_{req}) are given. The ratios ($\phi M_n^+/M_u^+$, $\phi M_n^-/M_u^-$, $I_{con}/I_{req-con}$, and I_{comp}/I_{reqd}) are also included in the table. The non-composite strength of the deck is based on the elastic section modulus (S) of the deck for both positive and negative bending. The composite capacity of the section is based on assuming full plastification of the section.

As shown in Table 6.1, the positive moment induced by the concrete self-weight is equal to 2.4kip-ft/ft and the negative moment is equal to 3.2 kip-ft/ft. The positive and negative moment capacities of the bare steel deck were calculated as 15.4 kip-ft/ft and 16.5 kip-ft/ft, respectively. In the composite phase, the shore removal caused a positive moment of 18.6 kip-ft/ft that must be carried by the composite section. The positive moment capacity of the composite section is equal to 39.4 kip-ft/ft assuming full plastification. The steel deck had a non-composite moment of inertia equal to 20 in.⁴/ft. The required non-composite moment of inertia was 1.57 in.⁴/ft. This requirement was based on a deflection limit of $L/240$ for a 15 ft span. In the composite phase the composite moment of inertia was equal to 73 in.⁴/ft, which was 3 times the required moment of inertia based on a $L/360$ limit for applied live loading of 40 psf.

6.2.2. Numerical Non-Linear Inelastic Analysis

The load-deflection behavior of the SC-DD system was predicted using the same fiber-based analytical approach used earlier for CC-DD Specimens in Chapter 4. A fiber model of the composite cross-section was developed and used to predict the section moment-curvature ($M-\phi$) response. The section curvatures were integrated numerically using the central difference method to predict the complete load-displacement response. This has been presented in detail in Section 4.2.2 and not repeated here for brevity. The preliminary analysis models for the SC-DD Specimen used nominal properties for the steel deck and concrete slab materials, assumed full composite action (i.e. no slip) between the deck and slab, and did not include the effects of construction loading or shore removal on behavior. This is similar to the assumption used earlier for the CC-DD specimens to predict their preliminary behavior in Section 4.2.2.

Results of Non-Linear Inelastic Analysis

Figure 6.3 shows the preliminary load-deflection behavior predicted for the SC-DD system based on the non-linear inelastic analysis procedure. The figure includes both Option 1 and Option 2 for the CC-DD systems described previously in Section 4.2.2. As shown, the predicted load capacity of the SC-DD system was equal to 395 psf. The predicted strength is greater than the design factored loads of 165 psf ($1.2D + 1.6L$). The strength of the SC-DD system is lower than that of the CC-DD System because of the removal of the bottom plate on the cross-section. The predicted deflection at assumed

lived loads of 40 psf is approximately 0.3 in., which is well under an $L/360$ limit (1 in. for a 30 ft span).

6.2.3. Finite Element Analysis

The load-deflection behavior of the SC-DD system was also predicted using the 3D finite element method. The FEM models were similar to those used earlier for the CC-DD Specimens in Chapter 4. The steel deck was modeled using 4 node S4 shell elements and the concrete slab was modeled using 8 node brick elements (C3D8). The steel deck and concrete surfaces were tied to each other to prevent slip. The steel and lightweight concrete material properties were specified as mentioned earlier in Section 4.2.3 using nominal material properties. The 30 ft span of the SC-DD floor system was simply supported as shown in Figure 6.4, which shows a picture of the FEM model. Figure 6.5 shows the load-deflection behavior predicted by the finite element analysis. It includes the predictions using the fiber model, the results from the finite element analysis using simplified geometry and fully detailed geometry, the nominal live loading, and the factored ultimate loading. As shown, the full geometry and fiber-based model compare well to one another for behavior and predicted capacity. The simplified geometry model under-estimates capacity by approximately 10%, which is similar to the CC-DD models. As mentioned earlier in Chapter 4, the simplified geometry ignores the flange stiffeners and side laps, but provides a conservative prediction of the load-deflection behavior. Again, it was difficult to for the FEM model to run to as high displacement levels as the fiber based analysis. This was due to convergence problems in the model at these higher load levels from the geometric and material non-linearity present in the model.

6.3. Experimental Setup

The experimental setup for investigating the behavior of the SC-DD System was very similar to that used for the CC-DD systems presented in Chapter 4. The loading and support frames used for applying loading and supporting the specimen ends were identical to previous specimens. The fixtures used to transfer the loads from the loading frames to the specimens were also identical. These included the spreader beam and cylindrical bearings providing contact between the hydraulic rams and spreader beams. The SC-DD Specimen had one line of shoring at the mid-span during the construction non-composite phase. Only one SC-DD specimen was tested. The SC-DD deep deck profile was already described previously in Section 3.3.2. It consisted of a 14 gage thick 7.5 in. deep deck profile with 3.5 in. of concrete cover on top. The same lightweight concrete mix was used as the previous CC-DD Specimens.

The experimental setup and instrumentation layout for the SC-DD specimen was almost identical to those used for CC-DD specimens. A 4 ft width of the SC-DD specimen was tested. Wood side forms were used in place of metal ones as the depth of the lightweight concrete changed to 11 in. and there were no metal forms available to accommodate the change in depth. Steel pour stops were used at the specimen ends and shear studs placed through pre-cut holes in the deck to connect it to the supporting beams.

Five 3/4 in. diameter, 9 in. long studs were welded to each support beam through pre-cut holes in the deck trough as shown in Figure 6.6. Displacement transducers were used to measure the displacement at the 6th point and mid-span during the construction phase. Strain gages located were located at the specimen sections at the third points and mid-span. These were used to measure the strains in the construction and composite phases. Figure 6.7 shows a picture of the specimen with side forms in place, sensors attached, and shoring set. The following section present descriptions of the SC-DD specimen testing and behavior during construction, ultimate loading, and vibration tests.

6.4. Experimental Results and Discussion

This section presents the experimental results and behavior of the SC-DD Specimen for the construction, ultimate loading, and floor vibration tests.. The results and discussion are separated into those for the construction phase testing and composite phase testing.

6.4.1. Construction Phase Results and Discussion

The construction phase testing of the SC-DD specimen was different from the previous CC-DD specimens. Since there was a line of shoring during construction, the strains and displacements from the concrete casting were quite small. Furthermore, as discussed previously, when the shore was in place, the deep deck of the SC-DD system behaved as a two-span continuous beam.

One aspect of behavior examined was the vertical displacement of the shore due to axial shortening of the shoring posts and the flexural displacement of the shoring beam. These vertical displacements may cause some differences in the expected behavior and strain distribution in the SC-DD specimen from the case of a rigid support. Figure 6.8 shows the measured vertical displacement of the shoring system during concrete casting and over the first twelve hours of curing. It is apparent from the figure that the shoring system is not a completely rigid support system. The final vertical displacement of the system settles to around 0.14 in. after the concrete casting. The vertical displacement of the shore slowly decreases and settles over the first twelve hours as the concrete begins curing.

Figure 6.9 shows the measured strains in the deck profile at mid-span (shoring location) during concrete casting and for twelve hours after casting. It can be seen that there is some negative moment occurring at this location as the top of the deck is in compression and the bottom steel is in tension. However, as the concrete began curing all the strains increase steadily during the first twelve hours, which is similar to the behavior observed for the CC-DD Specimens. The steady increase is caused by the thermal strains induced at elevated temperatures caused by the heat of hydration during curing. The strain data over the first few days of concrete curing and hardening is shown in Figure 6.10. As shown, the measured strains are highest around 8 hours after the concrete casting and decrease steadily over the next few days. The heat of hydration is quite high during the first few hours of concrete curing. Unfortunately, the temperatures

of the steel deck during curing were not measured. It was observed that a reasonable amount of heat was being generated in the specimen. Figure 6.10 also shows that the strains do reduce back close to initial values after a few days of curing, although one of the strain gages was damaged after about 3 days.

The next stage in the construction process was the removal of the shoring. After 7 days of curing, the shoring was removed and the specimen behavior was monitored continually until the load testing was done. The composite section resisted the load effects (strains and stresses) induced by the shore removal. Table 6.2 shows the change in strain at the top, web, and bottom of the steel deck at the mid-span section and sections located at 8 ft from the north and south supports. Figure 6.11 shows the mid-span displacement during casting, curing, and shore removal. As shown, the deflection immediately increases to around 0.45 in. Over the following week the deflection increased to around 0.65 in. This increase comes from creep effects on the composite section. The use of shored construction leads to more creep related effects as the entire composite section now must resist the concrete self-weight.

Figure 6.12, Figure 6.13, and Figure 6.14 show the measured strains in the steel deck after shore removal and thereafter. Figure 6.12 shows the strains at the bottom of the steel deck of the mid-span section. Similarly, Figure 6.13 and Figure 6.14 show the strains at the top and web of the mid-span section. All the figures show the increase in strains from shore removal has the most substantial effects on the specimen in the construction phase. After shore removal, the strain remained mostly constant until load testing.

Key Observations from Construction Level Testing

- 1) The use of shoring helps in limiting the strains induced on the section from the wet concrete weight.
- 2) The magnitude of strains induced on the composite cross-section are dominated from the shore removal process. These strains can be reduced further by using more than one line of shoring.
- 3) A final mid-span deflection of around 0.7 in. resulted from the construction process with maximum tensile strains of around 190 microstrain (5.5 ksi).
- 4) Creep effects increased displacement from 0.5 to 0.65 in. after shore removal.

6.4.2. Modal Impact Testing Results and Discussion

Modal impact testing was performed to determine the dynamic properties of the SC-DD specimen. These dynamic properties included fundamental (natural) frequencies and damping. Similar modal impact tests were conducted on the CC-DD specimens as explained in Chapter 4. The testing equipment, instrumentation, and data analysis were identical to those identified earlier in Section 4.4.2. Similar to previous specimens, three accelerometers were placed at 9 ft in from either support and at the mid-span. Hits were applied with a modal impact hammer at every foot along the length of the specimen. Five hits were applied per location and an average of the readings was used for final data processing. Figure 6.15 shows a typical measured frequency response function for modal

impact hits made at mid-span. As shown, the frequency response of the SC-DD specimen is similar to the FRF behavior of the CC-DD specimens. The first natural frequency (for the primary bending mode) of the SC-DD specimen was 5.98 Hz. This compares reasonably with the natural frequency of 5.9 Hz estimated with a simple SDOF model. Figure 6.15 shows that the second and third fundamental frequencies were estimated at 22.5 Hz. and 47.5 Hz, respectively.

The modal impact data was used to estimate damping using the half power method. The half power method was described previously in Section 4.5. The damping estimated for the first natural frequency of the SC-DD system was 0.98%. This was slightly higher than previous CC-DD systems. The increase is likely due to the additional 1 in. of lightweight concrete slab on the specimen. From a floor vibration standpoint, this additional damping may be advantageous in mitigating possible floor vibration issues.

Discussion of Modal Impact Results

As described above, the primary relevant dynamic property that could be determined from the modal impact tests were the natural frequencies of the SC-DD specimen. The results were also used to estimate the damping for the natural frequencies of the specimens. However, the dynamic behavior of a composite slab floor system in a building structure depends on the contributing mass and damping from the adjoining bays, the presence of partitions and other elements that could dissipate vibrations, and the structural configuration. These elements obviously could not be captured from the performed modal impact testing. Furthermore, the supporting girders for the SC-DD floor system will play a vital role in the dynamic behavior of the complete floor system. The SC-DD System alone may not be prone to annoying vibrations, but if the floor system is supported by relatively flexible girders then problems could arise.

The SC-DD Systems satisfy the key assumptions made by AISC and SCI in using their guidelines for floor vibration evaluation. These assumptions are (1) The first fundamental frequency is in the 4 – 10 Hz. range (2) the first frequency is adequately distanced from other frequencies such that modal coupling does not occur and (3) floor vibration induced by walking excitation is dominated by the first natural frequency and mode.

Key Observations and Discussion for Modal Impact Testing

- 1) The measured natural frequencies were close to those calculated using a simple SDOF model.
- 2) The first mode of vibration and natural frequency was much lower than higher modes.
- 3) The floor vibration behavior of the SC-DD system can be evaluated using guidelines published by the AISC and SCI.

6.4.3. Ultimate Load Test

An ultimate load test was conducted on the SC-DD specimen. As mentioned previously, the test was conducted using the same loading and support frames, hydraulic

rams and equipment, instrumentation layout, and data acquisition as the previously tested CC-DD specimens. The compressive strength of the concrete on the date of test was 5393 psi. This was determined by testing 4in. by 8 in. concrete cylinders. Uniaxial tension tests according to ASTM E8 (ASTM, 2004) were performed on machined tension coupons taken from the deck. These tests indicated a yield stress of 31 ksi for the deck. Additional concrete batch mixes, mill certifications and measurements from tension tests are given in Appendix C.

Displacement and Rotation Data

Figure 6.16 shows the applied load vs. mid-span displacement behavior of the SC-DD specimen. The figure includes the loads applied by the north and south hydraulic rams and their average values. There is some difference between the north and south applied loads that increase as displacement levels are increased. The discrepancy between the north and south begins around 4 kips of loading when flexural cracking was observed in the north span of the specimen. The figure includes the service level live loading ($LL=40$ psf) and the factored ultimate loading ($166 \text{ psf}=1.2D+1.6L$). The corresponding mid-span deflections were 0.5 and 2.0 in. As shown, some flexural cracking was observed after the service level live loading. After flexural cracking, the north loads are always smaller than the south loads as shown in Figure 6.16. There is a sudden large drop in the north load at 4.5 in. of vertical displacement. At this point a shear bond failure initiated at the north loading point. A shear crack formed under the loading point and propagated to the support through the shear interface. The north end of the concrete slipped towards the support.

The measured loads and mid-span deflections were used to estimate the stiffness of the specimen. Table 6.3 shows the flexural stiffnesses of the specimen before and after concrete cracking. The un-cracked stiffness was estimated based on the displacements from applied loads of 0-4 kips. The cracked stiffness was measured for loads between 4 and 8 kips. The stiffness was estimated as the north or south load value divided by the mid-span displacement. The values of the stiffness are given in Table 6.3. As shown, the average stiffness reduces by about 21% due to the concrete cracking.

Figure 6.17 shows the applied load vs. end slip data measured for the north and south ends. As shown, some elastic slip was observed at the north end for loads exceeding 6 kips (120 psf equivalent). This slip (with positive values) represents movement of the concrete slab towards the load point. The north end slip increases rapidly as the peak load is reached. Shear bond failure occurs reducing the applied load, increasing the mid-span deflections, and causing the concrete slab to slip back towards the support. Figure 6.18 shows a photograph of the north loading point just prior to shear bond failure. Figure 6.19 shows a photograph of the deflected shape of the SC-DD specimen. After the shear-bond failure, the north end shear studs provided some ductility, which is evident from the positive slope of the load-deflection curve after the sudden drop. The specimen capacity increased back up to about 11 kips (220 psf) with increasing deflections. The test was terminated at the maximum deflection of 8 in., corresponding to the stroke limit of the hydraulic ram.

As the specimen was being loaded in displacement control, a sizable horizontal crack began forming in the concrete at the north end support as shown in Figure 6.20. This

crack began forming just prior to the shear bond failure and continued opening as the displacements increased. This crack was different in appearance than those that occurred in the CC-DD specimens but had a similar effect of weakening the overall structure. The final capacity of the structure was approximately 11 kips (220 psf) and the mode of failure was shear bond, but with reasonable overall ductility due to the presence of end shear studs.

Figure 6.21 shows the average load vs. measured end rotations for the Specimen. The end rotations were approximately equal to each other up to around 5 kips of applied load. Beyond this point the north end rotations were larger than the rotations of the south end of the Specimen. The flexural cracking observed at the north end of the specimen was likely the cause. Clinometers were also used to determine the average curvature of the uniform moment region of the Specimen (between the load points). The clinometers were placed near the loading points of the specimen as described previously. The average curvature between the loading points was calculated using Equation 4.16. The mid-span moment vs. average curvature plot is shown in Figure 6.22.

The experimental results highlight a major difference between shored and un-shored construction with deep deck systems. The line of shoring reduced the construction load effects (deflections, strains, and stresses) on the long span system. However, the shore removal locked in strains and stresses in the composite deck system. The concrete slab had built-in tensile stresses that resulted in cracking at relatively low load levels. This can be reduced by adding more lines of shoring or increasing the overall depth of concrete. Adding shoring or increasing concrete depth will affect the overall economy of the system. These are issues that need consideration for optimizing the design of the system.

Strain Gage Data

Figure 6.23 shows plots of the strains measured in the steel deck and the concrete slab at the mid-span section at different load levels. The strain measurements are shown as variations over the section depth at different load levels. Figure 6.24 shows plots of the strains measured in steel deck and the concrete slab at the north load point. Figure 6.25 shows plots of the strains measured in steel deck and the concrete slab at the south load point. It is important to note that all the strains were re-zeroed at the beginning of the load test. Therefore, the plots show the strains induced in the composite section by applied loads.

Figure 6.23, Figure 6.24, and Figure 6.25 show that strain distributions are mostly linear over the cross-section. Non-linearity occurs as the loads are increased, and the slope of the strain diagram in the steel deck section becomes different from the slope of the strain diagram in the concrete slab. This indicates the occurrence of slip and partial composite action between the steel deck and the concrete slab. The figures also indicate that reasonable portions of the bottom of the deep deck had yielded at ultimate loads (although the entire cross-section had not yielded completely). The strain profile figures also show that there is a change in the slope of the strains within the steel deck especially at higher load levels. The likely reason for this is the occurrence of web distortion within the deck. Web distortion is when the webs of the steel deck displace out-of-plane. Figure 6.26 shows web distortion schematically. The web distortion occurred in this

specimen because there was not cellular plate on attached to the bottom of the deck, which helps in limiting web distortion. Table 6.4 reports the R^2 values for the strains shown in Figure 6.23, Figure 6.24, and Figure 6.25. As shown, the linearity of strain profiles measured by the R^2 value decreased as the loads were increased, especially for the north end (where significant slip and shear bond failure occurred).

Key Observations and Discussion for Ultimate Load Testing

- 1) The line of shoring placed at mid-span helped in controlling construction level deflections and strains on the specimen.
- 2) The specimen exhibited a shear bond failure with reasonable ductility beyond the occurrence of the separation between the deck and concrete. The shear studs helped in enhancing the ductility of the specimen.
- 3) The north end of the specimen had a reduced stiffness throughout the duration of the test. Cracking was exhibited at low load levels for this end of the specimen. The shore removal process 'locked in' stresses into the composite specimen – including the concrete. The cracking stress from applied load was thus lower than if the specimen would have been un-shored.

Table 6.1: Design checks for SC-DD System using code based approach

	Parameter	Construction Phase	Composite Phase
Strength	Positive Flexural Capacity (ϕM_n^+ kip-ft/ft)	15.4	39.4
	Required Positive Flexural Capacity (M_u^+ kip-ft/ft)	2.4	18.6
	$\phi M_n^+ / M_u$	6.4	2.1
	Negative Flexural Capacity (ϕM_n^- kip-ft/ft)	16.5	NA
	Required Negative Flexural Capacity (M_u^- kip-ft/ft)	3.2	NA
	$\phi M_n^- / M_u^-$	5.2	NA
Stiffness	Moment of Inertia for Section (in.^4)	20	73
	I_x / I_{req}	12.7	3

Table 6.2: Change in Microstrain readings from removal of shoring

Gauge Location in Cross-Section	Gauge Location along Specimen – Change in Microstrain from Shore Removal			
	Mid-Span East Side	Mid-Span West Side	8 ft from North Support	8 ft from South Support
Top of Steel	-36	-33	-16	-12
Web of Steel	48	31	32	32
Bottom of Steel	189	187	85	96

Table 6.3: Relative stiffness parameters of SC-DD Specimen

Type of Stiffness	North Load / Mid-Span Displacement (kips/in.)	South Load / Mid-Span Displacement (kips/in.)	Average Load / Mid-Span Displacement (kips/in)	Reduction in Stiffness from Concrete Cracking
Concrete Un-Cracked	5.3	6.3	5.8	21%
Concrete Cracked	4.3	5.04	4.6	

Table 6.4: R^2 values for strain distribution at various loading values for SC-DD Specimen

Average Load Value (kips)	Average Load / Measured Capacity	R^2 value for strains at south end	R^2 value for strains at mid-span	R^2 value for strains at north end
4	0.33	0.99	0.99	0.99
7.5	0.63	0.98	0.99	0.98
10	0.83	0.98	0.99	0.97
11.5	0.96	0.95	0.99	0.89

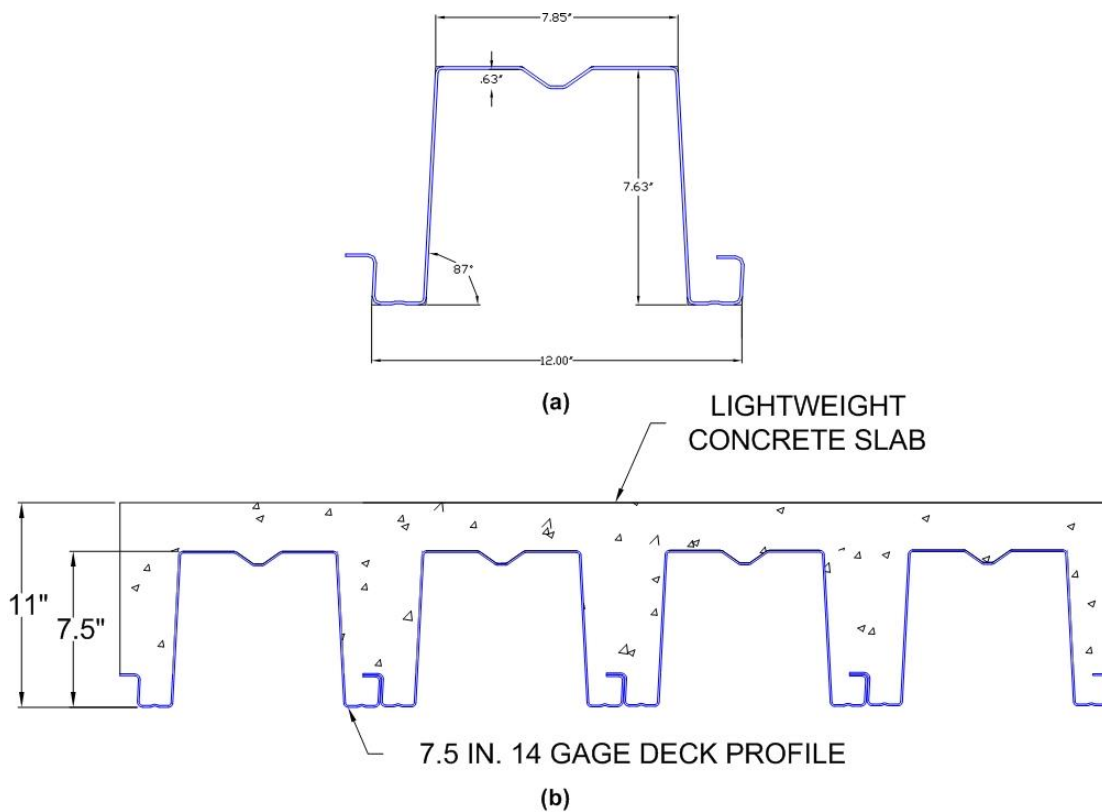


Figure 6.1: Schematic of SC-DD system showing (a) the deck profile, and (b) a cross-section with concrete cast

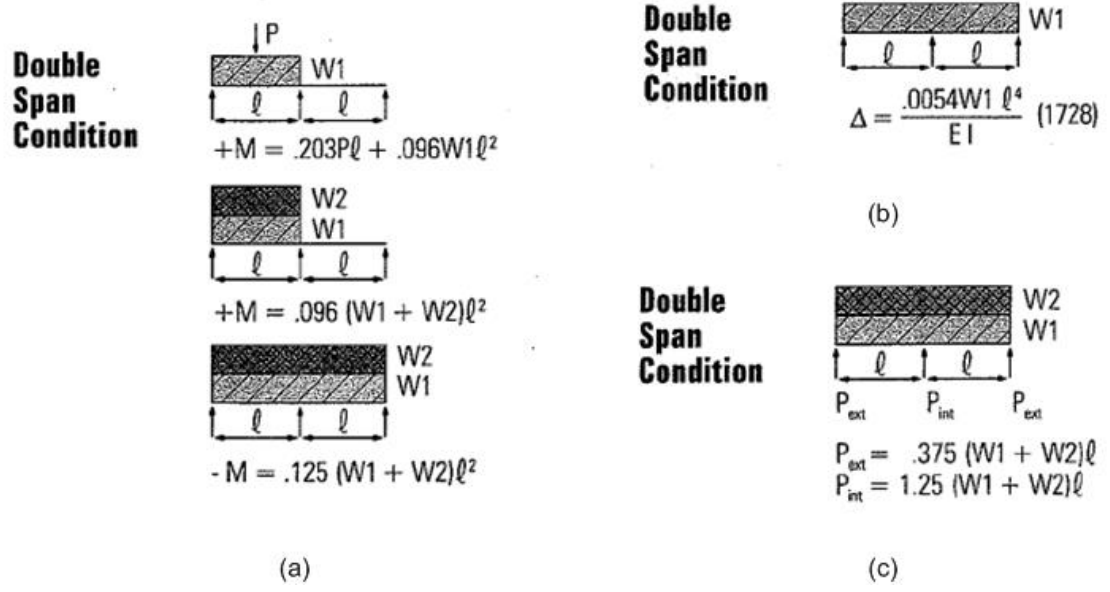


Figure 6.2: Structural analysis for two-span condition showing equations for calculating (a) positive and negative bending moments, (b) deflections, and (c) reactions (Steel Deck Institute , 2002)

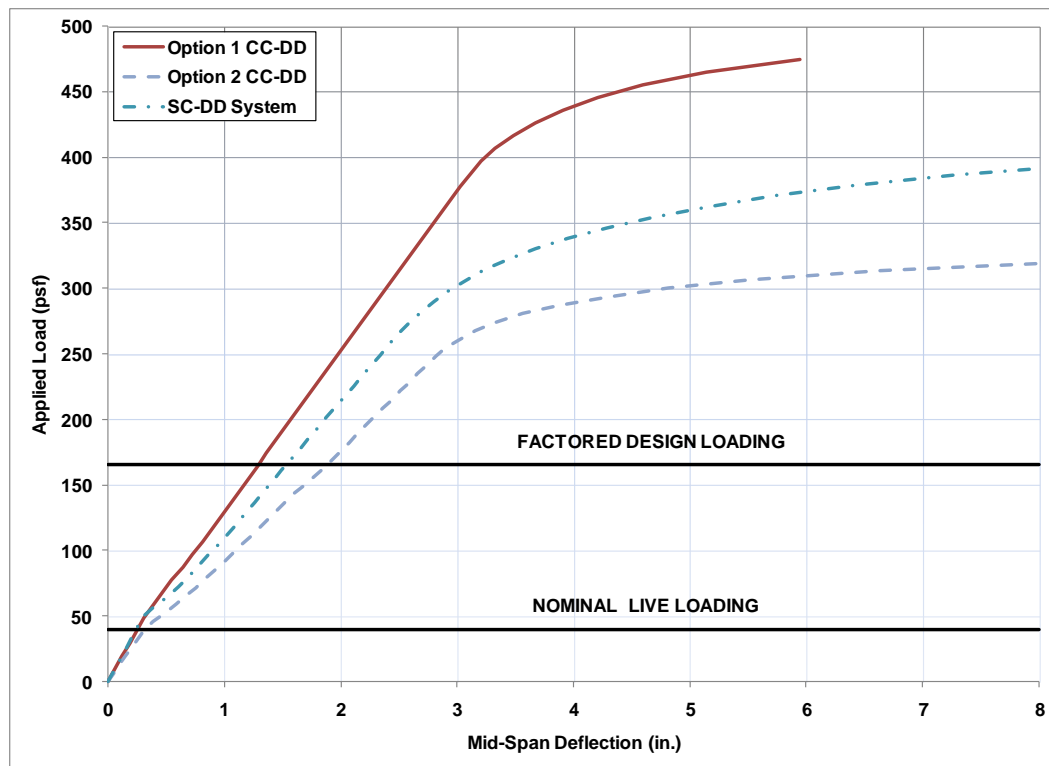


Figure 6.3: Non-Linear inelastic analysis results showing the CC-DD systems and the SC-DD system

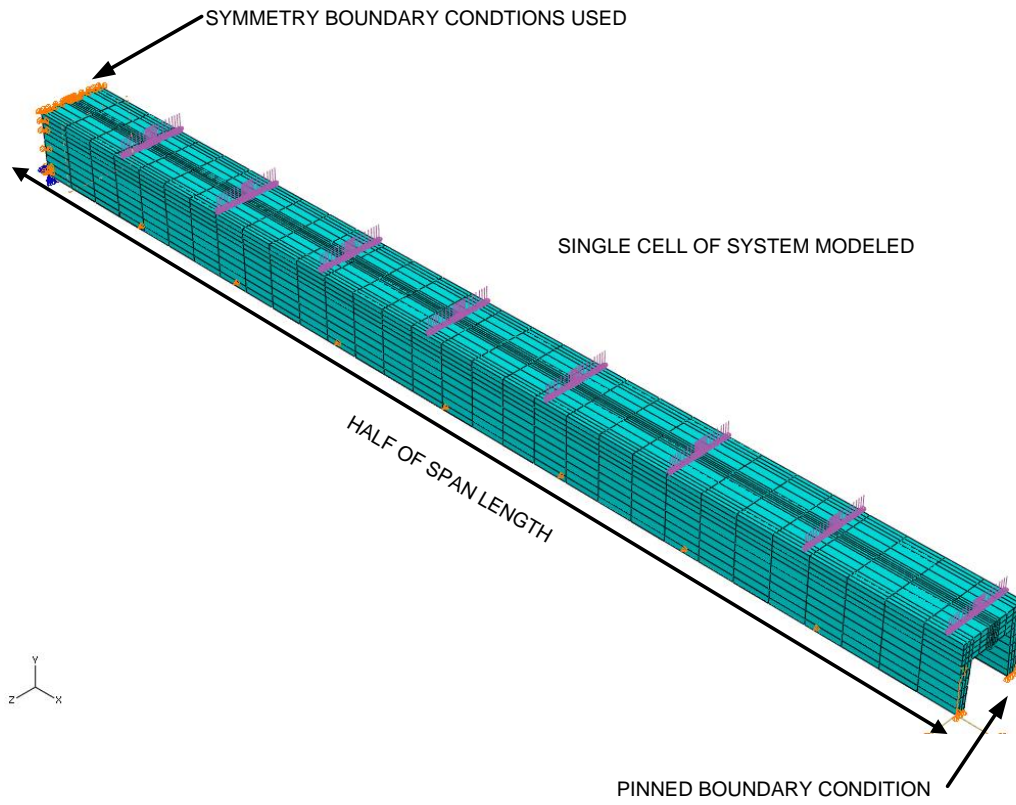


Figure 6.4: Schematic of meshed structural FEM models for SC-DD

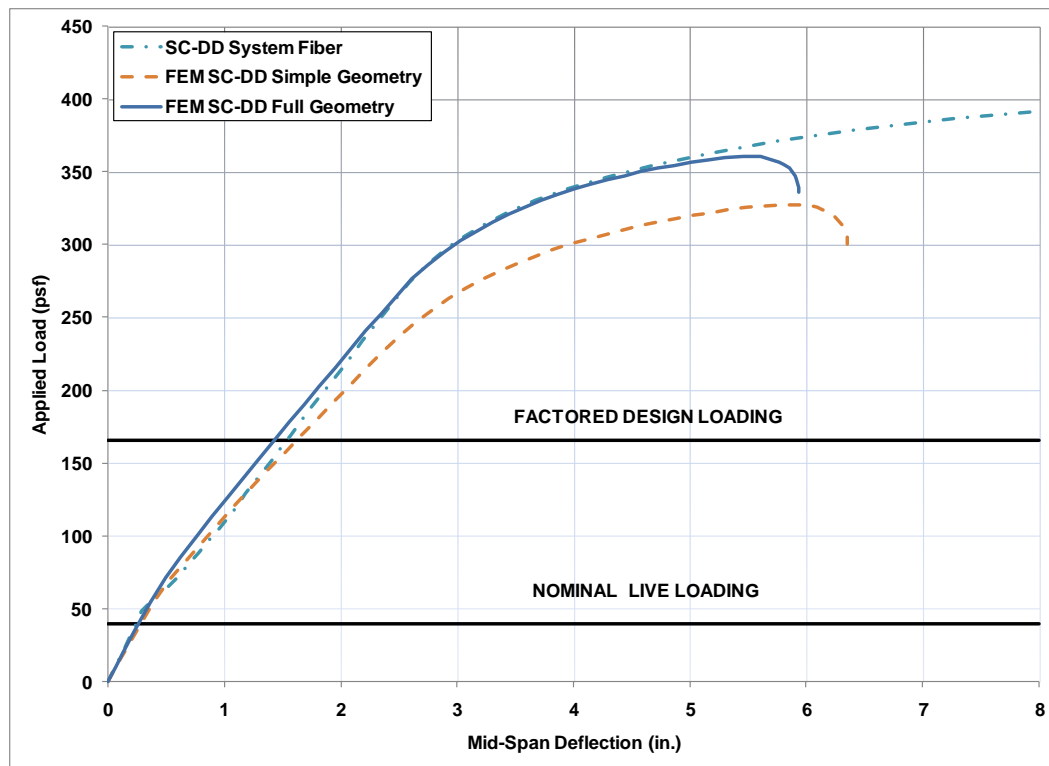


Figure 6.5: Comparison of FEM models and fiber based model for SC-DD System



Figure 6.6: SC-DD Specimen ends before concrete casting (note shear studs at ends)



Figure 6.7: SC-DD Specimen prior to concrete casting

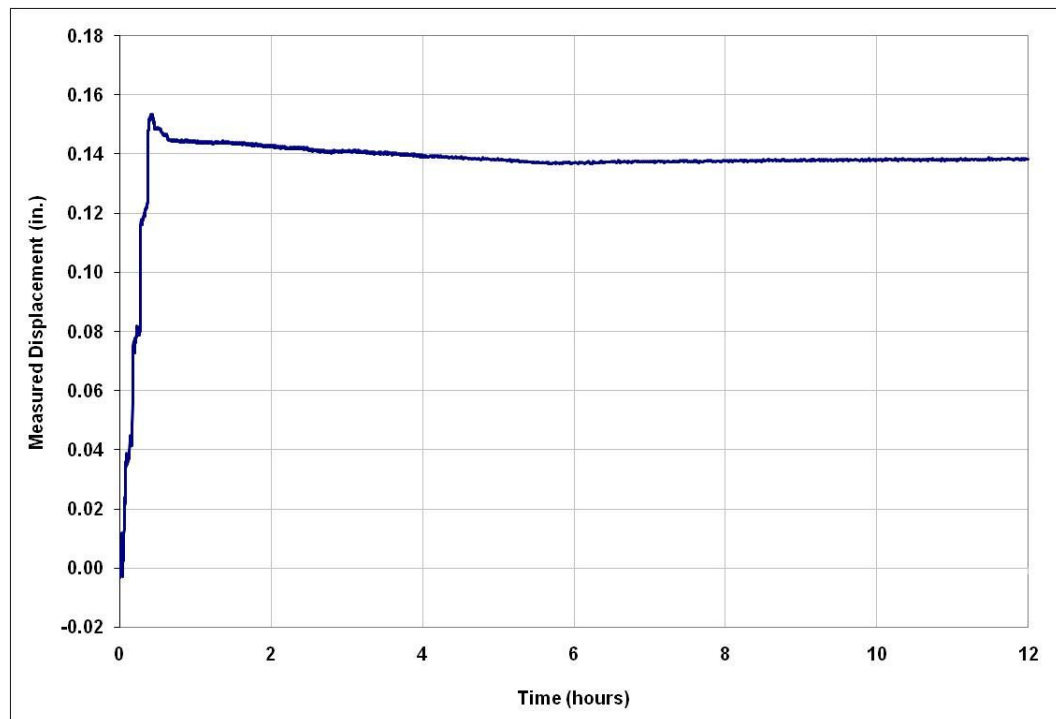


Figure 6.8: Vertical displacement of shoring system during concrete pour

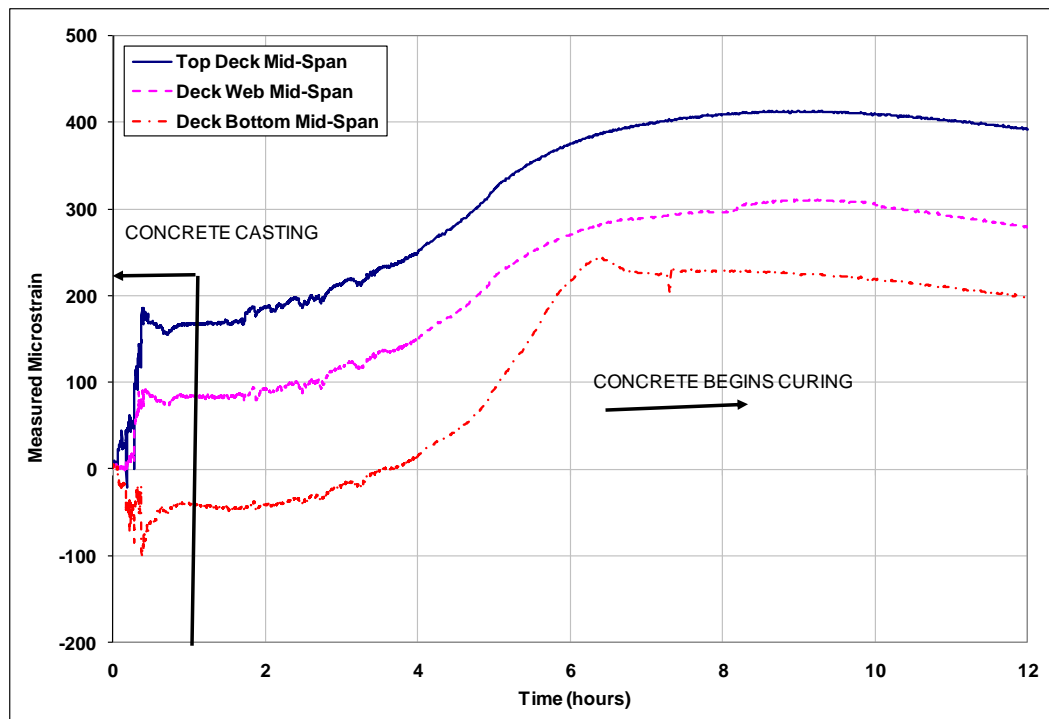


Figure 6.9: Measured strains in deck profile at mid-span during concrete pour and for first twelve hours

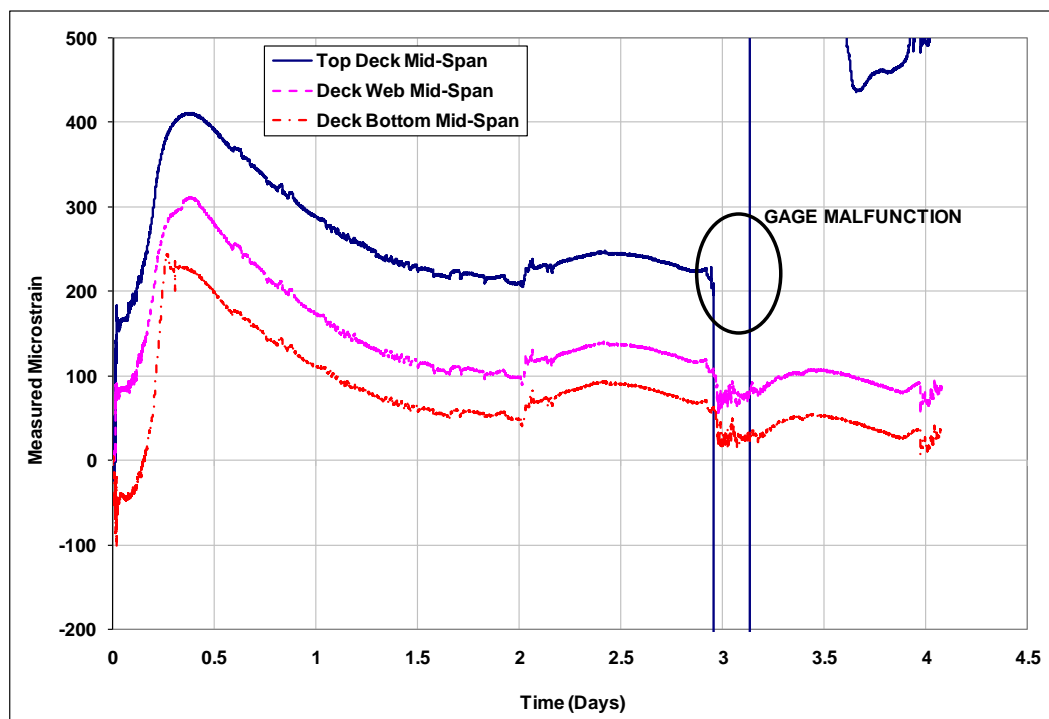


Figure 6.10: Measured strains at mid-span over first four days after concrete casting

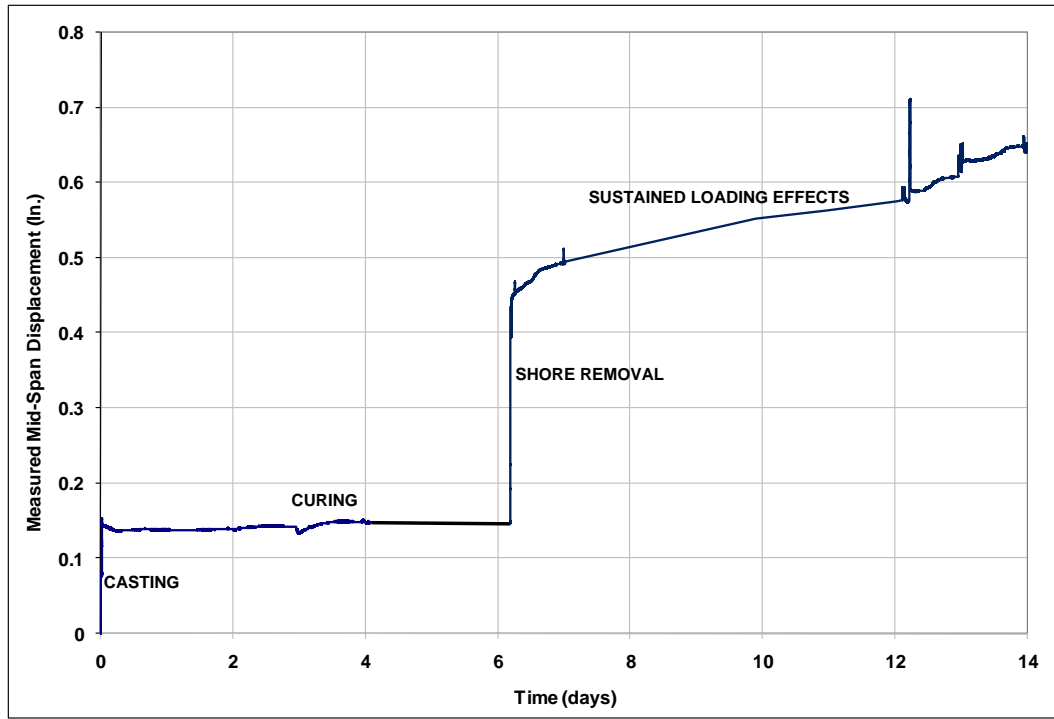


Figure 6.11: Measured mid-span deflection vs. time after concrete pour and shore removal for SC-DD Specimen

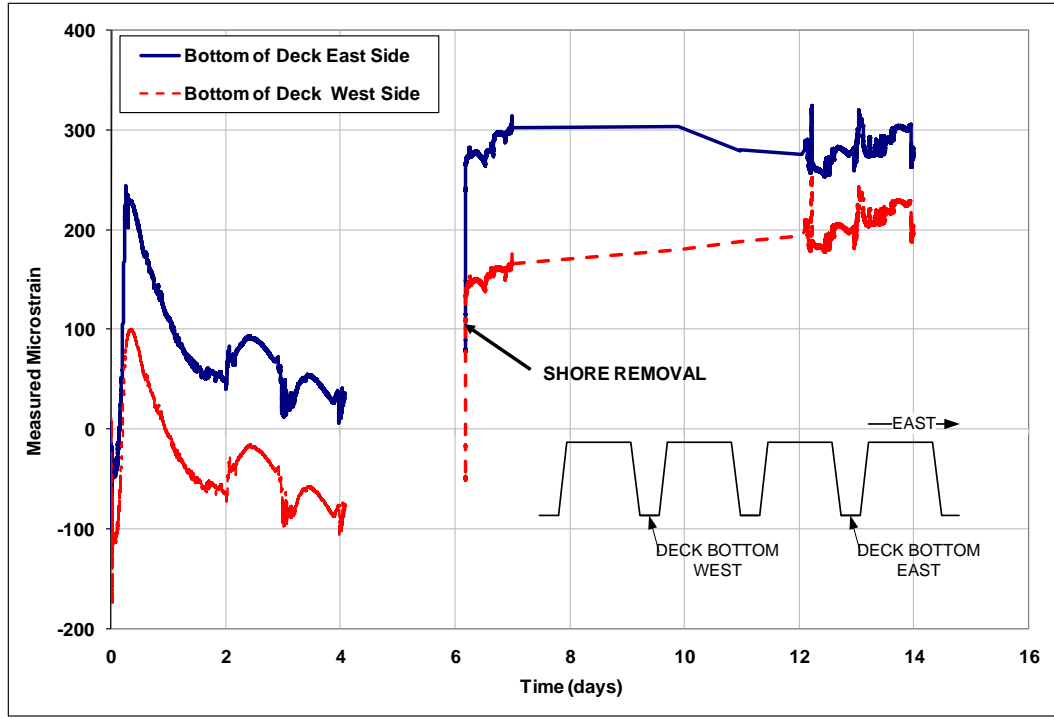


Figure 6.12: Measured strains vs. time for mid-span bottom gages

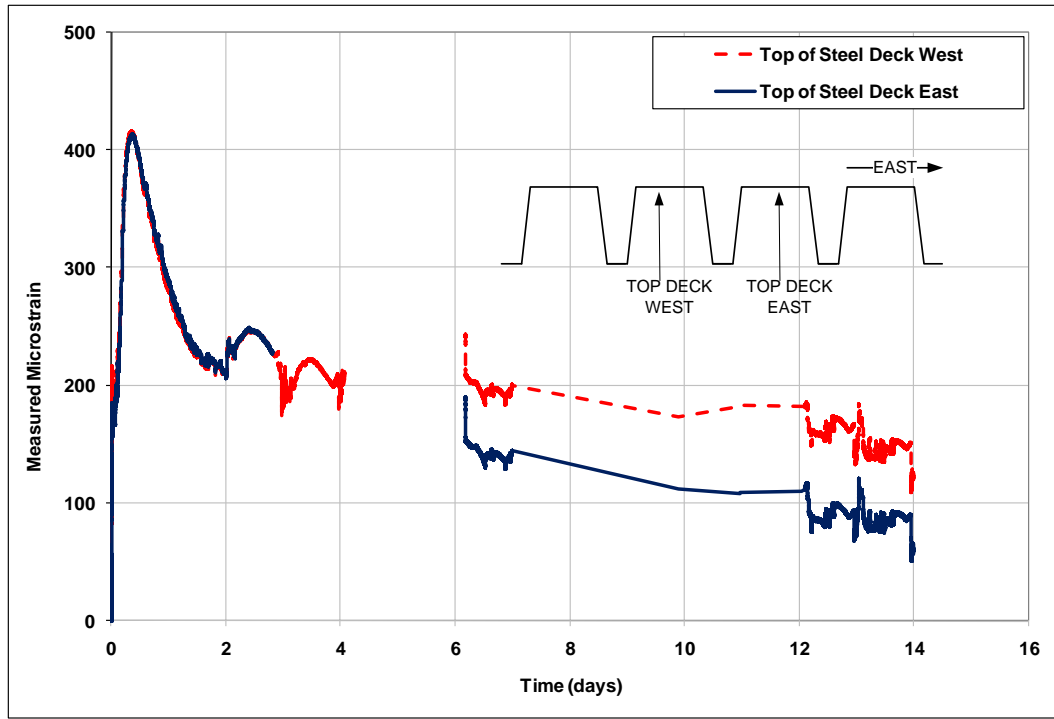


Figure 6.13: Measured strains vs. time for mid-span top gages

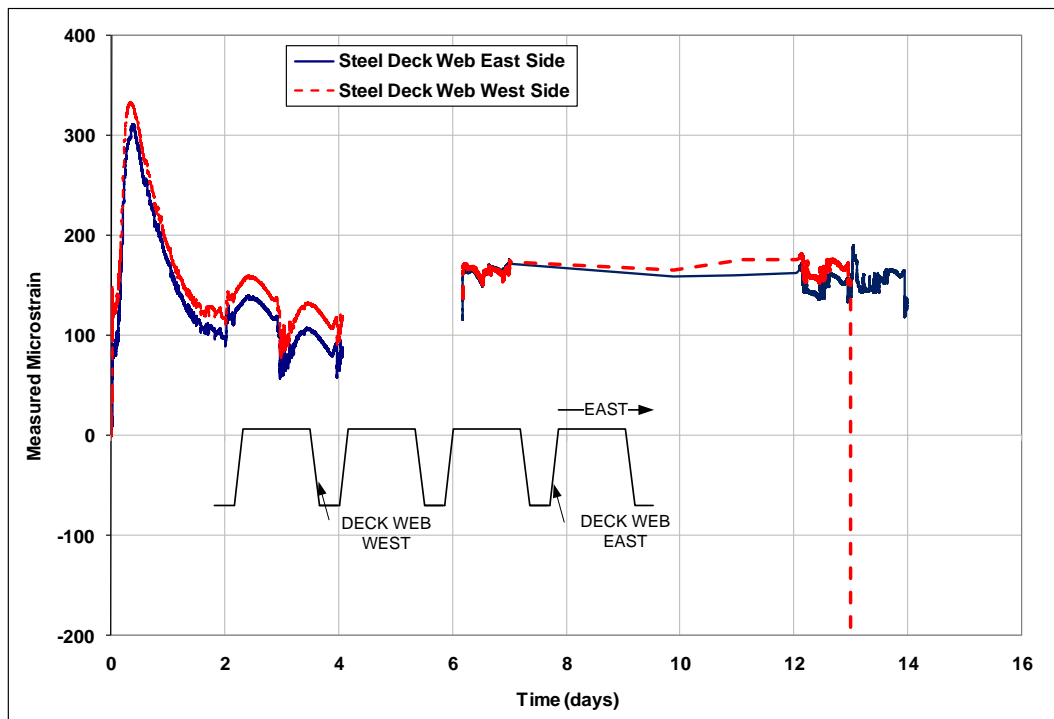


Figure 6.14: Measured strains vs. time for mid-span web gages

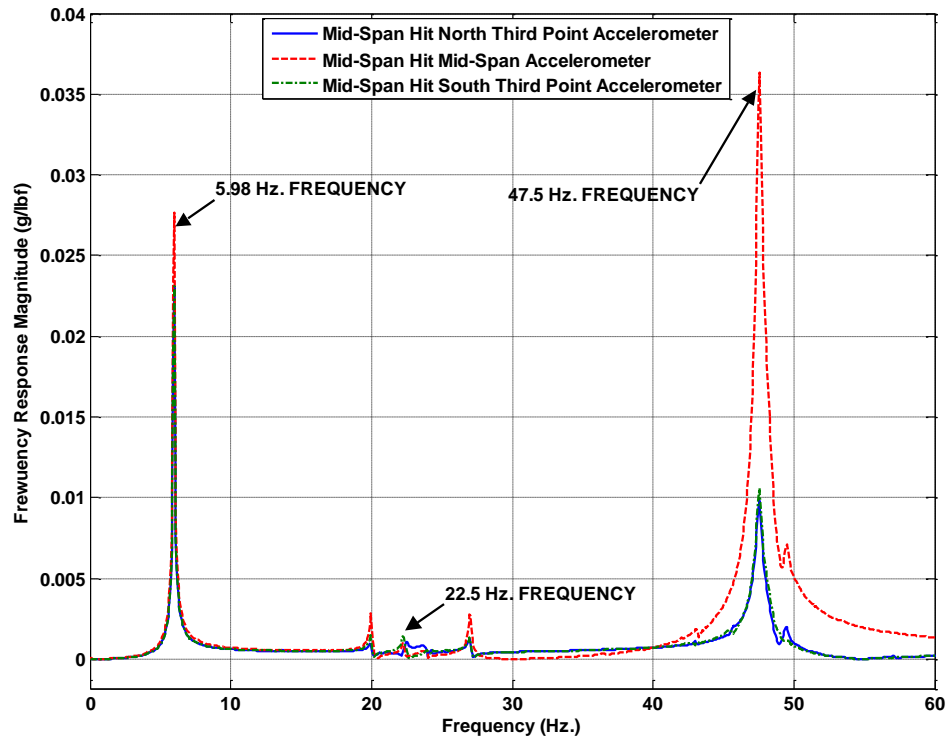


Figure 6.15: Frequency response plot for SC-DD Specimen taken from mid-span hammer hit showing data from south third point accelerometer, mid-span accelerometer, and north third point accelerometer

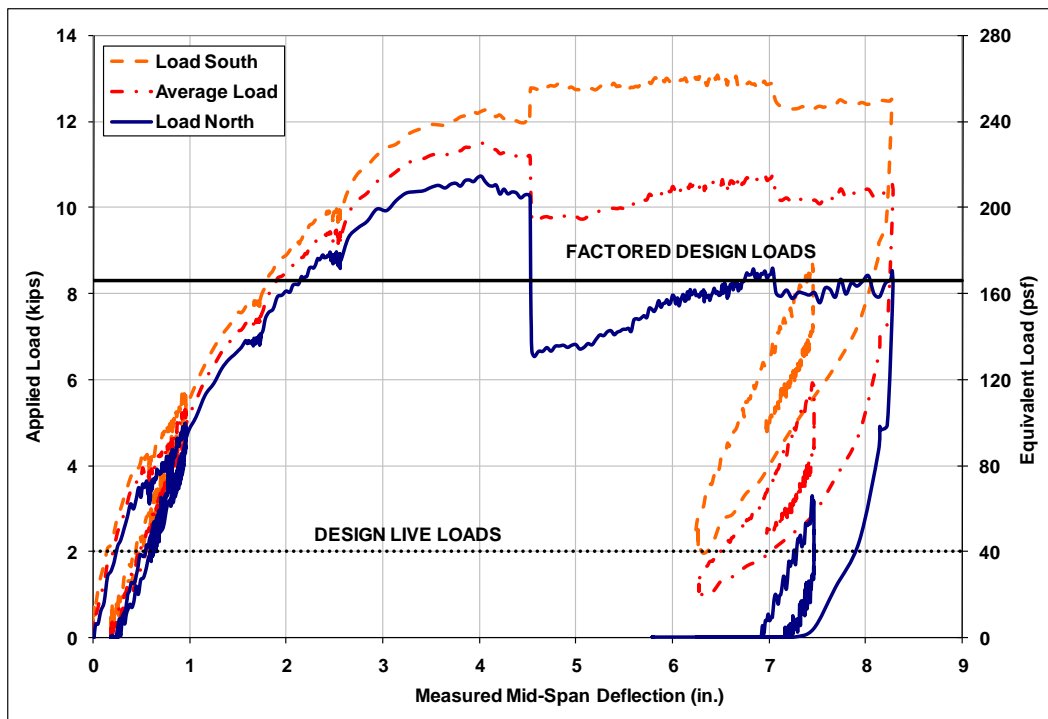


Figure 6.16: Applied load vs. mid-span deflection plot for SC-DD Specimen

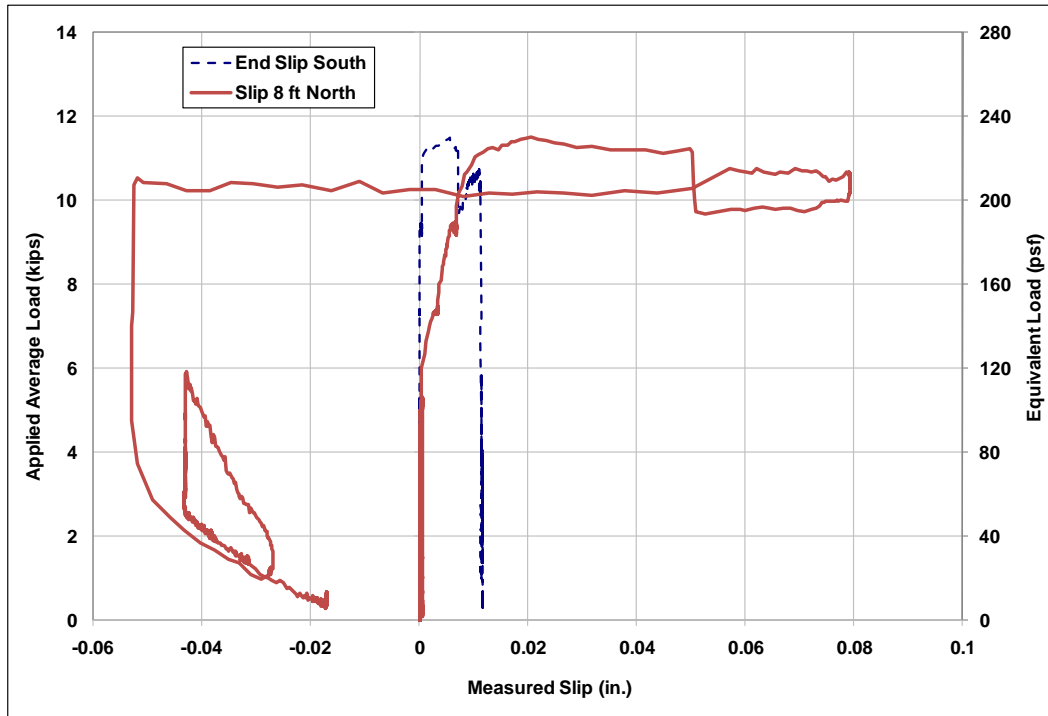


Figure 6.17: Average applied load vs. measured slip plot



Figure 6.18: View of north load point just prior to shear bond failure



Figure 6.19: SC-DD Specimen with approximately 11 kips (220 psf) applied and 4.5 in. of deflection



Figure 6.20: Concrete cracking at north support of SC-DD Specimen

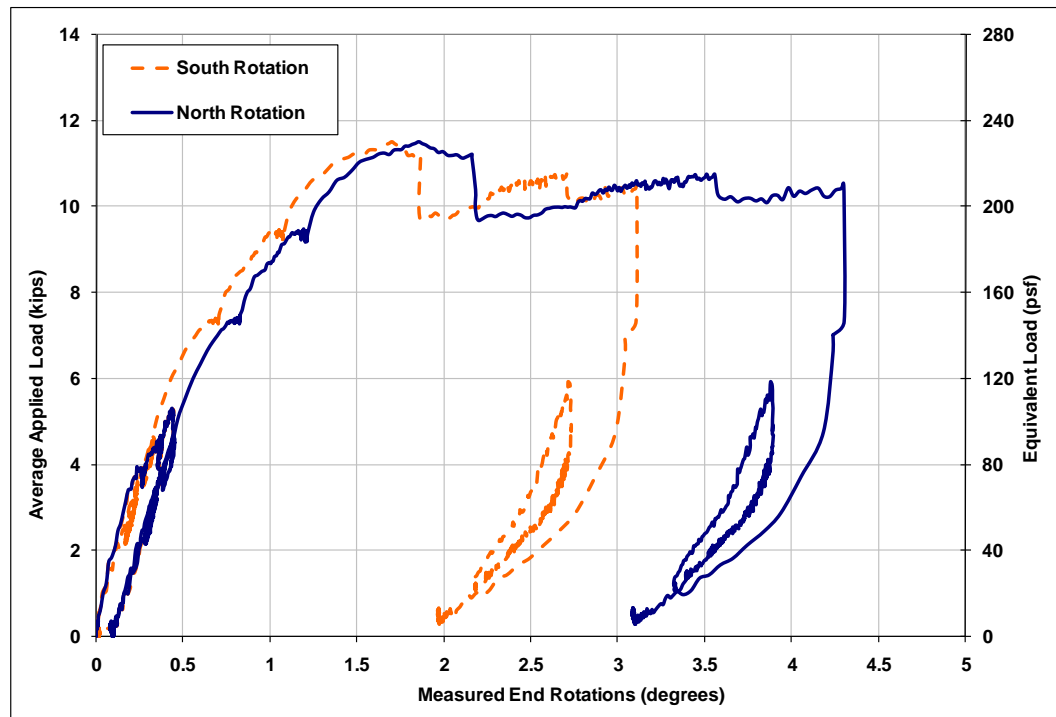


Figure 6.21: Average applied load vs. measured end rotation for SC-DD Specimen

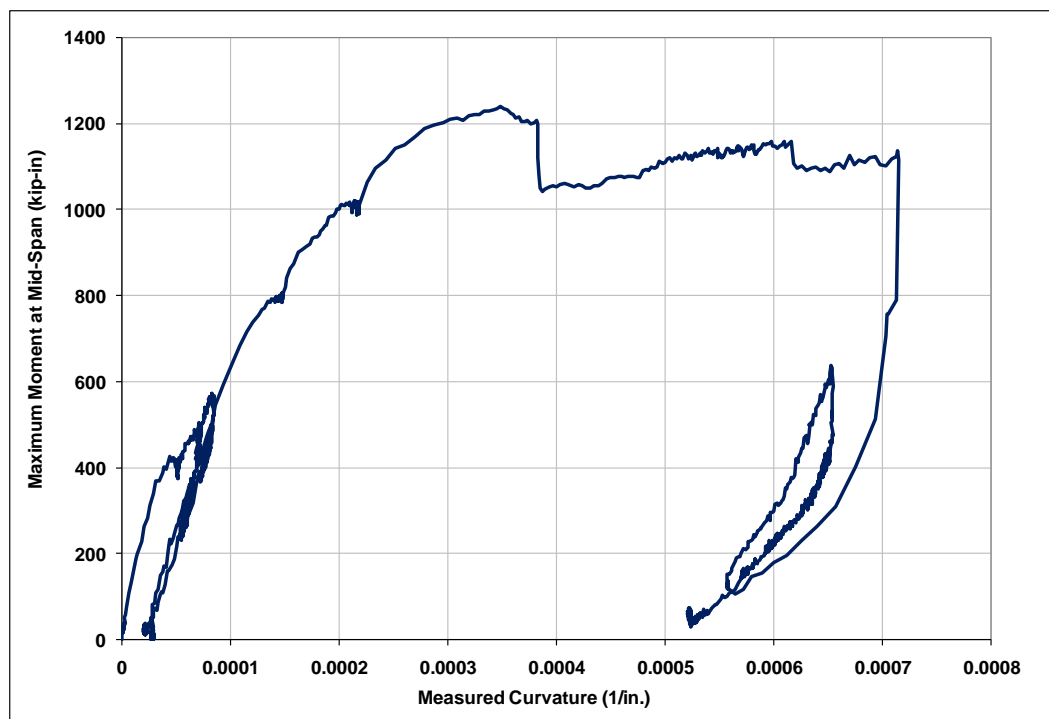


Figure 6.22: Plot of moment vs. measured curvature for SC-DD Specimen

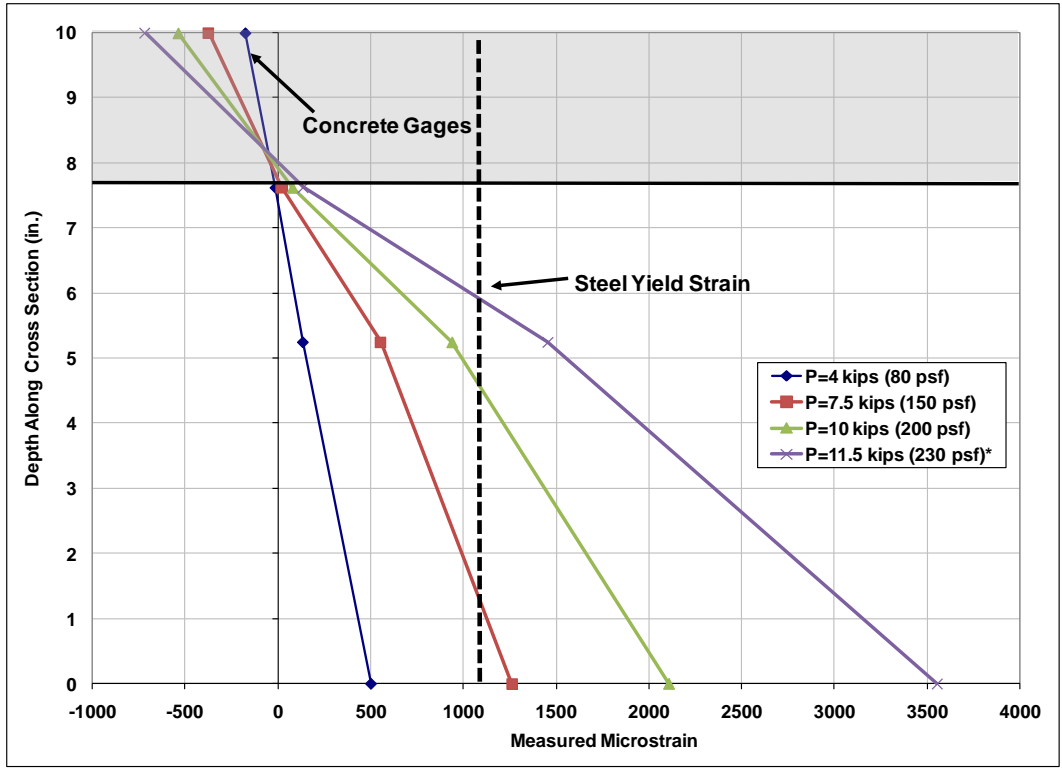


Figure 6.23: SC-DD Specimen strain gauge profiles through depth at mid-span for various load levels

*Indicates reading just prior to shear bond failure

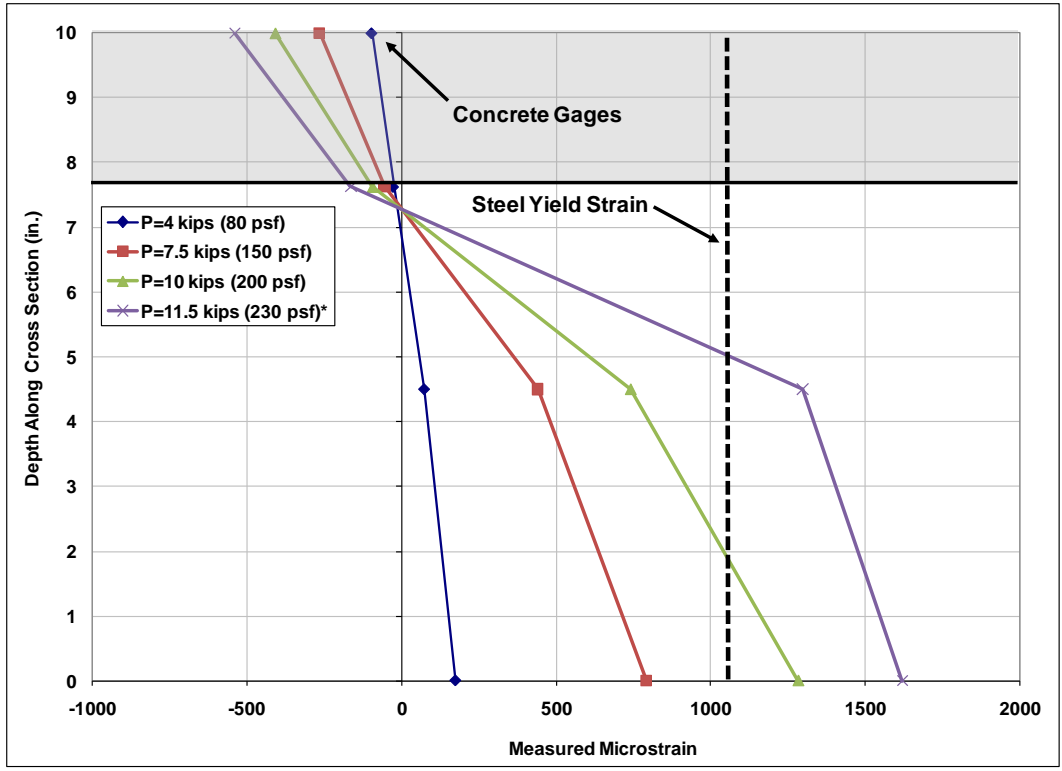


Figure 6.24: SC-DD Specimen strain gauge profiles through depth at north loading point for various load levels

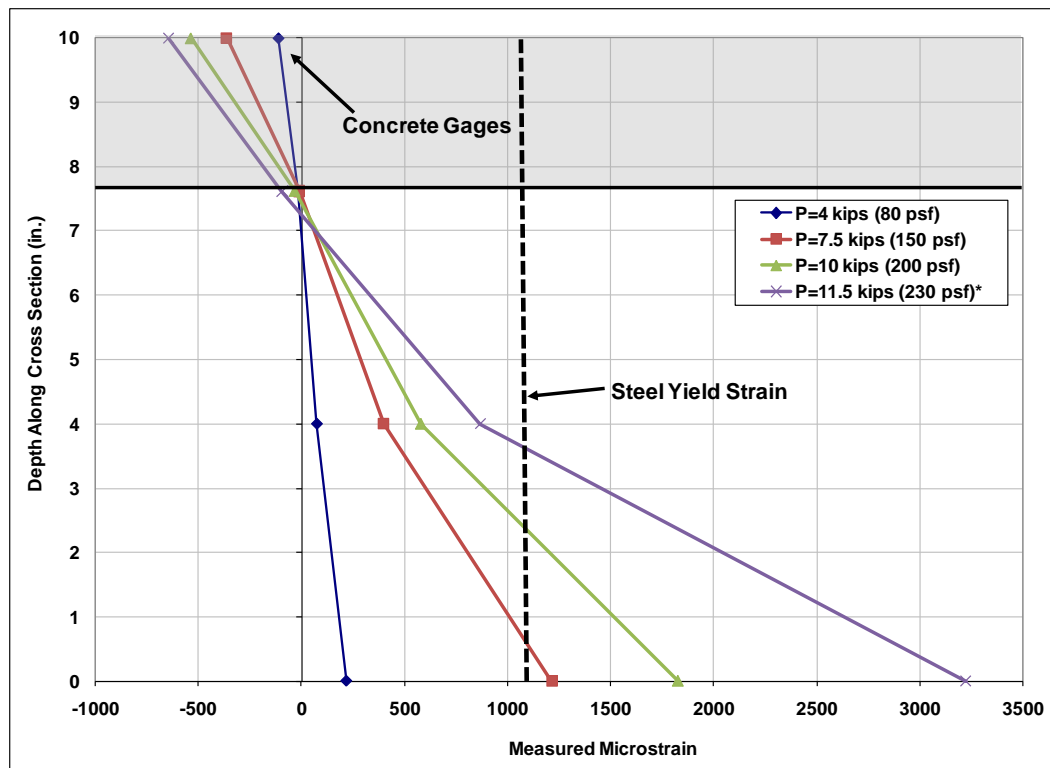


Figure 6.25: SC-DD Specimen strain gauge profiles through depth at south loading point for various load levels

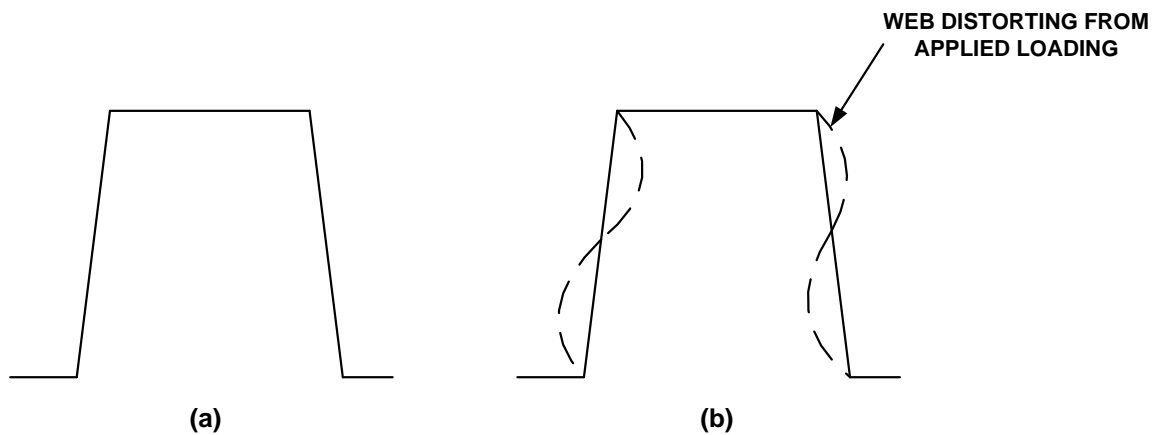


Figure 6.26: Schematic showing web distortion of deep deck cross-section

CHAPTER 7. REDUCED WEIGHT DEEP DECK SYSTEM

This chapter presents some further details of the previously described Reduced Weight Deep Deck (RW-DD) System. The system is summarized in Section 7.1. Details of the preliminary analysis and design are presented in Section 7.2. The details of the experimental setup are discussed in Section 7.3 and experimental results in Section 7.4

7.1. Summary of RW-DD System

The Reduced Weight Deep Deck (RW-DD) System was presented previously in Section 3.3.4 as an alternative composite steel deck-concrete system. This system was designed to reduce the self weight of a composite system while maintaining the desired composite strength and stiffness. The RW-DD system consisted of an existing 7.5 in. deep, 14 gage thick steel deck profile acting composite with a 2.5 in. thick lightweight concrete slab (115 pcf LWC). The concrete slab was on top of the steel deck only, i.e., no concrete was placed in the lower troughs of the steel deck. Furthermore, for the initial system design the deck profile would be inverted to put more steel area in tension. The concrete was prevented from flowing into the lower flutes by placing a lightweight filler material in them. Mineral wool, which is a common insulating and fireproofing material, was used as the lightweight filler material in the RW-DD system. The nominal density of the mineral wool was 10 pcf. A schematic of the cross-section is shown in Figure 7.1. The target span of the RW-DD system was 30 ft.

7.2. Preliminary Analysis and Design

The preliminary analysis and design of the RW-DD System was similar to that of the CC-DD and SC-DD systems. The same three approaches were used for analysis and design: 1) the design code-based approach, 2) non-linear inelastic analysis, and 3) 3D finite element modeling. The RW-DD was assumed to be a fully composite system for initial analysis and design.

7.2.1. Design Code Based Approach

The RW-DD System was first analyzed and designed using the code based approach that was similar to the approach used for the CC-DD and SC-DD systems. These approaches were described previously in Section 4.2.1 and Section 6.2.1 for the CC-DD and SC-DD systems, respectively. Both the construction and composite phases were

considered by this approach. Since un-shored construction was used the steel deck alone would resist the applied concrete weight. The composite level stiffness was estimated as the average of the cracked and un-cracked moments of inertia of the composite section. The composite strength was estimated assuming full composite action.

Table 7.1 summarizes the results of the code-based design and analysis for the construction and composite phases for the RW-DD system. Table 7.1 includes the flexural strength (ϕM_{n-con} , ϕM_{n-comp}) and stiffness (I_{cons} , I_{comp}) for the construction and composite phases. The ratios ($\phi M_{n-con}/M_{u*}$, $\phi M_{n-comp}/M_u$, $I_{con}/I_{req-con}$, and I_{comp}/I_{reqd}) are also included in the table. In these ratios M_{u*} , $I_{req-con}$, M_u , and I_{reqd} are the required flexural strengths and stiffnesses for the construction and composite phases. The table shows that the governing design parameter was the construction level stiffness with a $I_{con}/I_{req-con}$ ratio of 1.7.

7.2.2. Numerical Non-Linear Inelastic Analysis

The load-deflection behavior of the RW-DD system was predicted using the same fiber-based analytical approach used earlier for CC-DD Specimens in Chapter 4 and SC-DD Specimens in Chapter 6. A fiber model of the composite cross-section was developed and used to predict the section moment-curvature ($M-\phi$) response. The section curvatures were integrated numerically using the central difference method to predict the complete load-displacement response. This has been presented in detail in Section 4.2.2 and not repeated here for brevity. The preliminary analysis models for the RC-DD Specimen used nominal properties for the steel deck and concrete slab materials, assumed full composite action (i.e. no slip) between the deck and slab, and did not include the effects of construction loading or shore removal on behavior. This is similar to the assumption used earlier for the CC-DD specimens to predict their preliminary behavior in Section 4.2.2.

Figure 7.2 shows the preliminary load-deflection behavior predicted for the RW-DD system based on the non-linear inelastic analysis procedure. As shown, the predicted load capacity of the RW-DD system was equal to 340 psf. The predicted strength of the two CC-DD systems and SC-DD system are also shown in the figure for comparison. The predicted strength is greater than the design factored loads of 130 psf (1.2D+1.6L). The strength of the RW-DD system is lower than that of the CC-DD and SC-DD systems. However, it has a reduced self weight and still is shown to have more than twice the capacity required for design factored loads. The predicted deflection at assumed lived loads of 40 psf is approximately 0.35 in., which is well under an $L/360$ limit (1 in. for a 30 ft span).

7.2.3. Finite Element Analysis

The load-deflection behavior of the RW-DD system was also predicted using the 3D finite element method. The FEM models were similar to those used earlier for the CC-DD and SC-DD Specimens in Chapters 4 and 6. The steel deck was modeled using 4 node S4 shell elements and the concrete slab was modeled using 8 node brick elements

(C3D8). The steel deck and concrete surfaces were tied to each other to prevent slip. The steel and lightweight concrete material properties were specified as mentioned earlier in Section 4.2.3 using nominal material properties. The 30 ft span of the RW-DD floor system was modeled as simply supported as shown in Figure 7.3, which shows a picture of the FEM models. Figure 7.4 shows the load-deflection behavior predicted by the finite element analysis. It includes the predictions using the fiber model, the nominal live loading, and the factored ultimate loading. The FEM model predicts strength of 370 psf and a live load deflection of 0.35 in. The FEM model was able to run until higher displacement levels than those models for the CC-DD and SC-DD systems. This was likely due to the contact interfaces being simpler for this FEM model.

7.3. Experimental Setup

The experimental setup for the RW-DD system was similar to the setup used for the other deep deck systems with a few differences that are highlighted here. The first difference is at the end supports for the specimen. Since the deck profile was inverted there was more room for shear stud placement. Thus, two shear studs were placed per flute as shown in Figure 7.5. Mineral wool was placed in the lower flute of the specimen throughout its length with the exception of the 2 ft near the end supports. Concrete was cast above the deck and was placed in the lower flutes for the 2 ft from the end supports, where the mineral wool was not present. The side forms for this specimen were 2x6 lumber screwed into the edge side-laps of the deck. Figure 7.6 shows the specimen with mineral wool placed and side forms attached prior to the concrete pour. Other aspects of the test setup, instrumentation layout, and data acquisition were the same as those for the CC-DD and SC-DD specimens described previously in Section 4.4 and Section 6.3.

7.4. Experimental Results and Discussion

7.4.1. Construction Phase Results and Discussion

Table 7.2 summarizes the results from the construction phase for the RW-DD specimen. The table includes the results from the static construction loading test and concrete casting operation. As mentioned previously, the construction load test was conducted by placing 1 kip concrete blocks at third points. The concrete casting included the effects of the weight of the concrete and the construction workers. The residual displacements were measured upon removal of the construction loads (1 kip blocks) and also after the completion of the concrete casting operation.

As shown in Table 7.2, the RW-DD specimen had a mid-span displacement of 0.8 in. for construction loading. This displacement was recovered upon removal of the concrete blocks. The maximum tensile strain induced in the bottom plate was equal to 190 microstrain. During the concrete casting operation, the maximum displacement caused by the wet concrete and workers was equal to 1.2 in. The residual displacement caused

by the concrete weight alone was 1.1 in. The maximum tensile strain induced by the concrete casting was 340 microstrain. The corresponding stress was 10 ksi. The residual strain after completion of the concrete casting process was equal to 300 microstrain or 8.9 ksi. These results indicate that the RW-DD system perform adequately during un-shored construction. The maximum strains experienced during the concrete casting operation were well below the yield stress of the deck.

7.4.2. Modal Impact Testing Results and Discussion

The use of modal impact testing was implemented on this specimen to estimate the fundamental frequencies of the system. Accelerometers were placed at three points on the top of the specimen. The locations were at 3rd points and at mid-span. Hammer hits were done every foot along the specimen. The average of 5 hits was used at every location. The estimated first natural frequency of the system was 5.9 Hz. This compares reasonably well with the 6 Hz. frequency estimated using a simple SDOF model. Damping was estimated at 0.5% for the first frequency using the half power method. An FRF computed from a hammer hit at mid-span is shown in Figure 7.7. As shown, the second and third fundamental frequencies are estimated at 21.1 and 43.5 Hz., respectfully. Some small torsional frequencies from the specimen twisting occur around 28 Hz. This torsional frequency is occurring due to the small width of the Specimen and is not representative of a frequency within an actual floor system in a structure.

The output spectra for this specimen was investigated to look at what modes were dominate. The spectrum for two people walking on the specimen was investigated for this purpose. Figure 7.8 shows the output spectra for two people walking simultaneously on the specimen. As shown, the first mode has around 24 times more energy than the second mode and 60 times more from the third bending mode. The torsional mode at 28 Hz is more dominant then the second and third resonances. However, this frequency is unique to the type of specimen and would not be a concern in an actual structure. Thus, based on the output spectra it is believed the first fundamental mode dominates dynamic behavior for the RW-DD Specimen.

7.4.3. Ultimate Load Test Results and Discussion

An ultimate load test was conducted on the RW-DD specimen. As mentioned previously, the test was conducted using the same loading and support frames, hydraulic rams and equipment, instrumentation layout, and data acquisition as the previously tested CC-DD specimens. The compressive strength of the concrete on the date of test was 5633 psi. This was determined by testing 4in. by 8 in. concrete cylinders. Uniaxial tension tests according to ASTM E8 (ASTM, 2004) were performed on machined tension coupons taken from the deck. These tests indicated a yield stress of 31 ksi for the deck. Additional concrete batch mixes, mill certifications and measurements from tension tests are given in Appendix C.

The RW-DD Specimen had unexpected results with regards to the ultimate load test. Figure 7.9 shows the applied load vs. displacement data for the specimen. As shown, the

specimen exhibited expected linear-elastic behavior until approximately 7 kips (140 psf) of applied loading. At this point, the top concrete slab separated from the steel deck and buckled under the applied load. The failure occurred at 4 ft from the north end and is shown in Figure 7.10 and Figure 7.11. After the slab separated from the deck there was sudden drop in load of around 2 kips at each load point. Load was kept on the specimen until it reached approximately 3 in. of deflection. At this point the top slab had lifted significantly and the web of the steel deck had begun to buckle outwards near mid-span. The specimen was unloaded at this point and subsequently re-loaded to yield the load-deflection curve shown in Figure 7.9.

The failure mode of this specimen highlighted some shortcomings in the RW-DD specimen. First, no shear transfer mechanisms were placed on the deck. Additional shear transfer and bonding mechanisms like embossments or stand-off screws may be required for the RW-DD system to work as intended. The best means to evaluate this likely would require more investigation and testing. Rather than try and to develop a system with shortcomings of this nature, it was decided to shift focus on systems with more applicability in the near future.

Table 7.1: Design Checks of RW-DD System

System	Construction Phase				Composite Phase			
	ϕM_{n-con} (kip-ft/ft)	ϕM_{n-con} / M_u^*	I_{cons} (in. ⁴ /ft)	$I_{cons}/I_{req-con.}$	ϕM_n (kip-ft/ft)	$\phi M_n/M_u$	I_{comp} (in. ⁴ /ft)	$I_{comp}/I_{reqd.}$
RW-DD	15.4	2.25	20	1.7	38.5	2.75	49	2

Table 7.2: Summary of construction phase measurements for RW-DD Specimen

Parameter	Construction Loading	Concrete Pour
Max Deflection During Construction (in.)	0.8	1.2
Residual Mid-Span Deflection (in.)	0	1.1
Max Tensile Strain (μs)	190	340 (10 ksi)
Residual Tensile Strain (μs)	0	300 (8.9 ksi)

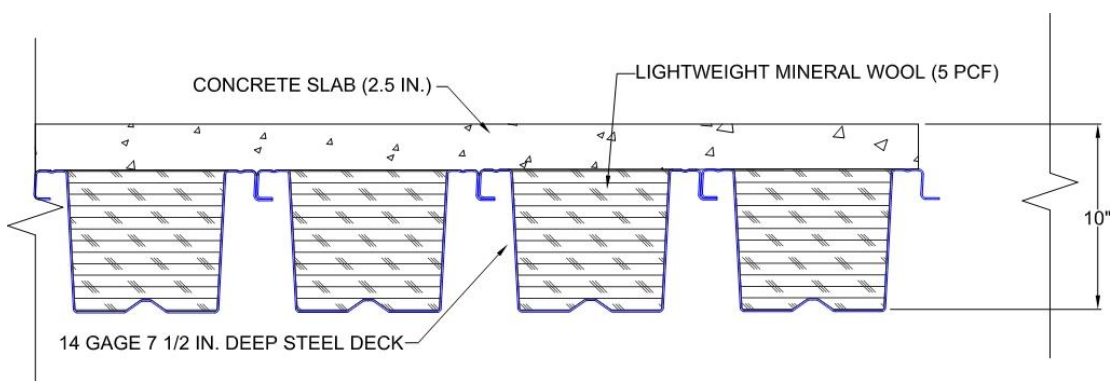


Figure 7.1: Reduced weight composite deck system

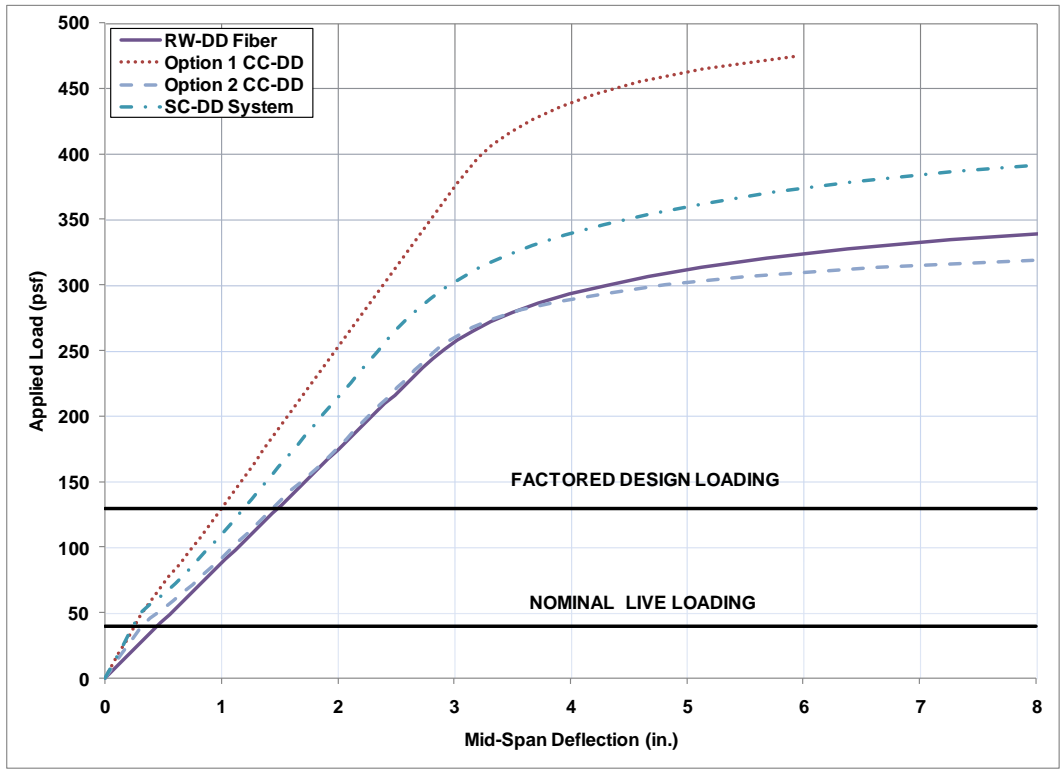


Figure 7.2: Predicted load vs. deflection behavior for RW-DD System for Non-linear inelastic analysis

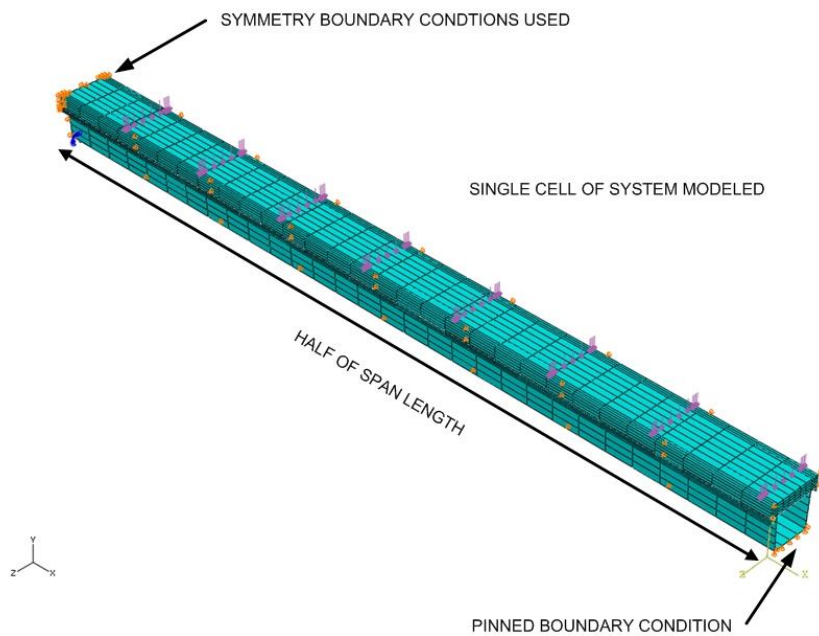


Figure 7.3: Schematic of meshed structural FEM models for RW-DD system

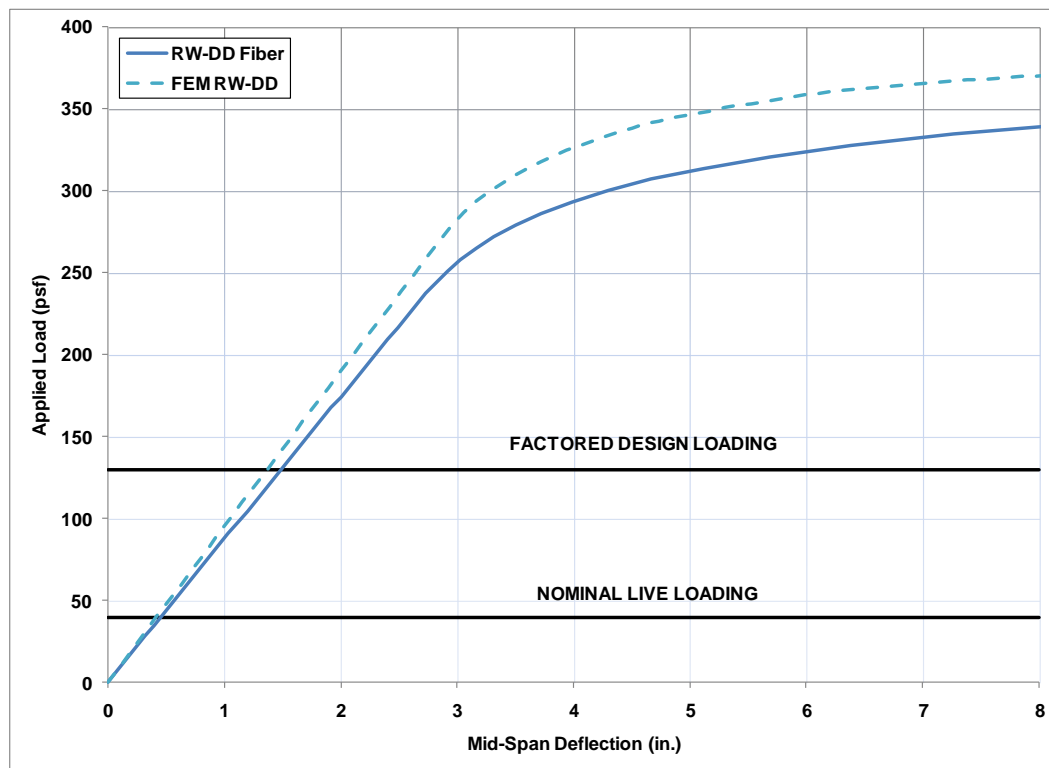


Figure 7.4: Predicted load vs. deflection behavior for RW-DD System for Non-linear inelastic analysis and FEM model



Figure 7.5: View of specimen with shear studs placed



Figure 7.6: End view of RW-DD System prior to concrete pour showing mineral wool placement

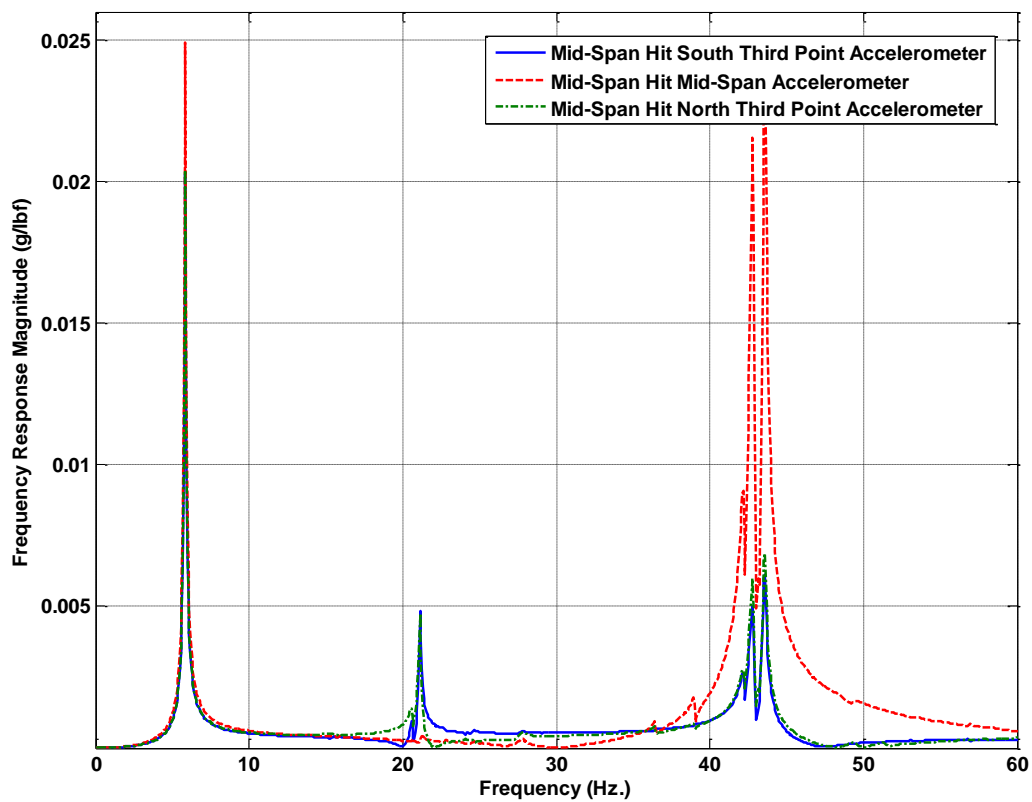


Figure 7.7: Frequency Response Function (FRF) for RW-DD System

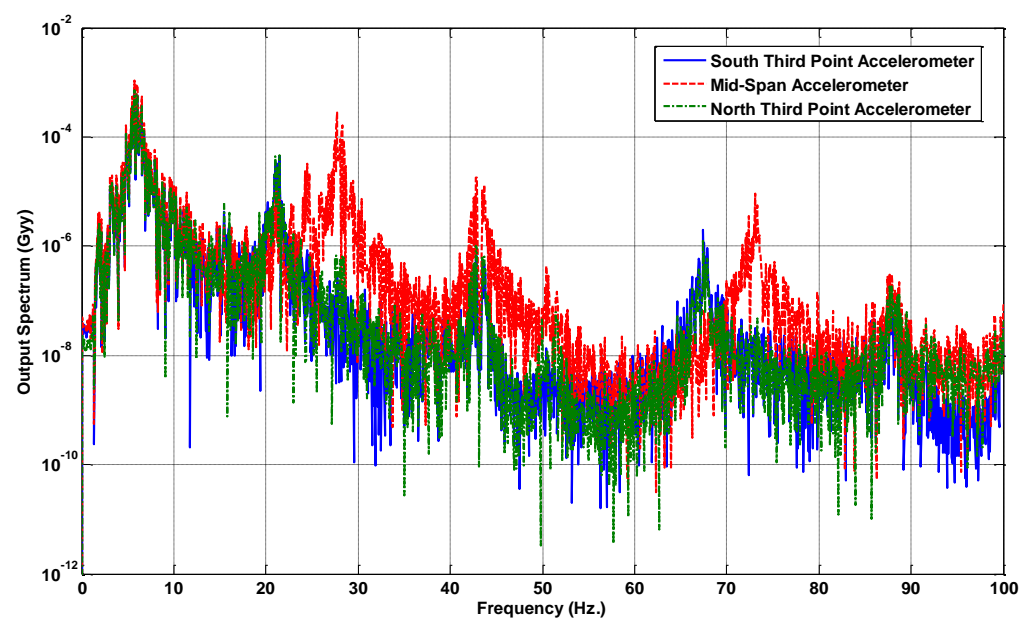


Figure 7.8: Output Spectrum for RW-DD Specimen from two people walking simultaneously (log scale)

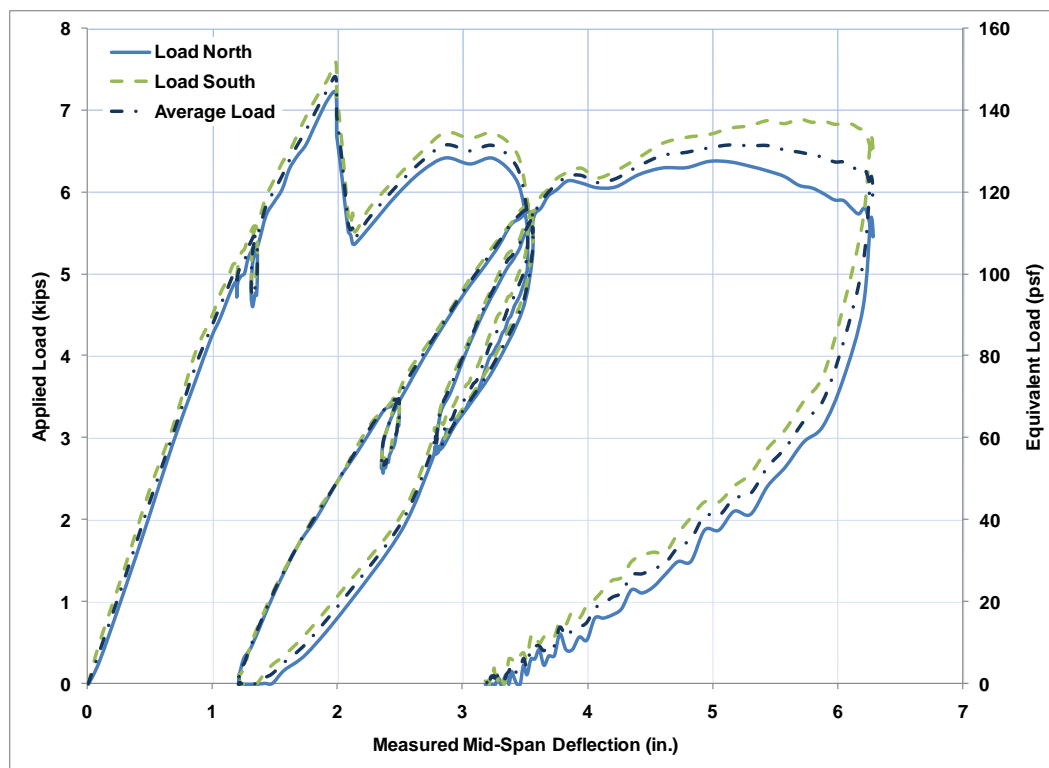


Figure 7.9: Applied load vs. measured mid-span deflection for RW-DD Specimen



Figure 7.10: Separation of concrete from steel and concrete buckling

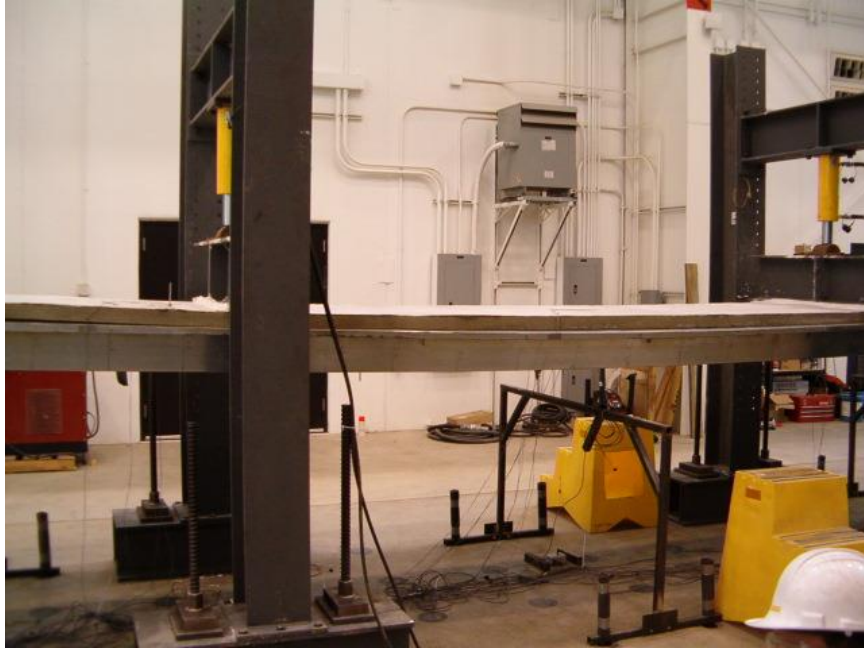


Figure 7.11: Displaced shape of specimen as failure occurred

CHAPTER 8. PRE-LOADED SELF-SHORED SYSTEM

This chapter presents further details on the Pre-Loaded Self-Shored (PLSS) System that was introduced earlier in Section 3.4. As mentioned earlier, the PLSS system optimizes the design and depth of the existing composite steel deck-concrete slab floor system by providing self-shoring in the construction phase. The flexural stiffness of the non-composite steel beam in the construction phase governed its design and depth (12-16 in.). The PLSS system optimizes this to 8 in. by providing self-anchored shoring in the construction phase as explained in this chapter. Section 8.1 presents the analysis and design of the PLSS system in the construction phase and also includes a design example. Section 8.2 presents the setup of the PLSS system in the laboratory and the experimental validation of the system. Section 8.3 presents the experimental results and discussion.

8.1. Analysis and Design of System – Construction Phase

The analysis of the PLSS system can be divided into three phases. Phase 1 consists of applying the upward force and displacement to the beam mid-span. This pre-loading force would be applied to the bare steel beam prior to any other attachments. Phase 2 consists of placing the steel deck and casting the concrete slab. Phase 3 involves removing the shoring system after the concrete had cured 7-14 days after casting. In the first two phases the non-composite steel beam and self-shoring system would be equivalent to a king-post truss, like that shown in Figure 3.18. The concrete casting process will lead to an increase in the force at the mid-span and the self-shoring mechanism. The force increase will depend on the stiffness of the jack (or king post/strut) and the tension members of the self-shoring system. The following subsections present the analysis and design of the PLSS system for the first three phases.

8.1.1. Phase 1

Phase 1 consists of applying an upward force at the beam mid-span using the self-shoring setup. The beam is assumed to be simply supported, i.e., there is no rotational fixity at the ends of the member. Figure 8.1 shows the free body diagram of the steel beam subjected to the upward force by the self-shoring system. Applying the upward force in the system induces axial tension and elongation in the tension members of the self-shoring system. The beam is subjected to axial compressive forces and a moment caused by the eccentricity of the tension force. Thus, in this stage the beam is actually a beam-column member and would need to be designed (checked) accordingly. The

flexural stiffness of the beam (K_I) for mid-span deflection is calculated using equation 8.1 and the upward deflection is (Δ_1) is calculated using equation 8.2.

$$K_1 = \frac{48EI_x}{L^3} \quad 8.1$$

$$\Delta_1 = \frac{PL^3}{48EI_x} \left(1 + \frac{d}{L} \frac{3}{\tan \theta} \right) \quad (a) \quad 8.2$$

$$\Delta_1 \approx \frac{PL^3}{48EI_x} \quad (b)$$

Where:

E	Elastic modulus of steel beam – assumed to be 29000 ksi
I_x	Moment of inertia of beam cross-section
L	Length of the beam
P	Applied upward force
d	Depth of the beam
θ	The angle between the horizontal plane of the beam and the tension members on the self shoring mechanism (see Figure 8.1).

In equation 8.2, d is the beam depth (approximately 8-10 in.) and the ratio of d/L is quite small. Hence, the mid-span deflection can be estimated using equation 8.2b as a reasonable approximation. The mid-span moment due to the pre-load (M_{pl}) can be calculated using equation 8.3.

$$M_{pl} = \frac{PL}{4} + \frac{Pd}{4 \tan \theta} \quad 8.3$$

8.1.2. Phase 2

Phase 2 analysis focuses on the effects of steel deck and concrete placement on the pre-loaded self shored beam. Casting concrete will cause an increase in the self-shoring force at the mid-span as the system compensates for the applied loading (self weight). This increase in the self-shoring force also increases the forces in the other components of the self-shoring system. The forces and displacements can be determined using the principles of compatibility and equilibrium and by estimating the stiffness of various components.

The stiffness of the self-shoring system depends on the axial stiffness of the diagonal tension members and the vertical compression strut. Axial shortening of the vertical compression strut is assumed to be small enough that it can be ignored in the analysis. The effective stiffness of the diagonal tension members for vertical displacement of the beam mid-span system can be calculated using equation 8.4.

$$K_s = \frac{2EA_r}{L_r} \sin^2 \theta = \frac{4EA_r \cos \theta \sin^2 \theta}{L} \quad 8.4$$

Where:

A_r	The cross sectional area of the tension members
L_r	Length of the tension members
L	Total length of the beam

This stiffness is in parallel with the flexural stiffness of the beam, which can be expressed using equation 8.5 for uniformly distributed loading (w).

$$K_{bm} = \frac{384EI_x}{5L^3} \quad 8.5$$

The total stiffness of the entire beam-shoring system for vertical displacement of the mid-span can now be calculated using equation 8.6.

$$K_2 = K_s + K_{bm} \quad 8.6$$

The mid-span displacement caused by placing the metal deck and the concrete slab can then be calculated using equation 8.7.

$$\Delta_2 = \frac{P_c}{K_2} \quad 8.7$$

Where:

P_c	The total weight of the concrete slab and the steel deck acting at the mid-span (shoring support). It is equivalent to 0.625 times the total weight of the slab
-------	---

The above expression gives the deflection for the second phase. The total deflection at this point will be the subtraction of the upward displacement from phase 1 and the downward displacement from phase 2, i.e., be $\Delta_1 - \Delta_2$. Where Δ_1 and Δ_2 are calculated using equations 8.2 and 8.7.

For this phase it is also important to estimate the forces in the self shoring system components and the beam member. The additional forces acting in the tension members of the self shoring system can be estimated by calculating the ratio of the self-shoring system stiffness to the overall system stiffness, and multiplying it by the load acting on the member as shown in equation 8.8.

$$\Delta P = \left(\frac{K_s}{K_2} \right) P_c \quad 8.8$$

Where:

ΔP The increase in the vertical force applied by the self shoring system and caused by the concrete casting.

Thus, the total force in each tension member (P_{tr}) of the self shoring-system can be calculated using equation 8.9.

$$P_{tr} = \frac{P + \Delta P}{2 \sin \theta} \quad 8.9$$

Figure 8.2 shows the free body diagram of the beam in this phase. It includes all the forces acting on the beam member from the loads and self-shoring system. The compressive force in the beam can be calculated using equation 8.10.

$$P_{tr} = \frac{P + \Delta P}{2 \tan \theta} \quad 8.10$$

The mid-span moment of the beam can be calculated using equation 8.11.

$$M_{ms2} = \frac{wL^2}{8} - \frac{(P + \Delta P)L}{4} - \frac{(P + \Delta P)d}{4 \tan \theta} \quad 8.11$$

Where w is the applied distributed loading.

8.1.3. Phase 3

The third phase during construction is the removal of the self-shoring system. The shoring system is removed after the concrete hardens (7-14 days after casting) and the beam section becomes composite with the steel deck-concrete slab. The effects of shore removal were simulated by applying negative (downward) load equal to $P + \Delta P$ at the mid-span of the composite beam. The downward deflection of the composite beam can be calculated using equation 8.12.

$$\Delta_3 = \frac{(P + \Delta P)L^3}{48EI_{comp}} \quad 8.12$$

Where:

Δ_3 The deflection due to shore removal

I_{comp} The moment of inertia of the composite beam. Assumed to be the transformed moment of inertia for an un-cracked section.

The final mid-span deflection (Δ_f) of the composite beam can be calculated using equation 8.13.

$$\Delta_f = \Delta_1 - \Delta_2 - \Delta_3 \quad 8.13$$

In phase 1, the steel beam will be subjected to a negative (hogging) moment at mid-span and the stresses will be tensile on top and compressive in the bottom flange. In phase 2, the steel beam will be subjected to a small positive moment at mid-span from the weight of the concrete slab casting operation and flexibility of the self-shoring system. In phase 3, the removal of the self-shoring will subject the composite section to positive moment at the mid-span. The total resultant stresses in the section can be calculated using superposition and mechanics as will be illustrated in Section 8.1.5.

8.1.4. Determination of ideal upward force and deflection

Equations 8.2-8.13 were used to develop a relationship between the initial pre-load (P) and the final deflection (Δ_f) after shore removal. This relationship is presented in equation 8.14.

$$P = \frac{I_x \left(\left(\frac{-48EI_{comp}\Delta_f}{L^3} \right) + P_c \left(-1 + \frac{96I_x - 60I_{comp}}{96I_x + 5A_r L^2 \cos \theta \sin^2 \theta} \right) \right)}{I_x - I_{comp}} \quad 8.14$$

This equation provides the relationship between P and Δ_f in terms of the applied concrete slab weight (P_c) and the bare steel and composite section properties (I_x , I_{comp}) and the self-shoring parameters (A_r and θ). Equation 8.14 can be used to calculate the value of P required to produce a target Δ_f . The target or ideal value for Δ_f after shore removal can be selected by the engineer in the design process, and equation 8.14 can be used to calculate the design P . If the target (or ideal) Δ_f is equal to zero, i.e., the floor has a level finish upon shore removal, then the corresponding value for the preload can be calculate using equation 8.15.

$$P_{\Delta_f=0} = \frac{P_c}{I_x - I_{comp}} \left(-1 + \frac{96I_x - 60I_{comp}}{96I_x + 5A_r L^2 \cos \theta \sin^2 \theta} \right) \quad 8.15$$

If the designer does not provide a preload (i.e. $P=0$) then the PLSS system will simplify to a king-post shoring system and the final deflection (Δ_f) after shore removal can be calculated using equation 8.16.

$$\Delta_f = \frac{P_c L^3}{48EI_{comp}} \left(-1 + \frac{96I_x - 60I_{comp}}{96I_x + 5A_r L^2 \cos \theta \sin^2 \theta} \right) \quad 8.16$$

This equation was obtained by substituting $P=0$ into equation 8.14. The designer has to check that Δ_f after shore removal is acceptable. As shown by equation 8.16, Δ_f depends on the applied loading (P_c), bare steel and composite section properties, and the king-post truss properties (A_r and θ). It is important to note that all the equations and calculations assumed downward displacements to be negative.

8.1.5. Analysis and Design of System – Composite Phase

For the post construction composite phase, the system it can be checked as a composite beam using the appropriate AISC specifications. The engineer designing the floor system for the intended structure can determine whether full composite action is needed in this phase. The system's susceptibility to floor vibrations can also be checked in this phase. AISC Design Guide 11 can be used to evaluate the systems overall susceptibility to floor vibration.

8.1.6. Design Example for Pre-Loaded Self-Shored System

This section presents a design example for the PLSS floor system. This design example will also be used later to design the test specimen for the PLSS system.

Given Parameters

Design a PLSS system with the given information:

- 30 ft span, 8 ft spacing (layout shown in Figure 8.3)
- 2 in. floor deck composite with 2.5 in. of normal weight concrete cover. Self weight of steel deck-concrete system = 45 psf.
- The angle of the shoring mechanism was assumed to be 8.5°
- Other loads acting on system:
 - Steel deck alone = 3 psf
 - Construction Live Load = 20 psf
 - Service Level Live Load = 40 psf
 - Partition Loads and Ductwork = 20 psf

Figure 8.3 shows the interior bay layout for the design example. The PLSS system was designed for all the interior beams. The interior (filler) beams were assumed to be W8x35 beam sections. The corresponding steel moment of inertia (I_x) was calculated as 120 in.^4 . The composite beam moment of inertia (I_x) was calculated as 550 in.^4 . The area of the tension members (A_r - per side) of the self shoring system was assumed to be 1.57 in.^2 . This corresponds to the use of 2 in. diameter steel rods (or two 1 in. diameter rods per side). The angle $\theta=8.5^\circ$ was assumed for the self-shoring system. It corresponds to a compression strut length of 26 in. below the beam depth. The assumed and calculated properties are listed below:

I_x	Moment of inertia for W8x35 beam = 120 in. ⁴
I_{comp}	Moment of inertia for composite section = 550 in. ⁴
A_r	Area of diagonal tension member = 1.57 in. ² (threaded rods assumed)
L	Length of W8x35 beam = 30 ft = 360 in.

Phase 1

The design example assumed that the target (ideal) displacement (Δ_f) was equal to zero, i.e., after shore removal the floor system will be level. Using equation 8.15, the preload force required to achieve this can be calculated as 3.25 kips.

$$P = \frac{I_x \left(\left(\frac{-48EI_{comp}\Delta_3}{L^3} \right) + P_c \left(-1 + \frac{96I_x - 60I_{comp}}{96I_x + 5A_r L^2 \cos \theta \sin^2 \theta} \right) \right)}{I_x - I_{comp}}$$

$$P = \frac{127in^4 \left(\left(\frac{(-48 \times 550in^4 \times 0)}{\left(30ft \times 12 \frac{in}{ft} \right)^3} \right) + 6.75 \left(-1 + \frac{96 \times 127in^4 - 60 \times 550in^4}{96 \times 127in^4 + 5 \times 1.57in^2 \times (360in)^2 \times \cos(8.5^\circ) \times \sin^2(8.5^\circ)} \right) \right)}{127in^4 - 550in^4}$$

$$P = 3.25kips$$

The corresponding upward deflection (Δ_f) of the beam mid-span will be equal to 0.87 in.

Phase 2

The downward deflection (D_2) after deck and concrete placement was calculated using equation 8.7 as 0.4 in. in the downward direction.

$$\Delta_2 = \frac{P_c}{K_2} = \frac{6.75kips}{17 \frac{kips}{in.}} = 0.4in.$$

The corresponding increase in the force (ΔP) applied by the self-shoring system can be calculated from equation 8.8 as 4.3 kips.

$$\Delta P = \left(\frac{K_s}{K_2} \right) P_c = \frac{10.9}{17} \times 6.75kips = 4.3kips$$

The total force in the tension members of the self-shoring system can be calculated using equation 8.9. as 25.5 kips.

$$P_r = \frac{P + \Delta P}{2 \sin \theta} = \frac{3.25 + 4.3}{2 \times \sin(8.5^\circ)} = 25.5 \text{ kips}$$

The compressive force in the steel beam can be calculated using equation 8.10 as 25 kips.

$$P_c = \frac{P + \Delta P}{2 \tan \theta} = \frac{7.55}{2 \times \tan(8.5^\circ)} = 25 \text{ kips}$$

The mid-span moment in the bare steel beam can be calculated using equation 8.11 as - 24.4 kip-ft.

$$M_{ms2} = \frac{wL^2}{8} - \frac{(P + \Delta P)L}{4} - \frac{(P + \Delta P)d}{4 \tan \theta} = \frac{0.36 \frac{\text{kips}}{\text{ft}} \times 30 \text{ ft}^2}{8} - \frac{7.55 \times 30 \text{ ft}}{4} - \frac{7.55 \times 8 \text{ in.}}{4 \times \tan(8.5^\circ)} = -24.4 \text{ kip} \times \text{ft}$$

The non-composite steel beam (W8x35) can be checked for the combined axial compression (P_c) and moment (M_{ms2}) using AISC Specifications (Chapter H, Equation H-1). The axial capacity of the W8x35 beam was calculated as the minor axis buckling strength of a column with an effective length equal to 30 ft. The flexural capacity of the W8x35 beam was calculated as that of a flexural beam with an un-braced length equal to 30 ft. The axial and flexural capacities (ϕP_n and ϕM_n) were calculated using AISC Specifications as 221 kips and 122 kip-ft.

$$\phi P_n = 221 \text{ kips}$$

$$\phi M_n = 122 \text{ kip} \times \text{ft}$$

Substituting these values into AISC interaction equation H-1.

$$\frac{P_r}{2\phi P_n} + \frac{M_r}{\phi M_n} = \frac{25 \text{ kips}}{2 \times 221 \text{ kips}} + \frac{24.4 \text{ kip} \times \text{ft}}{122 \text{ kip} \times \text{ft}} = 0.26 < 1$$

This confirms that the W8x35 beam will be adequate for this phase.

The last check is for the axial tension capacity of the threaded rods for tension. For this example, it is assumed the threaded rods have a yield strength of 65 ksi and tensile strength of 80 ksi. The axial tension capacity was calculated using equations D2-1 and D2-2 of the AISC Specification

$$\phi P_y = 0.9AF_y = 0.9 \times \left(2 \times \frac{\pi}{4} \times 1in. \right)^2 \times 65ksi = 92kips$$

$$\phi P_u = 0.75AF_u = 0.75 \times \left(2 \times \frac{\pi}{4} \times 1in. \right)^2 \times 80ksi = 94kips$$

These values are much greater than the applied force of 25 kips.

Phase 3

Within this phase the final deflection of the PLSS system is calculated. This final deflection corresponds to the deflection expected for the service life of the structure. As noted above, the transformed moment of inertia is used for finding the additional downward deflection in Phase 3. The transformed moment of inertia was found to be 550 in.⁴. Using the expressions shown above:

$$\Delta_3 = \frac{(P + \Delta P)L^3}{48EI_{comp}} = \frac{7.55kips \times \left(30ft \times 12 \frac{in.}{ft} \right)^3}{48 \times 29000ksi \times 550in.^4} = 0.46in$$

$$\Delta_f = \Delta_1 - \Delta_2 - \Delta_3 = +0.87in. - 0.4in - 0.46in = 0in.$$

This deflection found above (Δ_f) corresponds to that which can be expected prior to any additional loading being applied to the structure. So, any further deflections from additional loads or creep effects would add to this value for serviceability check. The final stage in the design for this system would be additional strength and serviceability checks for the composite section. These checks are well known so they are not presented here.

8.2. Experimental Setup – PLSS System

The experimental setup was designed to investigate the behavior of the PLSS system in both the construction and composite phases. The setup was designed for a floor system with a 30 ft span and 8 ft spacing between filler beams. The setup modeled the behavior of one of the filler beams from the design example given in the previous section. The behavior of the PLSS system in the construction phase when using the self-shoring system was of key interest to this research.

8.2.1. Overall Test Setup

As presented in the design example, the floor system is a conventional metal deck-concrete slab system supported by intermediate filler beams with 8 ft spacing. The experimental investigations focused on the PLSS filler beam behavior in the construction

phase (all three phases as described previously) and service phases. The test specimen was a W8x35 steel beam spanning 30 ft and simply supported at the ends. Eight foot long steel decks were attached to the top flange of the steel beam. The deck ribs were attached perpendicular (transverse) to the beam span, and had 4 ft overhangs on either side of the beam. The decks were attached to the beam top flange using $\frac{3}{4}$ in. diameter by 4 in. long shear studs. Twenty five shear studs were attached to each half of the beam length. This corresponds to an 80% partially composite design of the W8x35 beam. Figure 8.4 and Figure 8.5 show elevation and plan views of the W8x35 beam specimen. As shown, the W8x35 beam is connected to the supporting columns using all bolted double angle connections. Figure 8.6 shows additional design details of the double angle connection. The use of columns at the ends of the W8x35 beam instead of girders was for ease of construction and testing in the laboratory.

Self-Shoring Apparatus

The self-shoring system consists of a hydraulic ram for the vertical compression strut and two 1 in. diameter threaded rods for each tension member. Figure 8.7 (a-d) shows drawings and photographs of the end connection between the tension members and the beam bottom flanges. As shown in Figure 8.7, the threaded rods were attached to the beam ends using end clevis and pin connections. A 1 in. diameter clevis pin was used, and the 1 in. threaded rods were threaded into the end clevis. As shown in Figure 8.7 (c-d), angles (4x4x1/4) were attached to the bottom flanges of the W8x35 beam using two 5/8 in. diameter A325 bolts. These bolts were fully tensioned to the beam bottom flange.

The threaded rods were connected to intermediate turnbuckles, which then connected to a mid-span fixture. This mid-span fixture is shown in Figure 8.8 and Figure 8.9. As shown, the mid-span fixture consisted of a short W8x35 stub with stiffeners welded on either side of the web. As shown, the threaded rods were connected to this stub using clevis and pin connections. A steel spacing fixture was bolted on the top of the stub to achieve the target length. A 20 ton hydraulic ram was placed on top of the spacing fixture and used to apply an upward force. Alternatively, a simple screw jack can be used in its place. If the upward design force is zero, then the ram can be replaced with a column stub. Figure 8.10 shows a schematic of a possible fixture if the upward design force is zero. For the test specimen, the upward load was applied using the hydraulic ram and hand pump. The hydraulic pressure was monitored using a pressure transducer, and thus applied load was calculated.

Turnbuckles were used in the threaded rods to provide an alternative loading mechanism, where the upward load and member tension could be applied and also released by turning the turnbuckles. These turnbuckles can also be used for the alternate case where no pre-load is applied. In that case the turnbuckles can be used just to release the member tension after concrete casting during the shore removal phase.

Figure 8.11 shows an overall view of the beam with the self-shoring system in place. The system validated in the lab used a 20 ton hydraulic ram for the compression strut. This was done to utilize equipment available in the laboratory. Engineers can choose to design or use other equipment or the alternates proposed above. The target (or design) displacement of the beam mid-span (Δ_f) upon shore removal was assumed to be zero. Figure 8.12 shows a section view (schematic) of the composite beam upon shore

removal. As shown, the final depth of the floor system (including the filler beams) is equal to 12.5 in., which is quite competitive and comparable to the depth of the SC-DD system,

Instrumentation of Specimen and Composite Phase Loading Apparatus

The specimen was instrumented for both the construction and composite phases. In the construction phase, the mid-span displacement of the beam along with the displacement of the self-shoring fixture was monitored. Displacements were also monitored at third point on the specimen, where third points were measured as 10 ft from the support column centerline. Strain gages were attached on the top and bottom flange of the beam at mid-span. The mid-span self-shoring upward load, applied with the hydraulic ram, was monitored with a pressure transducer. A similar sensor layout was used for the composite phase. Transducers at the north and south ends to monitor slip between the steel beam and slab were used. A 1 in. stroke potentiometer was attached to the underside of the top flange of the W8x35 beam. A threaded rod was then run through the bottom of the steel deck which attached to a small steel angle. The slip gage plunger rested against the steel angle. Clinometers were attached at the beam ends to monitor end rotations. A photograph showing a slip transducer and clinometers attached to the specimen is shown Figure 8.13.

A concentrated load was applied at the longitudinal and transverse mid-span of the beam in the composite phase. The load was applied via the setup shown in Figure 8.14. As shown, threaded rods were run through hollow steel tube sections and into hydraulic rams on the top of the specimen. The hydraulic rams had load cells placed on top of them. The rams reacted against plates locked on the rods with nuts. The rods were locked into two additional tube sections at the base that were clamped to the strong floor via threaded rods. All threaded bars were 1 in. diameter and HSS sections were HSS8X4X1/2 sections. A bearing plate was placed on the top of the slab and directly over the wide flange beam to ensure no eccentric loading (in the transverse direction) was being applied. The specimen ended up being tested in two cycles. There was rotation of the slab that occurred during the first load cycle at high displacement levels. This caused the loading apparatus to rotate and bend the threaded rods. Therefore, a steel semi-circular bearing was placed on the specimen as shown Figure 8.14 (b). The cylindrical bearing help to keep the loading frame level if the slab rotated. Wooden 'catch' frames can also be seen in Figure 8.14 . These were placed to catch the specimen in the event of a collapse.

8.3. Experimental Results and Discussion – PLSS System

8.3.1. Construction Phase

As mentioned earlier, the construction phase for the PLSS System involved three different stages:

- 1) The application of the upward force to the steel beam and steel deck.
- 2) Concrete casting on the steel deck.
- 3) The removal of the self-shoring system after the concrete had cured for 7 days.

The construction phase testing monitored all three of these phases. Table 8.1 shows a summary of the construction phase results. As shown, the upward displacement of +1 in. was achieved by applying an upward force of 3.65 kips. The corresponding strain in the steel beam bottom and top flanges were equal to -370 and +330 microstrain. The calculated stresses were -10.7 and 9.5 ksi. As shown, concrete casting instantaneously reduced the beam deflection to 0.7 in. and increased the hydraulic ram force to 6.5 kips. The corresponding strains in the bottom and top flanges were -430 and +200 microstrain. The calculated stresses were -12.5 and 5.8 ksi. Seven days after casting, the beam deflection had reduced further to 0.6 in. (upward) and the hydraulic ram force had reduced to 6.3 kips, probably due to sustained load effects. Upon shore removal, the beam mid-span deflection reduced to -0.03 in. (downward), and the corresponding strains in the bottom and top flanges were equal to 100 and 180 microstrain. The calculated stresses were 2.9 ksi and 5.2 ksi.

The measured values compare reasonably with the initial analysis and design. The force estimated for subjecting the beam to a +1in. upward displacement was 3.25 kips, which is slightly less than the measured value of 3.6 kips probably because the actual clear beam span was equal to 29 ft and the connections had some small end restraint. The forces and displacements estimated earlier for the concrete casting and shore removal phases also compared well.

8.3.2. Composite Phase Results

Figure 8.15 shows the measured load vs. mid-span displacement behavior of the composite beam specimen. As shown, the figure includes the design live load levels (40 psf) and factored design live load levels ($1.2D+1.6L=142$ psf). The displacements at the live load and factored design load levels were 0.25 in. and 0.95 in., respectively. Figure 8.15 shows the overall capacity to be 36 kips or 300 psf equivalent. The figure also shows that there were some loading and re-loading for the specimen. The specimen was initially loaded and re-loaded a few times to ensure sensors were reading properly. It was cycled to 10 kips twice and then to 18 kips as shown in Figure 8.15. It was then loaded until 36 kips and around 4.5 in. of mid-span deflection. At this point the loading spreader beam was transverse rotating and becoming unstable. A cylindrical bearing was added to the loading setup and the specimen re-loaded as shown in Figure 8.15. The loading fixture with and without the cylindrical bearing was described previously in Section 8.2 and is shown in Figure 8.14.

Figure 8.16 shows the load vs. measured end rotations for the specimen. The end rotations were approximately equal to each other up to around 36 kips of applied load and 1.5 degrees of measured end rotation. At this point, the specimen was un-loaded and reloaded. Beyond this point the south end rotations were slightly larger than the rotations of the north end of the Specimen. It is likely that the south end had slightly more plastification occur at the time of un-loading. Also, prying action was observed at the

double angle connection for both the north and south end. This prying action is shown in Figure 8.17. This prying action may have initiated at the south end sooner than the north end, which possibly could have 'softened' the south ends response. Figure 8.18 shows the applied load vs. north and south third point displacements. As shown, the south portion of the specimen is observed to have larger displacements at the point of unloading and re-loading at 36 kips of applied load and 3 in. of displacement.

Figure 8.19 shows the load vs. end slip for the specimen. As shown, negligible slip occurred for loading up to 36 kips. This was the point of unloading corresponding to 3.5 in. of mid-span deflection. Upon re-loading more slip was observed as seen in Figure 8.19. Slip steadily increased until the test was terminated, when 0.17 in. of end slip had occurred. No shear stud failures or tearing of the deck was observed as slip increased. Hence, the system was quite ductile. The slip did recover when the specimen was finally un-loaded.

The overall response of the specimen is typical for composite steel-concrete beams. Even though the beam did not have enough shear studs for full composite capacity, it exhibited ductile behavior. An overall top view of the specimen at 6.5 in. of deflection is shown in Figure 8.20. There were some issues with the slab portion of the specimen rotating transversely as loading was applied. This was difficult to control due to the fact that there were 4 ft overhangs on either side of the specimen. This rotation can be seen in Figure 8.21. Overall, the specimen had adequate capacity and exhibited ductile behavior.

Key Observations of PLSS Test

- 1) The applied upward force in the self-shoring system needed to displace the steel beam upwards by 1 in. was 3.6 kips. This value compares reasonably with the 3.25 kips calculated from the analysis presented in Section 8.1.
- 2) The concrete casting operation reduced the mid-span deflection by 0.3 in. to 0.7 in. The force increase in the hydraulic ram was approximately 3 kips. These values compare well to the analysis values.
- 3) The shoring removal caused a residual mid-span deflection of -0.03 in. Hence, the system was essentially 'flat' after shore removal. Zero displacement was the target value.
- 4) The load-deflection behavior of the system was ductile with an estimated capacity of 36 kips or 300 psf equivalent.
- 5) The mid-span deflection for service level live loading was equal to 0.25 in. and for factored design loads was equal to 0.95 in.
- 6) The specimen experienced end slip at higher load and displacement levels. Slip increased steadily at higher loads but no shear stud or other slip related failures were observed.

Table 8.1: Construction phase results for PLSS System

Phase	Beam Displacement (in.)	Strain in Bottom Flange at Mid-Span	Strain in Top Flange at Mid-Span	Force in Hydraulic Ram (lbs)
Application of Upward Force	+1 (1)	-370	+330	3650
Concrete Pour	+0.7 (-0.3)	-430 (+60)	200 (-130)	6500 (+2850)
7 Days After Pour	+0.6 (-0.1)	-370	140 (-60)	6300 (-200)
Self Shoring System Removal	-0.03 (-0.63)	100 (+470)	180 (+40)	NA

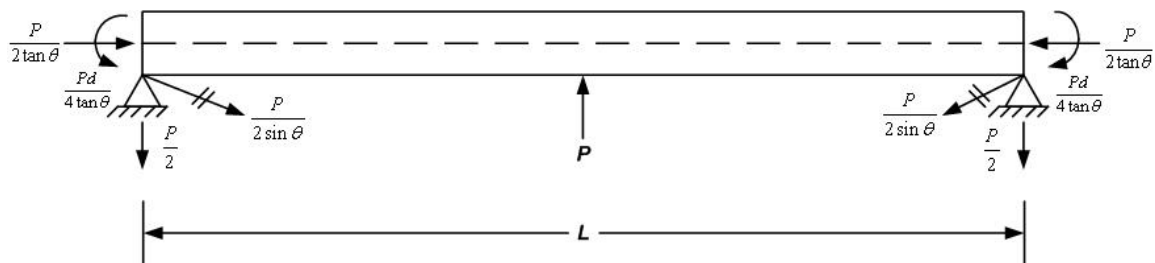


Figure 8.1: Free body diagram in phase 1

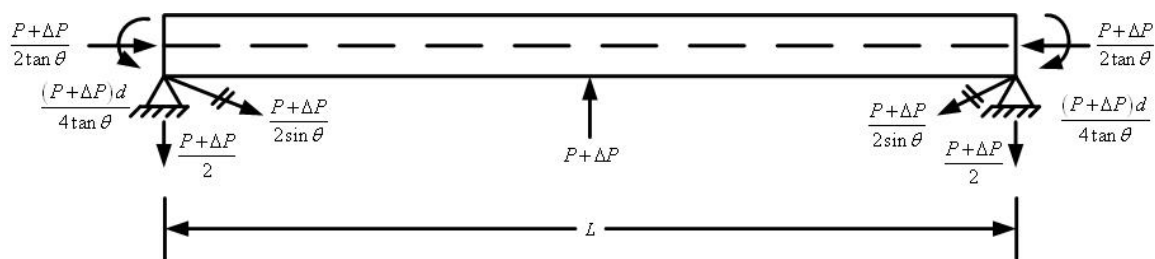


Figure 8.2: Free Body Diagram in Phase 2

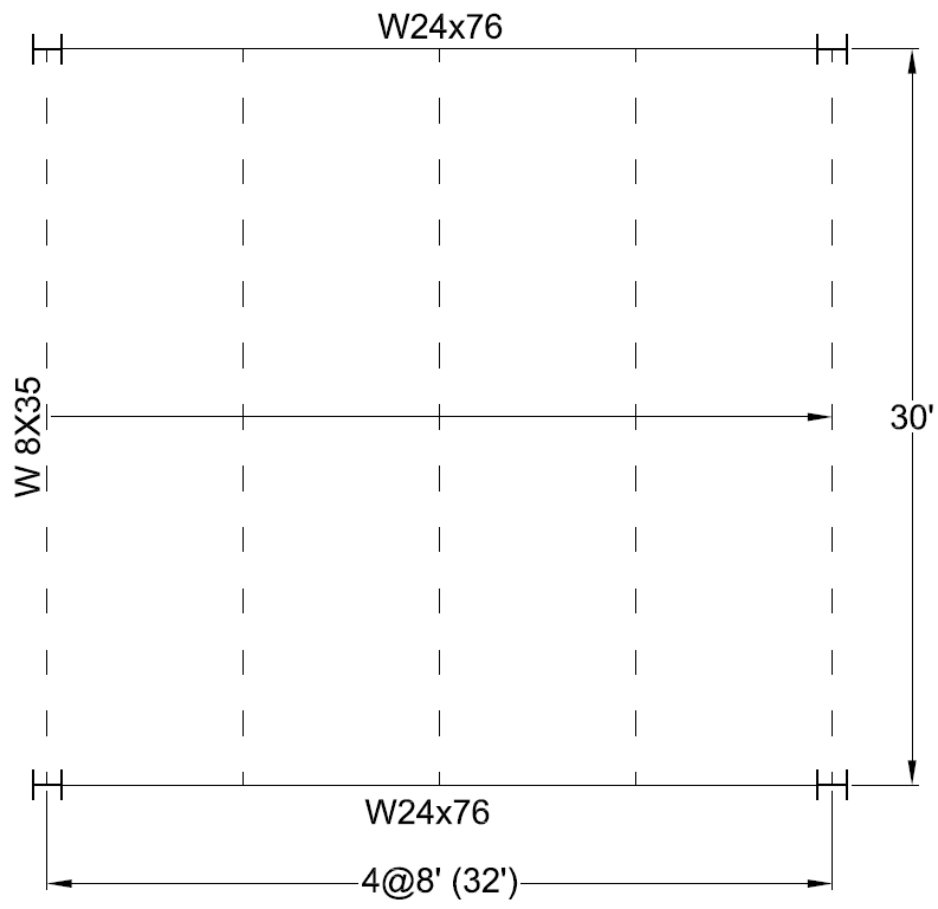


Figure 8.3: Interior bay layout for design example

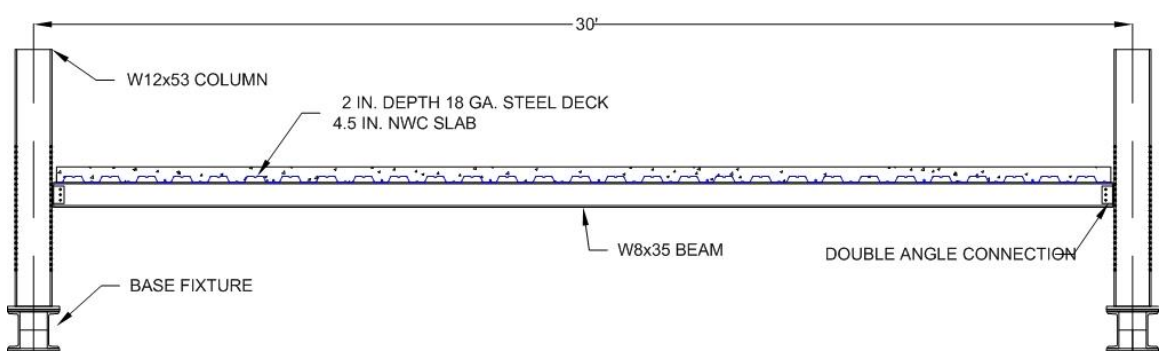


Figure 8.4: Side view schematic of self-shoring test setup

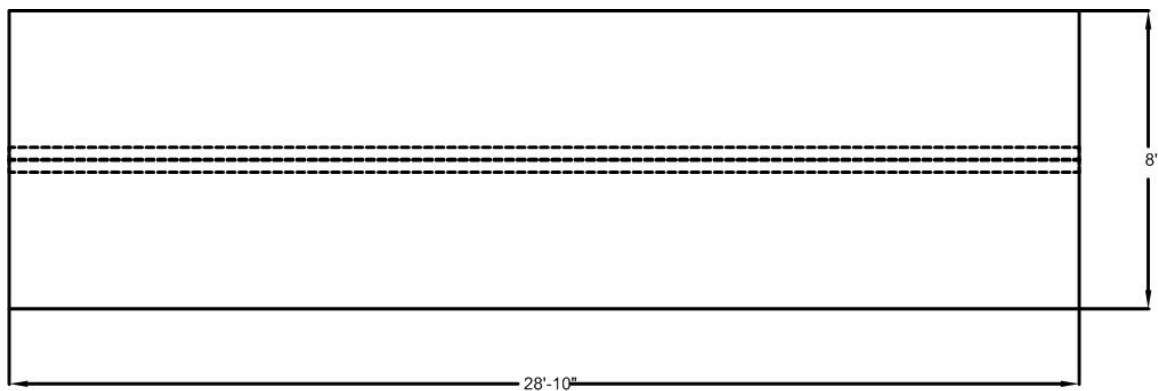


Figure 8.5: Top view schematic of PLSS test setup

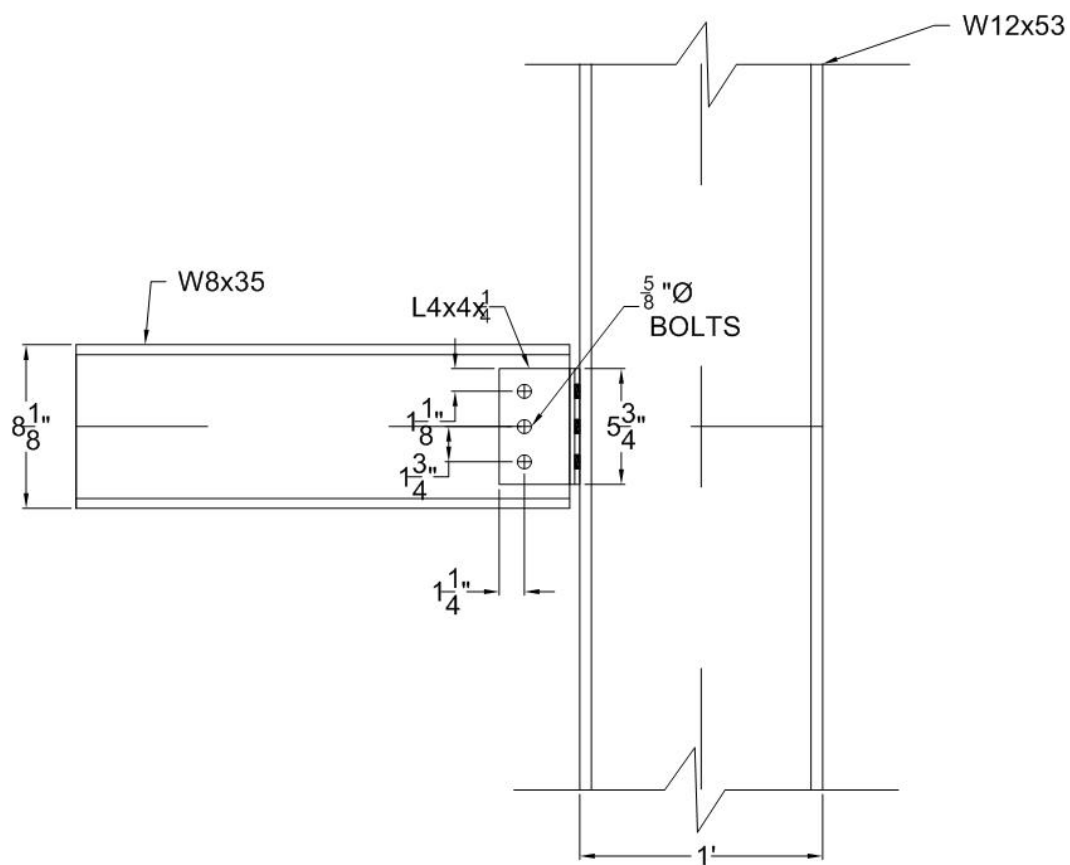


Figure 8.6: Side view of double angle connection on PLSS test setup

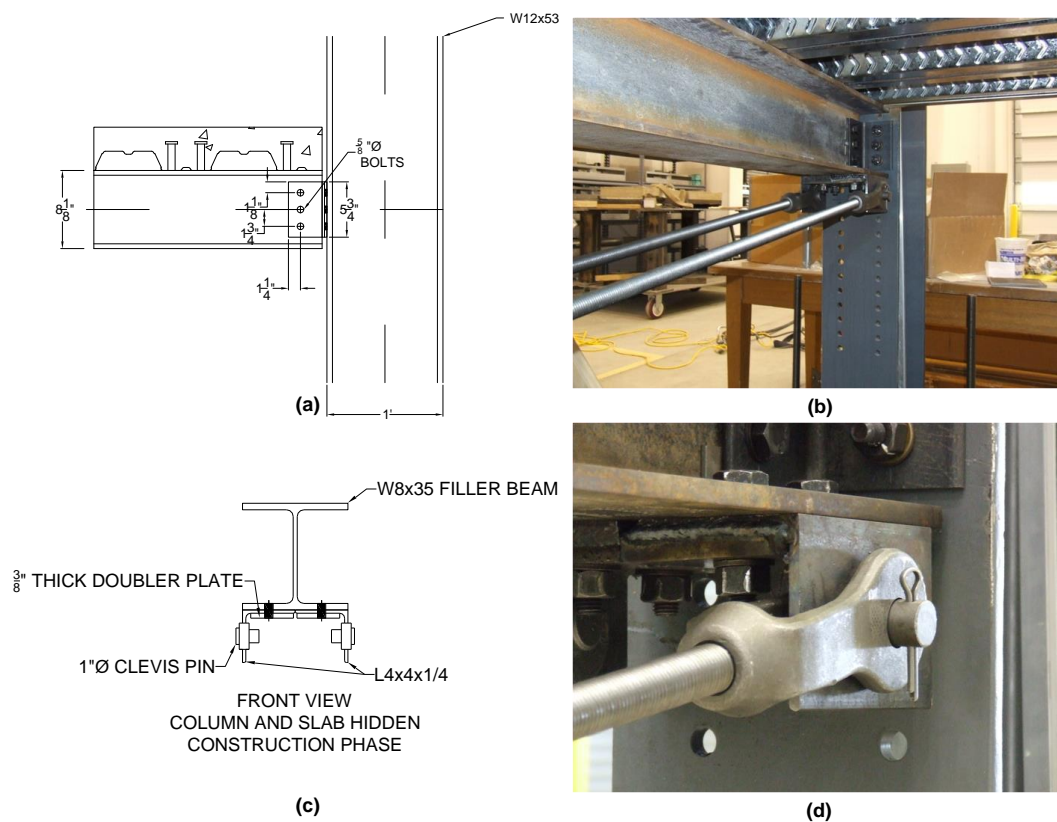


Figure 8.7: End fixture for self-shoring specimen showing (a) schematic of double angle connection, (b) photograph of double angle connection, (c) front view schematic of end fixture and (d) photograph of end fixture

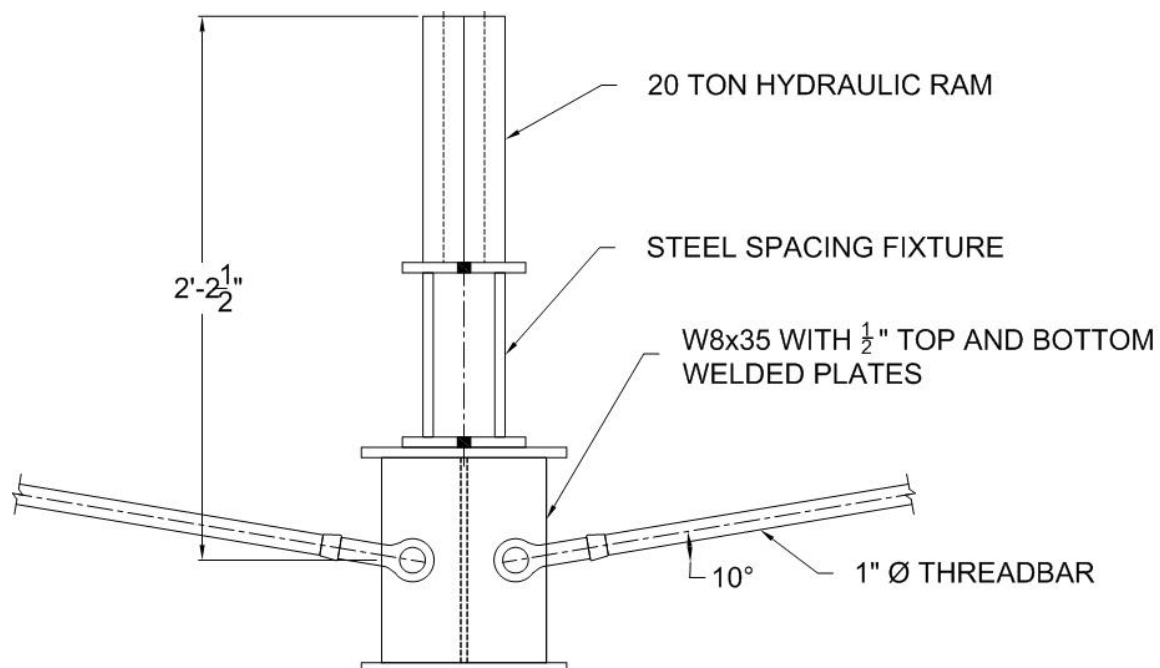


Figure 8.8: Schematic of mid-span fixture used on PLSS Specimen



Figure 8.9: Mid-Span fixture for PLSS lab specimen

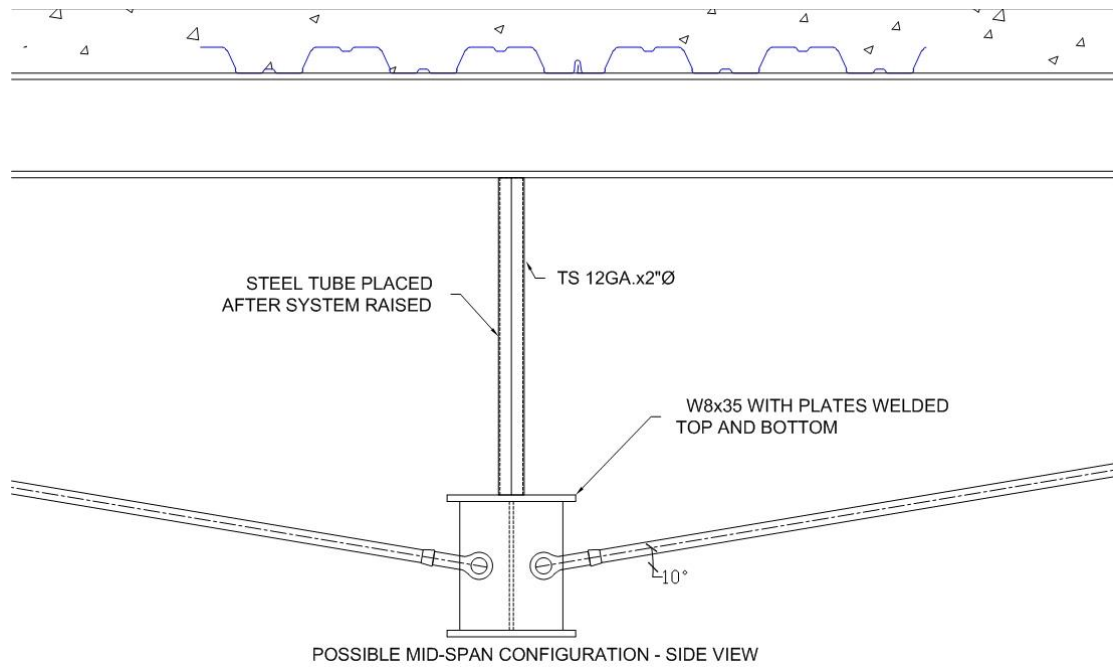


Figure 8.10: Possible mid-span configuration for PLSS system (assumed in design example)

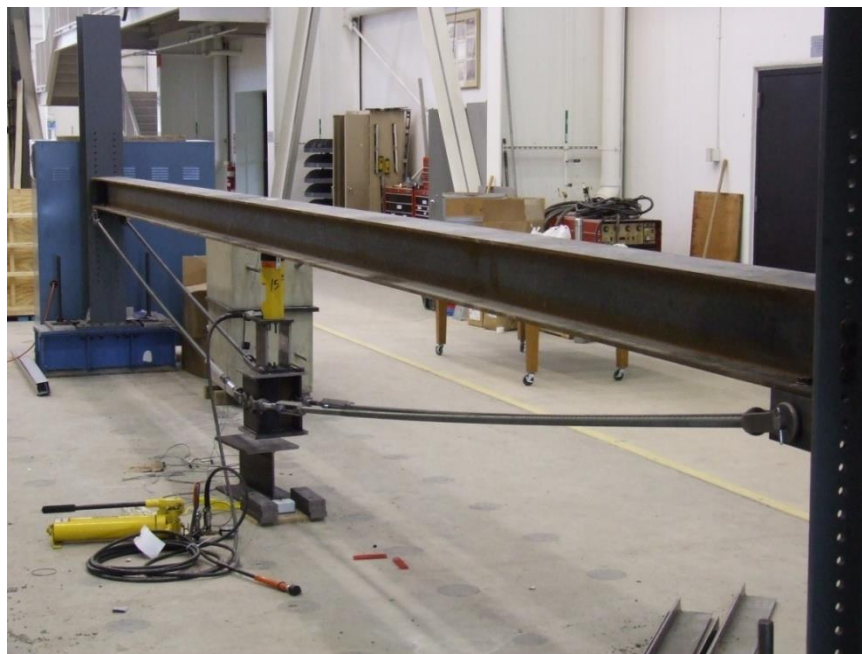


Figure 8.11: Photograph showing overall self-shoring apparatus

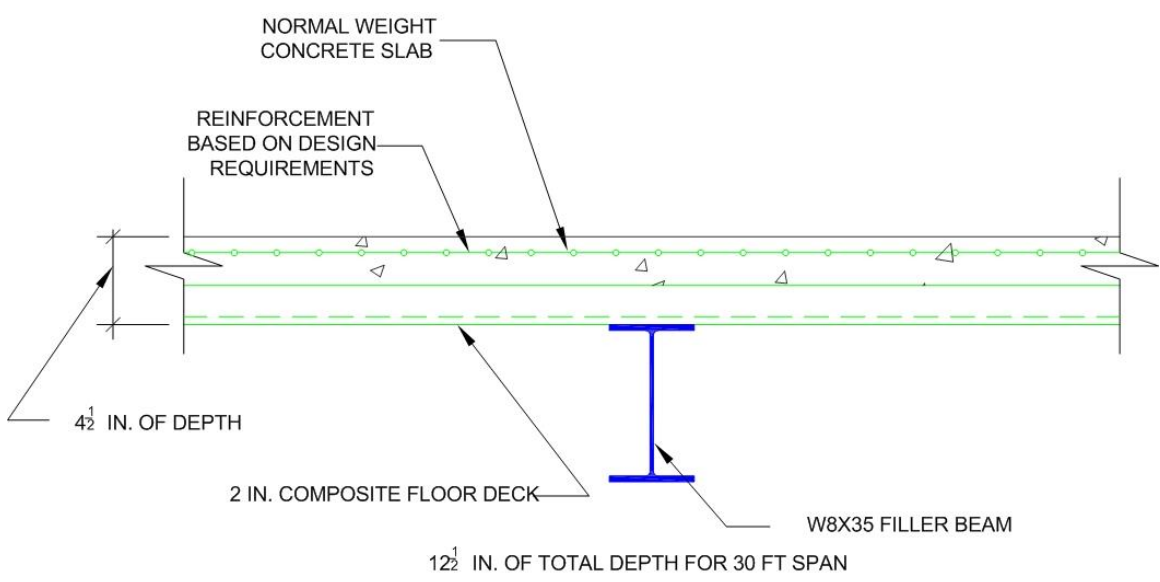


Figure 8.12: View of composite system after PLSS system removed

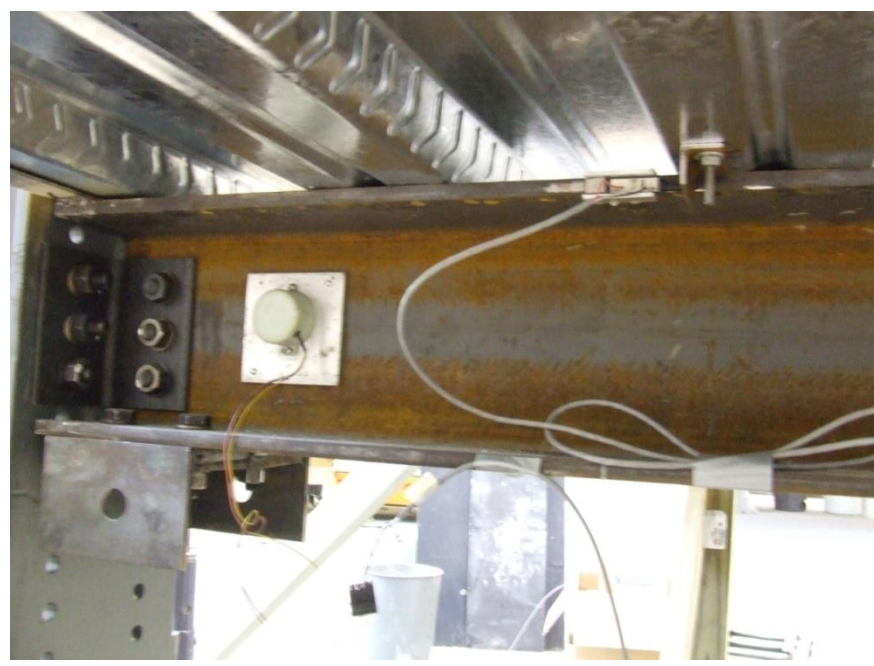


Figure 8.13: Photograph showing attachment of rotation clinometers and slip sensor



(a)



(b)

Figure 8.14: Loading frame for PLSS Specimen (a) in first load cycle and (b) second load cycle

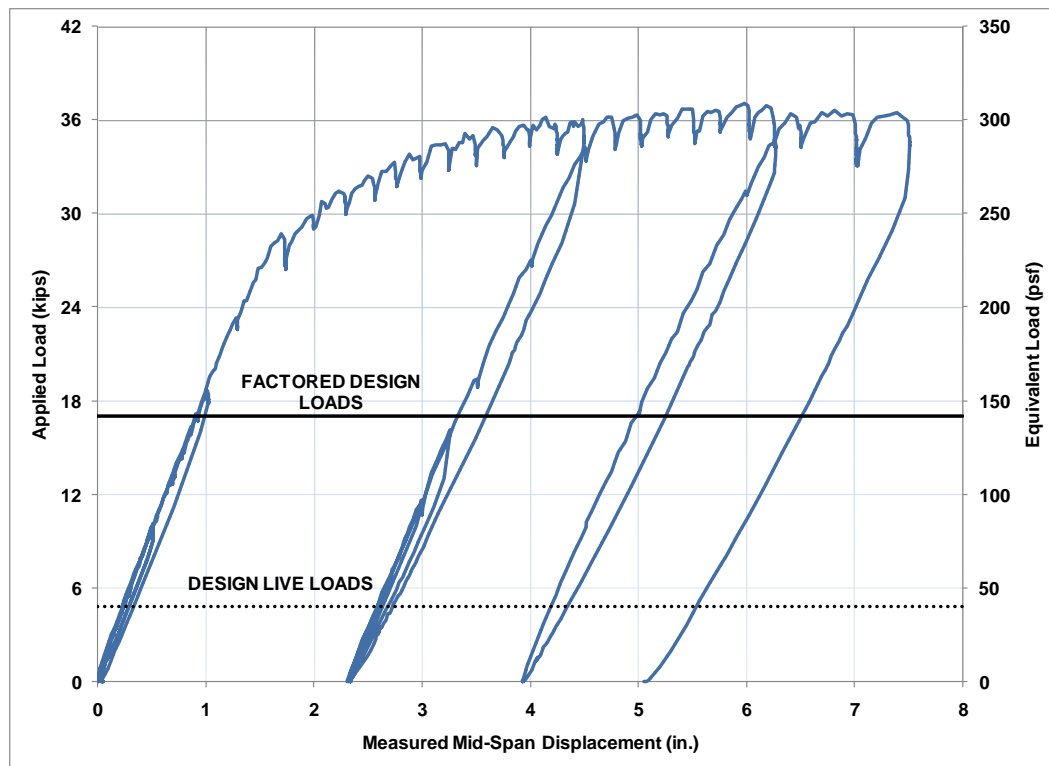


Figure 8.15: Measured load vs. mid-span deflection data for PLSS Specimen

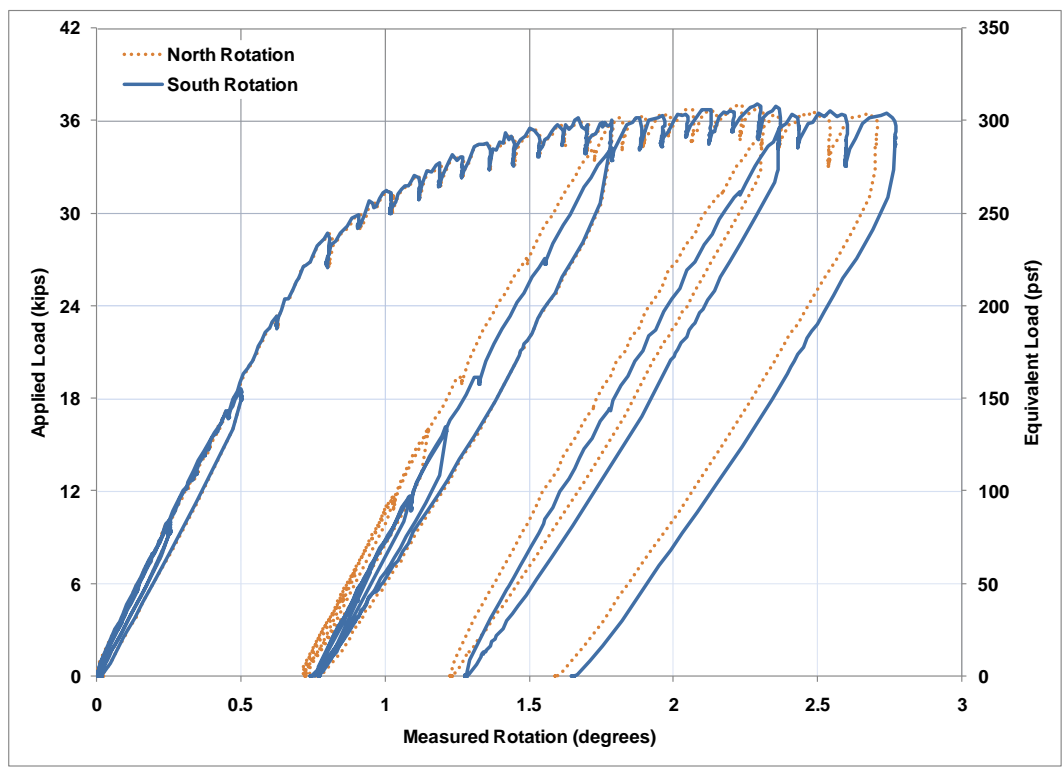


Figure 8.16: Measured Load vs. End Rotations for PLSS Specimen



Figure 8.17: Photograph showing prying action occurring at connection

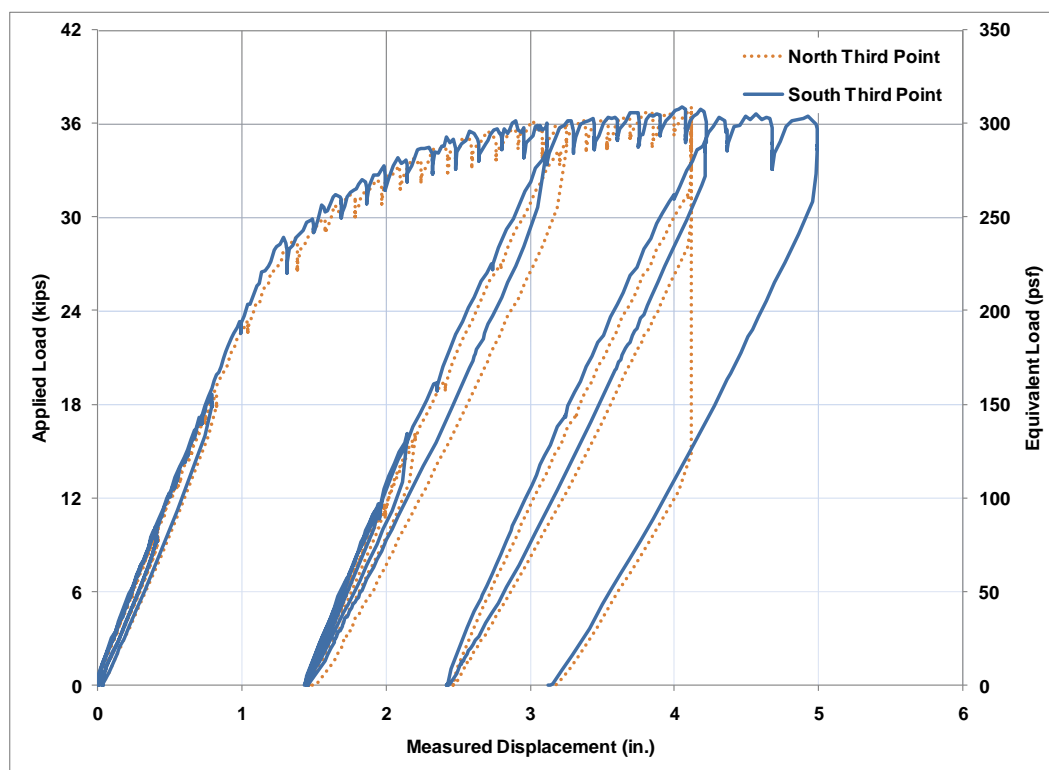


Figure 8.18: Measured Load vs. north and south third point displacements

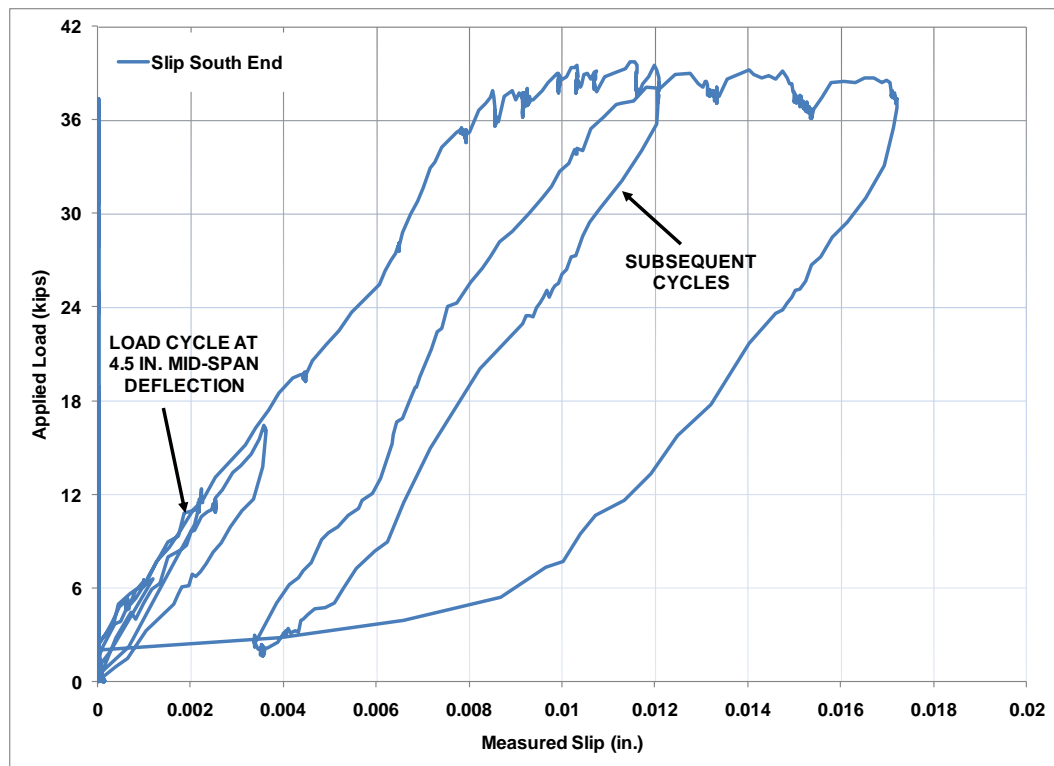


Figure 8.19: Applied load vs. measured end slip for PLSS Specimen



Figure 8.20: Photograph from above of PLSS Specimen at 6.5 in. of mid-span deflection



Figure 8.21: Side view of PLSS Specimen with 7.5 in. of mid-span deflection

CHAPTER 9. FURTHER ANALYSIS AND DESIGN STUDIES ON STRUCTURAL BEHAVIOR OF COMPOSITE DEEP DECK SYSTEMS

This chapter presents further analysis and design studies related to the structural behavior of composite deep deck systems. The studies are based on a combination of experimental observations, literature review, and engineering judgment.

9.1. Analysis of Ultimate Load Testing Results – Deep Deck Systems

The experimental testing of the composite deep deck (both CC-DD and SC-DD) systems highlighted some aspects that needed further research. These were the effects of construction loads and interfacial slip on the behavior of composite deep deck systems. The previously developed fiber models (Section 4.2.2) and FEM models (Section 4.2.3) were modified to account for the effects of construction loading and interfacial slip. This section compares the experimental results with those obtained analytically using models that:

- 1) Considered neither the effects of construction loading nor interfacial slip.
- 2) Accounted for construction load effects but not interfacial slip.
- 3) Accounted for interfacial slip but not construction load effects.
- 4) Accounted for the effects from both construction and interfacial slip.

9.1.1. Fiber Models and FEM Models – No Construction or Slip Effects

The modeling approaches described previously in Section 4.2.2 and 4.2.3 did not include the effects of construction or interfacial slip. The approaches were used directly to model and predict the behavior of the CC-DD specimens. The only modification was that the measured material properties were used in conjunction with the appropriate constitutive models defined previously in Chapter 4.

CC-DD Specimens Results and Discussion

Table 9.1 summarizes the values of the measured geometric and material properties for the CC-DD specimens. It includes the measured properties for specimens CC-DD-1 to CC-DD-4, described previously in Chapter 4. Figure 9.1, Figure 9.2, Figure 9.3, and Figure 9.4 shows comparisons of the applied load vs. mid-span displacement curves predicted by the analytical models with the experimental results for specimens CC-DD-1 through CC-DD-4, respectively. The figures include the load capacity (strength)

estimated using SDI (2002) procedures. The figures show that the models under-estimate the initial or un-cracked (UC) concrete stiffness. The predicted stiffness values compared to the experimental values are summarized in Table 9.2. The stiffness values shown are the applied average load over the mid-span deflection. The un-cracked (UC) stiffness was estimated for loading between 0 and 5 kips for CC-DD-1 to CC-DD-3. For CC-DD-4 UC stiffness was estimated for loading between 0 and 3 kips. The cracked (C) stiffness was estimated as the tangent stiffness for loading between 5 and 10 kips for the first 3 CC-DD specimens and between 3 to 8 kips for CC-DD-4.

Table 9.2 shows that the un-cracked stiffness is consistently under-estimated with the analytical models. The average difference is approximately 10% for both the FEM and fiber models compared to the specimens with shear studs (CC-DD-1, CC-DD-2, and CC-DD-4). The under-estimation of initial stiffness is probably a result of the boundary condition of the test specimens not being equivalent to an idealized 'pin' connection. The connection is providing some slight restraint to rotation initially as evidenced when comparing the models to test data. The non-studded specimen (CC-DD-3) had a difference of 13.5 and 15% in predicted stiffness for the fiber and FEM models. This larger difference is due to the puddle welds providing slightly more restraint than the shear studs. The stiffness predicted in the cracked phase was consistently over-estimated. These models did not consider any construction and interfacial slip effects, which could possibly affect this stiffness.

Table 9.3 shows the predicted strengths for the CC-DD specimens based on full composite models. As shown, the capacities are consistently over estimated using these models. The models over-estimate capacity between 20 and 30% for the specimens with shear studs. This was expected as no effects from the construction phase or interfacial slip were considered. In general, however, these models can be used to gain preliminary estimates of stiffness and an approximate but un-conservative range for overall strength. Comparisons with CC-DD- 3 were particularly poorer for strength estimation. This specimen had no shear studs and its failure was dictated by the onset of slip and an eventual shear bond failure. Therefore, these models without construction and interfacial slip effects are inadequate and un-conservative for modeling the composite deep deck specimens.

Shored Specimen (SC-DD) Results and Discussion

Figure 9.5 compares the load-deflection behavior for the SC-DD specimen and the prediction from the above model techniques. The predicted capacity and stiffness for the specimen compared to test data is summarized within Table 9.4. Figure 9.5 and Table 9.4 shows that both the fiber and FEM models over-estimate the capacity of the specimen. The fiber and FEM models over-predict strength by 37.7 and 39.5%, while the SDI method over-predicts by 52.7%. Hence, these models are inadequate and un-conservative for estimating capacity of the SC-DD specimen. Table 9.4 shows that the predicted UC stiffness is larger than the experimental value. This is contrary to the CC-DD specimen where stiffness was under-predicted. It is likely the concrete cracked from the removal of shoring, which caused the predicted un-cracked stiffness to be higher than the experimental value. While the construction level deflections are reduced from shoring, there are now initial strains in the concrete. This causes cracking to occur

sooner and can also reduce overall capacity of the system. These models do not consider this, and hence do not accurately predict the overall capacity of the system.

9.1.2. Fiber and FEM models accounting for Construction Effects

The next type of analytical model investigated for the composite deep deck systems included the effects of construction. The terminology of construction effects refers to a reduction in overall capacity based on what occurred in the construction phase. For the un-shored specimens this refers to the stresses that the deck experiences from the concrete casting operation. The maximum effect for a simple span configuration is at the longitudinal mid-span of the specimen.

Simplified Method for Accounting for Construction Effects – Fiber and FEM Models

The first method to incorporate construction effects into the analytical models reduced the yield stress that was used for input into the models based on the construction loading. For all un-shored specimens it was known that the weight of the wet concrete had to be resisted by the steel deck alone. The bending moment on these specimens came from the uniform loading the concrete applies to the deck. Thus, the moments at any point along the specimen can be found using principles of mechanics. Assuming a member with uniform loading w of length L , the moment at a point x along that length can be calculated using equation 9.1.

$$M_x = \frac{wx}{2}(L-x) \quad 9.1$$

Where M_x is the moment along the length of the beam.

Stresses can be found at any point knowing the distribution of moments and the section properties of the deck section. For the given deck cross-sections the section modulus (S_x) is known for both the top of the steel deck and bottom of the steel deck. Therefore, the stresses in the extreme compression and tension fibers can be calculated using equation 9.2.

$$\begin{aligned} \sigma_{top} &= \frac{M_x}{S_{x\text{top}}} \\ \sigma_{bott} &= \frac{M_x}{S_{x\text{bott}}} \end{aligned} \quad 9.2$$

Where:

σ_{top}	Stress at top fiber of deck at point x
σ_{bott}	Stress at bottom fiber of deck at point x
$S_{x\text{top}}$	Section modulus for the extreme compression fiber in the steel

S_{xbott} Section modulus for the extreme tension fiber in the steel

The distribution of extreme fiber stresses were found at 1 ft intervals along the span of the specimen lengths. The loading assumed on the deck was the weight induced by the concrete. These stress values were averaged to calculate the average stress at extreme tension and compression fibers in the steel deck over the entire length. These average values were then subtracted from the yield stress of the steel. This adjusted yield stress (f_{yr}) was then used as the yield stress assumed in the analytical models. A similar approach as above can be used for shored specimens. However, for the case of the shored specimens the stresses result from the shore removal and are exerted on the entire composite section. Thus, an equivalent section modulus can be found for the composite section and the same technique applied. The reduction of the yield strength to approximate construction effects was also implemented into the SDI models for estimating strength. The reduced SDI values are herein referred to as SDI-R.

Advanced Method for Including Construction Effects – Fiber Based Model Approach

Another way to account for the construction effects is to add the imposed stresses at each point into the final analysis. This was done in the fiber-based model for un-shored specimens as follows:

- 1) The moment-curvature behavior of the deck steel section alone was calculated using the same methodology as previously described in Section 4.2.2 for composite systems.
- 2) The moment-curvature relationship was used along with the central difference method to calculate the load-deflection behavior of the steel deck during construction. The applied loading was that simulating the effects of concrete weight.
- 3) The resulting moments were added as additional moments at each station along the length for the composite section analysis.
- 4) The displacement induced from adding the additional moments in the construction phase were subtracted to calculate the composite level displacements.

The above procedure allows for including the construction effects along the length directly.

A similar methodology can be used for shored systems as follows:

- 1) The composite section moment curvature can be used in conjunction with loading from shore removal to calculate the distribution of curvatures and moments along the length.
- 2) The moments at each station along the length were added as additional moments to the section for each increment of loading.
- 3) The induced deflection at zero loading was subtracted from the computed deflections at the applied load. This gives the composite level deflections.

Advanced Method for Including Construction Effects – 3D FEM Model Approach

The 3D FEM model developed also allows for the implementation of construction effects. Within *Abaqus* this was done using the *Model Change* keyword command. This command allows for temporarily removal of a model part, and reintroducing it later in the analysis. For the un-shored specimens, this command was used as follows:

- 1) The concrete slab portion of the model is removed in the construction phase.
- 2) The assumed uniform load of the concrete is then placed on the deck section alone in a separate analysis step.
- 3) In the next analysis step the concrete slab is re-introduced into the model.
- 4) For the final analysis step the model is run with the applied loading to determine overall behavior.

The use of the *Model Change* keyword command thus allows the construction level effects to be imposed on the un-shored specimens. For the shored specimens the *Model Change* command is not needed. An additional analysis step with the loading from the shoring is used prior to applying the imposed structural loading.

Results for Models Incorporating Construction Effects

The above techniques were implemented into the fiber based and FEM models for the CC-DD and SC-DD specimens. The results for the CC-DD Test Specimens 1-4 are presented in Figure 9.6 – Figure 9.9. The numbering of 1 and 2 in the figures corresponds to the models that used: (1) the simpler method of reducing the yield stress and (2) those that used the more complex methods. Figure 9.6 and Figure 9.7 show that the behavior predicted by the models for specimens CC-DD-1 and CC-DD-2 is still un-conservative. Figure 9.9 shows that the predicted behavior from the models compares well with CC-DD-4 experimental data. The construction effects were significantly greater for this specimen since it was made of thinner gauge steel. These comparisons were more relevant than those for systems with less severe construction effects (i.e., CC-DD-1 and CC-DD-2).

The predicted strengths using the models with construction effects are summarized in Table 9.5. The table indicates for CC-DD-1 and CC-DD-2 that the fiber based and FEM models are still relatively un-conservative in predicting strength. Table 9.5 shows that the SDI-R model predicts the strength of CC-DD-1 almost exactly, and it is slightly un-conservative for Specimen CC-DD-2 with a 7.6% over-prediction. The SDI-R model predicted the strength of CC-DD-4 conservatively 11% below the experimental capacity. Thus, the SDI-R model provides a good estimate of strength for specimens with shear studs at the ends. All other models were within 20% of the experimentally measured strength. Again, Specimen CC-DD-3 is difficult to discuss as it experienced a brittle shear bond failure, which could not be accounted using these models. The models accounting for construction effects were shown to be good predictors of strength for CC-DD Specimen 4. This specimen had higher construction level stresses and hence models that accounted for these effects were more effective in predicting strength than those with less significant construction effects (CC-DD-1 and CC-DD-2).

Shored Specimen Results – Models with Construction Effects

The shored deep deck specimen (SC-DD) was also analyzed using the fiber and FEM models that could account for construction effects. The summary of predicted strengths is summarized in Table 9.6 and the predicted load-deflection compared with the test data is shown in Figure 9.10. As shown, the models are mostly un-conservative for predicting strength. Table 9.6 shows that those models that account for construction effects by adding an additional moment in the first load step (method 2) are better predictors of strength. This is because these models are analytically inducing strains into both the concrete and steel initially. This is more representative of what is occurring for the shore removal process. This specimen did experience a shear bond type failure so predicting its strength based on these models also proves difficult.

9.1.3. Modeling Approaches for Partial Composite Action – Interfacial Slip in Fiber Based Model

The next step in analyzing the given test specimens was accounting for the effects of interfacial slip between the steel deck and concrete components. The fiber based models and the 3D FEM models were both modified to account for interfacial slip. Before explaining the details used in the modeling techniques, it is important to discuss how slip affects overall behavior and to provide relevant background as it pertains to the current specimens.

Background on Interfacial Slip

Interfacial slip is a design consideration for any system in which two or more materials are interconnected. Within civil structures the most commonly bonded materials are steel and concrete used within slab systems and various other structural systems. In a flexural member shear stresses develop at the interface of two materials as it is loaded. The section will act as a composite of the two materials if the interfacial bond can transfer these stresses. This can be visualized by looking at a differential element of a composite section like that shown in Figure 9.11. As shown in the figure, a differential element is subjected purely to bending. The top and bottom layer shown in the figure are assumed to be different materials bonded together. As the element undergoes flexure, the two separate materials induce interfacial shear stresses (τ) at the bonding surface. Once this interfacial stress τ is exceeded then the two materials will slip relative to each other.

Providing an exact model of the interfacial shear stress/slipping phenomenon is extremely difficult, if not impossible. The bond can be influenced by several factors based on the type of structural system being investigated. For example, with the deep deck systems investigated the interfacial bond stress is a function of normal force applied to the specimen, friction between the two materials, the bond between the steel and concrete, the shear studs at the ends, and curvature on the specimen. Therefore the bond model used in the current study had some simplifying assumptions.

Implementation of Slip Effects into Fiber Based Model

It is possible to implement the effects of interfacial slip into the previously developed fiber models. There are some underlying assumptions that do need to be stated in discussing the model. The first assumption is that once slip occurs both the steel and concrete components will have the same curvature (ϕ). This assumption will be valid as long as there is NO vertical separation between the two materials. For the specimens considered, no vertical separation was observed for the CC-DD specimens and SC-DD system. While both the concrete and steel sections have the same curvature, they will have separate strain profiles as shown in Figure 9.12. As shown, the strains are still assumed to vary linearly over the depth. There will now be a strain profile in the concrete portion and another in steel deck.

The second assumption made in developing the slip model was a rigid-plastic shear stress vs. strain relationship. This assumption indicates that when the stress at the interface reaches the limiting value no further increase in this value can occur. Also, prior to reaching the limiting value the shear interface has an infinite stiffness. That is, there is no elastic slip within the specimen. This relationship is shown in Figure 9.13. This is a valid assumption to make based on the measured slips from the experiments. For example, compare Figure 9.13 and the experimental measurement shown in Figure 4.52.

The above assumptions were used to set up the developed interfacial shear-bond model. Considering the test setup for the specimen, the bending moment and shear diagrams can be found as shown in Figure 9.14. In the shear span (length from the end of the specimen to the load application) there is a constant applied shearing force and linearly varying bending moment. The shear then drops to zero and the moment becomes constant in the area between load point, or the moment region. Therefore, the maximum shear forces will be generated in the shear span. The shear forces generated at the interface are in equilibrium with internal forces and moments as shown in Figure 9.15. In the figure:

τ_b	Interfacial shear stress at the interface
ΣF_c	Summation of internal forces within the concrete
ΣF_T	Summation of internal forces within the steel
M_i	The generated internal moment from the internal force couple
x	The shear span distance

The summation of forces in the concrete and steel should equal zero for the entire cross-section (internal force equilibrium). Additionally, the summation of the forces generated in the concrete and steel must equal the interfacial shear forces at the interface. Equation 9.3 states the equilibrium equation that can be used to relate the interfacial shear bond stress to the internal forces in the concrete and steel.

$$\tau_b \times A_s = \Sigma F_c = \Sigma F_s \quad 9.3$$

Where:

τ_b	Interfacial shear stress at the interface
----------	---

ΣF_c	Summation of internal forces within the concrete
ΣF_T	Summation of internal forces within the steel
A_s	The shear bond area of the specimen. This is total surface area over which bonding can occur. For the specimens considered, the shear bond area would be the length of the shear span multiplied by the deck cross sectional area divided by its thickness.

Hence, it is vital to determine what the interfacial shear stress is for the system. Two parameters are needed in determining this value. First, the type of loading must be known. For the test specimens 4 point loading was applied as shown in Figure 9.14. The second parameter needed is when a system is observed to have first slip. For the test specimens, this was the value of first measureable slip. This was determined by examining the slip data and observing where the measured slip began increasing at a steady rate as illustrated in Figure 9.16. Knowing this point, the load at which this occurs can be determined. For CC-DD- 2 (shown in Figure 9.16) the load at first slip is observed to be 21.6 kips. Knowing this load, the applied maximum moment can be determined assuming the moment distribution shown in Figure 9.14. Thus:

$$M_{\max} = 0.3PL = 0.3 \times 21 \text{ kips} \times 30 \text{ ft} = 189 \text{ kip} \cdot \text{ft} = 2268 \text{ kip} \cdot \text{in}.$$

The above value is now used in determining the internal force distribution of the cross-section at this point. This is done by taking the moment found from above and equating it to the internal moment of the cross-section and finding the corresponding normal force distribution in the concrete and steel components. The moment-curvature relationship for the fully bonded specimen can be used in determining this value. For the given 4 point loading condition, Equation 9.3 can then be used with the summation of internal forces at M_{\max} used to find the interfacial shear stress. This is possible since the shear force distribution is constant over the shear span in this case. For CC-DD Specimen 2, the summation of internal forces in the steel and concrete at this point were found to be 286 kips. Thus the interfacial shear stress can be calculated re-arranging equation 9.3 as:

$$\tau_b = \frac{\Sigma F_c}{A_s} = \frac{\Sigma F_s}{A_s} = \frac{286 \text{ kips}}{1439 \frac{\text{in}^2}{\text{ft}} \times 9 \text{ ft}} = 0.022 \text{ ksi} = 22 \text{ psi}$$

The above procedure can thus be summarized:

- 1) The moment-curvature relationship for the fully bonded specimen is calculated.
- 2) From test data, the load at first measureable slip is determined.
- 3) The applied moment at the interior end of the shear span is determined based on this applied force.
- 4) This applied moment is matched to the internal moment from the moment-curvature relationship.
- 5) For this internal moment, the internal force distribution is determined.

- 6) The interfacial shear stress is calculated using equation 9.3.

Modification to Procedure for Shored Specimen

The above procedure for finding the interfacial shear stress is valid if the system uses un-shored construction. There is a slight modification needed to the procedure if shored construction is used. During the shore removal process there are strains and stresses applied to the entire composite cross-section. Therefore, an additional moment is being applied to the section in conjunction to that being applied by structural loading. To account for this within the bond model, the additional moment from the shore removal must be added to the applied moment from loading in determining the interfacial shear stress.

This can be illustrated for the SC-DD test specimen as follows. First, the applied moment at the end of the shear span for shore removal can conservatively be estimated as:

$$M_{shore} = \frac{0.3P_{shore}L}{2} = \frac{0.3 \times 4.8 \text{ kips} \times 30 \text{ ft}}{2} = 21.6 \text{ kip} \cdot \text{ft} = 259 \text{ kip} \cdot \text{in}.$$

Where:

M_{shore} Applied moment from shore removal 9 ft in from the end. This corresponds to the length of the shear span.
 P_{shore} Applied loading from shore removal

This value is then added to the moment where first slip is observed. For the SC-DD Specimen slip was first observed at 11.2 kips. This corresponds to a moment at the load point of 1209 kip-in. Therefore, the total moment used to calculate the limiting shear stress becomes:

$$M_{total} = 259 \text{ kip} \cdot \text{in} + 1209 \text{ kip} \cdot \text{in} = 1468 \text{ kip} \cdot \text{in}$$

Solving for the interfacial shear stress:

$$\tau_b = \frac{\Sigma F_c}{A_s} = \frac{\Sigma F_s}{A_s} = \frac{187 \text{ kips}}{1439 \frac{\text{in}^2}{\text{ft}} \times 9 \text{ ft}} = 0.018 \text{ ksi} = 18 \text{ psi}$$

This would be the value used for the interfacial slip model.

Procedure for Implementing Model

Knowing the limiting interfacial shear stress value, slip can be accounted for and implemented into the fiber based model. The same basic fiber model was used with some modifications to account for the partially composite action that occurs once the limiting shear stress is exceeded. The procedure for how this was done for the test specimens is given below.

- 1) A curvature value is defined within the cross-section.
- 2) The strain at a reference depth is assumed. For the developed model the strain at elastic neutral axis depth was used. Other strains are computed based on this reference strain and the assumed curvature in step 1. The fiber stresses are calculated using appropriate material properties.
- 3) The internal forces in the cross-section are summed. If they do not sum to zero then the reference strain is changed until the solution approaches zero with a tolerance value of 1×10^{-6} .
- 4) The summation of the steel or concrete forces is checked against the limiting interfacial shear force. If the summation of the steel or concrete forces is less than the limiting value, interfacial slip has not occurred.
- 5) The moment and curvature at this point are tabulated, and the curvature is incremented if the limiting shear force has not been exceeded. Steps 1-4 are repeated while incrementing the curvature.
- 6) If the limiting shear force has been exceeded then slip has begun to occur. The cross-section is now separated into the concrete component and steel component.
- 7) The same curvature is assumed as in step 5.
- 8) A reference strain is assumed in the concrete portion of the cross-section.
- 9) The strain variation is computed based on the assumed curvature and reference strain. The sum of forces in the concrete must equal the magnitude of the limiting shear force ($\tau_b A_s$) by adjusting the reference strain. The concrete fiber stresses are calculated using the appropriate concrete material model.
- 10) A reference strain is then assumed in the steel portion of the cross-section. The strains in all fibers of the steel section are calculated, and the stresses are calculated using steel material properties.
- 11) The reference strain is iterated until the sum of the steel fiber forces becomes equal to the limiting shear force ($\tau_b A_s$) within a tolerance.
- 12) When both the steel and concrete forces sum to the limiting shear force then moments are summed in the cross section to calculate the moment corresponding to the curvature.
- 13) The curvature and moment values are tabulated and curvature is incremented. Steps 6-12 are repeated to develop the moment-curvature relationship of the cross-section.

The above procedure is valid when the shear force over the shear span is constant. If a loading condition was used that caused linearly varying shear over a span then the procedure would need to be modified to account for this variation.

9.1.4. Partial Composite Action – FEM Approach

The approach for modeling partial composite action in the FEM models involved the use of surface based interaction models. *Abaqus* allows for the definition of a variety of surface-to-surface bond models. The surface models considered for the deep deck systems were friction based models. The inputs for this model included a maximum shear stress (τ_{\max}), a coefficient of friction (κ), elastic slip tolerance, and the type of normal surface contact implemented. The model is shown schematically in Figure 9.17. From the figure an interpretation of some of the inputs can be made.

τ_{\max} Parameter

The maximum shear stress parameter is defined exactly as it was with the fiber-based model. Based on the test data, the force at which first measureable slip was obtained is used as the force causing slip. The corresponding applied moment can then be found. Based on the developed full bond fiber model the maximum shear stress is then found and input as τ_{\max} . The specimen slips as shown in Figure 9.17 once the maximum shear stress value is reached.

κ Parameter

The κ parameter for the slip model can be thought of as the initial stiffness for the surface model. The higher this value, the more ‘rigid’ the initial interfacial bond is. Therefore, if this value were set very high the model would approach that of the fiber based model. However, as this value increases it becomes more unlikely that the model will converge. A reasonable value needed to thus be chosen for this parameter.

Elastic Slip Tolerance

The elastic slip tolerance value is also related to the initial interfacial stiffness of the bond model. This term allows for small amounts of elastic slip to occur based on the input value. *Abaqus* sets this value to 0.5% of the total element length by default. This means that if a converged solution cannot be found at a certain step then *Abaqus* allows for a 0.5% times the element length amount of slip to occur. This helps the solution to converge, but can reduce accuracy if too much elastic slip is allowed to occur. Thus, smaller values can be used to increase accuracy but the solution may not converge.

Normal Surface Definition

The above terms related to the tangential surface interface. When using surface based models the normal (perpendicular) surface behavior must also be defined. The most common definition is that of a ‘hard’ contact. A hard contact attempts to keep over closure, or surface penetration, to a minimum. It does this by adjusting the surfaces, if one surface is believed to be penetrating another by more than an analysis default. The hard contact usually yields the most accurate results but can sometimes lead to convergence problems within the model. This is especially true when using friction models. Therefore, if convergence problems occur, then an Augmented Lagrange normal surface contact may be needed. This option allows for slightly more surface-to-surface penetration with the advantage of higher likelihood of convergence. The only way to

know which definition is more appropriate is by conducting analyses and checking for convergence.

The FEM models for the specimens were developed using the above parameters. One disadvantage of using the above interfacial slip model is that the model change method for accounting for construction effects could not be implemented along with it. This is because the surface-to-surface slip model could not converge when this option was used. Bringing the concrete into contact with the deformed steel deck in the model could not be done properly when the model change option was used.

9.1.5. Results of interfacial Slip (Partial Composite) Models

The above techniques for modeling interfacial slip effects were implemented into the developed fiber based and FEM models. The values of the limiting shear stress were input for both the fiber based and FEM models. The limiting values for the maximum shear stress were 22 psi for CC-DD specimens 1 and 2, 14 psi for CC-DD Specimen 3, 18 psi for CC-DD Specimen 4, and 18 psi for the SC-DD Specimen. For CC-DD specimen 1 accurate slip readings were not achieved from the test. Since it was the same as CC-DD 2, the same limiting shear stress was assumed. The slip models for the fiber based models were analyzed with no construction effects and with the two previously described methodologies for accounting for construction effects, i.e., the simple and detailed methods.

Fiber-Based Partial Composite Models

The load vs. deflection curves for the fiber based slip models and test data for the CC-DD Specimens are shown in Figure 9.18 - Figure 9.21. The slip models are denoted as Slip 1, Slip 2 and Slip 3. These numbers correspond to models that: (1) did not include construction effects, (2) included construction effects by reducing the yield stress, and (3) those that included construction effects using the more detailed method described previously. The figures show that the partial interaction models provide reasonable predictions of behavior and overall strength of the specimen. Table 9.7 summarizes the predicted strengths for the models along with the actual strengths. As shown, the models that included interfacial slip and construction effects all predicted capacities within 10% of the experimental capacity. Table 9.7 shows models for CC-DD-1 and CC-DD-2 were slightly un-conservative. The models with slip and construction predicted capacities that were 2.5 and 8.7% above the experimental values for CC-DD-1 and CC-DD-2, respectively. The predicted capacity for CC-DD-4 was conservative by 6.7%. This is likely because construction effects were more severe in this specimen (it used the thinner gage deck and bottom plate). CC-DD-3 (the non-studded specimen) was still quite un-conservative in terms of strength prediction. However, the developed model cannot predict shear bond failure in terms of a load capacity so this was expected.

The fiber based models with construction effects and slip closely approximate the overall load-deflection behavior of the specimens. They provide better comparisons than those models that did not include slip effects. This is illustrated by the load-displacement curves shown in Figure 9.18 - Figure 9.21. However, the load-displacement curves also show that all the tested specimens had higher initial stiffnesses than those predicted using

the models. This is likely an indicator that the end supports had some initial inherent restraint. These curves also help in validating a previously made observation during testing. For all studed specimens it was observed that a crack formed over the supports as load and deflection was increasing. The point at which this crack was observed occurs close to where the developed models ‘cross’ the test data on the load-deflection curves shown in Figure 9.18, Figure 9.19 and Figure 9.21. This is observed, for example, around 2 in. of deflection in CC-DD Specimen 2 in Figure 9.19. This change in stiffness observed here is thus believed to be a result of the combination of flexural concrete cracking and the crack that formed over the support. The developed models could not properly capture this stiffness reduction. There could be ways to modify the models to capture this effect, but it was not done within the current study.

The third specimen, without shear studs, shows different behavior based on the load-displacement data of Figure 9.20. While there is still a point where the analytical and test curves cross, what happens after this is of interest. The slopes of the analytical and test curves are quite similar at this point. This is because the slope change is occurring primarily due to effects of slip. The analytical models capture this behavior. However, the shear-bond failure cannot be modeled.

Results of Fiber Based Interfacial Slip Model for Shored Specimen

The interfacial slip fiber based model was also used in analyzing the shored specimen. The predicted load-displacement curves and experimental curve are shown in Figure 9.22. The numerical results from the analyses are shown in Table 9.8. Figure 9.22 shows slip models 1 and 2 reasonably predict overall strength, but are slightly un-conservative. Slip model 3 is conservative in strength prediction. Table 9.8 shows that the Slip 2 model over-predicted capacity by 5% and the Slip 3 model under-predicted capacity by 17%. The results show that the construction effects have a significant effect on overall capacity for shored specimens. While the model could not capture the shear-bond failure it can provide an idea of the strength of the system.

FEM Based Interfacial Slip Models

The above described FEM models were also analyzed for the deep deck test specimens. Numerous problems were encountered related to convergence and performance when analyzing these models. A typical load-displacement prediction of the models is shown for CC-DD Specimen 2 in Figure 9.23. The figure indicates that the overall prediction of the behavior is quite different than the experimental behavior. The model does an acceptable job of predicting capacity, but it does not accurately predict the structural behavior. The sharp drop in stiffness at low load levels in the model is the major problem with the model. The reason for this problem is that the assumed elastic stiffness (κ parameter defined previously) is not sufficiently accurate to model what is actually occurring in the specimen. The analytical results did not improve as the value of κ was increased. The highest value that could be used to obtain a converged solution was 5. For the test specimens it was desired to use a value of at least 100 to properly model the bond behavior. For this reason, the surface based FEM slip models were not further developed or calibrated for the deep deck specimens.

9.2. General Discussion of Structural Analytical Models for Deep Deck Systems

The above section presented analytical models for examining the structural behavior of composite deep deck systems. The models were checked with results from experimental testing. The following general discussion points can be stated based on the analysis

- 1) Models that do not account for construction or slip effects are un-conservative in predicting the overall capacity of the specimen.
- 2) The simple method for incorporating construction effects by reducing the yield stress did a reasonable job of estimating the strength for the un-shored specimens. It was particularly of merit for CC-DD Specimen 4 where construction level stresses were higher than other specimens.
- 3) The CC-DD test specimens had a small rotational end restraint initially. This is evident from comparisons of predicted and measured stiffness. For the specimens with shear studs at the end, the restraint was not significant to greatly affect overall behavior.
- 4) The partial composite CC-DD fiber based slip models that incorporated construction effects estimate strength for the studed specimens to a reasonable degree. They also accurately predict overall structural behavior of the specimens.
- 5) The FEM based slip models were shown to be inadequate for modeling structural behavior of the composite deep deck systems. They were computationally expensive and had numerous convergence problems. Thus, they were not further developed.

The above models were used in developing some simple design equations and recommendations for the CC-DD and SC-DD systems. These equations and recommendations are presented in Chapter 11.

Table 9.1: Geometric and material properties for CC-DD Specimens

Specimen Designation	Nominal Deck Depth (in.)	Total Slab Depth (in.)	Deck and Bottom Plate Thickness (Ga.)	Measured f'_c (psi)	Assumed Concrete Elastic Modulus (ksi)	Measured Yield Stress (ksi)	End Conditions
CC-DD-1	7.5	10	14/16	5767	3000	53 deck 46 bottom plate	Shear Studs/ Pour Stop
CC-DD-2	7.5	10	14/16	6222	3000	53 deck 46 bottom plate	Shear Studs/ Pour Stop
CC-DD-3	7.5	10	14/16	5295	3000	53 deck 46 bottom plate	Puddle Welds/ Pour Stop
CC-DD-4	7.5	10	18/20	5770	3000	46 deck 41 bottom plate	Shear Studs/ Pour Stop

Table 9.2: Predicted and Experimental un-cracked (UC) and cracked (C) stiffness for CC-DD Specimens

Specimen	Predicted Stiffness (kip/in)				Experimental Stiffness (kip/in)		% Difference			
	Fiber		FEM		UC	C	Fiber		FEM	
	UC	C	UC	C			UC	C	UC	C
CC-DD-1	7.7	6.25	7.1	6.3	7.9	5.65	-2.5	10.6	-10	11.5
CC-DD-2	7.5	6.2	7.1	6.3	8.15	5.8	-8	6.8	-13	8.7
CC-DD-3	7.4	6.2	7.1	6.3	8.4	6.1	-13.5	1.6	-15.5	3.3
CC-DD-4	6	4.5	5.8	4.6	6.6	4.45	-9	1.1	-12	3.4

Table 9.3: Predicted and Experimental capacities for CC-DD Specimens – Full Composite Models

Specimen	Predicted Strength (kips)			Experimental Strength (kips)	% Difference (relative to test)		
	Fiber	FEM	SDI		Fiber	FEM	SDI
CC-DD-1	30	29	28.8	24.5	22.4	18.4	17.6
CC-DD-2	31	29.2	29.1	23	34.8	27	26.5
CC-DD-3	29	26.2	28.2	18	61	45.5	56.7
CC-DD-4	19	18.5	20	15	26.7	23.3	33.3

Table 9.4: Capacity and stiffness prediction for SC-DD Specimen – Full Composite Models

Capacity (kips)		% Difference (relative to test)
Fiber	15.7	37.7
FEM	15.9	39.5
SDI	17.4	52.7
Experimental	11.4	NA
Un-cracked Stiffness (kips/in)		% Difference (relative to test)
Fiber	7.7	20
FEM	6.7	4.7
Experimental	6.4	NA

Table 9.5: Predicted and Experimental capacities for CC-DD Specimens – Full Composite Models with construction effects

Specimen	Predicted Strength (kips)					Experimental Strength (kips)	% Difference (relative to test)				
	Fiber 1	Fiber 2	FEM 1	FEM 2	SDI-R		Fiber 1	Fiber 2	FEM 1	FEM 2	SDI-R
CC-DD-1	26.8	27.5	26.5	26.9	24.5	24.5	9.4	12.2	8.2	9.8	0
CC-DD-2	27	27.5	26.8	27.3	24.75	23	17.4	19.6	16.5	18.7	7.7
CC-DD-3	26.5	27	26.2	26.6	24.1	18	45.5	50	45.5	47.8	34
CC-DD-4	14.1	15.2	15.7	16.5	13.3	15	-7	1.3	4.7	10	-11

Table 9.6: Predicted and Experimental capacities for SC-DD Specimen

Capacity (kips)		% Difference (relative to test)
Fiber 1	14	22.8
Fiber 2	12.8	12.3
FEM 1	14.8	29.8
FEM 2	13	14
SDI-R	14	22.8
Experimental	11.4	NA

Table 9.7: Predicted and experimental capacities for CC-DD Specimens models that account for interfacial slip and construction effects

Specimen	Experimental Capacity (kips)			Actual Capacity	% Difference		
	Slip 1	Slip 2	Slip 3		Slip 1	Slip 2	Slip 3
CC-DD-1	27	25	25	24.4	10.6	2.5	2.5
CC-DD-2	27	25	25	23	17.4	8.7	8.7
CC-DD-3	25	23	23	18	39	28	28
CC-DD-4	16	14	14	15	6.7	-6.7	-6.7

Table 9.8: Predicted and experimental capacities for SC-DD Specimen that account for interfacial slip and construction effects

Capacity (kips)		% Difference (relative to test)
Slip 1	12.5	9.6
Slip 2	12	5
Slip 3	9.4	-17
Measured	11.4	NA

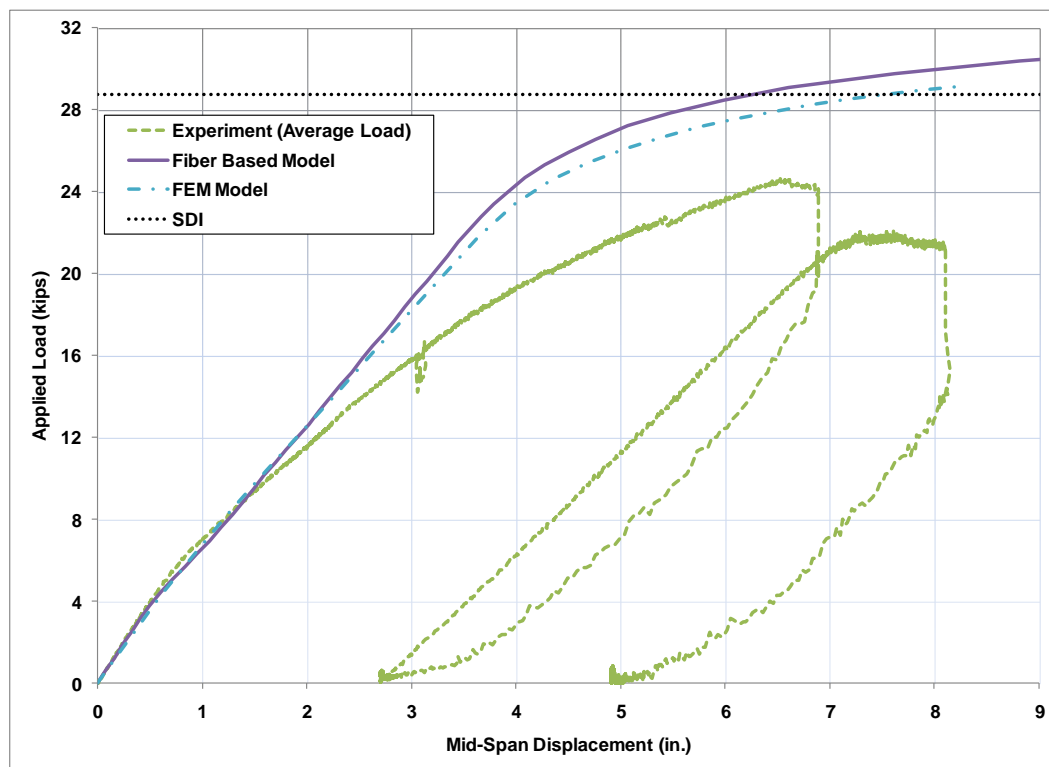


Figure 9.1: Comparison of analytical models to test results for CC-DD Specimen 1 – Models assuming no effects from concrete pour or interfacial slip

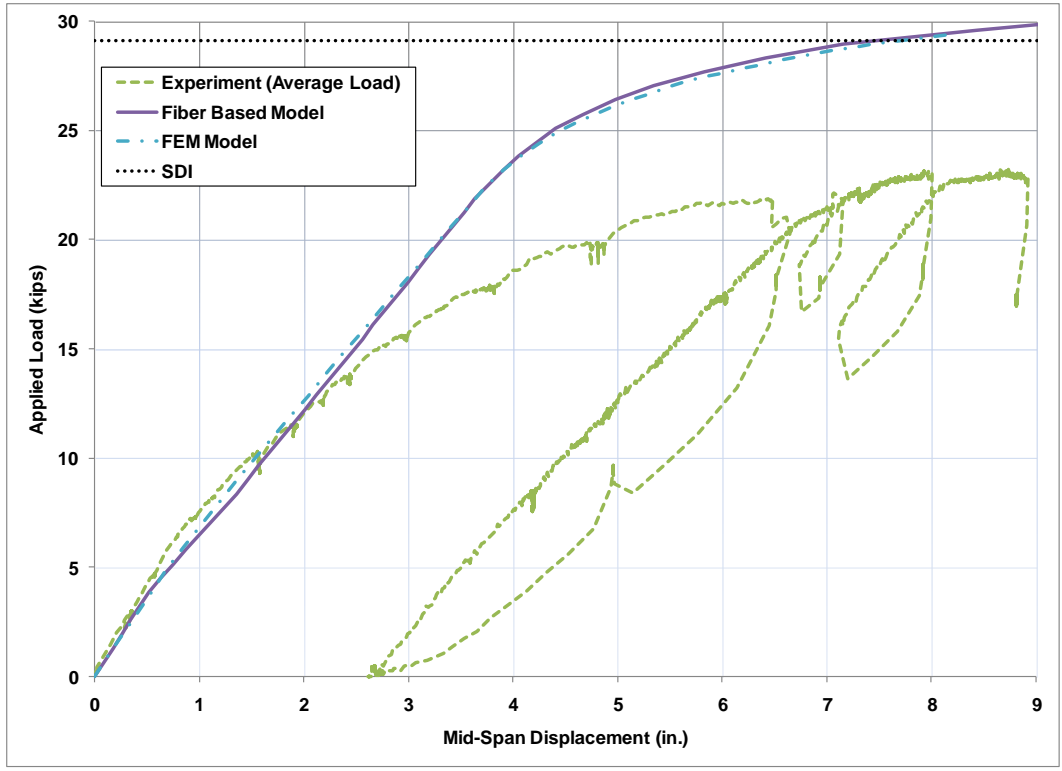


Figure 9.2: Comparison of analytical models to test results for CC-DD Specimen 2 – Models assuming no effects from concrete pour or interfacial slip

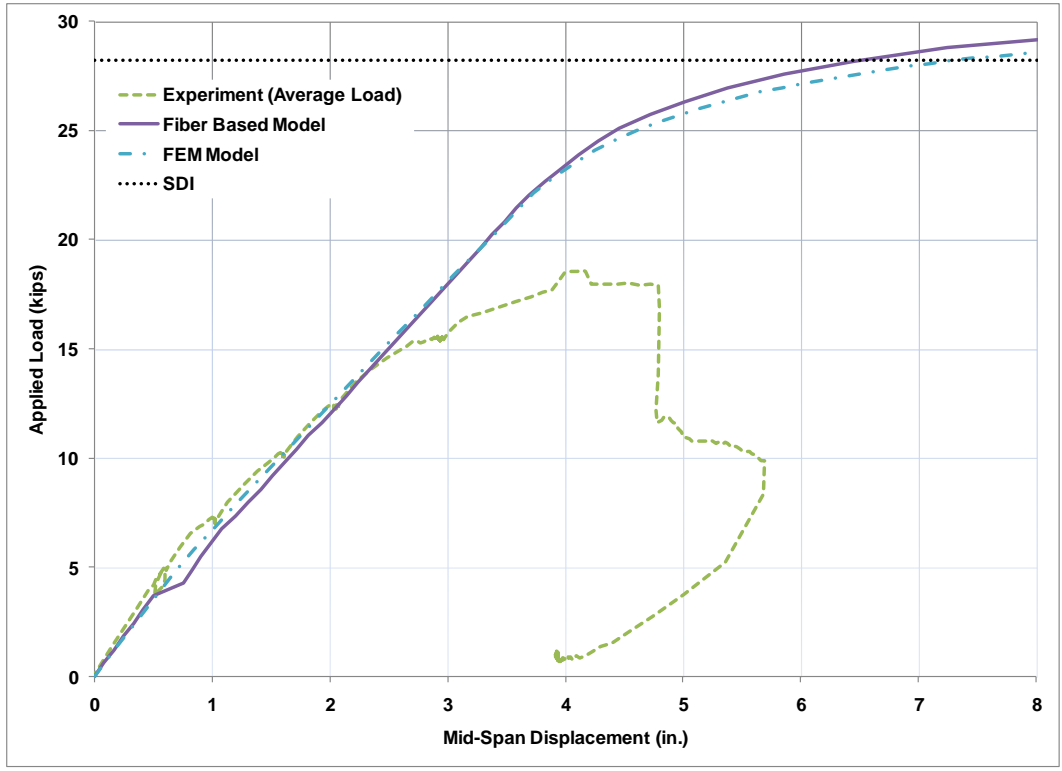


Figure 9.3: Comparison of analytical models to test results for CC-DD Specimen 3 – Models assuming no effects from concrete pour or interfacial slip

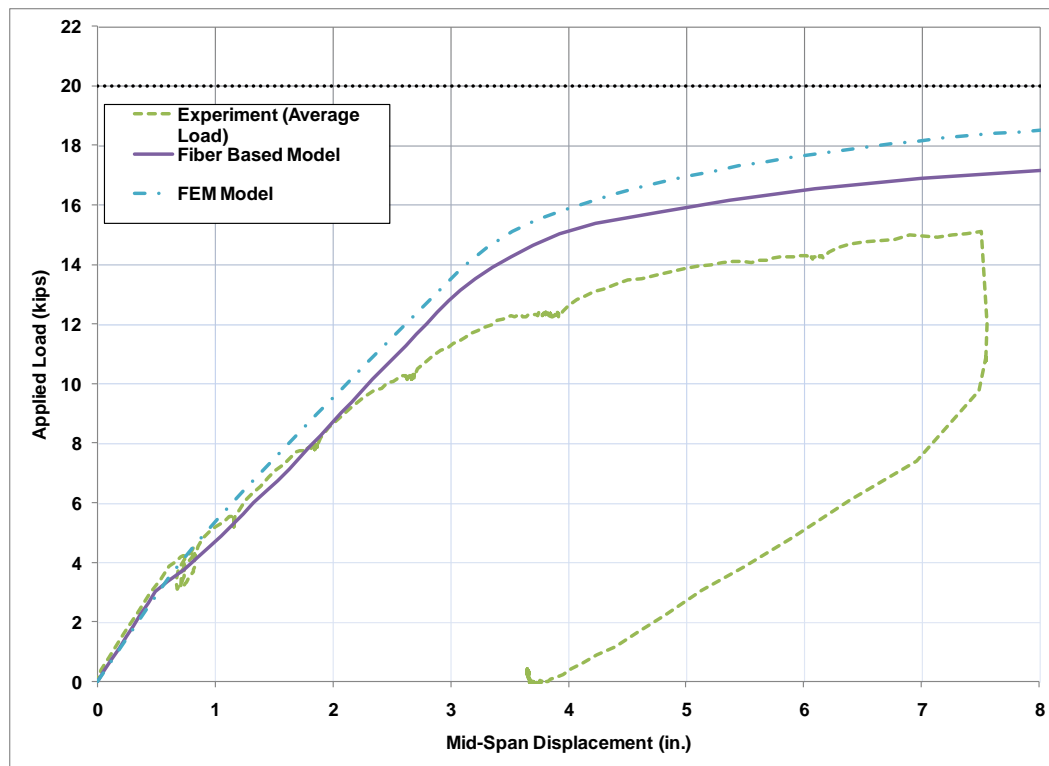


Figure 9.4: Comparison of analytical models to test results for CC-DD Specimen 4 – Models assuming no effects from concrete pour or interfacial slip

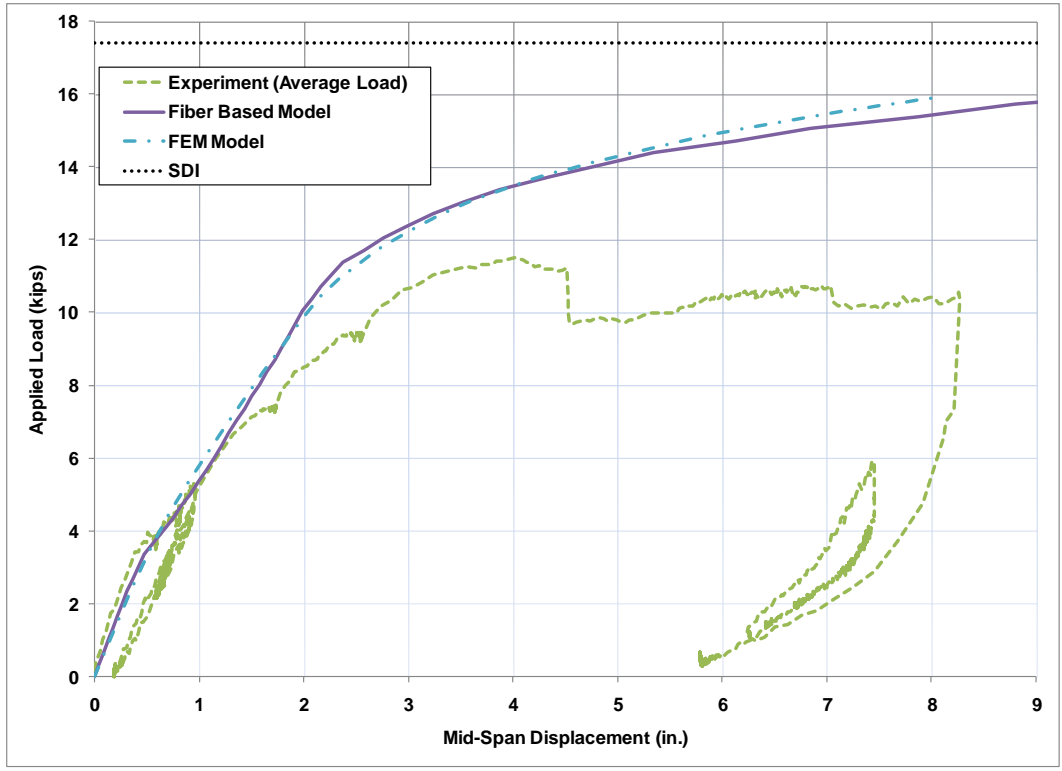


Figure 9.5: Comparison of analytical models to test results for SC-DD Specimen – Models assuming no effects from concrete pour or interfacial slip

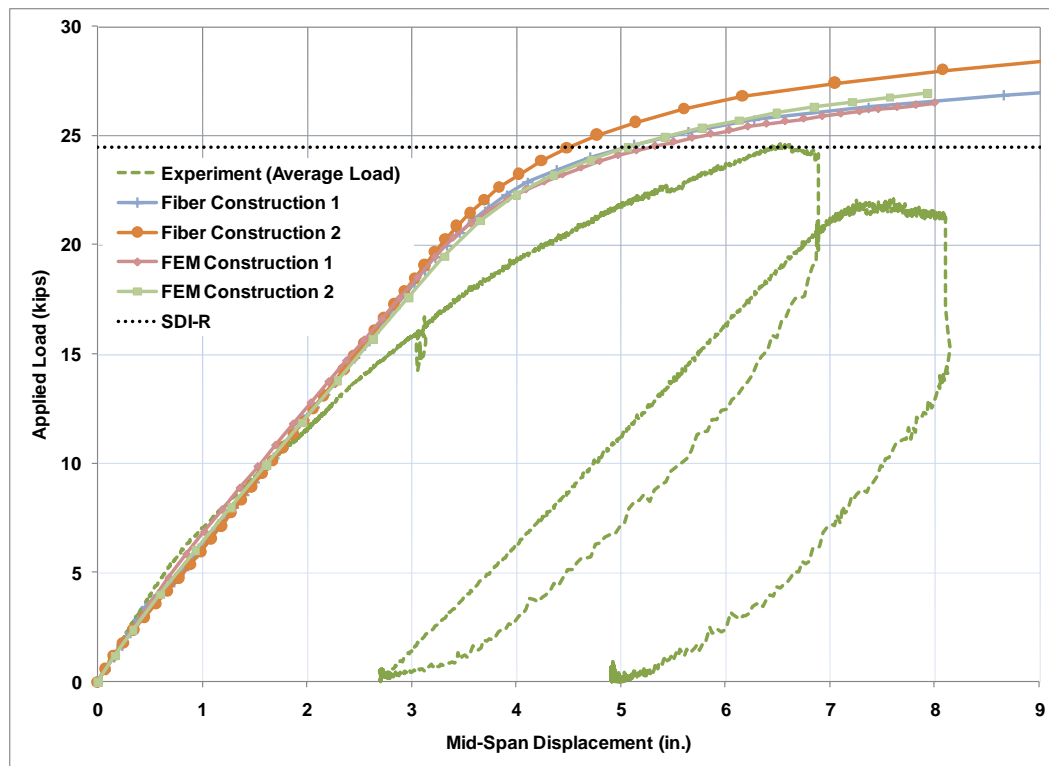


Figure 9.6: Comparison of models with construction effects included to test data for CC-DD Specimen 1

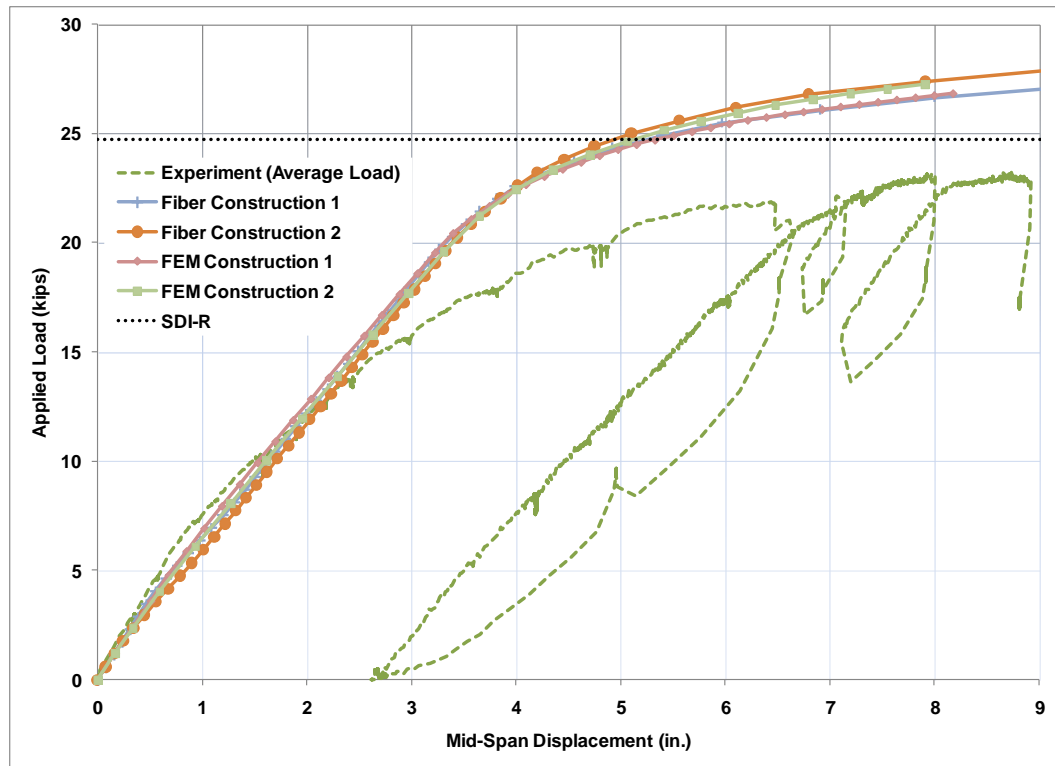


Figure 9.7: Comparison of models with construction effects included to test data for CC-DD Specimen 2

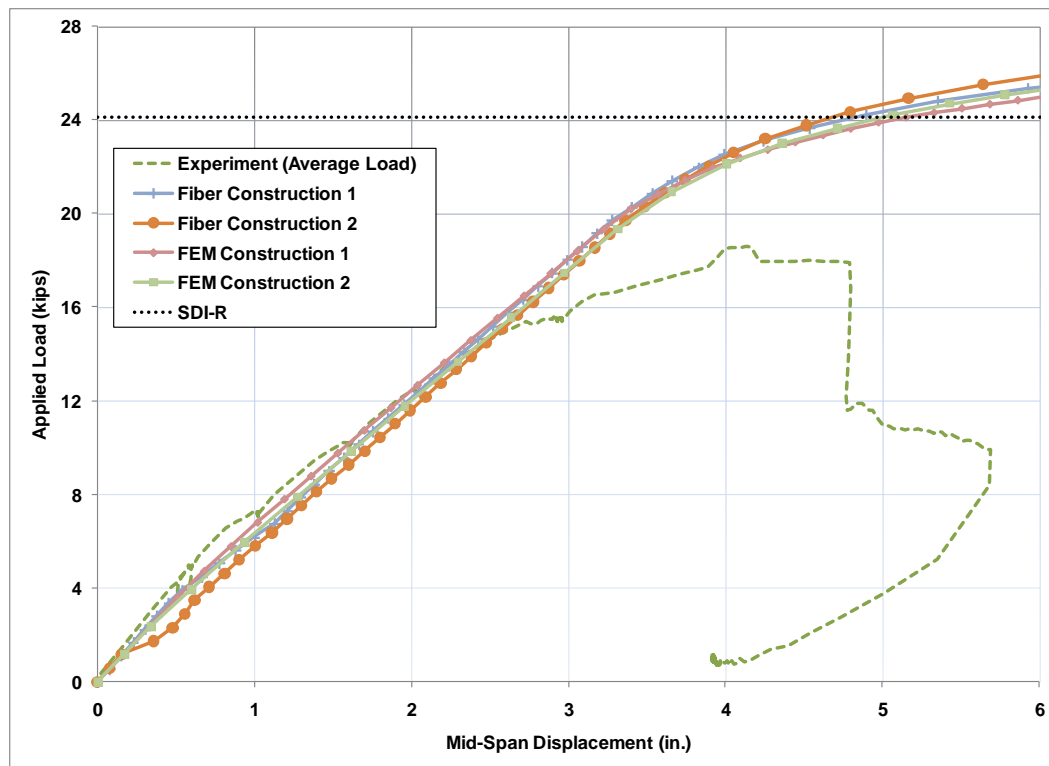


Figure 9.8: Comparison of model with construction effects included to test data for CC-DD Specimen 3

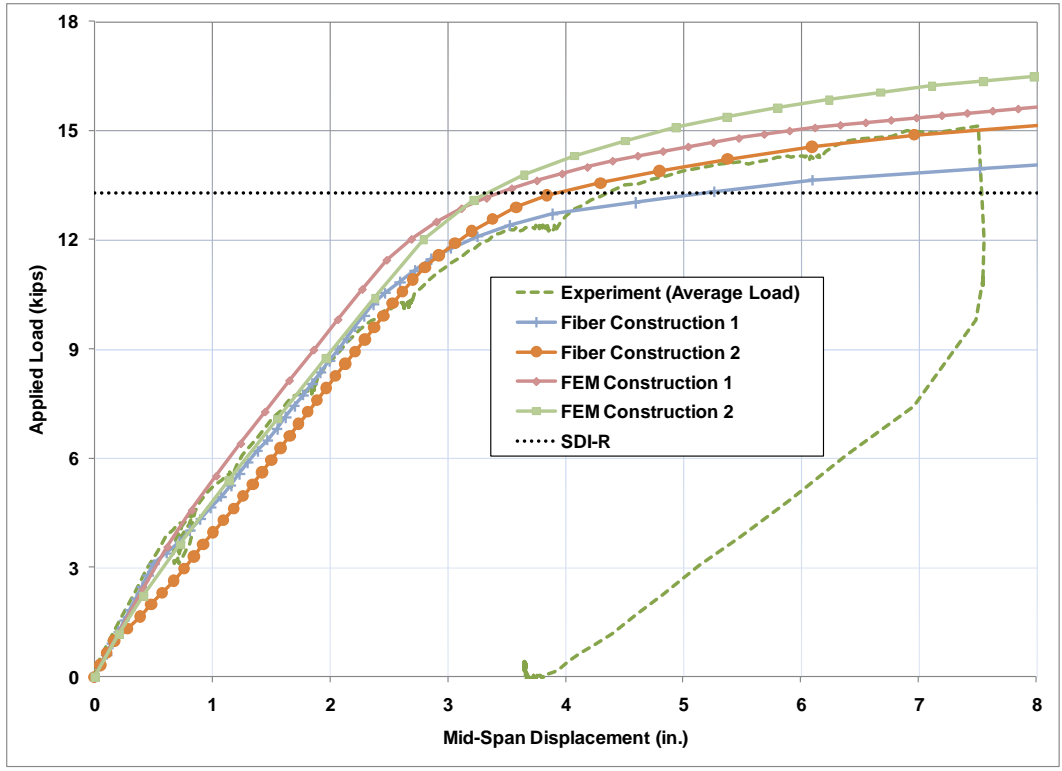


Figure 9.9: Comparison of model with construction effects included to test data for CC-DD Specimen 4

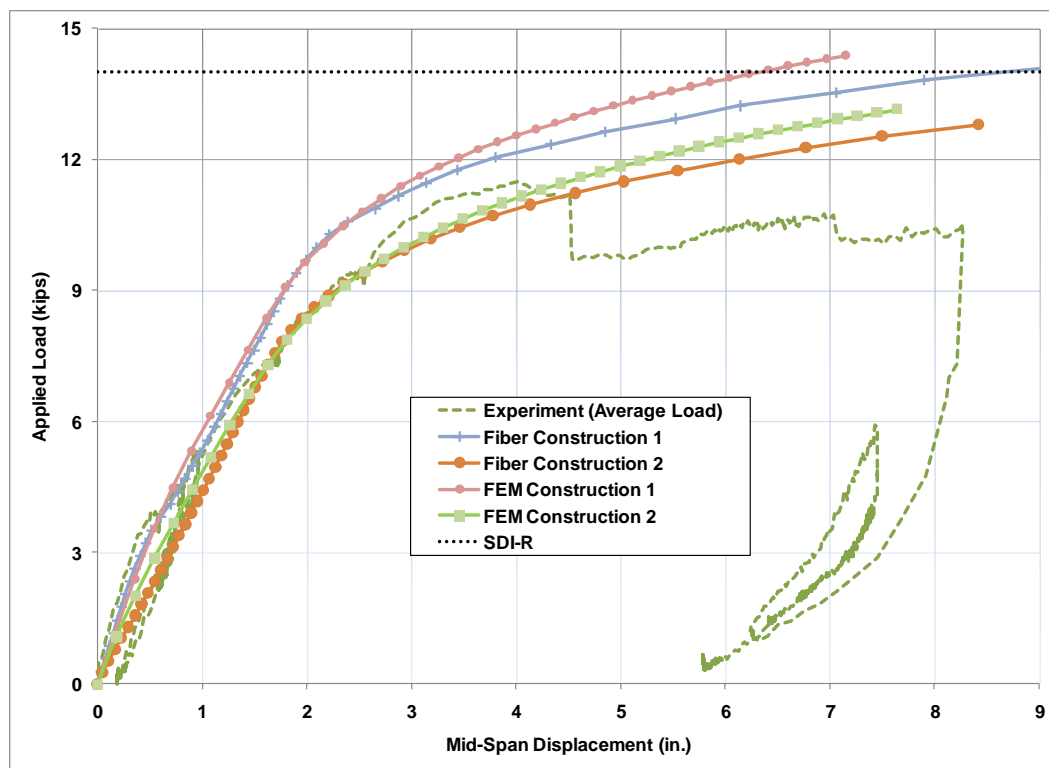


Figure 9.10: Comparison of model with construction effects included to test data for SC-DD Specimen

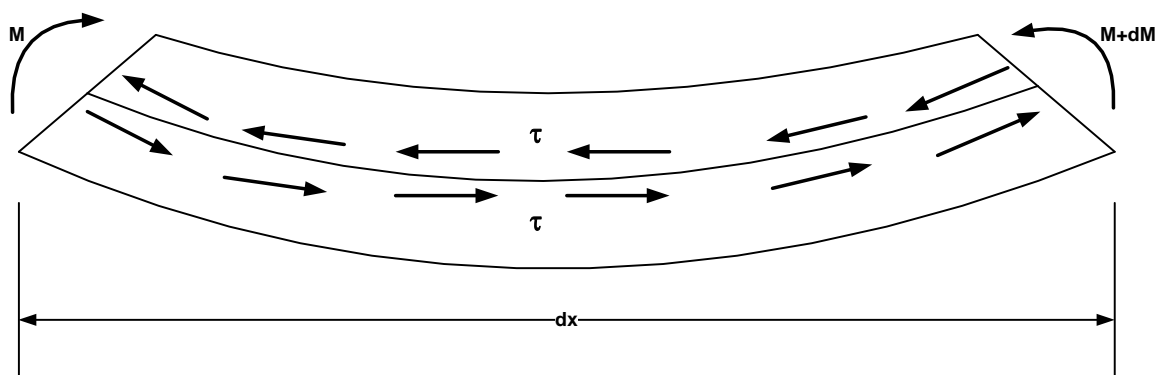


Figure 9.11: Differential element of composite cross section showing distribution of shear stresses at interface

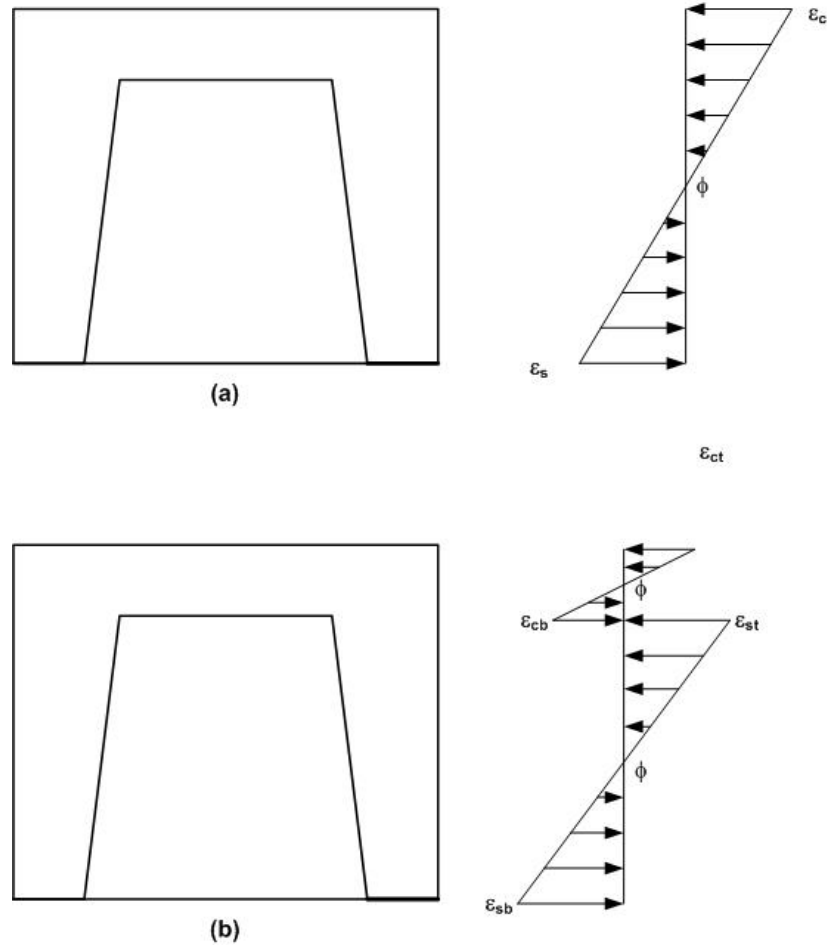


Figure 9.12: Distribution of strains for (a) fully composite section and (b) after slip occurs with two materials having the same curvature

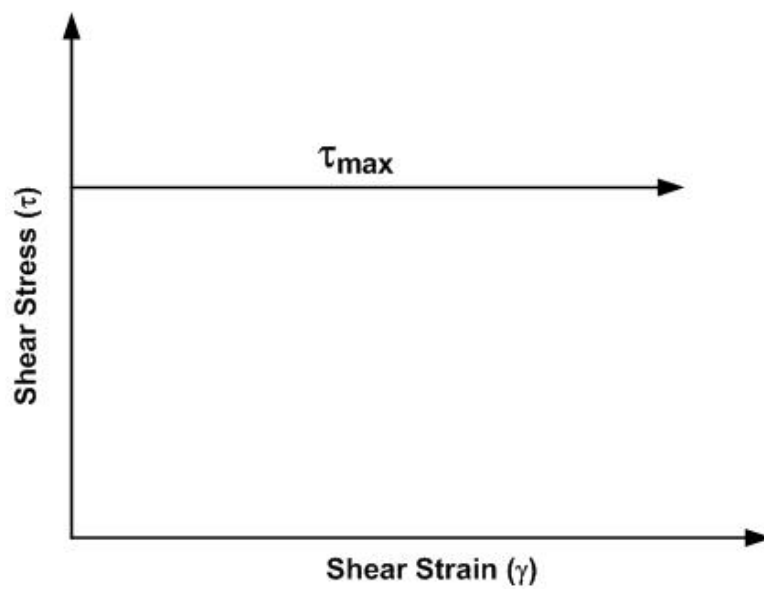
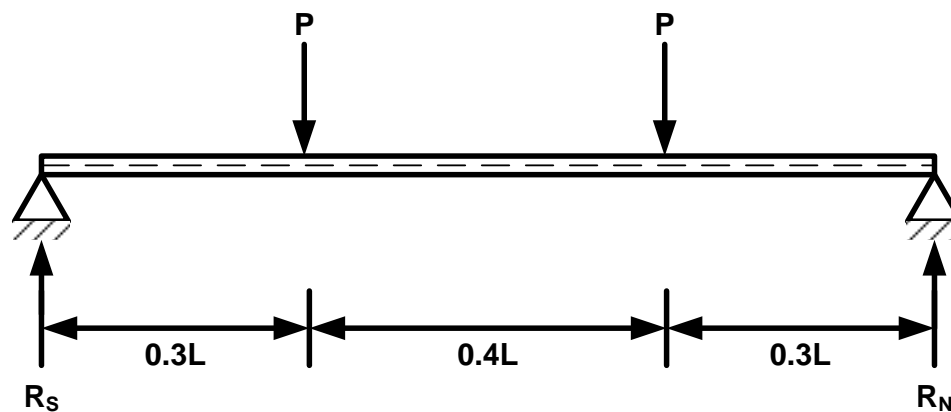
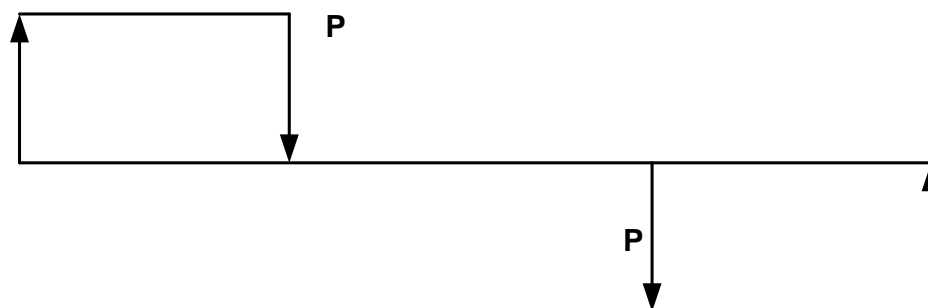


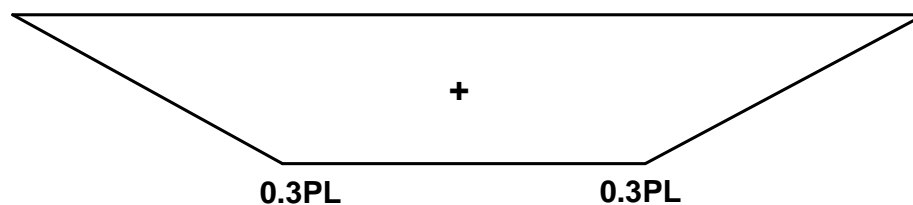
Figure 9.13: Rigid-Plastic relationship assumed for interfacial shear stress behavior



ASSUMED LOADING CONFIGURATION



SHEAR FORCE DISTRIBUTION



BENDING MOMENT DISTRIBUTION

Figure 9.14: Test configuration and resulting transverse shear and bending moment diagrams

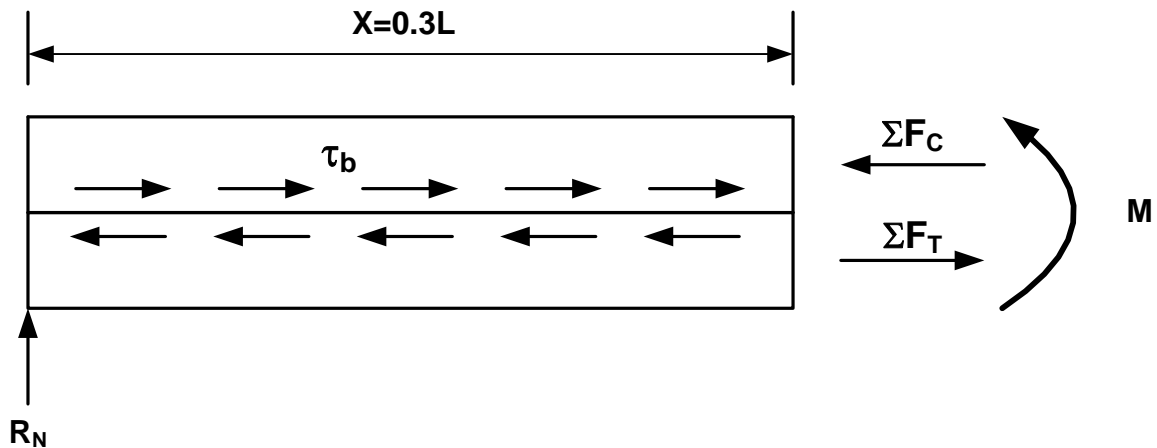


Figure 9.15: Internal force distribution for test specimens

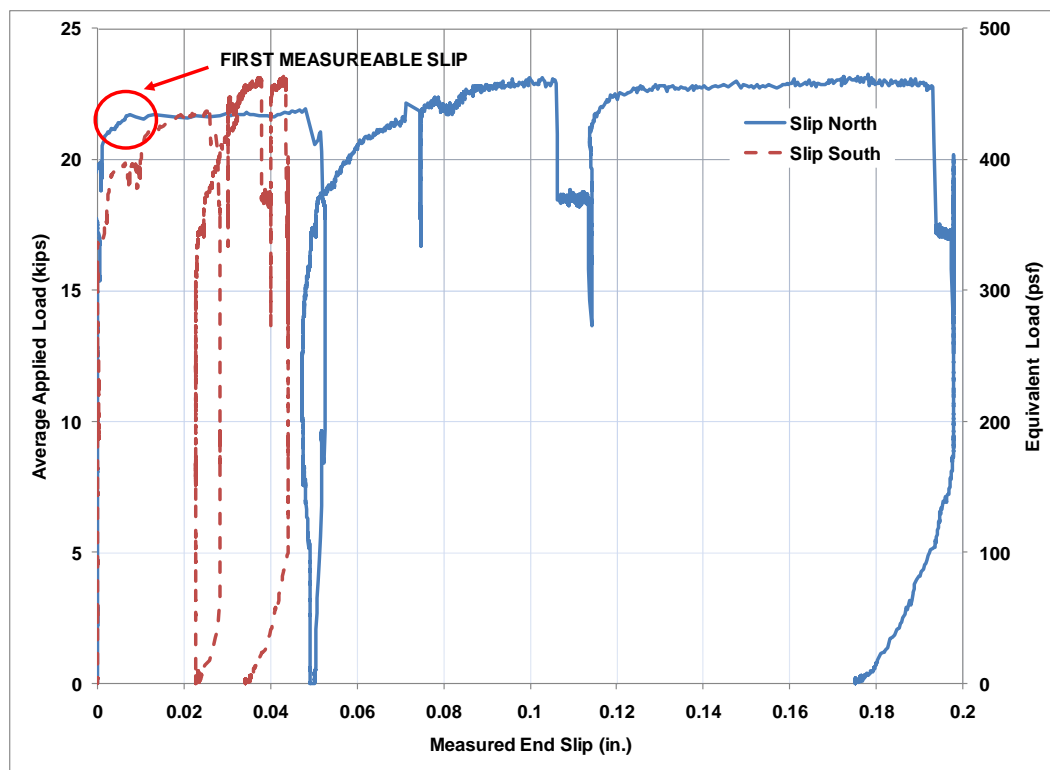


Figure 9.16: CC-DD Specimen 2 load vs. end slip plot showing indication of first measurable slip

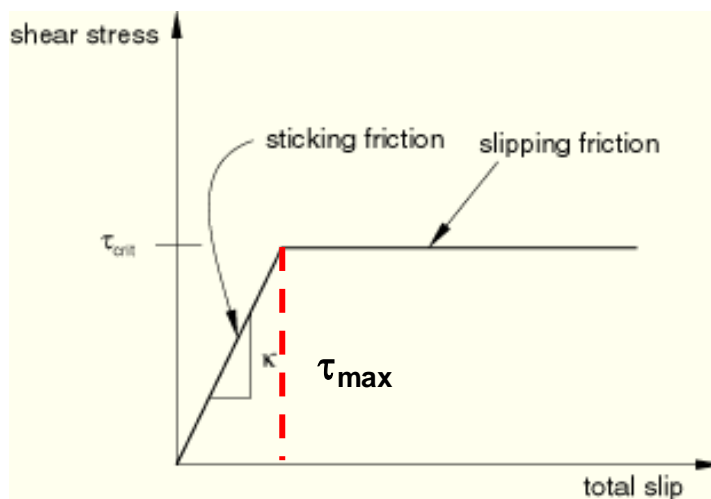


Figure 9.17: Shear bond surface model implemented in *Abaqus*

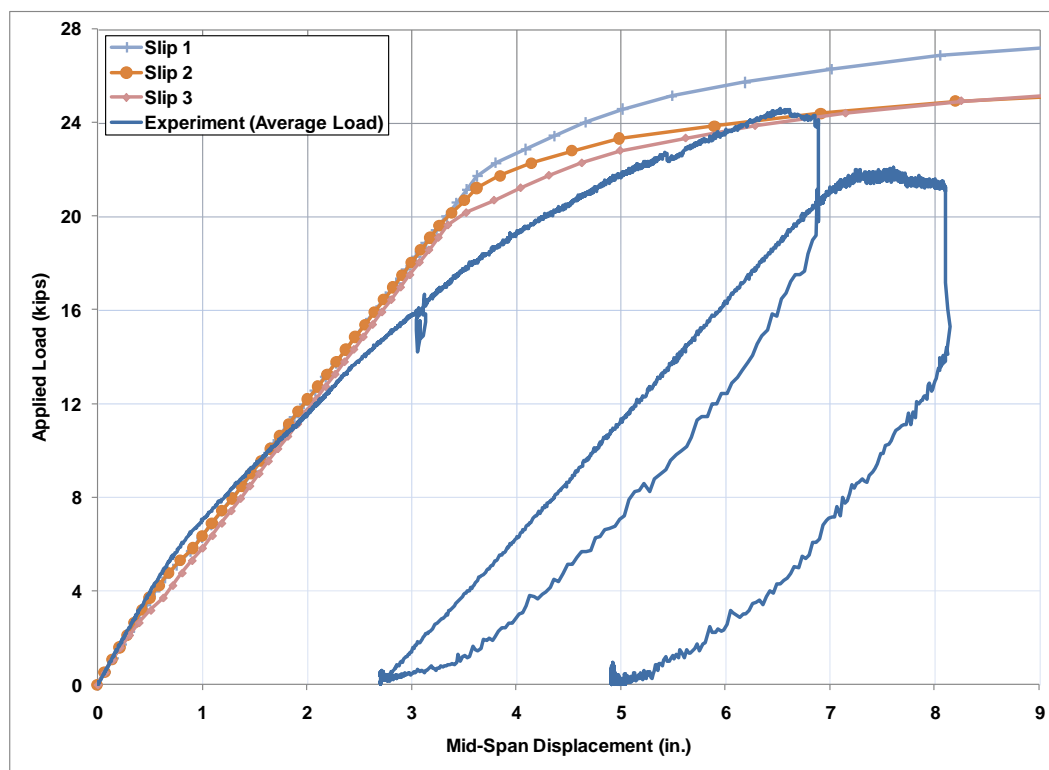


Figure 9.18: Load vs. mid-span deflection for interfacial slip models and CC-DD Specimen 1

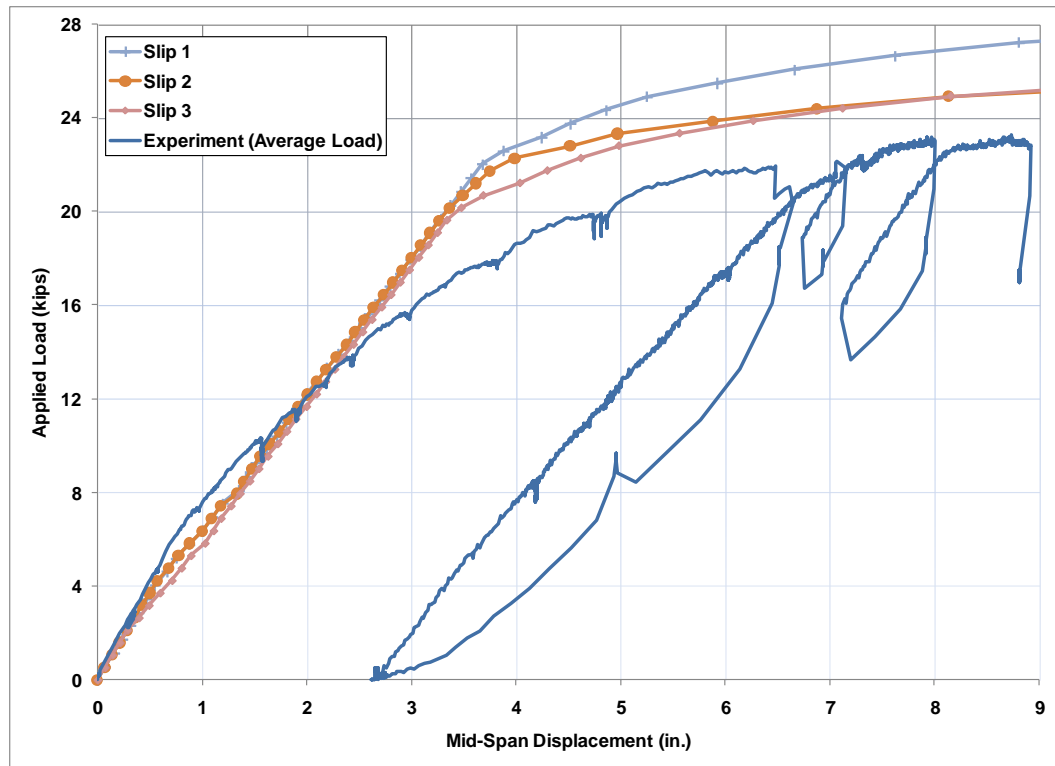


Figure 9.19: Load vs. mid-span deflection for interfacial slip models and CC-DD Specimen 2

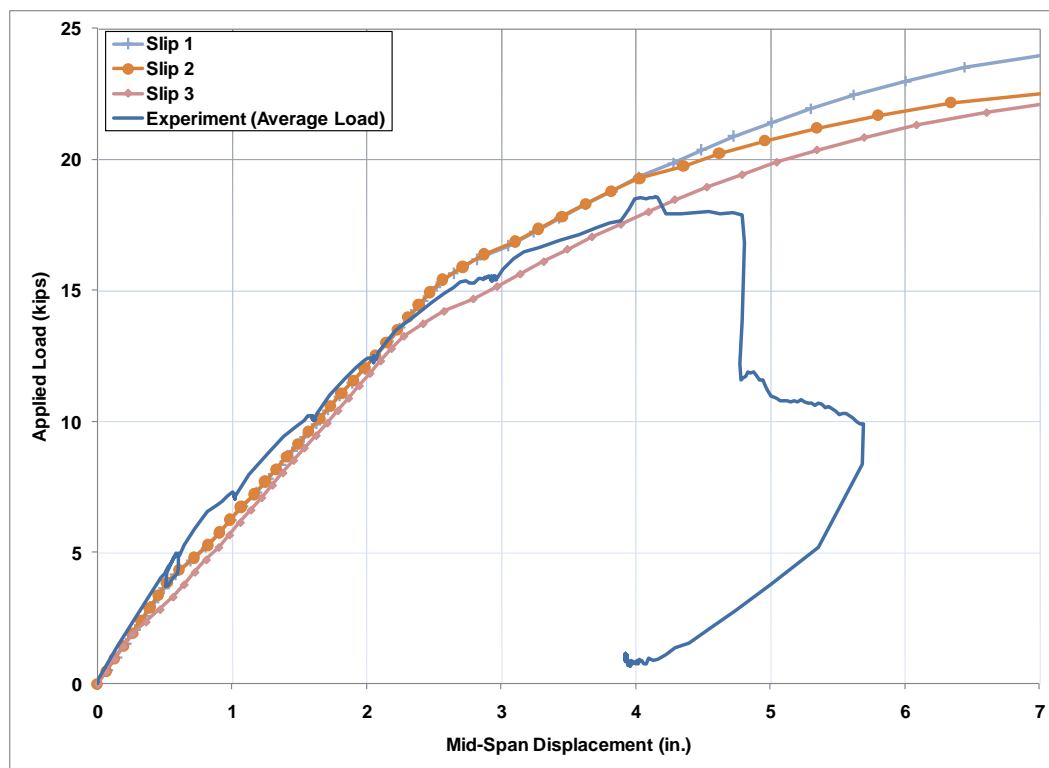


Figure 9.20: Load vs. mid-span deflection for interfacial slip models and CC-DD Specimen 3

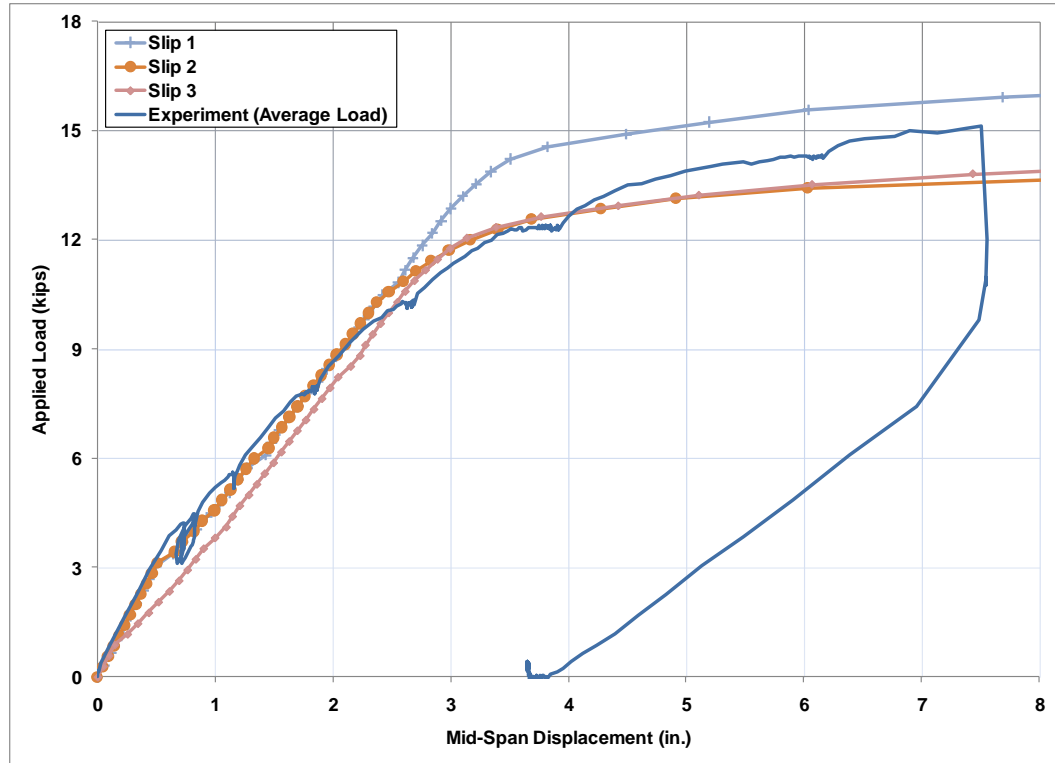


Figure 9.21: Load vs. mid-span deflection for interfacial slip models and CC-DD Specimen 4

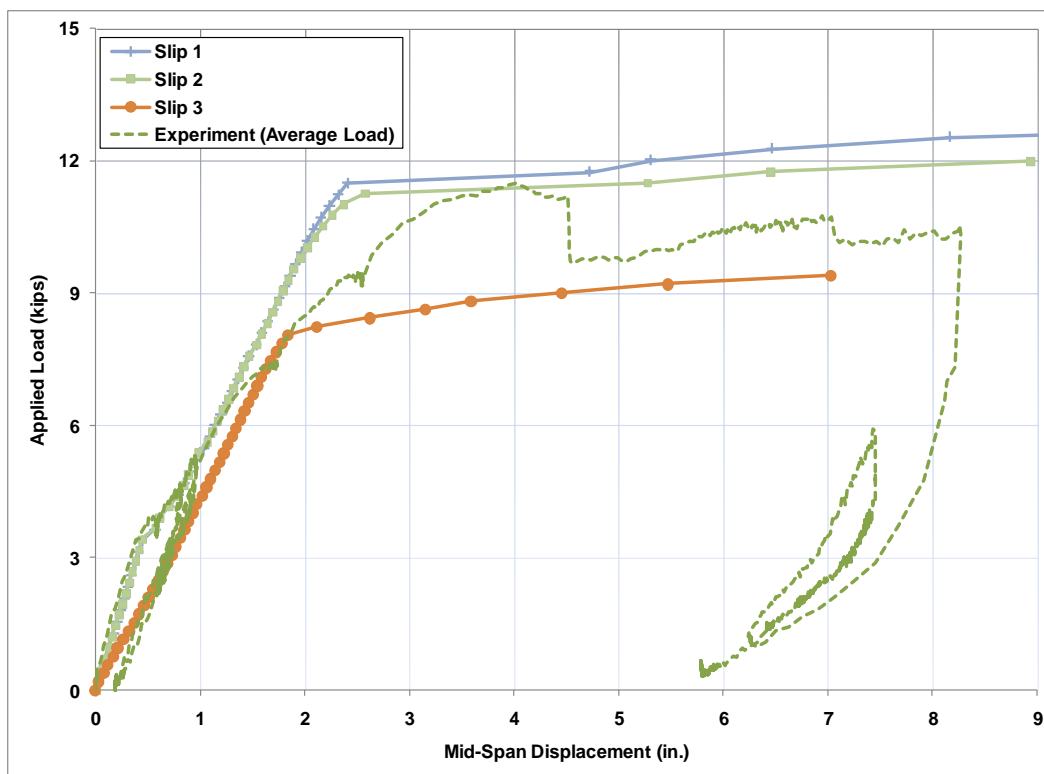


Figure 9.22: Load vs. mid-span deflection for interfacial slip models and SC-DD Specimen

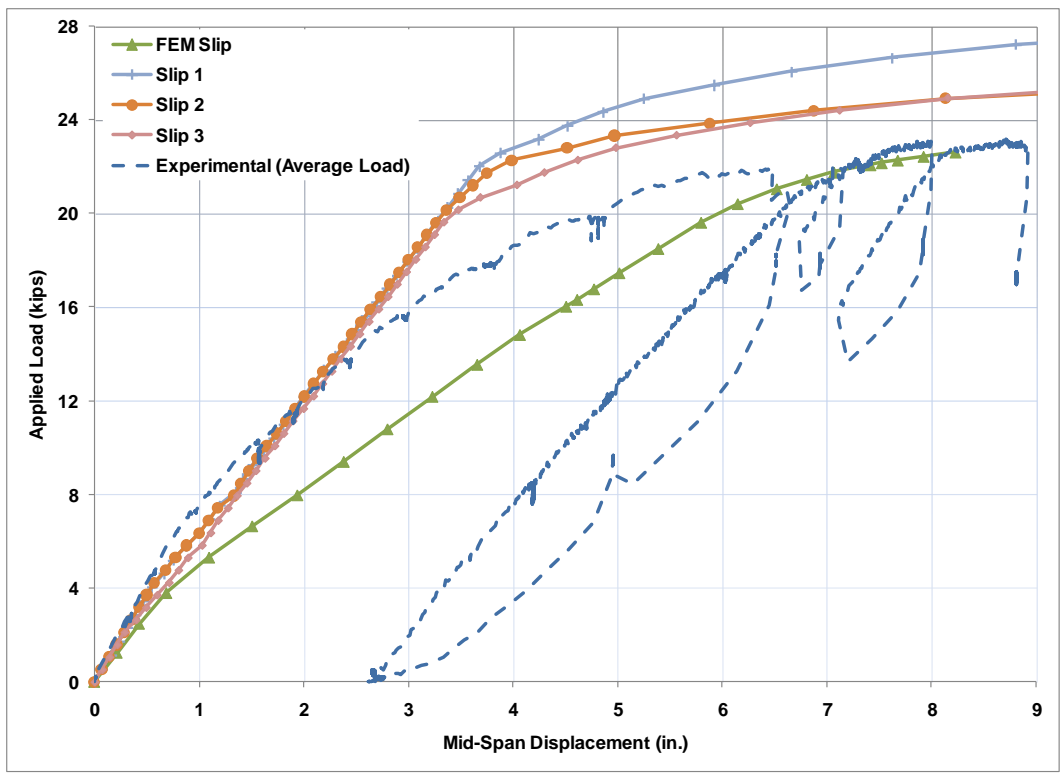


Figure 9.23: Comparison of fiber based slip models and FEM based slip model to test results – CC-DD Specimen 2

CHAPTER 10. COMPOSITE DEEP DECK FLOOR VIBRATION SYSTEM STUDY

10.1. Parametric Study Using US and UK Guidelines

Extensive data on the measured dynamic properties of the composite deep deck systems was collected via modal impact testing. This data is extremely valuable for understanding the fundamental behavior of the floor systems. However, if the system were to be used in an actual structure than a proper evaluation for floor vibrations is needed. This is because the system is now part of an entire structural system rather than an isolated beam in a laboratory. Since only a representative piece was tested in the lab, it is difficult to extrapolate the results and deem whether or not the system be acceptable when used in a structure. Thus, existing criteria on floor vibrations can be used in evaluating the current system. The benefit of performing testing is that it allows for measured quantities, such as natural frequency, to be compared with those suggested by existing guidelines and provide a basis for comparison on the collected data.

Criteria from two accepted design guides related to the mitigation of floor vibrations were used for investigating the current system. The first criterion used was based on recommendations from the American Institute of Steel Construction (AISC) publication *Design Guide 11: Floor Vibrations Due to Human Activity* (AISC 1997). The other design guides used for acceptability evaluation were published by the Steel Construction Institute (SCI) of the United Kingdom (UK). These guides were *SCI Publication 076: Design Guide on the Vibration of Floors* (1989) and *SCI Publication P331: Design Guide on the Vibration of Floors in Hospitals* (2004). The procedure for using these guidelines was summarized in Chapter 2.

The recommendations from these design guides were used to investigate the proposed deep deck floor systems as a full floor system that would be part of an actual structure. This theme structure was used for evaluating the floor system's susceptibility to floor vibrations. The structural and architectural layouts of the structure are given in Figure 10.1 and Figure 10.2, respectively. As shown in the figure, the structure has 30 ft spans which make it ideal for evaluating the proposed floor systems. Also, the structure is an eight story condominium building and therefore can be considered a residential application (which is the intended use for the proposed systems).

Three different deep deck systems were looked at for the study. They corresponded to those which were tested in the laboratory. The two different CC-DD systems tested were investigated. In this section CC-DD-1 refers to the CC-DD deck system with thicker steel components (correspond to CC-DD Specimens 1-3 that were tested). CC-DD-2 refers to the CC-DD system with thinner deck components (CC-DD Specimen 4 that was tested). Finally, the shored composite deck system was also investigated. It is referred to as the SC-DD System in this section.

10.1.1. AISC Guidelines

The AISC recommendations to prevent floor vibrations were described previously. The procedure is also summarized in Figure 10.3. For the given floor systems, this procedure was followed for evaluation of floor vibrations. The frequency measured from the modal impact testing and frequency estimated using the recommended design equation were both used and compared in evaluation. The AISC equation was always lower than that from experimental testing. This is because an additional applied load of 10 psf is assumed when using the AISC suggested equation. The AISC guidelines do not explicitly consider deep deck systems like the ones proposed in this study. Therefore, modifications to certain parameters were made based on engineering judgment to allow for evaluation of the floor system. Modifications to the effective widths and the resulting contributing masses and how a different assumption for the natural frequency changes overall results were investigated. These modifications are described below in the relative parameter studies shown below.

AISC Results – Parameter Study 1

The first parameter study in using the AISC criteria was done using the following assumptions:

- 1) The combined frequency calculated resulted from assuming simply supported deflected shapes for both the girders and floor slabs.
- 2) The effective widths used were those computed from equations 2.6 and 2.7.

Equation 2.4 was then re-arranged such that the required damping ratio was solved for. The equation was solved assuming that 0.005g was the acceptable acceleration (based on the ISO curves used for the criteria). From Table 2.2, it was seen that there is usually 2-5% damping present in a structure. 5% damping can be expected for a structure with full height partitions, which would likely be the case for the given structure. Therefore, in any case where damping above 5% is required the system would be deemed to be unacceptable for floor vibrations. A summary of the results with the above assumptions is given in Table 10.1.

It is seen that the required damping for the CC-DD systems when using the abovementioned assumptions is above 5%. This would indicate the floor system would be susceptible to floor vibration problems if all the above assumptions were valid. For the SC-DD system the required damping is 4.5%. The additional concrete is providing additional mass to the system and thus reducing the damping required to dissipate vibrations. The assumptions used in calculating the effective widths are likely not valid for the deep deck systems and this value would need to be estimated in some other manner. This was examined in the next parameter study for the systems.

AISC Results – Parameter Study 2

For this parameter study, the assumed effective width of the slab was changed for the system. Instead of using equation 2.6 for calculating the width, an effective width of the specimen length was assumed. The reasoning for using this new value was that equation 2.6 was not developed for the type of floor system being evaluated. Therefore, its applicability may come into question when being used for the current evaluation.

Secondly, ATC (1999) recommends using an effective width equal to the length of the floor system when hollow core pre-cast systems are used. While these types of systems are not identical to the given system, they share enough similarities to warrant adjustment to the width parameter. Table 10.2 shows the results using AISC guidelines with this new effective width assumption.

The floor system is now shown to require less than 5% damping to meet the AISC requirements. Thus, for the given structure the floor system would be deemed acceptable. The reason that the floor system is now acceptable is that the contributing mass is now almost twice of what it was in the previous case. What this would physically imply is that there is now twice the mass present, without reducing the stiffness, to reduce the motions present in the floor system. It is difficult to quantify if this effective width assumption is valid for our given system without testing a full scale system. However, the assumption of an effective width being at least that of the bay width seems reasonable.

AISC Results – Parameter Study 3

The final parameter investigated for use within the AISC guidelines is assuming a different fundamental frequency of the slab system. The effective width used was the same as used for Parameter Study 1. As was mentioned previously, the AISC specifications assume a simply supported deformed shape in computing the natural frequency of the floor and supporting members. However, guidelines from SCI (2004) recommend using a fixed-fixed boundary condition when calculating the frequency of the floor (for reasons given previously). The results from this Parameter study are summarized in Table 10.3.

The results show that when the fixed-fixed support deflected shape is assumed, the floor vibration requirements become less stringent. It is important to highlight that using this assumed frequency for the floor system is NOT recommended by the AISC guidelines and should therefore not be used in design. It is presented here solely for academic purposes. However, it illustrates the point that if this mode of vibration is observed in actual structures than perhaps the AISC guidelines should be modified to reflect this.

10.1.2. Steel Construction Institute Criteria

A similar procedure as outlined in *AISC Design Guide 11* is followed with some modifications when using the SCI recommendations for evaluating floor vibrations due to walking excitation. The outline for the SCI procedure was presented previously in Chapter 2. The SCI procedure was completed for two different sets of assumptions. The assumptions pertain to the computation of the effective length and width of the slab system. There are two different publications with different ways of calculating the effective width and length of the slab system. These recommendations for effective area were described in Chapter 2. Table 10.4 summarizes the results from both of these analyses. When looking at the results it is important to remember that the response factor (R) solved for should be less than 4.0 for residential applications (SCI, 1989). Table 10.4 shows that the response factor is less than 4.0 for cases assuming either 3 or 5% damping.

Hence, the SCI guidelines indicate the investigated floor systems would be adequate when looking at susceptibility to floor vibrations induced by walking excitation. The results obtained from the P331 guidelines were meant for considering a deep deck type floor system (the *Slimdek* system). Therefore, a reasonable amount of confidence can be placed in these results for the evaluation.

10.1.3. Discussion Points and Issues with Evaluation Guidelines

One important point of discussion is that U.S. guidelines do not explicitly consider any sort of deep deck systems. The lack of guidelines result because no deep deck system has been implemented for widespread used in the United States. It is likely that guidelines will not be published until a deep deck system is widely used in steel construction within the U.S. This makes evaluation of the proposed system difficult using these guidelines and leads to more questions than answers.

Another issue that needs to properly be considered is how the first natural frequency is computed. The calculation of the first natural frequency of the floor slab system is vital in performing a floor vibration evaluation. The frequency calculated within the U.S. guidelines assumes a simply supported deflected shape in calculating the first natural frequency of the floor system. However, work done in the UK has shown that the first frequency of the floor slab system approaches a fixed ended beam deflected shape. When this assumption is made a natural frequency of around two times that of the simply supported case is found. Drastically different results for acceptability can result depending on what frequency is assumed.

The guidelines from SCI Publication P331 bring forth an important aspect when considering floor vibrations. The publication essentially allows for the entire length of the structure to be used when finding the effective length of the structure. Therefore, the motion induced from an excitation source will produce a dynamic 'ripple' that will traverse the length of the structure as long as there is no obstruction to block its path. An obstruction being a sharp change in layout of the floor plan, or other means to stop the motion of the ripple. It can therefore be difficult in assessing for floor vibrations without knowing the layout of a structure. One part of the building may have no problems related to vibrations such as an interior bay. But, a corner bay in the same structure may have problems due solely to its location within the structure.

After performing the analysis and examining the guidelines it is believed that the guidelines published by the UK are likely more applicable for the current system than those published in the U.S. This is because the SCI guidelines have been calibrated such that a deep deck system can be evaluated. While the deep deck system they use is not the same as the proposed system, it shares enough similarities that the results found from the UK guidelines are likely more applicable than those found using AISC criteria.

10.2. Finite Element Investigation of Floor Vibrations for Deep Deck Systems

The above study on floor vibrations investigated how the systems could be analyzed using existing guidelines. However, the question arises as to how it may be possible to

develop a simple model in investigating a particular systems floor vibration behavior. The AISC and SCI guidelines provide for a simple equation in finding the first fundamental frequency of the system. This equation is based on a simple single degree of freedom model where an equivalent mass is found in estimating the frequency. For evaluation in a general sense, as was shown from the previous section, this estimated frequency should be enough in determining adequacy for most structures. However, an appropriate model is needed to model a particular floor layout in looking at dynamic response.

For the given deep deck systems this was done using the finite element method. The finite element software *Abaqus* was used. A simple ‘beam’ type model was first developed and checked. A complete bay was then modeled. Multiple bay models were then developed. Natural frequencies and modal mass participation factors were estimated using the various models. The modeling technique allows for an entire bay and floor layout to be modeled.

The basic model layout for the deep deck systems consisted of modeling the concrete and steel portions as shell elements and beam elements, respectively. The concrete was modeled using rectangular 3D shell elements where the thickness of the shell was defined as the thickness of the concrete above the steel deck. Stiffness contribution from the lower flute concrete was ignored in the model. Its stiffness contribution is minimal for the system since it lies mostly below the neutral axis and cracks in tension. However, the mass was scaled appropriately to account for the mass of the lower flute concrete. The element types used for the concrete portion were reduced integration shell or S4R elements. The steel deck was modeled as beam or B33 elements. The equivalent area and stiffness was used in the beam section definition. This is done within *Abaqus* using a generalized beam section definition. The slab section was then offset from the beam section by the vertical centroidal distances between the sections. The deck section and concrete were constrained to share the some relative motions. This was done using the ‘tie’ command in *Abaqus*. Figure 10.4 shows a schematic of the model for one unit width, or 2 ft. for the CC-DD specimens. As shown, the model is relatively simple to construct and can easily be expanded into a complete bay or multiple bays. Hence, the next step in developing the model is to extend it into an entire bay. For this example, a 30 ft by 30 ft. bay was developed. This is done by modifying the single cell model. First, the width of the top slab was extended to the entire width of the bay. This is a valid modification as long as the loads are small enough so that the concrete will not experiencing significant cracking. For the small loading assumed in vibration evaluation due to human excitation, this assumption is acceptable and commonplace. The deck elements are modeled as discrete (separate) sections. They are not interconnected with one another except through the top slab. Figure 10.5 shows a schematic of the entire bay model. It should be noted that the ends of the deck pieces are currently idealized as pins. This is representative of the case for a rigid girder. Therefore, the next step in the modeling process is adding the effects of support girders.

It is important to include the effects of girder stiffness into the model as it was shown in Section 10.1 that the girders play a very important role in dynamic behavior. These girders were input into the model as beam (B33) elements with 6 degrees of freedom. They were offset from the deck sections by the vertical centroid of the girder plus the

vertical centroid of the deck sections. The connection between the deck and girders was modeled using multi-point constraints (MPCs) within *Abaqus*. These are rigid links which constrain specified degrees of freedom within the model. Hence, the girders were assumed composite with the deck sections. The girder ends are then simply supported. Figure 10.6 shows the entire bay model with the flexible girders included. Girders are assumed to only run transverse to the decks. Girders were assumed to be W27x84 steel shapes (thought to be a reasonable cross-section for the given span and applied loads).

The final models included multiple bays. Each bay can modeled just like above and then combined within the model. Based on the studies done in Section 10.1, the concrete slab portions can be assumed continuous for the assumed forces imparted upon it. However, the deck sections are assumed discontinuous between bays. Thus, each deck section is assumed as 30 ft simple spans for the model. Figure 10.7 shows an example of a multiple bay model. As shown, the model is of a cruciform shape with 5 total bays. Another multiple bay model is shown in Figure 10.8. This model consists of 9 total bays of 30 ft by 30 ft dimensions each. The concrete is assumed to be continuous over the bays, while the deck pieces are modeled by B33 elements that are connected or constrained to the concrete slab.

10.2.1. Predicted Dynamic Parameters for Developed Models

The mode shapes and natural frequencies of the above models were estimated. *Abaqus* has a *frequency* analysis option that will determine the frequencies of the model. A Lanczos Eigensolver is used in finding the frequencies and the desired number of vibration modes can be specified. Initially, the first twelve modes were extrapolated for the models described in the previous section. These include: a) single cell model, b) entire bay with rigid girder model, c) entire bay with flexible girders model, d) the cruciform multi-bay model, and e) the 9 bay model. The properties of CC-DD System Option 1 described in Section 3.3 were used in defining the floor system component of the model. Table 10.5 summarizes the predicted resonant frequencies for the models. The mode shapes for these models are shown in Figure 10.9 through Figure 10.21. Figure 10.9 and Figure 10.10 present modes 1-6 and 7-12 for the single cell model. Figure 10.11 and Figure 10.12 present modes 1-6 and 7-12 for the single bay model with rigid supports. Figure 10.13 and Figure 10.14 presents modes 1-6 and 7-12 for the single bay model with flexible girder supports. Figure 10.15 and Figure 10.16 present modes 1-6 and 7-12 for the multi-bay cruciform model. Finally, Figure 10.17, Figure 10.18, Figure 10.19, Figure 10.20, and Figure 10.21 presents modes 1-4, 5-8, 9-12, 13-16, and 17-20 for the 9 bay model.

Table 10.5 and Figures 10.9-10.21 show that many different modes appear depending on the type of model. Many torsional modes are appearing between bending modes for the single cell model. The only two true bending modes present in the single cell model (Figure 10.9 and Figure 10.10) are mode 1 and mode 3. All other modes were combinations of torsional and bending as observed in the figures. This is consistent with what was observed from modal impact testing. These torsional modes are not truly representative of modes that would actually occur in large scale structure. The first bending mode predicted for the single cell model matches close to the single bay model

with the rigid support assumption. These two modes are 11 and 13% higher than that predicted from the single bay model with flexible girders included. The reduction in frequency illustrates Dunkerly's effect of the two separate frequencies of the floor system and girder combining.

The full bay models show more modes are appearing between the primary bending modes of the floor system. Both the rigid and flexible single bay models reflect this when examining the mode shapes in Figures 10.11-10.14. The modes are more closely spaced than that of the single cell model. This effect is seen even more so for the multi-bay modes where the first 12 modes are even more closely spaced.

It is obvious that looking purely at resonant frequencies and mode shapes will not provide enough information to make any certain comments on which modes are dominating response. Therefore, it is necessary to examine the modal participation factors for the modes and resonant frequencies. Modal participation was estimated with a modal effective mass parameter. The effective modal mass m_{ai}^{eff} for a particular mode α in a given kinematic direction i is defined by equation 10.1 (Simulia, 2007).

$$m_{ai}^{eff} = (\Gamma_{ai})^2 m_{\alpha} \quad 10.1$$

Where:

Γ_{ai} The modal participation factor for mode α in direction i

The modal effective mass can then be divided by the entire mass of the model to determine a particular mode's normalized modal effective mass. This parameter indicates how strong motion for the mode is in a particular direction. For the models the motion in the vertical direction was of interest. This would be the direction of motion in which vibration issues would occur. Also, if the normalized modal masses are summed their value should approach 1 if all modes that participate in that excitation direction have been extracted. If the summation of this value is much less than 1 it is likely that more vibration modes need to be determined.

The normalized effective modal mass parameters for the given models are shown in Table 10.6. As shown, for the single unit model and single bay models the first resonant frequency is seen to be dominant. The first resonant frequency is shown to have a normalized effective mass of 0.8 for the single cell model. The fifth vibration mode has a normalized effective mass value of 0.09. This corresponds to the first and third bending modes of the system. All other modal participations are essentially zero for the single unit model. This is consistent with modal impact testing where the first bending mode was around 10 times for dominant than third bending (see Figure 4.38). Also, when using the single cell model these two modes account for 89% of the modal participation. This indicates any higher modes contributions are likely negligible.

Table 10.6 shows that the first bending mode for the single bay model with rigid support assumptions has a normalized effective mass parameter of 0.8. Only the first mode is truly dominant when looking at the first 12 resonant frequencies for this model. The model gives us little more information than the unit cell model.

The modal participation of the first mode drops to 0.62 when a flexible girder is included in the single bay model as shown in Table 10.6. Mode 3 is shown to have 10%

participation and Mode 5 has 1%. Mode 3 is the second bending mode for the entire system and Mode 5 is the third bending mode for the system. Hence, the girder plays an important role in affecting multiple frequencies. Still, the first mode is observed to be dominant in the model.

The multiple bay models yielded quite interesting results. For the cruciform model, the first mode, which was first bending for the outer bays as seen in Figure 10.15, was found to have a normalized effective modal mass participation factor of 0.23. However, mode 9 seen in Figure 10.16 had a normalized mass participation factor of 0.32. This corresponds to a mode where the center bay slab portion is bending as a fixed end beam about the girders. This mode is shown to be quite similar to that recommended by SCI (2004) in evaluating the combined resonant frequency of floor systems. This indicates that this mode is more dominant than other modes within the system.

The nine bay model results are also shown in Table 10.6 . As shown, the summation of the normalized modal mass terms is 0.39. This value indicates that higher modes are contributing and need to be calculated. Therefore, the model was analyzed again, and the first 20 modes were found. These results are shown in

Table 10.7. The mode shapes for all 20 modes are shown in Figures 10.17-10.21. As shown, the summation of the normalized effective modal masses for the first 20 modes is 0.79. Modes 4 and 14 are shown to be dominant with normalized effective mass values of 0.35 and 0.37. Mode 4 is shown in Figure 10.17 and Mode 14 in Figure 10.20. Mode 4 is the combined frequency of the girders and floor system for Bay 5. The outer bays are also shown to be affecting the motion. Mode 14 is bending of the edge center bays (4 and 6 as identified earlier) about the edge girders. The bending of the floor system is seen to be close to a fixed-fixed bending condition about the girders. However, the flexibility of the girders does not allow for a complete fixed-fixed condition of the floor system. This mode is similar to that recommended by SCI in evaluating floor systems. This model also shows that all modes are close in frequency.

The above models have brought forth some important considerations when evaluating composite floor system for floor vibrations. These include:

- 1) A single cell model (analogous to the deep deck test specimens) is adequate for determining the first resonant frequency. Higher primary bending frequencies can also be determined adequately with this model.
- 2) Single bay models with assumed rigid end supports provide little more information than the single cell model.
- 3) Single bay models with flexible girders show Dunkerly's effect of the girder flexibility reducing the overall systems frequency.
- 4) Multiple bay models show that there are several closely shaped modes in an actual structure. Many of these modes have low participation in the overall dynamic response.
- 5) Effective modal mass parameters in the multi-bay models indicate that it is likely proper to use the SCI recommendations in estimating the dominant frequency of

the floor system for evaluation purposes. This frequency is based on the floor system (deck and concrete) bending about the girders with a mode shape similar to that of a fixed-fixed beam.

- 6) Multiple bay models qualitatively and quantitatively show how mass from multiple bays will contribute to the overall behavior.

10.2.2. Other Possible Applications of Modeling Technique

The developed models were used to show participation of various vibration modes for composite deep deck systems. However, the models could be used for other dynamic analyses in evaluating a particular composite floor system. One application could be applying certain forcing functions to the system and evaluating the dynamic response. This could be especially useful for a structure where floor vibration problems may be anticipated due to floor layout or intended use of the structure.

Table 10.1: Results from AISC Parameter Study 1

Floor Profile	Frequency Estimation	Effective Slab Width (ft)	Effective Girder Width (ft)	Combined Weight (kip)	Slab Frequency (Hz)	Girder Frequency (Hz)	Combined Frequency (Hz)	Required Damping at 0.005g (%)
CC-DD-1	Analytical	11.5	39.2	44.1	5.4	10.2	4.8	5.5
	Experimental	11.5	39.2	44.1	6.0	10.2	5.2	4.8
CC-DD-2	Analytical	12.2	37	41	5	10.5	4.5	6.5
	Experimental	12.2	37	41	5.8	10.5	5.0	5.2
SC-DD	Analytical	14.9	38.4	57.3	5.2	10.1	4.6	4.5
	Experimental	14.9	38.4	57.3	6.0	10.1	4.9	4.0

Table 10.2: Results from AISC Parameter Study 2

Floor Profile	Frequency Estimation	Effective Slab Width (ft)	Effective Girder Width (ft)	Combined Weight (kip)	Slab Frequency (Hz)	Girder Frequency (Hz)	Combined Frequency (Hz)	Required Damping at 0.005g (%)
CC-DD-1	Analytical	30	39.2	87.4	5.4	10.2	4.8	2.8
	Experimental	30	39.2	87.4	6.0	10.2	5.2	2.5
CC-DD-2	Analytical	30	37	82.1	5	10.5	4.5	3.2
	Experimental	30	37	82.1	5.8	10.5	5.0	2.8
SC-DD	Analytical	30	38.4	97.3	5.2	10.1	4.7	2.7
	Experimental	30	38.4	97.3	6.0	10.1	4.9	2.5

Table 10.3: Results from AISC Parameter Study 3

Floor Profile	Effective Slab width (ft)	Effective Girder Width (ft)	Combined Weight (kip)	Slab Frequency (Hz)	Girder Frequency (Hz)	Combined Frequency (Hz)	Required Damping at 0.005g (%)
CC-DD-1	11.5	39.2	44.1	12.1	10.2	7.8	1.9
CC-DD-2	12.2	37	41	11.1	10.5	7.7	2.2
SC-DD	14.9	38.4	57.3	11.5	10.1	7.6	1.6

Table 10.4: SCI Criteria Results

Floor Profile	SCI Guidelines	Effective Floor Width (ft)	Effective Floor Length (ft)	Combined Weight (kips)	Slab Frequency (Hz)	Girder Frequency	Combined Frequency	R factor (3%)	R factor (5%)
CC-DD-1	P076	30	57	112	12.1	10.25	7.8	3.5	2.1
	P331	10.5	170	119	12.1	10.25	7.8	3.3	1.9
CC-DD-2	P076	30	60	113	11.1	10.5	7.7	3.4	2.0
	P331	10.3	170	111	11.1	10.5	7.7	3.5	2.1
SC-DD	P076	30	60	133	11.5	10.1	7.6	2.9	1.7
	P331	10.3	170	131	11.5	10.1	7.6	3.0	1.8

Table 10.5: First 12 resonant frequencies for FEM models (no additional loading)

Vibration Mode	Predicted Resonant Frequency (Hz.)				
	Single Unit	Single Bay Rigid Girder	Single Bay Flexible Girder	Cruciform	9 Bay
1	6.05	6.14	5.45	5.28	5.288
2	15.26	6.42	6.78	5.28	5.298
3	20.5	8.12	8.99	5.48	5.299
4	30.6	10.6	11.1	6.47	5.32
5	45.8	13.8	13.6	6.75	5.48
6	46.2	18.4	14.4	6.87	6.0153
7	62.2	20.7	17.8	6.91	6.0158
8	76.3	21	18.9	7.81	6.43
9	78.6	22.4	21.4	8.65	6.61
10	95.7	24.5	24.1	8.84	6.84
11	113.1	24.9	25	9.16	7.3
12	113.5	28.2	26.6	9.3	7.57

Table 10.6: Modal effective mass ratios for various models – first 12 modes of vibration

		Effective mass of mode/total mass of system				
		Single Unit	Single Bay Rigid Girder	Single Bay Flexible Girder	Cruciform	9 Bay
Vibration Mode	1	0.80	0.80	0.62	0.23	0.000
	2	0.00	0.00	0.00	0.03	0.032
	3	0.00	0.00	0.10	0.05	0.000
	4	0.00	0.00	0.00	0.00	0.351
	5	0.09	0.00	0.01	0.00	0.005
	6	0.00	0.00	0.00	0.00	0.000
	7	0.00	0.00	0.00	0.00	0.000
	8	0.00	0.00	0.00	0.00	0.000
	9	0.00	0.00	0.00	0.32	0.003
	10	0.00	0.00	0.00	0.03	0.000
	11	0.03	0.00	0.00	0.00	0.000
	12	0.00	0.00	0.00	0.06	0.000
Summation		0.93	0.80	0.74	0.72	0.39

Table 10.7: Modal effective mass ratio for 9 bay model – first 20 modes of vibration

Vibration Mode	Resonant Frequency (Hz)	Effective mass of mode/total mass of system
1	5.288	0.000
2	5.297	0.032
3	5.299	0.00053
4	5.32	0.351
5	5.48	0.0049
6	6.0153	0.000
7	6.0158	0.000
8	6.43	0.000
9	6.61	0.00325
10	6.84	0.000
11	7.3	0.000
12	4.57	0.000
13	7.75	0.000
14	7.93	0.369
15	7.934	0.00099
16	8.19	0.0254
17	8.52	0.000
18	8.76	0.000
19	9.01	0.000
20	9.3	0.00052
Summation	NA	0.787

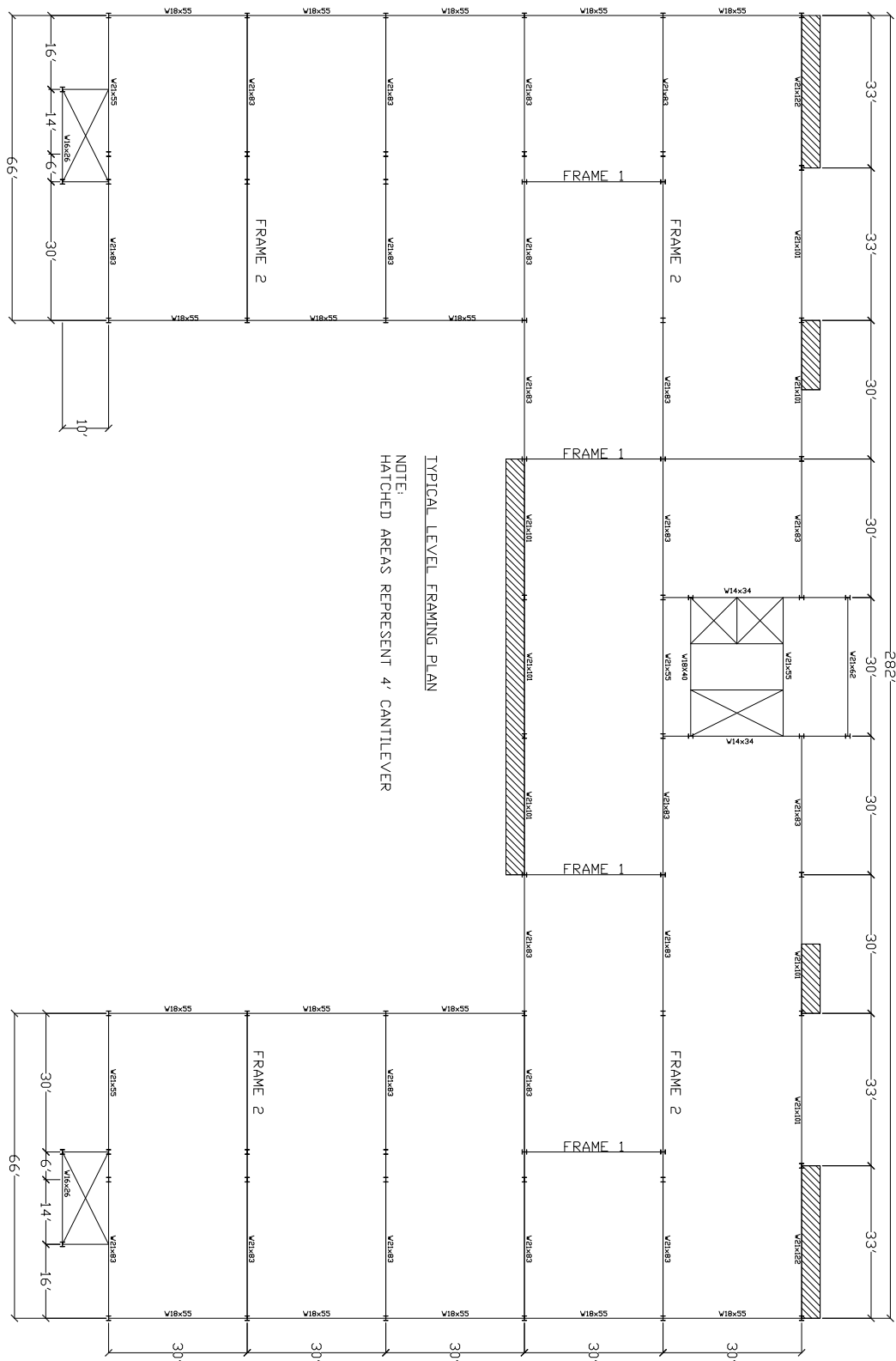


Figure 10.1: Typical Level Framing Plan – Structural (AISC 2004)

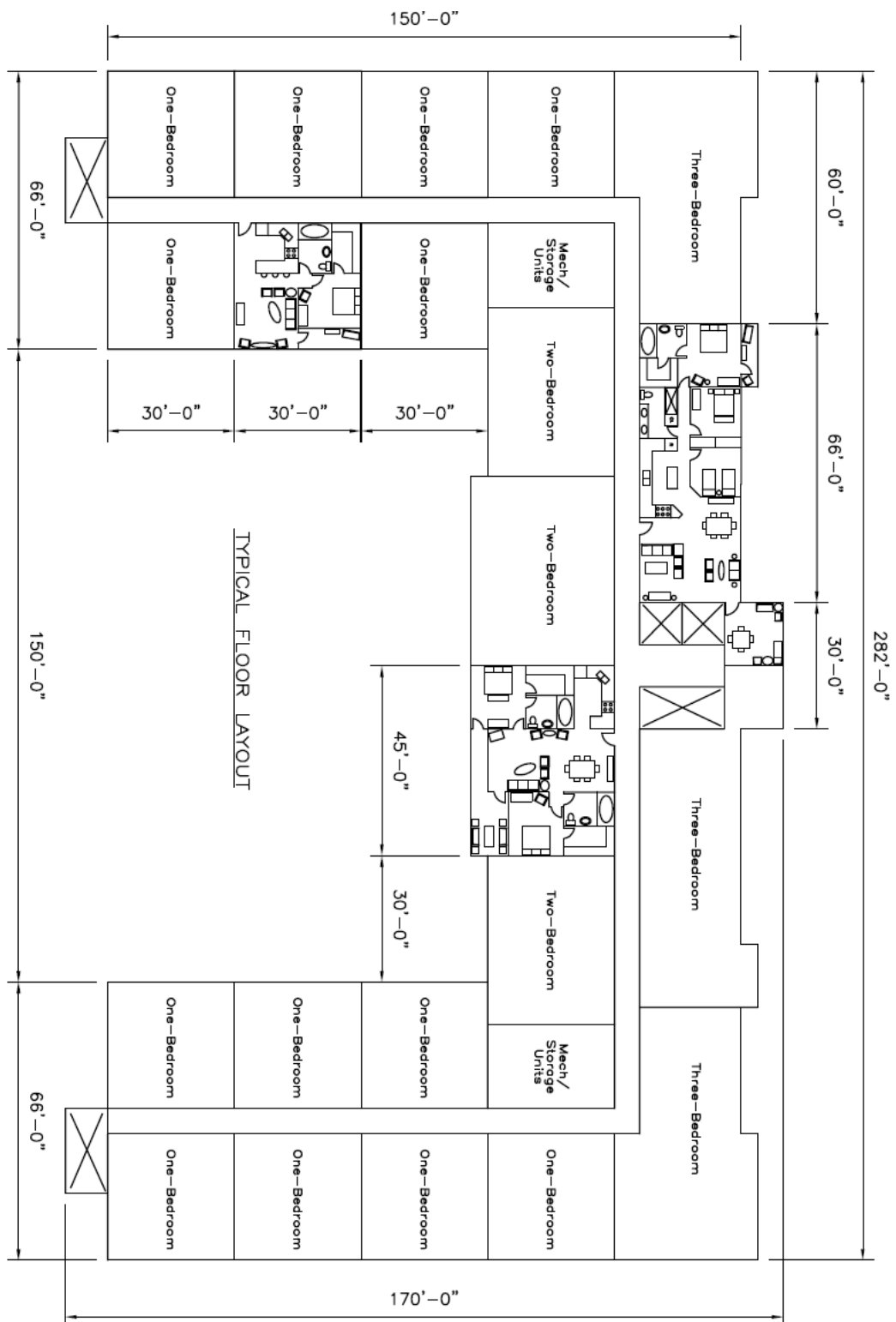


Figure 10.2: Typical Architectural Floor Plan for Prototype Structure (AISC 2004)

A. FLOOR SLAB

Determine unit weight and d_e = effective depth

$$\text{Calculate } D_s = d_e^3 / 12n$$

B. JOIST PANEL MODE

Calculate I_j (see Sections 3.5 and 3.6 if **trusses** or open web joists)

$$\text{Calculate } w_j \text{ and } \Delta_j = \frac{5w_j L_j^4}{384 E_s I_j}$$

$$\text{Calculate } f_j = 0.18 \sqrt{g / \Delta_j} \text{ and } D_j = I_j / S$$

$$\text{Calculate } B_j = C_j (D_s / D_j)^{1/4} L_j \leq 2 / 3 \times \text{floor width}$$

$$C_j = 2.0 \text{ for interior panels; } 1.0 \text{ for edge panels}$$

$$\text{Calculate } W_j = w_j B_j L_j \text{ (} \times 1.5 \text{ if continuous)}$$

C. GIRDER PANEL MODE

Base calculations on girder with **smaller frequency**.

Calculate I_g (see Sections 3.5 and 3.6 if truss or joist girder or if girder supports open web joists).

$$\text{Calculate } w_g \text{ and } \Delta_g = \frac{5w_g L_g^4}{384 E_s I_g} \text{ with correction if only one beam.}$$

$$\text{Calculate } f_g = 0.18 \sqrt{g / \Delta_g} \text{ and } D_g = I_g / L_j$$

Use average of supported joist span lengths,
if different, for L_j

For interior panel, calculate

$$B_g = C_g (D_j / D_g)^{1/4} L_j \leq 2 / 3 \text{ floor length}$$

$$C_g = 1.8 \text{ if shear connected; } 1.6 \text{ if not.}$$

For edge panel, calculate $B_g = 2 / 3 L_j$

$$\text{Calculate } W_g = w_g B_g L_g \text{ (} \times 1.5 \text{ if continuous)}$$

D. COMBINED PANEL MODE

If $B_j > L_g$, reduce Δ_g by $L_g / B_j \geq 0.5$

$$\text{Calculate } f_n = 0.18 \sqrt{g / (\Delta_j + \Delta_g)}$$

$$\text{Calculate } W = \frac{\Delta_j}{\Delta_j + \Delta_g} W_j + \frac{\Delta_g}{\Delta_j + \Delta_g} W_g$$

Choose β from Table 4.1 (0.02, 0.03, 0.05)

$$\text{Calculate } \frac{a_p}{g} = \frac{P_o \exp(-0.35 f_n)}{\beta W} \text{ where } P_o = 0.29 \text{ kN (65 lb)}$$

Compare with a_o / g from Table 4.1 (0.5%, 1.5%)

E. CHECK STIFFNESS CRITERION IF $f_n > 9 \text{ Hz}$ **F. REDESIGN IF NECESSARY**

Figure 10.3: Floor Evaluation Calculation Procedure (reproduced from AISC Design Guide 11, 2003)

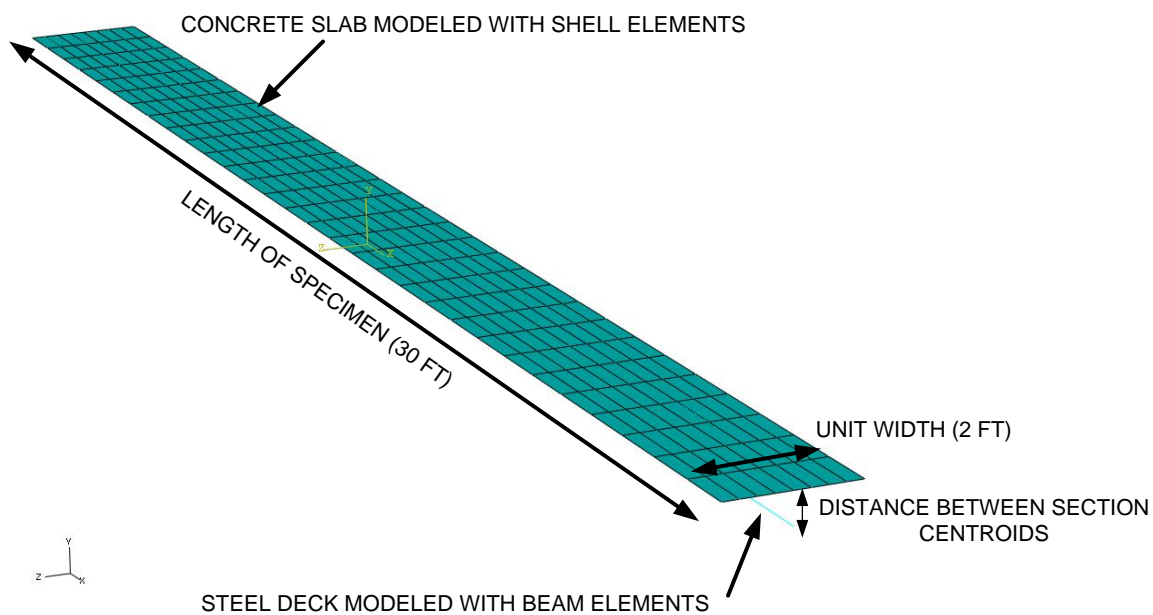


Figure 10.4: Schematic showing model of single cell for FEM model

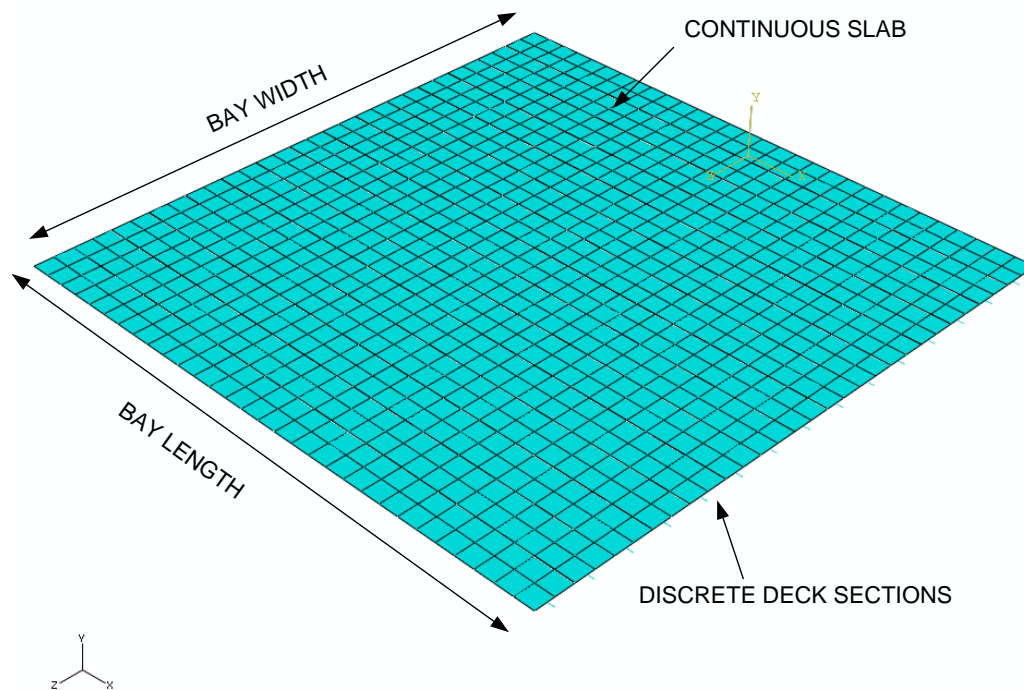


Figure 10.5: Schematic showing model of entire bay

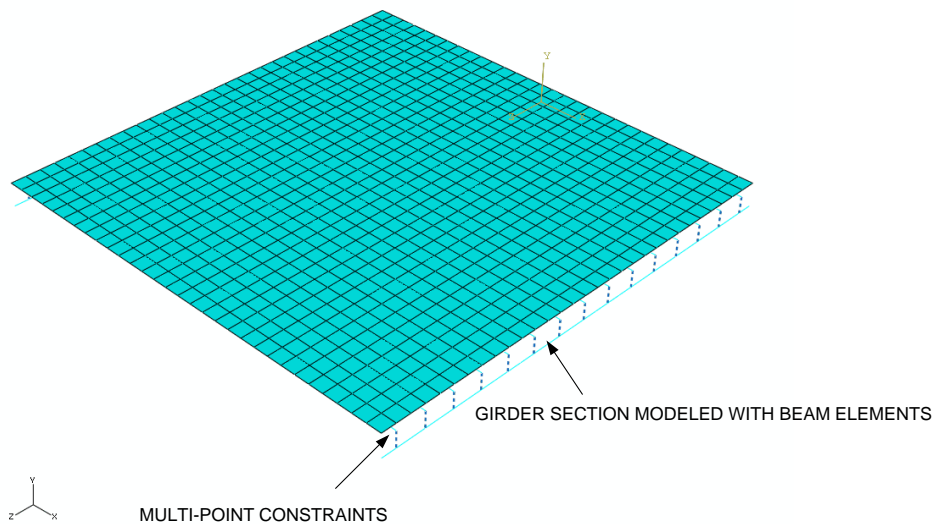


Figure 10.6: Schematic showing model of entire bay with flexible girder included

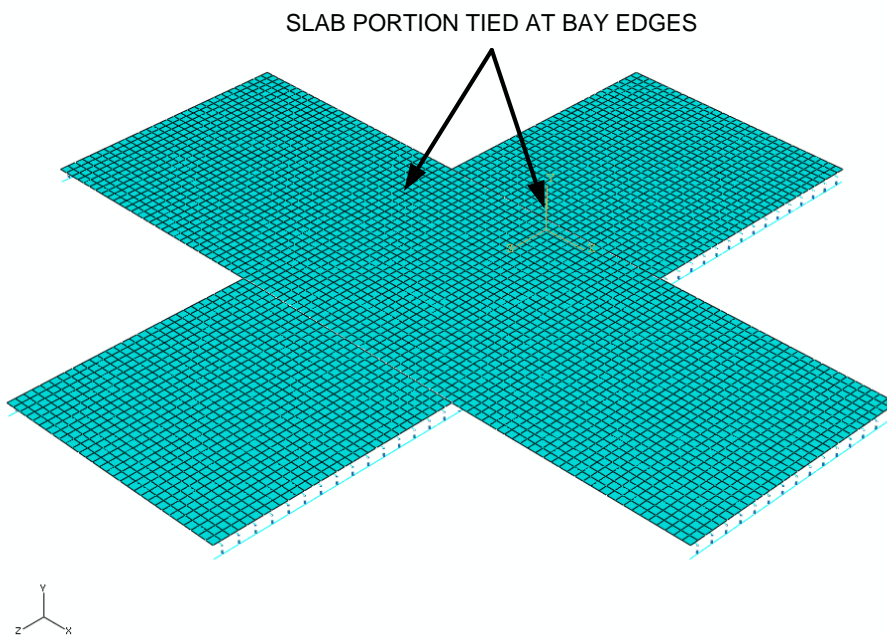


Figure 10.7: Schematic showing multiple bays modeled for vibrations

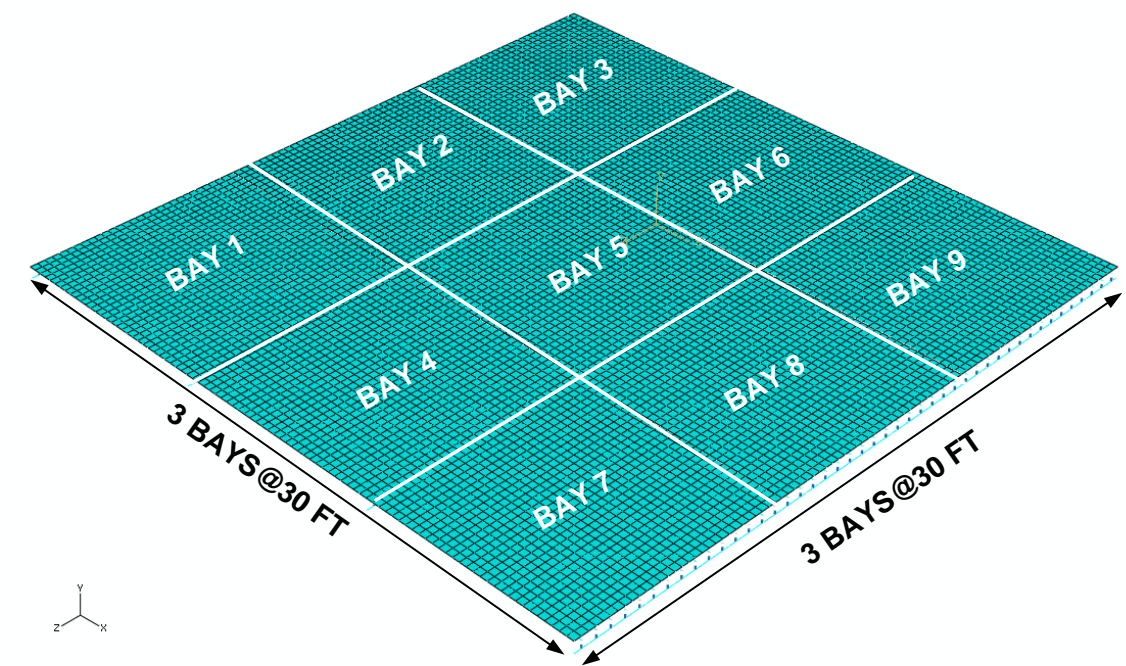


Figure 10.8: Schematic of 9 bay model

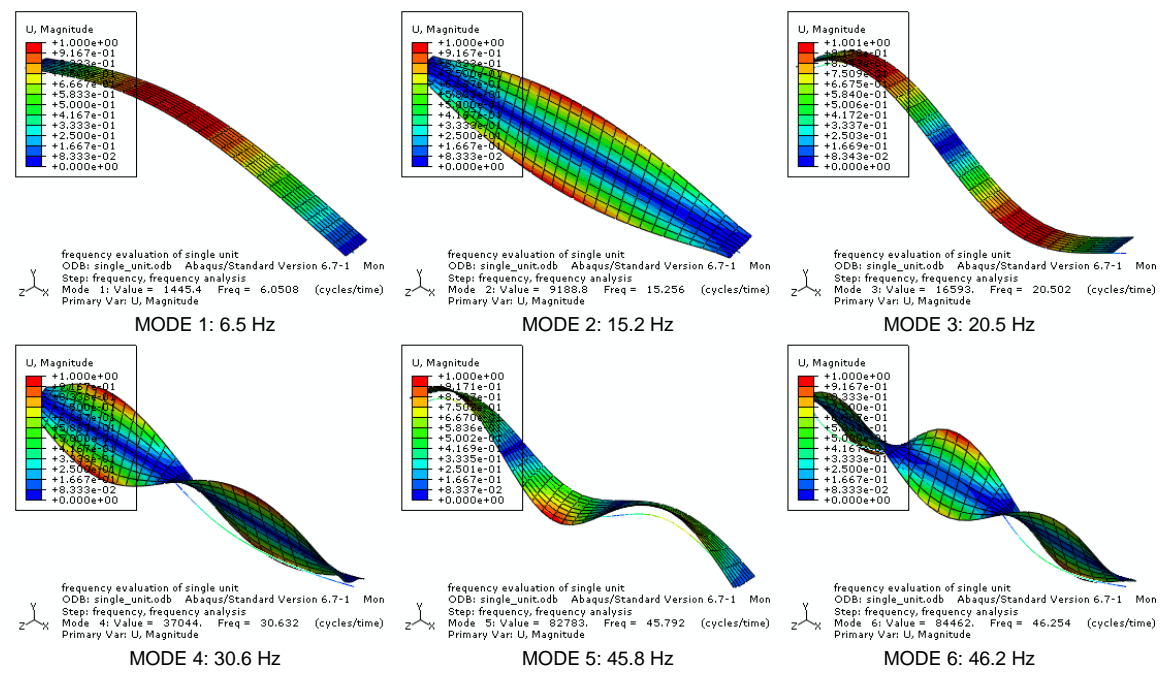


Figure 10.9: Modes 1-6 of vibration for single unit model

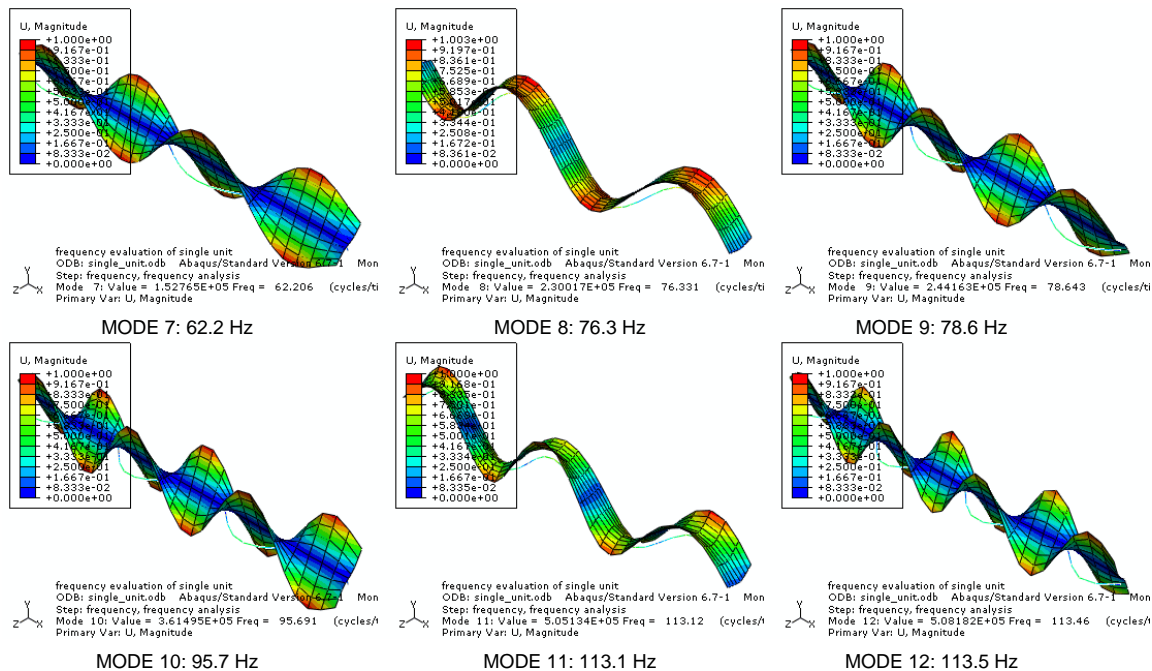


Figure 10.10: Modes 7-12 of vibration for single unit model

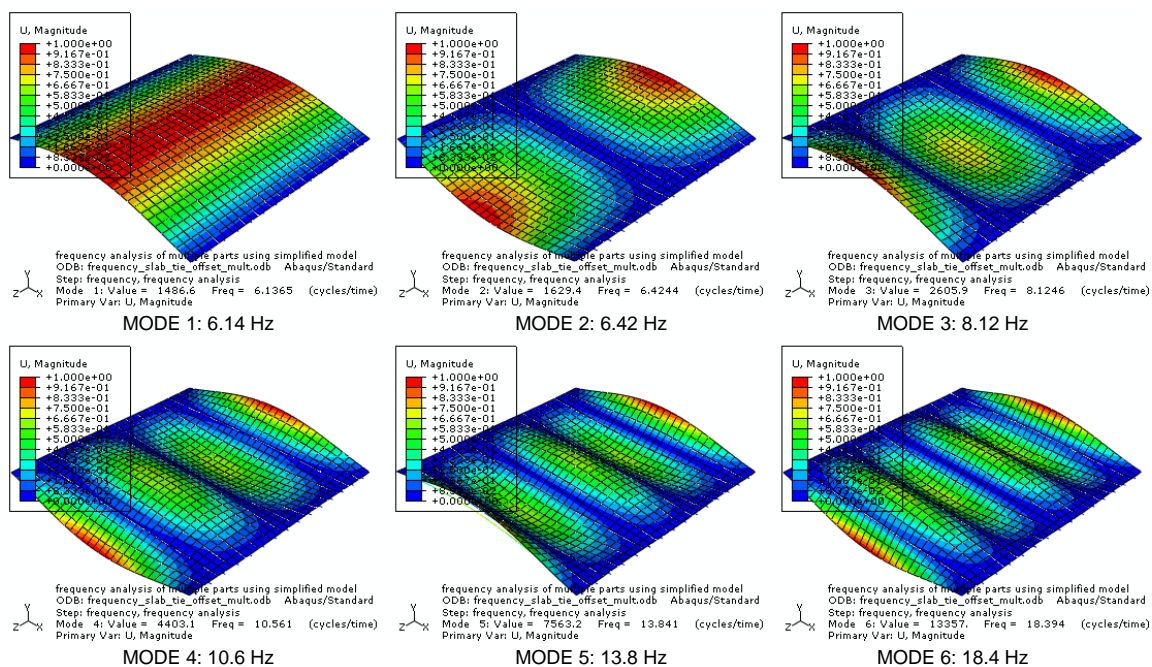


Figure 10.11: Modes 1-6 of vibration for single bay model with rigid supports

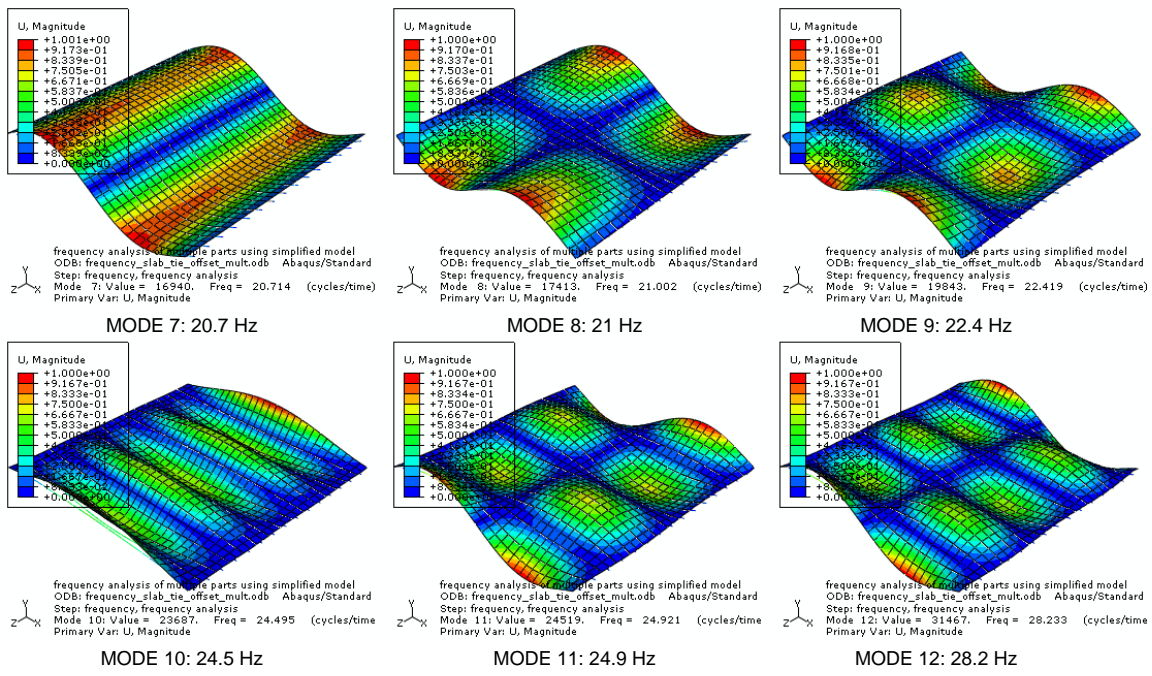


Figure 10.12: Modes 7-12 of vibration for single bay model with rigid supports

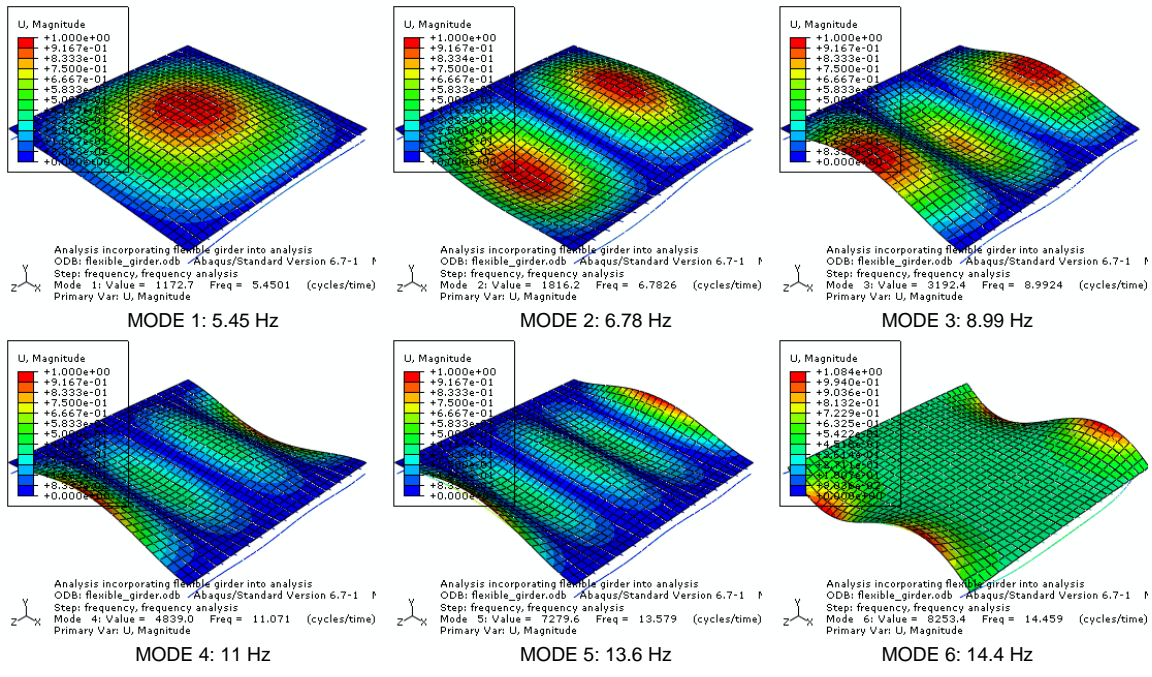


Figure 10.13: Modes 1-6 of vibration for single bay model with flexible girders

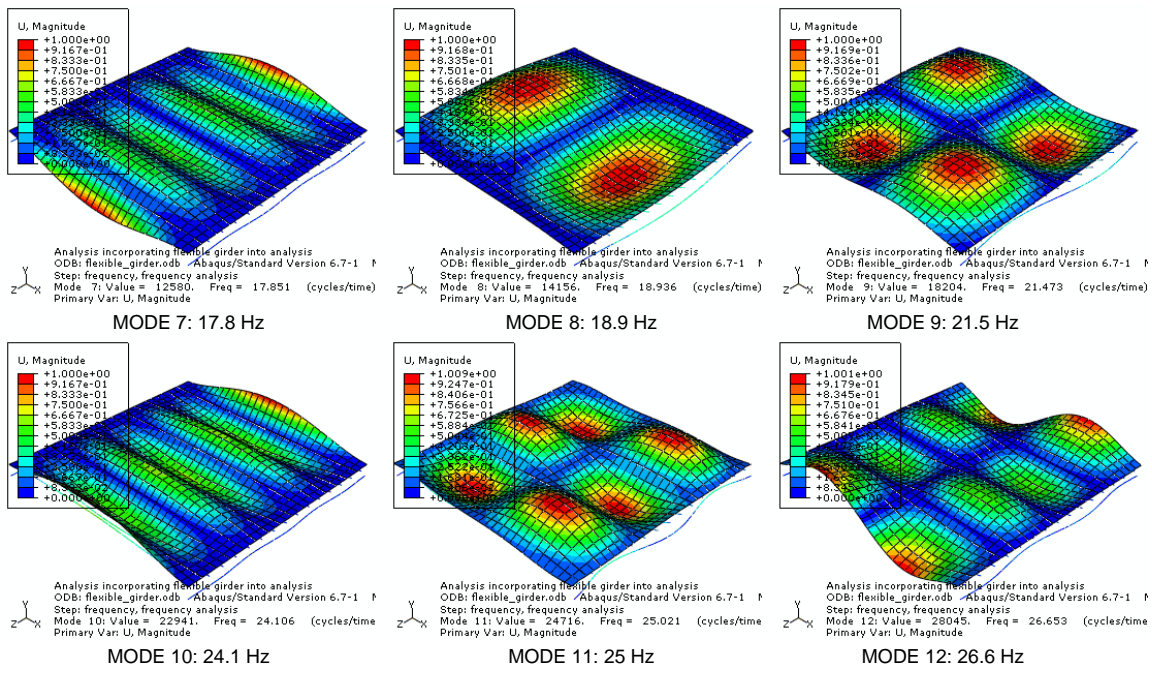


Figure 10.14: Modes 7-12 of vibration for single bay model with flexible girders

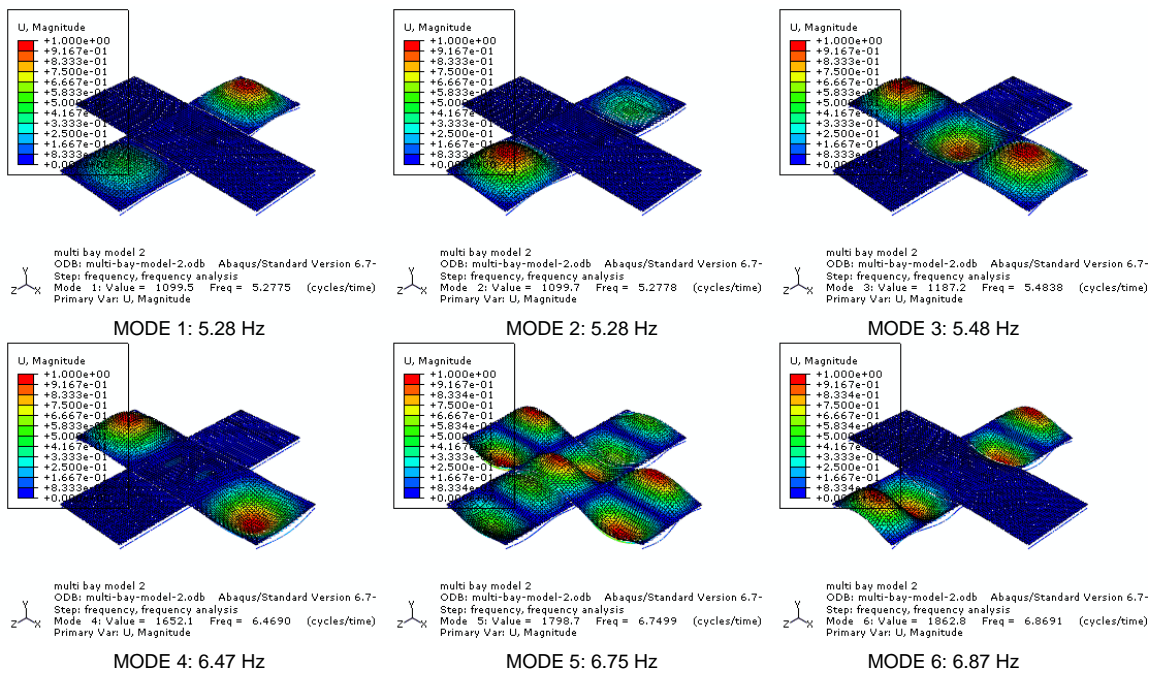


Figure 10.15: Modes 1-6 of vibration for multi-bay model

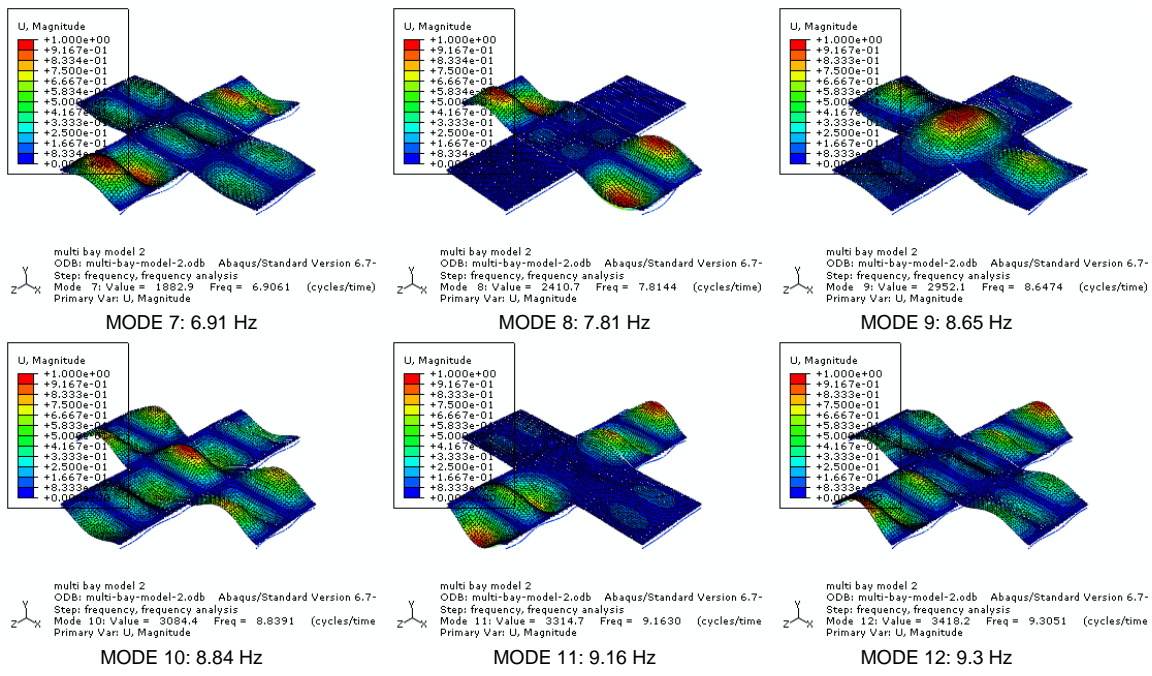


Figure 10.16: Modes 7-12 of vibration for multi-bay cruciform model

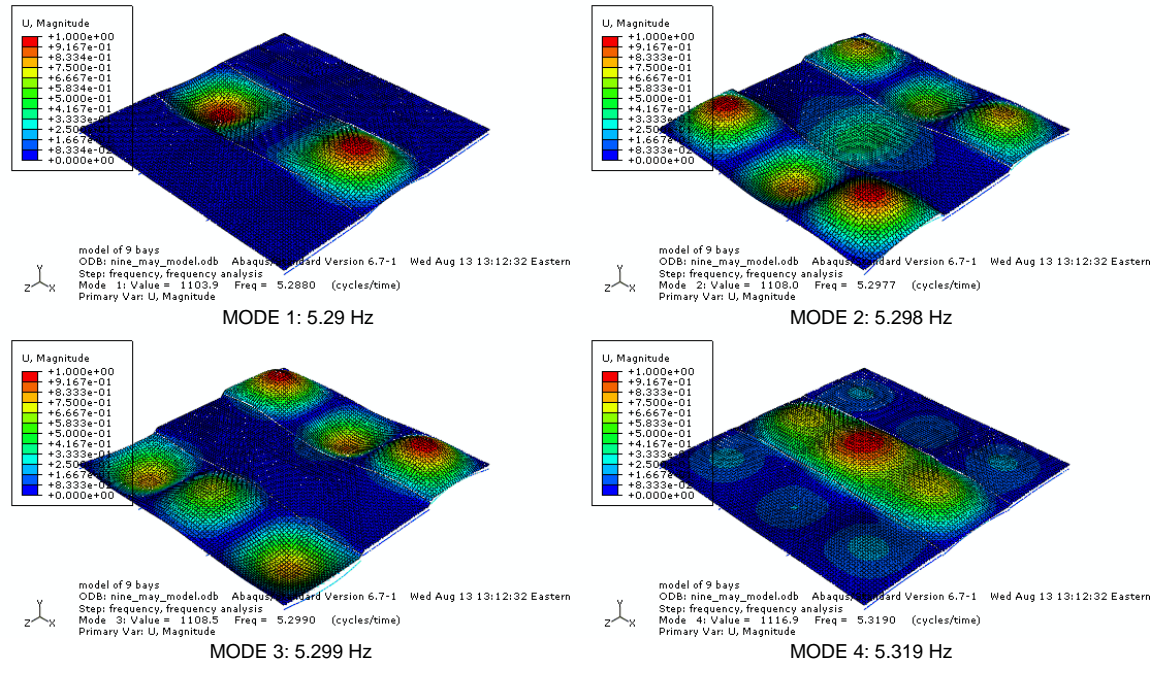


Figure 10.17: Modes 1-4 of vibration for 9 bay model

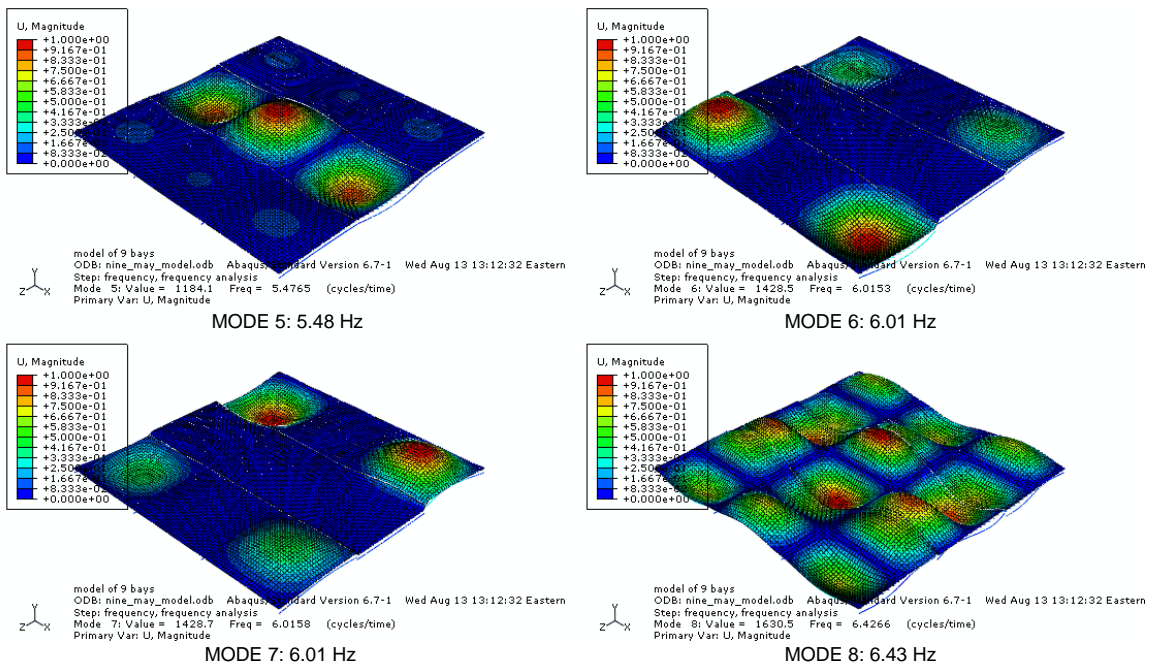


Figure 10.18: Modes 5-8 of vibration for 9 bay model

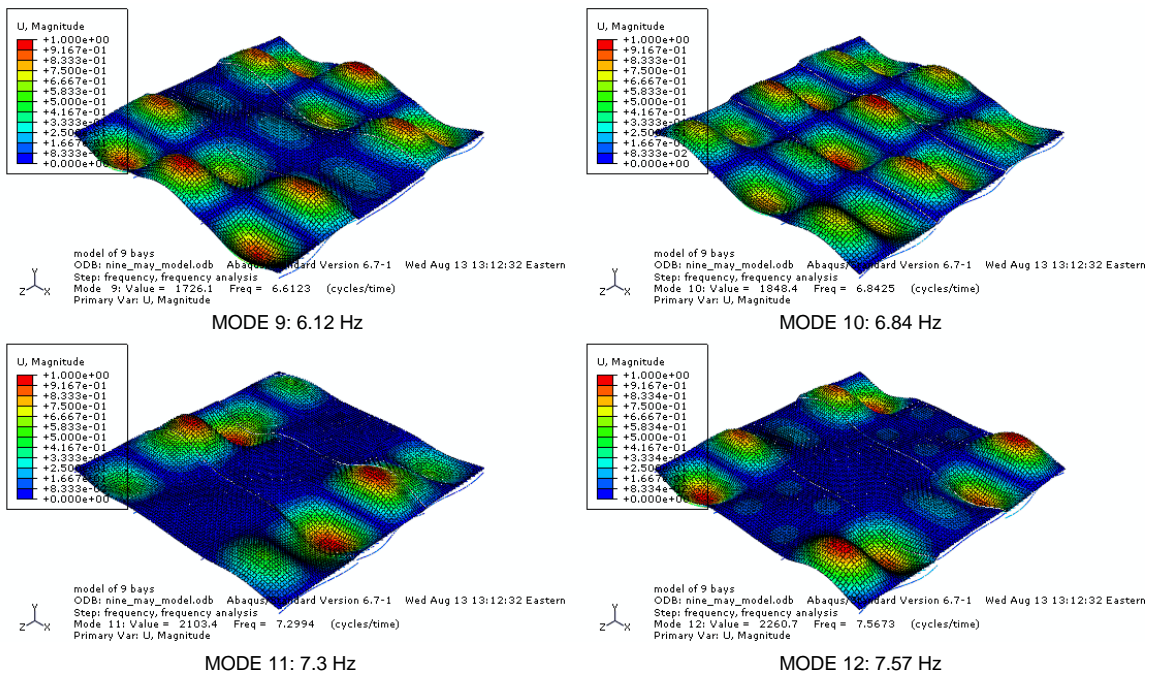


Figure 10.19: Modes 9-12 of vibration for 9 bay model

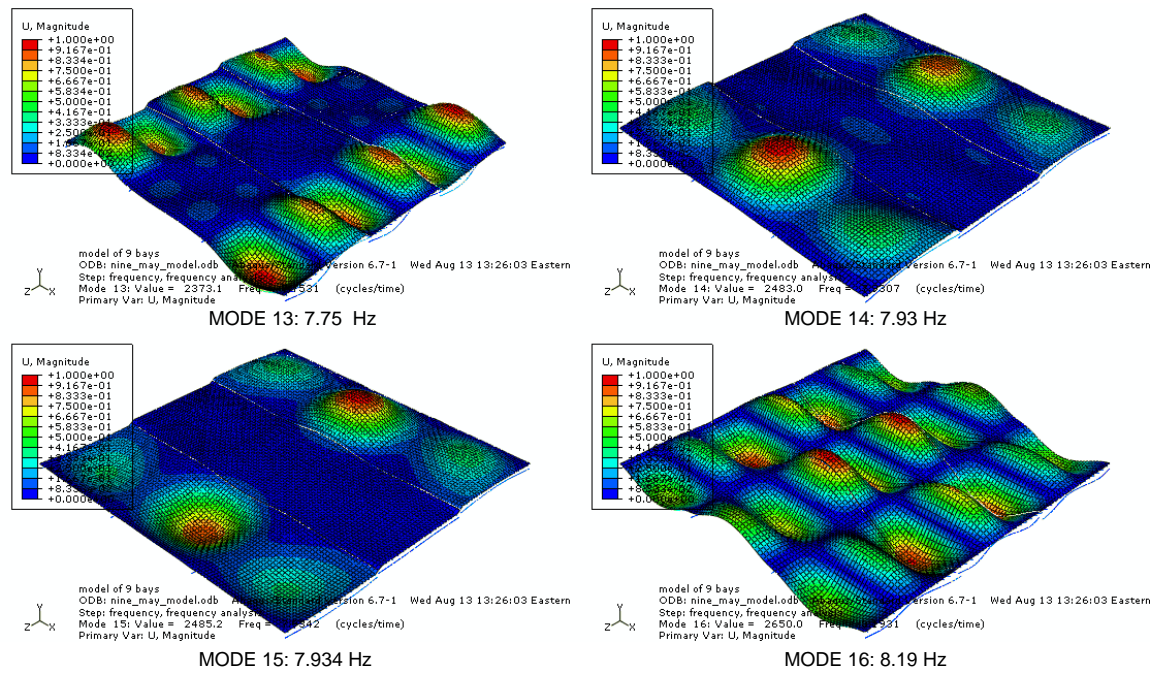


Figure 10.20: Modes 13-16 of vibration for 9 bay model

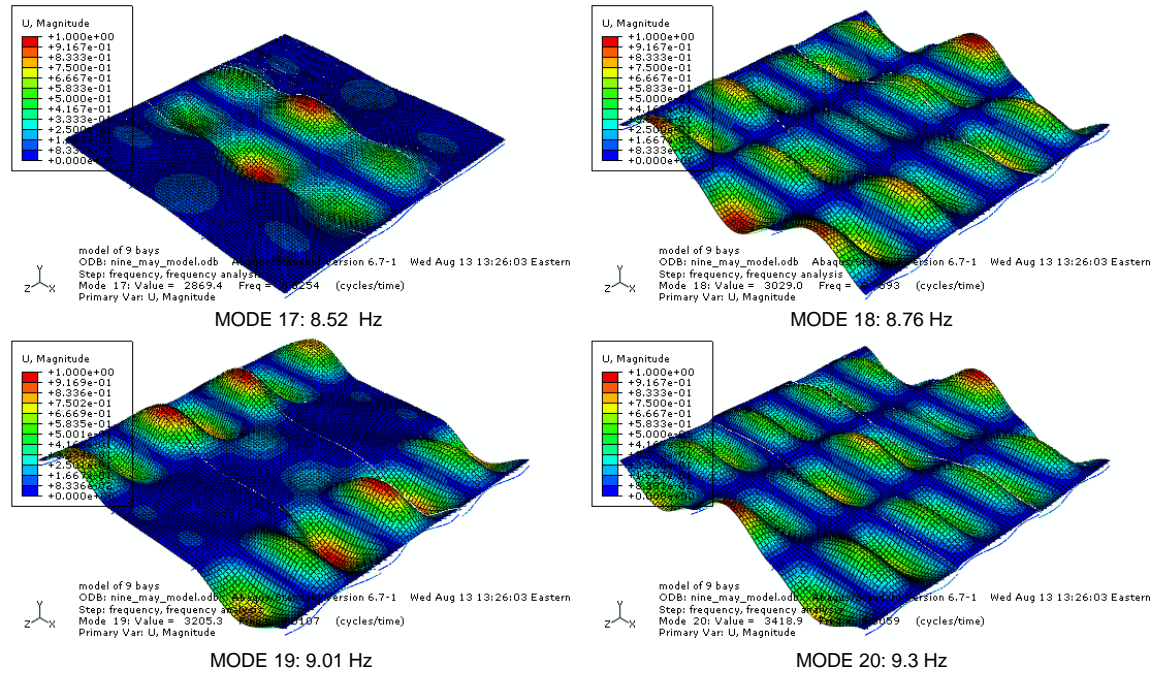


Figure 10.21: Modes 17-20 of vibration for 9 bay mode

CHAPTER 11. ANALYSIS AND DESIGN RECCOMENDATIONS FOR COMPOSITE DEEP DECK SYSTEMS

This chapter provides analysis and design guidelines for the developed deep deck systems. The guidelines are based on the experimental data collected and analytical models that were developed. Recommendations are made for evaluating overall strength, floor vibration considerations, and fire resistance.

11.1. Recommendations for Strength and Serviceability Evaluation of Composite Deep Deck Systems

This section provides details for evaluating the strength and serviceability of developed composite deep deck systems. Recommendations for analysis and design of deep deck systems are also given below. These are based on the experimental and analytical investigations performed on the deep deck systems. Discussion of the recommended analysis and design provisions is also given.

Preface to Recommendations – Shear Bond Discussion

The recommendations given below are based on the experimental and analytical work done within the current study. As mentioned previously, ASCE has standards for the structural design of composite slab system within Standard ASCE3-91(ASCE, 1992) for which SDI recommendations were based. Within these standards, evaluation of shear bond strength is given by a semi-empirical method. The method is known as the ‘m and k’ approach. For this method, the design shear-bond strength (ϕV_n) is based on equation 11.1.

$$\phi V_n = \phi \left[bd \left(\frac{m\rho d}{l_i} + k\sqrt{f'_c} \right) + \frac{\gamma W_s l_f}{2} \right] \quad (a)$$

$$\phi V_n = \phi \left[bd \left(\frac{4m\rho d}{l_i} + k\sqrt{f'_c} \right) + \frac{\gamma W_s l_f}{2} \right] \quad (b)$$

11.1

Where:

- ϕ Phi factor for shear-bond failure, equal to 0.75
- b Unit width of slab assumed to be 1 ft.
- d Effective depth of slab, distance from extreme concrete compression fiber to centroidal axis of the full cross section of the steel deck.

l'_I	Length of shear span
l_i	Length of span or shored span
m	Slope of reduced experimental shear-bond line
k	Ordinate intercept of reduced experimental shear-bond line
γ	Coefficient for proportion of dead load added upon removal of shore – more commonly known as a shoring factor. Table 11.1 shows shoring factor values.
W_s	Weight of slab
l_f	Length of span or shored span

Equation 11.1a is for simply supported spans for concentrated loading and 11.1b is for simply supported spans with uniform loading. 11.1b is based on experimental validation and mechanics principles, which showed for a uniformly loaded specimen that the shear span was observed to be 0.25 to 0.3 times the entire span length. Regression analysis showed $0.25L$ to be a better fit. The m and k terms are shown schematically within Figure 11.1. As shown in the figure, the y-axis is the ratio of the shear failure load from testing (V_e) to the width (b) times effective depth (d) times the square root of the concrete compressive strength (f'_c). The x-axis is the ratio of the reinforcement ratio (ρ), steel deck area (A_s) to effective concrete area (bd), to the shear span (l'_i) times the square root of the concrete compressive strength. The 'Region A' in the figure corresponds to specimens that are slender, large span to depth ratios, and have long shear spans, defined as longer than 36 in. 'Region B' corresponds to non-slender specimens, hence small span to depth ratios and short shear span. It is recommended that multiple specimens be tested in both the 'A' and 'B' regions to have some reasonable confidence in the resulting m and k parameters. A minimum of two specimens per region is required.

Equation 11.1 is thus observed to be semi-empirical with multiple test data points needed to use it. The predicted shear-bond capacity (ϕV_n) is dependent on the steel deck parameters ρ and d , the square root of the concrete compressive strength – which is an indirect measure of the concrete tensile strength of concrete, and the portion of the slab weight imposed on the composite specimen – represented by the γ factor. The equation attempts to provide a straight-forward evaluation of the shear bond capacity based on experimental testing. Multiple tests are required for each parameter of interest when using this approach. The approach is only valid when a shear-bond failure is forced to occur in the specimen.

The current project did not attempt to find the relevant m and k parameters needed for the shear-bond strength evaluation. There were several reasons for this, primarily the following.

- 1) The CC-DD specimens tested with shear studs were not observed to have shear bond failures. Their failure modes were dominated primarily by flexure. To force a shear bond failure in these specimens multiple specimens would be needed with small enough shear spans to force the failure. That was beyond the scope of this project.

- 2) The above ‘m and k’ method is calibrated to conventional metal deck concrete slab systems. It is likely that factors in the equations may change based on the new types of deck profiles and spans being investigated.
- 3) The design equations presented in this chapter are based on reducing the overall flexural capacity of the specimen. Those types of systems with brittle shear-bond failure were given more stringent reduction factors.

11.1.1. Composite Strength of Long Span Composite Deep Deck Systems

The following recommendations are made for composite deep deck sections that satisfy the following criteria:

- 1) Shear studs are placed at the ends such that at least one stud is placed per each unit width of the specimen.
- 2) Span lengths between 20 and 30 ft
- 3) The ratio of span length to section depth is 24 to 36 in the composite phase
- 4) Deck profiles are not embossed
- 5) Construction level deflections are limited to $L/200$
- 6) For cellular deck profiles, the interfacial shear stress found based on testing and using Equation 9.3 must be at least 80% of the maximum possible interface shear stress that could develop for a full composite section (80% composite action). For non-cellular profiles, the interfacial shear stress found based on testing and using Equation 9.3 must be at least 90% of the maximum possible interface shear stress that could develop for a full composite section (90% composite action).
- 7) The system analyzed is either uniformly loaded or point loaded with the shear span being no less than 0.3 times the length of the system.
- 8) The ratio of the steel deck area to the unit width times the effective depth (ρ) is less than the balanced reinforcement ratio (ρ_b) given in Equation 11.2.

$$\rho_b = \frac{0.85\beta_1 f'_c}{f_y} \left[\frac{\epsilon_c E_s (h - d_d)}{(\epsilon_c E_s + f_y) d} \right] \quad 11.2$$

Where:

β_1	0.85 for concrete with compressive strength 4000 psi and below. Reduced at a rate of 0.05 for each 1000 psi above 4000 psi, but greater than 0.65.
ϵ_c	Limiting concrete crushing strain – assumed to be 0.003 in./in.
h	Overall floor system depth
d_d	Depth of steel deck

If the above requirements are met the composite strength of the system can be evaluated with equation 11.3.

$$\phi M_{n1} = RF_1 \times \phi_f \times (M_{nSDI} - M_{shore}) \quad 11.3$$

Where:

ϕM_{n1}	Flexural moment capacity of composite CC-DD section
RF_1	Reduction factor to account for effects from construction and partial composite action. This value can be assumed equal to 0.8.
ϕ_f	Phi factor recommended for composite steel-concrete members with flexure dominated failures. Assumed to be 0.85.
M_{nSDI}	The capacity of the section as found per SDI recommendations.
M_{shore}	Additional maximum moment induced in composite system when shoring is used.

When all requirements except number 6 are met, then equation 11.4 can be used.

$$\phi M_{n2} = RF_1 \times \phi_{sb} \times (M_{nSDI} - M_{shore}) \quad 11.4$$

Where:

ϕ_{sb}	Phi factor recommended for composite steel-concrete members with shear bond type failures. Assumed to be 0.75.
-------------	--

Equations 11.3 and 11.4 are based on test observations and the analytical models developed. The reduction factor accounts for effects from construction loading and partial composite action resulting from interfacial slip. A value was chosen to ensure conservative strength estimations would be made. The M_{shore} term is used to include the effects of shoring. Table 11.2 shows the predicted strength of the shear studed specimens using Equations 11.3 and 11.4 and the partial composite models (described in Chapter 9) that accounted for construction effects. As shown, the design equation is conservative for all cases. The reduction factor is likely overly conservative, but for the limited amount of specimens tested it is believed appropriate.

The requirements given for using the above equations included a minimum shear bond stress that must be transferred between the deck and concrete interface. The specified minimum is based on experimental observation. All CC-DD specimens that met this minimum were able to develop failure modes that were primarily flexural in nature with good ductility. The SC-DD specimen was observed to have a shear bond failure, with reasonable ductility due to shear studs being present. This specimen did not meet the minimum interfacial shear stress requirement. Hence, equation 11.4 was used to evaluate the system. This equation is accounting for the shear-bond failure by using the more stringent phi factor.

Alternatively to using the above equation, a full section analysis can be done using strain compatibility and assuming full composite action. However, the final moment capacity found should be reduced by the phi factor and the reduction factor. Furthermore, if the yield stress of the section is reduced using the simplified method described in Section 9.1.2 the reduction factor can be changed accordingly based on that analysis. Shoring effects should also be properly accounted for in the analysis (if needed). The proposed partial interaction model can also be used in evaluating composite strength if test data is

available to input the maximum shear stress. It is recommended that construction effects are included when using the model.

All profiles that were tested had no embossments on the steel decks. Embossments are the most common way to provide additional shear bond capacity to deck profiles. If a deep deck profile was provided with embossments (or other means of enhancing the interfacial bond) the structural behavior would change. If end shear studs were used in conjunction with embossments equation 11.3 or 11.4 would still be valid, but would likely be too conservative. The more likely case would be the use of an embossed deck without end shear studs. The capacity and behavior of this deck would need to be validated experimentally.

Strength of Composite Deep Deck Systems without End Shear Studs

The above design equation was calibrated to those specimens that had shear studs placed at the ends. The end shear studs were observed to prevent a shear bond failure from occurring for cellular profiles and provide additional ductility for non-cellular specimens that had a shear-bond type failure. However, in the lab experiments the non-studded specimen was observed to have a brittle shear bond failure. The failure was sudden and brittle, which is not a desirable failure mode. The reduction in overall strength was approximately 20% as compared to the similar specimens that had shear studs placed at the ends. Based on these observations, the following recommendations are made when the given composite deep deck section satisfies the following criteria:

- 1) Un-shored span length between 20 and 30 ft
- 2) The ratio of span to depth is between 24 to 36
- 3) Deck is not embossed
- 4) Construction level deflections are limited to $L/200$
- 5) For cellular deck profiles, the interfacial shear stress found based on testing and using Equation 9.3 must be at least 60% of the maximum possible interface shear stress that could develop for a full composite section.
- 6) The ratio of the steel deck area to the unit width times the effective depth is less than the balanced reinforcement ratio given in Equation 11.2.
- 7) The system analyzed is either uniformly loaded or point loaded with the shear span being no less than 0.3 times the length of the system.

If the above requirements are met the composite strength of the system can be evaluated with equation 11.5.

$$\phi M_{n3} = RF_2 \times \phi_{sb} \times M_{nSDI} \quad 11.5$$

Where:

ϕM_n	Flexural moment capacity of composite section
RF_2	Reduction factor to account for effects from construction loads and partial composite action. In lieu of a more advanced analysis, can be assumed to be 0.65.

ϕ	Phi factor recommended for composite steel-concrete members with brittle shear bond failure. Taken as 0.75
M_{nSDI}	The capacity of the full composite section as found per SDI recommendations.

Equation 11.5 is quite similar to 11.3, with changes to the reduction and phi factors. These reduced values are accounting for the brittle type shear bond failure expected for these types of systems. Alternatively, a full section analysis can be done using strain compatibility and assuming full composite action. However, the final moment capacity found should be reduced by the phi factor and the 0.65 reduction factor. The equation predicts a capacity for CC-DD specimen 3 of 13.7 kips, which is quite conservative with a 23% under-prediction. However, the brittle failure mode is not desirable so conservative strength predictors are needed.

Requirement number five in using the equation is based on observation from CC-DD Specimen 4 (without end shear studs). The predicted shear stress at first slip for this specimen was 15 psi, which correlates to approximately 60% of the needed interfacial shear to achieve full composite behavior. In lieu of more test data and the brittle failure observed, it was decided to have this limitation in using the equation.

The proposed partial interaction model (presented in Chapter 9) is not as straightforward to apply in the case where a shear bond failure occurs. First slip was observed near 15 psi of interfacial stress, which can be used as input for the model (for the given profile). However, the shear bond failure mode experienced cannot directly be captured within the model. Further calibration of the fiber model to capture brittle shear bond failures is needed.

Discussion of Strength Prediction Equations

Three different strength prediction equations were presented for long span deep deck systems. The equations were separated into those systems with end shear studs that had flexural failures and those with shear bond failures with reasonable ductility, and those without end shear studs that had brittle shear-bond failures (no embossments were assumed). The systems with shear studs have less stringent strength reduction factors than those without. This is because non-studded specimens were observed to have both lower strength and ductility compared to similar specimens with shear studs. The equations are based on limited testing so further testing is recommended to further develop the equations.

11.1.2. Recommendations for serviceability criteria

Deflections

The recommendations for structural serviceability criteria, i.e. deflections, are the same as prescribed by the ASCE 3-91 standard (ASCE, 1992) and SDI recommendations (Steel Deck Institute, 2002). For the non-composite phase those recommendations presented previously in Section 4.2.1 and 6.2.1 are valid. For immediate deflections due

to live loading, the average moment of inertia from of a cracked and un-cracked section is recommended. For long term deflections, i.e. creep, recommendations from ASCE 3-91 can be used. The standard recommends that the additional deflection by creep should be calculated by multiplying the immediate deflection due to sustained load by the factor (λ) given in equation 11.6.

$$\lambda = \left[2 - 1.2 \left(\frac{A'_s}{A''_s} \right) \right] \geq 0.6 \quad 11.6$$

Where:

A'_s Area of that portion of steel deck that is in compression
 A''_s Area of that portion of steel deck which is in tension

Floor Vibrations

The recommendations for floor vibration evaluation for composite deep deck systems were given previously in Chapter 10. Evaluating deep deck systems for floor vibrations can be done using existing guidelines with slight modifications. If AISC Design Guide 11 (AISC, 2003) is used, the natural frequency of the floor system alone should be estimated assuming fixed-fixed boundary conditions. All other assumptions from the design guide can be applied. The provisions given in SCI Publication 331 (SCI, 2004) can be used directly. When using deep deck systems it is recommended that the first natural frequency of the floor system alone (i.e. without considering girders) should stay above 5 Hz as calculated by Equation 2.1 for those systems with 30 ft spans. This is valid for systems that have a self-weight of at least 50 psf.

11.1.3. Fire Resistance and Behavior

Elevated temperature behavior of CC-DD Specimens was investigated experimentally in the current study. Heat transfer testing and combined heating and loading tests were conducted as described in Chapter 5. The testing showed that the bottom cellular plate acted as a sacrificial layer when a system is subjected to heating from the underside. The depth of concrete helped in delaying the temperature rise through the depths of the system. When exposed to both heating and mechanical loading, a 20 ft long unprotected CC-DD system was able to sustain applied loading without an observable major failure. A subsequent loading test showed the specimen still retained around 70% of its original capacity. Hence, the CC-DD specimens showed good overall elevated temperature resistance. However, if the systems were to be used the fire ratings that were given in

Table 4.5 should still be used as a guideline until further testing could be done to validate performance based design requirements. Also, no elevated temperature testing was done on non-cellular profiles. This is recommended as future work.

Table 11.1: Shoring factors (ASCE, 1992)

Support During Concrete Placement	γ
Complete support over length	1.0
Un-shored	0
Shored at center	0.625
Shored at third points	0.733

Table 11.2: Predicted and actual capacities

Specimen	Fiber Model – Partial composite model (kips)	Proposed Equations (kips)	Actual Strength (kips)
CC-DD-1	25	19.5	24.4
CC-DD-2	25	19.5	23
CC-DD-4	14	11.8	15
SC-DD	9.4	9.1	11.4

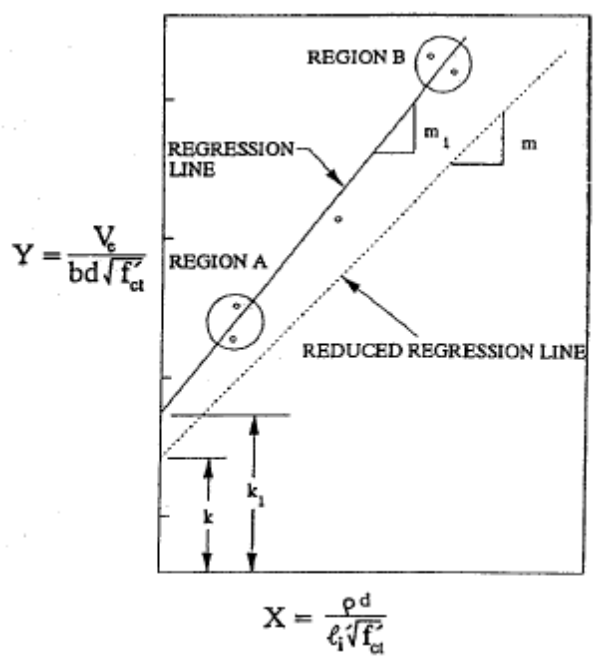


Figure 11.1: Typical shear-bond plot showing reduced regression line for m and k (ASCE, 1992)

CHAPTER 12. SUMMARY, CONCLUSIONS, AND FUTURE WORK

The current study consisted of the conceptual development, design, testing, and validation of innovative long span floor systems for multi-story steel construction. This was done systematically by first reviewing existing floor systems and research. Their salient features were identified along with advantages associated with them. Key issues related to existing floor systems were also identified. Several new types of long-span floor systems were initially developed based on the literature review and input from an oversight committee. Three types of floor systems were chosen for further development, which included large scale testing. These three types of systems were chosen based on their technological, economic, and feasibility merit. The following sub-sections summarize the research and relevant conclusions from the chapters of the dissertation.

12.1. Background and Literature Review

- 1) Performance objectives for long span floor systems were specified. These included the ability to: (i) achieve long spans of up to 30 ft. unsupported, (ii) achieve minimum floor-to-floor height requirements, (iii) utilize un-shored construction (preferred) or provide minimal shoring, (iv) achieve strength and serviceability criteria during the construction phase, (v) achieve strength and serviceability criteria during the service phase of the structure, (vi) achieve adequate performance with respect to floor vibrations, (vii) achieve adequate fire resistance, (viii) use relatively simple connection systems, (ix) provide cost-effective fabrication and erection, and (x) provide adequate diaphragm action for transferring lateral loads.
- 2) Several existing alternative floor systems were presented including the Stub Girder, *Slimdek*, and *Girder-Slab* floor systems. Previous research on long-span floor systems was also presented including the work on 20 ft long composite deep deck systems (Widjaja, 1997) and the Deck-on-Deck System (Hillman, 1990). A review of sandwich type structural systems was also described. The deep deck systems showed merit as long span floor systems.
- 3) A review of the state-of-the-art for floor vibration evaluation due to human induced motion was also given. It highlighted relevant AISC and SCI guidelines currently used in the United States and UK. Background to the guidelines was also provided. A review of the state-of-the-art for fire resistance on composite floor systems was also given. The review highlighted the differences between prescriptive and performance based design methodologies.

12.2. Overview of Developed Floor Systems

- 1) Two different designs of the sandwich type composite floor systems were presented. (1) The Double Skin Composite (DSC) system and (2) the profiled DSC System. The DSC System consisted of ¼ in. thick top and bottom steel plates with six in. of concrete sandwich between. The plates were bonded to the concrete with shear studs welded to the inside surfaces of the top and bottom plates. The Profiled DSC system used 2 in. deep cellular deck profiles top and bottom in lieu of the top and bottom plates. The shear transfer between the deck and concrete was assumed to be provided by the deck embossments. The systems were designed for 30 ft spans. Both of these systems were deemed un-economical in current steel construction and were not further developed.
- 2) Four different types of Advanced Metal Deck (AMD) Systems were presented for the intended spans of 30 ft. These were the: (1) Composite Cellular Deep Deck (CC-DD), (2) Shored Composite Deep Deck (SC-DD), (3) Sandwich Metal Deck (SMD), and (4) Reduced Weight Deep Deck (RW-DD) Systems.
- 3) The CC-DD system consisted of 7.5 in. deep cellular deep deck with a 2.5 in. lightweight concrete on top. Two different deck profiles were used. One deck profile had a 14 gage deck thickness and 16 gage bottom plate. The other had an 18 gage deck with 20 gage bottom plate, this option was more optimized with respect to material usage. The SC-DD system was a non-cellular 7.5 in. deep deck with 3.5 in. of concrete on top. A line of shoring was added at mid-span in the construction phase, which allowed for less steel material to be used.
- 4) The sandwich metal deck system utilized a cellular deck profile with a thin steel plate attached to the top of the deck profile also. A lightweight concrete topping was then placed atop the top plate. This system was deemed economically unfeasible and led to the development of the alternative RW-DD system.
- 5) The RW-DD system consisted of an inverted 7.5 in. deep deck profile with lower flutes of the deck filled with mineral wool material (instead of concrete) to reduce self-weight of the system. A 2.5 in. lightweight concrete slab was placed on top of the deck to complete the composite system.
- 6) The final proposed long span floor system presented was the Pre-Loaded Self Shored (PLSS) system. The PLSS system used existing composite steel deck profiles and reduced the depth of the intermediate steel floor beams. This was accomplished by applying a pre-load to the mid-span of the floor beam in the construction phase. The system used to apply the pre-load was self-supported by the steel beam. Hence, no shoring upon floors beneath was needed. The pre-loading can be removed upon adequate concrete curing, 7-14 days after casting.
- 7) The proposed systems were rated and evaluated by the researchers and oversight committee. The top four systems were chosen for further development. These were the CC-DD, SC-DD, RW-DD, and PLSS systems.

12.3. Composite Cellular Deep Deck Systems Experimental Validation

An experimental program was implemented to investigate the behavior of the developed CC-DD systems. The experiments included looking at structural behavior in

both the construction and composite phases for the systems. Modal impact testing was also done on the systems to determine natural frequencies and other dynamic properties. The testing matrix for the structural and modal impact testing was presented previously in Chapter 4 within

Table 4.8. The other aspects investigated experimentally were heat transfer behavior of the CC-DD systems and a combined heating and loading test of a CC-DD system. Details of these experiments were presented in Chapter 5. The experimental investigations indicated that:

- 1) Measured deflections and strains during the construction loading test and the concrete casting operation were within acceptable limits for all specimens. The cellular deep deck systems proved efficient in resisting the imposed construction (non-composite) loads for 30 ft spans. The optimized system, CC-DD specimen 4, had construction level deflections on the order of $L/200$. This was the most optimized design for construction and it used the least amount of steel material compared to the other specimens.
- 2) CC-DD specimen 3 exhibited slightly less deflection than specimens 1 and 2 during the concrete casting operation. The only difference between the specimens was the end support conditions. Specimen 3 was attached to the support beam only with puddle welds. The welds likely provided slightly more restraint to the end connection. Hence, if there is a desire to reduce construction level deflections then puddle welds in conjunction with shear studs are recommended.
- 3) The residual strains after concrete casting were measured and reported at least 24 hours after the initial concrete pour. The concrete heat of hydration caused thermal strains in the first few hours (12-24 hours) after casting. These thermal strains decreased as the concrete hardened and set, and the strains reduced to the residual value.
- 4) The measured natural frequencies were close to those calculated using a simple SDOF model for all specimens. Some likely non-linear behavior was observed in higher frequencies as indicated by some double peaks in the FRFs. However, these modes did not contribute significantly to the dynamic response of the specimens.
- 5) The first mode of vibration and natural frequency was much lower than higher modes for all specimens, and seemed to be the dominant mode for heel drop and modal impact excitation. Also, there was significant spacing between modes and the first mode was dominant. Hence, the floor vibration behavior of the CC-DD systems can likely be evaluated using guidelines similar to those published by the AISC and SCI.
- 6) Damping was estimated between 0.7 and 0.9% for the CC-DD Specimens at the first fundamental frequency. This is comparable to estimates made of existing composite flooring systems. The actual damping present in a structure would also be heavily dependent on the presence of non-structural elements, floor bay layouts, and occupancy.
- 7) A reduction in acceleration response and a decrease in damping were observed when additional mass was added to CC-DD Specimen 3. The frequency shift

occurred because the kinetic energy needed to bring the system to equilibrium increased. Furthermore, if we consider Equation 2.4 for evaluating the floor system, then if both the response and frequency of the system are reducing, then the amount of damping needed would also reduce.

- 8) The presence of shear studs at the support provided additional capacity and ductility to the CC-DD specimens. This was evident from comparing the results of Specimens 1, 2 and 4 to Specimen 3. The capacity of the non-studded Specimen 3 was around 20% less than the studded options (1, 2, and 4) and it experienced a brittle shear-bond failure. This type of failure is undesirable as it appears suddenly and with little warning. The failure occurred at 18 kips (360 psf), which is well above design loads and hence the specimen still had much reserve capacity. To avoid this failure mode either shear studs at the end should be used, or some other means to prevent the onset of slip that would cause the brittle failure mode.
- 9) All specimens with shear studs experienced cracks that opened over one of their support points. This crack formed probably due to the concrete bearing against the shear stud. As forces increased the interfacial shear demand increased. This increased the longitudinal forces induced on the shear studs. The force of the stud bearing on the concrete caused the concrete to split locally in the area of the stud. This crack could be prevented by providing some hoop type reinforcement around the shear studs. Preventing or delaying this crack would likely enhance capacity and overall behavior of the systems.
- 10) Strain observations indicated mostly linear behavior through the profile depths until higher load levels for shear studded specimens. Linearity in the strains dropped near ultimate loads and high levels of mid-span displacement. The drop in linearity indicates partial composite behavior of the specimen. The drop in linearity was more pronounced in the shear span region of the specimens, as was expected. The non-studded Specimen also experienced mostly linear strains up to near ultimate loads. However, the specimen experienced a sudden and brittle shear bond failure.
- 11) All specimens were observed to have reserve capacity for factored ultimate loads. CC-DD Specimen 1 and 2 were quite overdesigned while Specimen 4 had a more efficient design (for both the construction and composite level phases). Hence, the most efficient design would use the CC-DD Specimen 4 profile for the 30 ft span. Furthermore, using puddle welds and shear studs at the ends and providing some hoop reinforcement around the studs would likely yield the most desirable construction and composite level behavior.
- 12) Heat transfer CC-DD specimens with and without fire protection performed well under thermal loading. The behavior of the specimen with fire protection was excellent even after 3 hours of heating. The 1 in. thick AAC tiles are recommended for fire protection of CC-DD and comparable systems, particularly for the deep deck systems without a bottom plate. The behavior of the specimen without fire protection was also quite good after two hours of heating. The concrete slab temperature on top (unheated side) was less than 80°C after two hours of heating, which meets the thermal limits required by the ASTM E119

Standard test. Some minor cracking of concrete and moisture migration and evaporation from the cracks was observed. But, the temperatures were quite low (less than 80°C) compared to the E119 limit of 250°C for unrestrained ratings.

- 13) A combined heating and loading test was performed on a 20 ft CC-DD Specimen. The specimen was a 7.5 in. deep cellular deck profile with a 18 gage thick deck and 20 gage bottom plate. It had 2.5 in. of lightweight concrete on top.
- 14) For the combined heating and load test, a maximum mid-span displacement of 1 in. (downward) occurred from heating of the specimen. This displacement was a result of the thermal gradient in the specimen and end restraint present. After cooling, mid-span displacements equal to -0.35 in. (upward) were observed.
- 15) The combined heating and load specimen was able to resist the applied heating and load without experiencing failure criteria defined by ASTM E119 (ASTM, 2000).
- 16) A load test was conducted on the Specimen after heating and loading. It showed that the specimen retained 70% of its undamaged capacity. The reduction in capacity is a result of the bottom plate becoming a ‘sacrificial’ fire protection layer. The bottom plate properties were changed from the extreme temperatures, but it helped shield other material in the cross-section from damage. This inherent fire resistance is an advantage to using cellular deep deck systems.

12.4. Shored Composite Deep Deck (SC-DD) System Experimental Validation

Similar experimental investigations as for the CC-DD systems were also done for a shored deep deck system. The details of the testing are presented in Chapter 6. Testing for structural behavior and modal impact testing were done on the shored specimen. No elevated temperature was performed. The experimental investigation indicated that:

- 1) The use of shoring helped in limiting the construction strains induced on the section from the wet concrete weight.
- 2) The magnitude of strains induced on the composite cross-section are dominated from the shore removal process. These strains can be reduced further by using more than one line of shoring or more concrete depth.
- 3) The SC-DD system satisfied the key assumptions made by AISC and SCI in using their guidelines for floor vibration evaluation.
- 4) The specimen exhibited a shear bond failure with reasonable ductility beyond the occurrence of the separation between the deck and concrete. The shear studs helped in enhancing the ductility of the specimen.
- 5) The north end of the specimen had a reduced stiffness throughout the duration of the test. Cracking was exhibited at low load levels for this end of the specimen. This is because the shore removal process ‘locked in’ stresses into the composite specimen – including the concrete.
- 6) As the specimen was being loaded in displacement control, a sizable horizontal crack began forming in the concrete at the north end support. This crack began forming just prior to the shear bond failure and continued opening as the displacements increased. This crack was different in appearance than those that

occurred in the CC-DD specimens but had a similar effect of weakening the overall structure. The final capacity of the structure was approximately 11 kips (220 psf) and the mode of failure was shear bond, but with reasonable overall ductility due to the presence of end shear studs.

- 7) The line of shoring reduced the construction load effects (deflections, strains, and stresses) on the long span system. However, the shore removal locked in strains and stresses in the composite deck system. The concrete slab had built-in tensile stresses that resulted in cracking at relatively low load levels. This can be reduced by adding more lines of shoring or increasing the overall depth of concrete. Adding shoring or increasing concrete depth will affect the overall economy of the system. These are issues that need consideration for optimizing the design of the system.
- 8) Non-linearity in strain profiles occurred as the loads were increased, and the slope of the strain diagram in the steel deck section became different from the slope of the strain diagram in the concrete slab. This indicates the occurrence of slip and partial composite action between the steel deck and the concrete slab.
- 9) Strain profiles figures also showed a change in the slope of the strains within the steel deck especially at higher load levels. The likely reason for this is the occurrence of web distortion within the deck. The web distortion occurred in this specimen because there was no cellular plate attached to the bottom of the deck, which helps in limiting web distortion.

12.5. Pre-Loaded Self-Shored (PLSS) System

Analysis and design details and experimental investigation was presented for the PLSS System in Chapter 8. The relevant discussion points for the system are presented in this section, these include:

- 1) A design process for the PLSS system in the construction phase was presented. In the design of the PLSS system the engineer must consider the rise in force that will occur in the system from the concrete casting operation. The components of the PLSS system and steel beam it is acting upon must all be checked for appropriate limit states in the non-composite phase.
- 2) An equation was presented that solved for the initial upward force required to meet a target displacement after shore removal. This equation allowed for determination of all other design forces and displacements in the construction phase. An option where no upward force is applied was also presented. This option allows for using the system as a king post setup.
- 3) A design example was presented to show how the developed equations could be implemented. The results from the design example were used for the experimental validation of the PLSS system.
- 4) The applied upward force in the self-shoring system needed to displace the steel beam upwards by 1 in. was 3.6 kips for the test specimen. This value compares reasonably with the 3.25 kips calculated from the analysis presented in Section 8.1.

- 5) The concrete casting operation on the test specimen reduced the mid-span deflection by 0.3 in. to 0.7 in. The force increase in the hydraulic ram was approximately 3 kips. These values compare well to the analysis values.
- 6) The shoring removal on the test specimen caused a residual mid-span deflection of -0.03 in. Hence, the system was essentially 'flat' after shore removal. Zero displacement was the target value.
- 7) The load-deflection behavior of the system was ductile with an estimated capacity of 36 kips or 300 psf equivalent.
- 8) The mid-span deflection for service level live loading was equal to 0.25 in. and for factored design loads was equal to 0.95 in.
- 9) The specimen experienced end slip at higher load and displacement levels. Slip increased steadily at higher loads but no shear stud or other slip related failures were observed.
- 10) The test specimen observations compared well with the parameters predicted by the developed equations.
- 11) The PLSS system showed merit as a long span floor system. More work is needed to optimize the PLSS components and make it economically feasible in steel construction.

12.6. Analysis and Design Studies for Structural Behavior of Composite Deep Deck Systems

Chapter 9 presented analysis and design studies for the developed composite deep deck systems. A summary of the main points from the chapter are presented in this section.

- 1) Analytical models were developed that considered construction effects and partial interaction resulting from interfacial slip.
- 2) Those models that did not attempt to model construction or slip effects were shown to be un-conservative in predicting the overall capacity of composite deck specimens.
- 3) The simple method for incorporating construction effects, described in Section 9.1.2, by reducing the yield stress did a reasonable job of estimating strength for the un-shored specimens. It was particularly of merit for CC-DD Specimen 4 where construction level stresses were higher than other specimens.
- 4) The CC-DD test specimens had a small amount of end restraint initially based on comparisons from predicted stiffness and what was measured. For the studed specimens, the restraint was not significant enough to greatly affect overall behavior.
- 5) The partial composite CC-DD and SC-DD fiber based slip models that incorporated construction effects did a good job in estimating strength for the studed specimens. They also did a reasonable job in predicting overall structural behavior of the specimens.

- 6) The FEM based slip models were shown to not accurately capture the behavior of the deep deck specimens. They were computationally expensive and had numerous convergence problems. Thus, they were not further developed.

12.7. Floor Vibration Parametric Studies and FEM Modeling

Chapter 10 presented floor vibration parametric studies and FEM models for floor vibration evaluation. The main discussion points from this chapter are presented within this section.

- 1) The effective floor length in SCI Publication 331 allows for the entire length of the structure to be used when finding the effective mass of a floor system. This is saying that the motion induced from an excitation source will produce a dynamic 'ripple' that will traverse the length of the structure as long as there is no obstruction to block its path. An obstruction being a sharp change in layout of the floor plan, or other means to stop the motion of the ripple. Thus, it can be difficult in assessing for floor vibrations without knowing the layout of a structure. One part of the building may have no problems related to vibrations such as an interior bay. But, a corner bay in the same structure may have problems due solely to its location within the structure.
- 2) A single cell FEM model as described in Chapter 10 (analogous to the deep deck test specimens) is adequate for determining the first resonant frequency. Higher primary bending frequencies can also be determined adequately with this model. Single bay models described in Chapter 10 with assumed rigid end supports provide little more information than the single cell model. Single bay models with flexible girders show Dunkerly's effect of the girder flexibility reducing the overall system frequency.
- 3) Multiple bay FEM models developed in Chapter 10 show that there are many closely spaced modes in an actual structure. Many of these modes have low participation in the overall dynamic response. Effective modal mass parameters in the multi-bay models indicate that it is likely proper to use the SCI recommendations in estimating the dominant frequency of the floor system for evaluation purposes. This frequency is based on the floor system (deck and concrete) bending about the girders with a mode shape similar to that of a fixed-fixed beam. Multiple bay models qualitatively and quantitatively show how mass from multiple bays will contribute to the overall behavior.
- 4) Evaluating deep deck systems for floor vibrations can be done using existing guidelines with slight modifications. If AISC Design Guide 11 (AISC, 2003) is used, the natural frequency of the floor system alone should be estimated assuming fixed-fixed boundary conditions. All other assumptions from the design guide can be applied. The provisions given in SCI Publication 331 (SCI, 2004) can be used directly.
- 5) The developed FEM models were used to show participation of various vibration modes for composite deep deck systems. However, the models could be used for other dynamic analyses in evaluating a particular composite floor system. One

application could be applying certain forcing functions to the system and evaluating the dynamic response. This could be especially useful for a structure where floor vibration problems may be anticipated due to floor layout or intended use of the structure.

12.8. Analysis and Design Recommendations for Composite Deep Deck Systems

- 1) The traditional 'm and k' method for establishing shear-bond capacity of composite slabs was not used in the current study. Reasons include that many specimens are required for this methodology and this was beyond the scope of the current project. Also, for studed CC-DD specimens shear bond failure was not observed. To force a shear bond failure in these specimens multiple specimens would be needed with small enough shear spans to force the failure. That was beyond the scope of this project. The 'm and k' method is calibrated to conventional metal deck concrete slab systems. It is likely that factors in the equations may change based on the new types of deck profiles and spans being investigated.
- 2) Simple design equations were presented for evaluating the capacity of composite deep deck systems. The equations included reduction factors to account for construction effects and partial composite action. The equations were developed based on test observations and developed analytical models. More stringent reduction factors were applied to those systems expected to have a shear-bond type failure.
- 3) Recommendations for evaluating immediate and long term deflections were given. The use of recommendations given by SDI (Steel Deck Institute , 2002) and ASCE (ASCE, 1992) can be used for these parameters.
- 4) Evaluating deep deck systems for floor vibrations can be done using existing guidelines with slight modifications. If AISC Design Guide 11 (AISC, 2003) is used, the natural frequency of the floor system alone should be estimated assuming fixed-fixed boundary conditions. All other assumptions from the design guide can be applied. The provisions given in SCI Publication331 (SCI, 2004) can be used directly. When using deep deck systems it is recommended that the first natural frequency of the floor system alone (i.e. without considering girders) should stay above 5 Hz as calculated by equation 2.1 for those systems with 30 ft spans. This is valid for systems that have a self-weight of at least 50 psf.
- 5) The fire ratings that were given in Table 4.5 should be used as a guideline until further testing could be done to validate performance based design requirements.

12.9. Recommendations

12.9.1. Recommendations for Long Span Floor Systems

Based on the work done in this project, three types of systems are recommended for use as long span floor systems. These systems are:

- 1) Composite Cellular Deep Deck (CC-DD) systems. These systems can be designed to achieve 30 ft spans without the need for shoring. Existing profiles from CSI that were tested can be used. Other similar deep deck profiles whose properties are verified experimentally can also be used. The design and analysis procedures presented in this dissertation can be used for these types of systems. The use of shear studs at the ends or other means to transfer interfacial shear stresses is recommended if un-embossed deck profiles are to be used. In using these systems, considerations for fire resistance and floor vibrations should also be made as discussed in the relevant chapters of this dissertation.
- 2) Shored Composite Deep Deck (SC-DD) systems. The use of a single line or multiple lines of shoring can be used in conjunction with deep decks (4.5 to 7.5 in.) in achieving long spans. Consideration of the locked in stresses from shore removal need to be carefully considered in the design process. The use of shear studs at the ends or other means to transfer interfacial shear stresses is recommended if un-embossed deck profiles are to be used. The design and analysis procedures presented in this dissertation can be used for these types of systems.
- 3) Pre-Loaded Self-Shored (PLSS) System. The PLSS system can be implemented with conventional floor systems to help in reducing floor-to-floor heights. How the system would be implemented and used will vary depending on the project.

12.9.2. Recommendations for Future Work

Recommendations for future work include:

- 1) Further large scale testing of deep deck systems looking at different span lengths, span to depth ratios, decks with additional shear transfer mechanisms such as embossments, and different shear span lengths. Testing to validate the effective shear span of a uniformly loaded specimen should also be considered. This would especially be needed if a 'm and k' type method is desired for evaluating strength.
- 2) Dynamic testing on a full bay specimen (i.e., 30 ft by 30 ft). This would provide further insight into dynamic characteristics of long span composite deep deck systems.
- 3) Further development of the proposed FEM models for floor vibrations. This would include applying forcing functions and examining responses of a system within a given structure.

- 4) Comprehensive feasibility studies with respect to overall economy of using proposed long span systems. This would include costs related to fabrication and erection using the various systems.
- 5) Further investigation into using the proposed shear bond model for evaluation of composite deep deck systems.
- 6) Further performance based elevated temperature testing of the deep deck systems. Analysis to validate testing results should also be considered.
- 7) Studies on the best way to implement a PLSS type system in the field. This would include working with fabricators and erectors to determine most feasible and economical way to use a system of this nature.

LIST OF REFERENCES

- AISC. (2003). *AISC Design Guide 11: Floor Vibrations Due to Human Activity*. Chicago: AISC.
- AISC. (2003). *Fact for Steel Buildings*. Chicago, IL: AISC.
- AISC. (2003). *Steel Design Guide No. 19: Fire Resistance of Structural Steel Framing*. Chicago, IL: AISC.
- Allemang, R. J. (1999). *Vibrations: Analytical and Experimental Modal Analysis*. University of Cincinnati, Department of Mechanical, Industrial and Nuclear Engineering, Cincinnati, OH.
- Allen, D. E., Onsyko, D. M., & Murray, T. M. (1999). *ATC Design Guide 1: Minimizing Floor Vibration*. Applied Technology Council.
- Allen, H. G. (1969). *Analysis and Design of Structural Sandwich Panels*. Oxford, UK: Pergamon Press.
- Almusallam, T. H., & Alsayed, S. H. (1995). Stress-Strain Relationship of Normal, High-Strength and Lightweight Concrete. *Magazine of Concrete Research*, 47 (170), 39-44.
- American Concrete Institute. (2005). *Building Code Requirements for Structural Concrete*. Farmington Hills, MI: ACI.
- ASCE. (1992). *ASCE 3-91: Standard for the Structural Design of Composite Slabs*. New York, NY: ASCE.
- ASTM. (2000). *ASTM E119: Standard Test Methods for Fire Tests of Building Construction and Materials*. West Conshohocken, PA: ASTM.
- ASTM. (2004). *ASTM E8: Standard Test Methods for Tension Testing of Metallic Materials*. West Conshohocken, PA: ASTM International.
- ATC. (1999). *Design Guide 1: Minimizing Floor Vibration*. ATC.

- Avitable, P. (1998). Modal Space: Could You Explain Modal Analysis for Me? *Experimental Techniques*, 22 (2), 11-13.
- BEI Duncan. (2008). *Linear Position Sensors*. Retrieved 2008, from <http://www.beiduncan.com>
- Brigham, E. O. (1988). *The Fast Fourier Transform and its Applications*. Englewood, New Jersey: Prentice Hall.
- Buckner, C. (Ed.). (2002). Construction Considerations for Composite Steel-and-Concrete Floor Systems. *Journal of Structural Engineering*, 9 (128), 1099-1100.
- Cafco International. (2004, January). Blaze-Shield II Data Sheet C/F/C-1.
- Canam Steel. (2002). *Steel Deck Catalog*. Columbus, OH.
- Caverson, R. G., Waldron, P., & Williams, M. S. (1994). Review of Guidelines for Suspended Concrete Slabs. *Canadian Journal of Civil Engineering*, 21 (6), 931-938.
- Cedeno, G. A. (2006). *Behavior and Design of Composite Floor Systems Under Realistic Fire Loading*. Preliminary Examination Report, Purdue University, School of Civil Engineering, West Lafayette, IN.
- Colaco, J. P. (1972, July). A Stub-Girder System for High Rise Buildings. *Engineering Journal*, 89-95.
- Corus. (2002). *Composite Floor Decks*. UK: Corus.
- Davies, J. M. (2001). *Lightweight Sandwich Construction*. London, UK: Blackwell Science Ltd.
- Easterling, W. S. (2002). Long Span Composite Slabs - Extending the Reach of Steel Construction. Seattle, WA: AISC.
- Girder Slab Technologies. (2002). *Design Guide*. Cherry Hill, N.J.
- Hillman, J. R. (1990). *Innovative Lightweight Floor Systems for Steel Framed Buildings*. M.S. Thesis, Virginia Polytechnic Institute and State University.
- Hillman, J. R., & Murray, T. M. (1990). Innovative Floor Systems. *Proceedings of the 1990 National Steel Construction Conference*. Kansas City, MO: AISC.
- Huber, D. H., & Varma, A. H. (2005). *Annual AISC Project Progress Report*. Annual Progress Report, Purdue University.
- International Code Council. (2003). *International Building Code*. Oak Brook, IL: IBC.

- Kennedy, S. J., & Kennedy, L. K. (2004). *SPS Creates New Markets for Steel*. Intelligent Engineering, Ltd.
- Lawson, R. M. (2000). Fire Engineering Design of Steel and Composite Buildings. *Journal of Constructional Steel Research* , 57, 1233-1247.
- Lawson, R. M., & Mullet, D. L. (1999). *Design of Slimflor Fabricated Beams Using Composite Decking*. , U.K.Berkshire: Steel Construction Institute.
- Lawson, R. M., Mullet, D. L., & Rackham, J. W. (1997). *Design of Asymmetric Slimflor Beams Using Deep Composite Decking*. Berkshire, UK: SCI.
- Lee, J., & Fenves, G. L. (1998). A Plastic-Damage Concrete Model for Earthquake Analysis of Dams. *Earthquake Engineering and Structural Dynamics* , 27 (9), 937-956.
- Liddy, B. (2004, May). *Steel Interchange Discussion Board*. Retrieved from Modern Steel Construction website: http://www.aisc.org/MSCTemplate.cfm?Section=Steel_Interchange2&Template=/CustomSource/Faq/SteelInterchange.cfm&FaqID=2344
- McKinley, B., & Boswell, L. F. (2002). Behavior of Double Skin Composite Construction. *Journal of Constructional Steel Research* , 58, 1347-1359.
- Measurement Specialties. (2008). Retrieved 2008, from <http://www.meas-spec.com>
- Naccarato, P. (1999, December). New Alternative to Flat Plate Construction. *Modern Steel Construction* .
- Naccarato, P. (2001, May). Steel & Pre-cast Slab Construction System for Mid and High-Rise Residential Buildings. *Modern Steel Construction* .
- Naeim, F. (1991). *Design Practice to Prevent Floor Vibrations*. Structural Steel Education Council.
- National Instruments. (2008). Retrieved 2008, from <http://www.ni.com>
- Parkinson, D. L. (2002). *Performance Based Design of Structural Steel for Fire Conditions*. M.S. Thesis, Worcester Polytechnic Institute, Department of Fire Protection Engineering.
- Pavic, A., & Reynolds, P. (2002). Vibration Serviceability of Long-Span Concrete Building Floors. Part 1: Review of Background Information. *The Shock and Vibration Digest* , 34, 191.

- Pavic, A., & Reynolds, P. (2002). Vibration Serviceability of Long-Span Concrete Building Floors. Part 2: Mathematical Modeling Approaches. *The Shock and Vibration Digest* , 34, 279.
- PCB . (2008). Retrieved 2008, from <http://www.pcb.com>
- Popovics, S. (1973). A Numerical Approach to the Complete Stress-Strain Curve of Concrete. *Cement and Concrete Research* , 3, 583-599.
- Rainer, J. H., Pernica, G., & Allen, D. E. (1988). Dynamic Loading and Response of Footbridges. *Canadian Journal of Civil Engineering* , 15 (1), 66.
- SCI. (1989). *SCI Publication P076: Design Guide on the Vibration of Floors*. Nerkshire, UK: SCI.
- SCI. (2004). *SCI Publication P331: Design Guide on the Vibration of Floors*. Nerkshire, UK: SCI.
- SDI. (2002). *Design Manual for Composite Decks, Form Decks and Roof Decks-No. 30*. Fox River Grove, IL: SDI.
- Simulia. (2007). Abaqus Version 6.7 Analysis User's Manual.
- Steel Deck Institute . (2002). *Design Manual for Composite Decks, Form Decks, and Roof Decks - No. 30*. Fox River Grove, IL: SDI.
- Tanner, J. E. (2003). *Design Provisions for Autoclaved Aerated Concrete (AAC) Structural Systems*. The University of Texas at Austin.
- Thomson, W. T. (1988). *Theory of Vibration With Applications*. Prentice Hall.
- UL. (2003). *Fire Resistance Directory*. Northbrook, IL: Underwriters Laboratory.
- UniMeasure. (2008). Retrieved 2008, from <http://www.unimeasure.com/>
- Veitas, R. (2002, May). Slab Solution. *Modern Steel Construction* .
- Viest, I. M., Colaco, J. P., Griffis, L. G., Leon, R. T., & Wylie, L. A. (1997). *Composite Construction Design for Buildings*. New York, NY: McGraw-Hill.
- Wang, C. M., Padmanaban, K., & Shanmugam, N. E. (1995). Ultimate Strength Analysis of Stub Girders. *Journal of Structural Engineering* , 121, 1259-1624.
- Widjaja, B. R. (1997). *Analysis and Design of Steel Deck Concrete Composite Slabs*. PhD Thesis, Virginia Polytechnic Institute and State University, Blacksburg, VA.

Williams, M. S., & Waldron, P. (1994). Evaluation Methods for Predicting Occupant Induced Vibrations in Concrete Floors. *The Structural Engineer*, 72 (20).

Wright, H. D. (1991). The Design of Double Skin Composite Elements. *The Journal of Constructional Steel Research*, 19, 111-132.

Yoder, N. (2006). Modal Impact Viewer - Custom GUI for Matlab.

Appendix A.

Further Details on DSC Systems

Principles of Sandwich Panel Structural Behavior

There are many structural design details that need to be considered for DSC panels. The subsequent sections provide first the structural principles of sandwich panels, the design approach for a DSC system, and finally other issues of concern for the DSC panels being considered. These include determining the load capacity of DSC panels, deflection and vibration criteria, fire resistance, connection between the DSC panels, and possible connection layouts to girders and other structural members. The final proposed designs for a proposed DSC panel system are then described along with relevant issues.

The design of a sandwich panel for use as a flexural member is somewhat complex due to the contribution of the core material. If the stiffness is small enough, its contribution can be neglected. However, for the applications being considered is assumed the core will have enough stiffness to contribute significantly to overall behavior. Nonetheless, ordinary beam theory can be used to analyze sandwich structures with modifications to account for the core material. The following derivations will consider the case of a core material sandwiched between two flat plates. All derivations and equations come from Allen (1969) and Davies (2001).

Sandwich Panels with Flat Faces

Consider the beam panel given in Figure A.1. The flexural rigidity of this panel about the centroidal axis, denoted D , can be given as:

$$D = E_f \frac{bt^3}{6} + E_f \frac{btd^2}{2} + E_c \frac{bc^3}{12} \quad \text{A.1}$$

Where E_f and E_c correspond to the Young's Modulus of the face and core materials. The corresponding bending stresses in the faces and core can be found as:

$$\begin{aligned} \sigma_f &= \frac{Mz}{D} E_f \\ \sigma_c &= \frac{Mz}{D} E_c \end{aligned} \quad \text{A.2}$$

With the maximum bending stresses being defined as:

$$\begin{aligned} (\sigma_f)_{\max} &= \pm \frac{ME_f}{D} \frac{h}{2} \\ (\sigma_c)_{\max} &= \pm \frac{ME_c}{D} \frac{c}{2} \end{aligned} \quad \text{A.3}$$

The bending stresses can be seen to very familiar to common bending stress relations. The shear stresses are slightly more complex due to the contribution of the core material.

The shear stress distribution in sandwich beam with a core of significant rigidity is given in Figure A.3. The governing equation for shear stress known from mechanics can be applied and is given as:

$$\tau = \frac{VQ}{Ib} \quad \text{A.4}$$

Where,

V	The applied shear force
Q	The first moment of area of the section
I	Moment of inertia
b	Width of the section

For the sandwich beam, this equation must be modified to account for the modulus of elasticity of the different elements. This can be expressed:

$$\tau = \frac{V}{Db} \sum(QE) \quad \text{A.5}$$

$\sum(QE)$ represents the sum of all the products of Q and E for all parts of the section above the centroidal axis. This equation can be simplified to determine the shear stress at any level in the core, knowing that:

$$\sum(QE) = E_f \frac{btd}{2} + \frac{E_c b}{2} \left(\frac{c}{2} - z \right) \left(\frac{c}{2} + z \right) \quad \text{A.6}$$

Therefore, the shear stress in the core can be expressed:

$$\tau = \frac{V}{D} \left(E_f \frac{td}{2} + \frac{E_c}{2} \left(\frac{c^2}{4} - z^2 \right) \right) \quad \text{A.7}$$

It can therefore be noted that once applied loadings and forces are known, the corresponding bending and shear stresses can readily be achieved.

Overall deflections in a sandwich panel result from shear deformations from the core in addition to the bending deflections. The effect of core material shear deformations is illustrated in Figure A.4. In the figure it can be seen that the original coordinates $cdef$ move to the new coordinates $c'd'e'f'$ as result of the shear deformations of the core. Thus, overall deflections will be increased. For the present derivation of deflection, it is assumed that a uniformly loaded simply supported single span panel is being considered. Figure A.1 shows the case being considered. For this case, the bending deflection and shear deflection are calculated separately and then added together.

Using conventional beam bending theory, the bending deflection along anywhere throughout the length of the beam can be calculated as:

$$\Delta_b = \frac{wL^4 \xi}{24D} (1 + \xi)(1 + \xi - \xi^2) \quad \text{A.8}$$

This bending deflection can then be added to the shear component of deflection. The shear component of deflection is given as:

$$\Delta_s = \frac{wL^2 \xi}{2A_c G_{eff}} (1 - \xi) \quad \text{A.9}$$

Where A_c represents the area of the core and G_{eff} is the effective shear modulus of the concrete core. This effective modulus is found as:

$$G_{eff} = \frac{G_c}{1 + \frac{E_c c^2}{6E_f t(c+t)}} \quad \text{A.10}$$

Knowing both components of the deflection, they can directly be added together to obtain the total deflection. This is given as:

$$\frac{wL^4}{24D} \xi (1 - \xi) (1 + 4k + \xi - \xi^2) \quad \text{A.11}$$

Where ,

$$k = \frac{3D}{A_c G_{eff} L^2}$$

Finally, the maximum deflection can be found (occurring at mid-span) as:

$$\Delta_{max} = \frac{5wL^4}{384D} (1 + 3.2k) \quad \text{A.12}$$

The basic structural behavior has now been presented for a sandwich beam. It should be noted that the above derivations assumed full composite behavior between the core and face materials. It is also assumed that the top and bottom faces are of equal thickness and uniform cross section. This would be the case for the DSC elements being considered. Thus, this above derivation helps to describe the basic analytical model of a sandwich or DSC panel.

Load Capacity of DSC panels

The overall load capacity of a DSC panel subjected to flexural loading can readily be predicted as long as all modes of failure are properly considered. Research has shown that properly designed DSC experience a ductile failure, which is similar to under-reinforced concrete beams (McKinley and Boswell 2002). However, other failure modes can govern design and must be properly accounted for. Possible failure modes include:

- 1) Balanced failure – yielding of the steel plate followed by concrete crushing
- 2) Shear failure of the concrete
- 3) Local buckling of the compression steel plate
- 4) Shear slip of the plate from the core

It is obvious that failure mode 1 would be the most desirable to occur in a DSC specimen. Therefore, if the DSC panels are properly designed then their full composite strength can be utilized. Designing to utilize full strength and preventing premature failure is described below.

Moment Capacity

In determining the moment capacity of a DSC section, traditional reinforced concrete theory for a doubly reinforced (tension and compression reinforcement) section can be applied. Using Figure A.2 as a reference, the location of the neutral axis can be found using the following expression:

$$z = -n(t_1 + t_2) + \left[n(t_1 + t_2)^2 - n(t_1^2 - 2t_1c + t_2^2) \right]^{\frac{1}{2}} \quad \text{A.13}$$

Where,

z	depth of neutral axis relative to the bottom of the top plate
n	The modular ratio of steel to concrete
$t_1 = t_2$	plate thickness (assumed top and bottom plates are equal thickness)

Once the neutral axis location is determined the moment resistance of a DSC panel can be determined by taking moments about the concrete compressive force and solving such that:

$$M = \sigma_1 b t_1 \left(\frac{z}{3} + \frac{t_1}{2} \right) + \sigma_2 b t_2 \left(c - \frac{z}{3} + \frac{t_2}{2} \right) \quad \text{A.14}$$

Where σ_1 and σ_2 correspond to the top and bottom plate stresses that are occurring. If local buckling is prevented such that the full yield capacity of the steel is utilized in both the compressive and tension plates, the elastic moment resistance becomes:

$$M_e = \sigma_y b t_1 \left(\frac{z}{3} + \frac{t_1}{2} \right) \frac{z + \frac{t_1}{2}}{h_c - z + \frac{t_2}{2}} + \sigma_y b t_2 \left(c - \frac{z}{3} + \frac{t_2}{2} \right) \quad \text{A.15}$$

Once the yielding of the tension steel has occurred, the neutral axis shifts upward toward the compression plate. The ultimate moment capacity occurs upon the neutral axis reaching the bottom steel plate. Upon reaching this level, the moments can be summed about the compression plate and the ultimate moment resistance calculated as:

$$M_y = \sigma_y b t (c + t) \quad \text{A.16}$$

It can be seen that if yielding is allowed to occur in both the bottom and top plates, the moment capacity can be calculated using A.15 or A.16 based on the type of design being considered. However, if local buckling occurs in the top plate prior to yielding then A.14 should be used to predict the moment capacity.

Shear Failure of Concrete

Shear failure of the concrete core in a DSC panel is a very drastic and non-ductile failure. Thus, it is imperative that the panels be designed such that this does not occur. To properly account for this, it must be ensured that the concrete have adequate shear strength. In a DSC panel using shear stud or transverse double welded bars, the studs or bars can help in providing additional shear strength in addition to the strength of the concrete. However, this strength would only need to be utilized if the shear strength of the concrete was exceeded. Furthermore, once this limit state is approached the faces will likely slip with respect to the core and the onset of local buckling would occur.

Predicting the maximum shear stress in the concrete can be found by maximizing equation A.7. This is done by setting z equal to zero such that:

$$\tau_{\max\text{-concrete}} = \frac{V}{D} \left(E_f \frac{td}{2} + \frac{E_c}{2} \left(\frac{c^2}{4} \right) \right) \quad \text{A.17}$$

The shear resistance provided by the concrete can then be calculated by ACI provisions for shear strength. ACI 318-2002 provisions state that for normal weight concrete the unit shear stress can be expressed:

$$v_c = 2\sqrt{f'_c} \quad \text{units of force/area} \quad \text{A.18}$$

For lightweight concrete:

$$v_c = 1.5\sqrt{f'_c} \quad \text{A.19}$$

If LRFD design is to be used then appropriate phi (ϕ) factors be used in conjunction with desired load combinations. ACI recommends a ϕ factor of 0.75 be used in design for shear resistance in a flexural member.

Local Plate Buckling

The use of relatively thin steel plates in a DSC system could lead to local buckling of the compression plate. The prevention of plate buckling is controlled by the spacing of the shear transfer mechanism used and the overall thickness of the compression plate. If shear studs or double welded transverse bars are assumed, then the studs essentially act as partially clamped support conditions in preventing the plate from buckling. The concrete prevents the plate from buckling inwards (toward the concrete), which leads to a unilateral buckling problem.

Considering the above assumptions, the elastic buckling relationship for plate buckling can be used and is expressed:

$$\sigma_{cr} = k \frac{\pi^2 E}{12(1-\nu^2)(b/t)^2} \quad \text{A.20}$$

Where,

σ_{cr}	Elastic buckling stress
k	Constant depending on the type of stress, boundary condition, and b/t ratio
E	Young's Modulus
ν	Poisson's Ratio
b/t	width to thickness ratio of the plate (b corresponds to maximum spacing between studs forming the boundary)

It is common in plate buckling to define the ratio of critical buckling stress to yield stress (σ_{cr}/σ_y) as $1/\lambda_c^2$. Therefore, expression A.20 becomes:

$$\lambda_c = \frac{b}{t} \sqrt{\frac{\sigma_y (12)(1-\nu^2)}{\pi^2 E k}} \quad \text{A.21}$$

For the DSC panels in question, the maximum b/t ratio that can be achieved without local buckling occurring is desired. Therefore, knowing that $\nu = 0.3$ and $E = 29,000,000$ psi for steel:

$$\frac{b}{t} \leq 5120 \lambda_c \sqrt{\frac{k}{\sigma_{cr}}} \quad \text{A.22}$$

If residual stresses and imperfections are considered, it is usually assumed to take $\lambda_c = 0.7$ and thus:

$$\frac{b}{t} \leq 3580 \sqrt{\frac{k}{\sigma_{cr}}} \quad \text{A.23}$$

Where, the critical stress is in terms of psi.

Expression A.23 can be considered the maximum b/t ratio that can be used to achieve a critical stress value. The k term is somewhat difficult to determine for a DSC panel due to the boundary conditions and presence of the concrete. Prior research has shown that keeping the b/t ratio at a maximum of 67.5 will ensure full buckling strength can be utilized in the plates (Wright et al 1991). For 36 ksi yield steel, this implies that a k value of approximately 12.5 should be used. Therefore, for the designs considered this was the limiting value used in determining maximum stud spacing.

Whether yield stress needs to be achieved is a design issue that needs to be considered. If the yielding moment from expression A.16 is desired, then yield stress needs to be considered. However, if only the stress in the plates at a service level loading is desired then the stress found from A.3 in correspondence with the proper load combination can be used. The final design was based on allowing the plate to develop its full post buckling strength (σ_y).

Shear Slip Between Plate and Concrete

Another key design constituent for the DSC panels is achieving adequate transfer between the steel plates and concrete core. An adequate amount of shear studs must be present as to prevent slippage between the core and face plate. There are two methodologies that can be used for doing this design. The first is a mechanics based approach in which the shear is found using A.7 from above. The applied shear is based on the service loads applied to the system. The second method is a limit state approach where the maximum force created by either the tension in the steel plate or compressive force of the concrete is designed for.

If design is based on a mechanics approach the actual shear stress in the system is considered. The shear at the interface can be found using expression A.7 with applied service level loading being assumed. Once the shear stress is found, the corresponding shear flow can be found by multiplying by the width of the panel such that:

$$q = \tau b \quad \text{A.24}$$

Where q is the shear flow (force/length) and b corresponds to the width of the panel being considered. Once q is known, the spacing of studs can be found using:

$$s = \frac{q}{Q_n} \quad \text{A.25}$$

Where Q_n corresponds to the strength of the individual shear connector and s is the required spacing. If the panel is loaded uniformly, the shear will decrease linearly from

the end to mid-span. Therefore the spacing can be reduced based on this approach, however local plate buckling will govern this overall spacing.

The other approach to spacing shear connectors comes from the ultimate interface shear that can develop between the plate and concrete. This is the same approach used in designing shear stud spacing for composite floor construction in typical steel framing. The maximum shear at the steel-concrete interface is defined as the least of:

$$\begin{aligned}\tau_{\max} &= A_s f_y & (a) \\ \tau_{\max} &= 0.85 f_c' A_c & (b)\end{aligned}\tag{A.26}$$

Where A_c refers to the area of effective concrete in compression (above the neutral axis) and f_c' is the compressive strength of the concrete. This equation is a limit state equation and does not really consider the actual behavior of the system. For design, expression A.26 was checked against the requirements using the mechanics approach to ensure both limit states were accounted for. However, local plate buckling will likely govern more so than the above limits.

Other Design Considerations

Deflection

Often in long span flooring systems, deflection criteria governs design more so than strength criteria. For the DSC system, maximum deflections were checked using expression A.12 for applied service loads. The criteria set forth for acceptable deflections were $L/240$ for applied service dead loads and $L/360$ for applied live loading. These criteria are commonly used in composite construction for deflection evaluation.

Floor Vibrations

Note: Derivations and terminology related to floor vibrations are given in Chapter 2.

Floor vibrations are another design issue that must be considered for DSC systems. As noted before, floor vibrations in a residence are induced mainly from walking excitation and are evaluated accordingly. The same design equations can be used to evaluate DSC panels for floor vibration as traditional composite floors with some slight modifications. These modifications are as follows:

- 1) The effective weight of the DSC component is evaluated as $W_{DSC} = wB_{DSC}L_{DSC}$. Where B is equal to the length of the DSC panel being considered. This is based on recommendations set forth for hollow core slabs and are considered adequate for DSC panels (ATC, 1999).
- 2) In determining the vibration criteria, a required damping ratio was determined. Values under 5% are considered reasonable for residential structures. If a required damping ratio was higher than 5%, the design was deemed unsatisfactory.
- 3) As noted previously the overall frequency of a floor system within steel framing is a combination of the floor system itself, and the supporting girders. For the

current DSC designs it was assumed that deflections of the girder would be kept at an $L/360$ limit for applied service loading. It was also assumed that some composite action would occur at the girder, thus further stiffening the girder. For this reason, a maximum girder deflection of 0.5 in. was assumed in all vibration calculations.

Fire Resistance

Note: Derivations and terminology related to fire resistant design are given in Chapter 2.

While the proposed DSC panels are structurally efficient, there could be concern of the fire resistance of the system. This is especially true if the bottom steel plate is exposed to open flames. Cross sectional thermal analysis were conducted on the designed sections to determine the thermal conductivity of the DSC elements. These analyses were based on the ASTM E199 curve and looked at the time it would take for the top plate to reach 250° C.

Similar to conventional floor systems, UL approved designs could be used to provide additional thermal resistance if needed. Corus Construction reports that for their bi-steel panels an average fire rating of 30 minutes can be achieved with no additional protection. Similar performance could likely be expected for the proposed systems so it is likely additional fire protection could be needed.

Final Design

With design criteria described above, it is now possible to present the design of a DSC panel to be used as floor system within residential steel construction. The assumed layout for the DSC panels design is shown in Figure 3.2. As seen from the figure, all DSC panels were assumed to span 30 ft without any filler beams or other means of intermediate support. Typical residential loadings were assumed in the designs and are the same as assumed in the self shoring design. The DSC panels were designed according to abovementioned criteria and the final design is summarized below.

The cross section of the designed 30 ft long DSC panel is shown in Figure A.5. As seen from the figure, 6 in. of lightweight concrete (115 pcf) is sandwiched between ¼ in. top and bottom steel plates. The total self weight of the system is 75 psf. 2.5 in. long and ½ in. diameter shear studs are spaced transversely at 12 in and longitudinal spacing is shown in the figure. It should be noted that top and bottom studs may need to be staggered, depending on the maximum aggregate size of the concrete used. The governing design parameter for the stud spacing was local buckling of the steel plate. Thus, studs were spaced such that slippage would not occur and plates could reach yield.

The DSC panels were designed to reach full moment capacity based on expression A.15. The spacing of studs allows for the yield moment capacity to be reached with M_y being predicted as 330 ft-kips. Applying a 0.85 phi factor, this value becomes 280 ft-kips and the maximum applied moment was found to be 120 ft-kips. It can therefore be seen that flexural strength is not an issue if adequate composite action is ensured.

Serviceability criteria pertaining to deflections and floor vibrations were also checked for the DSC panels. Deflection at full service loads was estimated to be 1.1 in. for full service loads and 0.9 in. when looking at live loads only. These are within the limits set

forth of $L/240$ and $L/360$ respectively. Floor vibrations were evaluated considering both a panel frequency (only the DSC panels) and a combined mode including contribution from the girder. 4% damping is required for the combined mode and 3.7% if only the floor panels are considered. In a residential application this degree of damping is likely to occur from attachments and partitions within the bay.

The last design parameter investigated were the thermal properties of the DSC panel. To investigate the thermal properties of the DSC panel, a 2D thermal analysis was run in *Abaqus*. The ASTM E119 curve was used in the analysis. The parameter investigated was the time it takes for the top plate to reach 250°C and how fast the bottom plate and concrete heat up. Often fire ratings are established by the amount of time it takes for the top flange of the system to reach 250°C. Thus, the analysis was used to give estimate of the temperature resistance of the panels. Figure A.6 shows the time temperature curves of various constituents of the DSC panel. It can be seen from the figure that it takes 2.5 hours for the top plate to reach 250°C. The bottom plate reaches this temperature in 11 minutes while the 3 in. concrete depth level takes roughly one hour. This analysis shows the favorable insulation properties that are provided by the concrete, as proven by the time it takes for the top plate to reach 250°C. However the bottom plate heats up quickly and may likely need additional fire resistance. However, determination of true fire resistance is a parameter that would likely need to be investigated further.

Layouts and Connection Details

With the DSC panels now designed, it is necessary to address some of the placement and connection issues. As noted from the previous figures, panels were assumed have a six foot width. This width allows for fewer modules that would need to be placed in the field and helps cut down on fabrication costs. The first issue is transfer of lateral loads to allow for diaphragm action and provide some continuity to control vibrations. As noted in Figure A.5, a grout key can be present in the DSC panels to allow for diaphragm action if desired. Furthermore, a connection between adjacent plates can be made by the means of intermittent welded steel plates. An example of this type of connection is shown in Figure A.8. The welded plates will help in horizontal load transfer and aid in vibration control of the system. Also noted in the figure, a 1 in. thick layer of gypcrete or other similar material could be used on the top plate as a walking surface. The topping would not be needed for further strength or stiffness, as is often the case when pre-cast planks are used.

The connection to supporting girders is another aspect needing consideration. It is proposed initially to have the panels resting on the top flange of supporting girders, however other layouts are possible. One possible connection scheme involves welding the transverse edges of the DSC panels to the top flange of the girder, while leaving a slight separation between the transverse edges where grout could be placed. An example of this connection is shown in Figure A.9. It is believed this type of connection could provide some composite action to help stiffen the girder.

Issues and Discussion

A design for a structurally efficient DSC panel system utilizing lightweight concrete sandwiched between steel plates has been presented. The system has been shown to

perform well from a structural viewpoint and could present merit for use in multi-story residential steel construction. However, since a system of this nature has never been significantly used in the proposed context there are some issues that would need to be investigated.

The first and most obvious issue to consider would be the overall cost of a system of the nature. If the system could efficiently be fabricated and erected the cost may be within the limits of its intended multi-story residential use. The cost would likely be governed by how much of the system could be pre-fabricated prior to arrival at the job site. Previous research and current uses has shown the inherent strength and stiffness of these systems. Also, Corus Construction of the UK has shown mass production and implementation of a DSC system is feasible. Thus, if the DSC composite system could be fabricated and erected economically, it is a strong candidate for a long span slab system.

Profiled Double Skin Composite System

Structural Design Considerations and Load Capacity

Using the same basic formulation as used for the DSC system, a system of this nature was designed. As in other systems considered, the design accounted for strength, stiffness, floor vibrations and fire resistance. The fundamental difference in the design compared to the DSC system was in accounting for the profiled top and bottom faces. These profiled faces added an additional term to account for their bending resistance. The system could be separated into two components in which one component is a sandwich profile system with flat plates, and the other is the resistance provided by having profiled faces. Thus, the expressions for deflection and corresponding stress calculations needs to be modified.

Moment Capacity

The moment capacity of the profiled DSC system was predicted using a similar procedure as for the first DSC system. Steel was assumed to reach yield and moments were summed about the compression face, while taking the profiled faces into account.

Shear Failure of Concrete

Determining the applied shear stresses in the system was similar as to the first DSC system. Again, the profiled faces were accounted for in the calculations for the maximum applied shear stress. The resistance of the concrete was estimated using expression A.19.

Local Plate Buckling

The local plate buckling of the compression plate will likely be restrained by the continuous bond of the decks to the concrete and the moment of inertia inherent in the deck profile. Further studies are being conducted on this issue.

Shear Slip Between Profiled Face and Concrete

The amount of horizontal shear capacity provided by deck geometry and embossments needs to be carefully considered for this system. Shear slip tests on the

proposed profiles would need to be done to ensure enough shear resistance is provided by the profiles. If more capacity is needed, additional embossments could be used or shear studs could be placed at critical sections.

Serviceability Design Considerations

Deflection

The same deflection criteria used in evaluating the flat faced DSC system was used in evaluating the profiled system.

Floor Vibrations and Fire Resistance

Again, the same procedure as was used in the flat faced DSC system was used for the current system. For fire resistance, more work is currently in progress to evaluate this issue. It is believed that typical SFRM or other UL approved designs could be used to protect the system if needed.

Profiled DSC Panel Design and Layouts

Following the above procedure, designs considering both a 1.5 and 2 in. cellular deck were done. The design profile is shown in Figure A.10. For both systems, an overall depth of 9 in. was required with self weights between 84 and 87 psf for the 2 in. and 1.5 in. profiles. The design strengths and overall deflections are summarized in Table A.1. Checking floor vibrations shows that required damping ratios are 3% and 4% for the 1.5 in. deck profiles, respectively. It should be noted that these systems appear to have better characteristics from a floor vibration standpoint than the flat plate DSC system. While the natural frequencies are not much different, the added mass helps in damping the system. For fire resistance, SFRM could be used or other UL approved designs for traditional deck systems could be used.

This sandwich system could be laid out in a similar manner as the DSC panels. The panels could be placed side by side and a topping material placed over top of them. The side-lap connection may need to be modified to allow for shear transfer between the planks, or intermittently welded plates could be used (same as in the DSC system). The planks used would have to be either pre-cast with concrete (either onsite or before arriving) or shoring would be required. If pre-cast, the planks would simply be lifted and placed on the supporting girders. A plank to girder connection like that in the DSC system could be used.

Issues and Discussion

The above design is presented as an alternative to the DSC previously presented. Both systems use the same fundamental principles in their behavior and resulting designs. The cellular sandwich system is slightly heavier than the DSC system due to the fact that it is using less steel, but requires more concrete. From a fabrication standpoint, the cellular deck system may present an advantage from the standpoint that it uses existing profiles and may not require the use of additional shear studs. The main issues corresponding to the system are:

- 1) The current sidelap connections used on the deck profiles may inhibit casting of the concrete into the system. If system were to be cast by being laid on their side and concrete being added, the connection could become deformed and unusable. If a grout key could be added, it would help in transferring shear for diaphragm action. The use of intermittently welded steel plates is also a possibility.
- 2) Another main issue that needs to be addressed with this system is determining how much interface shear the deck profiles can transfer. If they do not possess enough capacity, then slip may occur and the system will lose much of its strength. Determining this capacity would likely require testing to determine the shear-slip behavior of the profiles.

The cellular deck sandwich system is a way to construct a sandwich system utilizing readily available products and technologies. While it is somewhat heavier than the DSC system, the additional mass enhances floor vibration resistance characteristics. It is also innovative in how it utilizes both sandwich construction and cellular steel decks in the structural system. If using a flat plate DSC type system were to be too expensive, the above system presents a viable alternative.

Table A.1: Design Forces for Cellular Sandwich System

Cellular Deck Profile	Moment Capacity (kip-ft/ft)	Maximum Applied Moment (kip-ft/ft)	Max Applied Shear Stress (psi)	Shear Strength of Concrete (psi)	Dead Weight Deflection (in.)	Live Load Deflection (in.)
1.5 in.	44.5	21.3	29	95	0.94	0.35
2 in.	44	21.3	29	95	1	0.38

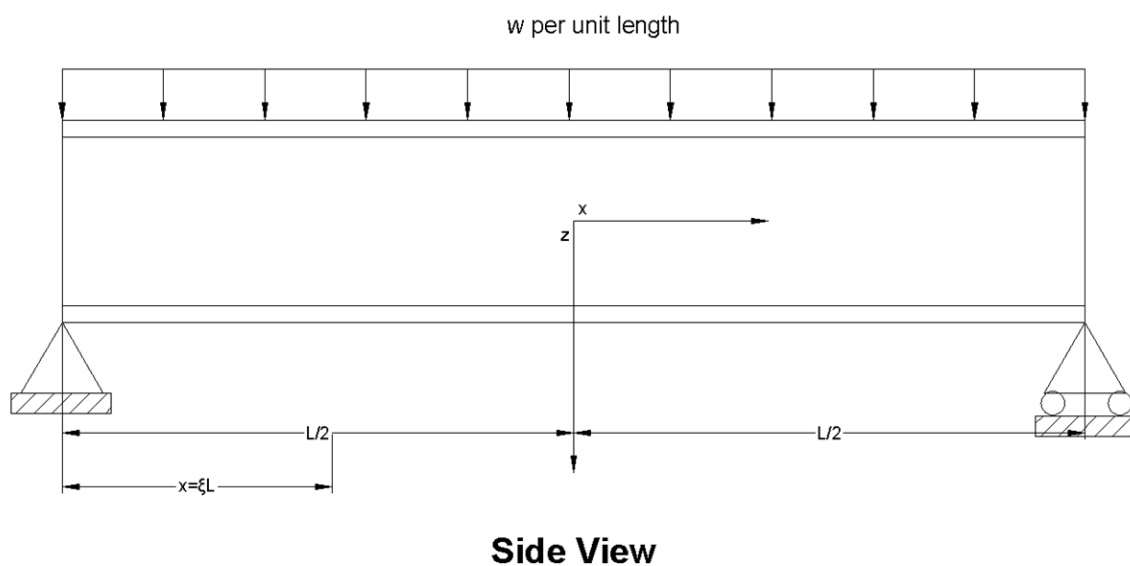


Figure A.1: Sandwich Beam Schematic

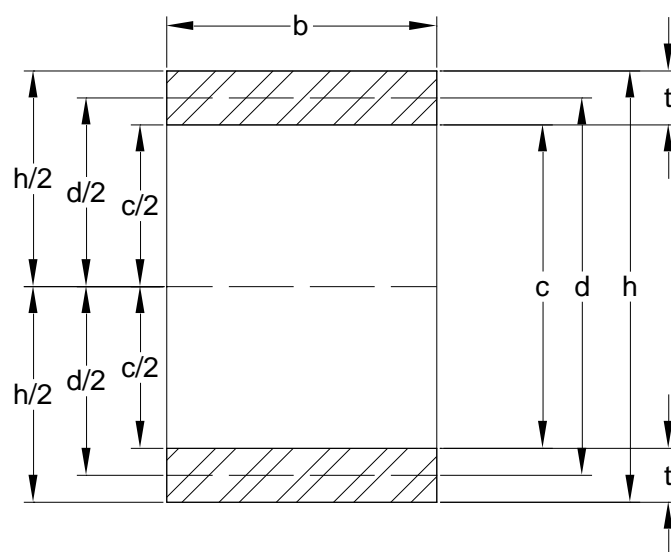


Figure A.2: Cross Section View of Sandwich Beam

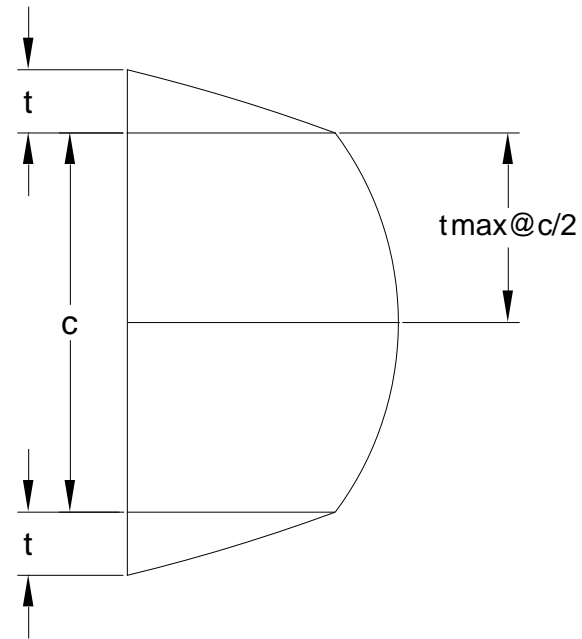


Figure A.3: Shear Stress Distribution in Sandwich Panel

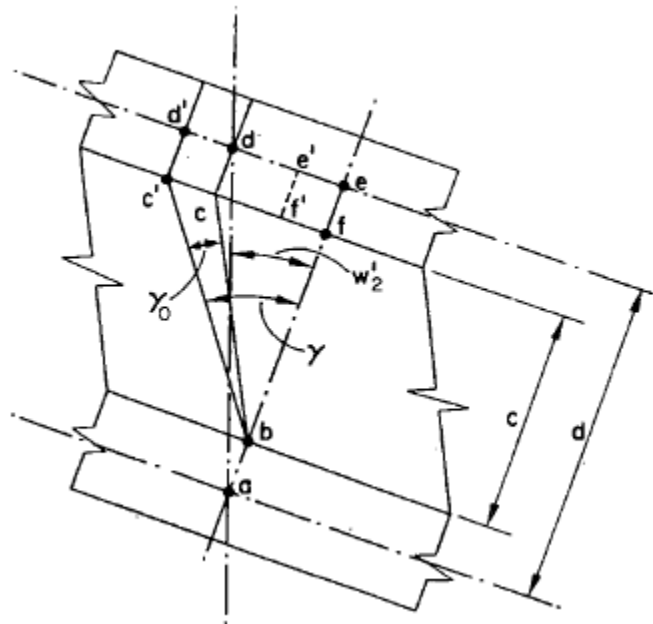


Figure A.4: Effects of Shear Deformations on Sandwich Panel (Allen H. G., 1969)

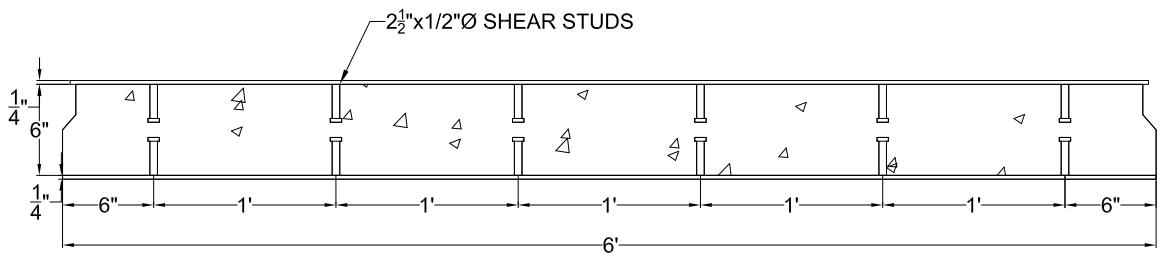


Figure A.5: Cross Section of DSC Panel

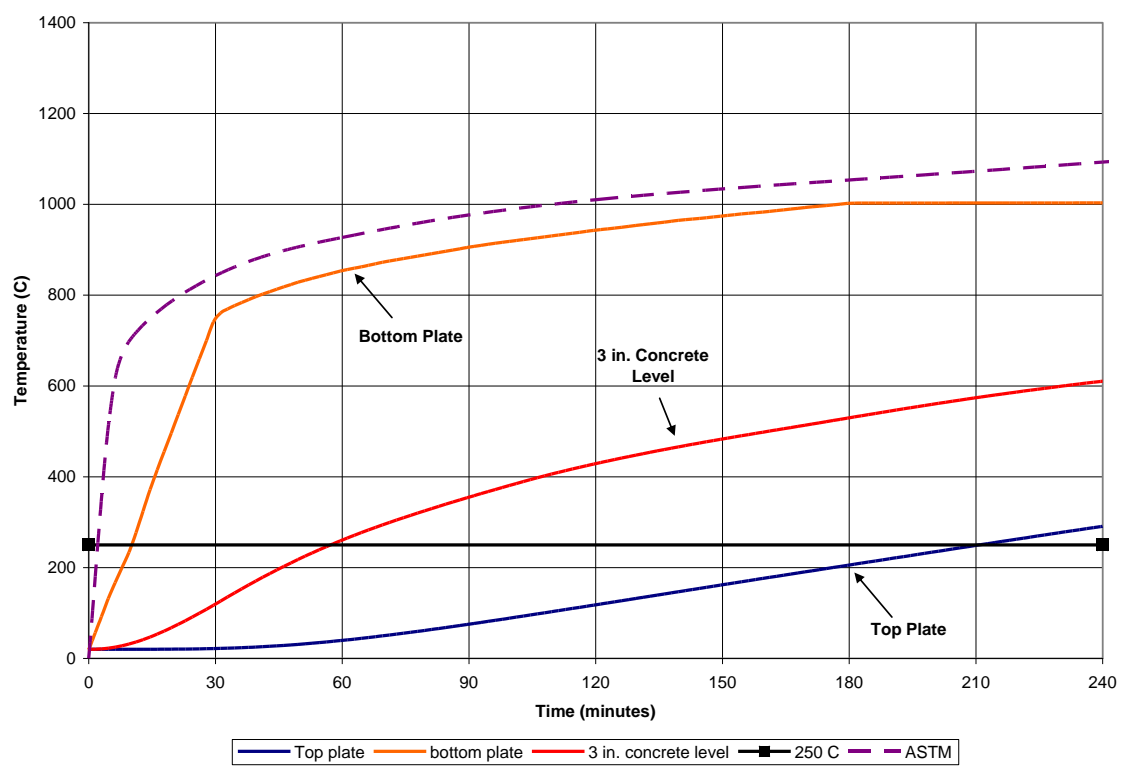


Figure A.6: Two Dimensional Thermal Analysis Results

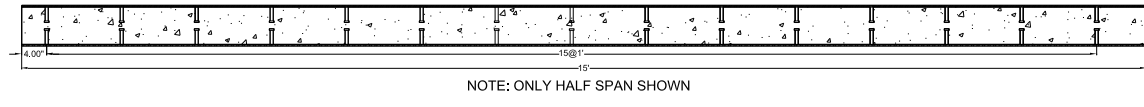


Figure A.7: Side View of DSC Panel

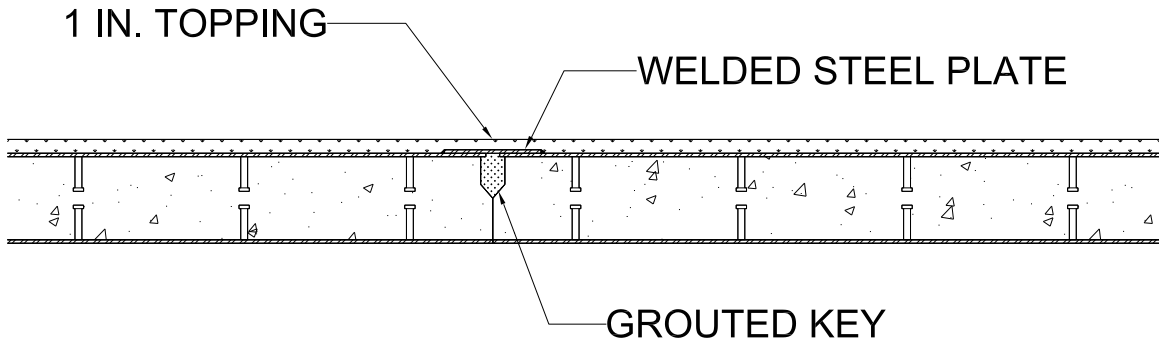


Figure A.8: Possible Connection Between Panels

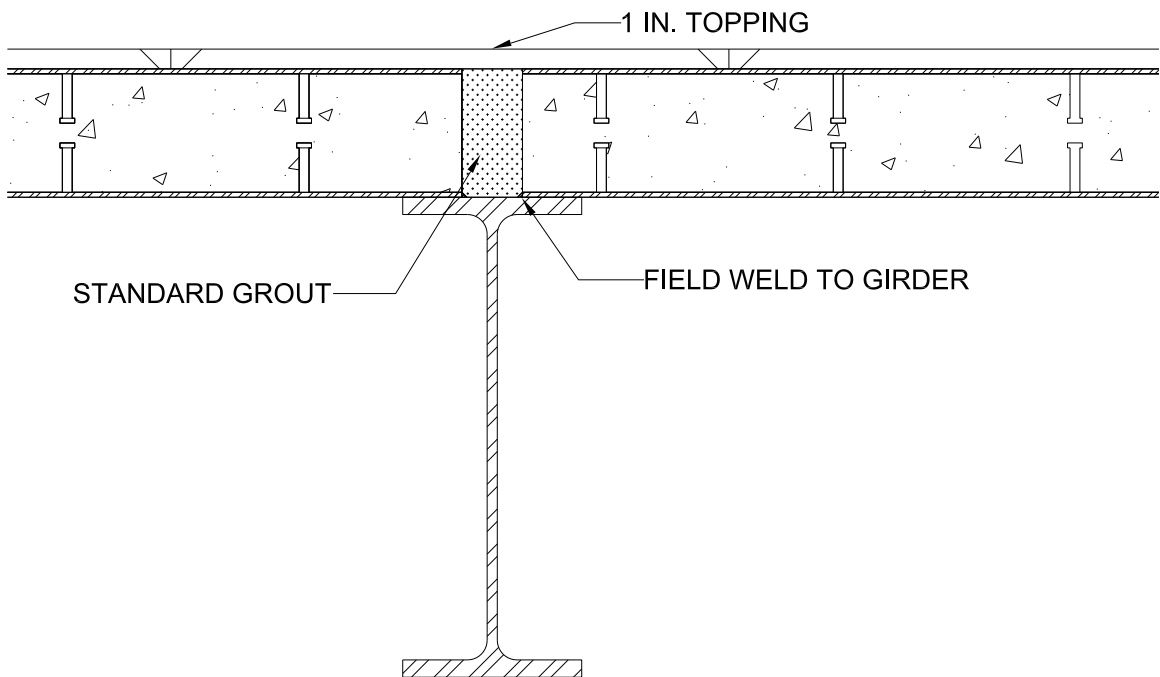


Figure A.9: Possible DSC to Girder Connection

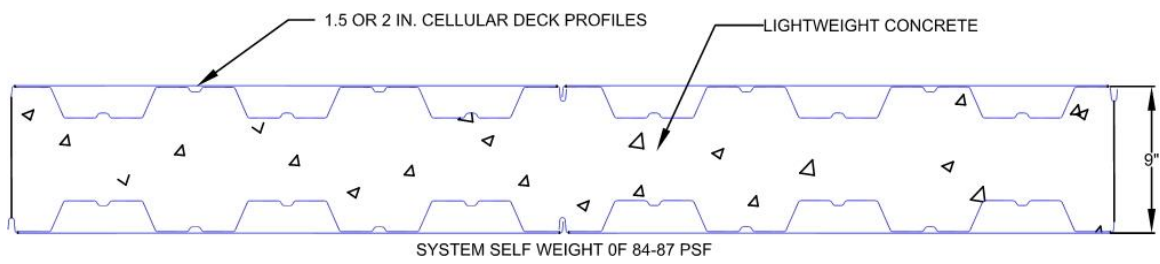
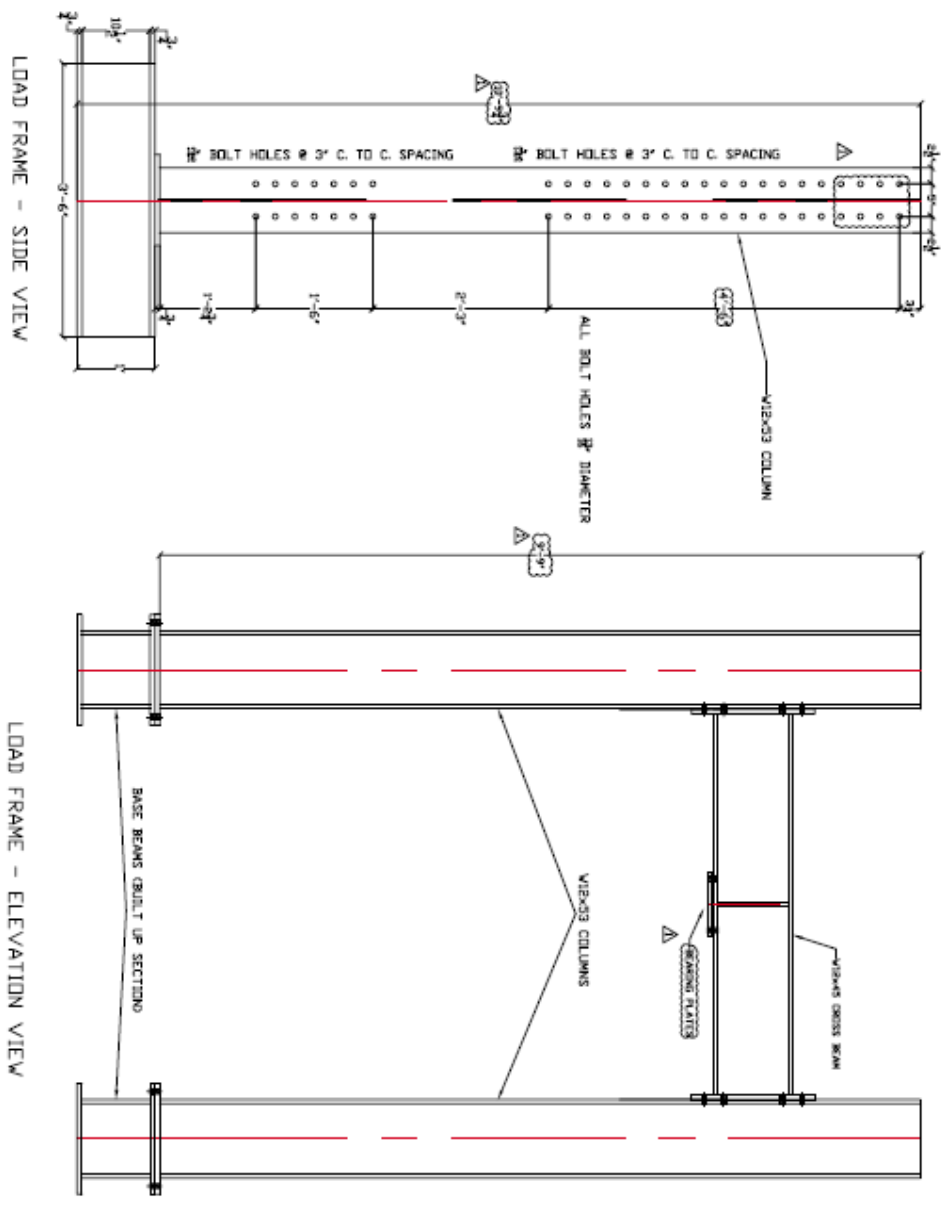


Figure A.10: Cellular Deck Sandwich System Profile

Appendix B.

Load Frame Drawings for Structural Test of CC-DD Specimens



LOAD FRAME - SIDE VIEW

LOAD FRAME - ELEVATION VIEW

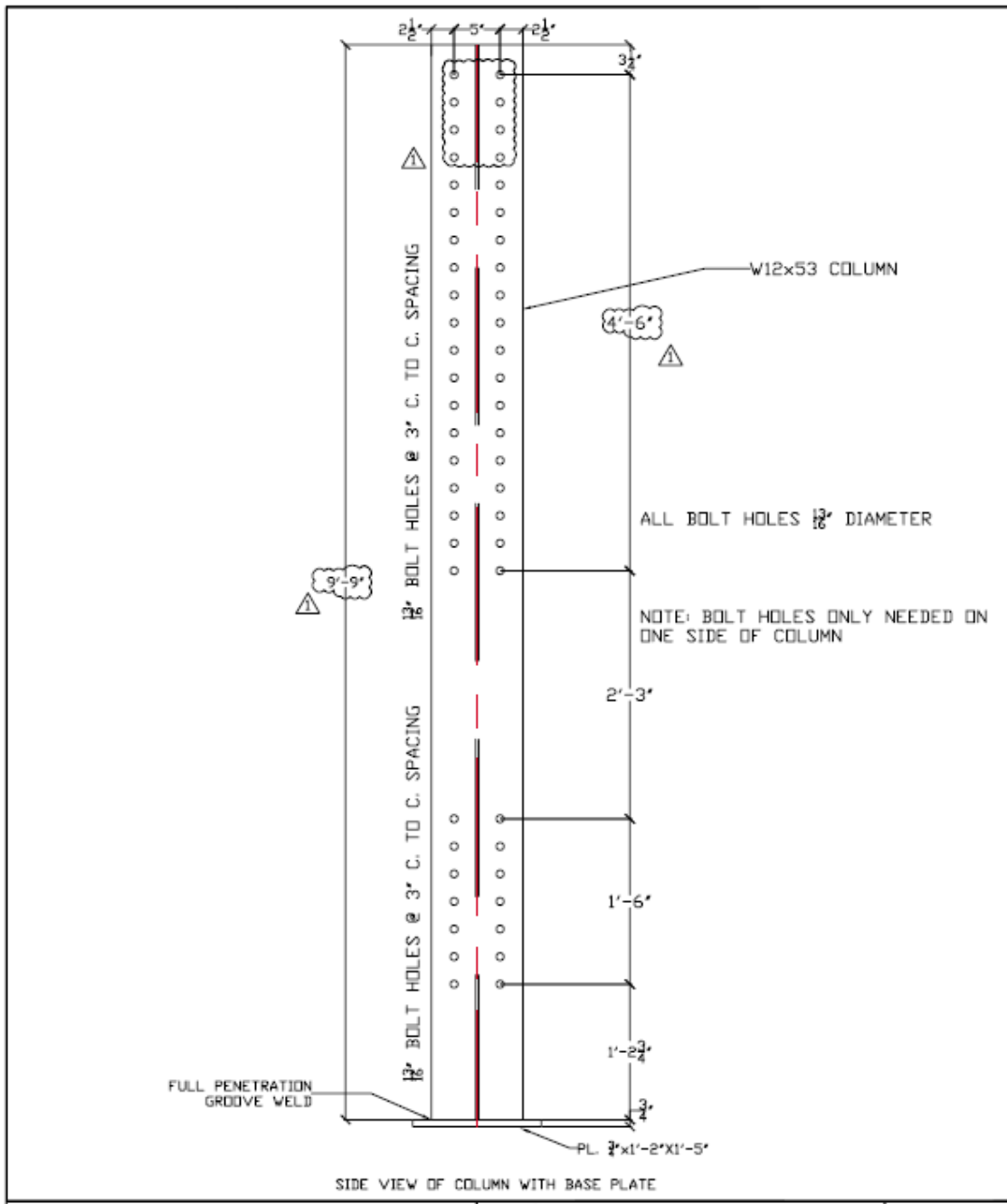
TEST LOAD FRAMES
 AISC MSR PROJECT
 BOWEN LAB

PURDUE
 UNIVERSITY



DEPARTMENT OF CIVIL ENGINEERING
 605 FRIEDLAND HALL
 WEST LAFAYETTE, IN 47907-1334
 PHONE: (765) 464-2544
 FAX: (765) 464-0380

DR	DWYN HENDER
CK	AMT VALINA
DATE	8/17/06
SCALE	N/A
FILE	REBERT 1 OF 8



TEST LOAD FRAMES
AISC MSR PROJECT

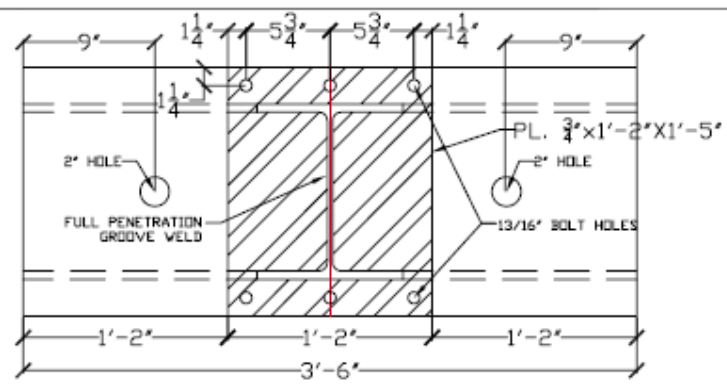
BOWEN LAB

REVISION 1 - 3/17/06

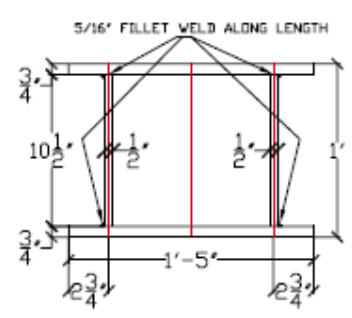


DEPARTMENT OF CIVIL ENGINEERING
650 STADIUM MALL DRIVE
WEST LAFAYETTE, IN 47906
PHONE: (765) 494-2224
FAX: (765) 494-0300

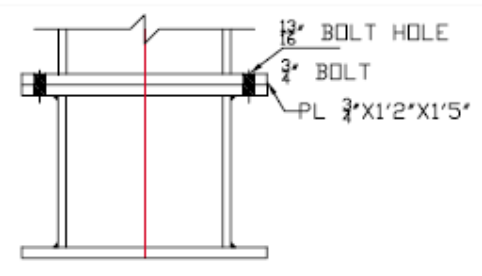
DR	DEVIN HUBER
CK	AMIT VARMA
DATE	5/17/06
SCALE	N/A
FILE	SHEET 2 OF 6



BUILT-UP SECTION TOP VIEW

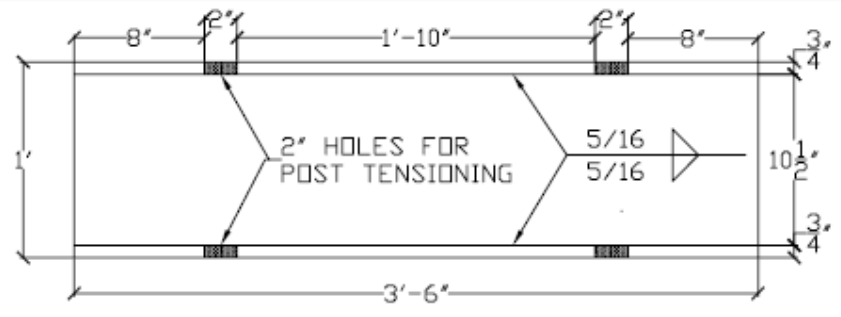


BUILT-UP SECTION FRONT VIEW (COLUMN NOT SHOWN)



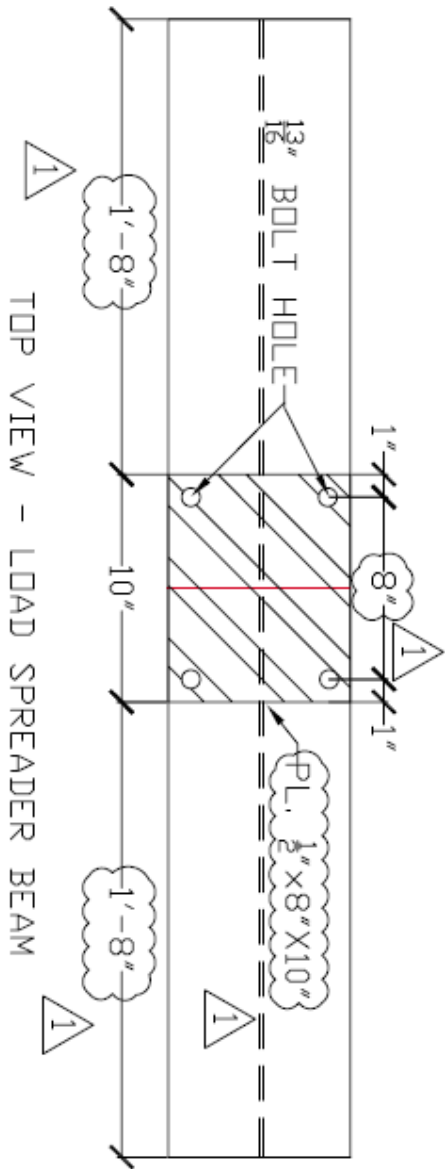
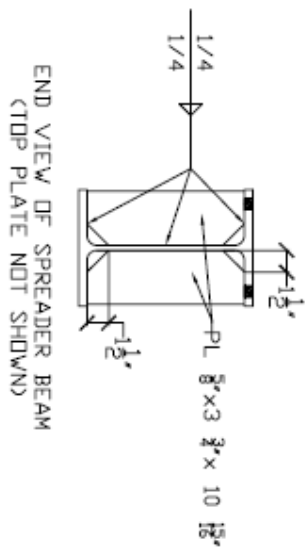
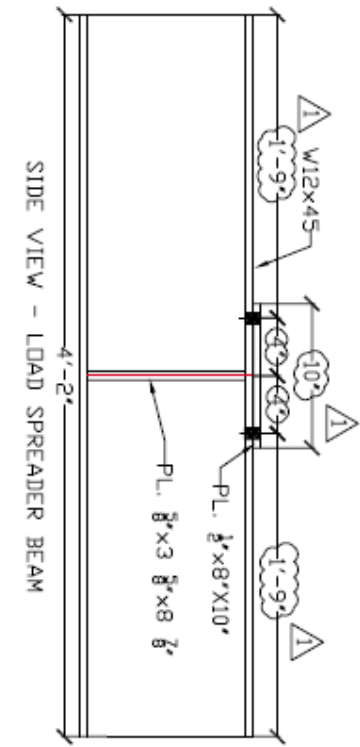
BUILT-UP SECTION FRONT VIEW (COLUMN SHOWN)

NOTE: ALL PLATE STEEL A36

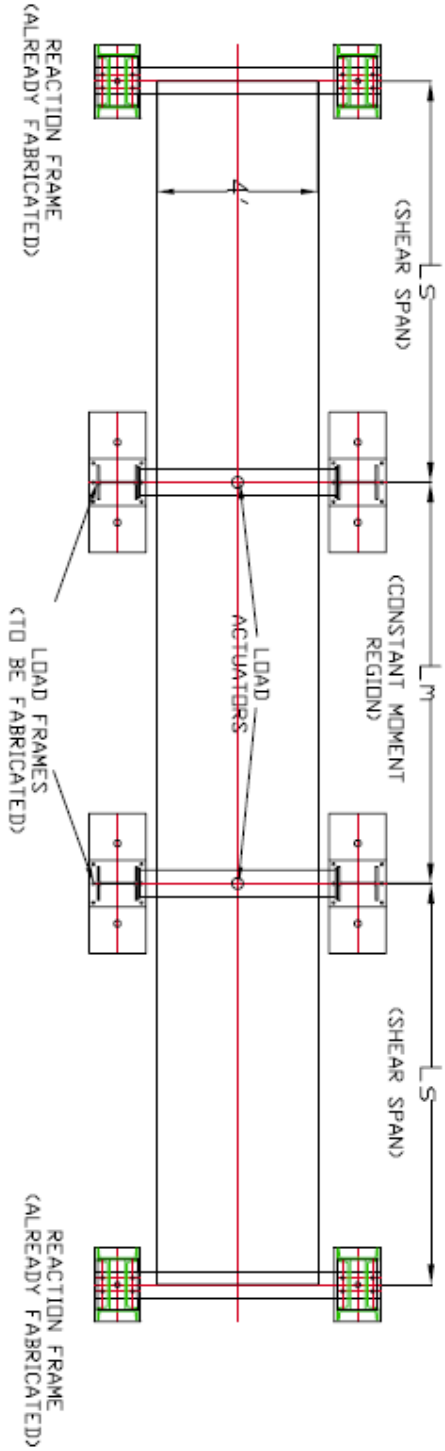


BUILT-UP SECTION SIDE VIEW (ATTACHED COLUMN BASE PLATE NOT SHOWN)
BASE BEAM (BUILT UP SECTION) DETAILS

<p>TEST LOAD FRAMES AISC MSR PROJECT BOWEN LAB</p>		<p>DEPARTMENT OF CIVIL ENGINEERING 550 STADIUM MALL DRIVE WEST LAFAYETTE, IN 47906 PHONE: (765) 494-2224 FAX: (765) 494-0310</p>	DR DEVEN HUBER
			CK ANIL VARMA
			DATE 5/17/06
			SCALE N/A
			FILE SHEET 4 OF 6

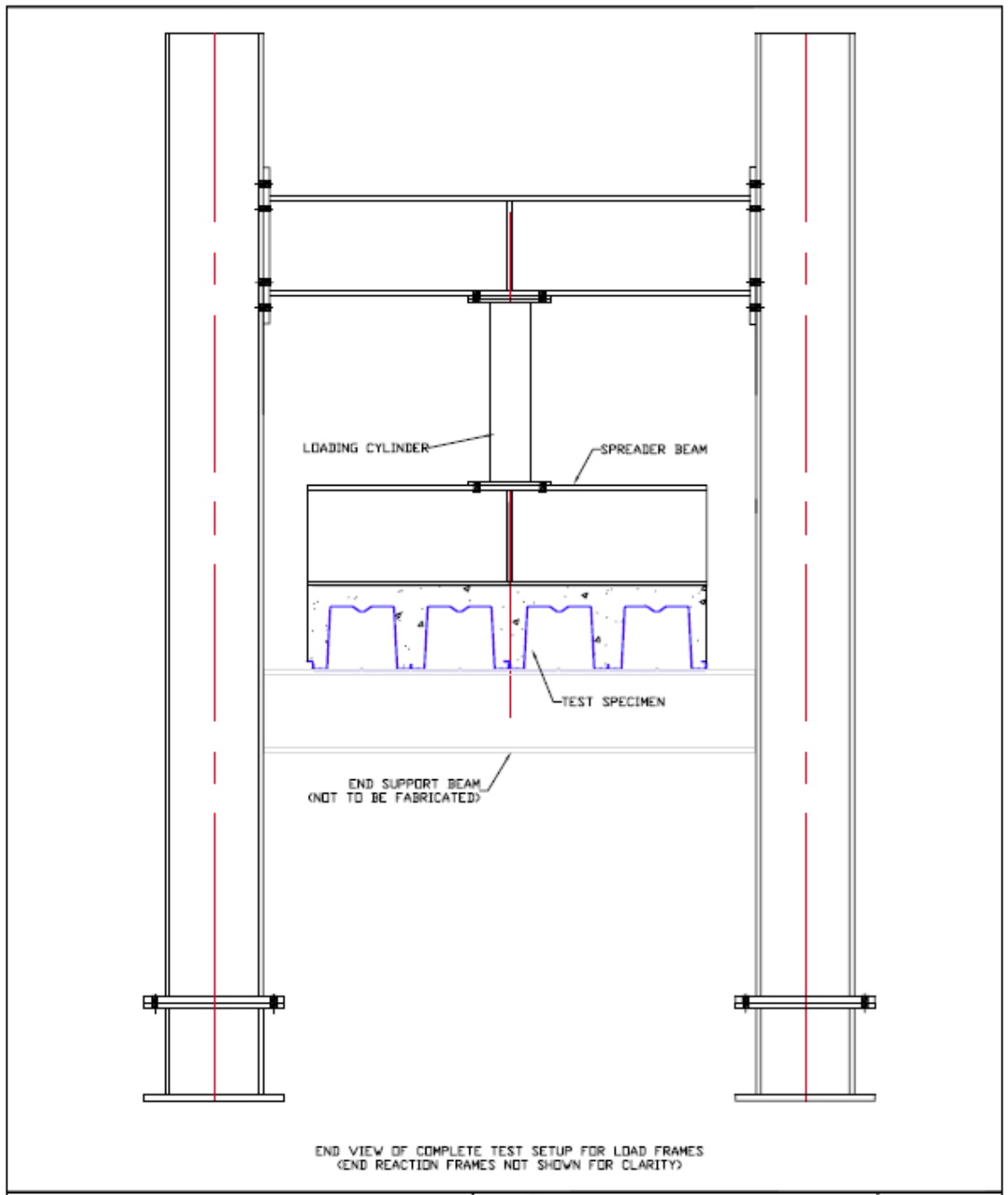


TEST LOAD FRAMES AISC MSR PROJECT BOWEN LAB		PURDUE UNIVERSITY		DEPARTMENT OF CIVIL ENGINEERING 605 FRIEDLAND HALL WEST LAFAYETTE, IN 47907-1334 PHONE: (765) 464-5244 FAX: (765) 464-0380	
REVISION 1 - 9/17/06	Δ				DATE: 9/17/06
SCALE: N/A	DRAWN: AMF/VAJMA				CHECK:
FILE:	SHEET: 5 OF 8				DATE:



OVERALL SCHEMATIC OF TEST SETUP

<p>TEST LOAD FRAMES AISC MSR PROJECT BOWEN LAB</p>	<p>PURDUE UNIVERSITY</p>	<p> DEPARTMENT OF CIVIL ENGINEERING 605 FRAZAR HALL, WEST LAFAYETTE, IN 47907-1336 PHONE: (765) 464-2544 FAX: (765) 464-0386</p>	<p>DR. DAWN HENDER PIE SCALE N/A DATE 8/17/06 FILE REBERT 6 OF 8</p>
--	-------------------------------------	---	--



TEST LOAD FRAMES
AISC MSR PROJECT
BOWEN LAB



DEPARTMENT OF CIVIL ENGINEERING
650 STADIUM MALL DRIVE
WEST LAFAYETTE, IN 47906
PHONE: (765) 494-3224
FAX: (765) 494-0310

DR	DEVIN HUBER
CK	ANIL VARMA
DATE	5/17/06
SCALE	N/A
FILE	SHEET 7 OF 8

BILL OF MATERIALS

PART	QUANTITY	DESCRIPTION
PL. $\frac{3}{4}$ "X1'-5"x3'-6"	8	FLANGES FOR BUILT UP SECTION
PL. $\frac{9}{16}$ "X10 $\frac{1}{2}$ "X3'-6"	8	WEBS FOR BUILT UP SECTION
PL. $\frac{3}{4}$ "X1'-2"x1'-5"	4	END PLATES FOR COLUMN TO BUILT-UP SECTION CONNECTION
PL. $\frac{3}{4}$ "X9"x1'-7"	4	PLATES FOR END PLATE CONNECTIONS
PL. $\frac{5}{8}$ "X3 $\frac{5}{8}$ "X10 $\frac{15}{16}$ "	8	STIFFENER PLATES FOR CROSS BEAM AND SPREADER BEAM
PL. $\frac{1}{2}$ "X8"X10"	6	BEARING PLATES FOR CROSS BEAM AND SPREADER BEAM
W12x53x9'-9"	4	COLUMN SECTIONS
W12x45x4'-10 $\frac{1}{2}$ "	2	CROSS BEAMS
W12x45x4'-2"	2	SPREADER BEAMS
$\frac{3}{4}$ "X2 $\frac{1}{4}$ " A325 BOLT	28	BOLTS FOR SPREADER BEAM BEARING PLATES AND BASE PLATE BOLTS
$\frac{3}{4}$ "X2 $\frac{1}{2}$ " A325 BOLT	32	BOLTS FOR END PLATE CONNECTION
$\frac{3}{4}$ "X2 $\frac{3}{4}$ " A325 BOLT	8	BOLTS FOR CROSS BEAM BEARING PLATES
$\frac{3}{4}$ " A563 GR. DH HEAVY HEX NUT	68	—
$\frac{3}{4}$ " F436 CIRCULAR WASHER	68	—

NOTE: ALL STRUCTURAL SECTIONS TO BE A992 STEEL AND PLATES TO BE A36 UNLESS NOTED OTHERWISE. ALL WELDS E70 ELECTRODES.

TEST LOAD FRAMES
AISC MSR PROJECT

BOWEN LAB

REVISION 1 - 3/17/08



DEPARTMENT OF CIVIL ENGINEERING
650 STADIUM MALL DRIVE
WEST LAFAYETTE, IN 47906
PHONE: (765) 494-3224
FAX: (765) 494-0310

DR	DEVIN HUBER
CK	AMIT VARMA
DATE	5/17/08
SCALE	N/A
FILE	SHEET 5 OF 6

Appendix C.

Mill Certifications for Steel Material, Tension Results for Steel Material, and concrete batch tickets.

Concrete Batch Mixes for Specimens

Batch tickets from the ready mixer are provided for some of the concrete pours that were done for the deep deck specimens and the PLSS Specimen.

TRUCK	USER LOGIN	DISP	TICKET NUM	TICKET NUM	TICKET ID	TIME	DATE
1677	USER		1814742	94275	92345	09:56	07/24/2006
LOAD SIZE	MIX CODE					SEQ	LOAD ID
5.00 yd	292					D	94542
MATERIAL	DESIGN QTY	REQUIRED	BATCHED	VAR	% VAR	%MOISTURE	ACTUAL WAT
HAYDITE	850 lb	4250 lb	4240	-10	-0.24%		
SAND-23	1400 lb	7280 lb	7240	-40	-0.55%	4.000% M	33.37 gl
CEMENT	650 lb	3250 lb	3240	-10	-0.31%		
SUPER1	7.00 /C	227.50 oz	228.00	0.50	0.22%		
AIR	0.10 /C	3.25 oz	3.50	0.25	7.69%		
WATER	245.0 lb #	945.0 lb	944.0	-1.0	-0.11%		113.12 gl
NON-SIMULATED NUM BATCHES: 1							
LOAD TOTAL: 15679 lb DESIGN W/C: 0.377 WATER/CEMENT: 0.378T DESIGN WATER: 146.8 gl ACTUAL WATER: 146.5 gl TO ADD: 0.3 gl							
SLUMP: 6.00 " WATER IN TRUCK: 0.0 gl ADJUST WATER: 0.0 gl /load TRIM WATER: 0.0 gl /yd							

Figure C.1: Concrete batch ticket for CC-DD Specimen 1

TRUCK	USER LOGIN	DISP	TICKET NUM	TICKET NUM	TICKET ID	TIME	DATE
1673	USER		1821630	97932	99488	10:37	05/16/2007
LOAD SIZE	MIX CODE					SEQ	LOAD ID
3.50 yd	292					D	101839
MATERIAL	DESIGN QTY	REQUIRED	BATCHED	VAR	% VAR	%MOISTURE	ACTUAL WAT
HAYDITE	850 lb	2975 lb	2940	-35	-1.18%		
SAND-23	1400 lb	5096 lb	5080	-16	-0.31%	4.000% M	23.41 gl
CEMENT	650 lb	2275 lb	2265	-10	-0.44%		
SUPER1	7.00 /C	159.25 oz	160.00	0.75	0.47%		
AIR	0.10 /C	2.28 oz	2.00	-0.28	-12.28%		
WATER	210.0 lb #	539.0 lb	526.0	-13.0	-2.41%		63.03 gl
NON-SIMULATED NUM BATCHES: 1							
LOAD TOTAL: 10022 lb DESIGN W/C: 0.323 WATER/CEMENT: 0.324T DESIGN WATER: 88.1 gl ACTUAL WATER: 86.4 gl TO ADD: 1.6 gl							
SLUMP: 6.00 " WATER IN TRUCK: 0.0 gl ADJUST WATER: 0.0 gl /load TRIM WATER: 0.0 gl /yd							
NOTE: Manual Feed Occurred.							

Figure C.2: Concrete batch ticket for CC-DD Specimen 4

TRUCK	USER LOGIN	DISP	TICKET NUM	TICKET NUM	TICKET ID	TIME	DATE
1639	USER		1822796	99044	100710	10:05	06/29/2007
LOAD SIZE	MIX CODE					SEQ	LOAD ID
5.00 yd	292					D	103089
MATERIAL	DESIGN QTY	REQUIRED	BATCHED	VAR	% VAR	%MOISTURE	ACTUAL WAT
HAYDITE	850 lb	4250 lb	4260	10	0.24%		
SAND-23	1400 lb	7280 lb	7240	-40	-0.55%	4.000% M	33.37 gl
CEMENT	650 lb	3250 lb	3260 *	10	0.31%		
SUPER1	7.00 /C	227.50 oz	228.00	0.50	0.22%		
AIR	0.20 /C #	6.50 oz	6.50	0.00	0.00%		
WATER	225.0 lb #	845.0 lb	838.0	-7.0	-0.83%		100.42 gl
NON-SIMULATED NUM BATCHES: 1							
LOAD TOTAL: 15613 lb DESIGN W/C: 0.346 WATER/CEMENT: 0.345T DESIGN WATER: 134.8 gl ACTUAL WATER: 133.8 gl TO ADD: 1.0 gl							
SLUMP: 6.00 " WATER IN TRUCK: 0.0 gl ADJUST WATER: 0.0 gl /load TRIM WATER: 0.0 gl /yd							

Figure C.3: Concrete batch ticket for SC-DD Specimen

TRUCK	USER LOGIN	DISP	TICKET NUM	TICKET NUM	TICKET ID	TIME	DATE
0412	USER	1636378	57632	63900		15:06	02/26/2008
LOAD SIZE	MIX CODE					SEQ	LOAD ID
3.00 yd	292					D	65413
MATERIAL	DESIGN QTY	REQUIRED	BATCHED	VAR	% VAR	XMOISTURE	ACTUAL WAT
HAYDITE	850 lb	2550 lb	2540 lb	-10	-39%		
SAND-23	1400 lb	4368 lb	4420 lb	52	1.19%	4.000% M	20.37 gl
CEMENT	650 lb	1950 lb	1940 lb	-10	-51%		
AIR	0.10 /C	1.95 oz	0.00 oz	-1.95	-100.00%		
SUPER1	7.00 /C	136.50 oz	136.00 oz	-50	-37%		
WATER	190.0 lb #	393.1 lb	372.0 lb	(-21.1	-5.37%		44.50 gl
NON-SIMULATED NUM BATCHES: 1							
LOAD TOTAL: 9281 lb DESIGN W/C: 0.292 WATER/CEMENT: 0.294T DESIGN WATER: 68.3 gl ACTUAL WATER: 64.9 gl TO ADD: 3.4 gl							
SLUMP: 6.00 " WATER IN TRUCK: 0.0 gl ADJUST WATER: 0.0 gl /load TRIM WATER: 0.0 gl /yd							
NOTE: Manual Feed Occurred.							

Figure C.4: Concrete batch ticket for combined heating and loading Specimen

TRUCK	USER LOGIN	DISP	TICKET NUM	TICKET NUM	TICKET ID	TIME	DATE
1639	USER	1636954	58246	64623		15:04	03/17/2008
LOAD SIZE	MIX CODE					SEQ	LOAD ID
4.50 yd	185					D	66071
MATERIAL	DESIGN QTY	REQUIRED	BATCHED	VAR	% VAR	XMOISTURE	ACTUAL WAT
P-GRAVEL	1850 lb	8325 lb	8300 lb	-25	-30%		
SAND-23	1400 lb	6552 lb	6580 lb	28	0.43%	4.000% M	30.33 gl
CEMENT	611 lb	2750 lb	2740 lb	-10	-36%		
REDUCER	2.00 /C	54.99 oz	55.00 oz	0.01	0.02%		
WATER	210.0 lb #	768.1 lb	776.0 lb	7.9	1.03%		92.99 gl
NON-SIMULATED NUM BATCHES: 1							
LOAD TOTAL: 18400 lb DESIGN W/C: 0.344 WATER/CEMENT: 0.376A DESIGN WATER: 113.2 gl ACTUAL WATER: 123.3 gl TO ADD: 0.0 gl							
SLUMP: 6.00 " # WATER IN TRUCK: 0.0 gl ADJUST WATER: 0.0 gl /load TRIM WATER: 0.0 gl /yd							

Figure C.5: Concrete batch ticket for PLSS System

Mill Certifications for steel deck components

Mill certification collected for all steel deck material is provided in this appendix.

02:57 03-10 To: 18035402246 From: NUCOR STEEL -HUGER Page 1 of 3

**FAX 1-803-540-2246 DELIVER TO: MATERIALS MANAGEMENT SYSTEMS, INC.

HQA

METALLURGICAL TEST REPORT
 Nucor Steel - Berkeley
 a division of NUCOR corporation

Phone: 843-336-6000
 Sales Fax: 843-336-6150

P.O. Box 2259
 Mt. Pleasant, SC 29465

Sold CONSOLIDATED SYSTEMS, INC. Ship CONSOLIDATED SYSTEMS, INC. Ship date 3/10/05
 To: P.O. BOX 1756 To: 650 ROSEWOOD DRIVE Bill of Lading # 439758
 ATTN: ACCOUNTS PAYABLE Vehicle # CSX7495050
 COLUMBIA, SC 29202 COLUMBIA, SC 29201

Gauge x Width .0710 MIN X 55.5000 MIN CRGALV P/O # 546305
 Description ASTM A653 S540 G90 No Welds Mill Order # 142232-1
 Testing performed: ASTM A653 S540 Part # 0710-55500-G090

(in percent)

Heat	C	Mn	P	S	Si	Cu	Ni	Cr	Mo	In	Al	V	Nb	N	Ti	B	Ca
1501957	.06	.38	.010	.003	.03	.09	.04	.04	.01	.007	.033	.001	.002	.007	.003	.000	.005

Coil Number	YIELD STRENGTH (ksi)		TENSILE STRENGTH (ksi)		ELONGATION	HARDNESS	VALUES	
	longitudinal	transverse	longitudinal	transverse	(% IN 2")	(Rockwell B)	n	r
465203.000	48.1	.0	60.6	.0	33	68	.1710	

Coil Numbers 465203.000

All material is sold subject to the description, specifications and terms and conditions set forth on the face and reverse side of Nucor Steel - Berkeley's sales order acknowledgment.

Tensile Testing is performed in accordance with ASTM A-370 specifications. Specimen is machined to standard rectangular test configuration (Figure 3 of ASTM A-370) with a 2" gage length. Yield Strength is determined at 0.2% offset.

This material has been produced in compliance with the chemistry and established rolling practices of the ordered specification. If material is ordered to a chemical composition only and if physical testing is not a requirement of the customer's order, testing is not performed by the producer.

We hereby certify the above information is correct as contained in the records of the corporation.
 Randall C Krause Rod Marrassini ** 100% MELTED AND MANUFACTURED IN THE USA **
 Hot Mill Metallurgist Cold Mill Metallurgist

Randall C. Krause

Figure C.6: Mill Certification for 14 gage deck material used in CC-DD Specimens

AK Steel RightFax 3/28/2005 8:18 AM PAGE 23/20 RightFax



AK Steel
CUSTOMER COPY

AK Steel Corporation
METALLURGICAL TEST REPORT
MIDDLETOWN WORKS
MIDDLETOWN, OH 45043

PAGE 1 OF 1
LOAD NO. 7346376
SRN NO. 7346376

C U S T O M E R	CONSOLIDATED SYSTEMS, INC PUR DEPT P O BOX 1756 COLUMBIA, SC 29202-1756	S CONSOLIDATED SYSTEMS, INC CSI H 650 ROSEWOOD DR P COLUMBIA, SC 29201 T O													
MILL ORDER NO. 47555453-0888	PROCESSOR ORDER NO. S46392	BUYERS ORDER NO. S46392	PART NO. 0570-55250-G090-CDRC	SEQ NO.											
16 GA ENGLISH UNITS .0570 MIN 55.2500 X COIL		-PRODUCT SIZE-													
CHEMICAL ANALYSIS OF LADLE TEST															
HEAT # 251370	C .19	MN .47	P .007	S .013	SI .005	CU .031	AL .044	CB .001	V .001	NI .014	CR .050	TI .001	N .0000	MO .004	B .000
LIFT ID: 552814-02AB	WGT: 23,450 LBS.		SHIPPING DATE: 03/27/2005												
PRODUCT DESCRIPTION															
ZINGRIP GALV SHT G90 SS GRADE 40 MIN SPANGLE CHEM TREATED DRY TEST REPORTS ASTM A653/A653M-04A GR 40 SS (AKS CODE T99)															
LONGITUDINAL KSI															
YIELD STRENGTH	47.7														
TENSILE STRENGTH	65.7														
% ELONG:	34.2														
WGT OF COATING TESTS: TOP (OZ/SQ FT): E: 0.48 C: 0.48 E: 0.48															
BOTTOM (OZ/SQ FT): E: 0.49 C: 0.48 E: 0.49					AVG: 0.97										
TOP (GM/SQ M): E: 146.00 C: 145.00 E: 147.00															
BOTTOM (GM/SQ M): E: 150.00 C: 147.00 E: 149.00					AVG: 295.00										
THE CHEMICAL ANALYSIS AND PHYSICAL OR MECHANICAL TESTS REPORTED ABOVE ARE CORRECT AS CONTAINED IN THE RECORDS OF THE CORPORATION ALL TESTING IS DONE IN ACCORDANCE WITH A.S.T.M. STANDARDS UNLESS OTHERWISE NOTED AK Steel Corporation MWQC#0004 REV:2, 7/98					THIS CERTIFIED TEST REPORT HAS BEEN DELIVERED TO A CONSIGNEE OF MATERIAL PURCHASED FROM AK Steel Corporation. TO AVOID THE POSSIBILITY OF ITS MISUSE ON REDELIVERY OF THE REPORT TO A THIRD PARTY MUST BE RECERTIFIED BY AND UNDER THE NAME OF SUCH CONSIGNEE. SIGNED <i>[Signature]</i> DATE 03/28/2005										

Figure C.7: Mill Certification for 16 gage bottom plate material used in CC-DD Specimens

United States Steel Corporation
01.000.072 (REV 3/02)

REG. JOB CONTRACT NO. _____

PRM: GER-M SWG: STEEL SOLD
FAIRFIELD WORKS
P.O. BOX 599
FAIRFIELD, ALABAMA 35064

SHIP DATE: 06-27-05
PURCHASE ORDER NO: 846556-01
BILL ORDER NO: BF80044
INVOICE NO: 488-319724

SOLD TO: CONSOLIDATED SYSTEMS INC
ATTN ACCOUNTS PAYABLE
COLUMBIA SC 29202-1756

SPEC: GALVANIZE CARBON ASTM A653-04A BR 40 APPROVED SS AS COATED
MSP: GF40SK55 SEMI-EXPOSED PRIME SIDE IN 860 REGULAR SPANGLE CHEM
TREAT DRY NO PICKLE WELDS YS MIN 40. KSI TS MIN 55. KSI EL MIN
INSP: 0.1 MILL INSPECTION RA/SN ALSO RA/LT REPORT TENSILES-KSI,

Metallurgical Test Report

THIS IS TO CERTIFY THAT THE PRODUCT DESCRIBED HEREIN WAS INSPECTED, SAMPLED, TESTED AND/OR THE SPECIFICATION AND FULFILLS REQUIREMENTS IN SUCH RESPECT.

PREPARED BY THE OFFICE OF:
R.W. FEWERS-GEN. MGR., B. A. DATE: _____

ITEM NO	GAGES	MATERIAL DESCRIPTION	QUANTITY	WEIGHT	HEAT NO.	TEST OR PICE IDENTITY	YIELD STRENGTH	ELONGATION %	
								IN 8"	IN 2"
01	.0450	46.5000 COIL	01	22570	X03616	6122066	52.0	29.7	
01	.0450	46.5000 COIL	01	22480	X03616	6122067	52.0	29.7	
01	.0450	46.5000 COIL	01	23230	C05911	6121704	62.5	28.1	
01	.0450	46.5000 COIL	01	23310	C05911	6121705	62.5	28.1	

YIELD STRENGTH @ 0.2% OFFSET
16 TEST REPORT SHALL NOT BE REPRODUCED WITHOUT THE PRIOR WRITTEN APPROVAL OF THE USS CORPORATION.
HEAT 13 049 011 011 013 02
HEAT 15 049 007 009 010 02
C/MEN PREPARATION AND TESTING PERFORMED IN ACCORDANCE WITH ASTM E8-03
3-01, ASTM E18-03, ASTM E1019-00 BY U.S. STEEL FAIRFIELD WORKS. IF ORDERED TO A J.I.S. SPECIFICATION THE
C/MEN PREPARATION AND TESTING IS PERFORMED IN ACCORDANCE WITH J.I.S. E2241 & E2241 USING A NO. 5
DE BY STAVELEY SERVICES GARY IN. IF MATERIAL IS ORDERED AS COATED PRODUCT AND FINISH IS NOT SPECIFIED
3ER- PRODUCTION AND TESTING PERFORMED BY DOUBLE G CALIBR FORMERLY...
11X
DECIMAL POSITIONS FOR ELEMENTS ARE INDICATED BY DOUBLE G CALIBR FORMERLY...
1429 70070000

Figure C.8: Mill Certification for 18 gage steel deck material used in CC-DD Specimens


United States Steel Corporation
Metallurgical Test Report

01.000.0772 (REV. 01/62)

THIS IS TO CERTIFY THAT THE PRODUCT DESCRIBED HEREIN WAS MFGD., SAMPLED, TESTED AND/OR INSPECTED IN ACCORDANCE WITH THE SPECIFICATION AND FILLS REQUIREMENTS IN SUCH RESPECT.
 PREPARED BY THE OFFICE OF: R.W. FLOWERS GEN. MGR., D. A.

NO. DATE PURCHASE ORDER NO. SHIPPER NO. MAIL ORDER NO. INVOICE NO.
 102844 05 21 04 8891411 488-271921
 22254HY TN

SHIP TO: CONSOLIDATED SYSTEMS
 2990 TEM TEX BLVD
 TERRELL TX 75160-1756

SHIP FROM: CONSOLIDATED SYSTEMS
 2990 TEM TEX BLVD
 TERRELL TX 75160-1756

DATE: _____

SPEC. GALVANIZE CARBON ASTM A653-02A GR 40 APPROVED SS AS COATED
 INSP. GF40SK35 SEMI-EXPOSED PRIME SIDE IN G90 REBULAR SPANGLE CHEM
 TREAT DRY NO PICKLE WELDS Y8 MIN 40. KSI TS MIN 55. KSI EL MIN
 16. % EL DIST 2 INCHES
 INSP:01 MILL INSPECTION RA/SN ALSO RA/LT REPORT TENSILES-KSI,

ITEM NO.	MATERIAL DESCRIPTION		QUAN- TITY	WEIGHT	HEAT NO.	TEST OR PECE IDENTITY	YIELD FL. KSI	TENSILE STR. KSI	ELONGATION % IN 8" IN 2"	% RED. OF AREA
	THICKNESS OR TENSIL	LENGTH								
01	.0340	48.0000 COIL	01	24340	X83403	8850903	50.0	57.5	33.4	
01	.0340	48.0000 COIL	01	24350	X83405	8850905	51.5 50.0	58.0 57.5	34.6 33.4	

YIELD STRENGTH @ 0.2% OFFSET
 THIS TEST REPORT SHALL NOT BE REPRODUCED WITHOUT THE PRIOR WRITTEN APPROVAL OF THE USS CORPORATION.

HEAT NO. X83405
 THE C HEAT 08 039 008 008 009 D1
 CU N S 3
 DO 03 006007 042005 0010003 001 001 002

SPECIMEN PREPARATION AND TESTING PERFORMED IN ACCORDANCE WITH ASTM E8-03. ASTM E646-00, ASTM E415-99, ASTM A343-01, ASTM E18-03, ASTM E1019-03, BY U.S. STEEL FAIRFIELD WORKS. IF ORDERED TO A J.I.S. SPECIFICATION THE SPECIMEN PREPARATION AND TESTING IS PERFORMED IN ACCORDANCE WITH J.I.S. Z2201 & Z2241 USING A NO. 5 TEST PIECE BY STAVELEY SERVICES BARK. IN. IF MATERIAL IS ORDERED AS COATED PRODUCT AND IDENTIFIED WITH A "C" NUMBER PRODUCTION AND TESTING PERFORMED BY DOUBLE G CHATING COMPANY JACKSON, MS.

MATRIX 040-581
 1250 700394250 035104
 DECIMAL POSITIONS FOR ELEMENTS ARE INDICATED BY THE LEFT MARGIN, VERTICAL DOTTED LINE OR DECIMAL POINT. 1 OF 1.

Figure C.9: Mill Certification for 20 gage bottom plate material used in CC-DD Specimens

Measured Mechanical Properties of Steel Material

This section presents results from tension coupon testing of the steel deck material. The main parameters of interest from these tests were the yield and ultimate stresses. All tests were performed according to ASTM Specification E8. An extensometer was used in measuring elongations. Both a strain gage and extensometer were used in estimating yield stress. The Extension Under Load Method given in Section 7.2.2 of the Specification was used in estimating yield stress. Sheet type coupons were machined with a 2.5 in. gage length and 0.5 in. gage width.

Table C.1: Measured yield stress and tensile stress for 14 gage steel material taken from CC-DD Specimens

Estimated Parameter	Coupon 1	Coupon 2	Coupon 3
Yield Stress Strain Gage (psi)	55333	51228	54301
Yield Stress Extensometer (psi)	52852	51220	54273
Tensile Stress (psi)	62822	60713	62762

Table C.2: Measured yield stress and tensile stress for 16 gage steel material taken from CC-DD Specimens

Estimated Parameter	Coupon 1	Coupon 2
Yield Stress Strain Gage (psi)	46420	45205
Yield Stress Extensometer (psi)	45777	44866
Tensile Stress (psi)	62575	60911

Table C.3: Measured yield stress and tensile stress for 18 gage steel material taken from CC-DD Specimens

Estimated Parameter	Coupon 1	Coupon 2
Yield Stress Strain Gage (psi)	43736	49017
Yield Stress Extensometer (psi)	43871	48725
Tensile Stress (psi)	62947	64966

Table C.4: Measured yield stress and tensile stress for 20 gage steel material taken from CC-DD Specimens

Estimated Parameter	Coupon 1	Coupon 2
Yield Stress Strain Gage (psi)	42453	41268
Yield Stress Extensometer (psi)	42616	38997
Tensile Stress (psi)	53420	51548

Table C.5: Measured yield stress and tensile stress for 18 gage steel material taken from CC-DD Specimens

Estimated Parameter	Coupon 1	Coupon 2	Coupon 3	Coupon 4	Coupon 5	Coupon 6	Coupon 7	Coupon 8
Yield Stress Strain Gage (psi)	31050	28630	30197	29759	30183	30470	32412	30930
Yield Stress Extensometer (psi)	31037	28468	29944	30169	30270	29294	32346	30778
Tensile Stress (psi)	42326	37731	39978	39597	41979	40944	42776	41806

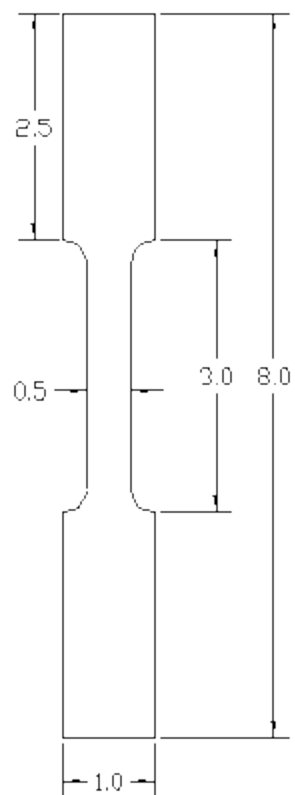


Figure C.10: Nominal dimensions of steel deck tension coupons

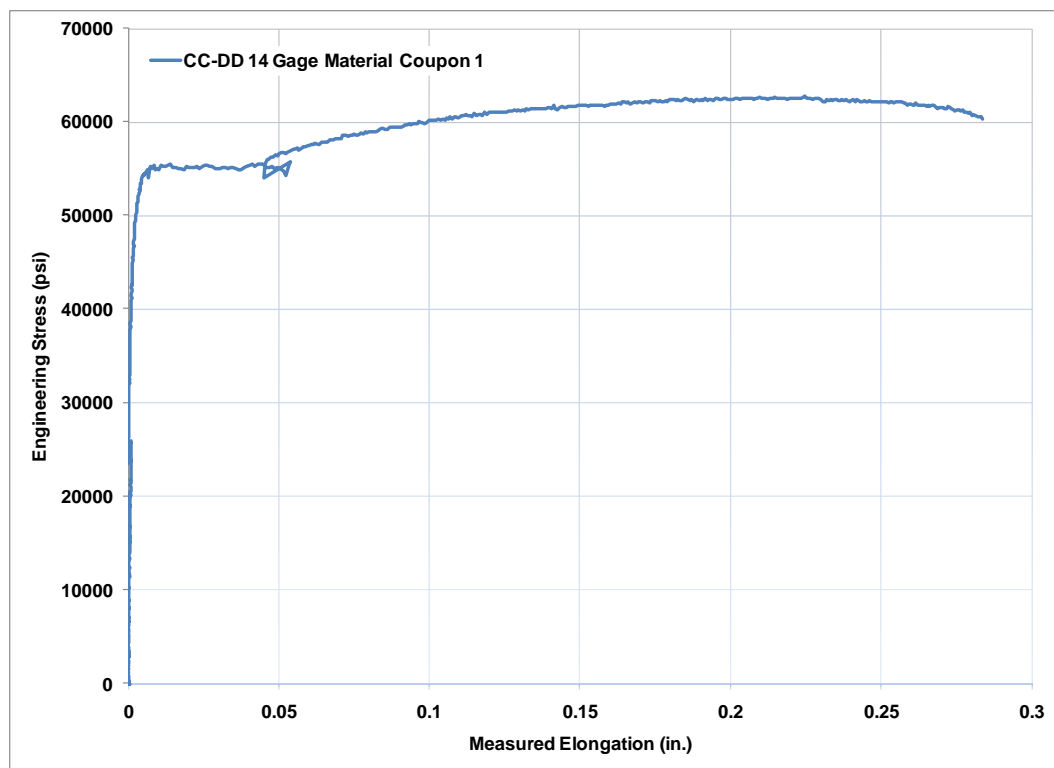


Figure C.11: Engineering stress vs. measured elongation CC-DD 14 Gage Material Coupon 1

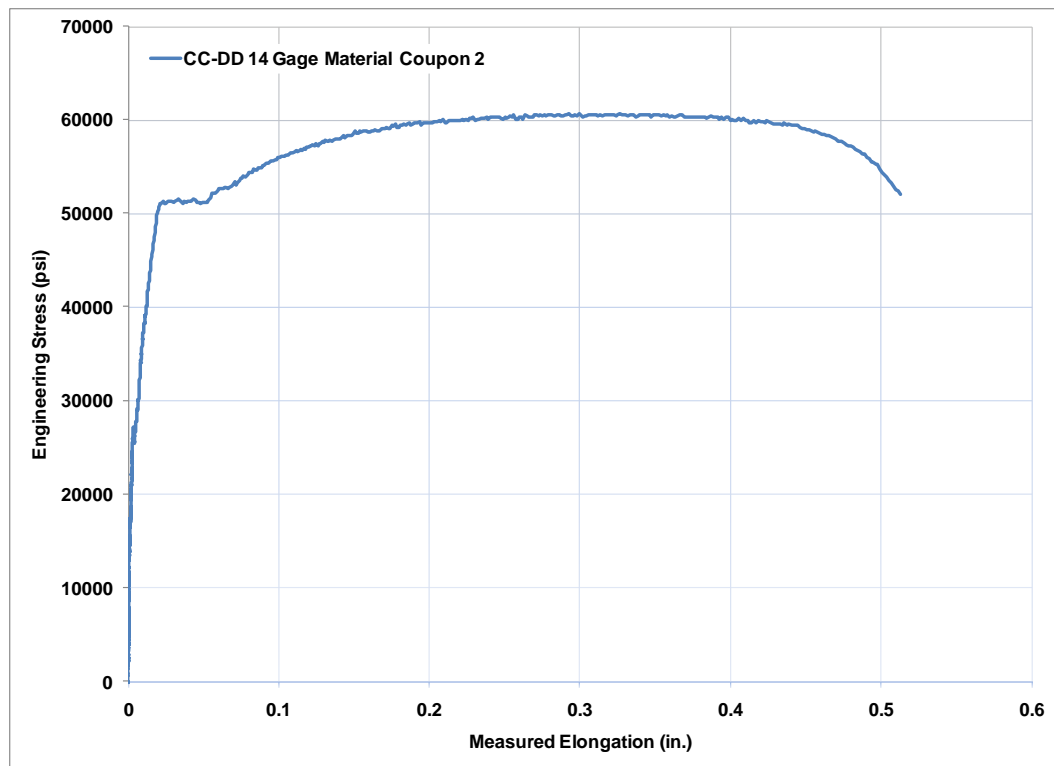


Figure C.12: Engineering stress vs. measured elongation CC-DD 14 Gage Material Coupon 2

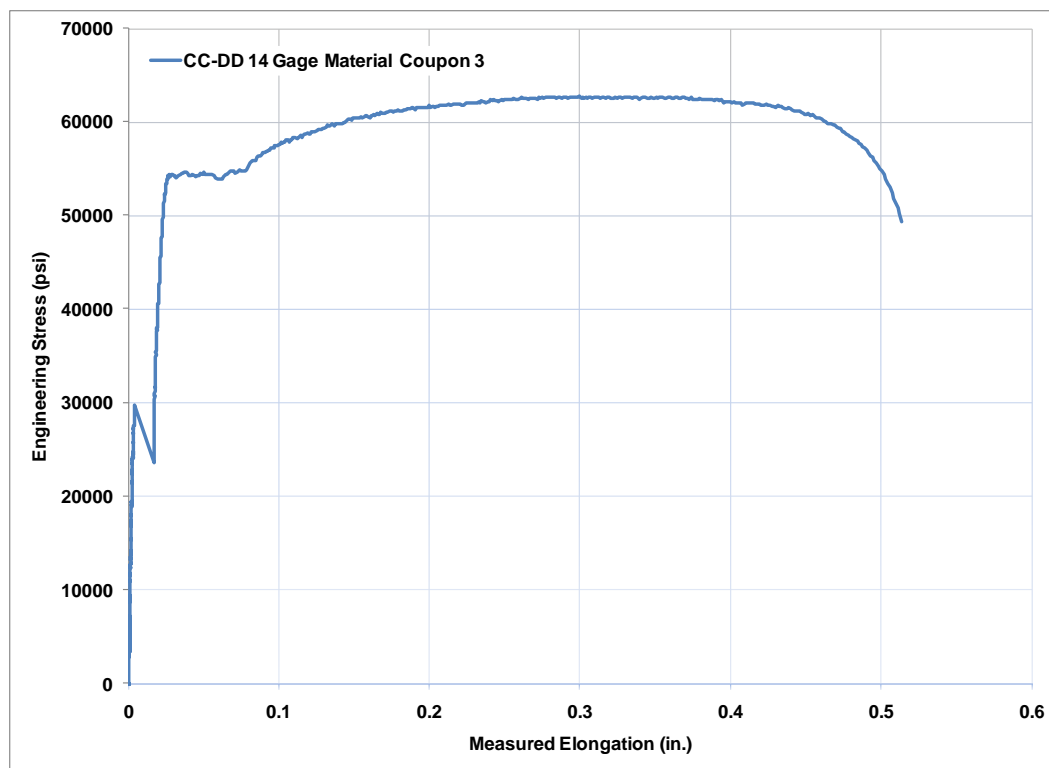


Figure C.13: Engineering stress vs. measured elongation CC-DD 14 Gage Material Coupon 3

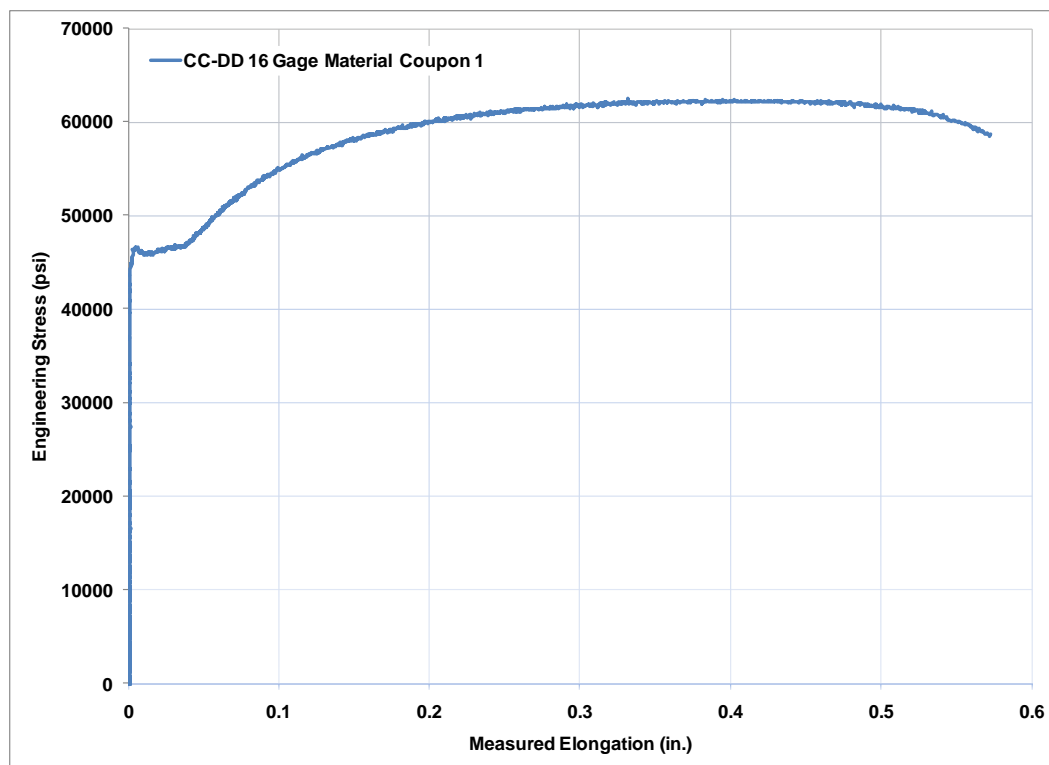


Figure C.14: Engineering stress vs. measured elongation CC-DD 16 Gage Material Coupon 1

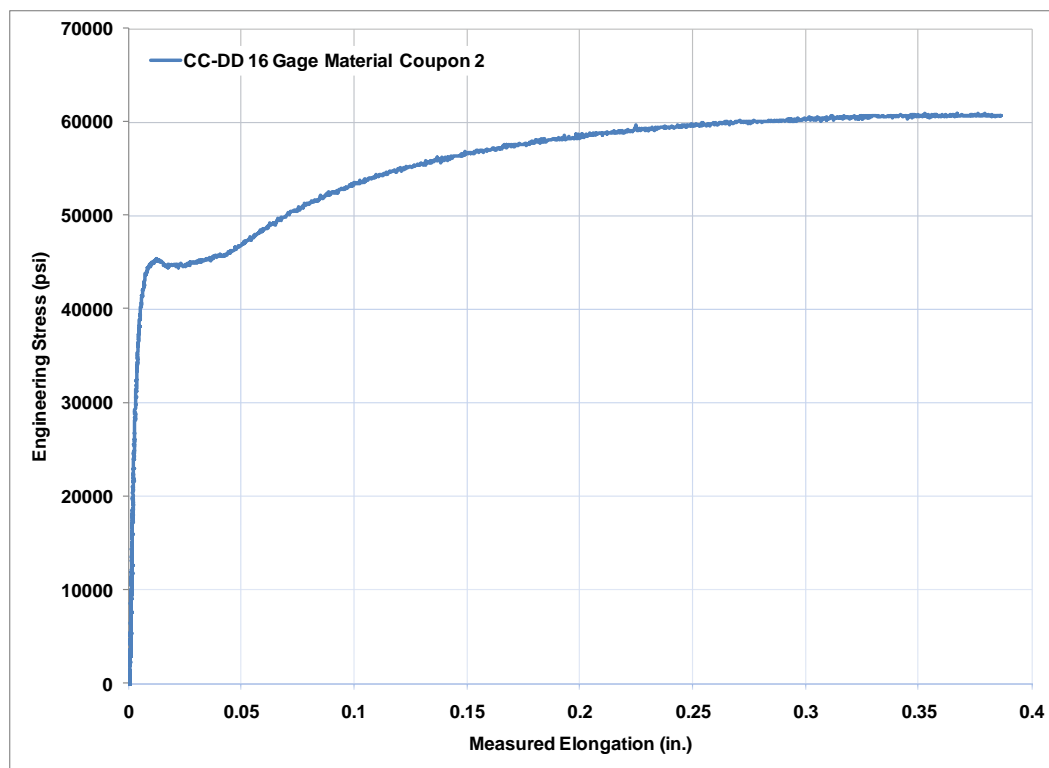


Figure C.15: Engineering stress vs. measured elongation CC-DD 16 Gage Material Coupon 2

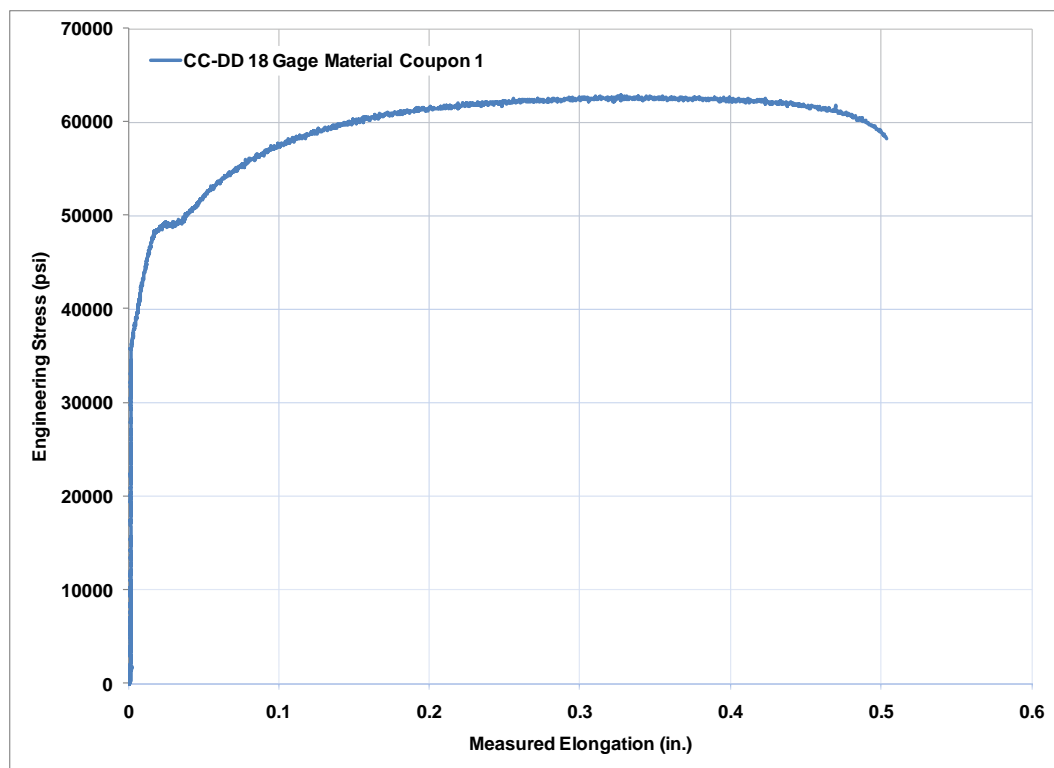


Figure C.16: Engineering stress vs. measured elongation CC-DD 18 Gage Material Coupon 1

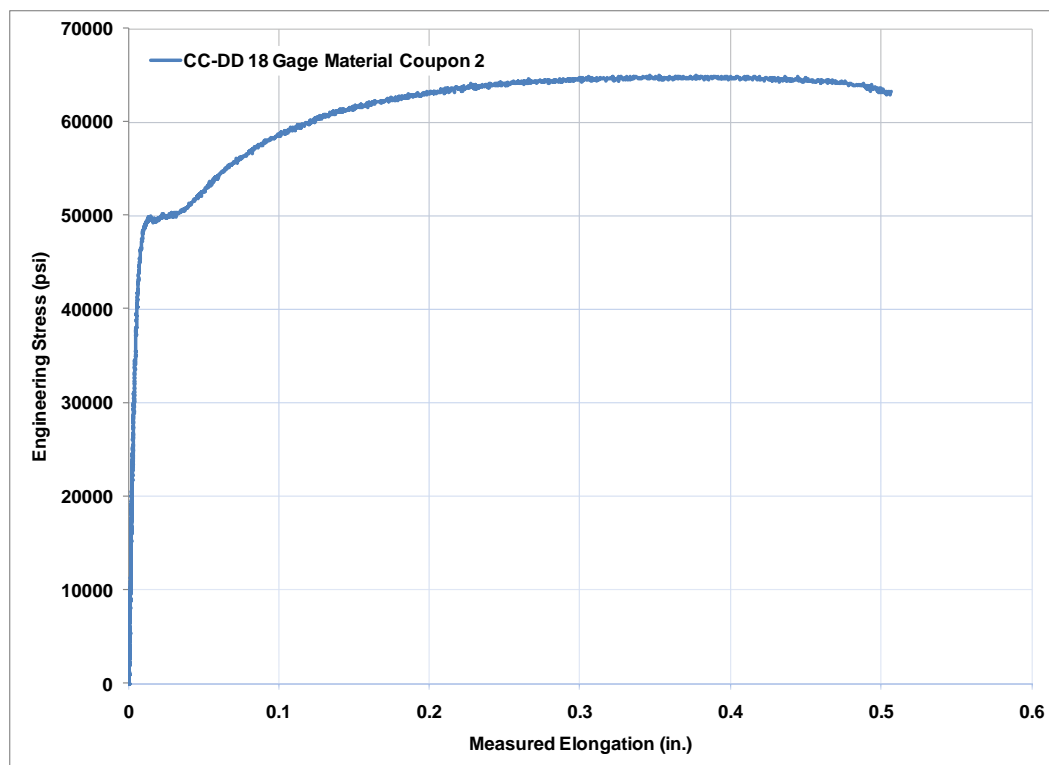


Figure C.17: Engineering stress vs. measured elongation CC-DD 18 Gage Material Coupon 2

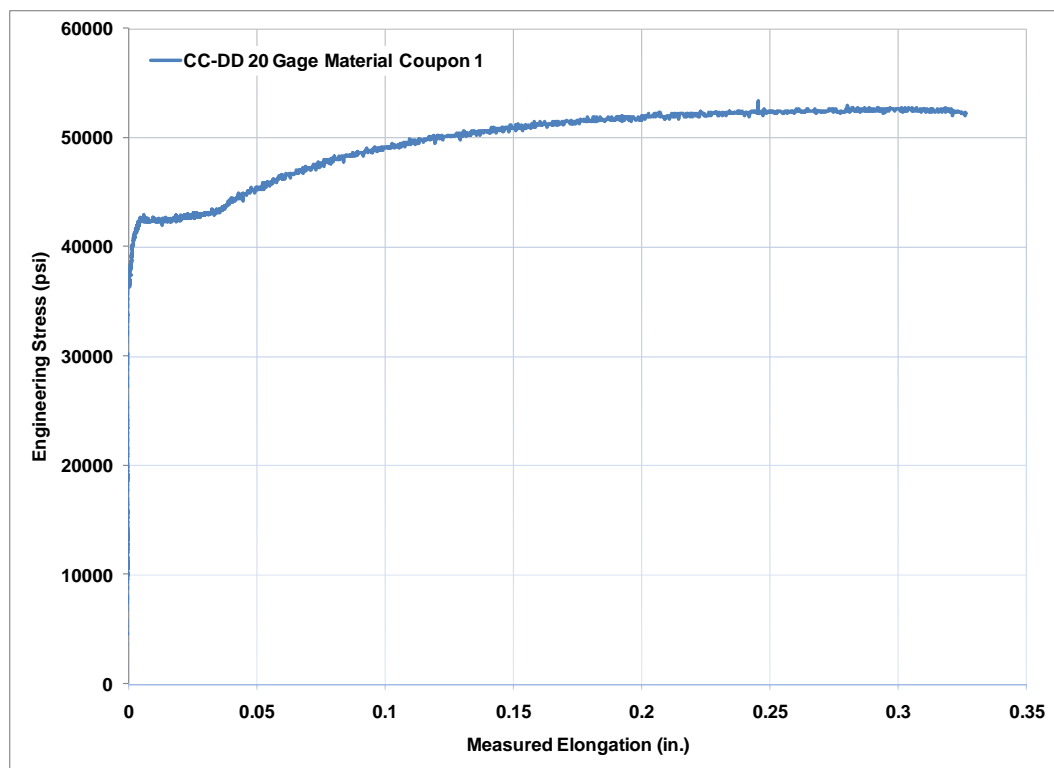


Figure C.18: Engineering stress vs. measured elongation CC-DD 20 Gage Material Coupon 1

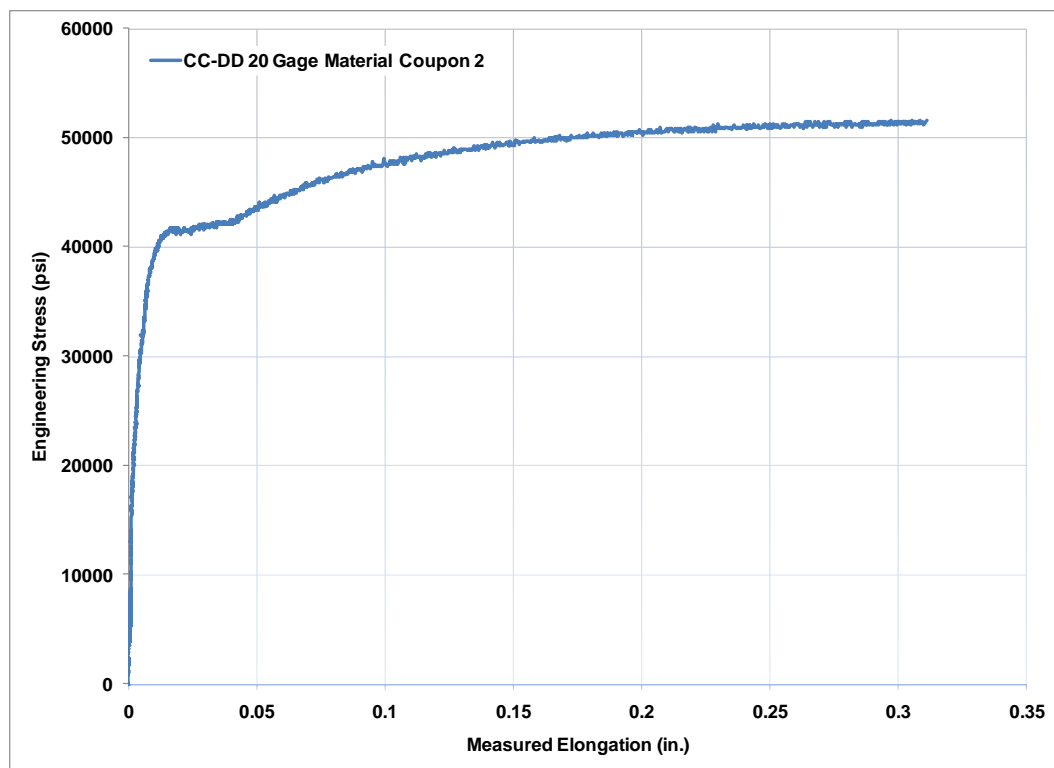


Figure C.19: Engineering stress vs. measured elongation CC-DD 20 Gage Material Coupon 2

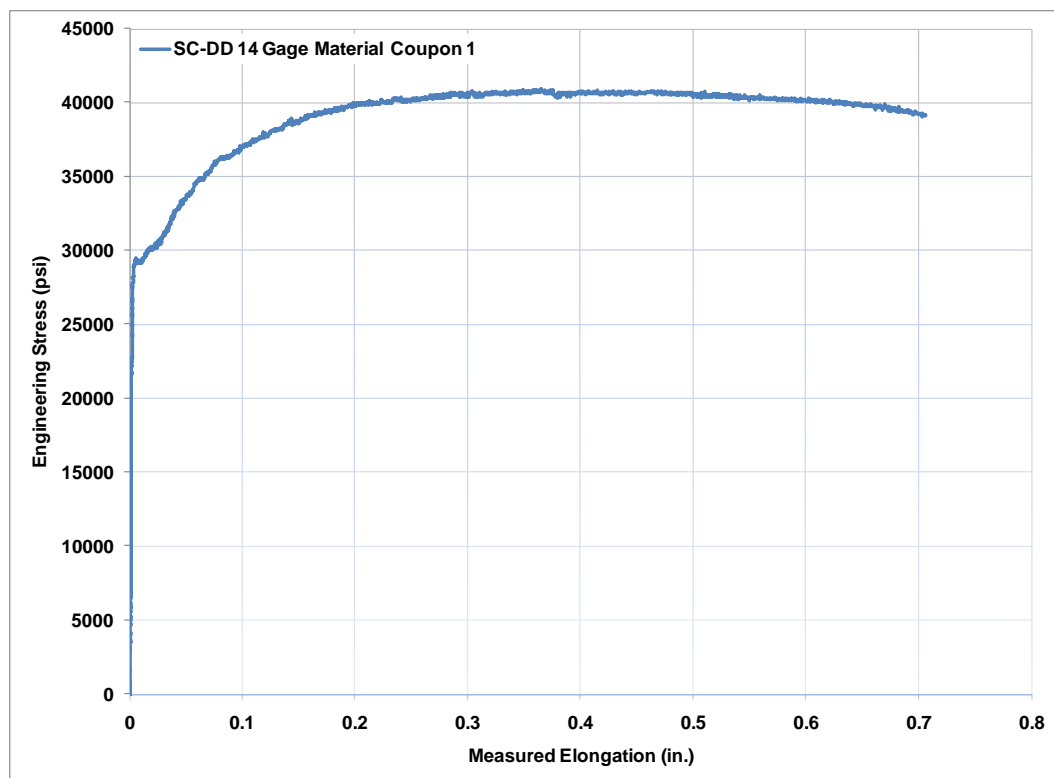


Figure C.20: Engineering stress vs. measured elongation SC-DD 14 Gage Material Coupon 1

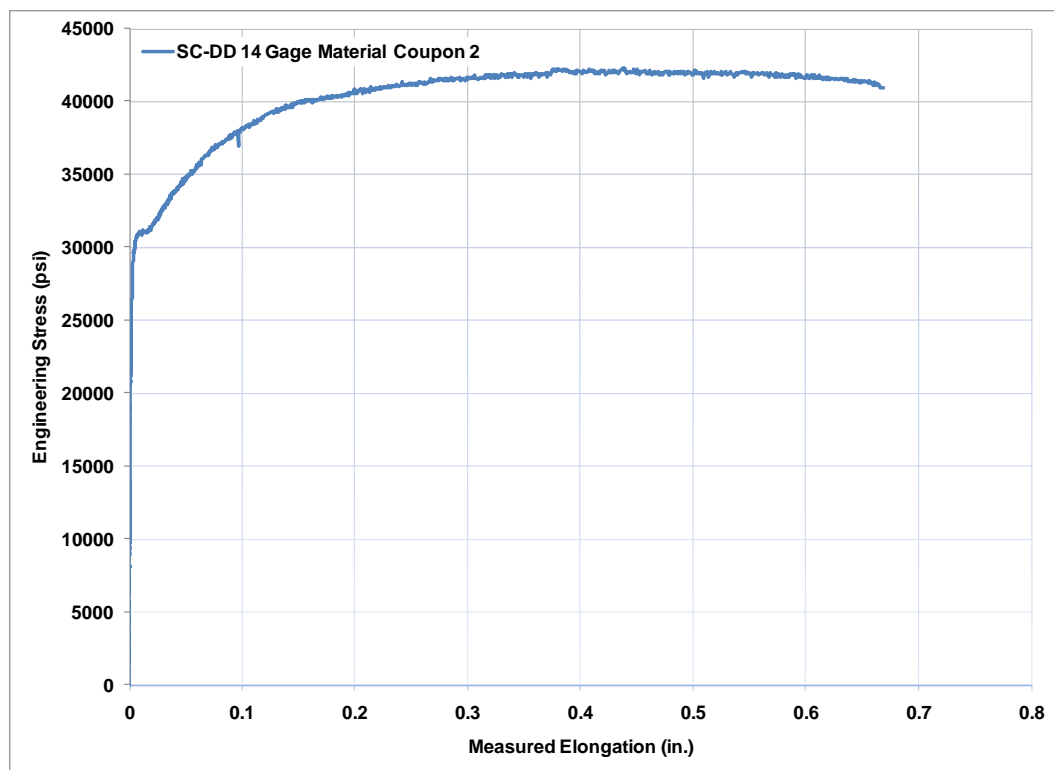


Figure C.21: Engineering stress vs. measured elongation SC-DD 14 Gage Material Coupon 2

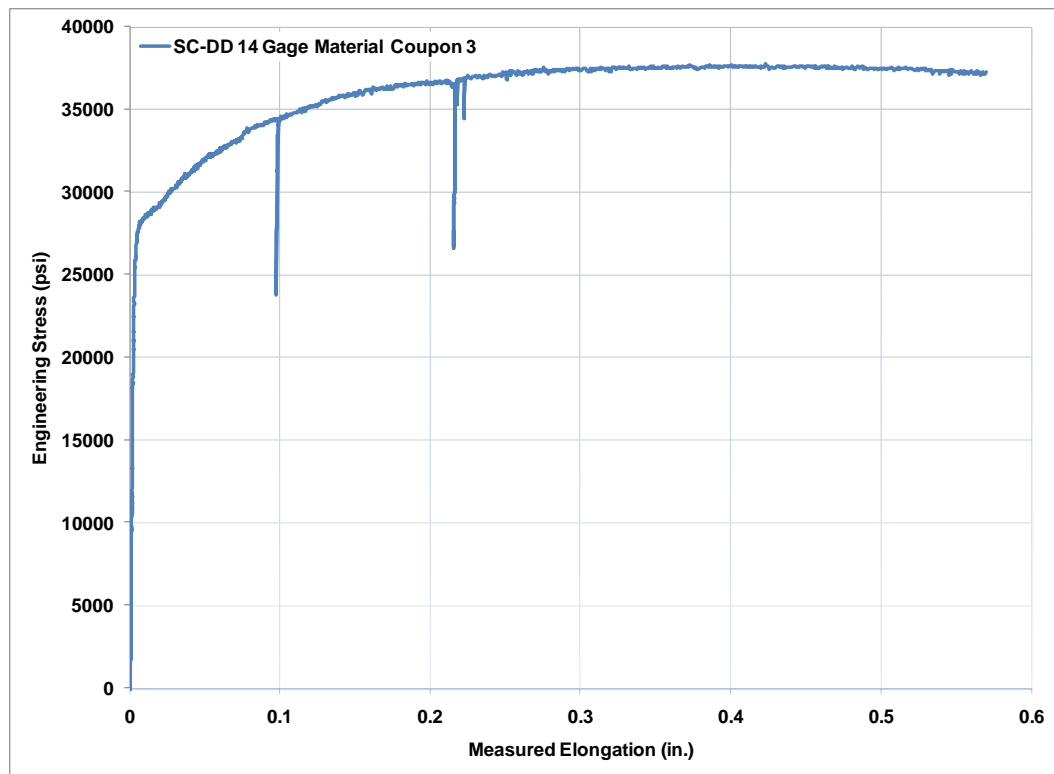


Figure C.22: Engineering stress vs. measured elongation SC-DD 14 Gage Material Coupon 3

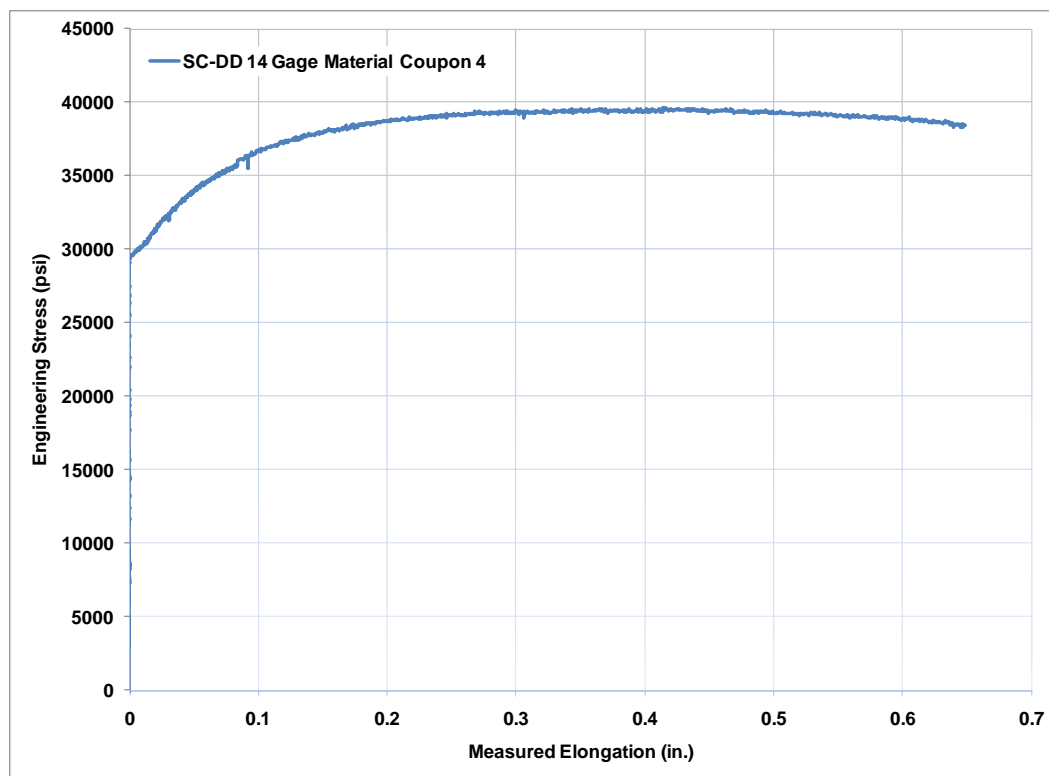


Figure C.23: Engineering stress vs. measured elongation SC-DD 14 Gage Material Coupon 4

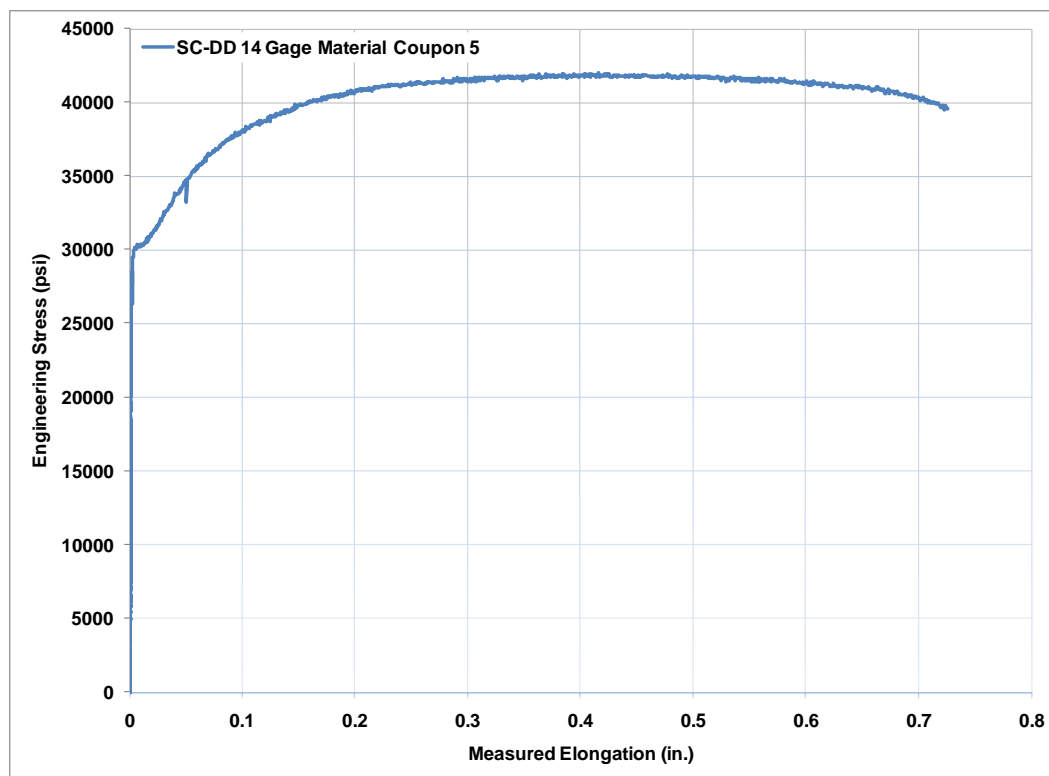


Figure C.24: Engineering stress vs. measured elongation SC-DD 14 Gage Material Coupon 5

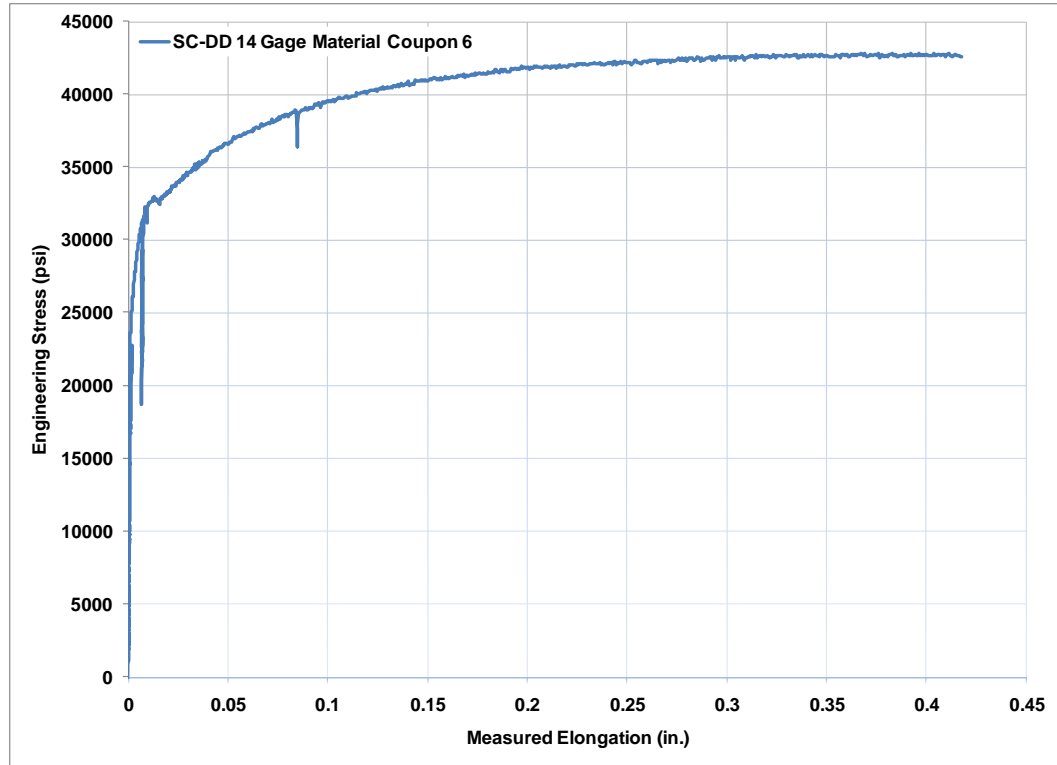


Figure C.25: Engineering stress vs. measured elongation SC-DD 14 Gage Material Coupon 6

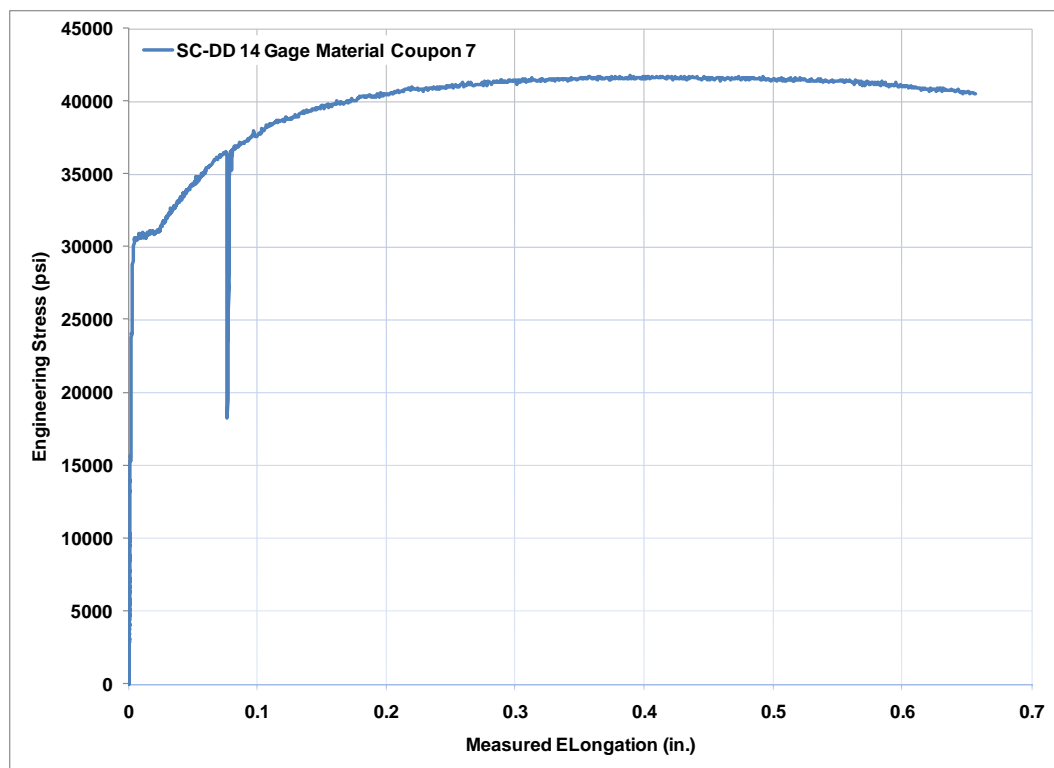


Figure C.26: Engineering stress vs. measured elongation SC-DD 14 Gage Material Coupon 7

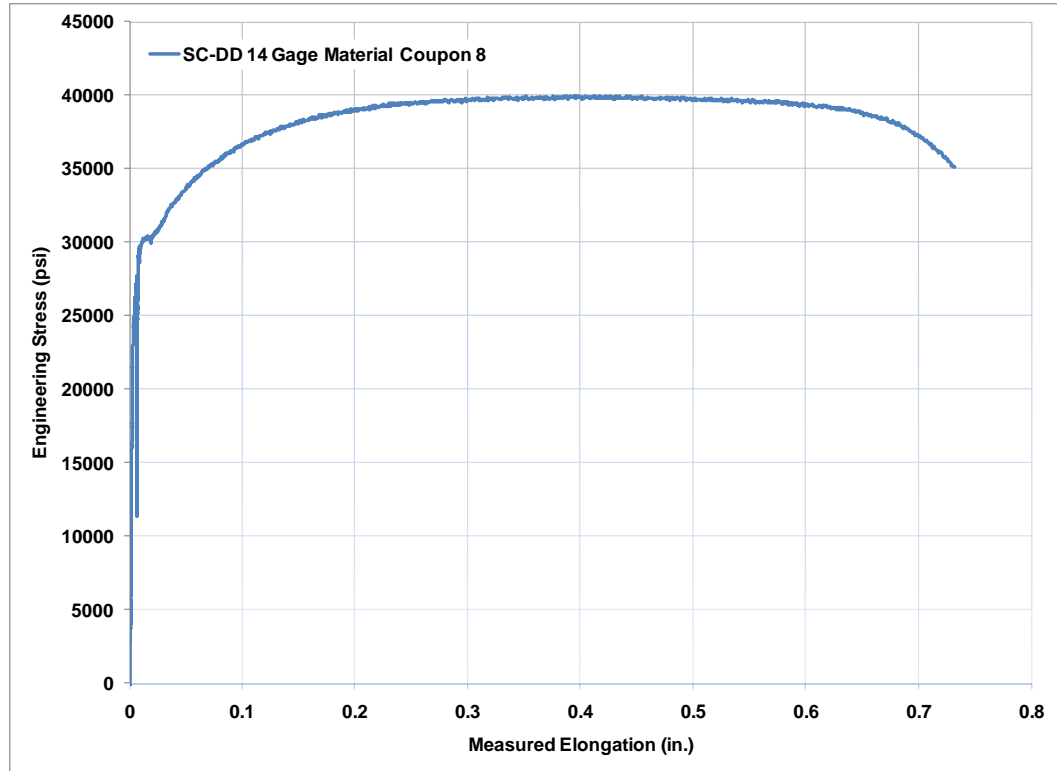


Figure C.27: Engineering stress vs. measured elongation SC-DD 14 Gage Material Coupon 8